SPIE. REMOTE SENSING SPIE. SECURITY+ DEFENCE

INTERNATIONAL YEAR OF LIGHT 2015

CO-LOCATED 2015 CONFERENCES

REMOTE SENSING. AND SECURITY+ DEFENCE.

TECHNICAL SUMMARIES

WWW.SPIE.ORG/RS

WWW.SPIE.ORG/SD

Centre de Congrès Pierre Baudis
Toulouse, France
Conferences: 21-24 September 2015

Exhibition: 22-23 September 2015

SPIE. REMOTE SENSING

2015 SYMPOSIUM CHAIR

CHARLES R. BOSTATER
Florida Institute of Technology,
Marine-Environmental Optics Lab & Remote Sensing Center, United States

2015 SYMPOSIUM CO-CHAIR

KLAUS SCHÄFER
Karlsruhe Institute of Technology, Institute of Meteorology and Climate Research, Germany

Cooperating Organisations

EARSC
European Association of Remote Sensing Companies

CENSIS Innovation Centre for Sensor and Imaging Systems

EARSeL

Optitec

EOS European Optical Society

BORDEAUX Route des Lasers THE PLACE TO BE

SPIE Remote Sensing Contents

9637: **Remote Sensing forAgriculture, Ecosystems, and Hydrology** 3
9638: **Remote Sensing of the Ocean, Sea Ice, Coastal Waters, and Large Water Regions 2015** 39
9639: **Sensors, Systems, and Next-Generation Satellites** 53
9640: **Remote Sensing of Clouds and the Atmosphere** 80
9641: **Optics in Atmospheric Propagation and Adaptive Systems** 96
9642: **SAR Image Analysis, Modeling, and Techniques** 104
9643: **Image and Signal Processing for Remote Sensing** 118
9644: **Earth Resources and Environmental Remote Sensing/ GIS Applications** 156
9645: **Lidar Technologies, Techniques, and Measurements for Atmospheric Remote Sensing** 179
9646: **High-Performance Computing in Remote Sensing** 189

SPIE. SECURITY+ DEFENCE

2015 SYMPOSIUM CHAIRS

DAVID H. TITTERTON
UK Defence Academy,
United Kingdom

REINHARD EBERT
Fraunhofer IOSB, Germany

Cooperating Organisations

EOS European Optical Society

BORDEAUX Route des Lasers THE PLACE TO BE

Optitec

SPIE Security+Defence Contents

9647A: **Unmanned/Unattended Sensors and Sensor Networks** 201
9647B: **Advanced Free-Space Optical Communication Techniques and Applications** 204
9648A: **Electro-Optical and Infrared Systems: Technology and Applications** 208
9648B: **Quantum Information Science and Technology** 217
9649: **Electro-Optical Remote Sensing, Photonic Technologies, and Applications IX** 223
9650A: **High-Power Lasers 2015: Technology and Systems** 234
9650B: **Technologies for Optical Countermeasures** 239
9651: **Millimetre Wave and Terahertz Sensors and Technology** 242
9652A: **Optics and Photonics for Counterterrorism, Crime Fighting, and Defence** 250
9652B: **Optical Materials and Biomaterials in Security and Defence Systems Technology** 259
9653: **Target and Background Signatures** 264

MANAGED BY
SPIE.EUROPE

SPIE Europe Ltd., a subsidiary of SPIE, is a not-for-profit UK-registered company serving SPIE constituents throughout Europe as an advocate and liaison to political and industry associations within the European optics and photonics community.

In addition to providing membership services, SPIE Europe Ltd. organises and manages internationally recognised conferences, education programmes, and technical exhibitions featuring emerging technologies in optics and photonics.

SPIE Europe, 2 Alexandra Gate, Ffordd Pengam, Cardiff, CF24 2SA;
Tel: +44 29 2089 4747 • Fax: +44 29 2089 4750
info@spieeurope.org

9637-2, Session 1

Estimation of crop parameters using multi-temporal optical and radar polarimetric satellite data

Julie Betbeder, Remy Fieuzal, Ctr. d'Etudes Spatiales de la Biosphère (France); Yannick Philippets, Ctr. d'Etudes Spatiales de la Biosphère (France) and Ecole Nationale des Sciences Géographiques (France); Laurent Ferro-Famil, Univ. de Rennes 1 (France); Frederic Baup, Ctr. d'Etudes Spatiales de la Biosphère (France)

Crop monitoring at a fine scale represents an important stake from an environmental point of view as it provide essential information to combine increase of production and sustainable management of agricultural landscapes. Crop identification and characterization can be carried out using accurate ground surveys, spatial modeling and/or remote sensing data.

Nowadays, remotely sensed images offer a unique opportunity to monitor cropland worldwide and to estimate crop parameters at a fine scale. Crop inventories and characterization are generally done using optical images. In some regions, microwave images provide a reliable alternative to optical time series whose accessibility is limited to cloud free periods. However, if some studies have already evaluated the sensitivity of backscattering coefficients to crops parameters, the potential of multitemporal polarimetric data is still unknown. Moreover, few studies were interested in the comparison of multitemporal optical and radar data for crop parameters estimation.

In the context of the actual and upcoming space missions such as Radarsat constellation, Sentinel 1 A/B or Sentinel 2, the objective of this study is to investigate the ability of SAR backscatter, polarimetric and optical time series to estimate crop parameters at a fine scale. To this end, an experimental campaign has been conducted by the CESBIO laboratory, over an agricultural area, during the year 2010 (Baup et al. 2012). This study focuses more particularly on two crop types: wheat and rapeseed.

During the crop vegetation cycles, a series of sixteen quad-polarization Radarsat-2 images were acquired in Fine-Quad-Pol mode, together with seventeen optical images (provided by Formosat-2, SPOT-4&5 sensors) at high spatial resolution (<20m). Synchronously to satellite acquisitions, ground surveys were conducted on 14 wheat fields and 4 rapeseed fields in order to monitor agricultural practices (irrigation, sowing, harvesting...), vegetation parameters (crop height, phenological stages, biomass and crop water content) and soil parameters (top soil moisture, surface roughness). Vegetation index and Leaf Area Index (LAI) were extracted from optical time series. Backscattering coefficients (?°HH, ?°VV and ?°HV) and polarimetric parameters were derived from the Radarsat-2 time series. From the 3X3 coherency matrix (T3) sixteen polarimetric parameters were extracted (Lee & Pottier, 2009): |T_11 | , |T_22 | ,|T_33 | (Pauli matrices), Entropy, Anisotropy, Alpha angle (Cloude-Pottier decomposition), Double bounce, Volume and Surface scattering (Freeman-Durden decomposition), the Shannon entropy, which corresponds to the sum of two contributions related to the intensity and the degree of polarization, the Span, the Radar Vegetation Index and the eigenvalues (?1, ?2 and ?2). The multitemporal signatures of SAR and optical parameters were analyzed, at a landscape scale, over the rapeseed and wheat monitored fields together with crop parameters (crop height, LAI, biomass).

Results show the high potential of backscattering coefficient ?°HV and of some polarimetric parameters (Cloude_Pottier decomposition) for crop parameters estimation (r? > 0.80). Multitemporal polarimetric signatures allow detecting crop phenological stages (e.g. rapeseed flowering period, crop senescence) as accurately or better than optical time series parameters which saturate. SAR parameters appear in this study to be a reliable alternative to optical data for crop parameters estimation, and/or to provide complementary information.

References

F. Baup, R. Fieuzal, C. Marais-Sicre, J.-F. Dejoux, V. le Dantec, P. Mordelet, M. Claverie, O. Hagolle, A. Lopes, P. Keravec, E. Ceschia, A. Mialon, et R. Kidd, « MCM'10: An experiment for satellite multi-sensors crop monitoring from high to low resolution observations », in Geoscience and Remote Sensing Symposium (IGARSS), 2012 IEEE International, 2012, p. 4849 4852.

Lee, J.-S. & Pottier, E. Polarimetric Radar Imaging: From Basics to Applications. (CRC Press, 2009).

9637-3, Session 1

Seasonal parameter extraction of paddy rice fields in West Java using multitemporal MODIS imagery datasets

Riswan S. Sianturi, Willem Nieuwenhuis, International Institute for Geo-Information Science and Earth Observation (Netherlands); Victor G. Jetten, Faculty of Geo-Information Science and Earth Observation (Netherlands)

West Java is one of main rice producing regions of Indonesia. Understanding of phenology and seasonal parameters of paddy rice field provide better information in assessing the sustainability of farming practices. This current study utilized multitemporal 8-day MODIS imagery datasets (MOD09A1) from 2010 to 2014 to map and characterize paddy rice field in West Java, Indonesia. Time series Enhanced Vegetation Index (EVI) datasets are derived and further smoothed by adaptive Savitzky-Golay filter the noise of the data. Seasonal parameters (e.g. Start of Season (SOS), End of Season (SOS), Length of Season (LOS), Peak) of paddy rice fields from time series EVI data were extracted using methodology from TIMESAT software. The results are further validated using primary and secondary datasets collected during fieldwork.

9637-4, Session 1

Using remote sensing to calculate plant available nitrogen needed by crops on swine factory farm sprayfields in North Carolina

Elizabeth Christenson, Marc Serre, The Univ. of North Carolina at Chapel Hill (United States)

Industrial-sized swine concentrated animal feeding operations (CAFOs) have well documented environmental consequences for ground and surface water quality. North Carolina (NC) is the second largest producer of hogs in the United States with Duplin county, NC having the densest hog population in the world. Waste from swine CAFOs is stored in open air lagoons and sprayed onto sprayfields as fertilizer. Swine CAFOs are regulated based on their ability to have nutrient management plans (NMPs) that have balanced plant available nitrogen (PAN), the estimated portion of nitrogen that remains available to for crops to use after nitrogen volatilizes into the atmosphere during irrigation. For balanced PAN, PAN in annual manure produced by swine must be less than the PAN annually utilized by crops grown on sprayfields. PAN needed by crops is dependent on crop and soil types. Objectives of this research are first to quantify the difference in hog manure PAN balance between CAFO point and sprayfield area locations at two sub-watershed spatial scales in Duplin

county, NC. In doing so, a review of all 485 active NMP permits in Duplin county was conducted, the first NC sprayfield spatial database created for over 24,000 permitted sprayfield acres, and summary descriptive characteristics of Duplin county NMPs presented. Second, a new, time-efficient remote sensing method was developed to identify PAN balance on sprayfields at two sub-watershed spatial scales in Duplin county for years 2008-2014. Using sprayfield location rather than CAFO point location markedly affected PAN balance at two sub-watershed scales. Many more shifts in PAN balance were observed at the catchment level compared to the larger sub-watershed scale. Using the annual remote sensing method instead of permit data to identify PAN balance along with sprayfield location information allowed calendar year identification for which crops were grown at sprayfield and sub-watershed scales. Comparatively, NMP PAN balance calculations are averaged annually and do not disaggregate by year or are able to identify calendar year for which a particular crop is grown. Many NMPs have a lot of potential crop options with a large range of PAN needed by crops. Although permitted data have more detailed crop information than remotely sensed data, PAN identification using remotely sensed data is more time efficient, internally consistent, easily publically accessible, and has the ability to identify annual changes in PAN balance at the sprayfield and sub-watershed levels. Once sprayfield location is known, remote sensing can be used to quantify PAN balance at the sub-watershed scale and better inform targeted water quality monitoring of swine CAFOs.

9637-5, Session 2

A critique of field spectroscopy and the challenges and opportunities it presents for remote sensing for agriculture, ecosystems, and hydrology *(Invited Paper)*

Alasdair Mac Arthur, The Univ of Edinburgh (United Kingdom)

This presentation will review the historic context, physical principles, modern evolution, and contemporary challenges of field spectroscopy and development of near-ground Earth observation (EO) for remote sensing (RS) agriculture, ecosystems, and hydrology.

There is evidence in the early modern French scientific literature (circa 1700) that relationships between the colour of leaves and their composition was being investigated. However, instruments capable of spectral measurements were not available at that time. Fast tract to the early 20th century and instruments were in evidence in scientific laboratories. In these laboratories spectral measurements were being made and relationships with photo-active pigments and wavelength regions established. The fundamental principle underlying spectroscopy, is that a) when light interacts with any surface there is a photon energy level and flux density change, b) that the light measured by the spectrometer will contain information of both the light source and the surface with which it has interacted,. Therefore, light has then becomes an 'information' carrier. From this information it may be possible to infer or estimate some properties of that surface. So in spectroscopy we measure the energy level, indicated by wavelength, and flux density of photons per unit time, often in relation to some standard reference to try to relate our measurements to those of others separated by space and time and spectroscopy has a well-documented pedigree.

In the 1950's the potential of spectrally sampling the Earth's surface from airborne platforms was realised. Consequently, through the 1960s field spectrometers began to be developed albeit either scanning instruments, with limited resolution and sensitivity, or recording a limited number of bands and both with limited spectral range to better understand the interaction of light with Earth surfaces and further understand the airborne images. With the dawn of the space age, there was the realisation that the Earth's surface could be classified using spectral information and these space-based observations could provide unprecedented insights into ecosystem distributions, Earth system process, and physical and chemical properties. This drove forward the development of field spectroscopy as a) there need to better understand the optical properties, both spectral and directional, of Earth surfaces and the physical and chemical properties that could be inferred and b) there was a need to calibrate and or validate space-based observations. These last needs arise because spectral sensors on satellites record 'at sensor' radiance and, as light will have interacted with the Earth's atmosphere after leaving the surface and will therefore carry information of these interaction as well as the surface information of interest to scientists. These interactions need to be accounted for. In addition, the calibration status and stability of sensors on board satellites needs to be verified after launch and as the sensors age. Field spectroscopy and field spectrometers have therefore developed to increase our understanding of the interaction of light with Earth surfaces and as a method of calibrating or validating (cal/val) observations from air- or space-borne sensors. Different instrument designs and measurement methods and measurement modes have developed and will be discussed.

From the early scanning spectrometers, field work was constrained by detector sensitivity, computing power, power consumption, portability and many other factors. However, over the last twenty years or so instruments have become ever more reliable and portable, leading to increasing use both to support science and as optical remote sensing teaching and training tools. The uncertainties associated with field spectral measurements are now widely recognised and field sampling methods and instrument continue to be developed to enable these uncertainties to be quantified and minimised. However, it is worth emphasising that field spectroscopy is a passive RS method relying on the ever changing Sun and sky as the source of light. As the energy level and flux density from the source changes so too will the reflected radiance that we wish to measure. This leads to a number of key challenges which need to be addressed if field spectroscopy is to provide reliable and replicable measurements. Much progress has been made and state-of-the-art field spectrometer systems and field methodologies are being developed to address these issues and will be introduced and discussed here. One major further constraint on the use of field spectroscopy has been the size of the field measurement support and the significant mismatch in scale between these and the air- and space-borne observations – the so called 'Remote Sensing Scaling Issue'. However, in the last two or three years even this issue has begun to be addressed with the development of unmanned aerial vehicles as platforms for lightweight and miniaturised spectrometers controlled by mico-computers. It is now possible to non-invasively sample terrestrial and hydrological ecosystems in a statistically robust manner and do so with supports similar in scale to those of air- and space-borne sensors. These developments will revolutionise the use of field spectroscopy to support empirical science and model development and validation and this case will be made here.

9637-6, Session 2

Determination of pasture quality using airborne hyperspectral imaging

Rajasheker Reddy Pullanagari, Gabor Kereszturi, Ian J. Yule, Mathew E. Irwin, Massey Univ. (New Zealand)

Pasture quality is a critical determinant which influences animal performance (live weight gain, milk and meat production) and animal health. Assessment of pasture quality is therefore required to assist farmers with grazing planning and management, benchmarking between seasons and years. Traditionally, pasture quality is determined by field sampling which is laborious, expensive and time consuming, and the information is not available in a real-time. Hyperspectral remote sensing has potential to accurately quantify biochemical composition of pasture over wide areas in great spatial detail. In this study an airborne imaging spectrometer (AisaFENIX, Specim) was used with a spectral range of 380-2500 nm with 448 spectral bands. A case study of a 1000 ha hill country farm in New Zealand is used to illustrate the use of

the system. Radiometric and atmospheric corrections, along with automatized georectification of the imagery using Digital Elevation Model (DEM), were applied to the raw images to convert into geocoded reflectance images. Then a multivariate statistical method, partial least squares (PLS), was applied to estimate pasture quality such as crude protein (CP) and metabolisable energy (ME) from canopy reflectance. The results from this study revealed that estimates of CP and ME had a R2 of 0.77 and 0.79, and RMSECV of 2.97 and 0.81 respectively. By utilizing these regression models, spatial maps were created over the imaged area. These pasture quality maps can be used for adopting precision agriculture practices which improves farm profitability and environmental sustainability.

9637-7, Session 2

An advanced fluorescence lidar system for the acquisition of interleaved active (LIF) and passive (SIF) fluorescence measurements on vegetation

Valentina Raimondi, Lorenzo Palombi, Paola Di Ninni, Istituto di Fisica Applicata Nello Carrara (Italy)

Fluorescence-based techniques have been regarded for a long time as a valuable tool to investigate the eco-physiological state of vegetation. Chlorophyll a, which emits a typical fluorescence in the red region of the e.m. spectrum, plays a key role in the photosynthetic process and its fluorescence is considered an effective proxy of photosynthetic activity of plants. Hence the interest for fluorescence-based techniques for the remote sensing of vegetation fluorescence as a means for large-scale monitoring of plants health.

Laser Induced Fluorescence (LIF) has been studied for several decades, both at leaf- and canopy-level by means of optical fibers-coupled instrumentation and fluorescence lidar systems. On the other hand, solar-induced fluorescence (SIF) has been the object of several scientific studies quite recently, with the aim to investigate the feasibility of measuring the fluorescence of vegetation using passive spectroradiometers and the so-called Fraunhofer Line Discriminator (FLD) method in view of global scale from satellite platforms.

This paper presents the main technical features and preliminary tests of a fluorescence lidar imager, recently upgraded so as to carry out interleaved LIF and SIF hyperspectral measurements at canopy level. The lidar imager uses as an excitation source a tripled Nd:YAG pulsed laser (8-mJ output energy, 5 ns width pulse, 15-Hz max. repetition rate). The laser beam is sent to a large scanning mirror controlled by a PC and used to obtain a 2-D mapping of the canopy. The signal is collected by a telescope (1000-mm focal length, f/4), filtered and focused on a optical fiber bundle coupled to the inlet slit of a flat field 300-mm focal length, f/3.9 spectrometer equipped with three different and selectable diffraction gratings (150 gg/mm, 600 gg/mm and 2400 gg/mm). The detector is a ICCD gateable camera. Nominal spectral resolution @ 435.8 nm is 0.51 nm/pixel, 0.12 nm/pixel and 0.02 nm/pixel depending on the used diffraction grating. In-house developed electronics and relevant GUI permit the acquisition of interleaved LIF and SIF spectra by driving the laser on/off operation mode, the selection of the suitable grating, the setting of the integration time and the synchronisation of the ICCD gate opening time in correspondence with the incoming signal. Interleaved LIF and SIF acquisition mode allows for the collection of remote LIF/SIF maps at canopy level with a spatial resolution of 1 cm at a distance of 10 m from the target. For each pixel of the map, the dataset consists of a LIF spectrum – from 570 nm to 830 nm with a spectral resolution of 0.5 nm - and of a radiance spectrum containing the O2-A and O2-B molecular oxygen absorption lines at 760 nm and 687 nm, respectively. The latter can be acquired either with a spectral resolution of 0.1 nm to detect simultaneously the O2-A and O2-B lines or with a spectral resolution up to 0.02 nm to obtain highly-resolved spectral features for polynomial regression data fit for SIF retrieval. In the latter case only one telluric line (either O2-A or O2-B) at a time can be monitored.

9637-8, Session 2

Estimation of leaf chlorophyll content in winter wheat using variable importance for projection (VIP) with hyperspectral data

Peng He, Xingang Xu, National Engineering Research Ctr. for Information Technology in Agriculture (China); Baolei Zhang, Shandong Normal Univ. (China); Zhenhai Li, Haikuan Feng, Guijun Yang, National Engineering Research Ctr. for Information Technology in Agriculture (China)

Accurate estimation of chlorophyll content has great significance in the study of the winter wheat. Selecting the closed related variable is important for indicating nutrition status and photosynthetic. Multiple linear regression analysis, e.g. stepwise regression analysis, and partial least squares regression (PLSR), is one approach to inverse the leaf chlorophyll content .The variable importance for projection is one of variable selection methods. The VIP technology based on the PLSR could be used to the little samples and strong correlations data.

In this study, the study area is located in national demonstration base of precision agriculture research. The data of two years,2011-2012 and 2012-2013 growing seasons, were selected to build chlorophyll model, which 186 sampling point was use to the model establishment during 3 growth periods including booting stage,anthesis stage and filling stage.The data of 2009-2010 growing season including 108 points was used to validate the model. Two methods, the variable importance for projection(VIP) and the grey relational analysis(GRA), were used to extract four kinds of hyperspectral features including the reflectance spectra and the first derivative spectra, vegetation indices and absorption and reflectance position. The best five variables of each feature were applied to estimate leaf chlorophyll content using PLSR respectively..

The results indicated that the spectral regions of green peak (520nm-550nm), and the red edge (710nm-780nm) were the most sensitive to chlorophyll. Most features in these regions presented a high correlation with chlorophyll, with a higher GRA and VIP values. Compared with the grey relational analysis, the VIP had a better prediction results. The method by VIP had the higher R2 and lower RMSE, except the VIP had the similar R2 and RMSE in vegetable indices. In addition, the performance curve with reflectance spectra by VIP (R2 =0.42; RMSE = 0.66mg/g) is better than the curve by the GRA (R2 = 0.17; RMSE = 0.79mg/g). The same result was demonstrated with the first derivative spectra, with R2 and RMSE values of 0.40 and 0.68mg/g, and 0.34 and 0.71mg/g for VIP and GRA, respectively. The VIP method selecting vegetable indices (R2 = 0.41; RMSE = 0.71mg/g) resulted in a lower estimation than that by GRA method (R2=0.52; RMSE=0.61). There was little error in vegetable indices because vegetable indices was so common that both methods were used to them. Above all, this study suggests that it is appropriate to the quantitative study of leaf chlorophyll content in winter wheat using VIP method.

9637-9, Session 2

Disease stress detection on citrus using a leaf optical model and field spectroscopy

Mrunalini R. Badnakhe, Surya S. Durbha, Jagarlapudi Adinarayana, Indian Institute of Technology Bombay (India)

As citrus is progressively contributing to horticultural production, wealth and economy of India, it is necessary to understand the factors impacting citrus production. Gummosis is one of the most serious diseases causing considerable loss of overall citrus production and yield quality. A qualitative and quantitative analysis of citrus leaf biochemical properties are necessary to monitor the crop health, disease /pest stress

and production. Leaf Chlorophyll Content (LCC) represents a one of the key biophysical factors which contributes in water, carbon, energy exchange processes. Leaf Chlorophyll Content gives interpretative information on leaf thickness, photosynthesis, respiration rate, etc. It dominates the spectral signal of leaf at visible range. Photosynthesis production in citrus will be disturbed as gummosis disease life cycle progresses. To evaluate the photosynthesis rate and disease stress, it is a prerequisite to retrieve the LCC. An emerging use of hyperspectral remote sensing provides a better solution for extracting specific leaf variables than other multispectral sensors. In this study the potential of PROSPECT biophysical modeling to predict LCC in citrus orchards was undertaken at different sites. This study derives the temporal analysis from June 2014 to March 2015. LCC were clearly influenced by the leaf optical properties. The main aim was to evaluate the relationship between the LCC and gummosis disease stress for citrus with its phenological stages. To address the challenge, Inversion PROSPECT model was used to extract the leaf parameters influencing disease. The hyperspectral data is collected from different citrus orchards using SVC GER-1500 Field Spectroradiometer within range 350- 1050 nm. A different approach is implemented with field hyperspectral data which runs using information extraction entirely from ground-based. The PROSPECT model was simulated for the reflectance spectra. This well known model is inverted with the ground truth hyperspectral reading. The testing was separately initiated for healthy and infected plant leaves. This leads to understand the disease stress on citrus leaves. For accuracy, raw spectra are filtered and processed which is an input parameter for Inversion PROSPECT model. Healthy and infected plant leaf biochemical parameters were extracted. Validation results are based upon knowledge bases of LCC for different phenological stages from literature. The accuracy is assessed with Root Mean Square Error (RMSE), Coefficient of Determination (R2) for comparison with total leaf chlorophyll content. The disease incidence surveillance data was also collected from same orchards. The disease incidence at the each citrus orchard is determined. The correlation of the LCC was estimated with disease incidence for each place to understand the dependency between LCC and disease stress. The work will be further extended with hyperspectral airborne imagery for regional scale. The spatial analysis can be initiated with in situ quantification of LCC. More advances in the retrieval of citrus leaf biochemical components will require novel use of existing remote sensing data within physically realistic canopy reflectance models along with the ability to exploit the enhanced spectral and spatial capabilities of upcoming satellite systems.

9637-10, Session 3

Complementing airborne laser bathymetry with UAV-based lidar for capturing alluvial landscapes

Gottfried Mandlburger, Technische Univ. Wien (Austria); Martin Pfennigbauer, Alexander Haring, Peter Rieger, Ursula Riegl, RIEGL Laser Measurement Systems GmbH (Austria); Martin Wieser, Philipp Glira, Technische Univ. Wien (Austria); Lukas Winiwarter, TU Wien, Department of Geodesy and Geoinformation (Austria)

Airborne laser bathymetry (ALB) has experienced a boost of attention in the past years through the introduction of topo-bathymetric systems being able to capture high resolution topography for shallow water areas and the surrounding littoral zones simultaneously. Another topic which is just in the process of revolutionizing certain areas of the surveying business is UAV-based laser scanning (ULS). In this paper we report on a surveying campaign employing both methods with the aim to assess how information gained from non-bathymetric ULS can support the ALB data.

We present an approach for analyzing the quality and validation process of water surface modeling in airborne bathymetric LiDAR by analyzing the results of a practical experiment of simultaneous airborne LiDAR survey with two different types of aircraft and sensors, an ALB system operated from a fixed-wing aircraft in 600 m altitude in concurrence with a small topographic LiDAR sensor on a high-performance unmanned aerial system platform. Analytic outcome and practicability of this approach for different environments in hydrology, ecohydraulics, and combined topo-bathymetric applications are discussed.

The first analysis relies on a dual-wavelength LiDAR survey (water penetrating green laser and near-infrared surface laser) carried out in a periodically surveyed test area in Austria (River Pielach) in order to monitor alluvial changes due to fluvial activity caused by high discharges in response to precipitation and/or snow melt events. The outcome of an airborne topo-bathymetric LiDAR system, the RIEGL-VQ-880G, employing a powerful 532nm visible green laser from 600m AGL is complemented by data from a low-altitude UAV-based LiDAR sensor working at non-penetrating wavelength (near infrared). It is investigated how the generation of the water surface model (WSM) and the calculation of refraction correction in airborne LiDAR can be improved making use of information gained through a simultaneously operated high density UAV-based LiDAR (RIEGL VUX-1 at 30 m AGL, field of view 270°, laser pulse repetition rate 550kHz). Its capability of registering short term changes of water levels considerably improves the reliability of the WSM, allowing to account for water surface movement tendencies over the duration of observation. Furthermore the findings can be used for refining the classification and modeling algorithms.

Furthermore, and in juxtaposition to the parallel dual-wavelength LiDAR data acquisition we discuss the tendencies of multi-sensor bathymetry in the UAV sector enabling high degrees of penetration and precision by close-to-surface sensor arrangements.

9637-11, Session 3

Olive trees LAI estimation using TLS and UAV

Rosanna Sciortino, Tiziano Caruso, Francesco Paolo Marra, Mauro Lo Brutto, Univ. degli Studi di Palermo (Italy)

The interactions between the vegetation and the atmosphere, the light radiation regimes through the vegetation canopies and the carbon, water cycles and fruit productivity depend significantly on the canopy architecture. The ability to accurately and rapidly acquire leaf area index (LAI), which can be defined as the total one sided leaf area per unit ground surface area (Bréda 2003; Wasseige et al. 2003), is an essential component of process-based ecological research facilitating the understanding of gas-vegetation exchange phenomenon at an array of spatial scales from the leaf to the landscape. LAI depends from the specie, developmental stage, seasonality and the management practices; it can be assessed directly by using leaf harvesting methods such as destructive sampling. However, direct measurements are difficult and labor-intensive.

Indirect LAI determination methods, in which leaf area is inferred from observations of another variable, are generally faster, amendable to automation, and thereby allow a larger spatial sample to be obtained. Recently LAI research focus has shifted from an empirical and statistical stage to process-based modelling stage due to the involvement of remotely sensed datasets and numerical ecological model implementation. Nevertheless, the use of indirect methods could affect the accuracy of LAI estimation. The first cause is the randomly distribution of tree foliage resulting in overlapping and clumping between the leaves of the canopy. If we want to obtain true LAI, these effects should be carefully considered and incorporated into the LAI estimations.

Accurate geometric information of trees could contribute to better describe the canopy shape and to understand the light regime within the canopy. Emerging 3D techniques as terrestrial laser scanning (TLS) or unmanned aerial vehicle (UAV) could be used to obtain very detailed 3D model of tree canopy and give new possibility in LAI measurement. Spatially 3D measurements extracted from TLS and UAV data

could became an indispensable component for modelling and simulation of ecological variables and processes.

In this paper, we evaluate the potential of TLS and UAV for canopy shape reconstruction and for LAI estimation in olive trees.

In particular, we compered the above mentioned indirect LAI measurements with the true direct LAI measurements of three years old potted olive trees. Point cloud density was an important parameter to estimate canopy shape showing statistically significant differences for the different resolutions tested.

The proposed methods could be applied to different areas, since they are not based on an empirical fit but on the analysis of the 3D canopy shape.

9637-12, Session 3

Evaluation of estimation of vegetation index by drones for different crops

Lúcio A. C. Jorge, Ricardo Y. Inamasu, Ziany N. Brandão, EMBRAPA (Brazil)

This research aimed to verify the precision and accuracy of orthomosaics generated automatically by aerial photography taken with an Unmanned Aerial Vehicle (UAV) in crop areas. It was verified the influence of the scale, depending on the flight height, the influence of the sunlight, and the phenological analysis obtained in agricultural areas with corn and cotton crops. Flight plans were drawn up in mission planner with pixhalk planner software. The camera on board UAV was the Canon S100, with a spatial resolution of 24 megapixel. To check the precision and accuracy of orthomosaics in crop areas, the flights were uniformly distributed in the study area with three-dimensional coordinates pre-marked targets read in the orthomosaic itself, and compared with the coordinates obtained by RTK positioning methods. The reflectance was measured by spectroradiometer FildSpec 3 and compared with obtained by drone. We have found that in those orthomosaics performed over the crop area without ground control points. It was observed that for a better estimate of vegetation index, the photographs needs to with larger scales (GSD of 5 cm) but there is a difficulty in finding homologous points. It did not occur when we used pictures with smaller scales (GSD 30 cm, or larger) for the generation of orthomosaics.

9637-13, Session 3

The inversion model of soil organic matter of cultivated land based on hyperspectral technology

Xiaohe Gu, Yancang Wang, Xiaoyu Song, Xingang Xu, National Engineering Research Ctr. for Information Technology in Agriculture (China)

Soil organic matter (SOM) is one of the most important indicators of cultivated land fertility, which has great influence on the other nutrient factors and physicochemical characteristics. Monitoring soil organic matter in the cultivated land quantitively and mastering its spatial change are helpful for the adjustment of fertility and sustainable development of agriculture.

The geostatistical method had been applied in the spatial pattern of SOM in large scale, which required plenty of field samples with great workload and poor timeliness. The hyperspectrum technology could be used to detect the targets quickly and nondestructively. The study aimed to develop a universal method to monitor SOM by hyperspectrum data, which could provide mechanism support for mapping SOM at county scale.

The Anping county of Hebei province in China was chosen as study area, where loam soil dominated in the cultivated land with the planting rotation of winter wheat and summer maize. The 32 SOM samples were collected in June, 2014, of which the hyperspectrum data was measured by the spectrometer named Field Spec Pro FR 2500. The spectrum range of the spectrometer is from 350 nm to 2500 nm with the interval of 1 nm.

The main idea of the study could be described as follows. Several mathematical transformations were used to improve the expression ability of hyperspectrum data. The correlations between SOM and the hyperspectrum reflectivity and its mathematical transformations were analyzed. Then the feature bands and its transformations were screened to develop the optimizing model of monitoring SOM based on partial least squares method (PLS). The in-situ sample was used to evaluate the accuracy of the model. The model stability was validated by the determination coefficient (R2). The prediction ability of the model was validated by the root-mean-square error (RMSE).

Results showed that the bands of 529 nm, 597 nm, 869 nm, 1168 nm, 1420 nm with different mathematical transformations had good correlation with SOM, which could be considered as sensitive bands. By the validation of in-situ samples, the inversion model with the one differentiation of logarithmic reciprocal transformation ( ) of reflectivity could reach highest correlation coefficient (0.643) with lowest RMSE (2.622 g/kg), which was considered as the optimizing inversion model of SOM. Taken the 11 unused samples as true value, the accuracy of the optimizing model was validated. The determination coefficient (R2) of testing samples was 0.602, while the RMSE was 2.65 g/kg. It indicated that the one differentiation of logarithmic reciprocal transformation of hyperspectrum had good response with SOM of cultivated land. Based on this transformation, the optimizing inversion model of SOM could reach good accuracy with high stability.

9637-14, Session 3

Mangrove species mapping in Kuala Sepetang Mangrove Forest: Perak using high resolution airborne data

Beh Boon Chun, Mohamad Zubir Mat Jafri, Hwee San Lim, Univ. Sains Malaysia (Malaysia)

Mangrove vegetation is widely employed and studied as it is a unique ecosystem which is able to provide plenty of goods and applications to our country. In this paper, high resolution airborne image data obtained the flight mission on Kuala Sepetang Mangrove Forest, Perak, Malaysia are used for mangrove species mapping. Maximum Likelihood Classifier in supervised classification was performed to classify the airborne data using Geomatica 2013 software package. The ground truth data are used to validate the classification accuracy. Higher kappa coefficient results (>80%) obtained in this study indicate that high resolution airborne data is reliable and suitable used for mangrove species mapping.

9637-16, Session 4

Introduction of a multifunctional tool for the evaluation of uncertainty and accuracy in multitemporal object-based land use classification

Patrick W. K. Knoefel, Fabian Löw, Julius-Maximilians-Univ. Würzburg (Germany); Henning Gerstmann, Markus Moeller, Martin-Luther Univ. Halle-Wittenberg (Germany); Xingmei Xu, Helmholtz-Zentrum für Umweltforschung GmbH (Germany); Christopher Conrad, Julius-Maximilians-Univ. Würzburg (Germany)

The aim of this study is the development of methods for the detection of optimal temporal windows for crop mapping in order to provide a more cost and calculation time efficient land use classification. One particular focus is set on the separation of cereal crops like winter wheat, barley, and rye

because the classification of this crop types is often limited by high spectral and phenological similarities. In context of the PhenoS project ("Phenological structuring to determine optimal acquisition dates for Sentinel-2 data for field crop classification"), a classification tool called MELanGe ("Multi-functional tool for the Evaluation of Land use classification and Geometric accuracy") was developed. Study regions of PhenoS are the German TERENO test-sites "The Harz/Central German Lowland" and "Demmin".

MELanGe uses, object based random forest (RF) classification to investigate the impact of image acquisition frequency and timing on crop classification accuracy. The required zonal information to train the RF classifier originates from the tool itself, it performs an automatic calculation of spectral metrics based on the selected objects. Here, different sampling methods for the selection of training objects were tested prior to implementation to improve the robustness of the classification results. In order to achieve the objectives of the PhenoS project a coupling of multi-temporal spectral characteristics and phenological events is promising. Therefore, new phenological metrics were developed and tested to improve the separability of the studied crop types. After the final compilation of the set of metrics MELanGe performs a permutation of RF classifications for all possible combinations of the available RapidEye time series recorded on the TERENO sites between 2010 and 2014. In an interactive part of MELanGe the user can simulate different data availability by selecting or deselecting specific time steps. It also allows the user to visualize the classification accuracy results of specific crop types, as well as the time step combinations with highest classification accuracies. The tool also provides the ability to investigate the geometric accuracy of the training objects in order to evaluate their impact on the classification accuracy. This is done using a metric which is characterizing the differences in size and position between training objects and reference segmentation results. These metric can be used to improve the reliability of object based land use classifications.

The accuracy assessment of the object selection methods demonstrates that stratified sampling methods leads to more robust classification results compared to random object selection for instance. In addition, an importance analysis of the used metrics for the best separability of the investigated crop types was performed. Furthermore, the results of the study indicate that classification and geometric accuracy evaluation provide a valuable addition to traditional accuracy assessments and helps the user to allocate error in crop maps.

9637-17, Session 4

A fast and versatile algorithm for object generic classification in RapidEye images

Salvador L. Esparza-Govea, Colegio de Postgraduados (Mexico); Fermin Pascual-Ramirez, Univ. Nacional Autonoma de Mexico (Mexico); Jose-Luis Oropeza-Mota, Mario R. Martinez-Menes, Carlos Castañeda-Ibañez, Colegio de Postgraduados (Mexico); Delfino Reyes-Lopez, BUAP (Mexico); Salvador Medina-Torres, UAIM (Mexico)

The use of imagery collected by sensors onboard of satellite platforms for knowledge of the land cover is particularly important due to its high spatial and temporal resolution. The process of identification or classification of objects in an image of this type can be performed using a variety of methodologies that are available in softwares for satellite imaging and platforms for development of geographic information systems. However, methods employed to date are based on algorithms that require training points, thorough understanding of field and statistical post-processing for the proper operation; this represents a disadvantage when large volumes of images are handled. In this paper, a development based on invariant behavior patterns of generic objects in the ranges of the electromagnetic spectrum analyzed by the RapidEye sensor is presented. RapidEye satellite imagery, characterized by high spatial and temporal resolution, are typically used in studies for crop monitoring and for planning and management of natural resources. Its spectral bands ranging from 440 nm to 850 nm wavelength in the optical bands visible (blue, green, red), red boundary and near infrared, of the electromagnetic spectrum are suitable for the activities described above. The development work was performed using spectral libraries JHU, USGS and JPL; convolutions of data were generated in the same spectral range of interest sensor bands using the 'Spectral Library Resampling' ENVI module. After adjusting the spectral libraries, both relative reflectance patterns between bands and absolute in each band of the reported objects were analyzed. Were selected 11 main groups of objetcs of interest: deep water, cursory water, soil, asphalt, high vegetation, medium vegetation, low vegetation, dark vegetation, cloud, shade and ice. With this information, was generated a classification algorithm based on the analysis derived from the information contained in spectral libraries; were proposed conditions based on Boolean operations to discriminate between objects. Subsequently, the algorithm was programmed and performance was tested by performing classification on a set of 17 satellite images obtained by the RapidEye satellite constellation in Europe, North America, Brazil, China, Malaysia and Australia; the shooting dates of the images were between April 2009 and June 2011. The images were converted to radiance and atmospheric correction was applied using the ENVI FLAASH module. Finally, when analyzing the results they showed an accuracy of 87.9% when compared to supervised classification with training sites based on photo interpretation using the maximum likelihood method. This leads to the conclusion that the algorithm developed was appropriate because satisfactory results were obtained when using it on a set of images.

9637-18, Session 4

An object-based image analysis approach for developing a green cadastre for monitoring of private urban gardens: case study of Hashemieh district, Mashhad, Iran

Hossein Vahidi, Wanglin Yan, Keio University (Japan)

This study aims to develop a geographical object based image analysis (GOBIA) approach to detect and delineate individual tree crown objects in the landscape by exploitation of Very High Resolution (VHR) imagery for the means of establishing a green urban cadastre for monitoring and preserving the trees in the urban private gardens. In the proposed framework, the classification strategy considers the different spectral, spatial and contextual characteristics of tree crowns in the private garden space to formulate the set of classification rules to identify the tree objects. The proposed OBIA framework is implemented on multi-temporal QuickBird Images from Hashemieh District, Mashhad, Iran as a good example of fast growing district in Mashad, Iran to detect and delineate the individual trees located in urban private gardens to create a pilot fine resolution tree inventory system for official and legal applications in the context of urban private gardens. Finally to assess performance of proposed OBIA framework an object based accuracy indicators have been used and the outputs have been evaluated.

9637-20, Session 4

Land usage analysis: a random forest approach

Nasru Minallah, Hidayat U. Rehman, Univ. of Engineering & Technology, Peshawar (Pakistan)

Land usage analysis takes advantage of the multi-band imagery for classification and recognition. Multi-bands data contains reliable information compared to the raw image formats e.g. RGB, HIS, HSV and other color spaces. In this paper, we advocate the usage of non-parametric machine

learning algorithms for land usage analysis. From the non-parametric algorithms, we propose a random forest approach for land use analysis. Our analysis is concerned with the classification of land into seven classes. We have shown that non-parametric classifier the "Random Forest" is well suited to the task of multi-band land usage analysis. In the experimentation setup, we have compared the random forest with the state-of-the-art classifiers. Based on the SPOT-5 imagery, we have shown that the random forest outperforms the state-of-the-art classifiers including Naïve Bayesian, Mutli-Layer Perceptron, Bayesian Network, SVM, Radial Basis Function Network (RBF) and Ada-boost. We further show that for the land use analysis, increasing the number of trees has no effect on the performance of the random forest and therefore the runtime of the random forest can be reduced compare to all the other classifiers. The best F-score is achieved using 4 trees and 10 Fold Cross Validation.

9637-21, Session 4

Likelihood-based image segmentation and classification of agricultural landcover in the Biddinghuizen study area, the Netherlands

Ali Ghofrani Esfahani, Univ. Twente (Netherlands); Ali Akbar Abkar, K.N. Toosi Univ. of Technology (Iran, Islamic Republic of); Mehnoush Ghofrani Esfahani, VU University Amsterdam, The Netherlands (Netherlands)

Remote sensing data are attractive for land cover classification, particularly in the agricultural regions, where most of the areas are flat. This paper presents a likelihood-based segmentation and classification method (LBSC) with ultimate goal of describing objects for remote sensing images. It is described as a function of likelihood of all objects and their parameters. The approach classifies not single pixel but groups of pixels that represent already existing objects in a GIS database while the variance in likelihoods will be reduced spectacularly. The training areas are derived automatically from the geographical information systems (GIS) database. After an introduction into the general approach, different input channels for the classification are defined and discussed. The result for a test Biddinghuizen region, includes a new approach for segmentation, which is based on criteria derived from local average likelihoods instead of local means or variances, making the segmentation method much less sensitive to radiometric outliers. Due to these capabilities the method represents a step towards optimization of remote sensing. To evaluate the approach, a software tool has been developed using ILWIS 3.7. Afterwards, further samples, which can improve the result of the classification, are tested. The classification with further samples in class of Peas performs much better than fewer samples in mentioned class. The case study presented remarkable increase in overall accuracy of land cover classification with further samples in Peas class with TM image which stand about 76% at the level of object. The addition of the training samples substantially reduced the misclassifications incurred due to the similarity in spectral characteristics of some classes in some areas. The present study also highlights the effectiveness of Likelihood-based classification and segmentation method to enhance the quality of land cover classifications in agricultural regions such as the Biddinghuizen. The results of this research are evaluated and compared.

9637-22, Session 4

RGB picture vegetation indexes for High-Throughput Phenotyping Platforms (HTPPs)

Shawn C. Kefauver, Univ. de Barcelona (Spain); George El-Haddad, Expert Software Engineering Consultant (Lebanon); Omar Vergara-Diaz, José Luis Araus, Univ. de Barcelona (Spain)

Extreme and abnormal weather events, as well as the more gradual meteorological changes associated with climate change often coincide with not only increased abiotic risks (such as increases in temperature and decreases in precipitation), but also increased biotic risks due to environmental conditions that are often favorable to the rapid spread of crop pests and diseases. Durum wheat is by extension the most cultivated cereal in the south and east margins of the Mediterranean Basin. It is of strategic importance for Mediterranean agriculture to develop new varieties of durum wheat with greater production potential, better adaptation to increasingly adverse environmental conditions (drought) and better grain quality. Similarly, maize is the top staple crop for low-income populations in Sub-Saharan Africa and is currently suffering from the appearance of new diseases, which, together with increased abiotic stresses from climate change, are challenging the very sustainability of African societies.

Current crop breeding methodologies, such as phenotyping, have been successful to a certain extent; however, the acceleration of breeding advances is urgently needed to confront the rapid rise in crop loss risk due to climate change. Current constraints in phenotyping under field conditions remain a major bottleneck for future breeding advances, but remote sensing-based High Throughput Phenotyping Platforms (HTPPs) show promise for rapidly developing disease-tolerant and weather-resistant crop varieties. Crop breeding progress in recent decades has been partly masked by climate change, but also a lack of understanding of the underlying physiological mechanisms. A deeper understanding of plant responses to a wide range of climate change risk factors will contribute to the long-term design of genotypes best suited in terms of production and quality.

As such, we are combining the use of remote sensing technologies for basic crop eco-physiological research and the more finalistic measures of accelerating current breeding programs on Durum Wheat with ITA (Technological Institute of Aragon, Spain) and INIA (National Institute for Agricultural and Food Research and Technology of Spain)in Spain and on Maize in collaboration with KALRO (Kenya Agriculture and Livestock Research Organization), and CIMMYT (International Maize and Wheat Improvement Center) in Kenya. So far, RGB pictures have proven cost-effective in studies assessing the effect of abiotic stresses, but have yet to be fully exploited to phenotype disease resistance. Recent analyses of durum wheat in Spain have shown RGB picture vegetation indices to outperform multispectral indices such as NDVI consistently in both yield prediction and disease detection. Towards HTTP development for breeding disease resistance in maize, similar RGB picture vegetation indices outperformed NDVI, with R2 values ranging from 0.33 to 0.65 compared to 0.56 for NDVI when compared to expert visual field assessments of MLN on a 1-5 scale. Specifically, hue, a*, u*, and Green Area (GA), as produced by the open-source software BreedPix and Fiji, performed better than NDVI. Future research plans along these lines of research include automated multi-rotor helicopter drones for more cost-effective and time efficient acquisition of meaningful phenotyping data and the development of open-source software, including color transform indices and spatial recognition of yield components.

9637-23, Session 4

Comparing Maximum Likelihood, Support Vector Machine, and neural networks classification algorithms for classifying tobacco crops in northwestern Pakistan

Shahbaz Khan, Aziz Ahmed, Muhammad Muaz, Manzoor Ali, Muhammad Yasir, Univ. of Engineering & Technology, Peshawar (Pakistan); Sadiq Ullah, Telecommunication Engineering Department (Pakistan)

Tobacco is one of the major cash crops in Pakistan and is widely grown in northwestern part of the country. Due to illicit tobacco trade in the market, the government faces annual tax losses amounting to USD 260 million. The existing approaches of yield estimations are manual and inaccurate to various degrees. Remote sensing based crop yield estimation is required to regulate tobacco farming with the help of better yield estimates. In this study, three highly accurate classification algorithms are compared in classifying different crops by the end of June, 2013 when tobacco crops are highly matured. Satellite imagery is acquired from SPOT-5 High Geometric Resolution (HRG) imagery with its 10m resolution multispectral bands merged into 2.5m resolution panchromatic band. As pre-processing, median filter is applied on the image and Normalized Difference Vegetation Index (NDVI) is added as additional layer. Supervised learning approach is adopted and 8 different classes are obtained by surveying different agricultural lands including tobacco, sugarcane, reaped fields, vegetables (immature), barren lands and settled areas. Furthermore, two classes are inferred from the imagery including 'interfering separations' and 'interfering settlements'. The inferred classes have mixed border pixels with tobacco crops and hence they were interfering in the classification results of tobacco. Separability factors like Jefferies-Matusita and Transformed Divergence algorithms are used to calculate separability between the training classes. Three pixel based classification algorithms including Maximum Likelihood (ML), Support Vector Machine (SVM), and perceptron feed-forward Neural Networks (NN) are used to classify the image. Thresholds of each class in all three classifiers are calculated with the help of Receiver Operating Characteristic (ROC) curve. Youden's Index and 450 slope iso performance lines are used to find the optimum thresholds on ROC curves. Grid search is used to optimize hyper-parameters in SVM and NN classifiers. In SVM, gamma parameter of the non-linear kernel (Radial Basis Function) and penalty parameters are optimized while in NN classifier; number of loops and number of hidden layers are optimized. Accuracy assessment of each classifier is performed through 1-fold cross-validation. The surveyed data is split into training and testing sets where 70% data is used only for training the classifiers and 30% data is used for plotting ROC curves, hyper-parameter optimization and accuracy assessment. Contingency table is used for deriving accuracy parameters including Overall Accuracy (OA), Kappa Coefficient (KC), Producer's and User's Accuracy (PA, UA) of individual classes. Results concluded that all 3 classifiers are highly accurate and minor difference exists in their classification accuracy. SVM classification supersedes with highest OA of 97.08% and KC of 0.963 while ML classification has OA of 96.23%, KC of 0.95 and NN classification has OA of 95.86% and KC of 0.947. In terms of tobacco crops, again SVM has highest PA of 98.12% while MLC has tobacco's PA of 91.73% and NNC has that of 95.53%.

9637-61, Session PS

Estimation spatiotemporal distribution of evapotranspiration using MODIS images and SEBS algorithm in Ghorveh and Dehgolan district

Kwestan Jalali, Islamic Azad Univ. (Iran, Islamic Republic of); Mohammad Hossein Mokhtari, Islamic Azad Univ (Iran, Islamic Republic of); Soodabeh Namdari, Jalal Karami, Islamic Azad Univ. (Iran, Islamic Republic of)

One of the ways to improve water management and ultimately increasing water use efficiency, is accurately estimated the evapotranspiration or amount of consumable water plants. Recently, has been developed using remote sensing data and has been used to estimate the amount of evapotranspiration on a Large surfaces. In this study, using the the surface energy balance system(SEBS) algorithm and MODIS images, the temporal and spatial distribution of evapotranspiration in the months of June to October period of 2010 in Ghorveh and Dehgolan district(East of Kordistan Province) was studied. The highest amount of evapotranspiration in terms of temporal were in June and the lowest in October and in terms of spatial the results indicate higher amount of evapotranspiration in good range and mix (agri-dry farming) land uses in which the density of vegetation is high and the temperature is low as in regression analysis of evapotranspiration and NDVI, high positive correlation coefficient and in regression analysis of evapotranspiration and temperature low negative correlation coefficient endorses this issue. In order to evaluate the accuracy of the SEBS model, actual evapotranspiration values from SEBS model were compared with values obtained from Inference method. The regression equations obtained maps from the two methods were indicated highly correlated values. In Comparison of mean evapotranspiration from basin using two methods in study days one fit correlation with 0.85 R2 value and 0.79 NS statistic shows Significant relationship between two methods and acceptable performance level of SEBS model, also the low RMSE error equal to 0.37 indicates high precision of SEBS model to estimate evaportranspiration in spatiotemporal scales.

Keywords: evaportranspiration, TERRA MODIS, Surface energy balance system (SEBS) Algorithm, Inference method.

9637-1, Session PS

An assessment of vegetation degradation in the semi-arid lands of Sudan using vegetation indices of multispectral imagery

Majdaldin Rahamtallah Abualgasim, GWT-TUD GmbH (Germany); Babatunde A. Osunmadewa, Check Abdel Kader Baba, Elmar Csaplovics, Technische Univ. Dresden (Germany)

Vegetation is one of the most dynamic element of the ecosystem. Hence, monitoring vegetation degradation through the use of various vegetation indices plays an important role in the quantitative assessment of its vigour which can be used for detecting land use change pattern and vegetation density in semi-arid region. In Sudan where fragile ecosystems are dominant and the vast majority of the rural population depend solely on agriculture and pasture as a means of living, the ecological pattern had been greatly impaired, resulting into loss of vegetation cover coupled with variation in climate. This study describes the use of normalized difference vegetative index (NDVI) to quantitatively examine the vigour of vegetation in Sudan through different vegetation indices. Cloud free multi-spectral remotely sensed data from LANDSAT Thematic Mapper (TM) for the dry season months of 1984 and 2009 were used in this study. In this study, vegetation indices (NDVI, SAVI, GSI) comprising of two or more spectral bands were used to examine vegetation degradation over 26 years. The normalized difference vegetation index (NDVI) was used to assess areas which had been undergoing changes over time. The results of this study shows conversion of vegetation cover to other land use type which is an indication of vegetation degradation. The results of the NDVI in 1984 (vegetated area) showed that an area of about 21% was covered by vegetation while 50% of the area were covered with vegetation in 2009. Similar increase in vegetated area were observed from the results of SAVI and GSI for 2009 respectively. Variation in the results of bare land /cultivated land was observed from the results of this study. An increase in area covered by sand land was observed from the results of soil adjusted vegetation index (SAVI) and topsoil grain size index (GSI). The result of SAVI showed that about 30% of the total area were covered with sand land in 2009 as compared to that of 1984 in which the area covered with sand land accounts for 27%. Also, the results of GSI showed an increase of about 54% in the area covered with sand land in 2009 and 52% in 1984. The results obtained from SAVI and GSI is an indication of loss in vegetal cover due to conversion of land such as agricultural activities and extensive rangeland expansion. Although, increase in vegetated area were observed from the result of this study, this increase has a negative impact as the natural vegetation are degraded due to human induced activities which gradually lead to the replacement of the natural vegetation with invasive of tree species (Mesquite). The

results of this study shows that vegetation degradation in the semi arid region of Sudan is associated with increase in sand land on expense of cultivable land. Hence, the study therefore suggest the use of different imagery with high resolutions to further analyse vegetation degradation in order to increase the validity and accuracy of vegetation change patterns and their relation to climatic variability in the semi-arid lands of Sudan.

9637-62, Session PS

Analysis of principal elements of land surface temperature retrieval from AVHRR over Tibetan Plateau

Qingni Huang, Guangzhen Cao, Lixin Dong, China Meteorological Administration (China)

Recently, Tibetan plateau (TP) has become a hot area of climate change research. And Land Surface Temperature (LST) is one of key factors in the research. In order to get a long time-series, high spatial resolution and high accuracy LST dataset, we carried out analysis of influence essential factor of LST retrieval from AVHRR oriented Tibetan plateau area. First?choose MODTRAN5.2 to simulate the impact of land surface, atmospheric, geometric factors on bright temperatures of channel 4 and channel 5 for special features of TP using stand atmospheric models. Result showed that emissivity, boundary temperature, water vapor amount and view zenith angle were the principal elements of bright temperature. Second an improved algorithm from Wanz-Dozier split window model was established considering these factors. At last, differences between LST retrieval result considering different factors were given.

9637-63, Session PS

Validation of land surface temperature products of Modis and FY3C over Tibetan Plateau

Qingni Huang, Guangzhen Cao, Guicai Li, Lixin Dong, China Meteorological Administration (China)

Land Surface Temperature (LST) is one of key factors in the climate change research. Its accuracy has an important impact on the trend of climate analysis result. In this study, we use ground weather station data per hour to validate daily LST products of Modis/Terra (MOD11A2) and FY3C/VIRR. Match of time and geographic situation were considered. In addition, factors of cloud and wind of the study area were also taken into account for LST products algorithm limit and situation of weather station. Ground measured data per half an hour of Pali grassland of Yadong from September 12 to October 25 of 2004 was used to validate accuracy these products.

9637-64, Session PS

Winter wheat GPC estimation with fluorescence-based sensor measurements of canopy

Xiaoyu Song, National Engineering Research Ctr. for Information Technology in Agriculture (China); Jihua Wang, Beijing Research Ctr. for Agricultural Standards and Testing (China); Xiaohe Gu, Xin-Gang Xu, National Engineering Research Ctr. for Information Technology in Agriculture (China)

Wheat grain protein content (GPC) is a key factor of wheat nutrition evaluation. It is important to determine wheat GPC before harvest for agriculture and food process enterprises in order to optimize the wheat grading process. This study focused on the wheat grain protein content (GPC) estimation based on wheat canopy chlorophyll parameters which acquired by hand-held instrument, Multiplex 3 (FORCE-A, Orsay, France). The wheat GPC estimation experiment was conducted in 2012 at the Xiaotangshan National Precision Agriculture Experimental Base in Changping district, Beijing. A square with area of 1.1 ha was selected and divided to 110 small plots by 10?10m in this study. In each plot, four 1-m2 area distributed in the square were selected for canopy fluorescence spectral measurements, physiological and biochemical analyses. The detection area of the fluorescence spectral sensor was circular with a 8 cm diameter at a distance of 10 cm from the light sources. Nine fluorescence spectral indices, including SFR_G, SFR_R, BRR_FRF, FER_RUV, FLAV, FER_RG, ANTH, NBI_G and NBI_R which combined by the red band at 680–690 nm and far-red band at 730–780 nm fluorescence excitation signal were used in this study. Measurements were performed five times at wheat tillering stage (April 12, 2012), jointing stage (April 27, 2012), heading stage (May 10, 2012), milking stage (May 24, 2012) and ripening stage (June 6, 2012), respectively. The wheat plant samples for each plot were then collected after the measurement and sent to Lab for leaf N concentration (LNC) and canopy nitrogen density (CND) analyzed. GPC sampling for each plot was collected manually during the harvested season. Four 0.3m?1m plots distributed in the square area were collected and mixed in laboratory to provide and GPC value for the plot. Then, statistical analysis were performed to detect the correlation between fluorescence spectral indices and wheat CND for each growth stage. The results showed that canopy-level fluorescence spectral parameters were more sensitive to CND than LNC at most wheat growth stages except at tillering stage. While CND were significantly correlated with GPC in all stages and the correlation coefficient values increased from 0.287 to 0.466 at tillering and jointing stage, then decreased to 0.377, 0.273 and 0.271 at heading, milking and rippening stage. The correlation results for the relationships of canopy-level fluorescence spectral parameters and GPC varied with wheat plant developing from Tillering stage to Rippening stage. But two Nitrogen Balance Indices, NBI_G and NBI_R were the more sensitive parameters than other fluorescence spectral indices in estimation of winter wheat GPC. The correlation coefficient values between NBI_G and GPC in different wheat growth stages were 0.364, 0.613, 0.708, 0.780 and 0.828 while the values between NBI_R and GPC were 0.558, 0.672, 0.614, 0.611 and 0.800. The study reveals that canopy-level fluorescence spectral parameters were better indicators for the wheat group activity and could be demonstrated to be good indicators for winter wheat GPC estimation.

9637-65, Session PS

Performance of fluorescence retrieval methods and fluorescence spectrum reconstruction under various sensor spectral configurations

Rong Li, Feng Zhao, BeiHang Univ. (China)

Solar-induced chlorophyll fluorescence is closely related to photosynthesis and can serve as an indicator of plant status. Several methods have been proposed to retrieve fluorescence signal (Fs) at specific spectral bands (e.g. around 687nm and 761nm, where solar irradiance is strongly absorbed by oxygen). Besides, the recently proposed method of Fluorescence Spectrum Reconstruction (FSR, Zhao et al., 2014) made possible the acquisition of fluorescence signal in its whole emission region of 640–850nm. Nevertheless, the precision of the fluorescence signal obtained through these methods is determined not only by the conditions of plants but also by sensor spectral configurations. Therefore, it is of significant importance to investigate the impact of sensor spectral characteristics on these Fs retrieval methods.

In this work, the performance of various Fs retrieval methods as well as FSR is investigated under different sensor spectral configurations by making use of simulated datasets with the known ‘true’ Fs. These datasets were simulated by the integrated radiative transfer and energy balance model, SCOPE (Soil Canopy Observation, Photochemistry and Energy fluxes,

van der Tol et al., 2009). Four commonly used Fs retrieval methods, namely the original Fraunhofer Line Discriminator method (FLD), the 3 bands FLD (3FLD), the improved FLD (iFLD) and the spectral fitting method (SFM), are investigated. Only oxygen A band (O2-A, 761nm) is used to evaluate the principle of FLD, 3FLD and iFLD, while five bands (centered at 656nm, 687nm, 719nm, 761nm and 823nm, respectively) are exploited for SFM and FSR. As to sensor characteristics, six spectral resolution (SR) levels (0.01nm, 0.1nm, 0.3nm, 1nm, 2nm, and 3nm) and five signal-to-noise ratio (SNR) levels (noise free, 100, 400, 1000, and 4000) are taken into account. The coefficient of determination (R2), the Root-Mean-Square Error (RMSE) and bias between the retrieved Fs and the 'true' Fs in the simulated dataset are calculated to assess the precision of the retrieval.

According to the results, SR and SNR both affect the retrieval accuracy, while SR plays a more significant role. Strong over-estimation, low R2 and high RMSE are observed for the original FLD method when data with low SR is exploited. Compared with the results of FLD, smaller absolute bias is obtained by 3FLD, though R2 is not improved. Similar precision with higher R2 (at least 0.99) as well as lower sensitivity to SR and SNR is achieved by iFLD and SFM, compared with those obtained by FLD and 3FLD. However, it should be noted that iFLD obtains these preferable results only when the spectral ranges for the interpolation of apparent reflectance are appropriately selected. Generally, SFM is more robust since the careful selection of spectral bands is not required. As to FSR, rather high accuracy of reconstructed Fs in the whole fluorescence emission region is obtained. The shape and magnitude of reconstructed Fs are generally consistent with the 'true' Fs distributions, with R2 higher than 0.95 except for the poorest sensor conditions (SR=2nm, SNR=100 and SR=3nm, SNR=100).

References

[1] Feng Zhao; Yiqing Guo; Wout Verhoef ; Xingfa Gu; Liangyun Liu; Guijun Yang. A Method to Reconstruct the Solar-Induced Canopy Fluorescence Spectrum from Hyperspectral Measurements. Remote Sens. 2010, 6, 10171-10192.

[2]Van der Tol, C.; Verhoef, W.; Timmermans, J.; Verhoef, A.; Su, Z. An integrated model of soil-canopy spectral radiances,photosynthesis, fluorescence, temperature and energy balance. Biogeosciences 2009, 6, 3109–3129.

9637-66, Session PS

Monitoring the ratio of leaf carbon to nitrogen in winter wheat with hyperspectral measurements

Xin-Gang Xu, Xiao-Dong Yang, Xiao-he Gu, National Engineering Research Ctr. for Information Technology in Agriculture (China); Hao Yang, Beijing Academy of Agriculture and Forestry Sciences (China); Gui-jun Yang, Xiaoyu Song, National Engineering Research Ctr. for Information Technology in Agriculture (China)

The metabolic status of carbon (C) and nitrogen (N) as two essential elements of crop plants has significant influence on the ultimate formation of yield and quality in crop production. Leaf is the major organ of plant photosynthesis and physiological activity, and in leaf tissues the ratio of carbon to nitrogen (C/N), defined as the ratio of LCC (leaf carbon concentration) to LNC (leaf nitrogen concentration), can help people to understand and quantify the carbon and nitrogen metabolism in crop plants, and is a good indicator for synthetically diagnosing the balance of carbon and nitrogen, nutrient status, growth vigor and disease resistance in crop plants. Thus, it is very significant for effective diagnosis and dynamic regulation of crop growth in field to monitor changes of leaf C/N quickly and accurately and in real time.

The traditional methods of determinating crop C or N status have relied substantially on sampling from fields and analysis in laboratories, but have the disadvantages of either destructive measurements with too much energy and time cost or hysteretic evaluations because of chemical assay in labs. In contrast, remote sensing of canopy reflectance acts an essential role in detecting physiological parameters of crop in field, with rapid and large-spatial-area measurement capabilities. Especially, hyperspectral remote sensing with hundreds of narrow bands can probe into the subtle changes of biochemical components (such as leaf chlorophyll content, nitrogen status and water stress) in crop, and markedly characterizes the non-destruction and quickness, and thus the estimates of biochemical parameters in crop plants by means of analyzing spectral characteristics to develop newly effective spectral variables for monitoring these parameters has become the focused interest in the evaluation of crop growth. Nowadays, the mechanism and methods of determinating leaf C/N with remote sensing techniques, especially ground-based hyperspectral measurements, are still placed in the exploring stage.

Some existing reports have showed that there are close relationships between chlorophyll, nitrogen (N) and C/N. In this study, some typical indices aimed at N estimation were tested to estimate C/N in winter wheat as well as several indices aimed chlorophyll evaluation. The multi-temporal hyperspectral data from the flag-leaf, anthesis, filling, and milk-ripe stages were obtained to calculate these selected spectral indices for evaluating C/N in winter wheat. The results showed that some tested indices such as MCARI/OSAVI705, MTCI and Rep-Le had the better performance of estimating C/N. In addition, GRA (gray relation analysis) and branch-and-bound method were also used along with spectral indices sensitive to C/N for improving the accuracy of monitoring C/N in winter wheat, and obtained the better results with R2 of 0.74, RMSE of 1.01. It indicates that monitoring of leaf C/N in winter wheat with hyperspectral reflectance measurements appears very potential.

9637-67, Session PS

Endmember identifcation from EO-1 Hyperion L1_R hyperspectral data to build saltmarsh spectral library in Hunter Wetland, NSW, Australia

Sikdar M. Rasel, Macquarie Univ. (Australia); Hsing-Chung Chang, Macquarie University (Australia); Timothy Ralph, Macquarie University (Australia) and Macquarie University (Australia) and Macquarie Univ. (Australia); Neil Saintilan, Macquarie University (Australia)

Saltmarsh is one of the important species of wetlands, however, it has been declared as an EEC (Ecological Endangered Community) in Australia. Remote sensing has been demonstrated as an efficient method to monitor the land cover, including vegetation. In order to correctly identify different saltmarsh species, development of spectral libraries of saltmarsh species is inevitable to facilitate advanced matching and analytical techniques to monitor this EEC. Hyperspectral remote sensing, with a capability to monitor more detailed changes in vegetation and species composition, can explore the area of wetland monitoring and mapping. Therefore, it can help wetland mangers to take initiative at relevant scales and resolutions. The hyperspectral imagery acquired by EO-1 Hyperion satellite comprises 242 bands in the wavelength ranging from 400 nm to 2500 nm, and a spatial resolution of 30 m. The benefits of Hyperion data to wetland have been studied at Hunter Wetland Park, NSW, and Australia. Hyperion data can be an effective tool to monitor saltmarsh community through the use of spectral signature (reflectance properties of an object in different wavelength). To reduce the systemic and random noise bad bands were excluded and vertical stripes were removed. The performance of this algorithm was tested using the Minimum Noise Fraction (MNF) transformation to identify any possible unwanted effect in the image. After exclusion of bad bands, atmospheric correction model was run to minimize residual atmospheric effect and to retrieve apparent surface reflectance for different land cover. Red edge part of the vegetation spectral profile was analysed to notice the effect of de-striping (removal of

vertical stripe) on vegetation spectral signature. Different land cover spectral profile were examined and subsequently large data dimensionality were reduced by Forward Minimum Noise Fraction (MNF) algorithm. Based on the eigenvalue and covariation matrix first 10 MNF bands were selected in Pixel Purity Index (PPI) to find out extreme pure pixel for each endmember within the saltmarsh community. To refine the endmember list, PPI selected pixels were compared with training pixels (reference pixels) to determine the threshold of PPI. Then extreme pure pixels were projected in n-D Visualizer in ENVI to identify final endmember for this community. At first four endmember including forest, saltmarsh, water and built up area were selected. Afterwards spectral profile of two saltmarsh species, Phragmitis australis and Sporobolus sp were identified.

9637-68, Session PS

The impact of different reference panels on spectral reflectance coefficients of some biological water pollutants

Agnieszka Jenerowicz, Piotr Walczykowski, Military Univ. of Technology (Poland)

Monitoring of water environment and ecosystem, detecting water contaminants and understanding water quality parameters are most important tasks in water management and protection of whole aquatic environment. Among many techniques available nowadays (e.g. biomonitoring, in- situ measurements) remote sensing methods not only offer possibilities for the understanding of a great number of changes in nature but also enable the monitoring of the state of water reservoirs, assessment several water quality parameters (e.g. chlorophyll and phycocyanin concentration, turbidity, total suspended matter, salinity, etc.) and level of physical, chemical or biological pollution. According to the European Union Water Framework Directive (2000/60/WE) biological pollutants can be defined as microbes that are harmful to humans and other forms of life (e.g. cyanobacteria, green algae, diatoms, etc.). Detection of biological contaminants, their distinction types indication play a very important role in preserving human health and water management. Different optical multispectral and hyperspectral instruments provide spatial and temporal data that are necessary for understanding changes that occur in aquatic environments and changes in water quality parameters, especially changes and level of biological water pollution. However to obtain accurate and precise results of determination of the level of biological contamination and to distinguish its type it is necessary to determine precisely spectral reflectance coefficients of several water biological pollutants with inter alia spectroradiometer. Determining spectral reflectance coefficients consists of measuring the intensity of the reflected electromagnetic radiation in specific wavelengths- these measurements are usually calibrated with a white reference panel. Within the “IRAMSWater - Innovative remote sensing system for the monitoring of pollutants in rivers, offshore waters and flooded areas” (PBS1/B9/8/2012) research project financed by the polish National Centre for Research and Development, there had been built a laboratory measuring station which enable the acquisition of spectral reflectance coefficients in stable conditions- it consists of a spectroradiometer (ASD Field Spec) and a lighting system mounted on a specially constructed platform. In this paper there is presented a methodology and preliminary results of acquisition of spectral reflectance coefficients with different reference panels (e.g. with 5%, 20%, 50%, 80% and 96% of reflectivity) of several biological pollutants, such as green algae, diatoms and cyanobacteria that originate from the Culture Collection of Baltic Algae (CCBA), University of Gdansk in Poland. The authors’ main task was to determine the precision and accuracy of measurements of different biological water pollutants with application of several reference panels (white and greys) and to select optimal reference standard, which would allow for distinguish different types of several biological contaminants. Moreover it was necessary to indicate the spectral range in which it is possible to discriminate investigated samples of biological contaminants- which is very important in optical remote sensing for choosing the right hyperspectral or multispectral sensors. By conducting many series of measurements of several samples of different types of biological pollutants, authors had concluded how the reflectivity of reference panel influences the accuracy of acquisition of spectral reflectance coefficients. Based on these measurements and their analyses it was possible to determine preliminary reflectivity values of reflectance panel (5% and 20 %), that would allow for discrimination between different species of investigated biological contaminants. This research was crucial in order to be able to distinguish several types of biological pollutants and to determine the useful spectral range for detection of different kinds of biological contaminants with multispectral and hyperspectral imagery.

9637-72, Session PS

Flow estimation using satellite-derived rainfall on inaccessible area

Joo-Hun Kim, Yun-Seok Choi, Kyung-Tak Kim, Korea Institute of Construction Technology (Korea, Republic of)

Because of the closed policy, it is very hard to get the water information for North Korea. Instead of gauge observations, information from satellites and global topographic data can be used to estimate water resources and flood disasters in North Korea in broad terms. The objective of this study is runoff analysis for the Dongsin-gun area, representative inaccessible region located at upstream of Chungcheon-gang(Riv.) in North Korea, using satellite-derived rainfall and global topographic data.

Xie et al.(2011) analyzed CMORPH data for average annual rainfall from 2000 to 2009 and showed the data could reflect the spatial distribution of rainfall very well. But they showed over estimated rainfall in tropical and subtropical regions and under estimated value in the middle to high latitudes zone.

Meteorological and Hydrological Bureau of North Korea reported the heavy rainfalls of Dongsin-gun(413mm), Songwon-gun(383mm), and Huicheon-si(322mm) in Jagang-do from 19 to 21 July, 2013.

Satellite-derived CMORPH data show 187.5mm of maximum rainfall and 163.2mm of watershed mean rainfall during the period. The CMORPH rainfall characteristics of this study corresponds well with the results from Xie et al.(2011).

Runoff analysis using the CMORPH data and DEM and GLCC(Global Land Cover Characterization) from global topographic of Global Map showed 2,333.7?/sec of peak runoff rate.

In the future, accuracy assessment of satellite rainfall and runoff analysis applying calibrated satellite rainfall data using rainfall gauge and radar will be carried out.

Acknowledgement

This research was supported by a grant (14AWMP-B079364-01) from Water Management Research Program funded by Ministry of Land, Infrastructure and Transport of Korean government.

9637-73, Session PS

Water level and SWH variations in the water reservoirs of the Volga river cascade on the base of SARAL/AltiKa satellite observations

Galina Rybushkina, Institute of Applied Physics (Russian Federation); Yuliya Troitskaya, Institute of Applied Physics (Russian Federation) and A.M. Obukhov Institute of Atmospheric Physics (Russian Federation)

In this work we study an applicability of new altimetric SARAL/AltiKa data for determining the water level and significant wave height (SWH) for large inland water bodies on the example of

water reservoirs of the Volga river cascade: Rybinsk, Gorky, Cheboksary, Kuibyshev, Saratov, and Volgograd reservoirs. The remote investigation of the water level of inland water (lakes, rivers, reservoirs) is one of the recent applications of satellite altimetry originally designed for measurements of the sea level. However one can face problems while employing standard altimetry algorithms, for the case of inland waters, especially for narrow elongated water bodies and rivers, where the distance between shores is less than 5-10 km. These conditions are typical, for example, for the majority of reservoirs of the Volga river cascade (with one exception, Rybinsk Reservoir). In this context, to explore the data of new altimetric satellite SARAL AltiKa for such water bodies is of considerable interest.

AltiKa is an innovating Ka-band altimeter system, dedicated to accurate measurement of ocean surface topography. It is the first oceanographic altimeter using such a high frequency (35.75 GHz). The Ka-band is much less affected by the ionosphere than one operating at Ku-band (on Jason-1,2 satellites) and has better vertical resolution, time decorrelation of echoes, spatial resolution and range noise. The radiometer included in the AltiKa operates in dual-frequency (23.8 and 37 GHz) to correct altimetry measurements from wet troposphere effects.

In this work the SARAL/AltiKa data from the GDR, SGDR and SIGDR datasets, containing information about 1 Hz and 40 Hz measurements are used. The water level variations in Volga reservoirs is calculated on the base of standard algorithm (GDR data) and the comparison with the Jason-2 satellite GDR data is made. The possibility of using the adaptive re-tracking procedure [1], previously developed for Jason-1,2 satellite data is studied. The method of re-tracking [1] is based on the analysis of the forms of reflected pulses in order to eliminate the influence of land on the tracking point calculations. The waveforms from SGDR and SIGDR SARAL/AltiKa datasets are analyzed and the reprocessing of the water level and SWH data is made. The results of calculation are compared with in situ observations, algorithm application has been shown to considerably increase the amount of actual data and significantly improve the accuracy of water level evaluation.

[1]Yu.Troitskaya et al., “Adaptive retracking of Jason-1 altimetry data for inland waters: the example of the Gorky Reservoir”, Int. J. Rem. Sens., vol. 33, pp. 7559-7578, 2012.

9637-74, Session PS

The applicability of FORMOSAT-2 images to coastal waters/bodies classification

Ana C. Teodoro, Lia Duarte, Pedro Silva, Univ. do Porto (Portugal)

Formosat-2, launched in May 2004, is a Taiwanese satellite developed by the National Space Organization (NSPO) of Taiwan [1]. The Remote Sensing Instrument (RSI) is a high spatial- resolution optical sensor onboard FORMOSAT-2 with a 2 m spatial resolution in the panchromatic (PAN) band and a 8 m spatial resolution in four multispectral (MS) bands from the visible to near-infrared region. The RSI images acquired during the daytime can be used for land cover/use studies, natural and forestry resources, disaster prevention and rescue work. Several studies are referred in the literature regarding the application of FORMOSAT-2 data. Cheng-Chien et al., [2] analyse a total of 16 pairs of FORMOSAT-2 images to monitoring the spatial and temporal variations of landslides in the catchment areas of reservoirs (Tseng-Wen Reservoir). However, the applicability of FORMOSAT-2 data regarding coastal area studies was not yet addressed. The main objectives of this work are to investigate the application of FORMOSAT-2 data in order to:

(2) Identify beach patterns;

(1) Correctly extract a sand spit boundary.

Different pixel-based and object-based classification algorithms were applied to three FORMOSAT-2 scenes (between 2014 and 2015) and the results were compared with the results already obtained in [3]. Analysing the results obtained, is possible to conclude that the FORMOSAT-2 data are adequate to an accurately identification of beach patterns. Also, a pixel-based (supervised classification) and an object-based classification were also applied to correctly extract a sand spit boundary (Douro river estuary, Porto, Portugal). The results were also compared with the results obtained in [4], where six IKONOS-2 images were processed. The results obtained with FORMOSAT-2 data were similar.

In conclusion, this research has demonstrated that the FORMOSAT-2 data and image processing techniques is an effective methodology to identify beach patterns and to correctly extract a sand spit boundaries. In the future more FORMOSAT-2 images will be processed and will consider the use of pan sharped images and data mining algorithms.

Acknowledgments

To “National Space Organization, National Applied Research Laboratories of Taiwan” for provided the FORMORSAT-2 data.

References

[1] Chen, K.-S., Wu, A.-M., Chern, J.-S., Chen, L.-C., Chang, W.-Y., “Formosat-2 mission: Current status and contributions to Earth observations,” Proc. IEEE, vol. 98, no. 5, pp. 878–891, (2010).

[2] Cheng-Chien L., Chjeng-Lun S., Jia-Chin L., An-Ming W., “Classification of non-vegetated areas using Formosat-2 high spatiotemporal imagery: the case of Tseng-Wen Reservoir catchment area (Taiwan),” International Journal of Remote Sensing Vol. 32, No. 23, 8519–8540 (2011).

[3] Teodoro, A.C., Pais-Barbosa, J., Gonçalves, H., Veloso-Gomes, F., Taveira-Pinto, F., “Identification of beach features/patterns through image classification techniques applied to remotely sensed data,” International Journal of Remote Sensing, 32(22), 7399-7422 (2011).

[4] Teodoro, A.C. and Gonc?alves, H., “A semi-automatic approach for the extraction of sandy bodies (sand spits) from IKONOS-2 data,” IEEE Journal of Selected Topics in Applied Earth Observations and Remote Sensing, 5 (2), 634-642 (2012).

9637-75, Session PS

Drought assessment using satellite-derived meteorological parameters and NDVI in Potohar region

Saad Ul Haque, Institute of Space Technology (Pakistan)

Pakistan faces a number of severe meteorological droughts due to various meteorological variations such as rainfall, air quality and related climate changes. The study area namely as and due to its unique topography, it lacks the network of canals system. Multi-temporal MODIS NDVI product 16-days composite for year 2000-2013 was used to identify any drought period in study area i-e, Potohar Plateau in the north of Pakistan.. There was an unexpected decrease in NDVI value in 2009-2010, which caused a short term drought. The minimum mean value for NDVI observed was 0.268 for the whole decade, where mean departure from minimum NDVI value was 0.063 reducing it to a value of 0.20. Meteorological parameters derived from NCEP satellite data such as Precipitation, Max. Temperature, Min. Temperature, Humidity and Solar Radiation were assessed for drought sensitivity for the past drought period 2009-2010. Further precipitation based drought index, known as the Standardized Precipitation Index (SPI) was also derived for 6 months. Maps for each parameter showing its intensity trend were generated for the drought period. For further investigation, the relationships between meteorological parameters were examined. A negative relationship between NDVI and SPI, in month of October was observed that triggered the condition of drought. A decreasing trend was also observed in relationship between NDVI and humidity. Further, Fuzzy Overlay analysis was performed after generation of Fuzzy membership function of these meteorological parameters. VCI was derived from NDVI that estimates the vegetation health. Finally, overall drought severity map was generated by combining VCI and Fuzzy overlay of meteorological parameters. This map gives a significant understanding about the areas under various degrees of drought stress.

9637-76, Session PS

Multisatellite data for estimating total discharge in the Volta River basin of West Africa

Vagner G. Ferreira, Hohai Univ. (China)

To date, the application of multi-satellite products to close the water budgets changes from basin to basin, and typically relies on the terrestrial water storage changes (TWSC) inverted from space-borne geodetic sensor. In this respect, we assessed the closure of the terrestrial water budget and the coupled atmospheric-terrestrial water budget methods, as well as the control of terrestrial water storage (TWS) gain over Volta Basin, West Africa. To achieve this, we explore the available satellite products: Gravity Recovery and Climate Experiment (GRACE)-derived TWSC; Tropical Rainfall Measuring Mission (TRMM)-measured rainfall; moderate-resolution imaging spectroradiometer (MODIS)-estimated evaporation; Satellite Altimetry; and atmospheric moisture storage and divergence (ERA-14 Interim reanalysis data). The closure of water budget methods has been validated by comparison with in situ discharge and hydrologic model prediction. The results indicate that the closure of water budgets over Volta Basin is not possible mainly due to nearly constant discharge (dominant annual signal of 0.77 mm/month peak-to-peak) and large errors in the data sets. The worst estimation is provided by using the coupled atmospheric-terrestrial budget method, probably due to the low quality atmospheric data (i.e., precipitable water and moisture flux divergence) since GRACE data are the same for both methods. The water storage anomalies due to the Lake Volta's water impoundment present a linear relationship with the observed discharge, showing a linear coefficient of 0.75. The discharge of Volta Basin is regularized; nevertheless it seems to be possible to use Satellite Altimetry to estimate discharge. With respect to the water storage increasing observed within Volta Basin, the significant accumulated water gain of 162.84 mm (67.97 km cubed) for the period of January 2003 - December 2013, where 48% is mostly controlled by Lake Volta.

9637-77, Session PS

Optimizing the impact of saline irrigation on water productivity in Rechna Doab (Pakistan) using RS, GIS and hydrological models under different irrigation scenarios

Qaisar Saddique, Northwest A&F Univ. (China)

Rational

A number of studies have been conducted in the past regarding the influence of waterlogging and soil salinity on crop yield. All these studies are agronomical in nature showing that there is a significance reduction of crop yield due to soil/water salinity (K. K. Datta and C. de Jong, 2002). Not a single study is reported which can quantify the impact of water/soil salinity on crop water requirement. Over irrigation or under irrigation can cause waterlogging and soil salinity respectively. At upstream of the canal system, farmers are applying abundant amount of water to leach the salts but there is not availability of water for the tail end farmers. They have no knowledge how much water is required to leach the salts. They have no knowledge about the optimal use of the available saline ground water in the form of tube-wells to leach the salts. They don't know the use of conjunctive irrigation (Qureshi et al, 2004). The water requirement is an important issue in recent research as it leads to water productivity. The idea behind the water productivity is to get the maximum yield with minimum amount of water (Dirk Zoebl, 2006). However the most important aspect will be to integrate RS, GIS and hydrological models. The spread of modeling techniques using distributed parameters has largely encouraged the use of input data from remote sensing (RS) with the support of Geographic Information System (GIS) for manipulating large data sets. Information such as land use, crop mapping, identification of irrigated areas and other crop related parameters are surveyed and monitored extensively in space-times by means of satellites (Bastiaanssen, 2000; Granger, 2000; Sarwar and Bill, 2002). A combined use of simulation models and remote sensing overcomes the shortcomings of low spatial coverage of point or field scale models and low temporal resolution of high spatial remotely sensed images.

Objectives of Study

• Mapping the salt affected soils using the RS techniques.

• Determination of net water applied in the both saline and non saline areas using inflow outflow method.

• Determination of water productivity using the crop yield data and total water application data.

• Analysis and modeling of the water application process under variation of irrigation methods, application strategies and field geometry at farmer field scale

• simulation strategies to improve the water productivity by application of balancing and application models regarding irrigation in the vegetation and leaching periods, and recommendation for best utilization of water resources

Methodology

- Differentiating the salt affected area from the unaffected area using RS techniques.

- Development of spatial database regarding the soil salinity, soil texture, cropping pattern, etc to use as a ground truth data for the mapping in RS.

- Inflow through artificial irrigation channels will be taken from the national and international organizations working there. If necessary at some point divers will be installed for cross checks.

- Outflow in the form of drains or the irrigation channels leaving the system will also be determined by the same way as inflow but the evapotranspiration data will be determined from RS techniques like SEBAL or SEBS.

- Inflow-Outflow methods will be used for water accounting.

- Yield data will be taken from the farmers or government organization for water productivity.

Results of water productivity will be compared for the saline and non saline areas in the Rechna Doab. Crop water requirement will be determined by using SWAP (or any other available/suitable model) and then optimised conditions will be developed under different irrigation scenarios by using this model.

- Recommending strategies will be developed for the sustainable management of land and water resources under different irrigation scenarios.

Scope of work

This research work aims to develop a methodological framework by combining RS, GIS and simulation models for better management and advanced planning of land and water resources in Rechna Doab.

9637-78, Session PS

Integration of remote sensing technology to geographic information system for sustainable planning of water resources

Nejat Evsahibioglu, Ankara Üniv. (Turkey); Egnar Ozdikililer, Istanbul Technical Univ. (Turkey)

Remote sensing provides much of the information that is input to a GIS, from global scale vegetation and climatic data to the roof outlines entered into a municipal GIS. As with other fields, to make effective use of remote sensing technology requires technically skilled personel as well as the appropriate tecnnology.

Remote sensing and GIS technology developed separately.

In part this was a result of the use of different technical skills. While a user of remote sensing teknology may develop expertise in sensor systems and image processing methods, the expert GIS user may become more familiar with principles of map projections, spatial analysis, and the design of spatial data bases. Although the technology may encourage different technical orientations, in both cases the user must understand the nature of the information being collected-the forestry, geology, building structures, roadway design and so on.

Ultimately, remote sensing and GIS teknology are both used to collect, analyze, and report information about the earth's resources and the infrastructure we have developed to use them. The two technologies provide complementary capabilities. Remote sensing analyses are improved by the verification data retrieved from a GIS, and GIS applications can benefit from the information that remote sensing can generate. Often the image data are the most current spatial information available for an area.The use of digital image data offers the additional advantage of a computer compatible format that can be input directly to a GIS.

The integrated use of remote sensing and GIS methods and technology can not only improve the quality of geographic information but also enable information previously unavailable to be economically produced. Over the past few years manufacturers have developed more sophisticated technology for integrating remote sensing systems and geographic information systems. The effective use of these tools, however, depends on user sufficiently knowledgeable to apply them.

The objective of this paper is to examine geographical information information system and its integration with Remote Sensing Technology for agricultural engineering applications in general but specifically related to water resources planning.

KEY WORDS: water resources, sustainable planning, remote sensing, geographic information systems

9637-79, Session PS

Changing planfoarm of Ichamati River and land use/land cover using RS and GIS techniques

Bikesh Sharma, Vidyasagar Univ. (India)

Analyzing the image of Ichamati river in North 24 Parganas District through the Year 1922 to 2013, it is found that significant changed has been occurred in eastern part of the river and less change is found in the middle part which is close to the Baduriya Town. Toposheet of the year 1922 is also compared with the image data to observe to change, soil types,meander etc. It is found from the study that there is a possibility of natural meander cut off at Near Chaura atBaduriya town.

Ichamati River had changed its course with time which were evident from temporal data (1922 – 2013) digitized from old toposheet and recent satellite imageries. Various natural and manmade phenomena were responsible for such changes of Ichamati River course. Analysis of topographical and remote sensing data on GIS platform helped in quantifying bank erosion vectors of Ichamati River. Present study also revealed:

• delineation of Risk zone areas due to bank erosion;

• that Baduria, Basirhat I & II and Hasnabad blocks were most affected by change of the Ichamati River channel during past 90 years.

• the LULC dynamics that affected geomorphological changes in and around Baduria, Basirhat – I & II blocks and Hasnabad in recent past.

Monitoring and modeling of erosion processes can help us better understand the causes, make predictions, and plan how to implement preventative and restorative strategies.

9637-80, Session PS

Comparisons of precipitation data from satellites and ground measurements over the North Korea

Yu-Ri Lee, Hyo-Jin Park, Dong-Bin Shin, Yonsei Univ. (Korea, Republic of); Joo-Hun Kim, Kyung-Tak Kim, Korea Institute of Construction Technology (Korea, Republic of)

Although many meteorological disasters, it is very difficult to get the water data of North Korea because of the closed policy. Then the satellite images can provide useful hydro-meteorological information of North Korea.

The objective of this study is to analyze the hydro-meteorological characteristics of inaccessible region by assessing the satellite-derived rainfall accuracy for water resources monitoring in North Korea.

27 gauges data distributed in North Korea(37.7 – 43 N, 124 – 131 E) were compared with TMPA(TRMM Multi-satellite Precipitation Analysis) 3B42, CMORPH(CPC MORPHing technique), and GSMaP(Global Satellite Mapping of Precipitation) derived form satellite images. The daily rainfall data from 2003 to 2013(2003 ? 2009 for GSMaP) were used and satellite rainfall data were calibrated using gauge data.

Correlation coefficients between rain gauges and satellite rainfall were calculated. The satellite rainfalls from TMPA 3B42 and CMORPH showed correlation coefficient over 0.6 with gauge data. GSMaP showed highest correlation coefficient over 0.8.

This study proved the applicability of satellite rainfall to rainfall monitoring of North Korea by analyzing correlation coefficient between satellite derived rainfall and ground observed data. In the future, satellite rainfall can be used in meteorological cooperation and disaster prevention joint research of South and North Korea.

Acknowledgement

This research was supported by a grant (14AWMP-B079364-01) from Water Management Research Program funded by Ministry of Land, Infrastructure and Transport of Korean government.

9637-81, Session PS

Derivation from the Landsat 7 NDVI and ground truth validation of LAI and interception storage capacity for Wetland Ecosystems in Biebrza Valley, Poland

Joanna Suliga, Vrije Univ. Brussel (Belgium); Jarosław Chormanski, Warsaw Univ. of Life Sciences SGGW (Poland); Sylwia Szporak-Wasilewska, Ma?gorzata Kleniewska, Tomasz Berezowski, SGGW (WULS) - Warsaw University of Life Sciences (Poland); Ann van Griensven, Vrije Univ. Brussel (Belgium) and UNESCO-IHE Institute for Water Education (Belgium); Boud Verbeiren, Vrije Univ. Brussel (Belgium)

Wetlands are of a great value and play a significant role in linking terrestrial and aquatic ecosystems, due to the fact these are providing a wide range of ecosystems services. Typically a hydrological modeling approach is used to gain understanding and support ecosystem management. Most of the hydrological models were, however, developed in the 90s and are usually not adapted to wetland conditions. Recently wetlands became a challenging topic of many researchers but due to the lack of data it is very difficult to design and use hydrological models. Therefore, there is a huge potential of improving and expanding the knowledge about and modeling of wetlands.

Interception storage capacity is often underestimated in hydrological modeling . In the case of wetlands, including

interception storage into calculations is even more challenging, because literature data hardly exists. Therefore, developing a quick, relatively cheap and accurate method of estimating interception storage for wetlands ecosystems is very useful.

This study includes the computation of interception storage capacity based on Landsat 7 images and groundtruthing measurements. The interception storage capacity storage for plant communities were estimated from field work conducted in Biebrza Valley (the biggest and best preserved peatlands in the European Union, located in the North-Eastern part of Poland). The method was based on collecting and weighting dry, wet and fully saturated samples of the most dominating species of sedges. With this experiment were also associated measurements of fresh and dry biomass and the leaf area index (LAI). Research was repeated three times during the same season (May, June and July 2013) to observe the temporal variability of the parameter caused by the vegetations development. Groundtruthing measurements were used to validate the estimation of parameters derived from images acquired in a similar period as the measurement campaigns. The use of remote sensing has as major advantage of being able to obtain an area covering spatially and temporally distributed estimate of the interception storage capacity.

Results from this study indicate that the interception capacity of wetlands vegetation is changing considerably during the vegetation season (temporal variability) and reaches its maximum value when plants are fully developed. Different areas depending on existing plant species are characterized with different values of interception capacity (spatial variability). There is a correlation between the increase of biomass and the increase of LAI (fresh biomass, n = 29, r = 0,63 and dry biomass, n = 29, r = 0,56) . There is a correlation between the increase of biomass (fresh and dry) and the increase of interception capacity (fresh biomass, n = 36, r = 0,59 and dry biomass, n = 36, r = 0,67).

This research frames within the INTREV - WetEco (INterception-TRanspiration-EVaporation; interdependencies of hydrological processes in WETland ECOsystems) and HiWET (High-resolution modelling and monitoring of Water and Energy Transfers in WETtland ecosystems) projects, funded respectively by National Science Centre (NCN) in Poland and BELSPO STEREO III.

9637-82, Session PS

Processing of airborne laser scanning data to generate accurate DTM for floodplain wetland

Sylwia Szporak-Wasilewska, Dorota Miroslaw-Swiatek, Mateusz Grygoruk, Warsaw Univ. of Life Sciences SGGW (Poland); Robert Michałowski, Ignacy Kardel, Warsaw University of Life Sciences (Poland)

Structure of the floodplain, especially its topography and vegetation, influences the overland flow and dynamics of floods which are key factors shaping ecosystems in surface water-fed wetlands. Elaboration of the digital terrain model (DTM) with very high accuracy is therefore crucial in hydrological modelling in river valleys which require detailed analysis of environmental impacts to ecosystems. In this study the research was conducted in the unique Central European complex of fens and marshes, in the Lower Biebrza river valley representing mainly peat ecosystems which according to Water Framework Directive are called “water-dependent ecosystems”. Development of accurate DTM in areas overgrown by dense wetland vegetation consisting of alder forest, willow shrubs, reed, sedges and grass is difficult, therefore to represent terrain in high accuracy the airborne laser scanning data (ALS) with scanning density of 4 points/m2 was used and the correction of the “vegetation effect” on DTM was executed. This correction was performed utilizing field measurements of vegetation height collected with GPS RTK (Real Time Kinematic) and remotely sensed images. The object based image analysis (OBIA) was used to classify different types of vegetation within research area. OBIA allowed partitioning remote sensing imagery into meaningful image-objects and assessing their characteristics through spatial and spectral scale. In order to develop the land cover map that takes into account the vegetation height, both laser scanning data and vegetation indices developed on the basis of airborne and satellite images were used in process of segmentation, attribution and classification. Several different vegetation indices were tested to distinguish different types of vegetation in wetland area. The digital terrain model was compared and examined within distinguished land cover classes (formed mainly by natural vegetation of the river valley) with elevation models from the ASTER-GDEM programme, SRTM and height models developed with limited number of ground points measured with GPS RTK.

9637-83, Session PS

Fires detection from hypespectral data using neural network approach

Alessandro Piscini, Stefania Amici, Istituto Nazionale di Geofisica e Vulcanologia (Italy)

This study describes an application of artificial neural networks for the recognition of burning areas using hyperspectral remote sensed data.

Satellite remote sensing is considered an effective and safe way to monitor active fires for environmental and people safeguarding.

Neural networks are an effective and consolitaded technique for the classification of satellite images. Moreover, once well trained, they prove to be very fast in the application stage for a rapid response.

At flaming temperature, thanks to its low excitation energy (about 4.34 eV), potassium (K) ionize with a unique doublet emission features. This emission features can be detected remotely providing a detection map of active fire which allows in principle to separate flaming from smouldering areas of vegetation even in presence of smoke.

For this study a normalised Advanced K Band Difference (AKBD) has been applied to airborne hyper spectral sensor covering a range of 400-970 nm with resolution 2.9 nm.

A back propagation neural network was used for the recognition of active fires affecting the hyperspectral image. The network was trained using all channels of sensor as inputs, and the corresponding AKBD indexes as target output.

In order to evaluate its generalization capabilities, the neural network was validated on two independent data sets of hyperspectral images, not used during neural network training phase.

The validation results for the independent data-sets had an overall accuracy round 100% for both image and a few commission errors (0.1%), therefore demonstrating the feasibility of estimating the presence of active fires using a neural network approach.

Although the validation of the neural network classifier had a few commission errors, the producer accuracies were lower due to the presence of omission errors. Image analysis revealed that those false negatives lie at the edges of fire fronts, and probably due to the detection threshold selected for discriminating pixels affected by active fires, so demonstrating that the accuracy in classification is strictly related to the sensitivity of the chosen model.

The proposed method can be considered effective both in terms of classification accuracy and generalization capability. In particular our approach proved to be robust in the rejection of false positives, often corresponding to noisy or smoke pixels, whose presence in hyperspectral images can often undermine the performance of traditional classification algorithms.

In order to improve neural network performance, future activities will include also the exploiting of hyperspectral images in the shortwave infrared region of the electromagnetic spectrum, covering wavelengths from 1400 to 2500 nm, which include significant emitted radiance from fire.

9637-86, Session PS

Assessment of the forest restoration process after a fire using decoding of high-resolution satellite images

Yurj P. Rozhkov, State Nature Reserve Olekminsky (Russian Federation); Maria Y. Kondakova, Hydrochemical Institute (Russian Federation)

The dynamics of forest fires, changing vegetation on burnt successfully traced multispectral satellite images taken at intervals of several years. The studies were conducted on the territory of the reserve "Olekminsky", burning at the site in 1985 with an area - 52200 hectares.

As a result, studies have identified the main trends recovery taiga forest after fires.

With the use of satellite image interpretation the study area, made in the range of 15 years (1995-2011) was traced dynamics of overgrowing of burning on the site of a fire in 1985: where and to what extent is a restoration of heathlands and woodlands resulting from fire.

A comparison of the processes of forest restoration after the fire using indices NBR, NDVI, SWVI, index overgrown wasteland. On vegetation index NDVI was an increase in the areas related to the 0-class destruction (NDVI range from 0.31 to 0.65) or highly productive forests. With 21,682 hectares in 1995 to 51,126 hectares in 2011 (up to 98% of the area burnt).

NBR on the index for the period 1995 to 2011. noted a sharp increase in the areas related to class 2 (undisturbed or reconstituted with a range of values from 0.41 to NBR 0.71) with 16,643 ha to 46,890 ha (up to 89% of the area burnt).

According to the index SWVI also significantly increase in the area, dating back to Class 2 (with high values of the index). The increase from 6421 ha in 1995 to 35,697 hectares in 2011 (up to 68% of the area burnt)

Depending on the extent of damage, the restoration of forest ecosystems after the fire passes at different speeds. The greater the proportion of post-fire wasteland, the more intense is restored. This can be judged by the nature of recovery curves "index overgrown wasteland" and "index burnt NBR».

Changes that occur in the structure of forests and heathlands in the process of overgrowing burnt, the tool allows you to define a "thematic difference."

Calculation of "thematic differences" with increasing time step (2001-1995gg, 2004-1995gg., 2006-1995gg, 2011-1995 gg.). Allowed for a more detailed classification than the classification drawn by ISODATA, and highlight the 4th grade. The first focus of the forest and heathland, which practically do not change in time. The second class - Wasteland - consists of two divisions - post-fire wastelands and deserts, associated with the natural features of the landscape. As overgrowing burning primarily on post-fire vegetation recovering wastelands, while the area of natural wasteland, almost no change over time.

The next class of "forest" is also composed of two divisions - "forests, which were not affected by fire" and "forests that have been passed by fire and restored."

9637-87, Session PS

Mapping areas invaded by Prosopis juliflora in Somaliland on Landsat 8 imagery

Felix Rembold, European Commission Joint Research Ctr. (Italy); Ugo Leonardi, Food and Agriculture Organization of the United Nations (Kenya); Wai-Tim Ng, Univ. für Bodenkultur Wien (Austria); Hussein Gadain, Food and Agriculture Organization of the United Nations (Kenya); Michele Meroni, European Commission Joint Research Ctr. (Italy); Clement Atzberger, Univ. für Bodenkultur Wien (Austria)

Prosopis juliflora is a fast growing tree species originating from South and Central America and with a high invasion potential in semi-arid areas around the globe. It was introduced to East Africa for the stabilization of dune systems and for providing fuel wood after prolonged droughts and deforestation in the 1970's and 1980's. In many dry lands in East Africa the species has expanded rapidly and has become challenging to control. The species generally starts its colonization on deep soils with high water availability while in later stages or on poorer soils, its thorny thickets expand into drier grasslands and rangelands. Abandoned or low input farmland is also highly susceptible for invasion as P. Juliflora has competitive advantages on native species and is extremely drought tolerant.

In this work we describe a rapid approach to detect and map P. Juliflora invasion at country level for the whole of Somaliland. Field observations were used to delineate training sites for a supervised classification of Landsat 8 imagery collected during the driest period of the year (i.e., from late February to early April). The choice of such a period allowed to maximise the spectral differences between P. Juliflora and other species present in the area, as P. Juliflora tends to maintain a higher vigour and canopy water content than native vegetation, when exposed to water stress. Although the canopy water content during the dry season is an important element for P. Juliflora identification and was the main driver for the selection of dry season imagery, we decided not to focus only on vegetation indices (VIs) but to use in the supervised classification all the spectral channels offered by Landsat-8. This follows a preliminary analysis performed by using vegetation indices only that showed reduced accuracy with respect to the methodology retained. In fact, the NDII (Normalized Difference Infrared Index) as well as other VIs like the Normalized Difference Vegetation Index (NDVI) and the normalized difference water index (NDWI) did not allow satisfactory separation of P. Juliflora from other vegetation types, including other tree species and irrigated crops, which also maintain high canopy water content during dry periods. A classification method including the near totality of the Landsat 8 spectral information was found to be more adequate as short wave infrared bands containing information about water content present are accompanied by the visible to near infrared bands related to specific leaf spectral signature and canopy density and structure. For the classification, the first seven bands plus NDVI were used, thus excluding the panchromatic, Cirrus and the thermal bands. The reasoning for including NDVI is to support the classification in easily distinguishing bare areas from vegetated areas .

The results of our classification map the current status of invasion of P. Juliflora in Somaliland showing where the plant is invading natural vegetation or agricultural areas. These results have been verified for two subsets of the whole study area with very high resolution (VHR) and prove that Landsat 8 imagery is highly adequate to map P. Juliflora at this scale. The produced map represents a baseline for understanding spatial distribution of P. Juliflora across Somaliland but also for change detection and monitoring of long term dynamics in support to P. Juliflora management and control activities.

9637-88, Session PS

Ecological changes detection in southern Algeria using remote sensing techniques: case of Oasis of Brezina

Taouaf Lakhdar, Ecole normale supérieure de Laghouat (Algeria)

Oases in the Sahara Desert are undergoing rapid physical and socio-economic changes. High spatial resolution remote sensing data from the Landsat Thematic Mapper have been used in an attempt to monitor these changes.

For studies of these changes we chosen the Oasis of Brezina in southwest Algerian an example of this phenomenon ,the variations of Average Difference Vegetation Index (NDVI) every Autumn in the last 20 years record a degradation since 2001 (the beginning of the dam Brezina) where data indicate the retreating number of palm trees from 28 000 to 18 000

between 2001 and 2013Several hypotheses are tested to find the cause, the pollution of water and increased salinity are tested , but the analysis and treatment were negative, with going back to data processing and area study shows that the main factor is the dam and the piece down the groundwater level, which was fed by the oasis which is due mainly to the geological nature of the area , we are proposed a New irrigation system to raise the groundwater level and in order to avoid such mistakes in the future development projects without a comprehensive study into account the characteristics of each region.

9637-89, Session PS

Spatio-temporal distribution of desert locust in Sudan

Mohammed A. Eltoum, Mohamedsalih D. Mohammed, Univ. of Khartoum (Sudan); Amna Ahmed Salih, Sudan national RemoteSensing authourity (Sudan)

Desert locust infestation is one of major pest infestation problems worldwide. Recently desert locust outbreaks were reported in many African countries. The main objective of this research was to study the spatial, geographical and temporal distribution of desert locust infestation in the Sudan, using remote sensing (RS) and geographical information System (GIS). Country map of Sudan, land cover map (FAO) and ancillary ground survey data from Plant Protection Directorate (PPD) were integrated and two maps were produced. These maps were Sudan desert locust summer breeding areas and Sudan desert locust winter breeding areas. The results of integrated data showed that winter breeding areas were located in the Red Sea State triggered by winter rain. Due to the rain fall in June, July and August , the summer breeding areas were located in Kordofan, White Nile, River Nile, Khartoum and Northern states and some parts of Eastern states.Land cover in these states were extracted from (FOA) Sudan land cover map .Four major classes were presented in the desert locust habitat in these araes mainly Herbaceous closed to - sparse in terrestrial and aquatic requlary flooded land, Agriculture in terrestrial and aquatic/requlary flooded land, Shrubs closed to -sparse in terrestrial aquatic requlary flooded land and Seasonal/perennial, natural/artificial waterbodies. Desert locust infestation were absent and seldom recorded in the Tree closed - to - spares in terrestrial and aquatic requlary flooded land class.Itis concluded that Sudan is threatened by desert locust which is triggered by rain fall in winter and summer breeding areas .The foodsecurity in Sudan is highly affected. A subset map of Sudan land cover map (Tokar Delta) was more investigated using Enhancet Vegitation Index of MODIS sattelite imge. The results indicate tha the magnitued of the problem will increase fellowing the detroioration of natural resorces in the land cover of these areas.The restoration of natural resources in these areas were recommended.

9637-90, Session PS

Dielectric properties of marsh vegetation

Tatiana D. Kochetkova, Valentin I. Suslyaev, Anna S. Shcheglova, National Research Tomsk State Univ. (Russian Federation)

INTRODUCTION. Changing climate and the exchange of carbon in the atmosphere are the subject of attention of scientists for many years. Ecosystems of forest and marsh complexes, particularly in Western Siberia, are a natural indicator of these processes. A study of the current state, mechanisms of their functioning and dynamics is an actual problem. The transformation of biota and subarctic landscapes, state of permafrost as a result of climate change in the current conditions and retrospective represent particular interest in the investigations. When continuous observations are conducted using remote sensing technology the issue of data recovery algorithms and dielectric models of investigated surface move into first place. It is necessary to take into account the vegetation cover for a more accurate interpretation of the data. Mosses, lichens and club mosses are widespread in the subarctic zone ecosystems. The present work is devoted to the measurement of the dielectric properties of mosses and lichens in the frequency range from 500 MHz to 18 GHz. Spectroscopic microwave dielectric model of wet soils is well proven in the SMOS retrieval algorithm. The similar approach was applied in this work for a marsh vegetation.

MATERIAL AND METHODS. Subjects of this research were three species of march vegetation – moss Dicranum polysetum Michx, club moss Diphasiastrum complanatum (L.) Holub and lichen Cladonia stellaris.

Samples of vegetation were collected in Tomsk region, Western Siberia, Russia. Complex dielectric permittivity was measured in coaxial section by Agilent Technologies vector network analyzer E8363B. Green samples was measured for some moisture contents from 100% to 3–5 % during a natural drying. The measurements were performed at room temperature, which remained within 21 ÷ 23 ° C.

RESULTS AND DISCUSSION.

The frequency dependence of the dielectric constant for the three species of marsh vegetation differ markedly.

The water in the vegetation can be in three states (phases): in the cells, in the cell walls, and in the intercellular space. Two break point were observed corresponding to the transition of water in the vegetation in various phase states.

Different parts of the complex permittivity dependency on moisture were fitted by line for all frequency points. The slope of the approximation line determined values of the dielectric constant of the liquid in a vegetation.

The complex permittivity spectra of water in the vegetation allow determining the most likely corresponding dielectric model of water in the vegetation by the method of hypothesis testing. It is the Debye's model.

Parameters of Debye's model were obtained by numerical methods for all of three states of water. This enables to calculate the dielectric constant of water at any frequency range from 500 MHz to 18 GHz,, and to find the parameters of the dielectric model of the vegetation.

To estimate the accuracy of the model was built the calculated values dependence on the measured values. There is a systematic error that can be taken into account. A high correlation coefficient was obtained for values of dielectric constant. The dielectric loss has a more greater spread, however a correlation coefficient greater than 0.6 indicates a sufficient degree of correspondence between the calculated and measured values.

9637-92, Session PS

Altimetry backscattering signatures at Ku and S bands over land and ice sheets

Fabien Blarel, Frédéric Frappart, Benoît Legrésy, Denis Blumstein, Frédérique Rémy, Christophe Fatras, Eric Mougin, Fabrice Papa, Observatoire Midi-Pyrénées (France); Catherine Prigent, Observatoire de Paris (France); Fernando Niño, Observatoire Midi-Pyrénées (France); Pierre Borderies, ONERA (France); Sylvain Biancamaria, Stéphane Calmant, Observatoire Midi-Pyrénées (France)

This study presents a comprehensive analysis of radar altimetry backscattering coefficients in different frequency bands over whole land surfaces. It uses backscattering coefficients from the most recent low resolution mode (LRM) radar altimetry missions launched since 2002, i.e., ENVISAT operating at Ku (13.57 GHz / June 2002-October 2010) and S (3.2 GHz / June 2002-February 2008) bands, Jason-2 operating at Ku (13.575 GHz) and C (5.3 GHz) bands since August 2002, and SARAL, the first altimeter to operate at Ka-band (35.75 GHz) since February 2013. The backscattering coefficients are acquired along the nominal orbit of these satellites and processed

using Ice-1 retracking scheme as it is commonly used for land surface studies and for consistency as it is available in the Geophysical Data Records (GDRs) of these three altimetry missions. The first step of this study is to define normalized altimeter tracks divided into cells of 1 kilometer length along track, for each orbit, in which the measurements are sorted every cycle. It permits then to produce maps of mean, standard deviation, seasonal average along the tracks during the whole observation period for each frequency. Maps of differences in backscattering are eventually computed for bi-frequency altimeters (i.,e., S-Ku and C-Ku using respectively ENVISAT and Jason-2 data). These maps are then used to characterize the radar responses of the surface for each frequency., in terms of either stability of the signal, amplitudes and seasonality of the variations, interannual trends, ... Time series over specific sites, characteristic of a eco-climatic region, will be also analyzed with the same purpose.

Early results show that the altimeter backscattered responses at Ka-, Ku-, C- and S- bands exhibit a wide range of spatial and temporal variations. Radar altimetry backscattering coefficients vary from 0 dB to 50 dB over the various land surfaces. The backscattered energy by each surface can be related to its soil roughness and soil dielectric constant and their variations against time. Over land surfaces not varying against time as stone and sand deserts and non-inundated evergreen tropical forests, radar altimeters exhibit quite stable responses. The higher frequencies (Ku and Ka) are yet more affected by changes in roughness caused by the wind regime over deserts. Besides, Ka-band demonstrates a strong sensitivity to moisture variations underneath the canopy of tropical evergreen forest. Over savannahs, radar altimetry confirms its strong potential for the monitoring of surface Soil Moisture in semi-arid areas already observed in previous studies. Differences in frequency C-Ku and S-Ku are likely to make easier the distinction between wet and dry soils and/or bare soil and vegetation areas. Backscattering coefficients also provide very useful information for detecting inundated areas in the altimeter groundtracks that could be used to identify altimetry echoes corresponding to a lake, a river or a wetland surface. If the use of radar altimetry for the monitoring of land surfaces currently suffers from its low spatial and temporal resolutions, the launch of Surface Water and Ocean Topography (SWOT) mission in 2020 will permit to overcome the limitations. Using the SAR interferometry technique at near nadir incidences, SWOT will provide backscattering coefficients in a swath of ~120 km with a spatial resolution of 100 m over land.

9637-93, Session PS

Comparing Citrus Tristeza Virus (CTV) and Phytophthora nicotianae infections on citrus plants using proximal sensing measurements

Stefania Gualano, Politecnico di Bari (Italy) and L'Istituto Agronomico Mediterraneo di Bari (Italy); Franco Santoro, L'Istituto Agronomico Mediterraneo di Bari (Italy); Eufemia Tarantino, Politecnico di Bari (Italy); Hanan Rafik, Anna Maria D'Onghia, L'Istituto Agronomico Mediterraneo di Bari (Italy)

Plant diseases influence the optical properties of the plants in different ways. Depending on the host pathogen interaction and disease symptoms, different regions of the reflectance spectrum are affected, resulting in specific spectral signatures of diseased plants.

CTV and Phytophthora nicotianae are the causal agents of the Tristeza and root rot diseases, these two pathogens are affecting the citrus trees and the diseases are showing similar symptoms in the field, such the tree decline, leaves discoloration and in some cases the death of the trees.

Due to the similar stress, in the thermo-conditioned greenhouse, an experiment was set up to compare reflectance data of citrus plants which were inoculated with Phytophthora and CTV.

Trials were carried out on Mexican lime seedlings (Citrus aurantifolia C; Swing), and on Navelina orange grafted onto sour orange (C. sinensis L.). For each species, 15 plants were inoculated with Tristeza-seedling yellows strain (SG 29 isolate), 15 plants were inoculated with P.nicotianae (isolate IAMB 77) by mixing the prepared inoculum to the growing media at a rate of 1% (v/v) and 15 healthy plants were used for control purpose.

All plants were grown in disinfected pots under controlled temperature conditions (25°C); they were regularly irrigated and fertilized to avoid any possible biotic or abiotic stress.

Spectral measurements were conducted for three months after inoculation for evaluating the differences between healthy and infected citrus plants and between CTV–infected, Phytophthora-infected. The reflectance data were acquired on leaves using Plant probe-leaf clip connecting directly hyperspectral spectroradiometer "FieldSpecHandHeld" by ASD (Analytical Spectral Devices, USA).

Plants were tested in the laboratory by Direct Tissue Blot Immunoassay (DTBIA) for CTV detection and by dilution method in corn meal agar selective media for Phytophthora infections.

The reflectance spectra of healthy leaves of both citrus species (Mexican lime and Navelina orange) are different from the spectrum of those infected by CTV or by P. nicotianae; the spectrum shows that the reflectance of uninfected leaves are relatively low in the visible parts of the spectrum.

In both citrus species, the average spectral reflectances of CTV-infected plants show a clear difference from that of Phytophthora-infected plants in the wavelength range between 375 nm and 1075 nm. All data will be analyzed using ViewSpec Pro software.

9637-94, Session PS

Forecasting of cereals yields in a semi-arid area using the agrometeorological model «SAFY» combined to optical SPOT/HRV images

Aicha Chahbi, Institut de Recherche pour le Développement (Tunisia) and Institut National Agronomique de Tunis (Tunisia); Mehrez Zribi, Ctr. d'Etudes Spatiales de la Biosphère (France); Zohra Lili Chabaane, Institut National Agronomique de Tunis (Tunisia); Bernard Mougenot, Ctr. d'Etudes Spatiales de la Biosphère (France)

In semi-arid areas, an operational grain yield forecasting system, which could help decision-makers to make early assessments and plan annual imports, is needed. It can be challenging to monitor the crop canopy and production capacity of plants, especially cereals. Many models, based on the use of remote sensing or agro-meteorological models, have been developed to estimate the biomass and grain yield of cereals. Remote sensing has demonstrated its strong potential for the monitoring of the vegetation's dynamics and temporal variations, mainly because it provides wide spatial coverage and has consistent internal datasets. Through the use of a rich database, acquired over a period of two years for more than 30 test fields, and from 20 optical satellite SPOT/HRV images, the aim of the present study is to evaluate the feasibility of two approaches: the agro-meteorological SAFY model "Simple Algorithm For Yield estimation" and combined use of the SAFY model with remotely sensed data, to estimate the dynamics and yields of cereals in the context of semi-arid, low productivity regions in North Africa.

The first approach is based on the application of the semi-empirical growth model SAFY, developed to simulate the dynamics of the LAI and the grain yield, at the field scale. The model is able to reproduce the time evolution of the leaf area index of all fields with acceptable error. However, an inter-comparison between ground yield measurements and SAFY model simulations reveals that the yields are under-estimated by this model. We can explain the limits of the semi-empirical

model SAFY by its simplicity and also by various factors that were not considered (fertilization, irrigation ...).

Therefore, we developed a new approach to improve the SAFY model. The grain yield is function of LAI area in the growth period between 25 March and 5 April. In fact, in the initial SAFY model, the grain yield is a function of the total dry ground phytomasse which correspond at the maximum of LAI. The SAFY model does not take into account the type of the cereal growth cycle. Hence the idea of the new approach is to consider the area of the LAI of the maximum period of growth in computing of the grain yield of cereals with SAFY model. This approach is robust, the measured and estimated grain yield are well correlated (R?céréale = 0.59, R?wheat= 0.62 and R? barley = 0.63).

Finally, this model is used in combination with remotely sensed LAI measurements. In an initial step, an exponential relationship is established between the NDVI and the LAI, both of which are derived from optical satellite data. An rms error equal to 0.78 is found when these remotely sensed parameters are validated through the use of ground measurements. This relationship allows the LAI to be mapped on cereal fields. Following calibration of the SAFY model through the use of multi-temporal LAI satellite maps and the determination of the LAI area of the maximum growth period, yield estimations are proposed for the entire studied site.

9637-95, Session PS

Winter wheat growth spatial variation monitoring through hyperspectral remote sensing image

Xiaoyu Song, National Engineering Research Ctr. for Information Technology in Agriculture (China); Ting Li, Hainan Normal Univ. (China); Jihua Wang, Beijing Research Ctr. for Agricultural Standards and Testing (China); Xiaohe Gu, Xin-Gang Xu, National Engineering Research Ctr. for Information Technology in Agriculture (China)

Crop growth diagnosis or evaluation was mainly relay on field survey, manual sampling and biochemical analysis in lab. It is difficult to master the real spatial variance character for the whole crop field because survey sample collection are restricted to the sampling interval or sampling density. Remote sensing technology provides an opportunity for crop growth spatial variance monitoring for its rapid development in recently years. Geostatistical analysis methods can be used to interpolate the measurements to create a continuous surface map or to describe its spatial pattern. Remote sensed imagery constitutes a record of distinct spatial properties of the Earth's surface. Images can be treated as "field" data depicted by varied digital numbers. These spectral values of pixels are spatially auto-correlated and their spatially dependent structures can be represented by variogram. This work aims at quantifying the winter wheat growth spatial heterogeneity captured by hyperspectral airborne images. The field experiment was conducted in 2001 and 2002 in at the National Experiment Station for Precision Agriculture in Changping district, Beijing. Airborne hyperspectral remote-sensing data were acquired at noon on 11 April 2001 using an operational modular imaging spectrometer (OMIS; Shanghai Institute of Technical Physics, Chinese Academy of Science, Shanghai, China), which has a ground resolution of 3 m and a spectral range of 0.46 to 2.48?m with 91 bands. Black and white calibration targets were deployed in the experimental area to support atmospheric correction using an empirical line method. In this work, from blue to near infrared reflectance data were the state variables used to describe the spatial heterogeneity of the winter wheat cover at the field level defined here as an area of few ha (1.2 to 13.2 ha). Totally 12 winter fields which covered by both dense and sparse winter wheat canopies were selected to analysis the winter wheat growth heterogeneity. The sample semi-variograms for all bands for each field were computed by Matheron's method of moments (MoM) estimator. Then the theoretical models were be fitted through the experimental data points to quantify spatial patterns with least squares algorithm for Spherical model, Exponential model and Guassian model. The optimization model was then selected after evaluated by R-square (Coefficient of determination) through method of maximum likelihood. Three key terms in each model, the sill, the range, and nugget variance were then calculated from the models. The study results showed that the sill, range and nugget for same field wheat were varied with the wavelength increasing from blue to near infrared. Although wheat growth in different fields showed different spatial heterogeneity, they all showed an obvious sill pattern. The minimum of mean range value was 13.14 meters while the maximum of mean range value was 63.75 meters. The mean sill and mean nugget value varied from 1.70 to 14.76, 11.30 to 68.46, respectively. This study indicate that remote sensing image is important for crop growth spatial heterogeneity study. But it is necessary to explore the effect of different wavelength of image data on crop growth variogram estimation and find out which band data could be used to estimate crop variogram reliably.

9637-96, Session PS

Application of agrometeorological spectral model in rice area in southern Brazil

Janice F. Leivas, Antônio Heriberto C. de Castro Teixeira, Ricardo G. Andrade, Daniel C. Victoria, Embrapa Monitoramento por Satélite (Brazil); Gustavo Bayma-Silva, Embrapa Satellite Monitoring (Brazil); Edson L. Bolfe, Embrapa Monitoramento por Satélite (Brazil)

Rice is one of the main grain crops produced in the world, being of great importance for the world food. Brazil is among the ten main world rice producers, with approximately 11 million tons. The southern region stands out to be 70% of rice production in Brazil, the culture system by irrigation. In this study, rice growing areas of Rio Grande do Sul were selected, using the shape of land use, scale 1: 100,000, provided by Brazilian Institute of Geography and Statistics (IBGE). Satellite images were used MODIS and meteorological data, available by National Institute of Meteorology (INMET). The period of analysis was crop season 2011/2012. The rice cycle in the Rio Grande do Sul State ranges between 100 and 140 days, the best time used for sowing from October to November. The period of maximum development of the rice occurs between the months of January and February and the harvest, occurring between the months of March to May. To obtain evapotranspiration was applied agrometeorological-spectral model SAFER (Simple Algorithm For Retrieving Evapotranspiration). From the analysis of the results, from planting and cultivation, the average was 1.93 ± ET 0.96 mm.day-1. In the the vegetative development period of rice, the daily ET has achieved 4.94 mm.dia-1. In the period of harvest, evapotranspiration daily average was 1.84 ± 0.80 mm.day-1. It is observed that at the beginning of the cycle, ET predominate refers to the evaporation of water, as observed NDVI values (Normalized Difference Vegetation Index) less than zero, characteristic of wetlands. With the development of culture, the spectral characteristics of the culture predominate. At the start of culture, ET is in mostly composed by the evaporation of the water surface, but as the culture grows and shades the water evaporation decreases, increasing transpiration canopy. In the period analyzed occurred severe drought which affected rice crops and reduced production of Rio Grande do Sul state in the 2011/2012 harvest to 7.672.809 tons. From results obtained, the estimation of evapotranspiration from satellite images may assist in monitoring the culture during the cycle and SAFER model proved effective on estimates evapotranspiration in areas planted with rice in Rio Grande do Sul state, assisting in estimates of productivity and crop yield.

9637-98, Session PS

Study of monitoring the freezing injury of winter wheat at over-wintering period based on HJ1A-HSI image

Junling Li, Henan Institute of Meteorological Science (China) and Key Lab. of Agrometeorological Safeguard and Applied Technique (China); Shuyan Li, Henan Institute of Meteorological Science (China)

At present, the remote sensing monitoring of winter wheat freezing injury uses mainly multispectral data, the lower spectral resolution could lead to the lower sensitivity of the result. HJ1A-HSI data have filled the blank of domestic data in the field of hyperspectral sensors; its 2- level products have been free distribution and have great application prospects. This paper studied the winter wheat freezing injury process of 2012-2013 in Linzhou and its surrounding areas of Henan province. Two HJ1A-HSI images before and after freezing injury were used as the research object, the hyperspectral remote sensing monitoring for winter wheat freezing injury was done based on Li Junling (2014) results of winter wheat freezing injury hyperspectral sensitive indices after data format conversion, striped removal, atmospheric correction, geometry correction and other pretreatment. Statistics results from the changes of sensitive indexes of VI3 ?VI3=SDr/SDb; SDb is the blue edge area; SDr is the red edge area?and VI5 [VI5=(SDr-SDb?/(SDr+SDb?] showed that the proportion of heavy freezing injury was almost identical and the percentage difference of mild freezing injury was 2.11%. Freezing injury distribution monitoring results showed that the two indexes distribution results had bigger differences. It is necessary to verify the reliability of the conclusions when freezing injury is occurring in the future. This paper studied the winter wheat freezing injury process of 2012-2013 in Linzhou and its surrounding areas of Henan province. Two HJ1A-HSI images before and after freezing injury were used as the research object, the hyperspectral remote sensing monitoring for winter wheat freezing injury was done based on Li Junling (2014) results of winter wheat freezing injury hyperspectral sensitive indices after data format conversion, striped removal, atmospheric correction, geometry correction and other pretreatment. The results showed that, this method was feasible. But the two sensitive indices of monitoring freezing injury distribution results were differences; we need to do on-the-spot investigation in the process in the future to verify the reliability of this study conclusion.

Because of the low signal-to-noise ratios of HJ-1A satellite HSI data and the influence of atmospheric scattering and absorption, data quality is reduced and the ability of reflecting different objects is reduced. The spatial resolution of HSI data is low (100 m), which limits its application in more fields. These problems need to be solved by the improved sensor parameters [19]. But the results showed that hyperspectral HJ-1 satellite HSI data could be used to monitor winter wheat freezing injury, the HJ-1 satellite HSI data had a great potential for agricultural meteorological disasters, and the method had a great application value with the HSI sensor gradually improving and perfecting.

9637-99, Session PS

Improving spatial heterogeneity of spring maize yield simulation at field scale by assimilating time series HJ-1 CCD data into WOFOST model

Zhiqiang Cheng, Jihua Meng, Institute of Remote Sensing and Digital Earth (China)

Regional crop yield prediction is significant to grain storage, agricultural production management and national agricultural decision-making. The crop growth model is currently widely used in crop yield prediction. But the model is limited when it is extrapolated to field scale to estimate regional crop yield due to the uncertainty or similarity of the input parameters. To a farmland with hundreds of fields, the crop model input parameters such as Sunlight, rain, temperature and field management are nearly identical, the soil condition may be different but soil parameters of every pixel or field is hard to acquire. So the crop model's performance of yield spatial heterogeneity simulation is relatively poor. Data assimilation method which combines crop growth model and remote sensing has been proven to be the most effective method in regional yield estimation. But the common assimilation methods still can't resolve all the problems since many designers are focusing on improving the mean yield precision rather than the variation. This paper presents a new method of assimilating the time series HJ-1 A/B data into the crop growth model WOFOST (World Food Studies) to improve the spatial heterogeneity of spring maize yield simulation. Firstly, the WOFOST model was selected to simulate the growing process of spring maize. The model was calibrated and validated by the field measured data in order to get the accurate average yield result. While the simulated result was still poor at the field scale due to the lack of essential varied parameters. Secondly, time series LAI was calculated from the HJ data by an empirical statistical model. Thirdly, a simple but effective method was built to assimilate the LAI into the WOFOST model. The core concepts of this method were formulas that aimed to improve yield spatial heterogeneity. Expressing details of ground objects clearly is one of the advantages of medium or high resolution remote sensing images. The formulas were built according to this ability of RS and they can also avoid image errors efficiently. Finally, several experiments have been made about spring maize in a farmland named Hongxing Farm, whose aims were to calculate the spatial heterogeneity. The calculated data were all collected at field scale including HJ-LAI data, yields simulated by WOFOST model with common assimilation method, yields simulated by WOFOST model with the new assimilation method and the observed yields. Through systematic evaluation, the result illustrated that the new assimilation method significantly improved the WOFOST model's ability to show the spatial heterogeneity of spring maize yield simulation. The coefficient of variation (CV) of the new method increased from 0.05 to 0.08 (accommodation coefficient of core equation was from 1 to 10), which was obviously greater than the common method (CV = 0.03) and close to the observed yields (CV = 0.08) and LAI data (CVmax = 0.09). The precision analysis was also made: the correlation of simulation yields and observed yields remains a high level (R2 = 0.52, RMSE = 697 kg/ha). In general, our results indicate that the new method is reliable to improve spatial heterogeneity with high prediction precision.

9637-100, Session PS

Delay-tolerant mobile network protocol for rice field monitoring using wireless sensor networks

Alexandre Guitton, LIMOS CNRS (France); Frederic Andres, National Institute of Informatics (Japan); Jarbas Lopes Cardoso Jr., Ctr. de Tecnologia da Informacao Renato Archer (Brazil); Asanee Kawtrakul, Kasetsart Univ. (Thailand); Silvio E. Barbin, University of Sao Paulo (Brazil)

The monitoring of rice fields can improve productivity by helping farmers along the rice cultivation cycle to determine when to harvest, when to treat the crops against disease, when to increase the water level, how to share observations and decisions made in a collaborative way, etc. However, the monitoring of large rice fields often involves costly techniques. In this paper, we propose an architecture to monitor a rice field by a wireless sensor network, as well as a delay-tolerant, mobile network protocol.

Our architecture consists in deploying few static, battery-powered, sensors in the rice fields (e.g., weather or soil sensors). These sensors are equipped with wireless communication devices with limited capabilities and limited communication range, which is not sufficient to allow the

network to be connected. Farmers are equipped with low-weight communication devices (such as smart phones). As farmers work in their fields, they get in range of the static sensors and collect data from then in a transparent manner. The collected data is aggregated or compressed, and is exchanged from farmer to farmer using a mobile network protocol, until it reaches a gateway node, which might be located in a nearby village. The collected data is then stored into a database, called the Cyberbrain Platform, and is analyzed. Cyberbrain generates farming advices for farmers, based on the historical data, and these advices are again propagated among the farmers through the mobile network protocol.

The plan of the paper is the following. In Section 2, we describe the related work on rice fields monitoring using a wireless sensor network. In Section 3, we illustrate our architecture and describe the delay-tolerant, mobile network protocol, which is a key component in our proposal. In Section 4, we evaluate the performance of the protocol through simulations, and we describe the current state of our experiment in a rice field in Thailand. Finally, in Section 5, we conclude our work.

The main challenges addressed by the paper are the following: (i) a sparse deployment of static sensors, which results into a disconnected network topology, (ii) few mobile farmers, whose movements are not predictable or controllable, (iii) a relatively large amount of data to transfer, especially when the static sensors are not visited often by the farmers.

The network protocol addresses these challenges using the following mechanisms.

- Static and farmer devices use a periodic announcement mechanism, where the periodicity is adapted to network conditions and gateway proximity (computed using GPS or estimated through the time of last contact).

- Farmer devices use a limited flooding mechanism, where each data is sent only to a limited number of neighbors, and for a limited number of hops.

- Static and farmer devices use data timestamping as well as aggregation to compress them. They also use a data priority estimation function, in order to decide which data to remove first from the memory of an overloaded device, as well as which data to send first to a new device that comes in range.

9637-101, Session PS

Supporting precision agriculture with comprehensive application of satellite remote sensing

Jihua Meng, Jin Xu, Zhiqiang Cheng, Wenquan Dong, Institute of Remote Sensing and Digital Earth (China); Yafang Li, China Univ. of Geosciences (China)

The factual base of precision agriculture (PA) - the spatial and temporal variability of soil and crop parameters within or between different fields has been recognized for centuries. Field information on seeding suitability, soil & crop nutrition status and crop mature date is needed for field management optimization. How to acquire the spatially and temporally varied field parameters accurately, efficiently and at affordable cost has always been the focus of the researches in the field. Satellite remote sensing has held out much promise for within & between-field monitoring, along with the promising development regarding spatial, temporal and spectral resolution in the last decade. Scientists from all over the world have provided a great deal of fundamental information relating spectral reflectance and thermal emittance properties of soils and crops to their agronomic and biophysical characteristics. This can make significant contribution in optimizing crop management as sowing, irrigation, fertilization and harvest. Studies on optimizing field management have been implemented throughout the world in the last twenty years. Yet most of these previous researches on applying remote sensing in precision agriculture only focused on how to acquire field and crop parameter with higher accuracy---necessary attention were not paid on how to use these information efficiently in optimizing field management. To solve this issue and promote the application of remote sensing in precision agriculture, a new technical frame was developed focusing on guiding field management (namely seeding, fertilization and harvest). This technical frame consists of 4 primary components: 1) satellite image pre-processing; 2) field seeding suitability evaluation; 3) soil & crop nutrition status monitoring and 4) crop mature date prediction. In the first component, remote sensing images from different sensors can be pre-processed with format conversion, radiation calibration, atmospheric correction and geometric correction. BRDF correction was also provided for images with wide swath. Fusion of images from different sensors was also implemented to produce images with both high spatial and high temporal resolutions. In the second component, soil moisture and surface temperature will be acquired from satellite images (depth of melt layer can be estimated if soil was frozen in previous winter). Together with the information on requirement of different crops in seeding, seeding suitability of different fields can be evaluated. Suggested seeding order and dates for all fields will be put forward. In the third component, the soil and crop nutrition status (nitrogen and chlorophyll concentration for crop; available nitrogen and organic matter content for soil) will be mapped with satellite image, and then been transferred to field/pixel scale fertilization prescriptions. In the fourth component, crop canopy/leaf water and chlorophyll content will be quantitatively mapped, along with the varying pattern of crop water and chlorophyll content during maturing process, crop mature date will be predicted 20 days before the harvest. The predicted optimal harvest date will be updated with the approaching of crop maturity. The concept and algorithm of this technical frame was introduced in detail in this paper. A case application of the technical frame in Northeast China was presented to demonstrate its effect.

9637-102, Session PS

Mapping crop based on phenological characteristics using time-series NDVI of operational land imager data in Tadla irrigated perimeter, Morocco

Jamal-eddine Ouzemou, Abderrazak El Harti, Faculté des Sciences et Techniques Béni-Mellal (Morocco); Ali EL Moujahid, Naima Bouch, Rabii El Ouazzani, COSUMAR SUTA (Morocco); Rachid Lhissou, El mostafa Bachaoui, Faculté des Sciences et Techniques Béni-Mellal (Morocco)

Morocco is a primarily arid to semi-arid country. These climatic conditions make irrigation an imperative and inevitable technique. Especially, agriculture has a paramount importance for the national economy. Retrieving of crops and their location as well as their spatial extent is useful information for agricultural planning and better management of irrigation water resource. Remote sensing technology was often used in management and agricultural research. Indeed, it's allows crops extraction and mapping based on phenological characteristics, as well as yield estimation. The study area of this work is the Tadla irrigated perimeter which is characterized by heterogeneous areas and extremely small size fields. Our principal objectives are: (1) the delimitation of the major crops for a good water management, (2) the insulation of sugar beet parcels for modeling its yields. To achieve the traced goals, we have used Landsat-8 OLI (Operational Land Imager) data pan-sharpened to 15 m. Spectral Angle Mapper (SAM) and Support Vector Machine (SVM) classifications were applied to the Normalized Difference Vegetation Index (NDVI) time-series of 10 periods. Classifications were calculated for a site of more than 124000 ha. This site was divided into two parts: the first part for selecting, training datasets and the second one for validating the classification results. The SVM and SAM methods classified the principal crops with overall accuracies of 85.27% and 57.17% respectively, and kappa coefficient of 80% and 43% respectively. The study showed the potential of using time-series OLI NDVI data for mapping different crops in irrigated, heterogeneous and undersized parcels in arid and semi-arid environment.

9637-104, Session PS

Identification and characterization of agro-ecological infrastructures by remote sensing

Danielle Ducrot, Ctr. d'Etudes Spatiales de la Biosphère (France); Sylvie Duthoit, Ecole d'Ingénieurs de PURPAN (France); Alexandre d'Abzac, Ctr. d'Etudes Spatiales de la Biosphère (France); Claire Marais-sicre, CESBIO (France); Véronique Cheret, Ecole d'Ingénieurs de PURPAN (France); Christophe Sausse, CETIOM (France)

Agro-Ecological Infrastructures (AEIs), which include many semi-natural habitats (hedgerows, grass strips, extensive grasslands, thickets, field margins) play a key role in the preservation of biodiversity, water quality, and the control of erosion. Indirect indicators of biodiversity based on AEIs are used in many national and European public policies. AEIs are useful to explain and analyze ecological processes, some of which may concern agronomy (pests' population dynamics and auxiliaries, ecosystem regulating services...). The identification and characterization of these landscape features are difficult and expensive, which limit their use for the different purposes mentioned above. Remote sensing has a great potential to solve this problem.

In this study, we propose an operational tool for the identification and characterization of IAEs. The method is based on segmentation, contextual classification and fusion of different temporal classifications to improve the classification performance. Experiments were carried out on a large number of satellite data (various temporal and spatial resolution: 20-m, 10-m, 5-m, 2.5-m, 50-cm pixel size) and on three different regions of France: Southwest (hilly or plain, wooded or cultivated), North (open field) and Brittany (meadows and farmland closed by hedges).

The results give a good idea of the potential of remote sensing image processing methods to map the fine agro ecological objects such as hedgerows, grass strips, forest edges, thickets and riparian forests..., among crops, meadows, and woodlands.

At 20-m spatial resolution, only the larger hedges and riparian forests are apparent. Classification results show that 10-m resolution (such as SPOT-5 imagery) is well suited for agricultural and AEI applications. Most hedges, forest edges, thickets are detected. The classifications obtain a high overall accuracy, allowing an agro-landscape characterization. The main limit of using this spatial resolution is found in too narrow hedges which are not revealed.

We confirm the importance of multitemporal data. 3-4 dates are recommended for satisfactory results for AEIs, the minimum being 2 dates. The future Sentinel satellites, which have a very high temporal resolution (about 5 days' revisit) and 10m spatial resolution, should be an answer to AEI detection.

The 2.50-m resolution classification is always more precise with more details than 10-m resolution. For example, there is no confusion between hedges and groves or wastelands that is found in 10-m resolution. But treatments are more complicated. At this scale the great amount of details requires more accurate ground truths. Moreover, the shadow induced by hedges, forests etc., must be taken into account on certain dates and imply additional operations.

At 50-cm resolution, the accuracy level of details is even higher; therefore this amplifies the difficulties previously reported. Inside forest, crop or grassland patches, small objects are visible due to the intrinsic heterogeneity of these patches: at this resolution the slightest variation is perceptible. The hedges are rather well detected, but they are not homogeneous: every detail appears and is classified as bush, tree or grass.

The results obtained allow calculation of statistics and metrics (as Fragstats software) describing landscape structures.

9637-105, Session PS

Early pest detection in soy plantations from hyperspectral measurements: a case study for caterpillar detection

Matías Tailanián, CSI Ingenieros (Uruguay); Enrique Castiglioni, Univ. de la República (Uruguay); Pablo Musé, Germán Fernández Flores, Gabriel Lema, Pedro Mastrángelo, Mónica Almansa, Ignacio Fernández Liñares, Germán Fernández Liñares, CSI Ingenieros (Uruguay)

Soybean producers suffer from caterpillar damage in many areas of the world. Estimated average economic losses are annually 500 million USD in Brazil, Argentina, Paraguay and Uruguay. Designing efficient pest control management using selective and targeted pesticide applications is extremely important both from economic and environmental perspectives. With that in mind, we conducted a research program during the 2013-2014 and 2014-2015 planting seasons in a 4,000ha soybean farm, seeking to achieve early pest detection.

Nowadays pest presence is evaluated using manual, labor-intensive counting methods based on sampling strategies which are time consuming and imprecise.

The experiment was conducted as follows. Using manual counting methods as ground-truth, a spectrometer capturing reflectance from 400 to 1100nm was used to measure the reflectance of soy plants. A first conclusion, resulting from measuring the spectral response at leaves level, showed that stress was a property of plants since different leaves with different levels of damage yielded the same spectral response. Then, to assess the applicability of unsupervised classification of plants as healthy, biotic-stressed or abiotic-stressed, feature extraction and selection from leaves spectral signatures, combined with a Supported Vector Machine classifier was designed. Optimization of SVM parameters using grid search with cross-validation, along with classification evaluation by ten-folds cross-validation showed a correct classification rate of 95%, consistently on both seasons. Controlled experiments using cages with different numbers of caterpillars - including caterpillar-free plants - were also conducted to evaluate consistency in trends of the spectral response as well as the extracted features.

Finally, in the 2014-2015 season, a SenseFly-Ebee drone was used for detecting stress using test cages in the soy plants field (four with pest infestation and four without pest), using NIR images at a 2cm/pixel resolution. Spectroscopy and drone results were qualitatively consistent. These preliminarily results are encouraging from a cost-effective remote sensing viewpoint.

9637-106, Session PS

Optical remote sensing of salt-affected soils

Rumiana Kancheva, Georgi Georgiev, Space Research and Technology Institute (Bulgaria)

Soil salinization as a result of natural or human-induces processes is a serious global-scale problem. Numerous efforts have been made in assessing and controlling soil salinity. Nearly sixty percent of the salt-affected soils around the world are in irrigated farmlands, and this trend is increasing. Salinization is a major reason for degradation of soil resources and decline of soil fertility. From an ecological and economic point of view it is extremely important to establish both the occurrence and distribution of soil salinization as well as the intensity of the process. Remote sensing techniques are widely used in soil surveys to detect and map salt-affected areas. However, many constrains in monitoring and evaluating the spatial and temporal variability of the salinization process have been found out. Difficulties arise also in applying remote sensing to the

assessment of slightly affected soils. The objective of this paper is to examine the spectral reflectance properties of soils with difeferent degree of salinization and the feasability of using spectral indicators derived ftom Vis/NIR field and airborne data as detectors of salr-affected soils and quantitative estimators of soil salinity level.

9637-108, Session PS

Assessing the quality of in-situ measurements of vegetation albedo for validating remote sensing products

Jennifer S. Adams, Jean-Luc Widlowski, Nadine Gobron, Corrado Mio, European Commission Joint Research Ctr. (Italy)

Vegetation albedo is an important component of the Earth's energy balance and climate system, defined as the fraction of shortwave radiation absorbed by a vegetated surface, and is routinely retrieved from space through remote sensing. Vegetation albedo products are regularly incorporated into environmental and climate monitoring and modeling, and can improve our knowledge and understanding of ecosystem and vegetation processes. Accordingly, it is essential that high quality accurate albedo products are provided to allow further understanding of such processes. However, it is often not possible to specifically know the quality of such albedo products, which can prove consequential in later integration into monitoring and modeling studies. Therefore, it is important to quantify the quality of these products at each step in the processing chain, thus providing traceable sources of quality and uncertainty.

Given the critical role of in-situ measurements in the processing chain, this study aims to examine the uncertainties and assumptions taken when using in-situ measurements of vegetation albedo to validate remote sensing albedo products. In reality, assessing traceable uncertainties of an in situ measurement (i.e. Where do the uncertainties arise from?) is difficult as it is a combination of many uncertainties. As a result, this study will use radiative transfer modeling to simulate in-situ measurements of albedo in controlled experiments in order to provide traceable uncertainties.

A 3D Monte Carlo Ray Tracing radiative transfer model (raytran) was used to simulate an albedometer; an in-situ measurement of albedo, which measures incoming solar radiation and surface reflectance. To simulate vegetation albedo, a variety of complex 3D vegetation canopies were used, some based on forest inventory data (i.e. Spatial structure of trees, tree structure, number of trees, spectral and illumination characteristics) and some based on computer generated scenes. To trace sources of uncertainty of in-situ albedo measurements, experiments were set up to examine sources of uncertainty such as solar zenith angle, placement of albedometer in the site (both horizontally in the canopy and vertically above the canopy), and ecosystem type.

Given that in-situ measurements must be made to within 3% accuracy (WMO) in order to be used to validate remotely sensed albedo products, the results from this study show some conditions in which this accuracy criteria can be, and can not be met. It has long been documented that the uncertainty of an in-situ measurement should actually be made on an individual bases accounting for all the relevant factors, some of which have been mentioned previously. As a result, this study aims to move towards providing 'standards' for using in-situ measurements to validate remotely sensed albedo products, whereby given a specified uncertainty, can this uncertainty criteria be met under a specific scenario, or not. Moving towards 'standards' subsequently allows users of remote sensing data to have an indication of the uncertainty of in-situ measurements and where these uncertainties originate, which can be appropriately incorporated into their models to better estimate vegetation and ecosystem processes.

9637-110, Session PS

Correlation between the recreational activities and productivity of coastal areas: a case study in the low-lying coastal stretch in the Bay of Bengal coast, india

Srikanta Sannigrahi, Indian Institute of Technology Kharagpur (India)

This paper presents a methodological approach for assess the impacts of coastal recreational activities upon spatial and temporal dynamics of coastal productivity. Several sources data were used for estimation the exact demising rate of floral distribution. From 1973 Multi Spectral Scanner 4 band to 2010 Enhance Thematic Mapper 7 band satellite data has been collected for assess the spatial and temporal changes. It further collaterally assess with Survey of India closed series (1973) and open Series (2005-06) topographical map. Only first four band had been selected for advance rationing operation. Out of 44 mouzas and major tourist destination plots of Digha-Shankarpur area, maximum recreational activity spot have been identified by using tourist potentiality mapping technique. Selected species identified for this purpose from Botanical Survey of India (BSI) databank. A Geographical Information System (GIS) based model Carnegie-Ames-Stanford Approach (NASA-CASA) were used for accurately estimate the Net Primary Productivity of coastal flora. Pre-field bio-climatic parameters assess through by MODIS Surface Reflectance Product (MOD09A1) data and it verified by ground truth observation. Landsat Thematic Mapper(TM)and Enhance Thematic Mapper(ETM+) based estimation of Net Primary Productivity has been coupled with the MODIS Normalized Difference Vegetation Index (NDVI) based NPP to check the accuracy of the model. Extent of land-use alteration has been assessed from 1980 to 2013 to calibrate it with the potential NPP losses of the region. Socio-economic parameters like Gross Domestic Product (GDP), level of urbanization, land-use change, Specific recreational based impact scenario map generated by applying field data and potentiometric future coastal recreational impact analysis. Future research will involve feasibility studies of different treatment schemes and the development of specific monitoring activities.Net Primary Productivity (NPP) is regarded as an ecological index of environmental quality and state of health to evaluate the sustainability of an ecosystem (Fang, 2000). NPP, the direct reflection of plant community productivity for a certain natural environment, is the basis of matter and energy cycle of the terrestrial ecosystem (Field et al. 1998). International Geographical and Biological Plan (IGBP), Global Change and Terrestrial Ecosystems (GCTE) and Kyoto Protocol all take it as their key research field (Steffan et al. 1998). Net primary productivity (NPP) is an important component of the carbon cycle and a key indicator of ecosystem performance. Vegetation also acts as a source, or sink, for the greenhouse gas CO2. Thus, the increasing intensity of human induced disturbance could be considered an important factor in the decrease in forest NPP in urbanized areas (Imhoff et al., 2004; Xu et al., 2007). Indications have shown that settlement, population, and Gross Domestic Product (GDP) have had a strongly negative impact on NPP in South-eastern China (Lu et al., 2010). The loss of NPP due to urban expansion could be estimated by integrating remote sensing with GIS techniques (Tian and Qiao, 2014). Traditionally, NPP has been estimated using climate productivity relationship models (Del Grosso et al., 2008; Pranuthi et al., 2012) and eco-physiological processing models (Li and Ji, 2001; Sasai et al., 2011). However, NPP estimation based on Remote Sensing (RS) and Geographic Information System (GIS) technology has been shown to have vast advantages over previous approaches, especially for the study of regional and global scales (Zhao et al., 2005; Prieto-Blanco et al., 2009b; Yuan et al., 2014).

9637-111, Session PS

Monitoring regional winter wheat late frost injury using remote sensing data, WOFOST model and SHAW model

Nian Wang, Junming Liu, China Agricultural Univ. (China)

Late frost injury is one of the major agro-meteorological disasters for winter wheat. The key in occurrence of such freezing injury is the growth period and leaf temperature, and winter wheat is most sensitive to low temperature following the jointing stage. The land surface temperature or air temperature retrieved by remote sensing data is rather different from the leaf temperature so that it cannot be directly used to monitor late frost injury. The crop growth model WOFOST can simulate the growth process of crops successfully and the soil-vegetation-atmosphere transmission model SHAW can simulate the process of water and heat movement in the canopy of crops efficiently. Combine with the spatiality and temporality of RS and the advantages of the procedure and mechanism of model to propose a method which integrates remote sensing data with WOFOST and SHAW models to monitor late frost injury of winter wheat. The winter wheat in Shangqiu areas of Henan Province, China is taken as object of the study. Firstly, MODIS NDVI curve filtered by Savitzky-Golay is used to determine the returning green stage and the heading stage while the jointing stage is calculated with the accumulated temperature method. Then, on the basis of research area is grouped into grids, WOFOST and SHAW are locally calibrated according to soil data, meteorological data and growth parameters of winter wheat. Data of maximum air temperature and minimum air temperature retrieved by MODIS LST product by statistical regression model are put into WOFOST and SHAW along with surface observation data. Variables including LAI, root depth and dry biomass simulated by WOFOST model are transmitted to SHAW model for internal coupling. SHAW model generates the leaf temperature profile in vertical direction of winter wheat canopy by using hour as the step size. Finally, according to comparing the simulated leaf temperatures with measured ones, the ability of simulating leaf temperature of SHAW will be validated. In addition, the minimum leaf temperature and information of winter wheat during the growth period will be used as the factors to monitor late frost injury, monitoring results of such method are validated by referring to the field measured data about the percentage of damaged ears and kernel number of residual ears at 18 sampling sites of Shangqiu. It turns out that: air humidity and wind speed are the main factors to deciding the gap size of leaf temperature and air temperature; SHAW model stimulates leaf temperature in canopy of winter wheat in an accurate manner with model efficiency equaling 0.88 and the coefficient of determination is 0.85; The critical leaf temperature for frost is changing with the number of days after jointing, the minimum leaf temperature simulated by coupling model decrease to be below critical line in the three freezing injuries (April 7, 10 and 21), the correlation coefficient of leaf temperature and kernel number of residual ears is 0.76. Studies show that it is practical to integrate remote sensing data with WOFOST and SHAW models for monitoring late frost injury of winter wheat.

9637-112, Session PS

Investigation variation of carbon dioxide based on GOSAT data in peninsular Malaysia

Chong Keat Sim, Hwee San Lim, Mohamad Zubir Mat Jafri, Univ. Sains Malaysia (Malaysia)

Carbon dioxide (CO2) is an inodorous and transparent gas, and naturally originates in our atmosphere. Due to its optical characteristics, CO2 is the most important greenhouse gas and play a key roles in climate change due to an effective thermal infrared (IR) radiation absorber. Satellite observations of atmospheric carbon dioxide (CO2) can significantly improve our knowledge about the sources and sinks of CO2. The remote sensing satellite, namely Greenhouse Gases Observing Satellite (GOSAT) was employed to investigate the spatial and variations of CO2 column-averaged dry air-mole fractions, denoted XCO2 over Peninsular Malaysia from April 2009 to December 2013. The analysis of CO2 in the study area shows the significant differences between northeast monsoon (NEM) and the southwest monsoon (SWM). During NEM season, cold air outbreaks from Siberia spreads to equatorial region in the form of northeasterly cold surge winds and associated with a low-level anticyclone over Southeast Asia. Inversely, air masses from the southwest contribute to long–range air pollution due to transportation of atmospheric CO2 by wind is associated with biomass burning in Sumatra, Indonesia. The GOSAT data and the Satellite measurements are able to measure the increase of the atmosphere CO2 values over different regions.

9637-113, Session PS

An assessment of the impact of climate change effects on forest land cover based on satellite data

Maria A. Zoran, National Institute of Research and Development for Optoelectronics (Romania); Adrian I. Dida, Univ. Transilvania Brasov (Romania)

Climate change affects forest both directly and indirectly through disturbances, that are a natural and integral part of forest ecosystems, and climate change can alter these natural interactions. Forest vegetation characteristics, including land cover and phenology, affect processes such as water cycle, absorption and re-emission of solar radiation, momentum transfer, carbon cycle, and latent and sensible heat fluxes. The climate system responds in complex ways to changes in forcing that may be natural or human-induced. Drastic climate change over the last decades has greatly increased the importance of global environmental study. In frame of this research, forest land cover changes monitoring through satellite remote sensing can continually observe various surface processes playing an increasingly important role in large-scale environmental monitoring. Satellite based derived biophysical parameters information for assessment of climate impacts on forest vegetation for sustainable management needs have to meet particularly high quality requirements. Forest vegetation and climate interact through a series of complex feedbacks, which are not very well understood. The patterns of forest vegetation are largely determined by temperature, precipitation, solar irradiance, soil conditions and carbon dioxide (CO2) concentration. Vegetation impacts climate directly through moisture, energy, and momentum exchanges with the atmosphere and indirectly through biogeochemical processes that alter atmospheric CO2 concentration. Changes in forest vegetation land cover/use alter the surface albedo and radiation fluxes, leading to a local temperature change and eventually a vegetation response. Forest vegetation-climate feedback regimes are designated based on the temporal correlations between the vegetation and the surface temperature and precipitation. The different feedback regimes are linked to the relative importance of vegetation and soil moisture in determining land-atmosphere interactions. Forest vegetation phenology constitutes an efficient bio-indicator of impacts of climate change and a key parameter for understanding and modeling vegetation-climate interactions. Climate variability and anthropogenic stressors have a great impact on the forest vegetation biophysical parameters dynamics. Satellite remote sensing is a very suited tool to assess the main phenological events based on tracking significant changes on temporal trajectories of Normalized Difference Vegetation Index (NDVI), Land Surface Temperature (LST) and land surface albedo, which are key biophysical variables for studying land surface processes and surface-atmosphere interactions. The aim of this paper was to investigate their pattern dynamics due to the impact of climate variations on a periurban forest Cernica-Branesti, placed to the North-Eastern part of Bucharest city, Romania. The forest vegetation analysis was based on derived biogeophysical

parameters from time-series satellite remote sensing MODIS Terra/Aqua and NOAA AVHRR data and in-situ monitoring ground data (as air temperature, aerosols distribution, relative humidity, etc.) over 2002–2014 period. Have been analyzed also other biogeophysical effects of forest land cover change particularly changes in the surface moisture budget leading to shifts in the ratio of latent and sensible heat fluxes and changes in rate of land surface temperature and precipitation. Specific aim of this paper is to assess, forecast, and mitigate the risks of climatic changes on forest systems.

9637-114, Session PS

NDVI trend at a global scale from 1982-2012 with climate changes

Meng Guo, Northeast Normal Univ. (China)

To understand the trends in vegetation cover and the impact of global climate change on vegetation growth, this research examines the spatial-temporal trends of global vegetation using the Normalized Difference Vegetation Index (NDVI) from the Advanced Very High Resolution Radiometer (AVHRR) Global Inventory Modeling and Mapping Studies (GIMMS) time series (1982-2006). Mann-Kendal (MK) trend test results indicate that of all the regions where trends that are significant at the 99% level are found, 83.57% exhibit positive trends, and only 16.43% show negative trends. The increasing NDVI trends primarily occurred in ecotones between grasslands and bare areas, and the decreasing trends occurred in grassland/vegetation or mosaic croplands/vegetation areas. In addition to the spatial distribution of the per-pixel NDVI trends, we examined the temporal trends of the NDVI of each continent using a linear regression model. The results indicate that the NDVI increased from 1982 to 2006 for every continent. It appears that the annual sum precipitation is positively correlated with the NDVI for all continents except South America. Temperature has no relationship with the NDVI for any continent except Australia. The NDVI decreases as temperature increases in Australia because of the higher evaporation rates in the arid and semi-arid regions of Australia.

9637-115, Session PS

Estimating canopy water content of wetland vegetation using hyperspectral and multispectral remote sensing data

Yonghua Sun, Capital Normal Univ. (China); Yihan Wang, Capital Normal University (China); Jin Huang, Capital Normal Univ. (China)

Currently one of the main scientific issues is to understand and quantify the impact of global climate change on the earth system. One of the challenges is to understand the role of terrestrial ecosystems and the changes they may undergo. The water cycle is one of their most important characteristics. Wetlands, which are described as a 'storage area of natural genes' and the 'kidney of the Earth', play an important role in water cycle. Water and vegetation is the key characteristics of wetland. In this respect, the canopy water content represents the health condition of vegetation and wetland itself. In this paper, we focus on innovative approaches for retrieving canopy water content from optical remote sensing data-multispectral and hyperspectral data.

Therefore, in this study, we selected Honghe National Nature Reserve (HNNR) (47°42?18?–47°52?N, 133°34?38?–133°46?29?E), which is a miniature of wetlands in the Sanjiang Plain, Northeast China as the study area. Field spectrum data, Landsat-5 TM images and ground truth data was used to estimate canopy water content of wetland vegetation. The analysis methods include three-edge parameters, narrow band vegetation indexes, absorption indexes from hyperspectral data and different vegetation indexes from multispectral data.

1. Canopy water content estimated model based on three-edge parameters (Table2, Fig.1, and Table3)

The correlation between the indexes ((SDr-SDb)/(SDr+SDb)?SDr/SDb) and canopy water content reach to a very significant test level.

2. Canopy water content estimated model based on narrow band vegetation index (Fig.2 and Table4)

Narrow band vegetation index?NDVI?is a normalized difference index between any two hyperspectral bands. In this study, 39340? ?(spectral resolution =5nm) NDVIs were built. According to correlation analysis, NDVI based on reflectance of 970nm and 900nm has the maximum correlation with canopy water content.

3. Canopy water content estimated model based on general vegetation index (Table5, Fig.3 and Table 6)

Based on previous literatures, 14 vegetation indexes(PVIHYP?ATSAVI?DSWI?LWVI1?LWVI2?MSI?NDII?NDWI?PRI?RVIHYP?RVSI?SIWSI?SRWI?WI)were used for estimating canopy water content(Detailed definition of the VIs were listed in Table 5).Finally, WI which was built by R900/R970 has the maximum correlation and was selected to build estimated model.

4. Canopy water content estimated model based on absorption features (Fig.4 and Table 7)

The article selected the absorption features around the 970nm and 1200nm, such as absorption depth, absorption width and absorption area. Absorption depth of 1200nm has the maximum correlation and was selected to build estimated model.

5. Canopy water content estimated model based on TM image

The article extracted 11 VIs from Landsat5 TM image. According to correlation analysis with survey data, NDII(?TM4-TM5?/(TM4+TM5)) was selected to build the estimated model. Based on the model, distribution map of canopy water content in HNNR was generated.

9637-25, Session 5

Satellites in agriculture: precision and commercialisation in Germany

Lisa M. Gutermuth, Humboldt-Univ. zu Berlin (Germany)

Satellite imagery has been used since the 1960s to monitor agricultural activities at a government and international level. It is only now that the image quality and of cost feasibility have made satellite imagery available to individual farmers in application to crop quality analysis and other measures relating to precision farming. The underlying reasoning for the propulsion forward of this technology to the level of individual producers has been in the name of food security; to use agricultural intensification through precise monitoring of field factors including plant rigor, pests, water needs, weeds, soil quality, etc. However, when looking at the goals of common agricultural policy at large, satellite imagery availability contributes greatly to some, while detracting from important aspects such as maintaining small farms and rural infrastructure, as well as encouraging agrobiodiversity and it's acknowledgement as a main facet of global food security. Through a technological assessment, both the actors and supply chains that enable satellite imagery to be available to individuals, as well as the social impact and ultimate impact on global food security of this new development will be presented.

It is with this in mind that this study will, in the first section, explain the development of the privatisation and eventual commercialisation of satellite imagery in agriculture in Germany. Second, present an overview of applications currently available for small farmers and channels of communication for adoption. Third, an examination of the oppositional relationship between agrobiodiversity and precision agriculture. Then finally, a summation of the implications of this new practice on a social level with regard to small farmers and rural infrastructure, as well as agrobiodiversity and food security.

The method study is a classical technology assessment outlining potential issues and background workings to be inform policy making with regard to satellite imagery availability and regulation for individual agricultural use. As such, although the study is focused on the German context, the

study maintains global perspective and is future-oriented.

Key findings are:

-Satellite imagery analysis has successfully been used to include measures of agrobiodiversity, as demonstrated by Karl Zimmerer's research using remote sensing to study potato varieties in South America. While this technology and method exists for research purposes, it has not yet been either marketed or incentivised by precision farming companies or through agricultural policy.

-The gradual privatisation of farm technology has led to a change in how farmers become aware and adopt new technologies. Rather than relying on agricultural extension services, the channels of communication have shifted to direct marketing from precision farming companies and satellite imagery providers. There are, however, implications to this shift: firstly, that logically companies are targeting larger farmers where they can make most profit, creating a technology gap, and secondly, that farmers are not necessarily receptive to these channels of communication, leaving precision agriculture initiatives at a loss as to why their products are not being adopted.

-The use of satellite imagery for field and crop analysis has not yet been divorced from industrial agriculture. While NDVI imagery can reveal spots on a field that require fertilizer, pesticides, or herbicides, it is still mainly with synthetic and chemical use. There is no reason why this can't be a gateway to enable the application of organic fertilizers, pesticides, and herbicides as by definition, less field inputs makes it more affordable, and the practice of precision agriculture is advertising environmental sustainability as a main feature and benefit of use.

9637-26, Session 5

Study on drivers of cultivated land change in urban fringe area based on the multiple regression model: a case study in Tiruverkadu, Chennai metropolitan area

Manonmani R, Anna Univ. Chennai (India)

Society utilizes the natural resources in many ways in order to improve the living standard of the common man. With increasing population, the pressure on natural resources increases and with improvement in living standards, the amenities required for such development increase. This leads to changes in land use practices in the region like increase in built up area, decrease in crop land and water body etc. Based on Remote Sensing & Geographic information system derived map, three change matrices were constructed for detecting land use change between 2004-2008 and 2008-2014. Decreased in crop land and increase in built were extracted from the 2004-2008 land use /land cover. In addition, socio-economic data and demography were used to analyze major driving forces triggering land use change between 2004-2008 through multiple regression model and predicted land use change between 2014. The predicted result was compared with satellite derived land use map of 2014.The result indicated that population density, work force, dependency rate and infrastructure are major driving forces contributing to land use change in the study area.

9637-28, Session 5

Analysing the impact of natural and anthropogenic stresses on crop production in Iraq using time series of remote sensing data

Sarchil Hama Qader, University of Southampton (United Kingdom); Jadunandan Dash, Peter Atkinson, Univ. of Southampton (United Kingdom)

In the arid and semi-arid regions of Iraq inter-annual variation in climatic factors (such as rainfall) and anthropogenic factors (such as civil war) pose a major risk for food security. For example, the 'Post-Gulf' war which started in 2003 lasted for around 8 years. During this time, due to political instability and insecurity, many farmers were unable to grow crops. This, in turn, affected the overall crop production of the country. In addition, due to its geographical location the region is affected by irregularities in precipitation resulting in the frequent occurrence of drought. The combination of these factors makes it challenging in this this region to sustain food production, and indeed in recent years there have been large fluctuations in food production. Therefore, an operational crop production estimation and forecasting system is required to help decision-makers make early estimates of the potential food availability and plan for annual imports.

Given the large uncertainties in ground data, to date there is no reliable system to estimate crop production in Iraq. Therefore, this study attempted to combine 8-day three Moderate Resolution Imagine Spectro-radiometer (MODIS) products such as MOD09Q1, MOD09A1 and MOD17A2 with detailed official crop statistics to develop an empirical, generalized method to estimate and forecast annual wheat and barley production. The research will mostly focus on crop related phenological information. Finally, climatic variables such as rainfall and temperature and data related to regional instability (for example, civil war) were evaluated to understand their influence on local crop production during the last decade.

9637-30, Session 6

Water balance indicators from MODIS images and agrometeorological data in Minas Gerais state, Brazil

Antônio Heriberto C. de Castro Teixeira, Janice F. Leivas, Ricardo G. Andrade, Daniel C. Victoria, Edson L. Bolfe, Embrapa Monitoramento por Satélite (Brazil); Gustavo Bayma-Silva, Embrapa Satellite Monitoring (Brazil)

Minas Gerais state, Brazil, has gained special severe water scarcity, demanding large-scale studies to subsidize water policies. The reflectance bands were from a MODIS product were used together with agrometeorological data in the state, for each 16-day periods during of year 2014, later extracting the main agriculture growing regions for water regional analyzes. Precipitation (Prec) data from 36 weather stations were interpolated, while for evapotranspiration (ET), the SAFER (Simple Algorithm For Evapotranspiration Retrieving) algorithm was used. The model input parameters, surface albedo (?0) and the Normalized Difference Vegetation Index (NDVI), were calculated from the bands 1 and 2, while the surface temperature (T0) was estimated as a residual in the surface radiation balance. These parameters were used together with reference evapotranspiration (ET0) for ET acquirements. The daily net radiation (Rn) was retrieved from ?0, air temperature (Ta) and atmospheric transmissivity (?sw), while the soil heat flux (G) was considered as a fraction of Rn. Two climatic indicators were applied, the Water Balance Ratio (WBr = Prec/ET) and the Water Balance Difference (WDd = Prec - ET). For soil moisture conditions, the evaporative fraction [Ef = ?E/(Rn - G)] and the evapotranspiration ratio (ETr = ET/ET0) were used, with the latent heat flux (?E) obtained by transforming ET into energy units. Analysing WDr and WDd, the most critical periods of water scarcity, corresponding respectively to their values lower than 1.0 and -10 mm, were from the end of April to the middle of October. Higher water availability, detected by these indicators higher than 1.5 and 10 mm, respectively, were from the middle of October to the end of December. These last conditions indicated good opportunity for water storage techniques for further use during low Prec values. Both, Ef and ETr were sensitive to deficits and excesses of water but with time gaps in relation to WDr and WDd, because of the necessary time for soil moisture storage to follow the rainfall events. Among the main agricultural regions, North, Northwest and Minas Triangle, the lowest Prec values, were respectively, for the first and the last ones, amounting

788 and 1068 mm yr-1. North and Northwest regions presented similar ET rates, around 795 mm yr-1, while in the Minas Triangle they were 868 mm yr-1. The largest WDr and WDd of 7.0 and 158 mm happened from the middle of November to the start of December in the Northwest agricultural growing region. However, according to the Ef and ETr values, after this period, the soil moisture storage increased only in the second half of December, when they reached to averages of 0.63. The largest Ef and ETr values, higher than 0.7 in May, did not coincided with the period of higher Prec, but with that of the lowest atmospheric demands in all agricultural growing regions, probably because irrigation also plays a hole. The indicators tested here can be implemented in the state of Minas Gerais, Brazil, for water policies under the actual conditions of severe water scarcity and competition among water sectors.

9637-31, Session 6

Evaluation of disaggregated thermal images for evapotranspiration estimation in Barrax test site

Mar Bisquert, Juan Manuel Sánchez, Univ. de Castilla-La Mancha (Spain); Vicente Caselles, Univ. de València (Spain); Ramón López-Urea, ITAP-FUNDESCAMP (Spain)

Evapotranspiration (ET) is a key parameter in climatological and hydrological models. Moreover, the knowledge of ET at a local scale in agricultural areas may improve the irrigation practices. An operative method using remote sensing techniques would provide spatial and temporal continuous ET data. However, there are limitations in remote sensing data, especially due to the spatial and temporal resolution of the images. For agricultural practices, high spatial and temporal resolution is desired, but nowadays no sensor offers both. The coming Sentinel-2 sensor will have a 3-5 days revisit cycle and 10-30 m spatial resolution in the visible and near infrared (VNIR) bands. However, no thermal band (TIR) will be available, which is the key input in the models for ET estimation based on the surface energy balance. Several disaggregation techniques have been developed in recent years to downscale the coarse spatial resolution of TIR bands to the higher VNIR resolution. Moreover, some works apply the disaggregation techniques to two different sensors. For example, using first the TIR and VNIR MODIS bands to train the method, and then apply it to the VNIR bands of Landsat images. The further aim of these works is to apply these procedures to high resolution VNIR sensors, such as the coming Sentinel-2, in combination with a coarser TIR resolution such as MODIS or the future Sentinel-3.

A simple disaggregation procedure is applied in this work to MODIS-Landsat images to derive TIR data at 30 m spatial resolution. The disaggregated temperatures are further used as inputs in the STSEB approach (Simplified Two Source Energy Balance) to estimate ET values. ET is also obtained from the Landsat original TIR data and compared to results above. Additionally, Landsat ET results are aggregated to MODIS resolution and compared to maps obtained from MODIS original images. The study area is placed in the Barrax experimental site "Las Tiesas", central Spain. This is an agricultural area with a wide crop variety. Ground measurements were available in three small fields of festuca, wheat and vineyard, including land surface temperature measured with an infrared radiometer, and ET measured by lysimeters installed in each field. MODIS resolution is too coarse to monitor these fields. These local ET measures are used to assess the results of the STSEB model from both disaggregated and original satellite scenes, and reinforce the potential of this technique to be applied to sensors with no TIR bands.

9637-33, Session 6

Study on spatial variations of surface parameters and heat fluxes during the HiWATER-MUSOEXE compaign

Zhi Qing Peng, Institute of Remote Sensing and Digital Earth (China) and Univ. of Chinese Academy of Sciences (China); XiaoZhou Xin, Institute of Remote Sensing and Digital Earth (China); Ti Zhou, Institute of Remote Sensing and Digital Earth (China) and Univ. of Chinese Academy of Sciences (China)

Evapotranspiration (ET) is an important component in land surface heat and water cycle. Remote sensing has long been identified as a technology capable of monitoring ET and scholars have achieved great advance upon models, methods and satellite data applications of remotely sensed estimating evapotranspiration in last decades. However, severe scale effect emerge since surface heterogeneity influence the driving force of evapotranspiration retrieval with remote sensing, and scientists have proposed some statistical methods to correct scale deviation by combining high spatial resolution satellite data with the lower ones for externalizing the inhomogeneity of parameters in mix pixels. Meanwhile several methods of quantifying spatial heterogeneity have proposed in remote sensing, but it's difficult to use them to estimate evapotranspiration by integrating them with retrieval models.

From May to September, 2012, Multi-Scale Observation Experiment on Evapotranspiration over heterogeneous land surfaces of The Heihe Watershed Allied Telemetry Experimental Research (HiWATER-MUSOEXE) designed two nested observation matrixes overlay space of 30 km?30km and 5.5 km?5.5km respectively within the oasis in Zhangye city to emphasize the research of heterogeneity of scale effect. In larger observation matrix, 4 automatic meteorological stations (AMSs) and 1 superstation is installed in the oasis–desert ecosystem and each one is supplemented with an eddy covariance (EC) system to record meteorological and soil variables for monitoring the spatial–temporal variation of ET and its impact factors. Within the oasis, an observing matrix composed of 17 EC towers and ordinary AMSs in which the superstation is included and 4 pairs of large aperture scintillometers (LAS) systems that span 2–3 km each are located in the irrigation district, where the land surface is heterogeneous, dominated by seed corn, corn interplanted with spring wheat, vegetables, orchards, and residential areas. 4 wireless sensor net (WSN) composed of 50 WATERNET nodes, 50 SoilNet nodes, 75 BNUNet nodes which observed soil parameters such as moisture and temperature and so forth, and 45 LAI measurement system nodes are deployed to capture the heterogeneity of soil moisture, soil temperature, land surface temperature, and LAI and so forth.

In order to develop more representative remotely sensed evapotranspiration retrieval models over heterogeneous surface, we utilize methods that could quantify parameters' heterogeneity and may be able to integrate retrieval models to analyze data during the HiWATER-MUSOEXE compaign. We dissect the spatial-temporal variation between heat fluxes and related surface parameters by combining observation variables with the passing by satellite and airborne data from the following prospects. (1) What's spatial distribution pattern exists between observed turbulent fluxes and land surface or meteorological parameters over heterogeneous covering? (2) How the regularity in (1) varying with time? (3) How spatial heterogeneity affect the relationship that mentioned in (1)? As the spatial variability of parameters spans a wide range of scales, we explore the spatial distribution relationship from different spatial scale between evapotranspiration and related parameters, the same as the relationship between heterogeneity and spatial resolution.

9637-34, Session 7

Testing two temporal upscaling schemes for the estimation of the time variability of the actual evapotranspiration

Antonino Maltese, Fulvio Capodici, Giuseppe Ciraolo, Goffredo La Loggia, Univ. degli Studi di Palermo (Italy)

Temporal availability of grapes actual evapotranspiration is an emerging issue since vineyards farms are more and more converted from rainfed to irrigated agricultural systems.

The manuscript aims to verify the accuracy of the actual evapotranspiration retrieval coupling a single source energy balance approach and two different temporal upscaling schemes.

The first scheme tests the temporal upscaling of the main input variables, namely the NDVI, albedo and LST; the second scheme tests the temporal upscaling of the energy balance output, the actual evapotranspiration.

The temporal upscaling schemes were implemented on: i) airborne remote sensing data acquired monthly during a whole irrigation season over a Sicilian vineyard; ii) low resolution MODIS products released daily or weekly; iii) meteorological data acquired by standard gauge stations.

Daily MODIS LST products (MOD11A1) were disaggregated using a DisTrad model, 8-days black and white sky albedo products (MCD43A) allowed modeling the total albedo, and 8-days NDVI products (MOD13Q1) were modeled using the Fisher model.

Results were validated in time and space. The temporal validation was carried out using the actual evapotranspiration measured in situ using a Flux tower installation and eddy covariance technique. The spatial validation involved airborne images acquired at different times.

Results indicated whether the upscaling of the input data or the output evapotranspiration performed better and a critical analysis with reference to agronomical activities, irrigation scheduling and rainfall events.

9637-37, Session 7

Modelling radiation and energy balances with Landsat 8 images under different thermohydrological conditions in the Brazilian semi-arid region

Antônio Heriberto C. de Castro Teixeira, Janice F. Leivas, Ricardo G. Andrade, Embrapa Monitoramento por Satélite (Brazil); Fernando B. Tangerino Hernandez, Renato Alberto M. Franco, São Paulo State Univ. (Brazil)

The quantification of the radiation and energy balances along the year is highly relevant under the Brazilian semi-arid conditions. Four Landsat 8 images were used together with nine agro-meteorological stations for modelling these balances in the Petrolina municipality, Northeast Brazil, along the year 2014. The SAFER (Simple Algorithm For Evapotranspiration Retrieving) algorithm was used to calculate the latent heat flux (?E). Having the measured values of incident solar radiation (RS?) and surface albedo (?0) from the visible bands of the satellite, the reflected solar radiation (RS?) was calculated. With measured air temperature (Ta) from the stations and surface temperature (T0) from the thermal bands of the satellite, the ongoing (RL?) and outgoing (RL?) long wave components were determined, by applying the Stefan-Boltzmann low. Net radiation (Rn) was acquired by the difference of all incident and outgoing radiation fluxes, soil heat flux (G) as a fraction of Rn and the sensible flux (H) as a residual in the energy balance equation. For classifying the vegetation into irrigated crops and natural vegetation, the SUREAL (Surface Resistance Algorithm) algorithm was used to determine the surface resistance (rs) and threshold values for rs were used to retrieve the energy fluxes for each of these ecosystems. First, the entire municipality was considered. For the shortwave radiation balance, RS? mean pixel values were between 19.0 and 24.7 MJ m-2 d-1; while those for RS? ranged from 3.6 to 4.8 MJ m-2 d-1, with ?0 between 0.18 and 0.20. Taking into account the longwave components, RL? mean values were from 33.0 to 34.9 MJ m-2 d-1, while for RL? they were between 39.5 and 44.2 MJ m-2 d-1. The values for all longwave components happened during the naturally driest and hottest periods of the year. Rn mean values ranged from 8.7 to 11.5 MJ m-2 d-1, representing 41 to 46% of RG, independently of the ecosystem. However, energy partition differed among them besides the thermohydrological variation along the year. Clearly one could see higher ?E for irrigated crops than for natural vegetation with some situations of heat horizontal advection increasing the values till 1.4 times larger than Rn. These last conditions are also related to negative H values, reaching up to - 5.5 MJ m-2 d-1. The average ?E ranges for irrigated and natural conditions, were respectively, 3.8 (43% of Rn) to 6.3 (56% of Rn) and 0.1 (1% of Rn) to 4.9 (42% of Rn) MJ m-2 d-1. The corresponding H values were 4.0 (41% of Rn) to 4.7 (53% of Rn) and 6.2 (54% of Rn) to 9.5 (96% of Rn) MJ m-2 d-1. There were no significant differences between the daily G for irrigated crops and for natural vegetation, staying in the small average range from 0.2 and 0.4 MJ m-2 d-1, only 3 to 4% of daily Rn. The models tested here with Landsat 8 images and agro-meteorological stations, can subsidize the monitoring of the energy exchanges between the mixed agro-ecosystems in the Brazilian semiarid, under conditions of climate and land use changes.

9637-38, Session 7

Assessment of crop evapotranspiration and irrigation water demand in the lower Niobrara River, Nebraska (USA) by combining remote sensing-based energy and water balances

Christopher M. U. Neale, Univ. of Nebraska Lincoln (United States); Isidro Campos, Patricio Grassini, Univ. of Nebraska-Lincoln (United States)

This research analyzes the use of remote sensing methodologies for the assessment of crop evapotranspiration (ET) and irrigation water demand in high-yield, center pivot-irrigated maize and soybean fields located in the Lower Niobrara River basin in Nebraska (USA).

The proposed methodology combines surface energy balance approaches (SEB) using thermal infrared imagery and soil water balance models (RSWB) based on remotely sensed reflectance-based crop coefficients, for a daily estimation of the soil water content in the crop root zone. This hybrid approach can strength the results from each model running separately. More than 300 fields were analyzed during the 2011-2013 growing season. This period allowed for testing the model under a range of meteorological conditions; including the severe drought of 2012 and the abundant precipitation of the 2013 growing season.

The input data includes agro-meteorological data obtained from ground stations, satellite images from the Landsat Thematic Mapper 5, 7 and 8 and information on the soil physical properties and crop production of the fields.

The results of the models are compared and discussed against actual seasonal applied irrigation amounts, derived from flow meters and/or producer's estimates. The modeled ET estimates were also compared with eddy covariance flux tower measurements at research fields close to Mead, NE. The approach allows for the estimation of seasonal crop water requirements and demonstrates the suitability of remote sensing approaches for benchmarking current irrigation management over large areas.

9637-40, Session 8

Determination of water body structures for small rivers using remote sensing data

Pierre Karrasch, Daniel Henzen, Sebastian Hunger, Max Hörold, Technische Univ. Dresden (Germany)

The diversity of habitats in water bodies like rivers is characterized by the state morphological and hydrological conditions. A high variability of water body structures features the high quality river waters. The good ecological status of water bodies is claimed in the European Water Framework Directive. For the assessment of this status the hydro-morphology is one of the most important supporting components for the classification of the ecological status of water bodies. Different analyses in Germany (e.g. of the Federal Ministry for the Environment, Nature Conservation, Building and Nuclear Safety) and other European states show that hydro-morphological limitations are primarily responsible for the insufficient quality of water bodies. Therefore the periodical monitoring is a mandatory measure in the scope of the European Water Framework Directive. In the last years different national initiatives, in Germany on the level of the federal states, have developed workflows and methods for obtaining water body structures. The most essential feature of these classification workflows is the subdivision into an on-site method and an overview method. Regarding the overview-method the use of Remote Sensing data and Remote Sensing methodologies becomes more important. Results of several studies show a certain added value for the extraction of parameters like degree of curvature, transverse structures or the land use and land cover in the shore area as well as in the close environment of the river. These studies often use single products, derived from satellite systems and the determination of the already mentioned parameters is oriented towards the manual predefined stretch of water based on the subjective evaluation and individual experiences of the operator.

As part of a comprehensive project of determination water body structures funded by the German Federal Ministry of Education and Research, an innovative approach of determination water body structures using different remote sensing data was developed. Concerning the structure of the overview method, the used parameters were determined independent from a particularly stretch of water. Therefore remote sensing data on different scales (satellite, aerial photographs, UAV data) as well as other topographic information (ATKIS, high resolution DTM) were merged into an integrative process of analysis using remote sensing and GIS methodology. These results allow a better definition of stretches of water based on real conditions of changing quality of water bodies. Thereby the decision about the length and position of a stretch of water is taken after a detailed analyses of water body structures. An additional challenge is the chosen study area of a low mountain range river. While large rivers are clear visible in remote sensing data, the usability and transformation of the well-established algorithms and workflows to small rivers need a further substantial research.

Finally the introduced process will help to support the determination of parameters of morphology of waters as an inherent part of water quality assessment according to the European Water Framework Directive.

9637-41, Session 8

Analysis of spatial dynamics of drought in southern Africa

Alzira G. Ramos, Rogers Hansine, Maria João Pereira, Amílcar Soares, Instituto Superior Técnico (Portugal)

The desertification problem in southern Africa, its causes and impacts demand the attention of many experts from various fields of studies. Available data demonstrates that both human activity and climate factors are the causes of land degradation in southern Africa. In this study we analyse short term climatic data for assessing drought dynamics in semi-arid areas in southern Africa. Specifically the study areas comprises southern Mozambique, southern Zimbabwe and northern South Africa.

We used the climatic data from the European Centre for Medium-Range Weather Forecasts (ECMWF). Such data prompted us to analyse the temporal and spatial dynamics of total precipitation between October of 1989 and September of 2014 throughout the region. The present study, sought to use free data to analyse the desertification issue in southern Africa. Hence, showing that countries that have few resources can replicate and furthering the analysis without the issue of financial constraints for obtaining data.

In this study we have used data on daily total precipitation to compute the number of days per year with precipitation below 1mm (RL1), then we analyse the dynamics of spatial dispersion of drought in both static component and dynamic component. The static component was attained through computing the averages values of RL1 over time and the dynamic component was acquired from the variances of RL1 on moving windows over time.

Our findings suggested high levels of consistency with previous analysis about the relationship between the spatial dynamic of drought and spatial variability of semi-arid areas over the region. Although, the static component indicated stable dry areas conditions, the dynamic component allowed us to follow fluctuations of drought variability patterns.

Both the static and dynamic component will be used to investigate the Sustainability of Desertification in the study area.

9637-42, Session 8

Inter-annual response of the rainfall-runoff relationship to wildfire in a Mediterranean forested watershed

Noa Ohana-Levi, Ben-Gurion Univ. of the Negev (Israel); Amir Givati, Water Authority (Israel); Arnon Karnieli, Ben-Gurion Univ. of the Negev (Israel)

Wildfire is an environmental disturbance occurring due to climatic and/or natural causes or anthropogenic effects. It can result in land cover changes (LCCs) followed by altered hydrologic responses to a specific precipitation regime. Quantifying and simulating the effects of these LCCs, was done by using the new Weather Research & Forecasting–Israel Hydrological Service (WRF-IHS) model.

An exceptional wildfire event occurred on Mount Carmel, Israel, between Dec. 2-6, 2010. Two years after this event, the winter was characterized by an above normal precipitation levels, causing unusually high discharge levels. This study focuses on the effects that the wildfire event had on the runoff regime in the Oren Watershed, located in the Carmel Forest, Israel. Three land cover (LC) maps were generated by classifying satellite images that were acquired by the Advanced Spaceborne Thermal Emission and Reflection Radiometer (ASTER) sensor. The images represented pre-fire status, immediate post-fire, and recovery. The WRF-simulated and measured rainfall were analyzed and compared. These rainfall outputs were used as inputs for the WRF-IHS model and two rainfall events were chosen for calibration. The WRF-IHS model simulations were conducted for three selected rainfall events with the three LC maps.

The results show a 25% reduction of forest cover between pre-fire and immediate post-fire images. The measures of both peak discharge and runoff volume showed a large increase (between 24 and 63%). For the recovery status simulations, most results showed a minor increase in the peak discharge and runoff volume (between 1 and 10%). Wildfires are a special and exceptional case of LCC, since they are usually the result of climate conditions, sometimes in addition to human disturbance and their effects on the watershed landscape are unplanned and immediate. Moreover, the findings show that higher amounts of rainfall will result in stronger impacts of the LC alterations caused by wildfire.

9637-43, Session 8

Analysis of water supply and demand in the Ghataprabha River basin

Rajat K. Panda, Nagarajan Ramakrishna, Indian Institute of Technology Bombay (India)

The water availability and demand assessment is carried out in the Ghataprabha river basin of Peninsular India. The area of the basin is 8578 km2. The basin is sub divided into 58 sub basins. The water availability is done with the help of Soil and Water Assessment Tool (SWAT). The various inputs like Land use/ Land cover (LANDSAT, 2000), precipitation, temperature, wind speed of data duration 1995-2009 is supplied to the model. The first two years are taken for the model warm up. 1997-2005 are considered for the calibration. Validation is done for the rest of the year i.e 2006-2009. The location of different dams and tanks and their capacity information is supplied to the model. Based on this information the model generates the runoff for different outlets. This runoff is compared with the collected runoff from the field for three sub basins. The model evaluation criteria are assessed with the recommend statistics. The result shows that the statistics are coming under the region of very good to satisfactory range. The basin comprising the LANDSAT imagery covers with multi-dates imagery available. The image normalization is done to rectify the radiometric errors present in the scenes. The different bands are stacked together to form the FCC of the study area. Two scenes are mosaicked together to get the whole stretch of the Ghataprabha basin. The land use/ Land cover classification is done using the Maximum likelihood classifier technique. The accuracy assessment is carried out using Kappa coefficient and error matrix which are beyond 0.70 and 0.80. The water demand is calculated for individual revenue villages within each sub basin, similarly the crop water requirement is calculated on sub-basin scale. The number of industries and their water use is calculated for each sub basin. Overall the water availability and demand assessment is carried out on each outlet. The result shows that the basin number 2, 6, 7, 17, 48, 54 have water deficit. Similarly the status is calculated for the drought year of 2003.

9637-44, Session 8

A multilevel and multiscale soil moisture and temperature regular monitoring network aim at multisatellite remote sensing application in Tibet Plateau

Lixin Dong, National Satellite Meteorological Ctr. (China)

The unique interactions among land surface, boundary layer, troposphere, and stratosphere over the Tibetan Plateau (TP) directly impact regional weather progress, global climate changes and its surrounding environment at a variety of spatiotemporal scales. Remote sensing, climate modeling and numerical weather prediction are expected to provide land surface hydro-meteorological data needed for these process studies. But the complex topography, poor environment and lack of observational data are the main restrict factors for the further science research on the TP. Satellite remote sensing is one of the important means of obtaining the observation data, but also due to the lack of observation data which match the pixels size of satellite data, the inversion accuracy of satellite remote sensing products in TP region is lack of an effective verification. Hence, the in situ observations are required to support their calibration and validation.

For this purpose, a multi-level and multi-scale soil moisture and temperature regular monitoring network was established on the central TP to support multiple satellite remote sensing application, climate modeling or assimilation, and land surface process studies. The regular monitoring network mainly measure two state variables (soil moisture and temperature) at four spatial scales (1, 5, 15, and 25 Kilometer) and five soil depths (2, 5, 10, 20, and 30 cm). And it include two levels (about 2 ? 2 pixels), so it could expand eight spatial scales (1, 2, 5, 10, 15, 30, 25, and 50 Kilometer). Meantime, the 1 and 5 Kilometer scale could match the pixel size of polar orbit satellite and geostationary satellite, respectively. The 1 and 2 Kilometer scale could match the pixel size (about 3 Km) of active microwave or radar satellite. The other scale could match the different pixel size of passive microwave products (L1, L2 and L3). The experimental area lie in the Qiangtang grassland of northern Tibet area, which is characterized by high altitude, flat terrain, homogeneous grassland types, high vegetation biomass, gentle soil moisture dynamic range, and typical freeze-thaw cycle. The network consists of 33 stations node with their elevation varying over 4400-4600 m. In addition, many auxiliary parameters of this network, such as the infrared radiation temperature, emissivity, soil texture, soil dielectric constant, air temperature, wind direction and speed, precipitation, snow, vegetation coverage and vegetation type etc. were measured at each station node of the regular sample area to support further studies. These parameters will help to analysis the change of multi-scale soil moisture and temperature in Tibetan Plateau. It is worth noting that different parameters will match different scales. For example, infrared radiation temperature is only measured in 1 and 5 Km scales to match the pixel size of polar orbit satellite and geostationary satellite, respectively.

In order to guarantee continuous and high-quality data, tremendous efforts have been made to protect the data logger. Firstly, the data logger is protected from rain erosion with an instrument protecting box installed on a steel bracket which high 1.5 meters. Secondly, the reinforced protective fence was established around 1.5 – 2 meters area in order to prevent external damage. Then, the soil moisture sensors were calibrated with traditional weighing method. And all of the data were transmitted by a wireless transmission system and the point measurements could be upscale the different satellite pixel scales. This research can provide reference for the quality assessment of remote sensing product and satellite data assimilation results in the TP area.

In this paper, a multi-level and multi-scale soil moisture and temperature regular monitoring network aim at multi-satellite remote sensing application in TP were detailed and the observation data with quality control were used to the verification for multiple satellite retrieval products (FY3, AMSR2 and SMOS) and assimilation results (ERA, NCEP reanalysis data). This study will contribute to the understanding of the quality of products in TP area and lays the foundation for the business application.

9637-45, Session 8

Monitoring irrigation volumes using high-resolution NDVI image time series: calibration and validation in the Kairouan plain (Tunisia)

Sameh Saadi, Institut National Agronomique de Tunis (Tunisia); Vincent Simonneaux, Gilles Boulet, Bernard Mougenot, Ctr. d'Etudes Spatiales de la Biosphère (France); Zohra Lili Chabaane, Univ. of Carthage (Tunisia) and Institut National Agronomique de Tunis (Tunisia)

In arid and semi-arid regions, water availability is a major limitation for agricultural development, hence efficient agricultural water management is a major issue, especially in irrigated areas. The design of tools that provide regional estimates of water balance may help the sustainable development of these areas. Remote sensing has long been used for computing evapotranspiration estimates, which is an input for crop water balance monitoring. Up to now, only medium and low resolution data (e.g. MODIS) are available on regular basis to monitor cultivated areas. However, the increasing availability of high resolution high repetitively VIS-NIR remote sensing, like the forthcoming Sentinel-2 mission to be launched in 2015, offers unprecedented opportunity to improve this monitoring.

In this study, regional evapotranspiration and crop water

consumption were estimated over an irrigated area located in the Kairouan plain (central Tunisia) using the FAO-56 dual crop coefficient water balance model combined with NDVI image time series providing estimates of the actual basal crop coefficient (Kcb) and vegetation fraction cover using the SAMIR software (Satellite Monitoring of Irrigation). The main purpose of the study was to assess the operationality and accuracy of the method at plot and perimeter scales, regarding especially the possibility of correct parameterization in a context of high land cover complexity (i.e. trees, winter cereals, summer vegetables).

Meteorological ground stations were used to compute the reference evapotranspiration and get the rainfall depths. Three time of high-resolution SPOT5 images have been acquired for the 2008-2009, 2011-2012 and 2012-2013 hydrological years (resp. nine, six and fourteen images). We also benefited from 14 SPOT4 images acquired in the frame of the SPOT4-Take5 experiment ansd delivered in top of canopy reflectance. The SPOT5 images were radiometrically corrected, first, using the SMAC6s Algorithm, then improved using invariant objects located on the scene. From these time series, a Normalized Difference Vegetation Index (NDVI) profile was generated for each pixel.

SAMIR was first calibrated based on ground measurements of evapotranspiration achieved using eddy-correlation devices installed on irrigated wheat and barley plots. For other crops for which no calibration data was available, parameters were taken from bibliography. Then, the model was run to spatialize irrigation over the whole area and a validation was done using cumulated seasonal water volumes obtained from ground survey for three irrigated perimeters. Although simulated irrigations are still to be improved at monthly scale and seasonal scale, the overall error for the whoe data sate was only 5%, showing little bias in the method.

In a subsequent step, we used medium resolution MODIS 16 days NDVI synthesis time series to compute 12 years of water consumption over the Kairouan plain. However, as medium resolution pixels are mixed regarding land cover, and as many SAMIR parameters are crop specific, we had to determine “equivalent parameters” in order to run SAMIR, which was achieved by calibrating the MODIS approach based on the previous high resolution data.

9637-46, Session 8

Assessment of drought in savannah region of Nigeria using geospatial techniques

Olusola Gbolahun Odunayo, Univ. of Lagos (Nigeria); Oluwatola Adedeji, Obafemi Awolowo Univ. (Nigeria); Linda Abegunde, NCRS (Nigeria)

Due to climate change and variability, drought has become a recurrent phenomenon in several countries across the globe most especially in the sub-Saharan Africa. Drought is a random, low profile natural disaster that evolves slowly which requires consistent and effective monitoring, and assessment. Frequent and severe drought has become one of the most important natural disasters in sub-Saharan Africa.

The primary goal of this study is to utilize AVHRR time series satellite data (1981-2000) and MODIES imagery (2001-2012) to develop a reporting system for the assessment and monitoring of historical drought development in Savannah region of Nigeria using the Vegetation condition Index (VCI) approach. The research also uses meteorological weather parameter rainfall data to establish a correlation relationship with vegetation health (NDVI). The study emphasize on the use of Geographic Information System and Remote sensing technology.

This research shows that there is a correlation relation of r2=0.6 between rainfall and vegetation health (NDVI). There was drought in Savannah region of Nigeria all through the period of study and about 11.93% were highly severe, 40.81% low severe, and 47.79% very low severe of the total area. Drought has been more persistent in the Sudan savannah. The drought had a wider spread in 2007 affecting all the savannah ecological zones in Savannah region. Overall drought had increased from 55.38% in 1982 through 1992, to 75.52% in the last decadal study which is between the years 2002 to 2012. The spatial distribution of drought had spread across the entire savannah.

Considering the spread and frequency of droughts in Nigeria, drought monitoring using remote sensing techniques could play an invaluable role for food security and drought preparedness.

9637-47, Session 9

Carbon cycle and ecosystem priorities for the next decade: outcomes of a workshop on earth science remote sensing needs

Scott Goetz, Woods Hole Research Ctr. (United States); Forrest G. Hall, NASA Goddard Space Flight Ctr. (United States)

Objectives:

The objectives of the TECLUB workshop were to: (1) engage the relevant Terrestrial Ecosystem, Carbon Cycle, Land cover/Land use Change and Biodiversity science communities to describe and prioritize measurements required to support research objectives of these communities, (2) identify notional technical approaches and analysis frameworks to acquire the needed measurements, and (3) produce a white paper useful for science practitioners and science policy communities, including the 2015 Decadal Survey panel(s), articulating the outcomes of the TECLUB deliberations.

Rationale:

The workshop objectives support those articulated in the 2010 NASA Earth science plan, “How is the Earth changing and what are the consequences for life on Earth?” NASA seeks to characterize, understand and predict the current and future state of global Earth systems by addressing three critical science questions; (1) How is the global Earth system changing? (2) What are the sources of change in the Earth system and their magnitudes and trends? (3) How will the Earth system change in the future?

Approach:

A two and one-half day workshop was held at the Goddard Space Flight Center beginning 28 October 2014, bringing together over 50 scientists. Three discipline teams and one measurement team were formed from the research community; a carbon cycle (CC) team, a Terrestrial Ecology /Biodiversity (TEBD) team, a Land cover/Land use Change (LCLUC) team, and a measurements (MMT) team. The MMT team was initially integrated with the three discipline teams, with the intent of addressing the nominal measurement requirements specified by the discipline teams. Discipline team breakout sessions were conducted, ensuring the teams sequentially addressed: (1) the most important societal issues, (2) science questions, (3) analysis frameworks and (4) measurement needs. Then the measurement team integrated and summarized the requirements from the discipline teams. This approach ensured measurement needs were linked in a traceable way to societal issues. Finally, the teams worked together post-workshop to prioritize the integrated measurement needs across disciplines, and completed the draft report.

Outcomes:

The TECLUB discipline groups developed a consensus vision for the next decade that considered not only global and regional measurement needs, but also the analysis framework research needed to translate those measurements into the answers and information required to address a broad array of societal issues and science questions. To address the compelling questions, the science community must better understand and quantify the state and dynamics of terrestrial ecosystems. The conclusions of this community’s workshop deliberations were that to meet this challenge, it will need (1) continuity in the current global observational data and

capabilities already in place, (2) improved temporal frequency and spatial resolution of those observations and (3) new kinds of observations now available using remote sensing technologies and approaches developed in the last decade. These broad categories of observations, identified by the discipline groups are needed to address key relevant science questions they identified. The measurement requirements identified will require both the continuation of existing remote sensing assets, as well as new measurements that can only be acquired using new technologies developed in the last decade.

9637-48, Session 9

Monitoring carbon stocks and change in Miombo woodlands using remotely-sensed reflected and emitted energy

Harun A. Makandi, Univ. of Dar Es Salaam (Tanzania, United Republic of)

Miombo woodlands have extractive, aesthetic, and ecosystem support values. Large scale, accurate, and repetitive estimation of carbon stocks in the woodlands adds green and existential values to their multi-layered value landscape. A combination of accurate base data and remote sensing with optical multispectral imagery makes such rigorous estimation possible. The imagery is available in multiple platforms, is freely available, and has a broad spatio-temporal coverage.

This study estimates above-ground biomass (AGB) in miombo woodlands, southern Tanzania by interpreting dominant surface-atmospheric processes. These correlate with AGB variability. They are latent heat flux, aerodynamic resistance, and thermal inertia. The greater their magnitude, the larger the AGB and carbon carbon per unit area in wet, transitional, and dry seasons respectively. By studying the processes as surrogates of AGB and forest carbon, we resolve problems of saturation of vegetation indices (VIs) from image reflectances and inability of VIs to measure biomass in leafless woodlands need solutions. This increases the potential of repetitively acquired datasets to fill for phenomena obscured by cloud contamination, and cross-platform application with LiDAR and radar remote sensing.

We derive the mentioned processes by combining the product and correlation of soil-adjusted vegetation indices and surface temperature from Landsat imagery. The processes are interpreted in land units aggregated using spatial filtering. We regress the resulting maps with known carbon stocks per ha. The known stocks are calculated from sampled DBH values in the forest and woodland patches in Liwale using miombo-specific allometric models.

Visual comparison of the derived process maps, Landsat composites, and NDVI maps with the known AGB quantities show processes correlate significantly with AGB than reflectances in the Landsat and NDVI. In particular, some areas with highest AGB/ha do not show at all in NDVI maps of the driest months from July to December, when most trees shed their leaves. During this time, the mapped thermal inertia of the collective tree trunks in the woodlands correlates with AGB. In the following stages of the study, process maps and known carbon/ha shall be regressed to register map prediction values to be presented in scatterplots. Then seasonal and change analyses shall also be done to assess the spatio-temporal dynamics of AGB and forest carbon stocks in the study area.

By focusing on processes rather than vegetation indices or thermal bands only, the saturation problem of reflectances in dense miombo woodlands is resolved. Thermal inertia in dry woodlands resolves the inability of VIs to detect biomass during dry season. This method greatly increases the potential usage of freely-available multispectral imagery for sustainable AGB and carbon stocks quantification in developing countries. Combined with finer scale field estimation and LiDAR, multispectral imagery contributes understanding spatio-temporal patterns of carbon landscape at multiple scales.

9637-49, Session 9

The variation of crop phenology in North China from 1982 to 2011: impacts on crop productivity

Xin Du, Institute of Remote Sensing and Digital Earth (China)

Over the next few decades, due to growing population and the use of agricultural products as biofuels, the world's farmers will face increasing pressure to grow more food on less land. Therefore, the increased demand for food supply worldwide calls for improved accuracy of crop productivity estimation. Agriculture plays an important role in China. China is one of the largest agricultural producers of wheat, rice, maize and soybean in the world. Thus it is significant to study the variations and drivers of crop productivity in China.

In this study, crop phenology (the start of the growing season (SOS) and the end of the season (EOS)) was detected using time-series satellite data, and the trend of crop phenology and historical change of crop productivity were studied from 1982 to 2011. Our objective was to show whether there were significant time trends in changes of crop phenology across North China, and whether these changes have had significant impacts on the crop productivity.

A crop phenology detection method based on a combination of the Whittaker smoothing and the logistic model was used to derive the start of the growing season (SOS) and the end of the season (EOS). The purpose of the Whittaker smoothing was used to remove noise produced by effects of atmospheric conditions and view-illuminations. The logistic function of time was used to fit each period's vegetation indices, either increase or decrease. The time of SOS in each crop season is defined as the local maximum value of the second derivative of increased fitted curve, and EOS is defined as the local maximum value of the second derivative of declined curve.

The vegetation indices derived from the visible and near infrared wavelength of canopy reflectance, such as normalize difference vegetation index (NDVI) and wide dynamic range vegetation index (WDRVI), can obtain a priory crop productivity. In this study, a year of crop productivity was considered as the mean of NDVI between SOS and EOS. For analysis the trend changes of crop productivity, the Mann-Kendall method, a non-parameters approach, was employed in this study. A linear regression analysis performed between crop phonological metric and crop productivity is examined to show how crop phonological metrics influence on the variation of crop productivity.

9637-50, Session 9

GLORI: a new airborne GNSS reflectometry instrument for land surface monitoring

Erwan Motte, Pascal Fanise, Mehrez Zribi, Ctr. d'Etudes Spatiales de la Biosphère (France)

GLORI (GLObal navigation satellite system Reflectometry Instrument) is a new receiver dedicated to the airborne measurement of surface parameters such as soil moisture and biomass above ground, as well as sea state(wave height and direction) above oceans. The instrument is based on the PARIS concept [1] using both the direct and surface-reflected L-band signals from the GPS constellation as a multistatic radar source.

The receiver is based on one up-looking and one down-looking dual polarization hemispherical active antennas feeding 1) a low-cost 4-channel Software Defined Radio direct down-conversion receiver tuned to the GPS L1 frequency and 2) a direct sampling 4 GSPS digitizing board. The reflected channels can be cross calibrated using a transfer switch. a commercial precision timing GPS Unit records raw data such as estimated doppler and code phase, satellites azimuth and elevation. Figure 1 is showing a block diagram of the instrument.

The raw measurements are sampled at 16.368MHz and stored as 2-bit, IQ binary data. In post-processing, GPS acquisition and tracking are performed on the direct up-looking signal while the down-looking signal is processed blindly using tracking parameters from the direct signal. The obtained direct and reflected code-correlation waveforms are the basic observables. The geophysical parameters inversion is to be performed using processing methods from the literature based on the coherence time, correlation power and polarization ratios of the waveforms [2].

The instrument was designed to be installed aboard the ATR42 experimental aircraft from the French SAFIRE fleet (www.safire.fr) as a permanent payload. The long term goal of the project is to provide real-time continuous surface information for every flight performed. The aircraft Inertial Measurement Unit records position and attitude information.

Four test flights were performed over the Toulouse Francazal Airport as well as a flight over the Gulf of Lion (Mediterranean Sea) region during the period 17-21 Nov 2014 (Figure 2). These flights were performed together with the KuROS radar payload [3]. Preliminary results demonstrate the instrument sensitivity to both ground and ocean surface parameters estimation.

A dedicated scientific flight campaign is planned at the end of second quarter 2015 over the Landes area (south west of France) with collocated measurement of biomass, soil moisture and roughness ground truth in order to better characterize the instrument sensitivity to these geophysical parameters.

References

[1] M.Martin-Neira. A Passive reflectometry and interferometry system (PARIS): Application to ocean altimetry. ESA J., 17:331-355, 1993

[2] Egido et Al., “Airborne GNSS-R Polarimetric Measurements for Soil Moisture and Above-Ground Biomass Estimation,” Selected Topics in Applied Earth Observations and Remote Sensing, IEEE Journal of , vol.7, no.5, pp.1522,1532, May 2014

[3] Hauser et Al. “KuROS: A new airborne Ku-band Doppler radar for observation of the ocean surface,” Geoscience and Remote Sensing Symposium (IGARSS), 2014 IEEE International, vol., no., pp.282,285, 13-18 July 2014

9637-51, Session 9

Assessment of seasonal trends in the derived guinea savannah zone of Nigeria using AVHRR NDVI3g time series for the period of 1983-2011: a regional case study of Kwara State

Babatunde A. Osunmadewa, Christine Wessollek, Pierre Karrasch, Elmar Csaplovics, Technische Univ. Dresden (Germany)

Analysis of seasonal change in vegetation dynamics is becoming increasingly important in order to examine trends in vegetation phenological pattern over a long period. Due to human perturbation and inherent climate variability, the vegetation phenological phenomena in the derived guinea savannah region of Nigeria had undergone transition over the last decades leading to shift in vegetation characteristics such as emergence and senescence (timing and progression) of plant development. In order to objectively examine trends in vegetation dynamic over the study area (Kwara state, Nigeria), the newest bi-monthly normalized-difference vegetation index (NDVI 3g) time series from Advanced Very High Resolution Radiometer (AVHRR) from 1983-2011 was used for this study. Seasonal variation in vegetation greenness were examined over the whole study area while variation in NDVI pattern were observed for selected locations in order to further understand the inter-annual changes in vegetation dynamics. Seasonal Trend Analysis technique was used in this study to examine the overall greenness, peak of annual greenness and timing of annual greenness in the seasonal NDVI cycle using four approach. The first approach of noise removal which is one of the challenges in time series analysis was done using the inverse T-mode principal component analysis (PCA) in IDRISI Terrset, the second approach of seasonal trend analysis uses harmonic regression for the extraction of both amplitude and phase (overall greenness and timing of peak of greenness) from the annual NDVI cycle, this involve the use of a robust non-parametric trend estimator (Theil-Sen median slope) which is not affected by outliers to determine the slopes for each of the yearly greenness parameter. This is done by calculating the rate of change in slopes between all pair wise combination and then assessing the median over time. The significance test for the NDVI time series which is the third approach in this study was done using the contextual mann-kendall (CMK) test to examine trend significance in the greenness parameter for the whole study area. This CMK test was necessary in order to remove serial auto correlation which might affect the results of the analysis. The result of this approach are significant images of p-value and z-significance which shows trend significance for the greenness parameter (p-value < 0.05). An interactive approach which is the last stage was used to further examine changes in NDVI greenness parameters over the 29 years because of the difficulties in interpreting the produced amplitude and phase maps. Temporal profiles showing intra-annual variability for the monthly median of the first and last period of the NDVI data set were analyzed for locations chosen across different land cover types. An overall peak of annual greenness in NDVI trend over the 29 years examined was verified by the results of this study. The result of the non-parametric trend test (Theil–Sen slope) showed consistent increase in NDVI trend (greenness) over time. Results of the seasonal NDVI curve also shows variation in timing of vegetation greenness which is an indication of transformation of land cover types for various activities or climatic variability.

9637-52, Session 10

Application of a regularized model inversion system (REGFLEC) to multi-temporal RapidEye imagery for retrieving vegetation characteristics *(Invited Paper)*

Rasmus M. Houborg, Matthew F. McCabe, King Abdullah Univ. of Science and Technology (Saudi Arabia)

Accurate retrieval of canopy biophysical and leaf biochemical constituents from space observations is critical to diagnosing the functioning and condition of vegetation canopies across spatio-temporal scales. Retrieved vegetation characteristics may serve as important inputs to precision farming applications and as constraints in spatially and temporally distributed model simulations of water and carbon exchange processes. However significant challenges remain in the translation of the remote sensing signals into useful biochemical, physiological or structural quantities and treatment of confounding factors in spectrum-trait relations. The utility of a REGularized canopy reFLECtance model (REGFLEC) inversion system for joint leaf chlorophyll (Chl) and leaf area index (LAI) retrieval from Landsat data was recently demonstrated (Houborg et al., 2015, Remote Sensing of Environment, 159, 203-221). REGFLEC represents a fully integrated system of radiative transfer models that can be applied over a diversity of land cover types, soil backgrounds and atmospheric conditions based on image-based methodologies, thereby removing the need for site-specific calibration. REGFLEC implements novel spatio-temporal constraints and ancillary information within a multi-step look-up table inversion approach in an attempt to mitigate the ill-posed inverse problem and properly discriminate contributions from the atmosphere, canopy and soil.

In this contribution, REGFLEC is extended to sensor systems with bands in the red-edge region for the first time, in order to capitalize on the improved sensitivity of red-edge bands over the full range of chlorophyll values and the reduced sensitivity to confounding factors. Application to time-series of 30m resolution hyperspectral (i.e. Hyperion) and 5m resolution multi-spectral (RapidEye) data streams is demonstrated over an irrigated agricultural region in central Saudi Arabia. The study identifies optimal sensor-specific

spectral band combinations and assesses improvements in LAI and Chl retrieval from utilizing the enhanced (compared to Landsat-like observations) radiometric information content within the framework of REGFLEC. Model performances are evaluated using in-situ measurements of LAI and Chl in fields of alfalfa, rhodes grass, carrot and maize. The development of observationally based vegetation retrieval capacities, effectively constrained by the enhanced information content afforded by bands in the red-edge, is a needed investment towards optimizing the benefit of upcoming satellite systems such as soon-to-be launched Sentinel-2, which will be delivering super-spectral data at resolutions down to 10m on a routine (5 – 10 day) basis.

9637-53, Session 10

Modelling canopy radiation budget through multiple scattering approximation: A case study of coniferous forest in Mexico City Valley

Jose L. Silvan Cardenas, Ctr. de Investigacion en Geografia y Geomatica “Ing. Jorge L. Tamayo” A. C. (Mexico); Nirani Corona-Romero, Ctr. de Investigacion en Geografia y Geomatica “Ing. Jorge L. Tamayo” A. C. (Mexico) and CENTROGEO (Mexico)

Hyperspectral remote sensing has been shown to be useful for several natural resources applications, including species identification, plant stress detection, plant biochemistry analysis, biophysical forest parameters estimation, carbon storage quantification, and so forth. Yet the analysis of such datasets has proven to be very difficult due to several noise sources such as water vapor and aerosols in the atmosphere. In particular, monitoring coniferous forests with these technology represents an additional challenge due to the complex structure of vegetation so that knowledge from spectral measurements in the ground cannot be linearly scaled up to understand the spectral characteristics of a forest canopy as recorded in remote sensing data (Dalponte, et al., 2013; Gong, et al., 1997). One successful approach to scale up the optical properties at canopy level is the theory of spectral invariants, which has enabled a simple parametrization of the radiation budged of broadleaved and coniferous canopies with great accuracy (Smolander & Stenberg, 2005). This spectral invariant theory, also called p-theory, has been extensively used for modeling canopy scattering in coniferous forest (Huang, et al., 2007; Luke?, et al., 2011; Knyazhikin, et al., 2011; Lewis, 2007).

In this article, we describe a method to relate airborne hyperspectral measurements of coniferous forests taken from a flying helicopter with the FieldSpec 4 (ASD Inc.) to those taken in the ground with the same instrument for vegetation and understory components, including leaf, bark, soil and grass. Hyperspectral data was recorded in the optical range from 350 to 2500 nm at 1nm spectral resolution on a coniferous forest dominated by Pinus hartweguii and Abies religiosa within a major forest reserve in the Southern Mexico City.

Measurements were analyzed through a previously developed multiple scattering approximation (MSA) model (Silván-Cárdenas & Wang, 2010), which generalizes the single-component canopy scattering model by Smolander & Stenberg (2005) based on the p-theory. This generalization allowed us to incorporate contributions from understory components, so that the canopy spectral reflectance is synthesized through a non-linear combination of pure spectral components (end-members), as well as through a set of photon recollision probabilities and interceptance fractions. Since the MSA does not prescribe a priori the end-members to incorporate in the model, a multiple end-member selection method (MESMSA) was developed and tested in this study.

Measurements were first adaptively filtered to remove oscillations caused by water vapor. Then, photon recollision probabilities and interceptance fractions were estimated by fitting the model to airborne spectral reflectance. Estimated values were then assessed using external sources including LiDAR altimetry data, a WorldView 2 image and co-located airborne video acquired during the helicopter flight. Preliminary results indicate that, unlike a previously tested linear spectral unmixing method, the MEMSA yielded estimated species cover fractions more accurately. In addition, the re-collision probabilities are being used to estimate leaf area index, but the validation of the latter product is still under development.

9637-54, Session 10

A robust sugarcane yield prediction method using time series satellite imagery

Yu Zhao, Hitachi, Ltd. (Japan)

As one of the most important agricultural derivatives, Ethanol production has been paid attention and there is increasing demand for quantity and quality incensement. Sugarcane, as one of the most mainstay crop in Brazil, plays an essential role in ethanol production. To monitor sugarcane crop growth and predict sugarcane crop yield, remote sensing technology plays an essential role and accurate and timely crop growth information is significant, in particularly for large scale farming. As the high cost and low data availability of high-resolution satellite images such as RapidEye, we focus on the time-series low resolution satellite imagery. In this research, vegetation index extracted from time-series LandSat8 satellite imagery was applied to monitor and estimate sugarcane’s yield.

We focused on the issues of sugarcane yield estimation. In conventional method, spectral features are extracted from satellite imagery while vegetation indices are calculated, and utilizing this data, Statistical regression is applied to estimate the yield. However, two key factors in this respect are still needed to be improved. Firstly, the calculation and utilization of the spectral features and vegetation indices need to be correspondence to the crop growth biological mechanism. In other word, the vegetation indices need to be able to make an interpretation of the crop growth. In the terms of matching of vegetation indices and crop growth biological model, yield would be estimated more accurate and robust. Secondly, statistical regression model need to be improved considering more other factors.

To estimate sugarcane yield more accurate and robust, we analyze the standard growth stage of sugarcane and to model the growth process, we have two key calculate process. The first is biometry analysis of sugarcane growth. Using ground data of sugarcane obtained from Brazil, we analyze sugarcane growth stage and growth characteristics in each stage. The variation of growing stalk, green leaves, dry leaves and moisture contents is analysis for our understanding of the whole internal change for sugarcane growth cycle. Secondly, NDVI time-series variation is extracted from time-series LandSat8 images and for each characteristic stages respectively, sugarcane growth model is developed based on the understanding of biometry analysis. Nevertheless, as statistical regression model, we improved mix model for the estimation using FPAR data extracted from MODIS satellite imagery.

The evaluation was performed through the sugarcane yield prediction using our proposed vegetation features in the growth stage when the whole dataset for modeling is available. We got precision of 85% which is about 20% higher than the conventional method. The validation results showed that prediction accuracy using our sugarcane growth modeling and improved mix model is satisfied and can be applied in practice of large scale sugarcane yield monitoring. The present method is able to greatly reduce data cost of monitoring especially usage of high resolution data without a big loss of accuracy, therefore is has great potential for construction of operational and dynamical monitoring solution. Another important contribution of our method is that we integrated biological model and statistical model for vegetation analysis.

9637-55, Session 10

Algorithm developing of gross primary production from its capacity and canopy conductance index using FLUX data and satellite data for global observing satellite data

Kanako Muramatsu, Nara Women's Univ. (Japan); Shinobu Furumi, Nara Saho College (Japan); Motomasa Daigo, Doshisha Univ. (Japan)

An algorithm for estimating gross primary production (GPP) from it's capacity and canopy conductance index for global observing satellite GCOM-C1/SGLI project is presented. The GCOM-C1 satellite will be launched by Japan Aerospace Exploration Agency in 2016 of the Japanese fiscal year. For land area observing, SGLI has six bands from visible to near infrared with 250m spatial?resolution. The characteristics of this GPP estimation method correspond to the photosynthesis process. The photosynthesis velocity depends on it's capacity and depression because of weather conditions. The capacity part depends on one of plant physiological parameters of chlorophyll contents of a leaf. In the previous study (J. Thanyapraneedkul et al., 2013), the framework of estimation method was developed how to determine the two parameters, initial slope and maximum of GPP capacity in the light saturation, of light-response curves of GPP capacity using FLUX data and satellite data. The initial slope was used as fixed values for each plant functional types. The maximum of GPP capacity at the light saturation was determined from the linear relationship between GPP capacity at 2000 (umol/m2/s) and Chlorophyll index (CIgreen) using green band developed by Gitelson et al. (1996). The relationship determined for nine plant functional types (J. Thanyapraneedkul et al., 2013, and Y. Mineshita et al., 2013) of needleleaf deciduous trees, broadleaf deciduous trees, needleleaf evergreen trees, C3 grass, crops, open shrubs, closed shrubs, mixed forest, and tropical rain forest were determined. The photosynthesis velocity's depression is controlled by the stomatal opening and closing. It is well known, that stomatal conductance of a leaf changes during a day, and it is the maximum during the morning and then it is lowered in the afternoon. In previous study, we focused on the daily changes of stomatal conductance of a leaf, and calculated the stomatal conductance daily changes using Baldocchi's model (1994) and studied the method to estimate stomatal conductance using thermal image and weather data, and lookup table. The result shows that the daily change pattern was estimated, but the absolute value of stomatal conductance had a pedestal.

In this study, we used FLUX data of open shrub (US-Ses) and MODIS reflectance data sets for developing algorithm for a canopy. Firstly, we studied how different in the daily changes between GPP capacity estimated from CIgreen and photosynthesis active radiation (PAR) using light response curves, and GPP observed by FLUX experiment. Then we estimated canopy conductance using FLUX data as a concept of big-leaf model of the Penman-Monteith equation (Monteith et al., 1973). We tried to estimate GPP as GPP capacity multiplied by the normalized canopy conductance, which is the value divided the value at the satellite observing time of 10:30. The results shows estimated daily change of GPP showed almost same as observed GPP. From this result, we defined canopy conductance index as the normalized canopy conductance by the value of satellite observing time at 10:30. The scaling up method and data availability for global observing satellite project were discussed.

9637-56, Session 11

Interpreting snowpack radiometry using currently existing microwave radiative transfer models

Do Hyuk Kang, NASA Goddard Space Flight Ctr. (United States); Shurun Tang, University of Michigan, Ann Arbor (United States); Edward J. Kim, NASA Goddard Space Flight Ctr. (United States)

The radiative transfer (RT) model to calculate a snow brightness temperature (Tb) is a critical part to retrieve terrestrial snow using remote sensing. RT model simulates the Tb based on a layered surface snow by utilizing a set of microwave radiative transfer formulas. However, even with the same snow inputs provided, the currently existing RT models such as Microwave Emission Model of Layered Snowpacks (MEMLS), Dense Media Radiative Transfer (DMRT-Tsang), and Helsinki University of Technology (HUT) models produce different Tb responses. To backwardly invert snow physical properties, the standard response from the various RT models needs to be established, or at least, the differences are to be quantitatively explained. To this end, the study evaluates the sources of perturbations in the RT models. Investigations are conducted by providing the same but gradual changes in snow inputs to 3 different RT models, by changing snow grain sizes, and densifications. For future applications to the remote sensing, frequencies used here are equivalent to the Advanced Microwave Scanning Radiometer-E (AMSR-E) at 6.9, 10.7, 18.7, 23.8, 36.5, and 89.0 GHz.

After applying an increasing snow grain sizes from 0 to 3 mm, it is found that HUT shows a fast asymptotic decrease of the Tb, while MEMLS and DMRT-Tsang follow the gradual decrease of Tb only with higher frequencies such as 36.5 and 89 GHz. DMRT-Tsang uniquely shows a Tb increase at the end at 89 GHz. In the case of snow density ranging from 50.0 to 600.0 km/m3, MEMLS and DMRT-Tsang show the constant Tb in the low frequencies until 23.8 GHz. But, HUT has convex Tb responses until 36.5 GHz. However, all the 3 models have Tb increases at 89 GHz. This paper focuses on scattering coefficient calculations to explain the role of the snow grain size. And, the density effects are evaluated by the real part of permittivity and Fresnel coefficient calculations of 3 various RT models.

Furthermore, the RT models are simultaneously shared and driven by the same snow physics model with the meteorological forcing datasets from the CLPX 2002-2003, and NoSReX 2009-2010. To describe special features of snow hydrological processes such as layer densification and snowmelt, the radiometric variables are traced by all the RT models. This study introduces a possible development of the depository of the subroutines to ultimately determine the Tb, which can allow a next generation of the retrieval algorithms of the terrestrial snow physical properties using the passive microwave remote sensing.

9637-57, Session 11

Country-wide analysis of TRMM data in monitoring rainfall during two consecutive years of anomalous floods in Pakistan

Shamsa Kanwal, The Hong Kong Polytechnic Univ. (Hong Kong, China); Bilal A. Munir, National Univ. of Sciences and Technology (Pakistan)

Uninterrupted availability of Tropical Rainfall Measuring Mission (TRMM) precipitation measurements at no cost is a very cost effective mean of rainfall and flood analysis. The intent of this study is to explore the country wide spatial and temporal distribution of the monsoon seasons in Pakistan in the two consecutive years of anomalous flood i.e. 2010 and 2011, using TRMM satellite based rainfall estimation. For this purpose, rainfall data from the TRMM product 3B42 version 7 with a spatial resolution of 0.25° x 0.25°, rainfall from countrywide 24 gauge stations for the monsoon season of the same period of study and elevation data was used. The two sources of data acquisition were compared to check the correlation among the datasets. Rain rates from 2010 were compared with those from 2011. These consecutive years were among the most susceptible in terms of flood disaster in Pakistan. The source

areas of flood in terms of high rain rates and elevation were identified. Spatial trend of rainfall was incorporated in terms of altitude difference of the areas in Pakistan. In 2010, there was an increase in the intensity of rainfall at slightly higher elevations than normal, which is due to the increase of moisture content in the atmosphere. Otherwise, it precipitated largely along the Himalayan foothills in the northeastern region of Pakistan. The temporal shift of intense precipitation during each week for July and August in 2010 and 2011 were analyzed. Results shows that intense rainfall occurred during last week of July and first two weeks of August. Overall monsoon rainfall for the entire country is higher for 2010 than 2011, and the total area in Pakistan receiving monsoon rain is much larger. While in 2011 it hit the Southern Punjab, Sindh and lower regions of the country. Through the evaluation of TRMM 3B42 V7 rain rate data with elevation data, a few key features stood out 1) the temporal pattern exhibited by the arrival of the monsoon seasons, 2) the largest average rain rate intensities, occur in Northern mountainous region in 2010 while in 2011, southern areas of Pakistan were more affected. As a result of this finding, it can be concluded that most of the precipitation which occurred during 2010 is a result of severe storms with deep convective cores.

9637-58, Session 11

Extracting fields snow coverage information with HJ-1A/B satellites data

Wenquan Dong, Jihua Meng, Institute of Remote Sensing and Digital Earth (China)

The distribution and change of the snow coverage are sensitive factors of climate change. In the northeast part of China, farmlands are still covered with snow in spring. Since sowing activity can only be done when the snow is melting, fields snow coverage monitoring provides reference for the determination of sowing date. Because of the restriction of the sensors and application requirements, current researches on remote sensing of snow focus more on the study of mesoscale and large scale, rather than the study of small watershed scale, and especially research on snow melting period is rarely reported.HJ-1A and HJ-1B satellites are parts of little satellite constellation, focusing on environment and disaster monitoring and meteorological forecast. Compared to other data sources, HJ-1A and HJ-1B satellites both have comparatively higher temporal and spatial resolution and are more conducive to monitor the variations of melting snow coverage at small watershed. This paper is based on HJ-1A/1B data, taking Hongxing farm of Bei'an?Heilongjiang Province?China as the study area. In this paper, we exploited the methods for extraction of snow cover information on farmland in two cases, both HJ-1A/1B CCD with HJ-1B IRS data and just HJ-1A/1B CCD data. The reason we chose the two cases is that, the two optical satellites HJ-1A and HJ-1B are capable of providing a whole territory coverage period in visible light spectrum in two days, infrared spectrum in four days. So sometimes we can only obtain CCD image. In this case, the method of normalized snow index cannot be used to extract snow coverage information. Using HJ-1A/1B CCD with HJ-1B IRS data, combined with the theory of snow remote sensing monitoring, this paper analyzed spectral response characteristics of HJ-1A/1B satellites data, then the widely used Normalized Difference Snow Index(NDSI) and S3 Index were quoted to the HJ-1A/1B satellites data. The NDSI uses reflectance values of Red and SWIR spectral bands of HJ-1B, and S3 index uses reflectance values of NIR, Red and SWIR spectral bands. With multi-temporal HJ satellite data, the optimal threshold of normalized snow index is determined to divide the farmland into snow covering area, melting snow area and non-snow area. The results are quite similar to each other and of high accuracy, and the melting snow coverage can be well extracted by two types of normalized snow index. When we can only obtain CCD image, we use supervised classification method to extract melting snow coverage. With this method, the accuracy of fields snow coverage extraction is slightly lower than that using normalized snow index methods mentioned above. And in mountain area, the snow coverage area is slightly larger than that is extracted by normalized snow index methods, because the shadows make the color of snow in the valley darker, the supervised classification method divides it into non-snow coverage area, while the normalized snow index method well weakened the effect of shadow. This study shows that extraction accuracy in both cases is assessed, and both of them can meet the needs of practical applications. HJ-1A/1B satellites are conducive to monitor the variations of melting snow coverage over farmland, and they can provide reference for the determination of sowing date.

9637-60, Session 11

Mapping of bare soil surface parameters from TerraSAR-X radar images over a semi-arid region

Azza Gorrab, Mehrez Zribi, Ctr. d'Etudes Spatiales de la Biosphère (France); Nicolas Baghdadi, Institut National de Recherche en Sciences et Technologies Pour l'Environnment et l'Agriculture (France); Zohra Lili Chabaane, Institut National Agronomique de Tunis (Tunisia) and Univ. of Carthage (Tunisia)

Surface soil moisture retrieval with meter-scale spatial resolution is appropriate for multi- domains particularly hydrology and agronomy. It allows water resources and irrigation management decisions, drought monitoring and validation of multi-hydrological water balance models. In the last years, various studies have demonstrated the large potential of radar remote sensing data, mainly from C frequency band, to retrieve soil moisture. However, the accuracy of the soil moisture estimation is affected by the influence of surface roughness parameter on backscattered radar signals. In recent years, different empirical, semi empirical and physical approaches are developed for bare soil conditions, to estimate accurately spatial soil moisture variability.

In this study, we propose an approach based on the change detection method for the retrieval of surface soil moisture at a higher spatial resolution. The proposal algorithm combines multi-temporal X-band SAR images (TerraSAR-X) with different continuous thetaprobe measurements. Seven thetaprobe stations are installed at different depths over the central semi arid region of Tunisia (9°23' - 10°17' E, 35° 1'-35°55' N). They cover approximately all the area of our study site and provide regional scale information. Ground data were collected over agricultural bare soil fields simultaneously to various TerraSAR-X data acquired during 2013-2014. More than fourteen test fields were selected for each spatial acquisition campaign, with variations in soil texture and in surface soil roughness. For each date, we considered the volumetric water content with thetaprobe instrument and gravimetric sampling; we measured also the roughness parameters with pin profilor.

To estimate soil moisture from X-band SAR data, we analyzed statistically the sensitivity between radar measurements and ground soil moisture derived from permanent thetaprobe stations. Our approaches are applied over bare soil class identified from an optical image SPOT / HRV acquired in the same period of measurements. Results have shown linear relationship for the radar signals as a function of volumetric soil moisture with high sensitivity about 0.21 dB/vol%. For estimation of change in soil moisture, we considered two options:

On the first one, we applied the change detection approach between successive radar images (Δ?°) assuming unchanged soil roughness effects. Our soil moisture retrieval algorithm was validated on the basis of comparisons between estimated and in situ soil moisture measurements over test fields. Using this option, results have shown accuracy (RMSE) of about 3.8 %. Secondly, we corrected the sensitivity of the radar backscatter images to the surface roughness variability. Results have shown a reduction of the difference between the retrieved soil moisture and ground measurements with an RMSE about 3.2%. Hence, it is essential to consider roughness effect in radar signal inversion at high resolution scale.

Conference 9638: Remote Sensing of the Ocean, Sea Ice, Coastal Waters, and Large Water Regions 2015

Wednesday 23 September 2015

Part of Proceedings of SPIE Vol. 9638 Remote Sensing of the Ocean, Sea Ice, Coastal Waters, and Large Water Regions 2015

9638-20, Session PS

Mangrove density mapping with multitemporal remote sensing data and mangrove development impact analysis seen from environmental and society aspects: case study in Sidoarjo, east Java

Akbar Cahyadhi Pratama Putra, M. Randy Aswin, Tantri Utami Widhaningtyas, Univ. Gadjah Mada (Indonesia)

Lapindo mudflow disaster in Sidoarjo, East Java requires mudflow flowed into the sea through the Brantas and Porong River. The impact of the mud is increasing the land area and the addition of the shoreline in Porong and Brantas estuary. Land that formed by the mud have been planted mangroves, that need to be mapped to know the density of mangrove due to the utilization of mud as mangrove cultivation by society and government. This research also aims to analyze the impact of the development of mangrove on the environment and the community around research sites. Remote sensing can monitor mangrove ecosystem and monitor the condition of trees on every year. The methods in this survey is using multi temporal data. The data that we used is image of Landsat 7 ETM+ with dry months of recording time in 2002, 2006, 2009, and 2014. Mangrove density can be identified using red and near infrared wavelength, uses NDVI transformation. NDVI results were used for the detection of mangrove density is the value 0 - 1. That is because the vegetation objects indexed 0-1, while the value (-1) - 0 is a non-vegetation objects. Transformation NDVI shows vegetation density seen from canopy density, it is not the density of each stem. The index value is close to 0 means the canopy density is low and close to 1 means the canopy density is high. For image processing used Envi 5.1, whether both of radiometric and geometric correction. The software also used for the classification levels of vegetation density. On Landsat 7 ETM vegetation index is generated from the difference between the band 4 and band 3 compared to total between the two bands. Analyze of the increasing mangrove impact conducted by interview and observation. The output of this research is map of mangrove development in the Brantas and Porong estuary, and mangrove development impact analysis. The development of mangrove ecosystems of both area and density from year to year experienced a significant increase. Within 5 years period, from 2009 to 2014 the growth of mangrove looks very high, where the mangrove ecosystem is growing around Brantas and Porong estuary. The increased mangrove ecosystems were affected by mud material deposition in Brantas and Porong estuary, that the mud is suitable medium for mangrove. The development of mangrove ecosystems reduce erosion along the waterfront and can be used as a barrier of heavy metals derived from the mudflow to the Madura Strait. Another benefit of mangroves is give protection for marine animals such as shrimp and fish, then there is a lot of potential fisheries in mangrove areas. That situation can be exploited by fishermen around the study area to exploit marine products without harming the environment. People realize that mangroves can be used as a barrier of abrasion and as a habitat for marine animals to grow, so there is a wider utilization of mangrove, which is used as a buffer zone area of the pond.

9638-21, Session PS

Study on the seasonal migration of surface suspended sediment in the Taiwan Strait based on remote sensing

Xiaohui Xu, The Third Institute of Oceanography,SOA (China); Jian Chen, Xiang Ye, The Third Institute of Oceanography, SOA (China)

Concentration of suspended sediment directly affects the optical properties such as transparency and water color, and aquatic environment as well. Understanding temporal and spatial distribution of concentration of suspended sediment is key point in coastal study. Remote sensing has been proven to be an effective means of monitoring suspended sediment. The Taiwan Strait is a typical regional of research on material distribution and transport. This paper selects the Taiwan Strait as study area, establishes inversion mode of suspended sediment by coupling field data with remote sensing reflectance from MODIS data in the Taiwan Strait. Monthly-averaged concentrations and seasonal changes of suspended sediment from 2002 to 2012 were calculated and analyzed by the mode, in the end, mechanism affecting variability of suspended sediment was discussed. The main results are as follows:(1) remote sensing reflectance at 555nm from MODIS data has high relativity with the field observed turbidity by regression equation of =0.8931e123.93x in which Y is TSM concentration, X is Rrs555 and R2 is 0.6836. (2)Suspended sediment in the Taiwan Strait has obviously spatial and temporal distribution characteristics, that higher concentration of suspended sediment is in coastal water and decreases from shore to sea, and highest concentration happens in winter.(3) Concentration of suspended sediment is mainly controlled by volume of runoff, wind and hydrodynamics, including wave, tide and circulation.

9638-22, Session PS

Restoration of cloud contaminated ocean color images using numerical simulation

Xuefei Yang, Shanghai Institute of Technical Physics (China); Zhihua Mao, The Second Institute of Oceanography, SOA (China) and Shanghai Institute of Technical Physics (China); Jianyu Chen, Haiqing Huang, The Second Institute of Oceanography, SOA (China)

It is very hard to access cloud-free remote sensing data, especially for the ocean color images. A cloud removal approach from ocean color satellite images based on numerical modeling is introduced. The approach removes cloud-contaminated portions and then reconstructs the missing data utilizing model simulated values. The basic idea is to create the relationship between cloud-free patches and cloud-contaminated patches under the assumption that both of them are influenced by the same marine hydrodynamic conditions. Firstly, we find cloud-free GOCI (the Geostationary Ocean Color Imager) retrieved suspended sediment concentrations (SSC) in the East China Sea before and after the time of cloudy images, which are set as initial field and validation data for numerical model, respectively. Secondly, a sediment transport model based on COHERENS, a coupled hydrodynamic-ecological ocean model for regional and shelf seas, is configured. The comparison between simulated results and validation images show that the sediment transport model can be used to simulate actual sediment distribution and transport in the East China Sea. Then, the simulated SSCs corresponding to the cloudy portions are used to remove the cloud and replace the missing values. Finally, the accuracy assessments of the results are carried out by visual and statistical analysis. The experimental results demonstrate that the proposed method can effectively remove cloud from GOCI images and reconstruct the missing data, which is a new way to enhance the effectiveness and availability of ocean color data, and is of great practical significance.

9638-23, Session PS

The spatial-temporal distribution of particulate organic carbon in the Pearl River Estuary

Dong Liu, Zhejiang Univ. (China); Qiankun Zhu, Jianyu Chen, Fang Gong, JiAn Wei, The Second Institute of Oceanography, SOA (China)

River estuaries are connector of terrestrial ecosystem and marine ecosystem. Riverine Particulate Organic Carbon (POC) was poured into oceans after a series of biogeochemical reactions in estuaries. POC plays an important role in sink of atmospheric CO2, global carbon cycle, etc. Satellite monitoring of POC in river estuaries will improve studying carbon dynamics in estuaries. Around river estuary, POC was sourced from terrestrial ecosystem and aquatic ecosystem; its distribution features might be complex and likely to change with time. POC concentration in ocean surface is determined by biological production, transformations to other carbon reservoir, export downward, etc. Based on samples from four cruises, representing four seasons, we discussed spatial-temporal distribution and remote sensing monitoring of POC concentration in the Pearl River Estuary (PRE). Field sampling showed that there was a wide range of POC concentration in the PRE. For all cruises, the POC concentration ranged from 0.113 mg/l to 1.402 mg/l, with minimum value in winter cruise and maximum value in summer cruise. Average POC concentration in winter cruise was 0.393 mg/l, and that in summer cruise was 0.592 mg/l.

Under the influence of East Asian Monsoon, the Pearl River Estuary, with most discharge from the Pearl River happen in the wet season etc., differs from non-monsoon river estuaries. Being affected by larger discharge from the Pearl River in the wet season, surface POC concentrations in summer were usually higher than those in other three seasons, similar, in the PRE. In the Lingdingyang Bay, POC concentrations in the west were higher than those in the east, especially in spring and autumn; however, this distribution patter was not obviously in summer. In the south of the Lingdingyang Bay, POC concentration decreased from the northwest to the southeast, with higher value in near shore waters; moreover, area of the region, where POC concentration was larger than 0.3 mg/l, in summer was larger than those in other three seasons. Besides, because of resuspension, POC concentrations at the bottom layer were usually higher than those at the surface layer. Taking the PRE as an example, remote sensing monitoring of POC concentration in case II water around estuary was also discussed. On the one hand, on the basis of Chlorophyll-a (CHLa) and Total Suspended Matter (TSM) concentrations inversed by published algorithms, we could estimate surface POC concentration through multiple linear regression equation: POC=0.042*CHLa+0.014*TSM+0.1595, R=0.9156. Source of POC in the PRE was complicated. Some is from terrestrial ecosystem produced majorly by photosynthesis of vegetation; other is from aquatic ecosystem produced majorly by photosynthesis of vegetation phytoplankton. On the other hand, great relationships between surface POC concentrations and total particle absorption coefficient at 667nm (TPabs(667)) and 678nm (TPabs(678)) were also found: POC=3.813*TPabs(667)+0.0684, R=0.8769 and POC=3.9175*TPabs(678)+0.0624, R=0.8745. They imply that surface POC concentration monitoring from space through bands at 667nm or 678nm might be possible. In the same season, discharge might significantly change POC distribution in the PRE. POC concentrations in the PRE are the results of complicated physical and biogeochemical effects. They might change spatially and seasonally.

9638-24, Session PS

Investigation of mechanisms of generation, development and evolution of vortex structures in the northeastern part of the Black Sea and in the southeastern part of the Baltic Sea

Olga Y. Lavrova, Space Research Institute (Russian Federation); Evgeny V. Krayushkin, Lomonosov Moscow State Univ. (Russian Federation); Nikolay N. Golenko, Maria N. Golenko, P.P. Shirshov Institute of Oceanology (Russian Federation)

The results of many-year satellite observations of meso- and submesosacle vortex structures in the north-eastern part of the Black Sea and in the south-eastern part of the Baltic Sea are presented.

The principal element of large-scale water circulation in the Black Sea is the Rim Current. Between the stream core and the sea shore one can regularly observe coastal anticyclonic eddies resulting from RC meandering. Such eddies have the typical size, approximately several tens of kilometers, and can be clearly distinguished on maps of Sea Surface Temperature and Water Leaving Radiance. Despite the fact that mesoscale vortexes in the Black Sea have been successfully studied for a long time, the mechanism of these circulations formation still has not been fully investigated. We attempted to use computer model KUST in order to determine hydrometeorological conditions which favor the generation of mesoscale eddies. Finer scale vortexes, so-called submesoscale eddies, have typical sizes less than the baroclinic Rossby radiuses, and are characterized by feeble thermal and optical contrasts and short life period. They can be detected either in radar images with high spatial resolution or in visible spectrum images in the sunglint area. Mechanisms of their formation are diverse and not always clear. In the test area located in the north-eastern part of the Black Sea general mechanisms could be the following: wind impulse, water flow around a cape, the Cape Indokopas, for instance, interaction of large-scale water circulations and their dissipation etc. In order to study the structure of submesoscale eddies, we conduct in-situ measurements of currents using ADCP, CTD, thermistor sensor, drifters. In-situ measurements allowed us to investigate three-dimensional structure of small-scale eddies and in some cases to retrace their evolution.

Currents in the south-eastern part of the Baltic Sea are formed only under the influence of wind field in contrast to the Black sea, for example, where the constant Rim Current flows. Water flow responds to the wind change for so called inertial period which lasts for 14 hrs. For the time equal to 2-3 inertial periods quasi-geostrophic currents develop almost completely; and when the wind is quite strong they take the shape of streams. Moreover, as west winds predominate in this area the downwelling streams take place more frequently. In this respect the downwelling system fulfills the functions approximately similar to the ones of the Rim Current. Characteristic feature of the south-eastern part of the Baltics is non-uniformity of coastal relief which, first of all, include the Hel Peninsula and the Cape Taran. Vortex structures appear when the streams of coastal current flow around these relief elements.

In order to find out what conditions and primarily wind conditions favor vortex formation both near capes and in the Gdansk Bay, the numerical simulation of currents in this region was performed. There was used a well-known and adapted for the Baltic Sea the Princeton Ocean Model (POM). Simulations were run in those cases when vortex structures were distinct in satellite images. The use of real wind field data with high spatial resolution allowed obtaining the field of currents similar to the ones observed in satellite images, depicting the same eddies and streams etc. In summer, 2014, in-situ measurements were carried out and helped to study the formation process, structure and evolution of the eddy occurred near the Cape Taran.

The study was completed with partial financial support from The Russian Scientific Foundation grant # 14-17-00555

9638-25, Session PS

Observations of SST diurnal variability in the South China Sea

Qianguang Tu, Delu Pan, Zengzhou Hao, Jianyu Chen, The Second Institute of Oceanography, SOA (China)

Four years of hourly sea surface temperatures (SST) observations from the geostationary satellite Multi-functional Transport Satellite (MTSAT) provide a unique opportunity to investigate the diurnal warming in the South China Sea (SCS). Firstly, a complementary quality control procedure is carried out base on the MTSAT appended quality flags to remove the outliers. The quality control procedure mainly consists of limit checks, temporal consistency check and reference check. Secondly, the quality controlled MTSAT SSTs are validated against the ENVISAT Advanced Along Track Scanning Radiometer (AATSR) archive to make sure an accurate and trustworthy diurnal estimation. The spatial and temporal collocated windows of MTSAT and AATSR are 0.05o and 30 minutes. The overall mean bias of MTSAT–AATSR is ?0.2°C, and the standard deviation reduces from 0.67°C to 0.5°C. Finally, the diurnal signals are estimated from hourly MTSAT SST by subtracting the Operational Sea Surface Temperature and Sea Ice Analysis (OSTIA) SST at the same day(?SST=MTSAT-OSTIA).The daily OSTIA SST products have zero mean bias and an accuracy of ~0.57 K compared to in situ measurements (Craig J. Donlon et al., 2012). They are free of any diurnal signal so that can be taken as reference fields for diurnal variability calculating. The spatial distribution and temporal variations of ?SST in SCS is then investigated. Seasonal mean of the maximum ?SST from June 2006 to June 2010 is greater than 0.5oC in large regions through the year. It is most pronounced in the northwest of the Luzon Strait and the shallow coast in spring when the surface wind becomes weak in the transition of the monsoon while smallest diurnal signals are found in the south of SCS in summer. The seasonal mean of the?SST at Luzon Strait reaches ? 1.5 °C in spring. These characteristics of the?SST spatial distribution are similar to those estimated from MODIS and AMSRE SST in the previous studies by Lin Rui et al. (2014). Moreover, the seasonal mean of events with daily anomalies exceeding 2K shows clearly diurnal cycle. It shows a morning cooling period with a minimum at around 0600 ~0700 local solar time except summer. A warming peak occurs between 1300 ~ 1400 LST that is about 1~2 h after the maximal sun elevation and a decrease starting from 1500 LST. This is the first study using geostationary satellite measurements to characterize and quantify the diurnal warming in SCS. The results would contribute to our estimation of air-sea heat and gas fluxes, optimal assimilation of satellite SST data into the weather and ocean model.

9638-26, Session PS

Estimation of marine primary production from MODIS data using phytoplankton absorption-based model

Ma Sheng, Wu Bin, Aerospace DongFangHong Satellite Co., Ltd. (China); Tao Zui, Institute of Remote Sensing and Digital Earth (China)

As the fundamental component of global biogeochemical cycling, marine net primary production (NPP) has been used to study the global climate processes for decades. The development of space-borne ocean color sensors can provide continuous and large-scaled observations of various seawater biophysical parameters, which correlate highly with NPP. Therefore, using these satellite data, many models have been developed to estimate the spatial and temporal dynamics of NPP. Among these models, the phytoplankton pigment absorption (aph) based model has been used for many regional waters. In this paper, an aph-based model was proposed with the correction by size types of phytoplankton. Chlorophyll data was used to classify the phytoplankton as three types according to its size of cell. Then different maximum quantum yield of the three types of phytoplankton were applied to calculate its NPP respectively. Sea surface temperature (SST) was also used to correct the photosynthesis efficiency in the southern ocean as its cold water. Following the NPP model, the monthly averaged data derived by Moderate Resolution Imaging Spectroradiometer (MODIS) was applied to estimate monthly NPP of global ocean for the period from January 2003 to December 2012. The model yields an annual integrated NPP of approximately 53 Pg C yr-1 for the global ocean over the period 2003-2012. The model results were validated by comparing it with in-situ NPP data collected by five programs. The averaged logarithmic bias was about -0.07, and the logarithmic root-mean-square error of the model was about 0.17. The model performance was also compared with the results of chlorophyll-based model (VGPM) and Carbon-based model (CbPM) in terms of spatial distribution and accuracy. From the comparison results, we can find that the spatial distribution of NPP derived by our proposed model is much similar to CbPM other than VGPM. Although much more additional studies should be conducted, the comparison results in this work showed that the proposed model can depict the seasonal NPP variation with improved accuracy, which will encourage researchers to estimate ocean NPP from satellite ocean color data.

9638-27, Session PS

Multisensor satellite survey of surface oil pollution in the Caspian Sea

Marina I. Mityagina, Olga Y. Lavrova, Space Research Institute (Russian Federation)

This paper presents the results of long-term satellite survey of the aquatic area of the Caspian Sea. Starting from 2009 up to the present moment a satellite survey of central and south-eastern regions of the Caspian Sea is carried out by the Space Radar Laboratory of the Space Research Institute of RAS. The main attention is focused on detecting oil pollution as well as biogenic and anthropogenic surface films.

Our study is based on high-resolution radar imagery data obtained by synthetic aperture radars onboard Envisat satellite (till the spring of 2012) and onboard Sentinel-1 satellite (since October, 2014). We used remotely sensed data in visual and IR bands from Multi- and Hyper-spectral sensors, which was taken nearly simultaneously with the satellite radar images in order to distinguish between different types of surface pollutants, understand a comprehensive figure of meteorological and hydrodynamic processes in test areas and discover the factors affecting pollutants spread and drift.

We present the results of our comparative analysis of oil film signatures in satellite radar, multi- and hyper-spectral data and discuss strengths and shortcomings of each data sources.

The most common SAR observations of sea surface areas covered by pollution films were analyzed. The large amount of data available allowed us to make generalizations and obtain statistically significant results on spatial and temporal variabilities of various films' manifestations.

The pattern of surface oil pollution of the Caspian Sea is found to be substantially different from those observed in other seas (e.g. in the Black and Baltic Seas). We attribute this difference to a unique characteristic of the Caspian Sea, namely the presence of big oil and natural gas fields on its bottom. We confirm that the exploitation of the oilfields in the sea as well as natural seepages and mud volcanoes at the sea bottom are the main sources of the Caspian Sea surface pollution. Illegal discharges in the Caspian Sea are not the main source of sea surface film pollution, but unfortunately their amount is increasing year-to-year.

We outline two areas of the most intensive pollution of the Caspian Sea surface. Those are oil-producing regions near the Absheron peninsula and the west bank of the South-Caspian depression.

We discuss the relations between manifestations of surface films and natural seepages and mud volcanoes activity. We then study the connection between natural seepages' and mud

volcanoes' manifestations and earthquake activity in South Caspian and adjacent areas. We discover a high correlation between the SAR manifestations of natural seepages and mud volcanoes and 3-4-magnitude earthquakes.

The work was supported by the Russian Science Foundation under the project # 14-17-00555. ASAR Envisat data were obtained under the ESA projects C1P.6342, Bear 2775 and C1P.1027.

9638-28, Session PS

Studying flow variability trough narrow straits via satellite multispectral and hyperspectral data: the Kerch Strait case

Marina I. Mityagina, Olga Y. Lavrova, Space Research Institute (Russian Federation)

The main goal of this study is to demonstrate the possibility of retrieving information about the flow formation in narrow straits from satellite multispectral and hyperspectral data.

We used the Kerch Strait connecting the Black Sea and the Sea of Azov as a subject area for the study. It is a shallow sound, 41 km long and 4.5-15 km wide.

The study is based on remote sensing satellite data taken by OLI Landsat-8, ETM+ Landsat-7, and TM Landsat-5 multispectral (MS) instruments and Hyperion and HICO hyperspectral (HS) sensors. The data from these sensors was analysed together with available meteorological data and data of in situ measurements using the distributed information system "See the Sea" (STS), which has been created by Space Research Institute of Russian Academy of Science as a tool to aid in complex analysis of satellite data for oceanographic studies. STS has specialized tools that enable MS and HS data analysis, such as: easy to use spectral bands selection and visualization, such as assessment of the spectral bands information content; composition of various color syntheses; sequential conjugation of the information derived from different bands; spectral radiance and spectral reflectance graph drawing; preparing specialized data products to provide data input for classification and analysis.

It was demonstrated that optical properties of the waters of the Black Sea and the Sea of Azov interacting in the Kerch Strait exhibit significant differences. These differences affect spectral reflectance and are instrumental in determining the direction of flows, revealing local currents at various temporal scales, and describing water exchange patterns between the Black and Azov Seas.

An impact of wind speed and direction on formation of flows through the strait was estimated. It was confirmed that hydrodynamical processes in the strait are heavily dependent on the wind speeds and that a sharp increase in wind speed can significantly change the direction of the flow.

Based on the satellite data, we classified the main types of flows through the straight according to their water transport directions: the Sea of Azov type, the Black Sea type, oscillating flows. Occasionally, two-way flows can be observed, which are clearly manifested in satellite images.

We drew conclusions on the frequency of occurrence for each of the flow types and determined the character of the flow variability through the Kerch Straight.

Satellite images revealed that waters of the Kerch Strait have higher turbidity than adjacent waters of both the Black Sea and the Sea of Azov. We conjecture that this increased turbidity can be generated by bottom resuspension at the strait due to strong local currents in shallow waters.

The work was partially supported by RFBR project 13-07-12017 ofi-m. HICO data was obtained under the agreement between the Naval Research Laboratory and IKI RAN.

9638-29, Session PS

Sea waves backscattering statistical characteristics experimental researches results in microwave band

Michael V. Potipak, Vladimir T. Lobach, Southern Federal Univ. (Russian Federation)

The paper discusses the flight tests results for sea surface parameters measurements with aboard microwave band gauges. A comparison of different remote sensing methods capabilities for measuring height, average wavelength and sea wave's general direction of propagation are made. The possibility of measuring sea surge intensity, sea surface 3-D parameter and sea wave energy spectrum in microwave band are shown. Methodological and instrumental measurement errors of sea wave's statistical characteristics are taking into account. The limitations of remote sensing methods for flight altitude, pitch and carrier roll are also discussed.

9638-30, Session PS

Dynamic of mangrove cover change with anthropogenic factors on small island, Spermonde Archipelago

Nurjannah Nurdin, Muhammad Akbar, Farida Patittingi, Hasanuddin Univ. (Indonesia)

Indonesia has lost more than 1.2 million hectare of mangrove since 1980 when mangrove forest cover was still 4.2 million hectare (FAO 2007). The mangrove forest in Tanakeke Island, the district of Takalar, South Sulawesi, Indonesia in the early 1980s was 1,770 hectares, and after a conversion into middle and failed fish farms, only 500 hectares remain. The phenomenon of mangrove forests degradation in Tanakeke Island needs to receive specific attention, considering that the island is one in South Sulawesi having precious mangrove forests in a coastal region. The phenomenon of mangrove forests degradation in Tanakeke Island needs to receive specific attention, considering that the island is one in South Sulawesi having precious mangrove forests in a coastal region. The objective of this study was to analyze dynamics of mangrove cover changes (41 years) using multi temporal and multi sensor Landsat imagery. To conduct the study, Landsat data, including four Landsat MSS (28 October 1972), a Landsat Thematic Mapper (TM) images (26 August 1993), a Landsat Enhanced TM Plus (ETM+) image (21 July 2003), and a Landsat 8 (Operational Land Imager, OLI) image (27 April 2013) were acquired from the United States Geological Survey (USGS). The methodology of this study consisted of two main steps: (1) image analysis: geometric correction of Landsat images, preliminary analysis, and classification; (2) ground truth; while the data processing was composed of five main steps: (1) geometric correction, (2) preliminary analysis, (3) image classification, (4) accuracy assesment, and (5) post classification. The combination of RS and GIS techniques can help to identify the spatial dynamics of mangrove cover in Tanakeke Island. There was a large change in the net area of Tanakeke Island mangrove. Factors influencing loss of mangrove in Tanakeke Island from the anthropogenic are conversion of mangrove for aquaculture, clearing of mangrove trees for charcoal production on a large scale, and utilization of mangrove trees for domestic use. An increase of mangrove from shallow water and aquaculture in the last 41 years (1972 to 2013) was caused by environmental factors including silty substrate, current, tidal, and wavelength. Natural growth of mangrove have been carried out some places in Tanakeke Island, but were far from compensating losses by deforestation.

9638-31, Session PS

Controlling factors analysis of aquatic pCO2 distribution in the Western Arctic Ocean in summertime

Xuelian Song, Yan Bai, Zengzhou Hao, Qiankun Zhu, Jianyu Chen, Fang Gong, The Second Institute of Oceanography, SOA (China)

The uptake of carbon dioxide (CO2) by the Arctic Ocean has been changing because of the rapid sea-ice retreat. Sea ice melting will produce more open water to absorb CO2 from atmosphere and improve the biological productivity. At the same time, the melting ice water will also affect the physical properties of the sea water. The Chukchi Sea is the only gateway of the warm and nutrient-rich Pacific Ocean water flowing into the North Pole, and the high productivity-water has great impact on the uptake of CO2 by the Arctic Ocean. We use the in situ underway data of temperature, salinity, aquatic partial pressure of CO2 (pCO2), as well as remote sensing data of sea ice concentration, chlorophyll concentration, temperature in August in 2008, 2011 and 2012 to analyze the major controlling factors of aquatic pCO2 in the Western Arctic Ocean. We analyze the aquatic pCO2 variation with thermodynamic effect (temperature), mixing of water mass (salinity), biological drawdown (chlorophyll), and sea ice concentration. The remote sensing data provide us a relative complete view on the variation in large scale. Since the underway measurements do not contain the biological data, we use the satellite-derived 8-day composite chlorophyll data to match the in-situ data. Meanwhile, the satellite-derived sea ice concentration data is also a good parameter to divide the study areas. According to the different controlling mechanism, the study area is divided into three parts: the area affected by the Pacific Ocean water (mainly in the Chukchi Sea), the area where sea ice mostly melted with weak biological production (the southern Canada Basin and the Western Beaufort Sea), the area mostly covered by sea ice (the Northern Canada Basin). The distribution of aquatic pCO2 showed a below-atmospheric pCO2 level in most of the Western Arctic Ocean. The salinity and temperature value in the Chukchi Sea are also higher than other areas because of the impact of the Pacific Ocean water. Aquatic pCO2 is lowest in the Chukchi Sea because Pacific Ocean water, with high nutrients and biological production, kept the Chukchi Sea unsaturated relative to atmospheric pCO2. The high aquatic pCO2 values (360-380?atm) exist in the Western Beaufort Sea and the region in 75-80°N, where sea ice partially melted; and the high pCO2 values is resulted from warming, CO2 invasion from the atmosphere, and a low biological production. The melting ice water leads to a strong stratification in the Western Beaufort Sea and the Southern Canada Basin which prevent the nutrient supplement from the low layer. The CO2 quickly invade into the sea water and make a balance with the atmosphere because of the low productivity and shallow mixing layer. For the Canada Basin, pCO2 in the Canada Basin is influenced by temperature change and sea ice cover which impede the air-sea exchange. Remote sensing data can help to under the pCO2 variation and its response to the global change; and it need to develop a remote sensing algorithm of pCO2 based on the quantification of the controlling processes.

9638-32, Session PS

Spectral separation of wind sea and swell based on buoy observations

Yan Liu, Zengzhou Hao, Fang Gong, Tianyu Wang, Jianyu Chen, The Second Institute of Oceanography, SOA (China)

Numerous studies have demonstrated the capability of spaceborne altimeter to provide precise measurement of significant wave height (SWH). However, these altimeters record the information coexisting of swells from distant sources and wind seas generated locally, which presents a challenge for research such as air-sea interaction and coastal engineering. Identification and separation analysis of wave components of the wind sea and swell provide a more realistic depiction of the sea state and a better understanding of the characteristics of the two waves. Therefore, our study focuses on separating different waves to make a preparation for future applications in the field of remote sensing. This paper describes a method for partitioning wind seas and swells from the aspect of wave spectrum. The spectral separation method is composed of two stages. In the first stage, a separation frequency is determined by the optimum spectral partitioning technique. Data from the National Data Buoy Center (NDBC) are used to illustrate applications to various spectral separation techniques in this paper: 1) Initial Wave Steepness Method (STPN). This method separates wind sea and swell by the peak frequency of a defined steepness function which required only non-directional wave data.2) Modified Wave Steepness Method (MSTPN). On the basis of initial steepness method, this method improves by taking external information, such as the wind speed, into consideration. In the second stage, the SWHs of wind sea and swell are calculated respectively from frequency spectrum after separation. Results demonstrated that STPN often overestimates the SWHs of wind seas. Although MSTPN improves the performance from STPN, its results are still not good enough under condition of light winds. Considering limitations in aforementioned separating methods, the empirical coefficient C for determining the separating frequency is tested for more accurate results. Also, this paper gives a description of correlation between SWH and wind speed under the wind sea condition. Results show that SWH and wind speed of wind sea have a good quadratic fitting relationship. Comparisons among correlations from different separation techniques are made later for the choice of the optimum approach. The bias error and root-mean-square error (RMSE) are also computed for evaluating the accuracy of the correlation. In addition, this work would also provide a reference for extracting the wave component of wind sea from the satellite spectral data. And a practical method for deriving the wind sea SWHs from observations of scatterometer would be realized.

9638-33, Session PS

Evolutionary detectability of ocean and inland water variation from multidecadal satellite altimetry

Kuo-Hsin (Steven) Tseng, Guan-Ting Liu, National Central Univ. (Taiwan); C. K. Shum, The Ohio State Univ. (United States)

Since the successful observation of sea surface height (SSH) by TOPEX/Poseidon in the early 90's, a series of altimetry satellites have been dedicated to a continuous monitoring of ocean and inland water variation as well as detecting marine surface/bathymetry features globally. The unprecedented accuracy the altimetry satellite achieved has progressed towards centimeters level and the spatial coverage has been extended to a few kilometers from coastline by means of different ranging approaches. In this study, we compared a number of radar and laser altimetry satellites, namely TOPEX/Poseidon, Jason-1/-2, Envisat, ICESat, Cryosat-2, SARAL/AltiKa, from the aspect of their electromagnetic signal (single/dual-frequency radar band or green/red beam laser), coastal ocean detectability (footprint size and sampling rate), waveform retracking methodology (Brown model, specular, threshold and other empirical algorithms), and their ultimate water level accuracy over a variety of geographical locations and surface types (nearshore, snow-covered, and frozen waterbody).

By inspecting radar waveforms shapes and utilizing an approach called subwaveform-filtering (SF) method, a preliminary result concludes the detectability of water level in coastal area is from 7–10 km offshore by conventional Ku/C band radar approach (i.e., Envisat and Jason-2) to 1–2 km by Ka band SARAL/AltiKa. The SF method basically adopts far offshore waveform samples as reference to detect outlying waveform gates except for nominal tracking position, where the

anomalous waveform peaks are subject to land contamination in the radar footprint. The method is also applicable while there are ice floes interfering the retrieval of water surface in radar echoes.

Also, the accuracy of water level estimate has been improved from Envisat or Jason-2's 10–30 cm level to <10 cm by single band SARAL/AltiKa or SAR altimetry operated by Cryosat-2, in multiple coastal areas and Great Lakes in North America. The improvement in accuracy over Great Lakes region is by virtue of Ka band radar that is less penetrative into snow layer and thus keeps measurements more stable in contrast to Ku/C band radar. Furthermore, the detectability of small inland water bodies, or narrow rivers, becomes more accurate as the pulse repetition frequency (PRF) increases from Envisat's 1.8kHz to Jason-2's 2kHz and SARAL/AltiKa's 3.8kHz. In conclusion, the advance in satellite altimetry technology has evidenced its capability in measuring water level and its usefulness to serve as reliable virtual gauges for remote areas. It also reveals the prospect of future missions such as Sentinel-3 and SWOT, which extend the time series to synoptically observe global sea level and hopefully in the broader context of hydrosphere.

9638-34, Session PS

Study on extracting and verifying internal wave parameter of SAR image

Juan Wang, Jingsong Yang, The Second Institute of Oceanography, SOA (China); Junde Li, Second Institute of Oceanography,SOA (China); Lin Ren, Gang Zheng, The Second Institute of Oceanography, SOA (China)

Synthetic Aperture Radar (SAR) is a form of radar which is used to create images of an object. It can operate in all weather conditions. Oceanic internal waves are often observed by SAR. So SAR provides a new technique for measuring internal wave in a large area. And it is complementary to traditional measurements. The procedures are given in this paper for extracting the direction, wavelength, amplitude, speed and depth of internal waves. Some ENVISAT SAR images of South China Sea are used to extract the parameters in this paper. And a few HJ-1 and MODIS optical images are used to assist. Then some in-situ data from buoy is used to verifying the extraction results. The times of in-situ data and SAR image are similar. It is shown that: 1) The internal wave parameter can be extracted from SAR images, although sometime the extraction needs other data. 2) The error of wave direction between SAR and in-situ is less than 15 degree. The error of wave amplitude between SAR and in-situ is less than 15m, the relative error is less than 20%. 3) The wavelength of internal wave can't be measured by buoy. The wave depth, measured by buoy, is the depth where the Velocity of flow is maximum. It isn't the depth of internal wave.

9638-35, Session PS

GEOBIA and ontology-based sea area usage monitoring using remotely sensed imageries

Helingjie Huang, Jianyu Chen, The Second Institute of Oceanography, SOA (China)

Remote sensing is the best means of the global surface observation to date. The trend of higher spatial resolution of remote sensing imagery, makes it possible to move analysis unit from single pixel to image object made up of a set of relatively homogeneous pixels. Object based image analysis (GEOBIA) build a bridge between raster image and GIS contributing to synthesis multisource data. Ontology, a technique of knowledge representation in information science, would advance to it. Although the role of ontologies in GIS is not a new topic, few works have discussed how ontologies, considered from the perspective of a remote sensing specialist, can contribute to advancing remote sensing science. From reality world to meaningful objects, it involves how to generalize the reality depending on different research purpose and different understanding. Determining which characters of one geographic kind is the essential characters that differ from all the others, is related to epistemological and ontological aspects.

The sea area is an essential basic resource just as the same as the land. The information of sea area use is of great significance to the economy, environment, natural disasters, national defense and so on. The dynamic sea area usage monitoring system (DSMS) was formed in China since 2009. Remote sense is one of the most important means to detect the change information of dynamic monitoring of sea utilization. It can realize comprehensive, rapid, accurate, dynamic monitoring, and greatly enhance the management of sea area level.

This study concentrates on describing coastal entities from the view of GEOBIA in ontology modeling manners. GEOBIA benefits from image segmentation producing more information than single pixel analysis, such as geometry, texture, radiometry and even spatial relationships between two objects or among multi-objects. The spectral rules and topological spatial relationships dominate the knowledge part guiding interpretation course. Our works focus on salt fields, one of the major type of sea area use classification in the coast of China. Because of the high salinity, the spectral features of the salt field in the coastal areas are greatly different from marine water bodies and other ground objects spectral features. The salt field is man-made, so, it has regular arrangement and significant geometric characteristics. In the remote sensing images, the above characteristics are also shown as significant texture features (chessboard-like texture and stripe-like texture). Experiments on remote sensing images of a coastal zone of Jiaozhouwan, Shangdong Province, China is presented to show the relevance of the study.

9638-36, Session PS

Comparison of three airborne laser bathymetry data sets for monitoring the German Baltic Sea Coast

Yujin Song, Joachim Niemeyer, Leibniz Univ. Hannover (Germany); Wilfried Ellmer, Bundesamt für Seeschifffahrt und Hydrographie (Germany); Uwe Soergel, Technische Universität Darmstadt (Germany); Christian Heipke, Leibniz Univ. Hannover (Germany)

Various methods have been developed to measure the water depth and shape of the seabed using ship-based remote sensing techniques such as single-beam echo sounder, multi-beam echo sounder and side-scan sonar. An accurate description of the seabed is essential for enabling the precise and secure navigation of ships as well as a reliable coastal monitoring and management. However, it is difficult to obtain such information about the seabed especially in shallow water zones because these areas are not accessible for vessels in many cases due to the water depth. Airborne laser bathymetry (ALB) is a measurement technique particularly suitable for data acquisition at the shallow water zones. This technique has become increasingly important in recent years due to improved hardware and better processing software.

In this paper we report on practical experience gaining in the project 'Investigation on the use of airborne laser bathymetry in hydrographic surveying', in which the applicability of the ALB monitoring for the German Baltic Sea Coast is being analyzed in cooperation with BSH (Federal Maritime and Hydrographic Agency). Between 2012 and 2014, three flight campaigns were performed close to the island of Poel. The first data set was gathered by a Riegl VQ-820-G sensor in November 2012. The second and third data sets were acquired by a Chiroptera sensor of Airborne Hydrography AB in September 2013 and May 2014, respectively. The delivered data sets were classified into the five classes water surface, seabed, underwater vegetation, underwater object and onshore by the data providers. Simultaneously with the flight campaigns the Secchi depths were measured. This indicator describes the water

turbidity and is defined as the maximum depth at which the human eye is able to detect a specific disk in the water.

We examine the 3D points classified as seabed under different conditions during the data acquisition, e.g. the turbidity level, the date of flight and the flight altitude. The analysis comprises the point distribution, point density and the area coverage in several depth levels.

In addition, we analyze the vertical accuracy of the 3D points classified as seabed. For this purpose, the seabed points are compared to echo sounding data, which were acquired over about 20 years by BSH. The echo sounding data are available for the entire test area (except the very shallow water zones). Only small differences in elevation between both data sets can be observed demonstrating that the bathymetric models of both techniques are compatible to each other in our case.

Finally, the results of the three flight campaigns are compared to each other and analyzed with respect to the different conditions during the data acquisitions.

9638-37, Session PS

Laboratory investigation of wind wave breaking modulation in the inhomogeneous current field

Victor V. Bakhanov, Nikolai A. Bogatov, Alexei V. Ermoshkin, Olga N. Kemarskaya, Institute of Applied Physics (Russian Federation)

A experimental laboratory study of the effect of a horizontally inhomogeneous current on breaking statistics of wind waves was carried out. Were creating a current having the same direction as wind waves with positive and negative gradients and a current of the counter direction with a negative gradient. The wind speed varied from 10.4 to 20.1 m/s based on a standard height of 10 m.

A current was formed by a water pump and diffuser. The subsurface current parameters in the measurement area varied due to diffuser motion along the channel or varying the pump voltage (as a result, the velocity of water outflow from diffuser changed). The maximum current velocity near the surface was 27 cm/s. The maximum current gradient was equal to 0.09 1/s.

The current velocity was recorded by acoustic current meter (ADV), while the free surface deviation by string wave gauges. Breaking parameters were determined by X- and Ka-band scatterometers and a web camera installed inside the channel.

The codirected current reduces the wind wave amplitude for all wind speeds, while the frequency of the spectral density maximum of wind waves remains the same. The frequency of the recorded by radar wind-wave breaking also decreases for positive, negative, and zero gradients.

In the case of counter directions, for light winds in the presence of a current the wind wave amplitude reduces, the wind wave spectrum displaces in the direction of lower frequencies. At higher wind speeds, there were neither differences in the surface wave spectra in the presence and absence of a current, however, an increase in the frequency of the recorded by radar wind-wave breaking is observed.

From the analysis of the experimental Doppler spectra of radar signals in the X and Ka bands of VV and HH polarizations, which are scattered by a rough water surface in the presence of currents, one can draw several conclusions.

1. The Doppler spectrum maximum does not correspond to the free resonance ripple. The Doppler shift is determined by the velocity of the long wave with the Bragg ripple frozen into it.

2. The Doppler spectrum shift caused by the effect of the current is in good qualitative and quantitative agreement with theoretical predictions. If the current has the same direction as the wave, the shift of the Doppler spectrum maximum is positive; in the case of counter directions, the shift is negative relative to the background state of the Doppler spectrum.

3. If the current has the same direction as the wave, the radar signal power proportional to the effective scattering cross section of a rough surface decreases compared to the background value, while in the case of counter directions, it increases.

These laboratory investigations are carried out in the interests of the remote diagnostics methods development of inhomogeneous currents at higher wind speeds.

9638-38, Session PS

Field study of inhomogeneous currents, related to bottom topography, display on radar and satellite images

Nikolay A. Bogatov, Victor V. Bakhanov, Alexei V. Ermoshkin, Olga N. Kemarskaya, Institute of Applied Physics (Russian Federation)

This work deals with the data processing results of the complex subsatellite measurements taken in the White Sea in 2010 – 2011 in the summer from a board of research vessel “Ecolog”. The areas containing such features of bottom topography as underwater mountains and slopes were chosen for researches. The main research areas were chosen in the south and the southeast from the Solovetsky Island. The main interest of work is the transformation of sea waves in the field of inhomogeneous currents. Inhomogeneous currents were produced by means of tidal currents on bottom topography features. Characteristic speeds of tidal flow for these areas varied from 0.5 to 2 m/s. Simultaneous measurements of current profile, atmosphere parameters and surface wave’s intensity were taken. 3 cm X-band and 8 mm Ka-band skatterometrs (horizontal or vertical polarization, depending on installation) and 3 cm radar station (horizontal polarization) based on marine radar were used as onboard radar means. The analysis contact measurements and data from marine radar established that observed features on radar panoramas are related to inhomogeneous currents produced by bottom topography and tidal flow. The experimental data were compared with the satellite images. Images were obtained from the satellite TerraSAR-X on two polarizations: vertical (VV) and horizontal (HH). The method allowing in the presence of VV and HH polarizations to divide resonant (breg) and mirror components of the radar signal reflected from a sea surface was applied to process the satellite images. Breg component is related to a sea surface roughness while mirror component is related to surface wave’s breakings. Thus, obtaining mirror component of the signal reflected from a sea surface, it is possible to allocate sea surface regions with intensive sea wave’s breakings. After analyzing the results of the satellite images processing and measurements from the vessel, it was found that the presence of an inhomogeneous current leads to a change in the intensity of the breaking waves. The areas of characteristic features observation on satellite images are in good agreement with the bottom topography. At the same phase of the tide, the properties of the inhomogeneous currents vary slightly. This allows using radar techniques for sea topography monitoring.

9638-40, Session PS

Prediction models for CO2 emission in Malaysia using best subsets regression and multi-linear regression

Chun Ho Tan, Mohamad Zubir Mat Jafri, Hwee San Lim, Univ. Sains Malaysia (Malaysia)

This paper present the prediction models which analyze and compute the CO2 emission in Malaysia. Each prediction model for CO2 emission will be analyzed based on three main groups which is transportation, electricity production and consumption as well as residential and industry. The prediction models was generated using data obtained from World Bank Open Data. Partial least square and best subset method will be used to remove irrelevant data and followed by multi linear regression to produce the prediction models. From the results, high

R-square (prediction) value was obtained and this imply that the models are reliable to predict the CO2 emission by using specific data.

9638-41, Session PS

Combining bathymetric lidar and WorldView-2 satellite imagery for classifying benthic habitats using OBIA A

Ayin M. Tamondong, Mia Shaira Estabillo, Ivy Elaine Cadalzo, Charmaine Cruz, Julius Michael Hipolito, Gay Amabelle Go, Ariel Blanco, Univ. of the Philippines (Philippines)

The objective of this research is to combine bathymetric LiDAR (Light Detection and Ranging) point cloud data and WorldView-2 high resolution multispectral satellite imagery in classifying benthic habitats such as corals and seagrasses. The LiDAR data was obtained using an Optech Aquarius ALTM. LiDAR derivatives (mean depth, standard deviation of depth, plan curvature, profile curvature, rugosity, slope and slope of slope) were produced and these were combined with the multispectral bands of WorldView-2. These derivatives describe the complexity and structure of the seafloor. Rugosity can be used as a predictor of seagrass distribution in different bottom type variation. The slope defines the structure of the seafloor while the slope of slope has the ability to capture fine scale topographic complexity. Depth summary statistics, such as the Mean Depth and the Standard Deviation of the depth, are useful predictors in understanding the benthic zones, particularly in habitat classification. These derivatives were produced using different tools in ArcGIS. Principal Components Analysis was utilized to reduce the redundant information and produce uncorrelated data. The WorldView-2 data was corrected for radiometric and atmospheric inconsistencies using ENVI. To classify the benthic habitats, an object based image analysis approach was used using eCognition. Training and validation data sets were gathered using handheld GPS points and video tows geotagged using a dual frequency GPS receiver. The study area is a portion of the Lingayen Gulf. It is situated at the north of Dewey and east of Binabalian in Bolinao, Pangasinan, Philippines. The classification of WorldView-2 yielded the highest overall accuracy with 95.35% and kappa statistic of 0.93 while the LiDAR data produced 83.22% and kappa statistic of 0.75. Combining the WorldView-2 and LiDAR derivatives yielded an overall accuracy of 93.64% with a 0.9 kappa statistic. From this study, we can conclude that of WorldView-2 and bathymetric LiDAR derivatives can be utilized in creating benthic habitat maps and that object based image analysis is a useful tool for classifying such data sets.

9638-1, Session 1

Analysis of bistatic EM scattering by a polluted sea surface *(Invited Paper)*

Helmi Ghanmi, Ali Khenchaf, Fabrice Comblet, Ecole Nationale Supérieure de Techniques Avancées Bretagne (France)

In this paper, we study and analyze the influence of the presence of the pollutant on the electromagnetic (EM) signature of sea surface. We firstly analyze the pollutant effect on the geometrical and dielectric properties of the sea surface. Then we evaluate the EM scattering coefficients of a sea surface polluted by petrol emulsion or covered with oil layer observed in bistatic configuration. The bistatic scattering coefficients of a clean and a polluted sea surface are computed by using the rigorous Forward-Backward Method (FBM) and the asymptotic models (Small Perturbation Method (SPM), Small Slope Approximation (SSA) and Two Scale Model (TSM)). The models used for the numerical simulation of bistatic scattering coefficients of clean and polluted sea surface have been analyzed as a function of various acquisition parameters such as (wind speed, sea state, pollutant type, incidence angle, scattering angle, radar frequency and polarizations).

The presence of the pollutant on sea surface has an important effect on the geometrical and physical properties of a sea surface. When the wind velocity is relatively low, the oil forms a layer up the sea surface. In this case, the oil damps the surface roughness spectrum. Nevertheless, when the wind speed is high, the emulsion of oil with sea water is occurred and thus the dielectric properties of sea water are changed. Therefore, regardless of the choosing a sea spectrum, the dielectric constant of sea water is the only parameter that is truly related to the pollutant. More precisely, the dielectric constant has been considered as function of the oil percentage in seawater. Thus, the main goal of this work is to analyze precisely the scattered EM field by a clean and a polluted sea surface. The results obtained using the FBM have been compared with those given by the asymptotic models in several configurations and for different parameters.

Figure1 ((a), (b)) shows that the emulsion of petrol and sea water causes a reduction scattering coefficients of the sea surface. Namely, this reduction is essentially due to the emulsion effect on the dielectric properties of the sea surface. For the sea surface contaminated by pollutant film (c) a significant difference between the scattering coefficients of the clean and the polluted sea surface (for the scattering angles less than 40°). This difference is essentially due to the pollutant influence on the sea roughness and the dielectric constant of the pollutant.

In our previous work we have studied the variation of the bistatic EM scattering coefficients of clean and polluted sea, only by using the FBM method. Thus, more simulations and discussions on the EM scattering coefficients (of clean and polluted sea) simulated with the FBM and the asymptotic methods will be shown in the final paper. Some comparisons with experimental results will also be presented.

9638-2, Session 1

Assessment of the corrected CMOD6 GMF using scatterometer data

Anis El Youncha, Xavier Neyt, Royal Military Academy (Belgium)

An assessment of the agreement between ERS scatterometers (ERS-1 and ERS-2) and the Metop scatterometers (ASCAT-A and ASCAT-B) is essential for the consistency of the C-band scatterometry dataset.

An empirical correction of the CMOD5.n Geophysical Model Function (GMF) has been suggested recently by KNMI.

This correction was derived from the comparison of the ASCAT backscatter measurements and the CMOD5.n model.

Taking ASCAT's measurements as reference, the differences between the CMOD5.n and ASCAT measurements were attributed to GMF errors.

ERS-1, ERS-2, ASCAT-A and ASCAT-B are C-band fan-beam scatterometers covering overlapping incidence angle range.

Thus, their backscattering coefficients, over the common incidence angle range, can be compared.

During these C-band scatterometry missions, different calibration campaigns have been carried out mainly relying on ground active transponders and natural distributed targets e.g., rainforest.

Additionally, these missions differ in time with some overlapping periods.

Therefore, an assessment of the agreement between ERS measurements and the corrected CMOD5.n (equivalently ASCAT) is important for the validation of the applicability of the corrected GMF to the whole C-band scatterometry dataset.

The aim of this paper is the assessment of the corrected CMOD5.n GMF using ERS-1 and ERS-2 ocean backscatter measurements.

9638-3, Session 1

On the measure of sea ice area from sea ice concentration data sets

Mauro Boccolari, Univ. degli Studi di Modena e Reggio Emilia (Italy); Fiorigi F. Parmiggiani, Istituto di Scienze dell'Atmosfera e del Clima (Italy)

The measure of sea-ice cover, trends and variability provides a fundamental information on the climatology of the Arctic region. Sea-ice cover is conventionally measured by two parameters: i) Sea Ice Extent (SIE) given by the sum of all pixels whose Sea-Ice Concentration (SIC) is above 15%; and ii) Sea Ice Area (SIA) given by the sum of all pixels whose SIC is above 15% x pixel SIC. From a physical point of view, SIA is the really important parameter to be investigated. In addition to the conventional rule to compute SIA, a new one has been introduced, derived from the discrimination between thin and compact ice from microwave observations of antarctic polynyas; by this new method, SIA is given by the sum of all pixels whose SIC is above 70%.

Aim of this study is to compare the trends of the monthly time series of three Arctic areas according to these two rules and to prove similar performances. SIC data computed through the ARTIST Sea ICE (ASI) algorithm and provided by the Institute of Environmental Physics of the University of Bremen, were used. The three areas chosen for our analysis were: the whole Arctic Ocean and two Arctic sectors of different morphology, the East Greenland Sea, as a typical open sea, and the Beaufort Sea, as a typical closed sea. The study covers the period January 2003 -- December 2014, i.e. the period in which the SIC data set of the University of Bremen is built using the new AMSR passive microwave sensor. This study investigates the differences in SIA long term trends as computed with the two methods outlined above and indicates that they give very similar results. We suggest that the 70% threshold rule can be used in future studies of the Arctic sea-ice cover because it provides a well defined border between sea and ice.

9638-4, Session 1

Monitoring of landfast sea ice in West Antarctica using multisensor data and machine learning approaches

Miae Kim, Jungho Im, Hyangsun Han, Ulsan National Institute of Science and Technology (Korea, Republic of); Hyun-Cheol Kim, Korea Polar Research Institute (Korea, Republic of)

Landfast sea ice (hereafter fast ice) is the sea ice attached to coastal features such as shoreline, grounded icebergs, and glacier tongues with no or little motion. Fast ice plays an important role in various geological and biological processes in the Antarctic. It is known that fast ice acts as an important interface between ice sheet/shelves and ocean/pack ice. As fast ice persists over several years, it typically has physical forcing to ice shelves, acting as a buttress to them. In addition, fast ice provides an extensive habitat and breeding places for many organisms living in the Antarctic. Since fast ice is closely related to the polar and global climate systems, monitoring fast ice is necessary to better understand the Antarctic and global climate systems. In spite of the importance of fast ice, fast ice in the Antarctic has not been much studied especially in the West Antarctic. As fast ice is one of the crucial indicators of changes in the Antarctic, the spatiotemporal variation of fast ice should be carefully examined. Due to the harsh environment of the Antarctic, it is hard to obtain in situ measurements. Remote sensing data techniques can be as an alternative in this regard.

The objective of this study was to develop an automated West Antarctic fast ice monitoring approach using machine learning methods through the synergistic use of multi-sensor data. A total of 13 variables including sea ice concentration and 8 dual polarization frequency channels from the Advanced Microwave Scanning Radiometer for EOS (AMSR-E), day/nighttime ice surface temperature from the MODerate resolution Imaging Spectroradiometer (MODIS), ice velocity from the Special Sensor Microwave/Imager (SSM/I), and polarization ratio (PR) and spectral gradient ratio (GR) calculated from AMSR-E brightness temperatures were used to identify fast ice in the West Antarctic. Since there is no available in situ fast ice data in the Antarctic, we collected reference data for the West Antarctic fast ice using MODIS data based on the visual interpretation method used in Fraser et al. (2010), who mapped fast ice extent in the East Antarctic. Two rule-based machine learning methods used in this study were decision trees and random forest. MODIS Antarctic ice shelf images of 250m spatial resolution were used to validate the fast ice maps. Results showed that random forest produced better performance than decision trees in mapping fast ice of the West Antarctic. As both models provided information on variable contribution to fast ice mapping, relative variable importance was further examined. The spatiotemporal variations of fast ice extent in the West Antarctic were also explored using two metrics representing fast ice residence time—simple frequency and weighted averaged residence time.

9638-5, Session 2

Simulation of infrared emissivity and reflectivity of oil films on sea surfaces

Nicolas Pinel, Goulven Monnier, ALYOTECH France (France); Irina Sergievskaya, Institute of Applied Physics (Russian Federation); Christophe Bourlier, L'Univ. Nantes Angers Le Mans (France)

This paper presents a fast realistic simulation of the infrared emissivity and reflectivity of oil films on sea surfaces.

For a fast sea surface generation, the sea spectrum is divided into two parts, a low frequency (LF) and a high frequency (HF) part, with a windowing Hann function to make the transition between the two spectra [1]. Then, after the two generations, the whole surface is reconstructed by interpolating the LF grid at the HF grid sampling step, and by making copies of the HF grid. Validation process [1] made it possible to establish that the surface slope PDF and the surface slope autocorrelation function were well reconstructed provided that the windowing function is applied.

For being able to have a fast simulator, the electromagnetic (EM) modelling is based on a two-scale model [2] approach: the surface is not generated following the common constraint $\Delta x=\Delta y\approx ?/10$, but at a much looser spatial sampling step. To our knowledge, this approach was initially proposed for radar microwave applications, where the EM wavelength belongs to the decimetre or centimetre scale: for instance, in X band (frequency f≈10 GHz), the radar wavelength is ?≈3 cm. In this context, a looser constraint in the order of $\Delta x=\Delta y\approx 6?$ can be applied [3, 4]. At such frequencies, the non-resolved part is dealt with by using the small perturbation method, contrary to the resolved part which is dealt with based on the geometric optics (GO) approximation. Also, the choice of the cut-off between the resolved and non-resolved parts has a significant influence on the prediction of the scattered intensity [3, 4].

By contrast, at optical wavelengths, the problem becomes simpler, as the sea surface electromagnetic scattering can usually be described by the GO only, even at low grazing angles [5]. Then, the constraint about the choice of the cut-off separating the resolved and non-resolved parts is expected to be much looser. That is why recent simulations [6, 7] use surface sampling steps that can reach at least the decimetre; this approach is widely used in physically based rendering, and in particular in computer graphics [8]. In this paper, following previous work, this two-scale approach is elected [7]. The non-resolved part is dealt with by calculating the GO associated contribution from integrating the surface slope spectrum in the non-resolved region.

The incorporation of the oil pollution at the sea surface is made based on [9], in which the impact of the oil film at the sea surface on the surface spectrum and consequently on the EM

scattering behaviour is described. For short, the damping of the surface heights by the presence of the oil film is modelled by the model of local balance (MLB). For modelling the EM scattering from the oil film on the sea surface, the two air/oil and oil/sea interfaces are assumed to be parallel (fully-correlated) interfaces. Like for the clean sea surface, they are assumed to be locally flat. Then, the scattering behaviour is described by considering the air/oil/sea layer as a Fabry-Perot interferometer.

References:

[1] N. Pinel, G. Monnier, J. Houssay, "Fast simulation of a moving sea surface remotely sensed by radar", in International Radar Conference, Lille, France, 2014

[2] G. Valenzuela, "Theories for the interaction of electromagnetic and oceanic waves - A review", Boundary Layer Meteorology, vol. 13, pp. 61-85, 1973

[3] J. T. Johnson, R. T. Shin, J. A. Kong, L. Tsang, K. Pak, "A numerical study of the composite surface model for ocean scattering", IEEE Transactions on Geoscience and Remote Sensing, vol. 36, pp. 72-83, 1998

[4] G. Soriano and C.-A. Guérin, "A cutoff invariant two-scale model in electromagnetic scattering from sea surfaces", Geoscience and Remote Sensing Letters, vol. 5, pp. 199-203, 2008

[5] H. Li, N. Pinel, C. Bourlier, "Polarized infrared reflectivity of 2D sea surfaces with two surface reflections", Remote Sensing of Environment, vol. 147, pp. 145-155, 2014

[6] K. Caillaut, S. Fauqueux, C. Bourlier, P. Simoneau, and L. Labarre, "Multiresolution optical characteristics of rough sea surface in the infrared," Applied Optics, vol. 46, pp. 5471-5481, 2007

[7] G. Monnier, S. Vince, and J. Houssay, "Real time modelling of multispectral ocean scenes," in International Symposium on Optronics in Defence and Security, Paris, France, Feb. 2010

[8] L. Simonot, "Photometric model of diffuse surfaces described as a distribution of interfaced Lambertian facets," Applied Optics, vol. 48, pp. 5793-5801, 2009

[9] N. Pinel, C. Bourlier, and I. Sergievskaya, "Unpolarized emissivity of thin oil films over anisotropic Gaussian seas in infrared window regions," Applied Optics, vol. 49, pp. 2116-2131, 2010

9638-6, Session 2

Spreading of oil films on the sea surface: radar/optical observations and physical mechanisms

Stanislav A. Ermakov, Institute of Applied Physics (Russian Federation) and Volga State Univ. of Water Transport (Russian Federation); Ivan Kapustin, Irina Sergievskaya, Institute of Applied Physics (Russian Federation); Jose da Silva, Univ. do Porto (Portugal)

Slicks on the sea surface are one of the most common features on the sea surface at low to moderate wind speeds. Slicks can be associated with different dynamic processes in the ocean and atmosphere near surface layers, such as non-uniform surface currents, internal waves, wind shadowing areas, etc. A significant part of marine slicks is due to surface films of anthropogenic origin that appear on the water surface as a result of accidental or deliberate oil spills. The shape of oil slicks depends on different factors determining film spreading, which are surface and interfacial tension coefficients, near surface currents and wind waves. Note that the slick shape is an important characteristic that can be used to identify the nature of slick signatures in radar or optical images of the sea surface and possibly to describe them quantitatively.

Theory of oil slick spreading under the action of surface tension forces was developed e.g. by Fay (1969). The slick shape for this case is circular and the slick radius grows with time at the late stages of spreading as t3/4 . However, as evidenced by observations, oil slicks even at low wind conditions have an oval shape, with the long axis directed approximately along the wind. Currently, however, there is a lack of data of systematic experiments with slicks, and the very physical mechanisms of slick spreading are still not well understood.

This paper presents results of controlled experiments with oil spills, and a possible physical mechanism of slick asymmetry is discussed.

Experiments with oil spills were carried out in different water bodies and different environmental conditions – from an Oceanographic Platform on the Black Sea, and from a vessel on the Gorky Water Reservoir (GWR). Oleic acid was used to deploy films on the water surface. Characteristics of oleic acid films, in particular, the surface tension coefficient as functions of surfactant concentration were studied in laboratory conditions before the experiments. Slick shapes and their time evolution were studied using a photo camera and satellite radar images obtained by TerraSAR-X. In the satellite experiments several slicks were prepared consecutively when spilling a given volume of oil at predetermined time intervals before the satellite overpass. Some experiments were carried out with oil spilled from a small motor boat, in which case the slick shape was registered with GPS when the boat was moving along the slick border.

It is obtained that a long-to-short axis ratio of slicks weakly depends on spreading time but grows with wind speed. For instance, this ratio was 2-2.5 at wind speeds of 2-3 m/s and about 5 at wind speeds of 5-6 m/s.

A physical mechanism of slick deformation due to mean surface currents induced by surface wind waves is proposed. Namely, drift currents induced by oblique propagating surface waves increase in the area of slicks due to enhanced wave damping and these currents result in film compression in the cross wind direction. The currents at upwind and downwind sides contribute to the slick drift. Theoretical estimates of slick compression are presented and compared with experiments.

9638-7, Session 2

On discrimination between film slicks and "look-alikes" on the sea surface in multifrequency radar images

Irina Sergievskaya, Stanislav A. Ermakov, Ivan Kapustin, Institute of Applied Physics (Russian Federation)

Increasingly in recent years analysis of satellite radar and optical images of ocean surface is used for diagnosis of surface processes and, in particular, detection of film pollutions. Film slicks appear in the sea surface radar images as dark patches at moderate incidence angles (larger than 30-35 degrees). Usually it is considered to be established that there is a film (for example oil spill or biogenic films) on the sea surface in the area of reduced wave intensity under some additional arguments, e.g. proximity of oil platform/oil transportation routes or seafood farms etc. Remote sensing experience shows that the risk of the wrong decision is high because of some "look-alike" phenomena, for example, wind shadowing zones. A new approach for better discrimination between film slicks and "look-alikes" is developed using information about variations of wave intensity at several wavelengths in a cm-dm range of wind wave spectrum. The wavelengths are thus selected so that films and "look-alike" phenomena would manifest themselves in radar images in different ways at least at one of the selected wavelengths. The used wind wave model takes into account the influence of near surface wind, wave damping due to elastic films (if the latter are present on the surface) and nonlinear wind wave interactions. Analysis of the influence of film parameters and observation conditions on the depression of NRCS contrast and estimation of characteristics of potential "look-alikes" leading to the same depression effect are carried out. The used radar model takes into account Bragg and specular scattering mechanisms, the latter is usually small compared to the Bragg mechanism at moderate incidence angles for "non-slick" surface, but gives noticeable contribution to radar backscattering from slick areas when cm-scale ripples are strongly depressed.

An experimental verification of the main provisions of the new approach was done during some field experimental campaigns. Firstly, results of recent field experiments on radar probing of film slicks using satellite synthetic aperture radar TerraSAR-X and X-band scatterometer mounted on board a research vessel are compared with the theoretical calculations. The experiments were carried out with surfactant films with pre-measured physical parameters at low to moderate wind conditions. Some surfactants with different parameters were used. Satisfactory agreement between model and experiment is demonstrated and the information on NRCS depression can be used for better interpretation of signatures appeared in radar imagery of the sea surface. Secondly, some results of old field experiments using optical devices are analyzed, too. The optical spectrum analyzer developed in IAP RAS was allowed to register up the dramatic difference in the spectral contrasts of the film and wind slicks in dm-cm wave range, which are in satisfactory agreement with the theoretical calculation using the model mentioned above.

Thus recognition capabilities of different near-surface phenomena are clarified and the best conditions to their discriminations are determined. The work was supported by the Russian Ministry of Education and Science (Contract No. 14.607.21.0055, RFMEFI60714X0055), RFBR (Project 14-05-00876).

9638-8, Session 2

Application of compressive sensing to radar altimeter design

Yunhua Zhang, Xiao Dong, Wenshuai Zhai, Ctr. for Space Science and Applied Research (China)

Satellite altimeter has been proven to be the major microwave sensor which can accurately measure the range between the satellite and the average sea surface, and after precise orbital determination of the satellite, then the average sea surface height (SSH) with centimeter level accuracy can be retrieved. There is a common problem for satellite altimeters, i.e. the signal bandwidth for ocean surface measurement and that for continent surface measurement have to be different. This is because continent surfaces vary largely from where to where, but the ocean surfaces are quite smooth, in order to keep a robust tracking, the signal bandwidth for continent surfaces should be smaller so as to get larger time window, while the signal bandwidth for ocean surfaces can be much larger for only smaller time window is needed. If we want to increase the sampling time window (STW) without reducing the signal bandwidth, then the increase of data rate is unavoidable and this will lead to unrealizable data transmission.

In this paper, we propose to apply the compressive sensing (CS) technique to the design of satellite radar altimeter. We does not need to switch to a smaller signal bandwidth when the surface changes from ocean to continent, but just increase the STW and keep the same data rate as that for ocean observation so as to keep a robust tracking.

The rising slope of the echo waveform received and processed by an altimeter contains important information about the sea surface, e.g. the larger the slope of the waveform, means the smoother the sea surface. Besides, the half-power point of the slope refers to the range information. For satellite altimeter, due to the rising slope just occupies fewer range bins compared with the whole range bins illuminated by the long pulse signal, i.e. the signal is sparse in this sense, thus compressive sensing technique is applicable. In this sense, the echo data is sparsely sample according to a random scheme, so the data amount is reduced correspondingly. Altimeter echoes are simulated and the waveforms are constructed by using the traditional method as well as by CS method, they are very well agreed with each other. The advantage of using CS is that we can increase the sampling time window without increasing the data, thus the tracking capability can be enhanced without sacrificing the resolution. As we know, the sparse signal reconstruction by CS is very time consuming, it is not appropriate to apply CS to reconstructing the echo waveform of altimeter in real time. Fortunately, Fast Fourier Transformation (FFT) is still applicable to obtain the echo waveform by just zero-padding to the absent samples (the positions are exactly known) although the noise floor of the reconstructed waveform becomes larger. So, for this altimeter FFT based algorithm is used for tracking the slope of echo waveform with subsampled and recorded data, in the ground data processing system, CS is used to reconstruct the exact waveform which will be used for follow on processing.

9638-9, Session 3

Multiband algorithm for the estimation of chlorophyll concentration in the Chesapeake Bay

Alexander Gilerson, The City College of New York (United States); Michael Ondrusek, NOAA National Environmental Satellite, Data, and Information Service (United States); Maria Tzortziou, Robert Foster, Ahmed El-Habashi, The City College of New York (United States); Surya Prakash Tiwari, Red Sea Research Ctr. (Saudi Arabia); Samir Ahmed, The City College of New York (United States)

Chlorophyll-a concentration [Chl], one of the main products retrieved from the ocean color satellite imagery, is usually estimated from the ratio of reflectances in the blue-green bands which provide reasonable accuracy for open ocean waters though much less so in coastal waters because of contamination of the blue and green reflectance signals from CDOM absorption and mineral scattering.

Recent advances in the development of atmospheric correction models over coastal zones have inspired further development of retrieval algorithms for turbid productive waters. One of such approaches is based on the two- or three band ratio algorithms in the red/NIR part of the spectrum, which require 665, 708, 753 nm bands (or similar). Recent studies by many research groups around the world showed that relatively universal two- and three bands algorithms developed by us work well in various waters in the US, Israel, China, Russia, etc. The critical 708 nm band for these algorithms is available on MERIS and is expected to be on Sentinel 3 but is not available on MODIS and VIIRS sensors, which limits applications of this approach.

The VIIRS band set in the visible -NIR part of the spectrum includes 410, 443, 488, 551, 671 and 745 nm bands. Our recent work on validation of the VIIRS sensor based on data from our Long Island Sound Coastal Observatory (LISCO) located in coastal Western Long Island Sound, showed that VIIRS and MODIS remote sensing reflectance data are often associated with significant errors at 412 and 443nm bands, so preferably these bands should be excluded from the algorithms for coastal waters.

We report on one of the alternative approaches which was recently explored by us where an unusual combination of the 745nm band with blue-green-red bands was the basis for the new algorithms. Several multi-band algorithms which include ratios Rrs488/Rrs551, Rrs488/Rrs671, Rrs551/Rrs671 together with Rrs671/Rrs745 ratio were developed with the main focus on the Chesapeake Bay (USA) waters. Algorithms were tested on the specially developed synthetic datasets, well representing the main relationships between water parameters in the Bay taken from the NASA NOMAD database and available literature, and field data collected by our group during a 2013 campaign in the Bay, as well as NASA SeaBASS data from other groups and matchups between satellite imagery and water parameters measured by the Chesapeake Bay program. Our results demonstrate that the coefficient of determination can be as high as R2 = 0.78-0.93 for the new algorithm in comparison with R2 = 0.58-0.62 for the standard OC3V algorithm for the same field dataset.

Substantial improvement was also achieved by applying a similar approach (inclusion of Rrs671/Rrs745 ratio) for MODIS and VIIRS matchups especially when the time difference between satellite and in situ data was reduced to less than 1

hour. Expansion of the algorithms to other coastal waters is considered.

9638-10, Session 3

Neural network algorithms for retrieval of Harmful Algal Blooms in the West Florida Shelf from VIIRS satellite observations and comparisons with other techniques, without the need for a fluorescence

Ahmed El-Habashi, Samir Ahmed, The City College of New York (United States)

We describe a new approach that uses the Ocean Color Remote Sensing Reflectance readings (OC Rrs) available from existing Visible Infrared Imaging Radiometer Suite (VIIRS) satellite channels to detect and retrieve Karenia brevis (KB) Harmful Algal Blooms (HABs) that frequently plague the coasts and beaches of the West Florida Shelf (WFS), often resulting in ecological and health concerns and impacting tourism and local economies. Effective KB HAB detection and tracking approaches are needed for use with VIIRS so that NOAA can extend its HAB monitoring capabilities to VIIRS and continue to support local authorities in their forecasting of beach conditions, including health warnings etc. Unfortunately, VIIRS, unlike MODIS, does not have a 678 nm channel to detect chlorophyll fluorescence, which is used in fluorescence height (FLH) algorithm or in the Red Band Difference algorithm, both of which, when coupled with the known low backscatter characteristics of the KB microorganism, have been shown to help in effectively detecting and tracking KB HABs in the WFS. To overcome the obstacle that this lack of a fluorescence channel on VIIRS poses, the alternative approach, described here, bypasses the need for measuring chlorophyll fluorescence, and is therefore important for enabling the extension of KB HABs satellite monitoring capabilities in the WFS to VIIRS. The essence of the approach uses neural network (NN) algorithms, previously reported by us, which we have developed and trained, using a wide range of suitably parametrized synthetic data typical of coastal waters, to form a multiband inversion algorithm which models the relationship between Rrs values at the 486, 551 and 671nm bands that are available on VIIRS (and the 488, 547 and 667nm bands available on MODIS) against the values of phytoplankton absorption (aph), CDOM absorption (ag), non-algal particles (NAP) absorption (aNAP) and the particulate backscattering bbp coefficients, all at 443nm. This then permits, in principal, retrievals of these parameters from VIIRS and MODIS observations, without the need for Rrs retrievals at the chlorophyll fluorescence band (at 678 nm) and, which because it (the fluorescence band) does not exist on VIIRS, provided the impetus for this work. The retrieved aph , can in turn be converted to an equivalent chlorophyll concentration [Chl] by dividing retrieved aph by the specific phytoplankton absorption, which is region specific, and can be determined from previous in-situ sampling observations. Then making use of the fact, used in fluorescence height and red band difference techniques, that KB is known to have low scattering properties (e.g at 551nm) it is shown that suitable threshold criteria can be applied to the both (aph) retrieved by the NN algorithm from the VIIRS 486, 551 and 671nm bands, and which is proportional to chlorophyll concentration [Chl] together with the VIIRS measured Rrs backscatter values and use these threshold criteria to effectively detect the intensity of KB HAB blooms in the WFS and to delineate and track them. These retrievals are then compared with [Chl] retrievals from VIIRS using the blue-green OC3 algorithm and again combined with the same 551 nm backscatter measurements to apply threshold criteria and effectively detect and track KB HAB blooms.

9638-11, Session 3

Detection of ocean thermal fronts using thermal IR imagery

Irina Gladkova, Fazlul Shahriar, The City College of New York (United States); Alexander Ignatov, NOAA National Environmental Satellite, Data, and Information Service (United States); Yury Kihai, Global Science & Technology, Inc. (United States)

Customarily, ocean front detection from satellite observations is done on cloud- and ice-free sea surface temperature (SST) imagery. However, cloud and ice masks may not be fully accurate. As a result, thermal fronts derived from “cloud-cleared” IR imagery, may include, in addition to ocean features, also ocean/cloud and cloud/cloud boundaries. More importantly, false alarms (i.e. when ocean features are mistakenly screened out as cloud) often occur, preventing identification of thermal fronts under masked area. We explore an approach that does not require pre-computed clear-sky and sea-ice masks, but rather performs the search on the full water domain and relies on large scale statistics of thermal IR measurements and derived SST field, and their patterns including gradients, connectivity, bimodality of the SST distribution in the vicinity of the thermal front, etc. Ocean thermal fronts are manifested in gradient of various strength, length and width. To account for scale variations, we use several front enhancements pre-processing procedures. Our multi-scale approach is based on derivative of Gaussian kernel at various scales as well as eigenvalues of the Hessian matrix. The algorithm has been tested on the SST product derived from the Visible Infrared Imager Radiometer Suite (VIIRS) onboard the Suomi National Polar-orbiting Partnership (S-NPP) satellite launched in October 2011, in full VIIRS swath including the bow-tie regions, and will be also applied to the data of the Moderate Resolution Imaging Spectroradiometer (MODIS) onboard Terra and Aqua satellites, and Advanced Very High Resolution Radiometers (AVHRR) onboard NOAA and Metop satellites.

9638-13, Session 3

Revealing the influence of various factors on concentration and spatial distribution of suspended matter based on remote sensing data

Olga Y. Lavrova, Space Research Institute (Russian Federation); Dmitry M. Soloviev, Marine Hydrophysical Institute (Russian Federation); Marina I. Mityagina, Alexey Y. Strochkov, Tatiana Y Bocharova, Space Research Institute (Russian Federation)

The report provides results of the research on the influence of various hydrometeorological factors on distribution of suspended matter carried by river flows into the sea. The research is based on remote sensing data received in various bands of electromagnetic spectrum. Evaluation of suspended matter concentration and integral estimation of water turbidity were performed based to the data from sensors MODIS, MERIS and OLI. In case of MODIS data suspended matter distribution area was determined by means of color-synthesized satellite images (combination of spectral bands 1-4-3 (RGB)). The maps of Sea Surface Temperature (SST), Chlorophyll-a Concentration (CHL) and Water Leaving Radiance (WLR) were generated by the standard NASA algorithms with translation in actual values of Total Suspended Matter (TSM). For MERIS Envisat data the recommended ESA algorithms, integrated into appropriate software suites, were used to evaluate concentration of CHL and TSM. The distinctive characteristic of MERIS spectrometer is the possibility to calculate TSM concentration in absolute units (g/m3) and compile maps with spatial resolution of 260 m. On the grounds of double-band data from TIRS Landsat-8 SST magnitudes were determined with maximum spatial resolution (50 meters and higher). The special research was

conducted with OLI Landsat-8 sensors and with Hyperion and HICO hyper-spectrometers, it was aimed at finding spectral bands and bands combinations that would be the most informative for revealing suspended matter and obtaining parameters equivalent to its concentration.

The examined zones were the plumes of Vistula River, Danuba River and mountain rivers of Georgia. Results of satellite data processing were used for detecting the impact of various natural factors, such as precipitation, rivers flows, wind-driven water circulation and vortex activity, on suspended matter proliferation. Water circulation is known to determine suspended solids distribution in surface sea layer. Discharge flow of river waters rich in suspended matter is spread under the influence of coastal currents, functioning as a kind of their unique tracer agent. Mapping of zones characterized by maximum propagation of suspended solids in different seasons was performed for the examined areas.

Two case studies are considered in the report: proliferation of the Vistula River plumes in May, 2010, and propagation of the Vistula Lagoon plume in July-August of 2014. One of the most extensive and most damaging floods in the last 100 years occurred in May 2010 on the River Vistula, the longest river flowing into the Baltic Sea (Zaj?czkowski1 et al, 2010). Moreover, there is provided comparison analysis of the results obtained on the basis of data from MERIS, ASAR Envisat, MODIS Aqua and ETM+ Landsat-7 with results of in-situ measurements, represented in this article.

In July-August of 2014 we conducted field measurements in the south-eastern part of the Baltic Sea near the Baltic Channel from a small boat using CTD probes and Acoustic Doppler Current Profilers (ADCP). Mainly clear weather that lasted for more than 2 weeks in late July – early August, 2014, allowed us to track proliferation of turbid desalinated waters flowing from the Vistula Lagoon in the south-eastern part of the Baltic Sea in visible spectrum images daily received from MODIS Terra/ Aqua and Landsat-7/8 sensors. Hydrological structure measurements, conducted from small vessels simultaneously with satellite observations in the Vistula Lagoon, the Baltic Channel and coastal area of the Baltic Sea, revealed that the influence of the plume (distribution area of which was determined through satellite images) can be noticed in temperature and salinity fields as well as in sound signal scattering, most likely resulting from water turbidity. Plume waters from the Channel hardly reached the depth more than 5 m.

Joint analysis of satellite data and numerical modeling results made it possible to estimate the wind contribution to the plume propagation. Wind turned out to be of greatest importance as it forms the field of basic currents in this region. However, unless circulation processes dominating during the observation period are considered, numerical simulation results can substantially differ from satellite data.

The study was completed with partial financial support from The Russian Scientific Foundation grant # 14-17-00555.

9638-14, Session 3

Optical multispectral remote sensing of ocean surface

Victor I. Titov, Institute of Applied Physics (Russian Federation)

The principles of optical multispectral remote sensing of ocean surface from UV to IR are discussed. The mechanism of sea wave visibility taking into account sky radiance and own radiance of sea surface for various angles of incidence is investigated. The deposit of subsurface backscattered radiance to the radiance of sea surface is calculated also. The measured and modeled sky radiance distribution was used in the calculations.

The principles for retrieving of sea roughness characteristics, pollutions of sea surface and near surface winds by its manifestations on waved surface under grazing angles based on the comparison of measured and modeled surface radiance is discussed.

A set of original optical multispectral devices for recoding RTI images using linear arrays of CCD-photodiodes was created. The set consist from synchronized optical receivers with narrow band optical interference filters. It is possible to form images of sea surface for various optical wave lengths from UV to near IR with spectral resolution about 5 nm -10 nm.

The methods are verified in natural conditions using developed set of multispectral optical devices. The experiments were conducted simultaneously with the optical set and the buoy equipped with wave-recording gauge and wind sensors placed on various height above sea level.

9638-15, Session 4

Surface and subsurface optical and acoustic sensing in support of coastal waterway dredging

Charles R. Bostater Jr., Florida Institute of Technology (United States)

Airborne, Satellite and In-Situ optical and acoustical imaging provides a means to characterize surface and subsurface water conditions in shallow marine systems. An important research topic to be studied during dredging operations in harbors and navigable waterways is the movement or fluid motion of fluidized bottom material before, during and after dredging operations. The fluid movement of the surficial sediment materials in the form of flocs and mud is important to estimate in order to model the transport of solids material during dredging operations. Movement of highly turbid bottom material, sometimes called near bottom nephelomtric layers, reduces the penetration of light reaching the water bottom and benthic living marine resources, particularly submerged aquatic vegetation. Monitoring and measurement systems used Indian River Lagoon are discussed. Newly developed passive SONDES and subsurface imaging are described. Methods and techniques for quantifying the mass density flux of particulate matter demonstrate the use of multiple sensor systems for environmental monitoring to assess directional reduction of fluid solids movement and motion in terms of flux density. Airborne imaging of dredge sites provide wide area surveillance during these activities.

The passive SONDES are used to measure horizontal and vertical mass flux (mass/area x time). These passive SONDES can be directionally oriented and are deployed during optical imaging of the near bottom flocs, particles and colloidal material motion using subsurface time dependent imaging. The newly developed imaging system allows one to estimate particle velocity. These newly developed instrument systems are deployed with simultaneous acoustic sensors that record acoustic bottom reflections. Airborne imagery collected during the dredging operations allow for wide area monitoring for subsurface feature detection.

9638-16, Session 4

Subpixel mapping of water boundaries using pixel swapping algorithm (case study: Tagliamento River, Italy)

Milad Niroumand Jadidi, Alfonso Vitti, Univ. degli Studi di Trento (Italy)

Taking the advantages of remotely sensed data for mapping and monitoring of water boundaries is of particular importance in many different management and conservation activities. Imagery data are classified using automatic techniques to produce maps entering the water bodies analysis chain in several and different points. Very commonly, medium or coarse spatial resolution imagery is used in studies of large water bodies. Data of this kind is affected by the presence of mixed pixels leading to very outstanding problems, in particular when dealing with boundary pixels. As a matter of fact, a considerable amount of uncertainty in the presence of mixed

pixels inescapably occurs when conventional hard classifiers (e.g., maximum likelihood, support vector machines) are applied.

In this study, Linear Spectral Mixture Model (LSMM) is used to estimate the proportion of water in the boundary pixels. In this way, firstly by applying an unsupervised clustering the water body is identified approximately and a buffer area considered ensuring the selection of entire boundary pixels. Endmembers are derived from the image using Pixel Purity Index (PPI) and then LSMM is applied on this buffer region to estimate the fractional maps. However, resultant output of LSMM does not provide a sub-pixel map corresponding to water abundances in boundary pixels. To tackle with this problem, pixel swapping algorithm is used to allocate sub-pixels within mixed pixels in such a way to maximize the spatial proximity of sub-pixels and pixels in the neighborhood. Towards this end, each pixel is divided into nine sub-pixels. Sub-pixels are then arranged using the proportions obtained from LSMM. This leads to a synthetic amplification of the spatial resolution with a Zoom Factor (ZF) of 3.

The boundaries of a part of Tagliamento River (Italy) is mapped in sub-pixel resolution (10m) using a 30m Landsat image. To evaluate the proficiency of the proposed approach for sub-pixel boundary mapping, the image is also classified using a conventional hard classifier (maximum likelihood). A high resolution image of the same area is also classified with the maximum likelihood classifier and used as a reference for accuracy assessment. According to the results, sub-pixel map shows about 8 percent higher overall accuracy than hard classifier and fits very well in the boundaries with the reference map. Although this method is applied for mapping of river boundaries, it is applicable for other large water bodies such as shoreline detection issues.

9638-18, Session 4

Estimation of river discharge based on remote sensing of a river plume

Alexander Osadchiev, P.P. Shirshov Institute of Oceanology (Russian Federation)

Earth-observing satellites provide effective instruments for global monitoring of coastal zones adjacent to river estuaries. Particularly they can be used to identify buoyant river plumes formed by interaction between river and sea waters. The resulting spatial characteristics of a plume can be employed as indicators of the related river discharge.

A new method of reconstructing the volume of river discharge using satellite imagery and numerical modelling is presented in this work. Firstly, the spatial surface spread of the plume generated by the considered river discharge is identified using satellite imagery of the coastal zone adjacent to the river estuary. Secondly, the inverse problem of obtaining the discharge rate of the river (or rivers) that formed the examined plume is solved. For this purpose a series of numerical simulations of the river runoff spread are performed under a wide range of the prescribed external forcing conditions (e.g., wind, coastal circulation, tides, waves) and river discharge parameters (e.g., river inflow velocity, river discharge rate). We assume that the results of river plume simulation performed under real forcing conditions (including the sought-for real discharge), i.e., “modeled” plume, will be similar to the plume observed in satellite image, i.e., “satellite” plume. Varying the configuration parameters of the model we can improve the accordance between the model results and the satellite image to achieve the prescribed level of accuracy. As a result we will obtain the approximate value of the river discharge as one of the parameters of the best-fitting configuration.

The developed method was applied for several rivers feeding the Eastern part of the Black Sea. Identification of spatial structures of the studied river plumes was based on surface distribution maps of yellow substance, colored dissolved organic matter and chlorophyll a were retrieved from MERIS/EnviSat satellite imagery using MERIS Case-2 Regional water processing module. The model was verified against the in situ measurements and showed good capability to produce realistic results. Then using the model we evaluated the influence of the short-term and annual precipitation conditions on the variability of river discharge inflowing from the Russian coast to the Black Sea.

9638-19, Session 4

Coastal water quality monitoring using geostationary ocean color imager (GOCI) satellite data and machine learning approaches

Eunna Jang, Jungho Im, Sunghyun Ha, Ulsan National Institute of Science and Technology (Korea, Republic of)

Coastal regions are important to human society as they provide various resources and marine transportation. Due to various human activities, coastal pollution has become one of serious environmental problems in the world. In particular, the vast industrial complexes have been developed in coastal areas of South Korea and large quantities of industrial wastewater and sewage from them flow into the ocean through the coast. In order to monitor water quality especially in coastal areas, many countries have developed their own water quality index (WQI) using in situ measurements. While a water quality index itself is a controversial term as some scientists argue that an index cannot represent water quality, it is a very effective way to manage coastal regions using such an index. The current ecology-based standard on ocean water quality in South Korea considers water depth, tide, and current to identify five ocean divisions. The standard consists of five levels from the best (i.e., excellent) to the worst (very poor) based on WQI, which is a function of five water quality-related factors. The factors are chlorophyll concentration (Chl-a), secchi disk depth (SD), bottom dissolved oxygen (DO), dissolved inorganic nitrogen (DIN), and dissolved inorganic phosphorus (DIP). While in situ measurements can be used to calculate accurate WQI, it is difficult to provide spatially continuous coverage of such an index. Thus, satellite-based WQI estimation could be an alternative as some satellite sensors collect data over vast areas at very high temporal resolution (~hours).

The purpose of this study was to monitor coastal WQI using Geostationary Ocean Color Imager (GOCI) satellite data and machine learning approaches in Korean peninsula. GOCI, launched in June 2010, is the first geostationary ocean color observation satellite in the world. GOCI collects data hourly for 8 hours a day at 6 visible and 2 near-infrared bands at a 500 m resolution with 2,500 x 2,500 km square around Korean peninsula. In this study, two schemes were examined to monitor coastal WQI from GOCI data. The first scheme was to estimate the four water quality-related factors (Chl-a, SD, DIN, and DIP excluding DO) using GOCI-derived radiance data and their ratios based on machine learning approaches, and the second scheme was to directly estimate WQI values calculated from in situ measurements. In situ measurements of the water-quality-related factors collected in coastal areas of South Korea from May to September between 2011 and 2013 were used to implement two schemes. Three machine learning approaches including random forest, support vector regression, and Cubist were used to estimate water quality-related factors and WQI. Results showed that scheme 2 produced relatively higher accuracy than scheme 1, implying that it would be possible to operationally monitor coastal WQI using GOCI data. Among the three machine learning approaches, random forest outperformed the other two models regardless of the scheme applied. Relative variable importance identified by model was examined, and spatiotemporal variations of GOCI-derived coastal WQI were also explored.

Conference 9639: Sensors, Systems, and Next-Generation Satellites

SPIE. REMOTE SENSING

Monday - Thursday 21–24 September 2015

Part of Proceedings of SPIE Vol. 9639 Sensors, Systems, and Next-Generation Satellites XIX

9639-1, Session 1

Overview of ESA Earth observation missions *(Invited Paper)*

Roland Meynart, European Space Research and Technology Ctr. (Netherlands)

No Abstract Available

9639-2, Session 1

The flexible combined imager onboard MTG: from design to calibration

Yannig Durand, Pascal Hallibert, Mark Wilson, Mounir Lekouara, Semen Grabarnik, Donny M. Aminou, Paul Blyhte, European Space Agency (Netherlands); Bruno Napierala, Jean-Louis Canaud, Olivier Pigouche, Julien Ouaknine, Bernard Verez, Thales Alenia Space (France)

The Meteosat Third Generation (MTG) Programme is being realised through the well-established and successful Cooperation between EUMETSAT and ESA. It will ensure the future continuity with, and enhancement of, operational meteorological (and climate) data from Geostationary Orbit as currently provided by the Meteosat Second Generation (MSG) system.

The industrial Prime Contractor for the Space segment is Thales Alenia Space (France) with a core team consortium including OHB-Bremen (Germany) and OHB-Munich (Germany). This contract includes the provision of six satellites, four Imaging satellites (MTG-I) and two sounding satellites (MTG-S), which will ensure a total operational life of the MTG system in excess of 20 years.

Technically a clear baseline has now been established for both MTG-I and MTG-S satellites, and confirmed through rigorous Preliminary Design Review (PDR) process that was formally concluded during 2013. Dedicated reviews have been held for all the main elements including the core instruments (Flexible Combined Imager (FCI) and Infrared Sounder (IRS)), the Platform (which is largely common for the two satellites), the Lightning Imager (LI) and the MTG-I and MTG-S satellites as a whole. The satellites and instruments are at the moment in preparation for the Structural and Thermal Models (STM).

The FCI is designed to provide images of the Earth every 10 to 2.5 minutes in 16 spectral channels between 0.44 and 13.3 ?m, with a ground resolution ranging from 0.5 km to 2 km. The on-board calibration is based on the use of a Metallic Neutral Density (MND) filter for VIS/NIR channels and a blackbody for the IR channels.

This paper will introduce the overall FCI instrument design and its calibration concept covering VIS/NIR and IR domains and will describe how the use of the MND made it possible to correct efficiently the radiometric medium and long term drifts of the IR3.8 channel. This paper will also show how this calibration process using the MND has enabled to explore further the radiometric correction applied to the other IR channels.

9639-3, Session 1

CNES Cal/Val expertise centre for Sentinel-2 in orbit tests (TEC-S2): architecture and data processing

Julien Nosavan, Thierry Trémas, Jean-Louis Raynaud, Ctr. National d'Études Spatiales (France)

In partnership with the European Commission and in the frame of the Copernicus program, the European Space Agency (ESA) is developing the Sentinel-2 optical imaging mission devoted to the operational monitoring of land and coastal areas.

The Sentinel-2 mission is based on a satellites constellation offering a unique combination of global coverage with a wide field of view (290km), a high revisit (5 days with two satellites), a high spatial resolution (10m, 20m and 60m) and multi-spectral imagery (13 spectral bands in visible and shortwave infra-red domains).

The Centre National d'Etudes Spatiales (CNES) supports ESA/ESTEC to insure the Calibration/Validation commissioning phase during the first three months in flight, providing refined Ground Image Processing Parameters and leaving then the floor to the ESA operational processing center after the commissioning phase.

This paper provides an overview of the Technical Expertise Center Sentinel-2 (TEC-S2) which is the CNES expertise center in charge of the Calibration/Validation activities during the In Orbit Tests.

It describes first the functional breakdown and the IT architecture put in place regarding to Sentinel 2 calibration needs and CNES organization. A focus is made on the data processing in terms of volume and performances with a good opportunity for parallelization related to the structure of S2 images products (12 detectors to cover the 290 km swath and 13 spectral bands).

Then as a second step, it will provide the first feedback on TEC-S2 operation experience and in particular the first results on data processing performances.

9639-4, Session 1

Sentinel-2 radiometric image quality commissioning: first results

Sophie Lachérade, Vincent Lonjou, Ctr. National d'Études Spatiales (France); Morgan Farges, Capgemini Technology Services (France); Philippe Gamet, Sébastien Marcq, Jean-Louis Raynaud, Thierry Trémas, Ctr. National d'Études Spatiales (France); Philippe Martimort, Claudia Isola, François Spoto, European Space Research and Technology Ctr. (Netherlands)

In partnership with the European Commission and in the frame of the Copernicus program, the European Space Agency (ESA) is developing the Sentinel-2 optical imaging mission devoted to the operational monitoring of land and coastal areas.

The Sentinel-2 mission is based on a satellites constellation deployed in polar sun-synchronous orbit. Sentinel-2 will offer a unique combination of global coverage with a wide field of view (290km), a high revisit (5 days with two satellites), a high spatial resolution (10m, 20m and 60m) and multi-spectral imagery (13 spectral bands in visible and shortwave infra-red domains). The first satellite, Sentinel-2A, is planned to be launched in June 2015.

The Sentinel-2A Commissioning Phase starts immediately after the Launch and Early Orbit Phase and continues until the In-Orbit Commissioning Review which is planned three months after the launch.

The Centre National d'Etudes Spatiales (CNES) supports ESA/ESTEC to insure the Calibration/Validation commissioning phase during the first three months in flight. This paper provides first an overview of the Sentinel-2 system and a description of the products delivered by the ground segment associated to the main radiometric specifications to achieve.

Then the paper focuses on the preliminary radiometric results obtained during the in-flight commissioning phase. The radiometric methods and calibration sites used in the CNES image quality center to reach the specifications of the

sensors are described. A status of the Sentinel-2A radiometric performances at the end of the first three months after the launch is presented. We will particularly address in this paper the results in term of absolute calibration, pixel to pixel relative sensitivity and MTF estimation.

9639-5, Session 1

Sentinel-2/MSI absolute calibration: first results

Vincent Lonjou, Sophie Lachérade, Bertrand Fougnie, Philippe Gamet, Sébastien Marcq, Jean-Louis Raynaud, Thierry Trémas, Ctr. National d'Études Spatiales (France); Philippe Martimort, Claudia Isola, François Spoto, European Space Research and Technology Ctr. (Netherlands)

Sentinel-2 is an optical imaging mission devoted to the operational monitoring of land and coastal areas. It is developed in partnership between the European Commission and the European Space Agency. The Sentinel-2 mission is based on a satellites constellation deployed in polar sun-synchronous orbit. It will offer a unique combination of global coverage with a wide field of view (290km), a high revisit (5 days with two satellites), a high resolution (10m, 20m and 60m) and multi-spectral imagery (13 spectral bands in visible and shortwave infra-red domains).

CNES is involved in the instrument commissioning in collaboration with ESA. This paper reviews all the techniques that will be used to insure an absolute calibration of the 13 spectral bands better than 5% (target 3%), and will present the first results if available. First, the nominal calibration technique, based on an on-board sun diffuser, is detailed. Then, we show how vicarious calibration methods based on acquisitions over natural targets (oceans, deserts, and Antarctica during winter) will be used to check and improve the accuracy of the absolute calibration coefficients. Finally, the verification scheme, exploiting photometer in-situ measurements over Lacrau plain, is described. A synthesis, including spectral coherence, inter-methods agreement and temporal evolution, will conclude the paper.

9639-6, Session 2

The NASA Earth Science Flight Program: an update *(Invited Paper)*

Steven P. Neeck, NASA Headquarters (United States)

Earth's changing environment impacts every aspect of life on our planet and climate change has profound implications on society. Studying Earth as a single complex system is essential to understanding the causes and consequences of climate change and other global environmental concerns. NASA's Earth Science Division (ESD) shapes an interdisciplinary view of Earth, exploring interactions among the atmosphere, oceans, ice sheets, land surface interior, and life itself. This enables scientists to measure global and climate changes and to inform decisions by government, other organizations, and people in the United States and around the world. The data collected and results generated are accessible to other agencies and organizations to improve the products and services they provide, including air quality indices, disaster prediction and response, agricultural yield projections, and aviation safety. ESD's Flight Program provides the space based observing systems and infrastructure for mission operations and scientific data processing and distribution that support NASA's Earth science research and modeling activities. The Flight Program currently has 21 operating Earth observing space missions, including the recently launched Global Precipitation Measurement (GPM) mission, the Orbiting Carbon Observatory-2 (OCO-2), the Soil Moisture Active Passive (SMAP) mission, and the International Space Station (ISS) RapidSCAT and Cloud-Aerosol Transport System (CATS) instruments. The ESD has 22 more missions and instruments planned for launch over the next decade. These include first and second tier missions from the 2007 Earth Science Decadal Survey, Climate Continuity missions and selected instruments to assure availability of key climate data sets, operational missions to ensure sustained land imaging provided by the Landsat system, and small-sized competitively selected orbital missions and instrument missions of opportunity belonging to the Earth Venture (EV) Program. Some examples are the NASA-ISRO Synthetic Aperture Radar (NISAR), Surface Water and Ocean Topography (SWOT), ICESat-2, SAGE III on ISS, Gravity Recovery and Climate Experiment Follow On (GRACE FO), Tropospheric Emissions: Monitoring of Pollution (TEMPO), Cyclone Global Navigation Satellite System (CYGNSS), ECOsystem Spaceborne Thermal Radiometer Experiment on Space Station (ECOSTRESS), and Global Ecosystem Dynamics Investigation (GEDI) Lidar missions. An overview of plans and current status will be presented.

9639-7, Session 2

Landsat 8: status and on-orbit performance

Brian L. Markham, NASA Goddard Space Flight Ctr. (United States); Julia A. Barsi, NASA Goddard Space Flight Ctr. (United States) and Science Systems and Applications, Inc. (United States); Ron A. Morfitt, U.S. Geological Survey (United States); Mike Choate, Stinger Ghaffarian Technologies, Inc; Contractor to USGS/EROS (United States); Matthew Montanaro, Center for Imaging Science, Rochester Institute of Technology (United States); Terry Arvidson, Lockheed Martin, Goddard Space Flight Center (United States); James R Irons, NASA Goddard Space Flight Ctr (United States)

Landsat-8 has been operating successfully on-orbit since February 2013. It has two Earth imaging sensors on-board: the OLI which covers the visible, near-IR and SWIR spectral regions in 8 spectral bands at 30 meter resolution and one panchromatic band at 15 meter resolution; and TIRS which has two thermal spectral bands at 100 meter resolution. The OLI instrument has been extremely stable on-orbit radiometrically and geometrically and has exceeded the vast majority of the performance requirements. Likewise TIRS has been very stable on orbit and meets most of its performance requirements. The only exceptions for TIRS is some out-of-field ghosts which impact the absolute calibration and flat fielding of the TIRS data. Algorithms are being developed to reduce the impact of these ghosts on the data quality.

TIRS also experienced an anomaly in the on-oboard electronics associated with the encoder that provides the pointing angle for the TIRS scene select mirror. This resulted in a switch to the TIRS side B electronics in March 2015.

9639-8, Session 2

The Global Ecosystem Dynamics Investigation-GEDI

Ralph Dubayah, Univ. of Maryland, College Park (United States); Scott Goetz, Woods Hole Research Ctr. (United States); J. Bryan Blair, NASA Goddard Space Flight Ctr. (United States)

Spaceborne lidar has been identified as a key technology by the international ecosystem science community because it enables accurate estimates of canopy structure and biomass and forms the basis for fusion approaches that extend the capabilities of existing and planned optical and radar missions. The Global Ecosystems Dynamics Investigation Lidar (GEDI Lidar) was recently selected by NASA's Earth Ventures Instrument (EVI) program. The scientific goal of GEDI is to characterize the effects of changing climate and land use on ecosystem structure and dynamics to enable radically improved

quantification and understanding of the Earth's carbon cycle and biodiversity. From its vantage point on International Space Station, GEDI Lidar provides high-resolution observations of forest vertical structure and addresses three, core science questions: What is the aboveground carbon balance of the land surface? What role will the land surface play in mitigating atmospheric CO2 in the coming decades? How does ecosystem structure affect habitat quality and biodiversity? GEDI informs these science questions by making over 15 billion lidar waveform observations per year. These canopy measurements are then used to estimate biomass and to quantify changes in biomass resulting from disturbance and recovery. GEDI further marries ecosystem structure from lidar with ecosystem modeling to predict the sequestration potential of existing forests and to evaluate the impact of policy-driven afforestation and reforestation actions on sequestering additional carbon. Lastly, GEDI's observations of ecosystem structure provide a mapping of critical habitat metrics at the fine scales required for understanding the patterns, processes, and controls on biodiversity and habitat quality. The selection of GEDI Lidar, when combined with the rapid advancement of new radar missions and the availability of long-term land cover archives from passive optical sensors, ushers in an exciting new era of land surface imaging with far ranging consequences for forest science.

9639-9, Session 2

Earth radiation budget continuity observations: the Radiation Budget Instrument (RBI)

Kory J. Priestley, NASA Langley Research Ctr. (United States); Mohan Shankar, Science Systems and Applications, Inc. (United States); Anum Barki, NASA Langley Research Ctr. (United States); Elena M. Georgieva, NASA Goddard Space Flight Ctr. (United States); Melissa Yang, Barry Dunn, NASA Langley Research Ctr. (United States)

Radiation Budget Instrument (RBI) will be one of five instruments hosted aboard the NOAA JPSS-2 spacecraft; a polar-orbiting sun-synchronous satellite in Low Earth Orbit (LEO). The primary RBI mission goals and objectives are to measure the reflected sunlight and thermal radiation emitted by the Earth and provide transparent product consistency to the CERES data sets. RBI will provide configurability and capability to enable swath (elevation scanning cross-track), bi-axial (both elevation and azimuth scanning), and Earth pointing modes of operation. RBI also operates in a calibration mode, where various internal calibration sources, the moon, and a diffuse solar image are viewed. Operators can execute scans in two ways via Ground station communication. Commands may be initiated by a defined execution sequence or from upload timelines for autonomous execution sequences. There are non-operational modes, including Survival, System Boot, Safe Hold, Idle, Outgas, Diagnostic, for commissioning, dealing with anomalies, and maintenance.

The RBI consists primarily of a Cross-Track Scan Module (CSM), Azimuth Rotation Module (ARM), Electronics Unit (EU), Optical Module (OM), internal Calibration Targets, and structural elements. The EU contains several CCAs, including the single board computer (SBC), which controls operations and communication of the RBI. The SBC hosts the flight software, contains the volatile and non-volatile memory, and internal buss communications hardware.

RBI will provide an independent measurement of the broadband reflected solar radiance and Earth's emitted thermal radiance by using the three spectral bands (Shortwave, Longwave, and Total) that will have the same overlapped point spread function (PSF) footprint on Earth. RBI accomplishes this by having the optical module with three co-aligned telescopes that have fields of view (FOV), detector time constants, filtering, cross-track scan rates, and sampling rates to match the RBI PSF to the heritage CERES PSF. The Field of Regard (FOR) scanning capability is similar to CERES and provides cross-track and bi-axial scanning for full Earth disk coverage extending to deep-space as well as enabling solar and lunar calibration verification as required by the user.

RBI has multiple on-orbit calibration sources in order to provide high quality calibrated data products. These stable on-orbit references will ensure that calibration stability is maintained over the RBI sensor lifetime. To ensure NIST-traceable calibration in space the RBI sensor is designed to use a visible calibration target (VCT) and an infrared calibration target (ICT) containing phase change cells (PCC) to enable calibration of blackbody temperature sensors. The VCT is a thermally controlled integrating sphere with space grade Spectralon covering the inner surface. The two sides of the sphere will have fiber-coupled laser diodes in the UV to IR wavelength region. An Electrical Substitution Radiometer (ESR) on the integrating sphere will monitor the long term stability of the sources and the possible degradation of the Spectralon in space. In addition the radiometric calibration operations will use a solar calibration target (SCT) with multiple Spectralon diffusers to provide accurate measurements of solar degradation. Also RBI makes use of space-looks as a cold reference on each Earth scan.

9639-10, Session 3

Overview of Japanese Earth observation programs *(Invited Paper)*

Haruhisa Shimoda, Tokai Univ. (Japan)

Seven programs, i.e. TRMM, ADEOS2, ASTER, GOSAT, GCOM-W1, GPM and ALOS-2 are going on in Japanese Earth Observation programs. PR on TRMM and ASTER on EOS-Terra are operating well except SWI channels of ASTER. ASTER SWI channels have stopped the operation because of a refrigerator failure in 2009. ADEOS2 was failed, but AMSR-E on Aqua was operating until 14, Oct. 2011. AMSR-E has stopped at that time because of the antenna driving mechanism's torque increase. Now, AMSR-E instrument has been on from March 2012 without antenna rotation and antenna rotation has been started from Dec. 2012 with 2rpm. The fuel of TRMM has been exhausted and the height of TRMM is decreasing. We hope TRMM can continue observations until middle of coming April. GCOM-W1 was launched on May, 2012.GCOM-W1 carries AMSR2. The orbit is A-train and has higher resolution than AMSR-E. GOSAT was launched on 23, Jan., 2009. GOSAT carries 2 instruments, i.e. a greenhouse gas sensor (TANSO-FTS) and a cloud/aerosol imager (TANSO-CAI). TANSO-FTS is a Fourier transform spectrometer (FTS) and covers 0.76 to 15 ?m region with 0.2 cm-1 resolution. TANSO-CAI is a 5 channel push broom scanner to observe aerosols and clouds. Both sensors are operating well. SMILES was on JEM of ISS. SMILES is a sub-millimeter limb sounding instrument using super conducting mixer and measures stratospheric ozone and related compounds. Unfortunately, SMILES stopped its operation on 21, April, 2010. ALOS was launched on 24, Jan., 2006 and stopped on 22, April, 2011 by power anomaly. ALOS carried three instruments, i.e., PRISM, AVNIR-2 and PALSAR. PRISM is a 3 line panchromatic push broom scanner with 2.5m IFOV. AVNIR-2 is a 4 channel multi spectral scanner with 10m IFOV. PALSAR is a full polarimetric active phased array SAR. GPM core satellite is a joint project with NASA and carries two instruments. JAXA has developed DPR. DPR has Ka band channel in addition to Ku band channel. NASA has developed GMI which is a microwave imager. GPM core satellite was launched on February 2014 and operating well. ALOS-2 was launched on 24, May 2014. ALOS-2 carries PALSAR-2, which is a L-band SAR. PALSAR-2 has full polarimetric mode as PALSAR. In addition, the spatial resolution of PALSAR-2 is higher than PALSAR. The highest resolution is 3m X 1m. Next generation satellites will be launched in 2016-2019 timeframe. They are GCOM-C1, EarthCare, GOSAT-2 and Advanced Optical Satellite (AOS). GCOM-C1 will carry SGLI. SGLI has polarization channels. GCOM-C1 will be launched on 2016. Another project is EarthCare. It is a joint project with ESA and JAXA is going to provide CPR with NICT. EarthCare will be launched on 2018. GOSAT-2 is a follow on of GOSAT and will carry 2 instruments, i.e. TANSO-FTS2 and TANSO-CAI2. FTS2 is an improved version

of FTS on GOSAT, but CAI2 is a 10 channel ultra violet to near infrared imager. GOSAT-2 will be launched on 2018. AOS will carry a panchromatic camera and a multi-spectral camera and will be launched on 2019.

9639-11, Session 3

ASTER VNIR 15 years growth to the standard imaging radiometer in remote sensing

Masaru Hiramatsu, Hitomi Inada, NEC Corp. (Japan); Fumihiro Sakuma, Masakuni Kikuchi, Japan Space Systems (Japan)

The Advanced Spaceborne Thermal Emission and Reflection Radiometer (ASTER) Visible and Near Infrared Radiometer (VNIR) is the remote sensing equipment which has 3 spectral bands and one along-track stereoscopic band radiometer. ASTER VNIR planed long life design (5 years more), it is successfully achieved.

ASTER VNIR has been imaging the World-wide Earth surface multiband images and the Global Digital Elevation Model (GDEM). VNIR data creates detailed world-wide maps and change-detection of the earth surface as utilization transitions and topographical changes.

ASTER VNIR geometric resolution is 15 meters; it is the highest spatial resolution instrument on NASA's Terra spacecraft. Then, ASTER VNIR was planned for the geometrical basis map makers in Terra instruments. After 15-years VNIR results growth its data to be the standard maps for space remote-sensing.

This paper presents VNIR's feature items during 15-year operation as change-detection images , DEM and calibration result.

9639-13, Session 3

ALOS-2 initial results

Yukihiro Kankaku, Masanobu Shimada, Japan Aerospace Exploration Agency (Japan)

The Advanced Land Observing Satellite-2 (ALOS-2) was successfully launched on 24th May, 2014. The mission sensor of ALOS-2 is the Phased Array type L-band Synthetic Aperture Radar-2 (PALSAR-2) which is the state- of-the-art L-band SAR system. After the launch, the solar array paddle and the PALSAR-2 antenna were deployed successfully during the critical phase in three days, and we confirmed no problem with the functions of the satellite. After that, during the initial checkout phase, we confirmed the performance of PALSAR-2 such as spatial resolution and swath width for each observation mode, NESZ (Noise Equivalent Sigma Zero), data compression, and so on. Especially, the maximum transmitting power was over 6 kw by Gallium Nitride (GaN) amplifier in Transmitting and Receiving Modules (TRMs). PALSAR-2 is the first user of GaN in the space. This technology contributes to realize high NESZ. Furthermore, we confirmed about 50 minutes' continuous observation. This capability is higher than the other SAR satellites, and ALOS-2 can afford to provide global observation data. And also, we confirmed the functions of the ALOS-2 bus system such as high bit rate data downlink using 16QAM, sufficient power supply, agile attitude control, accurate position determination, and autonomous orbit maneuvering. As the result of the initial checkout, we confirmed that ALOS-2 were able to start the nominal operation from 20th August 2014. The Basic Observation Scenario (BOS) started at the end of initial check out phase in order to archive the base map for interferometry and for global data acquisition, PALSAR-2 observes the Japan area frequently and the global world area with specific observation modes regularly.

After the check out phase, the initial calibration and validation phase started and we optimized the parameters for the dual receiving system to realize the wider swath width than that of the single receiving system. The dual receiving system is adopted for all modes except the Fine mode succeeding to ALOS/PALSAR. JAXA had verified the characteristics of PALSAR-2 products with support of Calibration and Validation Science Team (CVST). As the result, we confirmed higher cross talk between H and V polarization, and better NESZ against the specification.

In parallel with the calibration and validation activities, ALOS-2 had conducted emergency observations for several disasters like a flood, land slide impacted by typhoons, and volcano eruptions requested by disaster related organizations.

As the results of the initial calibration and validation, we confirmed the good performance of the satellite and PALSAR-2, and released the PALSAR-2 standard products via AUIG2 web site from 25th November 2014. In this paper, the result of ALOS-2 first year operation is described.

9639-14, Session 3

On-orbit performance of the Compact Infrared Camera (CIRC) onboard ALOS-2

Michito Sakai, Haruyoshi Katayama, Eri Kato, Yasuhiro Nakajima, Toshiyoshi Kimura, Japan Aerospace Exploration Agency (Japan); Koji Nakau, Hokkaido Univ. (Japan)

Compact Infrared Camera (CIRC) is a technology-demonstration instrument equipped with an uncooled infrared array detector (microbolometer) for space application. Microbolometers have an advantage of not requiring cooling system such as a mechanical cooler, and is suitable for resource-limited sensor system. Another characteristics of the CIRC are its use of athermal optics and a shutterless system. The CIRC achieves a small size (approximately 200 mm), light mass (approximately 3 kg), and low electrical power consumption (<20 W) owing to these characteristics. The main objective of the CIRC is to detect wildfires, which are major and chronic disasters affecting various countries of Southeast Asia, particularly considering the effects of global warming and climate change.

One of the CIRCs was launched in May 24, 2014 as a technology-demonstration payload of Advanced Land Observation Satellite-2 (ALOS-2). Since the initial functional verification phase (July 4-14, 2014), the CIRC was demonstrated a function according to its intended design. We also confirmed the noise equivalent differential temperature (NEdT) of the CIRC observation data is less than 0.2K, the temperature accuracy of within ±4K, and the spatial resolution is less than 210m in the calibration validation phase after the initial functional verification phase. The CIRC also detected wildfires in various areas and observed the volcano activities and urban heat islands in the operational phase. The other CIRC will be launched in 2015 onboard CALorimetric Electron Telescope (CALET) of the Japanese Experiment Module (JEM) at the International Space Station (ISS). Installation of CIRCs on the ALOS-2 and on the JEM/CALET is expected to increase observation frequency.

In this paper, we present the on-orbit performance including observational results of the CIRC onboard ALOS-2 and the current status of the CIRC onboard CALET .

9639-15, Session 4

Current status of the Global Change Observation Mission 1st-Water "SHIZUKU" (GCOM-W1) and the Advanced Microwave Scanning Radiometer 2 (AMSR2)

Takashi Maeda, Keiji Imaoka, Misako Kachi, Hiroyuki Tsutsui, Marehito Kasahara, Norimasa Ito, Taikan Oki, Haruhisa Shimoda, Japan Aerospace Exploration Agency (Japan)

Japan Aerospace Exploration Agency (JAXA) launched the Global Change Observation Mission 1st - Water (GCOM-W1) or "SHIZUKU" (meaning "droplet" in Japanese) in 18 May 2012 (JST) from JAXA's Tanegashima Space Center. GCOM-W1 is not a name of single satellite mission. It is a part of global and long-term observation program with two complementary medium-sized satellites (GCOM-W and GCOM-C series) and three generations (10-15 years) for stable data records. The GCOM-W1 satellite is the first generation of GCOM-W series. The GCOM-W1 satellite joins to NASA's A-train orbit since June 2012, and its observation is ongoing. The GCOM-W1 satellite carries the Advanced Microwave Scanning Radiometer 2 (AMSR2). AMSR2 is multi-frequency, total-power microwave radiometer system with dual polarization channels for all frequency bands, and successor microwave radiometer to the Advanced Microwave Scanning Radiometer for EOS (AMSR-E) loaded on the NASA's Aqua satellite launched in May 2002. AMSR-E halted its scientific observation on October 2011 because torque to maintain the rotation speed in regular observations (40 rotations per minute) reached the design limit. However, AMSR-E restarted observation in the slower rotation speed (2 rotations per minute) in December 2012. Currently, cross-calibration between AMSR-E and AMSR2 is underway.

AMSR2 is designed almost similarly as AMSR-E, and has a conical scanning system with large-size offset parabolic antenna, a feed horn cluster to realize multi-frequency observation, and an external calibration system with two temperature standards. However, some important improvements are made. For example, AMSR2's main reflector is expanded from 1.6 m of AMSR-E to 2.0 m to observe the Earth's surface in higher spatial resolution, and 7.3-GHz channel is newly added to detect radio frequency interferences at 6.9 GHz.

JAXA started distribution of AMSR2 brightness temperature products to public since January 2013 after initial calibration/validation period through the GCOM-W1 Data Providing Service (https://gcom-w1.jaxa.jp/). After that, algorithms to retrieve 8 standard geophysical values (water vapor, cloud liquid water, precipitation, sea surface temperature, sea surface wind speed, sea ice concentration, snow depth, and soil moisture) were modified, and distribution of the (standard) products of these standard geophysical values (standard products) to public was also started since May 2013. In March 2015, all standard products including brightness temperature products have been updated.

After starting distribution of AMSR2 products, JAXA keeps validation of these products in order to improve their accuracy, and development of retrieval algorithms for more challenging geophysical values (research algorithms) in cooperation with other researchers and projects. In this paper, we present the current operation status of AMSR2.

9639-16, Session 4

Current status of the dual-frequency precipitation radar on the global precipitation measurement core spacecraft

Kinji Furukawa, Tomomi Nio, Toshiyuki Konishi, Riko Oki, Takeshi Masaki, Takuji Kubota, Japan Aerospace Exploration Agency (Japan); Toshio Iguchi, Hiroshi Hanado, National Institute of Information and Communications Technology (Japan)

The Dual-frequency Precipitation Radar (DPR) on the Global Precipitation Measurement (GPM) core satellite was developed by Japan Aerospace Exploration Agency (JAXA) and National Institute of Information and Communications Technology (NICT). The GPM is a follow-on mission of the Tropical Rainfall Measuring Mission (TRMM). The objectives of the GPM mission are to observe global precipitation more frequently and accurately than TRMM. The frequent precipitation measurement about every three hours will be achieved by some constellation satellites with microwave radiometers (MWRs) or microwave sounders (MWSs), which will be developed by various countries. The accurate measurement of precipitation in mid-high latitudes will be achieved by the DPR. The GPM core satellite is a joint product of National Aeronautics and Space Administration (NASA), JAXA and NICT. NASA developed the satellite bus and the GPM microwave radiometer (GMI), and JAXA and NICT developed the DPR. JAXA and NICT developed the DPR through procurement.

The configuration of precipitation measurement using an active radar and a passive radiometer is similar to TRMM. The major difference is that DPR is used in GPM instead of the precipitation radar (PR) in TRMM. The inclination of the core satellite is 65 degrees, and the flight altitude is about 407 km. The non-sun-synchronous circular orbit is necessary for measuring the diurnal change of rainfall similarly to TRMM.

The objectives of the DPR are

(1) to provide three-dimensional precipitation structure including snowfall over both ocean and land,

(2) to improve the sensitivity and accuracy of precipitation measurement,

(3) to calibrate the estimated precipitation amount by MWRs and MWSs on the constellation satellites.

The DPR consists of Ku-band (13.6 GHz) precipitation radar (KuPR) and Ka-band (35.5 GHz) precipitation radar (KaPR). The KuPR unit will measure 2.6m X 2.4m X 0.7m in size. The KaPR unit will measure 1.3m X 1.5m X 0.8m in size. Both KuPR and KaPR have almost the same design as TRMM PR.

GPM core observatory was successfully launched by H2A launch vehicle at 3:37 (JST), Feb. 28, 2014. DPR function and performance verification was conducted at NASA GSFC. DPR function verifications show that DPR functions are normal. DPR performances are almost same as the results taken on the ground. The results of orbital checkout show that DPR meets its specification on orbit. After completion of initial checkout, DPR entered Normal Operations and Initial Calibration and Validation period was started. JAXA conducted internal calibrations, external calibrations and phase code changes to mitigate KuPR sidelobe clutter effect. JAXA evaluated these operations results and concluded that DPR data could go public. DPR products released to the public on Sep. 2, 2014 and Normal Observation Operation period was started. JAXA is continuing DPR trend monitoring, calibration and validation operations to confirm that DPR keeps its function and performance on orbit. Current status and early phase results of GPM/DPR will be reported.

9639-17, Session 4

EarthCARE/CPR design results and PFM dvelopment status

Kenta Maruyama, Eichi Tomita, Hirotaka Nakatsuka, Yoshihisa Aida, Yoshihiro Seki, Kazuyuki Okada, Yoshiya Iide, Nobuhiro Tomiyama, Japan Aerospace Exploration Agency (Japan); Nobuhiro Takahashi, Yuichi Ohno, Hiroaki Horie, Kenji Sato, National Institute of Information and Communications Technology (Japan) and Japan Aerospace Exploration Agency (Japan)

Earth Clouds, Aerosols and Radiation Explorer (EarthCARE) is a Japanese-European collaborative earth observation satellite mission aimed to deepen understanding of the interaction process between clouds and aerosols and their effects on the Earth's radiation. The outcome of this mission is expected to improve the accuracy of global climate change prediction.

The EarthCARE spacecraft, which weighs approximately 2,250kg and goes along a Sun-Synchronous 400km-hight orbit around the Earth, accommodates four instruments which are to observe the Earth's clouds, aerosols and radiation. The observation data acquired simultaneously by the four sensors will be processed into a variety of synergy products including vertical profiles of clouds and aerosols, microscopic cloud parameters, radiation fluxes and so on. As one of those instruments, the Cloud Profiling Radar (CPR) is the world's

first space-borne Doppler cloud radar jointly developed by the Japan Aerospace Exploration Agency (JAXA) and the National Institute of Information and Communications Technology (NICT). The CPR which has a 2.5m-diameter main reflector and W-band 1.5kW transmitter and receiver, will provide the vertical velocity as well as the vertical structure inside clouds. The other payloads on the satellite are the Atmospheric Lidar (ATLID) for vertical structure measurement of clouds and aerosols, the Multi-Spectral Imager (MSI) for horizontal distribution measurement of clouds and aerosols, and the Broad-Band Radiometer (BBR) for measurement of radiation fluxes at top of the atmosphere. ATLID, MSI, BBR and the base-platform of the spacecraft are developed by the European Space Agency (ESA).

In Japan, the critical design review of the CPR has been completed in 2013 and CPR proto-flight model is currently being manufactured, integrated, and tested. After handed-over to ESA, the CPR will be installed onto the EarthCARE satellite with the other instruments. After that the CPR will be tested, transported to Guiana Space Center in Kourou, French Guiana and launched by a Soyuz launcher in JFY2017.

In this paper, the current status of CPR proto-flight test will be reported.

9639-18, Session 4

Development and pre-launch test status of Second Generation Global Imager (SGLI)

Yoshihiko Okamura, Kazuhiro Tanaka, Japan Aerospace Exploration Agency (Japan); Takahiro Amano, Koichi Shiratama, Tamiki Hosokawa, NEC Corp. (Japan)

The Japan Aerospace Exploration Agency (JAXA) is pressing forward with the Global Change Observation Mission (GCOM) for long-term monitoring of earth environment. GCOM consists of two series of medium-size satellites, GCOM-W (Water) and GCOM-C (Climate). The first satellite, GCOM-W with Advance Microwave Radiometer -2 (AMSR-2), was already launched in 2012 and is observing continuously. The second satellite is GCOM-C which will carry the optical radiometer, Second Generation Global Imager (SGLI).

SGLI is the wide FOV multi-spectral optical sensor in the wavelength range of near-UV to thermal infrared. SGLI consists of two sensor units, Visible Near Infrared Radiometer (SGLI-VNR) and Infrared Scanning Radiometer (SGLI-IRS). SGLI will provide high accuracy measurements of Ocean, Atmosphere, Land and Cryosphere.

Manufacturing of the key flight parts and sensor system integration of SGLI flight models were completed. Sensor system proto-flight tests (PFTs) are on-going including optical characterization tests such as radiometric tests using integrating sphere and geometric and MTF tests using collimator.

This paper describes development and pre-launch test status of SGLI flight model. Especially we focus on the pre-launch radiometric performances such as the spectral response characteristics and signal to noise ratio. We conducted several radiometric tests using integrating sphere and collimator system, and the test results show that the SGLI performances meet the high radiometric specifications.

Characterization results of onboard calibrators such as internal lamp/LED units and blackbody are also presented. In orbit we plan to perform the solar and lamp/LED calibration once per month for the visible to shortwave infrared bands and the blackbody/deep space calibration at every scan for thermal infrared bands.

9639-19, Session 5

The results of the critical design of GOSAT-2: mission and satellite

Masakatsu Nakajima, Hiroshi Suto, Kazuhiko Yotsumoto, Takehiro Miyakawa, Kei Shiomi, Yukie Yajima, Japan Aerospace Exploration Agency (Japan)

Over six years observation of GOSAT (alias “IBUKI”) launched on January 23, 2009, have made the importance and availability of the measurements of the greenhouse gases from space points to us.

On the other hand, although GOSAT has accomplished the accuracy targets which is highest ever for any observations from space with involvement of the information of the boundary layer, the accuracies were not enough for the political and scientific use. So it was desired to improve the measurement accuracies. Through the GOSAT operation, we learned a lot of things on the instrument, software, processing algorithm and operation; and we have recognized what we should improve in the following mission. To elucidate the carbon cycle more precisely, our experiences regarding observation performances as well as hardware design were reflected on the mission requirements on GOSAT-2.

The principal requirements are measuring the CO2 concentration with the accuracy of 0.5 ppm at 500km and 2,000km mesh spatial resolution over the land and ocean, respectively and 1 month average, estimating the net flux with the error of 100% and measuring the Carbon Monoxide as the correlated matter of the anthropogenic emission of the greenhouse gases to study the detection of that.

Through the preliminary design, the requirements for mission instruments hardware including software and satellite system had been defined.

To improve the measurement accuracy, the signal to noise ration will be increased by the extension of the aperture size and cooling the after optics as well as the thermal detectors. And to increase the number of the useful data, GOSAT-2 will equip the function to avoid the clouds using the images obtained by the monitor camera in FTS.

To observe the carbon monoxide, spectral range of the 2.0?m band will be extended to 2.3?m.

The pointing angle in the along track direction will be extend from 20 degrees of GOSAT to 40 degrees to expand the observation area over the ocean where the sun glint is observed. This will make it possible to increase the number of the observation points over the ocean and contribute to the global observation including the ocean.

The cloud and aerosol imager data on GOSAT have been used to compensate the FTS data for the aerosol and to detect clouds. The one on GOSAT-2 will be enhanced the aerosols measurements abilities to detect the flow of the PM2.5 which is the critical issues not only in Japan but also in the world. New observation channels are added and the viewing angles will be changed to + and - 20 degrees from nadir of GOSAT.

In addition, the GSD of the 1.6?m bands is twice of the one of GOSAT.

To increase the observation angle of each point, the satellite recurrent cycle will be increased from 3 days to 6 days.

Now GOSAT-2 is in the critical design phase, and the current status and details of the mission instruments and satellite system design will be shown in this presentation.

9639-20, Session 5

Concept study of a vegetation lidar on International Space Station

Toshiyoshi Kimura, Tadashi Imai, Daisuke Sakaizawa, Takashi Kobayashi, Junpei Murooka, Japan Aerospace Exploration Agency (Japan)

Vegetation observation in global scale is one of the suitable

missions for satellite, because of its observation uniformity and wide observation range. So far, VNIR Imagers, such as MODISs on Aqua and Terra, AVNIR2 on ALOS, L-band SAR, i.e. PALSAR on ALOS, and Laser Altimeter, i.e. GLAS on ICESAT, were mainly used for the purpose and got good results. However, recent reports say that there are still large uncertainties of carbon flux estimations in the interaction between ground and atmosphere. That is because of the uncertainties of "change of land use", in other words, "change of biomass" such as deforestation. Biomass estimation needs not only area of the forest but also its height information with topological features. In that sense, active sensors such as L-band SAR and LIDAR are highly expected for precise height measurement. However, the L-band SAR has some saturation point in the measurement at around 100Mg/ha. That means dense forest, such as in tropical regions, has some difficulties. On the other hand Laser Altimeter or simply LIDAR is able to measure the height of such dense forest, using its small foot print. This leads that the combination of the LIDAR and L-band SAR and/or VNIR imagers compensate each other for precise biomass measurement. Currently JAXA is working for a concept study of vegetation LIDAR named MOLI (Multi Observation LIDAR and Imager), flying on the International Space Station. MOLI will be the first Earth Observation LIDAR in Japan, The unique points of MOLI are the dual beams with enough small and close footprints to determine incline of the ground. This feature reduces height error reasonably. Full wave analysis technique is also under development to distinguish canopy heights, crown depth and other forest features. Currently Bread Board Model of MOLI Laser Transmitter is being tested under vacuum condition. Target launch year of MOLI is 2019.

9639-21, Session 5

Planned submillimeter limb sounder (SMILES-2) for measurement of temperature, wind, and chemical species in the middle atmosphere

Satoshi Ochiai, Yoshinori Uzawa, Yoshihisa Irimajiri, Philippe Baron, National Institute of Information and Communications Technology (Japan); Toshiyuki Nishibori, Japan Aerospace Exploration Agency (Japan); Takeshi Manabe, Osaka Prefecture Univ. (Japan); Akira Mizuno, Tomoo Nagahama, Nagoya Univ. (Japan); Yasunori Fujii, National Astronomical Observatory of Japan (Japan); Makoto Suzuki, Japan Aerospace Exploration Agency (Japan); Masato Shiotani, Kyoto Univ. (Japan)

Submillimeter-wave limb sounder has a potential for precise observation of temperature and wind of the atmosphere in a wide range of altitude, as well as observation of the profiles of atmospheric minor chemical species, such as ozone, and chlorine or bromine compounds. A simulation study shows that a limb sounder can measure the atmospheric temperature with a precision of 2 K in the range from the lower stratosphere to an altitude above the mesosphere by observing the oxygen-line limb-emission at 487 GHz, if the sounder has enough sensitivity, frequency resolution, and apropriate scanning ability. The wind speed along the line-of-sight, similarly, is estimated to be measured with a precision of 2 m/s. The height resolution of those measurements depends on the antenna aperture of the limb sounder and can achieve 2 - 4 km with a reasonable size of instrument. The sounder equipped multiple frequency bands including oxygen band has the capability in measuring height-profile of several important atmospheric constituents for chemistry and transport in the stratosphere and mesosphere.

We propose a submillimeter limb-sounding mission based on superconducting technology, which can realize those temperature, wind, and chemical species measurement. The planned sounder of this mission will equip SIS and HEB receivers. The SIS is a superconducting device and provides the lowest-noise heterodyne receiver in this frequency range. We use SIS mixer to measure a band of oxygen line, probably at 487 GHz, and two or three few-GHz-width bands within 520 - 650 GHz for measurement of other stratospheric and mesospheric chemical species. The HEB mixer, which is also superconducting device with good performance in higher frequency, will be used for observation of OH (1.8 THz) and O-atom (2.06 THz) lines. The SIS and HEB mixers will be cooled down to 4 K by a mechanical cooler of Joule-Thomson cycle that will utilize a heritage of JEM/SMILES mission. Although lifetime of JEM/SMILES had not been so long, a recent ground test of JT-cycle cooler demonstrated its reliability and a lifetime of more than 3 years. The target of the total mission weight, which includes 80-cm size offset Cassegrain reflector, is expected to be about 150 kg, so that the mission has a possibility of being boarded on Japanese small satellite platform.

In this paper, we will report the current status of our design study of this mission. A very rough sketch of the diagram of the mission instrument will be presented. At this moment some components in the diagram might be needed to be developed or qualified for space use. The paper will discuss our plan of few years study of technical readiness toward making a proposal of the mission to Japan Aerospace Exploration Agency.

9639-22, Session 5

Sensitivity study of SMILES-2 for chemical species

Naohiro Manago, Chiba Univ. (Japan); Hiroyuki Ozeki, Toho Univ. (Japan); Satoshi Ochiai, Philippe Baron, National Institute of Information and Communications Technology (Japan); Makoto Suzuki, Japan Aerospace Exploration Agency (Japan)

Theoretical sensitivity study of sub-mm limb sounder SMILES-2 (4K cooled, Tsys=150 K) proposal was conducted. BrO lines at 525.2 GHz and HOCl lines at 613.6 GHz were confirmed to have comparable theoretical sensitivities to those of SMILES and less spectral interferences by other species. 5 bands configuration (487±2, 527±2, 614±2, 626±2, 649±2 GHz) should have SMILES-like sensitivity and Aura/MLS-like chemical species coverage.

The 5 sub-mm bands will have 4 GHz band-width and 500 kHz spectral sampling using FFT spectrometer technique. The 487 GHz band can provide temperature and wind speed using 487.249 GHz O2 line, H2O, O3 and HO2. The 527 GHz band can provide BrO, O3, N2O, H2CO, NO2, HO2, 18OOO, 18OOO, and O18OO. The 614 GHz band cam [rovide O3, HOCl. The 624 GHz band can provide O3, H37Cl, H35Cl, HO2, HNO3, and BrO. The 649 GHz band can provide O3, ClO, HO2, NO and BrO.

Two THz bands are under consideration to retrieve OH (1.8 THz) and O-atom (2.06 THz) using 4 K cooled Hot Electron Bolometer detector (Tsys = 1300 K), which can provide OH and O-atom in the mesosphere and lower thermosphere.

Observations of species such as, (i) OH and HO2, (ii) N2O, NO, NO2, and HNO3 will improve our understanding of atmospheric chemistry. Oxidation process of CH4 can be investigated using H2CO data with O-atom, Cl (estimated from ClO).

9639-23, Session 5

Measurement of stratospheric and mesospheric winds with a submillimeter wave limb sounder: results from JEM/SMILES and simulation study for SMILES-2

Philippe Baron, National Institute of Information and Communications Technology (Japan); Naohiro Manago, Chiba Univ. (Japan); Hiroyuki Ozeki, Toho Univ. (Japan); Yoshihisa Irimajiri, Yoshinori Uzawa, National Institute

of Information and Communications Technology (Japan); Donal Murtagh, Chalmers Univ. of Technology (Sweden); Masato Shiotani, Kyoto University (Japan); Satoshi Ochiai, National Institute of Information and Communications Technology (Japan); Makoto Suzuki, Institute of Space and Astronautical Science (Japan) and Japan Aerospace Exploration Agency (Japan)

This presentation will assess the wind measurement performances of SMILES-2, a satellite project studied in Japan [1]. The considered instrument is an heterodyne submillimetre limb sounder. The satellite will be the successor of SMILES which operated from the Japanese Experiment Module (JEM) of the International Space Station between 2009/09 and 2010/04. Good quality winds in the stratosphere and mesosphere were successfully retrieved from JEM/SMILES though the instrument were not designed for such purpose [2].

Winds are an important target of SMILES-2 and a simulation study is conducted to optimize the instrumental setting and to find the most favourable spectroscopic lines for wind observations. In the presentation we will present the latest results obtained from JEM/SMILES in order to illustrate the capabilities of such instrument to measure winds and the scientific importance of such measurements. The discussion will include the comparison with atmospheric models. The simulation study for SMILES-2 will be described including the retrieval method (same as the one used for processing JEM/SMILES data) and the instrumental characteristics considered for the project. The wind measurement performances will be assessed for the spectroscopic lines of interest for SMILES-2. They cover the spectral ranges 500-700 GHz and 1.8-3 THz and include species such as H2O, O3, O2, atomic oxygen or OH. The performances are characterized by the retrieval errors induced by the measurement noise, the vertical resolution and the altitude range of good sensitivity. As for the instrumental characteristics, we will focus on the system temperature, the receiver bandwidth, the spectral resolution, the heterodyne mode (single or double side band), the antenna aperture and the scan velocity. The objective is to measure wind with a precision of 2-5 m/s and a vertical resolution better than 10 m/s. The first results show that middle stratospheric and lower mesospheric winds measurement needs a relatively large bandwidth (4-8 MHz) and a coarse spectral resolution (1-2 MHz) while middle and upper mesospheric winds measurement needs a small bandwidth (<1 GHz) and a high spectral resolution (0.125 MHz). The advantages and disadvantages of using a 4-K cooled instrument such as JEM/SMILES will be discussed.

References:

[1] N. Manago, H. Ozeki, and M. Suzuki. Band selection study for the SMILES-2, Proc. In 28 Taikiken symposium, 2014

[2] P. Baron, D. P. Murtagh, J. Urban, H. Sagawa, S. Ochiai, Y. Kasai, K. Kikuchi, F. Khosrawi, H. Kornich, S. Mizobuchi, K. Sagi, and M. Yasui. Observation of horizontal winds in the middle-atmosphere between 30S and 55N during the northern winter 2009-2010. ACP, 13(13), 2013.

9639-24, Session 6

Visible and infrared detector developments supported by the European Space Agency

Nick Nelms, Kyriaki Minoglou, Christoph Voland, Yves Levillain, Roland Meynart, Jean-Loup Bézy, Mustapha Zahir, Bruno Leone, Alessandra Ciapponi, Pierre-Elie Crouzet, European Space Agency (Netherlands)

The European Space Agency plays a significant role in the area of remote sensing and is rigorously developing new technologies in support of this activity. Detectors are a performance limiting component and the Agency is particularly interested in the continuous improvement of available detector capabilities across the spectrum, with a high concentration of effort in the visible and infrared wavebands.

Charge-coupled devices (CCD) continue to dominate in the visible waveband but developments for this mature technology are tending towards customization of detector formats for specific missions, although specific activities are in progress related to particular process variations and anti-reflection coatings. Consequently, the majority of our developments in the visible are targeted at improving the performance of CMOS image sensors in order to exploit their potential advantages for future missions.

In the infrared, mercury cadmium telluride (MCT) hybrid arrays are beginning to secure their position as the choice of imaging detector for NIR to VLWIR operation. Based on internal roadmaps, the Agency is pursuing a number of developments over this range aimed at improving different performance parameters including array size, dark current, quantum efficiency and read-noise. It is, however, recognized that other materials have potential in the infrared and we are also further investigating III-V compound semiconductors and Type-II superlattice structures.

This paper sets out the requirements for current and future missions and presents details of the Agency's current and planned detector developments in the visible and infrared wavelength parts of the spectrum.

9639-25, Session 6

Low dark current MCT-based focal plane detector arrays for the LWIR and VLWIR developed at AIM

Kai-Uwe Gassmann, Sebastian Kaspar, Detlerf Eich, Wolfgang P. Fick, Heinrich Figgemeier, Stefan Hanna, Karl-Martin Mahlein, Wilhelm Schirmacher, Richard Thöt, Joachim C. Wendler, AIM INFRAROT-MODULE GmbH (Germany)

Cryogenically cooled Hg_(1-x)Cd_xTe (MCT) quantum detectors are unequalled for applications requiring high imaging as well as high radiometric performance in the infrared spectral range. Compared with other technologies, they provide several advantages, such as the highest quantum efficiency, lower power dissipation compared to photoconductive devices and fast response times, hence outperforming micro-bolometer arrays. However, achieving an excellent MCT detector performance at long (LWIR) and very long (VLWIR) infrared wavelengths is challenging due to the exponential increase in the thermally generated photodiode dark current with increasing cut-off wavelength and operating temperature.

Dark current is a critical design driver, especially for LWIR / VLWIR multi-spectral imagers or hyper-spectral Fourier spectrometers operated at high frame rates and moderate signal levels.

Consequently, low dark current (LDC) technologies are the prerequisite for future scientific space and earth observation missions.

Aiming, for example at exoplanet or earth atmospheric spectral analysis, significant improvement in LWIR / VLWIR detector material performance is mandatory. LDC material optimization can target different directions of impact: (i) reduction in dark current for a given operational temperature to increase SNR and reduce thermally induced signal offset variations. (ii) operation at elevated temperatures at a given dark current level to reduce mass and power budget of the required cryocooler and to reduce cryostat complexity. (iii) increase the accessible cut-off wavelength at constant detector temperature and dark current level.

AIM will present its latest results on n-on-p as well as p-on-n low dark current planar MCT photodiode focal plane detector arrays at cut-off wavelengths >11 µm at 80 K. Dark current densities below Tennant's 'Rule07' have have been demonstrated for n-on-p devices. Slightly higher dark current densities and excellent cosmetics with very low cluster and point defect densities have been demonstrated for p-on-n devices.

This work has been carried out under ESA contract ESTEC 4000107414/13/NL/SFe.

9639-27, Session 6

NGP, a new large format infrared detector for observation, hyperspectral and spectroscopic space missions in VISIR, SWIR and MWIR wavebands

Anne Delannoy, Céline Riuné, Bruno Fièque, Philippe Chorier, SOFRADIR (France)

SOFRADIR is one of the leading companies involved in the development and manufacturing of infrared detectors for space applications. As a matter of fact, SOFRADIR is involved in many space programs in visible and SWIR spectral ranges. Most of these programs concern hyperspectral imagery observation of the earth but also some scientific applications. For more than 10 years, the Saturn generation detector (VISIR or SWIR) of Sofradir was the basis of numerous space missions.

In order to answer future mission needs which require larger detector for better spatial and spectral resolutions while complying with all specifications reflecting the state of requirements for space detectors, SOFRADIR has developed a new detector in a frame of an ESA R&T program, named Next Generation Panchromatic Detector (NGP). While designed for VISR and SWIR spectral ranges, this detector is also studied to be extended in MWIR spectral range. In this paper, NGP detector will be described as well as its performances. Space applications using this detector will be presented also showing appropriateness of its use to answer space programs specifications, as for example those of Sentinel-5.

9639-28, Session 6

Multiband CMOS sensor simplify FPA design

Bill W. Wang, CMOS Sensor Inc. (Taiwan); Jer Ling, National Space Organization (Taiwan)

Push broom multi-band Focal Plane Assemblies (FPA) design needs to consider optics, image sensor, electronics, mechanics as well as heat transfer requirements. Conventional FPA use two or several CCD devices as an image sensor. The CCD image sensors require several high speed, high voltage and high current clock drivers as well as analog video processors to support their operation. Signal also needs to be digitized using external sample / hold and digitized circuit. These support circuits are bulky, consume a lot of power and must be shielded and placed in close to the CCD to minimize the introduction of unwanted noise. The CCD also needs to consider how to dissipate power. The end result is a very complicated FPA design, hard to make due to more weighs and drawing more power requiring complex heat transfer mechanisms. In this paper, we integrate microelectronic technology and multi-layer soft / hard board technology for the electronic design. Since its simplicity and integration, the optical, mechanical and thermal design will become very easy. The whole FPA assembly and dis-assembly only take about a few days.

A space qualified multi-band CMOS image sensor (C468) was developed for the incorporation of clock drivers, timing generators, signal processing and digitization onto the same IC with the image sensor photodiodes. This keeps noise to a minimum while providing high functionality at reasonable power levels. The C468 device used CSI's proprietary wafer butting technology and MSOC technology to combine five long sensor arrays into a 121 mm x 23 mm of monolithic silicon chip. The device is composed of one Panchromatic (PAN) sensor and four different Multi-Spectral (MS) sensors. The PAN sensor has 12,000 pixels with pixel-pitch of 10 ?m; operated at integration time of 297 μm ± 5%, 80 MHz clock, and 12 bit of ADC. Four different MS are Blue (B), Green (G), Red (R) and Near Infrared (NIR) bands. Each band has 6,000 pixels with pixel pitch of 20 ?m; operated at integration time of 594 μm ± 5%, 40 MHz clock, and 12 bit of ADC. Both PAN and MS pixels are continuous with no gaps in the sensor direction. The distance between two neighboring band is 4 mm. The device is mounted on a multi-layer PGA ceramic package with size of 155 mm x 60 mm. All pixels are manufactured on same wafer, no registration error will occur between band to band and not any elevator variation between pixel to pixel. The multi-layer ceramic package was designed with built in de-couple capacitor for power supply and resistor network for LVDS. The input and output of C468 are either LVDS or digital output. A soft / hard board is used to send the signal to operate sensor and receive the data from C468 sensor. No connector is required within FPA electronics to increase the reliability. Since its integration design, a lot of room is clear for thermal design. The optical and mechanical design becomes very straight forward. The flight model FPA has passed all reliability tests.

The FPA was designed and developed for the NSPO Earth observation satellite, Formosat-5, expected to be launch to 720 km altitude orbit in 2016. The ground resolution for PAN and MS is 2 meter and 4 meter, respectively. The detail device structure and device performance will be present on the paper.

9639-29, Session 7

A 400 KHz line rate 2048 pixel modular SWIR linear array for earth observation applications

Ankur Anchlia, Rosa M. Vinella, Kristof Wouters, Daphne Gielen, Peter Hooylaerts, Xenics NV (Belgium); Pieter Deroo, Xenixs NV (Belgium); Wouter Ruythooren, Koen van der Zanden, Jan P. Vermeiren, Xenics NV (Belgium); Patrick J. Merken, Xenics NV (Belgium) and Royal Military Academy (Belgium)

In this paper, we report a family of linear imaging FPA's sensitive in the [0.9 - 1.7um] band, developed for high speed applications for earth observation and micro-gravity applications; such as LIDAR, wavelength references and OCT analyzers. Fast linear FPA's can also be used in a wide variety of terrestrial applications, including high speed sorting, electro- and photo-luminesce and medical applications.

The arrays are based on a modular ROIC design concept: modules of 512 pixels are stitched during fabrication to achieve 1024 and 2048-pixel arrays. In principle, this concept can be extended to 3072, 4096 pixels or any multiple of 512 pixels, the limiting factor is, however, the pixel yield of a long InGaAs array and the CTE differences in the hybrid setup. Each 512-pixel module has its own on-chip digital sequencer, analog readout channel and 4 output buffers. All the modules in a ROIC (1024 or 2048) work in parallel without any interaction among them, except the start time synchronization achieved with an external signal. This modular concept enables a long-linear array to run at a high line rate of 400 KHz of 512-pixel module irrespective of the array length, which limits the line rate in a traditional linear array.

The pixel has a pitch of 12.5um, both square (12.5um) imaging and rectangular (250um) spectroscopy pixels are implemented. The detector frontend is based on CTIA (Capacitor Trans-impedance Amplifier), having 5 selectable integration capacitors [redacted]. An auto-zero circuit limits the detector bias non-uniformity to 5-10mV across broad intensity levels, limiting the input referred dark signal noise to 20e-rms even at long integration time of 3ms. To limit the CTIA noise, the noise bandwidth is tuned automatically with chosen integration capacitance to meet the required settling time and not to avoid excess of bandwidth. An on-chip CDS that follows CTIA facilitates the removal of integration cap KTC noise and OTA offsets and most of the 1/f noise. [redacted]. One of the unique characteristics of these FPAs is the possibility to have different gains per pixel, a boon for applications with a large variation in signal level.

The ROICs have flip and hold column buffers to have better charge transfer efficiency and class AB output buffers for power efficiency. At a master clock rate of 60MHz and a minimum integration time of 1.4us, the FPAs reach the highest line rate of 400 KHz. To achieve this line rate, they work only in Integrate-While-Read (IWR) mode, and they have operations done in parallel in the CTIA and CDS stages. They have also split column output busses to reduce the loading on column amplifiers (power efficiency; analogous to bit-line splitting in memories).

Power consumption is normally an issue at such high line rates, especially when the ultimate target is to reach long-linear imaging arrays through stitching. So, a lot of attention has been given into making the modules power efficient by using class AB-type CDS OTA, flip-and-hold column buffers and class AB output buffers, and by splitting the column output bus to reduce loading.

9639-30, Session 7

Sensor system development for the WSO-UV (World Space Observatory–Ultraviolet) space-based astronomical telescope

Chris Hayes-Thakore, Stephen N Spark, Peter Pool, Andrew Walker, e2v technologies plc (United Kingdom); Matthew Calpp, Nick Waltham, Rutherford Appleton Laboratory (United Kingdom); Andrey Shugarov, Institute of Astronomy RAS (Russian Federation)

E2v is currently developing a sensor solution for the WSO-UV (World Space Observatory – Ultraviolet) programme, a Russian led 170 cm space astronomical telescope. This is a fully integrated sensor system for the detection of UV light across 3 channels: VUVES high resolution spectrometer (115 – 176 nm); UVES high resolution spectrometer (174 – 310 nm) and Long-Slit Spectrometer (LSS) (115 nm – 310 nm). This paper will describe the systematic approach and technical solution covering mechanical, thermal and vacuum analysis, showing how this is consistent with the CCD performance requirements and the overall environment requirements that the delivered system will experience through ground test, integration, storage and flight.

9639-31, Session 7

InAs photodiode for low temperature sensing

Xinxin Zhou, Jo Shien Ng, Chee Hing Tan, Univ of Sheffield (United Kingdom)

Radiation thermometers are used to monitor the temperature of an object without making physical contact. The temperature is calculated algorithmically from the measured infrared energy from the object over a specific wavelength range. Photon detectors are widely used in radiation thermometers due to higher sensitivity and faster response times than thermal detectors. Si and InGaAs photodetectors have been widely used as high temperature sensors in radiation thermometry with an operation wavelength of 0.9 micron and 1.6 micron, respectively. The measuring temperature range is limited to 400 degree centigrade and 150 degree centigrade for Si and standard InGaAs respectively. Long wavelength detectors need to be selected for lower temperature applications or to account for material optical transmission properties. PbSe photoconductors are used to sense target close to room temperature. However due to growth issues large size PbSe arrays are not available, although PbSe linear arrays grown by chemical bath deposition are commercially available. Additionally, they suffer from longer response time than photodiode as well as high 1/f noise.

Recently, InAs have been demonstrated as a promising material for infrared sensing. InAs photodiodes are seen as a viable technology for low temperature sensing due to high sensitivity and fast response. With a bandgap of 0.36 eV, our InAs photodiodes show a cutoff wavelength of 3.6 micron at room temperature, providing a high peak responsivity of 1.28 A/W at 3.35 micron at 0 V. This yields a peak detectivity value of 6.8?109 cm.Hz1/2/W which is higher than commercial uncooled InAs photodiodes. Our InAs also shows good linearity and photocurrent uniformity. By performing thermometry measurement, the InAs photodiodes can be used for sensing targets at 50 degree centigrade with a temperature error of 0.17 degree centigrade.

To further improve the device performance, cooled detectors could be used in the low temperature sensing applications. Therefore, by cooling InAs photodiodes from 295 to 200 K, the device dark current reduced by 3 orders of magnitude while the output photocurrent decreased by around 50 % due to the blue-shift of the cutoff wavelength. These lead to a significant increase in the signal-to-noise ratio. At a blackbody temperature of 37 degree centigrade the temperature error improves by 10 times from 0.46 to 0.048 degree centigrade, confirming the potential of using InAs for low temperature sensing, including human body temperature measurement.

9639-32, Session 7

Extended scene wavefront sensor for space application

Thierry T. Bomer, Karen Ravel, Gilles Corlay, SODERN (France)

The spatial resolution of optical monitoring satellites increases continuously and it is more and more difficult to satisfy the stability constraints of the instrument. The compactness requirements induce high sensitivity to drift during storage and launching. The implementation of an active loop for the control of the performances for the telescope becomes essential, in the same way of astronomy telescopes on ground.

The active loop requires disposing of informations in real time of optical distortions of the wavefront, due to mirror deformations. It is the role of the Shack-Hartmann wave front sensor studied by Sodern. It is located in the focal plane of the telescope, in edge of field of view, in order not to disturb acquisition by the main instrument. Its particular characteristic, compared to a traditional wavefront sensor is not only to work on point source as star image, but also on extended scenes, as those observed by the instrument.

The exit pupil of the telescope is imaged on a micro lenses array by a relay optics. Each element of the micro lenses array generates a small image, drifted by the local wavefront slope. The processing by correlation between small images allows to measure local slope and to recover the initial wavefront deformation according to Zernike decomposition.

Sodern has realized the sensor dimensioning and has studied out the comparison of various algorithms of images correlation making it possible to measure the local slopes of the wave front. Simulations, taking into account several types of detectors, enabled to compare the performances of these solutions and a choice of detector was carried out.

This article describes the state of progress of the work done so far. It shows the result of the comparisons on the choice of the detector, the main features of the sensor definition and the performances obtained.

9639-87, Session 7

Quantum efficiency performances of the NIR European Large Format Array detectors tested at ESTEC

Pierre-Elie Crouzet, Ludovic Duvet, Fritz De Wit, Thierry Beaufort, S. Blommaert, Bart Butler, G. Van Duinkerken, Joerg Ter-haar, J. Heijnen, Cornelis van der Luijt, Hans

Smit, European Space Research and Technology Ctr. (Netherlands)

The Payload Technology Validation Section at ESTEC has the goal to validate new technology for future or on-going mission. In this framework, a test set up to characterize the quantum efficiency of near-infrared (NIR) detectors has been created. In the development plan of a NIR European Large Format Array ("LFA"), 3 deliverables detectors coming from SELEX-UK/ATC (UK) on one side, and CEA/LETI- CEA/IRFU-SOFRADIR (FR) on the other side were characterized.

The quantum efficiency of an HAWAII-2RG detector from Teledyne was as well measured. The capability to compare on the same setup detectors from different manufacturers is a unique asset for the future mission preparation office.

This publication will present the quantum efficiency results of a HAWAII-2RG detector with a 2.5um cut off compared to the LFA European detectors prototypes developed independently by SELEX-UK/ATC (UK) on one side, and CEA/LETI- CEA/IRFU-SOFRADIR (FR) on the other side.

9639-51, Session PS

Overview of test and application of the multispectral camera on ZY-3 Satellite

Weijun Cai, Beijing Institute of Space Mechanics and Electricity (China)

ZY-3 satellite is the first high-precision Stereo-mapping satellitefor civilian purposes in China, which was launched in 9 Jun 2012. The Multi-Spectral Camera mounted on the satellite can acquire 4 multi-spectral bands. It has served steadily on orbit for more than three years. End to 22 Mar 2015 the satellite had produced more than 822730 images, include 212386 Multi-Spectral images, the multi-spectral data is more than 133TB. The telemetry data and the images shows that the imaging quality and the stability of interior orientation elements all satisfied the requirements of the mission.

In 2013 several field experiments have been organized in several provinces in China and Perth in Australia. The field experiment include geometric precision calibrating and radiation calibrating, the results of the experiments showed that the geometric and radiation performance of the Multi-Spectral Camera is perfect.

The high-precision multi-spectral images and the quantitative remote sensing data have been used widely in China. Including mapping, resource exploration, natural disasters Emergency response and so on. Substantial applying research projects about the ZY-3 satellite images are in progress. So the application of the satellite will be wider and wider.

The paper presents an overview of the test and calibration results of the camera, and with the present situation of the application, put forward some views about the subsequent camera.

9639-73, Session PS

ASTER 15 years challenging trail on-orbit operation

Masakuni Kikuchi, Fumihiro Sakuma, Kenji Tatsumi, Japan Space Systems (Japan); Hitomi Inada, Yoshiyuki Itou, NEC Corp. (Japan); Shigeki Akagi, Mitsubishi Electric Corp. (Japan); Hidehiko Ono, Fujitsu Ltd. (Japan)

ASTER (Advanced Spaceborne Thermal Emission and Reflection Radiometer) is a high-resolution optical sensor system that can be observed in a wide region from the near-infrared and the short wavelength infrared to the thermal infrared with 14 spectral bands on board of NASA's Terra spacecraft for EOS " A mission to planet earth ". Especially ASTER provides the capability useful for rock identification, mineral exploration and geologic structure. The features of ASTER sensor system are ; wide spectrum of wavelength (0.52?0.86?m, 1.6?2.43?m, 8.125?11.65?m), stereoscopic data in a single orbit using the near-infrared bands, high geometric and radiometric accuracy, worldwide coverage and GDEM (Global Digital Elevation Model) product generation.

ASTER was achieved 5 years mission success on orbit operation normally which is the specified target after launched on December, 1999. And after through 10 years continuous orbit operation, ASTER has still operating the long life observation of extra success to be 15 years in total on December, 2014. As for ASTER instrument that is composed of 3 radiometers ; VNIR (Visible and Near Infrared Radiometer) 3 bands, SWIR (Short Wavelength Infrared Radiometer) 6 bands, TIR (Thermal Infrared Radiometer) 5 bands, overall ASTER long life data taken by 15 years onboard operation has been reviewed from the point of view of as the health and safety check by TLM data trend, the function and performance evaluation by observation data trend, the onboard calibration and verification by periodic CAL data trend. As a result of this, the radiometric degradation of VNIR & TIR and the temperature rise of SWIR detector were identified as significant challenges. It was clarified the countermeasure plan towards the end of mission and also verified the novel lessons learned as follows ; VNIR lessons learned is a necessity of plume shield for thrusters firing during the initial orbit control, contamination measures by outgassing from silicone material of the optical system and calibration part, application of the sensitivity correction by the integration of onboard calibration and vicarious calibration. SWIR lessons learned is a new knowledge about the deterioration of cryogenic stress-strength properties of thermal lubricant, realization of robust design concerning the thermal interface between the detector and the cooler, ensuring a sufficient design margin for long life to the life limited items. TIR lessons learned is a necessity of plume shield for thrusters firing during the initial orbit control, contamination measures by outgassing from silicone material of the optical system and calibration part, consistency of the sensitivity correction by the cross-validation of onboard calibration and vicarious calibration.

9639-74, Session PS

The laser array generator for the Chang'E-3 lunar rover

Chunhui Wang, Hui Zhang, Beijing Institute of Space Mechanics and Electricity (China)

The laser array generator (LAG) is one of the sensors on the Chang'E-3 Lunar Rover , which launched on December 2, 2013 and landed on December 14, 2013. LAG cooperates with cameras for autonomous obstacle avoidance. LAG transmits sixteen continuous laser beams toward the front of the rover and the laser footprint on the lunar surface is photographed by the cameras. Images photographed by the cameras are processed and used for obstacle identification in order to rapid autonomous obstacle avoidance. This paper describes the sensor design, prelaunch testing, calibration, and results of postlaunch testing.

9639-75, Session PS

ASTER system operating achievement for 15 years on orbit

Hitomi Inada, Yoshiyuki Itou, NEC Corp. (Japan); Masakuni Kikuchi, Fumihiro Sakuma, Kenji Tatsumi, Japan Space Systems (Japan); Shigeki Akagi, Mitsubishi Electric Corp. (Japan); Hidehiko Ono, Fujitsu Ltd. (Japan)

ASTER (Advanced Spaceborne Thermal Emission and Reflection Radiometer) System is operating more than 15 years since launched on board of NASA's Terra spacecraft in December 1999.

ASTER System is composed of 3 radiometers (VNIR (Visible and Near Infrared Radiometer), SWIR (Short-Wave Infrared Radiometer), and TIR (Thermal Infrared Radiometer)), CSP (Common Signal Processor) and MSP (Master Power Supply).

This paper describes the achievement and successful result of ASTER System long term operation since the initial checkout operation (ICO).

In the initial checkout phase, ASTER System was successfully confirmed for the actuation, function and performance, and was successfully operated for recovery from some anomaly as TIR CPHTS fluctuations.

During the normal operation phase, ASTER system was successfully operated with full observation mode. In 2003, ASTER was successfully operated for the deep space calibration and the lunar calibration in order to evaluate the absolute response for the Terra onboard sensors including ASTER.

Over the 5 years mission life, ASTER System restarted several times because the anomaly of that SWIR detector temperature had increased. However SWIR detector temperature could not be get recovered. As the result, the SWIR observation data became unusable.

In the continuous operating phase, ASTER System was successfully operated such as; the special calibration to evaluate the contamination for the VNIR and TIR degradation, and the stopping operation of the onboard data processor for SWIR in order to save the data transfer rate.

ASTER system had totally checked the instrument health and safety check using telemetry data trend evaluation, the function and performance check using observation data, and the periodic onboard calibration.

This paper also describes the future operating plan based on the interface coordination status with the Terra spacecraft operation team.

9639-76, Session PS

Comparison of different water infrared emissivity retrieval methods with the theoretical model

JiAn Wei, Difeng Wang, Jianyu Chen, The Second Institute of Oceanography, SOA (China); Yan Bai, Xianqiang He, Jianyu Chen, The Second Institute of Oceanography, State Oceanic Administration (China)

Ground surface temperature is a vital parameter, not only in hydrological and agricultural studies but also in meteorological and climatological analysis. However, the Knowledge of surface emissivity in the thermal infrared (TIR) region is a required magnitude for the determination of temperature from TIR radiance measurements. If emissivity is not well determined, it can cause a significant systematic error in obtaining the surface temperature. Currently, emissivity, in the thermal infrared region, is still required as a critical factor to quantitative analyzing thermal characteristic of the targets, which focus on the estimation of actual land surface temperatures from at-surface radiometric temperatures, the calculation of effective emissivity of heterogeneous and rough surfaces at the pixel spatial and spectral resolutions, the simultaneous recovery of temperature and emissivity based on multi-spectral techniques and the calculation of the longwave effective radiance and the evapotranspiration of terrestrial surfaces from the radiation budget at surface. Often, the surface emissivity may be supplied by ground measurements. The main aim of this paper is to compare different methods for measuring accurate water surface emissivity in the laboratory, namely, the Absolute Emissivity method (AE) and the Temperature and Emissivity Separation (TES) algorithm. Firstly, a briefly description to the principle of the two measure methods was introduced. The multispectral radiometer CE312-2, with five narrow bands, with effective wavelengths at 8.420, 8.676, 9.145, 10.567, and 11.296?m, similar to the Advanced Space borne Thermal Emission and Reflection Radiometer (ASTER) TIR bands, and a broad band in the 8–13?m range, which was used to operate the measurements in the laboratory, and surface emissivity values were determined through the absolute emissivity method and the Temperature and Emissivity Separation (TES) algorithm, respectively. Pure water and sea water temperature are constant, both contained in the thermostatic water bath and regulated at a stable value, which emissivity were measurements in different view angles that range from nadir to 70°. Then, the comparison between the two measurements were made, and the retrieved emissivity value of the different methods were compared with the emissivity theoretical model (ETM). Next, assessments and analysis about the measurement accuracy of two methods were presented. For the results of the evaluation of those measurements, the profound reasons were provided by analyzing the environment condition effect and the sensitivity of the measure methods, during the measurements. The measurements show that for the emissivity derived with the AE method agree with those derived with the TES algorithm for the 10.576 and 11.296 ?m bands. However, the emissivity for the shorter wavelength bands are lower when derived with the AE method than those with the TES algorithm. The emissivity measured by CE 312 radiometer agree within very small difference with the emissivity theoretical model spectrum for the 11.296, and 10.6?m bands. Nevertheless, for the shorter wavelength bands, the difference appeared slightly bigger, with the larger value most likely caused by the deviation when gauging the water surface temperature and the input threshold value of the methods, while different wavelengths have different response.

9639-77, Session PS

Auroral activities observed by SNPP VIIRS day night band during a long period geomagnetic storm event on April 29-30, 2014

Xi Shao, Univ. of Maryland, College Park (United States); Changyong Cao, NOAA National Environmental Satellite, Data, and Information Service (United States); Tung-chang Liu, Univ of Maryland College Park (United States); Bin Zhang, Univ. of Maryland, College Park (United States); Wenhui Wang, ERT, Inc. (United States); Shing F. Fung, NASA Goddard Space Flight Ctr. (United States)

The Day Night Band (DNB) of the Visible Infrared Imaging Radiometer Suite (VIIRS) onboard Suomi-NPP represents a major advancement in night time imaging capabilities. The DNB senses radiance that can span 7 orders of magnitude in one panchromatic (0.5-0.9 ?m) reflective solar band and provides imagery of clouds and other Earth features over illumination levels ranging from full sunlight to quarter moon. When the satellite passes through the day-night terminator, the DNB sensor is affected by stray light due to solar illumination on the instrument. With the implementation of stray light correction, stray light-corrected DNB images enable the observation of aurora occurred at the nightside in the high latitude regions during geomagnetic storms and substorms. In this paper, DNB observations of aurora activities are analyzed during a long period (~ 24 hours) of geomagnetic storm event occurred on Apr. 29-30, 2014. The storm event is triggered by a weak solar coronal hole stream with the Bz component of the interplanetary magnetic field (IMF) pointing southward for ~ 24 hours. During this event, the geomagnetic storm index Dst reached -67 nT and the geomagnetic aurora electrojet (AE) index increased and reached as high as 1200 nT with large amplitude fluctuations. The event occurred during new moon period and DNB observation has minimum moon light contamination. During this event, auroras are observed by DNB for each orbital pass on the night side (~local time 1:30am) in the high magnetic latitude region in the southern hemisphere. These auroras are produced by optical emission induced by ionization and excitation of atmospheric constituents due to interaction of electrons precipitated along night side magnetic field lines with the atmosphere. The radiometrically calibrated DNB observations allow us to quantitatively analyze

the large-scale spatial distribution and temporal evolution of aurora during geomagnetic storm. Since DNB imagery has a high spatial resolution (750m), it also allows us to analyze fine details of aurora.

9639-78, Session PS

A improved method of fuzzy support degree based on uncertainty analysis

Yuan Huang, Jing Wu, Lihua Wu, Dong Wei Sheng, National Univ. of Defense Technology (China)

In a measurement system with distributed sensor processes, multisensor association is necessary. Association algorithms based on fuzzy set theory has been developed to solve the multisensor association problem, it has created a new branch of multisensor association. In general , association algorithm based on fuzzy set theory include three steps: First, Each sensor forms an opinion about the fuzzy proposition , named fuzzy support degree; Second, Define fuzzy distance measures between fuzzy sensor opinions; Finally, Choose the suitable fusion algorithm. There are many research on fuzzy distance measures and fusion algorithm, few pays attention to form the opinion about the fuzzy proposition. As the first step of the association algorithms , form the opinion accurately is meaningful and can affect the final fusion results.

Most multisensor association algorithms based on fuzzy set theory forms the opinion of fuzzy proposition using a simple triangular function. There exist two problems. First, it does not take the randomness of measurements into account, it is suitable for single measurement with unknown sensor variance, because no more information can be exploited, but it necessary to consider the uncertainty of measurements if the number of measurements is more than one. The uncertainty of measurements is defined as the correlation degree between measurements and targets. Second, the variance of sensors supposed to be known in the triangular function, but in fact the exact variance is difficult to acquire, indeed, the estimation errors is huge using sample variance to evaluate the real.

This paper discuss about two situations with known and unknown variance of sensors. First, with known variance and known mean(it is rational to model the measurements as Gaussian sequence). In this situation, a single measurement is enough. This paper proposes a different method, where the uncertainty of measurements is evaluated using error probability. It is easy to calculate the error probability with the known distribution. Second, with unknown variance and known mean value. The measurements originating from a sensor is often a small sample, that means the number of measurements is small. Traditional gray auto correlation method is expert in evaluating the uncertainty of small sample by calculating auto correlation. In this paper, we replace the sample mean in the gray auto correlation function with the real sensor mean value to analysis the uncertainty which is the correlation coefficient between targets and measurements actually. Finally, form the opinion about the fuzzy proposition in terms of weighting the opinion of all the sensors based on the result of uncertainty analysis.

Monte Carlo simulation studies on typical object recognition task. The task is to discriminate between two objects, labeled A and B. We have compared the result using the simple triangular function with the method this paper proposed. Sufficient simulations on some typical scenarios are performed, and the results indicate that the method presented is efficient.

9639-79, Session PS

Simulation with hyperspectral data of new Earth observation satellite missions

Dražen Skoković, José A. Sobrino, Juan Carlos Jimenez-Muñoz, Guillem P. Sòria, Yves Julien, Univ. de València (Spain)

In the near future, three new earth observation satellite missions will be launched to provide visible (VIS), near infrared (NIR), middle infrared (MIR) and thermal infrared (TIR) data: VENμS, Ingenio and Sentinel-3. VENμS Superspectral Camera (VSSC) is a sensor with 12 VIS-NIR spectral bands and 5.3 m of spatial resolution. Ingenio satellite carry onboard a high-resolution Primary Payload (PP) instrument with 4 VIS-NIR bands and 10 m of spatial resolution. Finally, Sentinel-3/Sea and Land Surface Temperature Radiometer (SLSTR) is a low spatial resolution sensor with 7 VIS-NIR-MIR spectral bands that will provide data at 500 m. Another 2 TIR spectral bands are included in the SLSTR instrument with spatial resolution of 1000 m.

The knowledge of the expected data before the launch of these missions is essential and simulated data are necessary to understand the response of the sensors. High spatial resolution images based on Compact Airborne Spectrographic Imager (CASI) and on Airborne Hyperspectral Sensor (AHS) data was used to aggregate to the scale of the low resolution sensor. Up-scaled to the nominal resolution of the simulated sensors was performed using simple linear averaging within no overlapping windows.

Multiple images was obtained in the campaigns performed in three Spanish test sites to simulate a Top of Atmosphere (TOA) radiances. CASI instrument, that has multiple and discrete image bands (between 400 nm and 1000 nm) and with 1 m of spatial resolution, was used to simulate VIS and NIR data of VSSC, PP instruments and three first SLSTR bands. Data of AHS sensor (5 m of spatial resolution and 48 MIR-TIR bands) was used in the simulation of the last 6 bands of SLSTR. The simulated data have been performed pixel by pixel using the filter function response for all sensors.

TOA radiances obtained for the different sensors can be used as a database to test and improve new algorithms for the implementation of products of level-2 or level-3.

9639-80, Session PS

Rugged: an operational, open-source solution for Sentinel-2 mapping

Luc Maisonobe, Jean Seyral, Guylaine Prat, Jonathan Guinet, Aude Espesset, CS Systèmes d'information (France)

Rugged, an open-source library for pixel geolocation, is at the heart of the Sentinel-2 Payload Data Ground Segment (PDGS) processing. The PDGS is in charge of processing the data acquired by Sentinel-2 high-resolution multi-spectral instrument (MSI). It aims at providing the end-users with orthorectified top-of-atmosphere reflectance images projected in UTM coordinates and tiled according to the Military Grid Reference System (MGRS) which divides the Earth in 100km square tiles.

Rugged is an intermediate-level library written in Java, which provides the tools to build a viewing model for any spacecraft instrument. The application to Sentinel-2 viewing model is implemented outside the library which aims at remaining mission-independent.

Rugged performs sensor-to-terrain mapping taking into account ground Digital Elevation Models, Earth rotation with all its small irregularities, on-board sensor pixel individual line-of-sights, spacecraft motion and attitude. The intersection of the line-of-sight with the DEM is based on an improved version of Duvenhage's algorithm (2009). Several Earth rotation models are available, from legacy models (Lieske 1976, Wahr 1980) to the most modern one (Capitaine 2006). IERS corrections for precession, nutation, rotation and pole wander are all taken into account in order to best position our planet before computing the intersection with the ground. Corrections for physical effects such as light-time correction and aberration of light are also applied.

Rugged mainly provides direct and inverse location, i.e. it allows to compute accurately which ground point is viewed from a specific pixel in a spacecraft instrument, and conversely which pixel will view a specified ground point. Direct and

inverse location can be used to perform full ortho-rectification of images and correlation between sensors observing the same area.

Implemented as an add-on for Orekit (Orbits Extrapolation KIT; a low-level space dynamics library), Rugged also offers the possibility of simulating satellite motion and attitude auxiliary data using Orekit's full orbit propagation capability. This is a considerable advantage for test data generation and mission simulation activities.

Together with the Orfeo ToolBox (OTB) image processing library, Rugged provides the algorithmic core of Sentinel-2 Instrument Processing Facilities. The S2 complex viewing model - with 12 staggered pushbroom detectors and 13 spectral bands - is built using Rugged objects, enabling the computation of rectification grids for mapping between cartographic and focal plane coordinates. These grids are passed to the OTB library for further image resampling, thus completing the orthorectification chain. Sentinel-2 stringent operational requirements to process several TeraBytes of data per week represented a tough challenge, though one that was well met by Rugged in terms of the robustness and performance of the library.

For more details, ckeck the website at www.orekit.org/rugged

9639-81, Session PS

Pixel partition method using Markov random field for measurements of closely spaced objects by optical sensors

Xueying Wang, Jun Li, Weidong Sheng, Wei An, National Univ. of Defense Technology (China); Qinfeng Du, College of Electronic Science and Engineering,National Univ of Defense Technology (China)

In Space-based optical system, during the tracking for closely spaced objects, the method with a constant false alarm rate(CFAR) detecting brings either more clutter measurements or the loss of target information , that depends on the false rate. To solve this problem, CSOs' feature on space-based optical sensor's pixel-plane were analyzed, then a pixel partition method using Markov random field(MRF) is proposed, simulation indicate: the method proposed provides higher performance than traditional method, especially when the signal-noise-rate is poor.

The energy distribution of the CSOs' on sensor's pixel-planes shows that Markov random field can describe the point-spread-function of optical sensors, and the noise and clutter have nothing to do with their neighbor pixel, that's quite different with pixel that carry the CSOs' energy. The different can be used to tell targets from clutter.

9639-82, Session PS

Calibration of the videospectral system for the space experiment "Uragan" onboard the ISS

Yury Krot, Leonid V. Katkovsky, Boris Beliaev, Belarusian State Univ. (Belarus); Anton Martenov, Belarusian State University (Belarus)

Aerospace Researches Department of the Institute of Applied Physical Problems at the Belarusian State University has developed videospectral system intended for ecological space experiment on the board of the ISS. This system has been used on the ISS since December 2014. The system includes the color (RGB) photocamera module of high spatial resolution, three CCD-array spectrometers MP-15 with the spectral resolution not worse than 5 nm, video-tracking camera, power control system, internal computer. For simultaneous registration the color images and about 290 spectra per one image the system has a common input lens Hasselblad HC 4,5/300 with an internal central electromechanical shutter. In standby mode the shutter is closed. The exposure time is determined by internal phototransistor.

Radiation flux transmitted through the input lens is divided into two parts by the beam splitter: the first part of the radiation is directed and focused on the color photodetector array Kodak KAF40000, the second part is focused on second plane intended for the spectral channel to obtain the spectra with a spectral resolution of 5 nm. Input ends of the imaging fibers are located at the second focal plane intended for the spectral channel. Imaging fibers transmit an image from the second focal plane to entrance slits of the spectrometers.

The polychromators of every spectrometer includes the imaging fiber, the entrance slit, concave holographic diffraction grating, and CCD-array photodetector. Light is transmitted through imaging fibers to the polychromators. Input of the imaging fiber is located at the focal plane of the input lens whereas its output is located at the entrance slit. Thereby the CCD-array of each spectrometer records the spectral distribution along lines and the spatial distribution along the columns. Astigmatism is typical aberration of polychromators based on concave spherical gratings: rays in the meridional and in the sagittal planes are focused at different points.

Estimated astigmatic line segment in a photodetector plane is about 2 mm, and height of the entrance slit is 20 mm. This means that polychromator provides about only 10 spectra of spatially separated areas. The method of improving the spatial resolution has been proposed: a separated focusing in the tangential and sagittal planes. This method consists in a shift of the output of the imaging fiber on specified distance from the entrance slit along the optical axis.

Laboratory experiment shows the significant improvement (up to 10 times) of the spatial resolution determined by the astigmatic grating for the central area of the entrance slit without loss of spectral resolution. In this case the entrance slit operates as one-dimensional aperture to obtain high spectral resolution.

The videospectral system has been calibrated by metrology complex. The method of the second diffraction order correction without using filters has been proposed. It consists in additional experiment using a monochromator and data processing to determine a dependence of second-order intensity on first-order intensity. The first data of the videospectral system application on board the ISS have confirmed the optical characteristics of image and spectral channels.

9639-83, Session PS

Monte Carlo-based multiphysics coupling analysis of x-ray pulsar telescope

Sheng Lian Li, Loulou Deng, Zhiwu Mei, Fuchang Zuo, Hao Zhou, Beijing Institute of Control Engineering (China)

An X-ray pulsar-based navigation is a novel celestial navigation technology for the spacecraft orbiting the Earth, probing the deep space or flying interplanetary. The complete navigation solutions, such as position, velocity, attitude and time, can be provided. This navigation technology is now the research hotspot within the domain of the satellite autonomous navigation.

X ray pulsar telescope is the basis for X-ray pulsar-based navigation. X-ray pulsar telescope is a classical complex space optical payload, which involves optical, mechanical, electrical and thermal disciplines. Actually, the X ray pulsar telescope will endure the strong impact during the launch of rocket and harsh space environment during the orbit service stage. Since there are many disciplines and different coupled relationships are involved in the X ray pulsar telescope. The multi-physics coupling analysis (MCA) plays an important role in improving the in-orbit performance of X ray pulsar telescope.

However, the conventional MCA methods encounter two serious problems in dealing with the X ray pulsar telescope. One is that both the energy and reflectivity information of X-ray can't be taken into consideration during the design

process, which always misunderstands the essence of X ray pulsar telescope. Another is that the coupling data can't be transferred automatically among different disciplines, leading to computational inefficiency and thus increases the design cost and the development cycle.

Therefore, a new MCA method for X-ray pulsar telescope is proposed based on the Monte Carlo method and the full reflective theory of X-ray. The main idea, procedures and operational steps of the proposed method are addressed in detail. Firstly, this method takes both the energy and reflectivity information of X-ray into consideration simultaneously. And formulate the thermal-structural coupling equation and multi-physics coupling analysis model based on the finite element method. Then, all the thermal-structural, thermal, and structural analysis under different working conditions have been implemented. Secondly, the mirror deformation can be obtained using construction geometry function. Meanwhile, the polynomial function is adopted to fit the deformed mirror and meanwhile evaluate the fitting error. Thirdly, the focusing performance analysis of X ray pulsar telescope can be evaluated by the RMS and maximum radius of dispersion spot employing the proposed method. Finally, a Wolter-I X ray pulsar telescope is taken as an example to verify the proposed MCA method. The simulation results show that the thermal-structural coupling deformation is bigger than others, the vary law of deformation effect on the focusing performance has been obtained. The focusing performances of thermal-structural, thermal, structural deformations have degraded 30.01%, 14.35% and 7.85% respectively. The RMS of dispersion spot are 2.9143mm, 2.2038mm and 2.1311mm. As a result, the validity of the proposed method is verified through comparing the simulation results and experiments, which can be employed in the reliability-based design of X ray pulsar telescope.

9639-84, Session PS

Application of high-precision matching about multisensor in fast stereo imaging

Hui Jing Zhang, Academy of Opto-Electronics (China) and Chinese Academy of Sciences (China); Mei Zhou, Haohao Wu, Dandan Zhang, Academy of Opto-Electronics (China)

Now most of the linear array active and passive imaging sensors integrate range data of LiDAR (Light Detection And Ranging) with texture information of visible light camera to get the stereo image of targets. Obtaining the accurate matching relationship of the source data is the guarantee of active and passive fast stereo imaging. High precision matching of linear array multi-sensor is the key to ensure fast stereo imaging. This paper has presented the general principle of active and passive imaging sensor, designed a high precision matching calibration system of linear array multi-sensor based on large-diameter collimator combined with assisted laser light source, and put forward an optical axis parallelism calibration technology suitable for linear array active and passive imaging sensor. This technology makes use of image acquisition system to obtain spot center, in order to match multi-linear array laser receive and transmit optical axes. At the same time, this paper uses linear visible light sources to extract the optical axis of the laser, then completes the parallelism calibration between lasers receive and transmit optical axes of multi-linear array sensors and active and passive optical axis. The matching relationship between the visible pixels and LiDAR (Light Detection And Ranging) detecting sensors can be obtained when using this technique to calibrate the active and passive imaging sensor. This paper has also described the general flow of fast stereo imaging processing of active and passive imaging sensor. And the obtained relationship is applied to the fast stereo imaging experiment of active and passive imaging sensor and gained good imaging effect. At the same time, contrast experiment without accurate input relationship was implemented; the comparative results showed that high precision matching of linear array multi-sensor can significantly improve the fast stereo imaging effect.

9639-85, Session PS

Applicability research of ALDC camera for the application of unmanned aerial vehicle

Chou Uong Choi, Ho Hyun Jeong, Pukyong National University (Korea, Republic of); Jinwoo Park, Pukyong National Univ (Korea, Republic of); Hoyong Ahn, Pukyong National University (Korea, Republic of)

A smart camera is having a dedicated processor and a lot of sensor(GPS, Accelerometer, 3Axis-magnetic, light, gyroscope, gravity, rotation, etc) in each unit. and, it can collect lens distortion and image stabilization, etc.

The existing camera was not able to perform prompt image processing without having dedicated processor. In addition, as the high-resolution digital image got accessible, the technology of digital camera ranging from computer vision to such specialized area as digital photogrammetry has been applied in many ways. (Hwan-hee Yoo etc, 2003). When it comes to digital photogrammetry, in particular the frequency of high-resolution non-metric camera usage has constantly increased (Jeong Su etc, 2005).

The purpose of the study is to evaluate applicability of the image by UAV with a built-in smart camera to examine generation of DEM according to the correction of camera distortion. A pair of the secured image goes through triangulation process for geometric correction. This process is dividedly proceeded with the case of concerning camera calibration date, and the case without concerning. Accuracy evaluation on each case is also undertaken. At this time differences in the result according to camera calibration data, and orthoimage is created through orthometric correction process utilizing DEM by TLS technique, and its accuracy is estimated by check point. It is also evaluated by comparing between TLS and DEM.

9639-86, Session PS

S-NPP VIIRS day-night band on-orbit calibration and performance update

Kwofu V Chiang, Hongda Chen, Science Systems and Applications, Inc. (United States); Chengbo Sun, Global Science and Technology, Inc. (United States); Samuel Anderson, Science Systems and Applications, Inc. (United States); Xiaoxiong Xiong, NASA/GSFC (United States)

The Suomi-NPP VIIRS instrument has been successfully operating on orbit since October, 2011. The Day-Night Band (DNB) onboard S-NPP VIIRS is a panchromatic channel covering wavelengths from 0.5 to 0.9 micron that is capable of observing the Earth scene in visible/near-Infrared spectral range at spatial resolution of 750 m. The DNB operates at low, mid, or high gain stages, and it uses an onboard solar diffuser (SD) for low gain stage calibration. The SD observations also provide a mean to compute gain ratios between low-to-mid and mid-to-high gain stages. With its large dynamic range and high sensitivity, the DNB detectors can make observations during both daytime and nighttime. This paper describes the DNB on-orbit calibration methodology used by the VIIRS Characterization Support Team (VCST) in supporting the NASA earth science community with consistent VIIRS sensor data records (SDRs) made available by the Land Science Investigator-led Processing Systems (SIPS). We will update the status of DNB calibration and characterization of its performance, including the SD degradation, detector gains and gain ratios trending, stray light contamination and its correction, as well as other performance metrics.

9639-33, Session 8

Comparison of S-NPP VIIRS and PLEIADES lunar observations

Xiaoxiong J. Xiong, NASA Goddard Space Flight Ctr. (United States); Sophie Lachérade, Bertrand Fougnie, Ctr. National d'Études Spatiales (France); Jon P. Fulbright, Zhipeng Wang, Science Systems and Applications, Inc. (United States)

The first Visible Infrared Imaging Radiometer Suite (VIIRS) instrument was launched on-board the Suomi National Polar-orbiting Partnership (NPP) satellite in October 2011. S-NPP VIIRS has 15 reflective solar bands (RSB), including a Day-Night band (DNB), covering wavelengths from 0.41 to 2.2 microns, and 7 thermal emissive bands (TEB) with wavelengths from 3.7 to 12.2 microns. Designed and operated with a strong MODIS heritage, the VIIRS RSB are calibrated on-orbit by an on-board solar diffuser in each orbit. On a regular basis, lunar observations are scheduled and implemented to independently monitor the RSB radiometric calibration stability. Since launch, more than 28 scheduled lunar observations have been made by the SNPP VIIRS, nearly all with phase angles from -51.5 to -50.5 degrees. Additional lunar observations at different phase angles are also collected from time to time for different spectral bands. The PLEIADES system consists of two satellites, PLEIADES-1A and PLEIADES-1B launched at the end of 2011 and 2012, respectively. Each instrument has 5 reflective solar spectral bands: four (blue, green, red and near-infrared) with a 2.8 m spatial resolution and one panchromatic channel with a 70 cm vertical viewing resolution. PLEIADES RSB are calibrated using observations of Pseudo Invariant Calibration Sites (PICS), such as African desert sites, Antarctica, ocean sites and the Moon. Since launch PLEIADES-1A and PLEIADES-1B have collected more than 1500 images of the Moon covering the phase angle range of ±115 degrees, which are dedicated to sensor calibration and to sensitivity studies of different lunar calibration methods. This paper provides an overview of SNPP VIIRS and PLEIADES lunar observations, an assessment of their calibration differences, inter-comparison strategies implemented, and future effort to be carried out. Also discussed in this paper are lessons learned that can potentially benefit other earth observing sensors and improve the radiometric accuracy of existing lunar model(s).

9639-34, Session 8

S-NPP VIIRS SDR calibration assessment and improvement

Kwofu V Chiang, Ning Lei, Jon Fulbright, Samuel Anderson, Science Systems and Applications, Inc. (United States); Sergey Gusev, Chengbo Sun, Global Science and Technology, Inc. (United States); Xiaoxiong Xiong, NASA/GSFC (United States)

The Visible Infrared Imaging Radiometer Suite (VIIRS) onboard the Suomi-National Polar-orbiting Partnership (S-NPP) satellite has successfully operated for more than three and a half years since its nadir door open on November 21, 2011. The VIIRS has 22 spectral bands: 5 Imagery bands (I-bands, 375 m), 16 Moderate resolution bands (M-bands, 750 m), and 1 panchromatic Day-Night band (DNB, 750 m). These bands are calibrated in two different categories: the reflective solar bands (RSB) (M1-M11, I1-I3, and DNB) covering wavelengths from 0.41 to 2.3 micron are calibrated with a set of solar diffuser (SD) and solar diffuser stability monitor (SDSM); the thermal emissive bands (TEB) (M12-M16 and I4-I5) covering wavelengths from 3.7 to 12 micron are calibrated with a blackbody (BB). In support of improved environmental data records (EDRs) and quality assessment, the NASA VIIRS Characterization Support Team (VCST) promotes the generation of a well-calibrated VIIRS sensor data records (SDRs) through the use of on-board calibrators (OBCs) with stable performance and consistent calibration methods for RSB and TEB. The improvements of SDR on-orbit calibration methodology and coefficients look-up-tables (LUTs) update will be described in this paper. Challenges and future improvements for SDR radiometric calibration will also be discussed.

9639-35, Session 8

A summary of the joint GSICS – CEOS/IVOS lunar calibration workshop: moving towards intercalibration using the Moon as a transfer target

Sebastien C. Wagner, Tim J. Hewison, EUMETSAT (Germany); Thomas C. Stone, U.S. Geological Survey (United States); Sophie Lachérade, Bertrand Fougnie, Ctr. National d'Études Spatiales (France); Xiaoxiong J. Xiong, NASA Goddard Space Flight Ctr. (United States)

In December 2014 experts from 14 different agencies and departments attended the joint GSICS – CEOS/IVOS Lunar Calibration Workshop meeting organized by EUMETSAT in collaboration with USGS, CNES and NASA. Altogether, this represents potentially more than 25 instruments capable of observing the Moon.

The main objectives of the workshop were i) to work across agencies with the GSICS Implementation of the ROLO model (GIRO) - a common and validated implementation of the USGS lunar radiometric reference, ii) to share knowledge and expertise on lunar calibration and iii) to generate for the first time a reference dataset that could be used for validation and comparisons. This lunar calibration community endorsed the GIRO to be the established publicly-available reference for lunar calibration, directly traceable to the USGS ROLO model. However, further effort is required to reach inter-calibration between instruments, in particular for each instrument team to accurately estimate the over-sampling factor for their images of the Moon.

A way forward to develop a cross-calibration algorithm and GSICS inter-calibration products is proposed. This includes key issues of fixing the GIRO calibration to an absolute scale, addressing spectral differences between instruments, and improving the existing calibration reference, which translates into future updates of the GIRO. The availability of extensive Moon observation datasets will help to further improve this reference and is expected to grow with the availability of additional lunar observations from past, current and future missions. All participants agreed on EUMETSAT pursuing its efforts in developing and maintaining the GIRO in collaboration with USGS to ensure traceability to the reference ROLO model.

9639-36, Session 8

Assessment of MODIS on-orbit spatial performance

Daniel Link, Science Systems and Applications, Inc. (United States); Xiaoxiong J. Xiong, NASA Goddard Space Flight Ctr. (United States); Zhipeng Wang, Science Systems and Applications, Inc. (United States)

The Terra and Aqua satellites are part of NASA's Earth Observing System and both satellites host a nearly-identical Moderate Resolution Imaging Spectroradiometer (MODIS). Of the 36 MODIS spectral bands mounted among four Focal Plane Assemblies (FPAs), two have a 250 meter spatial resolution at nadir. Five bands have a spatial resolution of 500 meters, while the remaining bands make observations at 1 kilometer resolution. MODIS is equipped with a suite of on-board calibrators to track on-orbit changes in key sensor performance parameters. The Spectro-Radiometric Calibration Assembly (SRCA) contains a calibration source that allows on-orbit assessment of MODIS spatial performance. When compared against pre-launch characterization, on-orbit calibration operations provide information on current

band-to-band registration (BBR), FPA-to-FPA registration (FFR), detector-to-detector registration (DDR), Modulation Transfer Function (MTF), and Instantaneous Field-of-View (IFOV). We present the methodology of the on-orbit spatial calibrations and the results of these key spatial parameters. The MODIS spatial characteristics, measured on-orbit, are compared against design specifications and pre-launch measurements. Though the MODIS instrument was designed to fulfill a six year mission on-orbit, Terra and Aqua MODIS have been successfully producing results for over 15 and 13 years, respectively. A spatial calibration event is scheduled for each instrument approximately four times each year. BBR results show Terra MODIS bands are still within their 200 m specification. Aqua BBR has shown similar stability on-orbit. We present instrument MTF and note its change over time. The MODIS instrument experiences seasonal temperature cycles as well as a gradual temperature increase over time. We note the relationship between MODIS instrument temperature and trends in spatial characteristics.

9639-37, Session 8

Cross-calibration of the reflective solar bands of Terra MODIS and Landsat 7 Enhanced Thematic Mapper plus over PICS using different approaches

Amit Angal, Jake Brinkmann, Science Systems and Applications, Inc. (United States); Nischal Mishra, South Dakota State Univ. (United States); Daniel Link, Science Systems and Applications, Inc. (United States); Xiaoxiong J. Xiong, NASA Goddard Space Flight Ctr. (United States); Dennis L. Helder, South Dakota State Univ. (United States)

Both Terra MODIS and Landsat 7 (L7) Enhanced Thematic Mapper Plus (ETM+) have been successfully operating for over 15 years collecting valuable measurements of the earth's land, ocean, and atmosphere. The land-viewing bands of both sensors are widely used in several scientific products such as surface reflectance, normalized difference vegetation index, enhanced vegetation index etc. A synergistic use of the multitemporal measurements from both sensors can greatly benefit the science community. Previous effort from the MODIS Characterization Support Team (MCST) was focused on comparing the top-of-atmosphere reflectance of the two sensors over Libya 4 desert target. Uncertainties caused due to the site/atmospheric BRDF, spectral response mismatch, and atmospheric water-vapor were also characterized. In parallel, an absolute calibration approach based on reference radiometer was also developed for the Libya 4 site by the South Dakota State University's Image Processing Lab. Observations from Terra MODIS and Earth Observing One (EO-1) Hyperion were used to develop the model and results were validated with number of sensors including Landsat 7 ETM+. Recently, there has been an update to the MODIS calibration algorithm, which has resulted in a newly reprocessed collection 6 level 1B calibrated products. Similarly, a calibration update to some ETM+ bands has also resulted in long-term improvements of its calibration accuracy. With these updates calibration differences between the spectrally matching bands of Terra MODIS and L7 ETM+ over the Libya 4 site are evaluated using both approaches discussed earlier. Results from other stable African desert sites using the MCST-approach are also presented.

9639-38, Session 9

Evaluation of VIIRS and MODIS thermal emissive band calibration consistency using Dome C

Sriharsha Madhavan, Aisheng Wu, Jake Brinkmann, Brian N. Wenny, Science Systems and Applications, Inc. (United States); Xiaoxiong J. Xiong, NASA Goddard Space Flight Ctr. (United States)

The S-NPP Visible Infrared Imaging Radiometer Suite (VIIRS) instrument is designed based on MODIS heritage and uses a similar on-board calibrating source - a V-grooved blackbody for the thermal emissive bands (TEB). Except for the 10.7 μm band, the central wavelengths of the rest of the VIIRS TEB match well with MODIS. To ensure the continuity and consistency of data records between VIIRS and MODIS TEB, it is important to assess any systematic differences between the two instruments for scenes with temperatures significantly lower than blackbody operating temperatures at ~290 K. In previous studies, the MODIS Calibration and Characterization Support Team (MCST) at NASA/GSFC uses recurrent observations of Dome C, Antarctica by both Terra and Aqua MODIS over the mission lifetime to track their calibration stability and consistency. Near-surface temperature measurements from an automatic weather station (AWS) provide a proxy reference useful for tracking the stability and determining the relative bias between the two MODIS instruments. In this study, the same approach is applied to VIIRS TEB and the results are compared with those from the matched MODIS TEB. The relative spectral response (RSR) differences are accounted for in the calculation of the radiance using MODTRAN simulations. The results of this study provide a quantitative assessment for VIIRS TEB performance over the first three years of the mission.

9639-39, Session 9

Tracking Terra MODIS on-orbit polarization sensitivity using pseudo-invariant desert sites

Aisheng Wu, Xu Geng, Science and Systems Applications, Inc. (United States); Andrew Wald, Global Science & Technology, Inc. (United States); Amit Angal, Science Systems and Applications, Inc. (United States); Xiaoxiong J. Xiong, NASA Goddard Space Flight Ctr. (United States)

The Moderate-Resolution Imaging Spectroradiometer (MODIS) is currently flying on NASA's Earth Observing System (EOS) Terra and Aqua satellites, launched in 1999 and 2002, respectively. MODIS reflective solar bands (RSB) in the visible wavelength range are known to be sensitive to polarized light based on prelaunch polarization sensitivity tests. The polarization impact is dependent on scan angle and mirror side. After about five years of on-orbit operation, it is found that a few shortest-wavelength bands of Terra MODIS show increased polarization sensitivity. In this study, we examine the impact of polarization on measured top-of-atmosphere (TOA) reflectances over pseudo-invariant desert sites. The standard polarization correction equation is used in combination with simulated at-sensor radiances by the Second Simulation of a Satellite Signal in the Solar Spectrum (6SV), Vector Radiative Transfer Code. Key Mueller matrix elements describing the polarization and gain correction of these bands are derived over the mission lifetime. Results indicate that the polarization sensitivity increases with scan mirror's angle of incidence (AOI) and relatively large impact is observed from mirror side 2. At the end of 2009, it reaches a peak at approximately 30% at 0.41 μm and stabilizes since then.

9639-40, Session 9

Radiometric calibration and performance trends of the Clouds and Earth's Radiant Energy System (CERES) instruments onboard the Terra and Aqua spacecraft

Mohan Shankar, Science Systems and Applications, Inc. (United States); Kory J. Priestley, NASA Langley Research Ctr. (United States); Nathaniel P Smith,

Science Systems and Applications Inc (United States); Natividad M. Smith, Susan Thomas, Dale R. Walikainen, Science Systems and Applications, Inc. (United States)

The Clouds and Earth's Radiant Energy System (CERES) instruments are part of NASA's Earth Observing System (EOS) missions to study the impact of clouds on the earth's radiation budget. These were based on instruments that were flown previously on the Earth's Radiation Budget Experiment (ERBE). CERES enables the measurement of the reflected shortwave radiation as well as the outgoing emitted longwave radiation from the earth, which are two components of the radiation budget. There are currently five CERES instruments making these measurements from earth's orbit- Flight Models (FM) 1 and 2 on Terra (operational since March 2000), FM 3 and 4 on Aqua (operational since July 2002) and FM5 on Suomi NPP (operational since December 2011). Each CERES instrument comprises three sensors that make measurements in different wavelength bands- a Shortwave sensor that make measurements between 0.3 and 5 microns, a Window sensor that measures the atmospheric water-vapor absorption band between 8 and 12 microns, and a Total Sensor that measures all incident energy (0.3 to >100 microns). The required accuracy of CERES measurements of 0.5% in the longwave and 1% in the shortwave is achieved through an extensive pre-launch ground calibration campaign as well as on-orbit calibration and validation activities. The on-orbit calibration is carried out using the Internal Calibration Module (ICM), which consists of a quartz-halogen tungsten lamp to calibrate the Shortwave sensor, blackbodies to calibrate the longer wavelengths, and a Mirror Attenuator Mosaic (MAM), which is a solar diffuser plate that is used to calibrate both the Shortwave and Total sensors. The sensor calibrations using the ICM provide information about the on-orbit changes in the sensors' radiometric gains from pre-launch values. Several validation studies that involve trending the radiances of specific earth scenes help to monitor the behavior of the instrument in various spectral bands. These validation studies helped to identify degradation observed in the measurements when viewing ocean (blue) scenes and the appropriate correction has been applied. The CERES Edition-4 data products for the instruments on Terra and Aqua (FM1-FM4) contain the most recent calibration updates that have been applied. One issue that was identified with the Edition-3 data products was that for the instruments on Aqua, the trends of the daytime longwave radiance anomalies (deseasonalized monthly average radiances) for ocean and land scenes were not consistent with each other. This pointed to the fact that there was some spectral abnormality in the near IR wavelength regions of the Total sensors' spectral response. The calibration approach that went into the deriving the Edition-3 data products assumed that degradation was present only in the wavelengths toward the blue end of the spectrum. As a result of this observation, the calibration approach has been updated to account for spectral changes in the longer wavelengths as well. In this paper, we discuss the updated calibration methodology used in the generation of the Edition-4 data products as well as the validation studies to demonstrate the improvements in the trends observed.

9639-41, Session 9

Landsat-8 calibration inter-consistency with ocean color missions

Nima Pahlevan, NASA Goddard Space Flight Ctr. (United States) and Sigma Space Co. (United States); John R. Schott, Rochester Institute of Technology (United States)

Over the past two years, the Operational Land Imager (OLI) onboard Landsat-8 has offered remarkable, high-quality observations over coastal/inland waters, which have significantly expanded the relevant science and applications of the Landsat mission. This study provides an update on OLI's radiometric performance over bodies of water through the analysis of near-simultaneous nadir overpasses with dedicated ocean color missions, including the Moderate resolution Imaging Spectroradiometer (MODIS) and the Visible Infrared Imaging Radiometer Suite (VIIRS). The inter-comparisons are performed across the OLI's entire Field Of View (FOV) to derive gain factors specific to various subsections of the focal plane. The analyses help to validate OLI's routine calibration procedure and complement ongoing vicarious calibration exercises. It is found that, for the visible and near-infrared channels, the OLI radiometric responses, on average, are well in agreement (within ±2%) with the TOA radiances estimated by the ocean color satellites. However, the TOA radiance at the new 443-nm band is found to be, on average, 3.4 % larger than those measured by the ocean color sensors. When the MultiSpectral Instrument (MSI) onboard Senstinel-2 is launched, a similar approach may be applied to ensure consistency with OLI (and other ocean color missions) for coastal/inland water applications.

9639-42, Session 9

The geostationary operational environmental satellite R-series advanced baseline imager: detector spectral response effects on thermal emissive band calibration

Aaron J. Pearlman, ERT, Inc. (United States); Francis P. Padula, GeoThinkTank, LLC (United States); Xiangqian Wu, National Oceanic and Atmospheric Administration (United States); Changyong Cao, NOAA National Environmental Satellite, Data, and Information Service (United States)

The Advanced Baseline Imager (ABI) will be aboard the National Oceanic and Atmospheric Administration's Geostationary Operational Environmental Satellite R-Series (GOES-R) to supply data needed for operational weather forecasts and other science applications, which depend on high quality data. Unlike the heritage operational GOES systems that have two or four detectors per channel, ABI has hundreds of detectors per channel requiring orders of magnitude more calibration coefficients. This increase in number of detectors poses new challenges for next generation sensors as each detector has a unique spectral response function (SRF) even though only one SRF per band is used operationally. The instrument vendor derived the baseline operational SRFs by propagating the spectral reflectances/transmittances of the optical components and detector quantum efficiencies in the ABI optical train to obtain the SRF for each band. Since this process does not account for each detector independently, it yields an SRF that is effectively an average SRF across all detectors instead of a unique spectral response based on each one. Using measured system-level SRF data from pre-launch testing, we have the opportunity to characterize the calibration impact using measured SRFs – both per detector and as an average of detector SRFs similar to the operational version. For the ABI's ten thermal emissive bands (TEBs), the responses to the reference internal blackbody determine the calibration coefficients and are dependent on the SRFs. We applied the measured detector SRF data to the TEB calibration pre-launch test data taken in a thermal vacuum testing environment thereby propagating the SRFs through the calibration process. We compared the retrieved brightness temperature values using the average SRF with those using the detector SRFs, expressed as differences in retrieved brightness temperatures. The observed brightness temperature trends showed structure across the array with magnitudes as large as ~80 mK for band 7 (3.90 μm), ~100 mK for band 12 (9.61 μm), and ~200 mK for band 14 (11.2 μm). The temperature differences between detector and average SRFs produced the structure expected using a simulated ideal blackbody as the calibrator. The pre-launch TEB calibration test uses an external reference in order to determine the expected calibration bias between the internal blackbody the reference blackbody. We determined this bias using the detector SRFs and found that the bias depends on whether the non-linearity of the instrument response is taken into account in the calibration process. Further understanding of this bias could lead to refinements of the blackbody thermal

model and a better understanding of causes of the measured non-linearity. This work shows the calibration impacts of using an average SRF across many detectors instead of accounting for each detector SRF independently in the TEB calibration. Note that these impacts neglect effects from the spectral sampling of Earth scene radiances that include atmospheric effects, which may further contribute to artifacts post-launch and cannot be mitigated using detector SRFs. This work enhances the ability to diagnose anomalies on-orbit and reduce calibration uncertainty for improved system performance.

9639-43, Session 10

Selenographic coordinate mapping of lunar observations by GOES imager

Xi Shao, ERT, Inc. (United States) and Univ. of Maryland, College Park (United States); Xiangqian Wu, National Oceanic and Atmospheric Administration (United States); Fangfang Yu, ERT, Inc. (United States)

Radiometric stability of the lunar surface, its lack of atmosphere and smooth reflectance spectrum makes the moon surface an ideal target for calibrating satellite-based multi-band imagers. Lunar calibration for solar bands has been an important part of trending the instrument radiometric performance. The lunar disk-equivalent irradiance has been used to trend the on-orbit degradation of the GOES imager and its performance is largely affected by the uncertainties embedded in the lunar irradiance model in characterizing its dependence on lunar phase and libration, as well as the satellite measurements. On the other hand, the lunar view by GOES imager provides opportunity to perform radiometric calibration of GOES imager using lunar radiances of selected locations on the Moon. In order to do so, the GOES lunar observations need to be mapped onto selenographic coordinate, i.e. latitude and longitude in moon-centered coordinate. In this paper, algorithms and procedures are developed to map GOES lunar images onto selenographic coordinate. Each individual lunar observation is corrected with progressive shift in east-west scan direction, oversampling factor and distortion of lunar image to result in a disk-shaped moon image. Both controlling point and landmark matching are applied to determine rotation angles and three consecutive rotations are performed to map lunar observation onto selenographic coordinates. Lunar observations of GOES-12 are processed and regions of interest (ROIs) are identified. Solar zenith angle and viewer zenith angle-dependence of lunar radiances at ROIs are analyzed. It is found that lunar radiance depends strongly on Sun-Moon-Satellite geometry and knowledge of BRDF of lunar surface can enable trending of radiometric performance of GOES imager with lunar radiance.

9639-44, Session 10

Preparation of a new autonomous instrumented radiometric calibration site: Gobabeb, Namib Desert

Claire L. Greenwell, Agnieszka Bialek, Amelia Marks, Emma R. Woolliams, National Physical Lab. (United Kingdom); Béatrice Berthelot, Magellium (France); Aimé Meygret, Sébastien Marcq, Ctr. National d'Études Spatiales (France); Marc Bouvet, European Space Research and Technology Ctr. (Netherlands); Nigel Fox, National Physical Lab. (United Kingdom)

A new permanently instrumented radiometric calibration site for high/medium resolution imaging satellite sensors is currently under development, focussing on the visible and near infra-red parts of the spectrum. It will become a European contribution to the CEOS (Committee on Earth Observation Satellites) initiative RadCalNet (Radiometric Calibration Network of automated instruments). The aim of this network is to provide daytime nadir top of atmosphere spectral reflectances in 10 nm steps every thirty minutes, at coordinated sites around the world, to facilitate satellite L1 radiance comparison and calibration. In addition to the requirements of RadCalNet, which will initially be limited to nadir, the Gobabeb site will provide off-nadir measurements to increase the number of matching overpasses. The site is being established as part of a collaborative project between ESA and CNES, partly in preparation for the Sentinel-2 satellite, in conjunction with NPL and Magellium.

In the first stage of this project, Magellium performed a study using pre-defined objective criteria to identify sites with optimum characteristics for radiometric calibration. An area close to Gobabeb Research Centre, Namibia, at 23°34'S, 15°03'E was chosen from a shortlist. The exact location of the permanent monitoring instrumentation will be defined following an initial site characterisation.

To achieve SI traceability with a robust uncertainty budget for in-situ measurements on this site, NPL has performed a detailed characterisation and calibration of instruments and artefacts to be used on the site. These include the instrument intended for permanent autonomous operation: a CIMEL sun photometer; those intended for the initial characterisation of the site: two ASD FieldSpec spectroradiometers and GRASS (Gonio RAdiometric Spectrometer System): a system for measuring HDRF (Hemi-spherical Directional Reflectance Factor); and the in-situ SI traceable standards (Spectralon™ panels and tarpaulins). The tarpaulins will be used to estimate variability due to instrument operator differences during ground reflectance measurements.

The laboratory-based preparation of the CIMEL sun photometer and the ASD FieldSpecs included absolute radiometric calibration (in radiance mode only), temperature response, spectral response (using an NPL tuneable laser system), and stability over time. The stability of the CIMEL instrument was found to be better than 0.18 %, and agreement within 1.8 % of the manufacturer's radiance calibration coefficients was found for all channels, except for 414 nm. NPL's calibration has reduced the uncertainty associated with these coefficients by a factor of 2. Only the longer wavelength channels showed temperature sensitivity; the shorter wavelength channels were unaffected over the tested temperature range of 8 °C – 35 °C. The GRASS spectrometer will undergo a similar set of tests before deployment. The reflectance standards (Spectralon™ panels and tarpaulins) will be calibrated using NPL's National Reference Reflectometer facility. Radiance factor will be measured for nadir viewing angle, and illumination angles that match the solar geometry at common satellite overpass times. In-situ measurements are also intended to be conducted at these times.

This presentation will cover the calibration and SI-traceability of these instruments. It is anticipated that a discussion on how these instruments performed when used in the site characterisation will also be included.

9639-45, Session 10

Development of a sensor web for vicarious-sites measurement based on self-calibrating LED radiometers

Roberto Filippo, Emanuele Taralli, Mauro Rajteri, Giorgio Brida, Istituto Nazionale di Ricerca Metrologica (Italy); Simon R. G. Hall, Agnieszka Bialek, Claire L. Greenwell, Nigel Fox, National Physical Lab. (United Kingdom)

Earth Observation is a major source of information for climate change research, monitoring and most importantly, for development of mitigation strategies that will minimise future damage caused by these changes. The harsh and challenging environment of space clearly limits the exact knowledge of instruments' performance during their operational phase. To obtain quality assured global and local products, satellites require improved and continuous radiometric calibration and validation uncertainty and traceability through all stages of data production: pre-flight and post-launch, and all the intermediate processing steps. These aspects are addressed

within the European Metrology Research Programme MetEOC I and II (Metrology for Earth Observation and Climate).

Instrumented test site based vicarious calibration of satellite radiometric sensors has already proven its efficacy (see the work of the Remote Sensing Group at the University of Arizona), however the high cost of instrumentation, transportation and labour has pushed the development of unattended cost effective radiometers based on LEDs as radiation detectors. This concept has shown some limitations mainly due to the variability of measurement results.

We have developed a multi-band ground viewing radiometer, based on LEDs, that addresses the issue of measurement instability through a self-calibration feature, a high resolution precision analog-to-digital converter, and temperature monitoring for data correction. The goal is to perform autonomous measurement of surface spectral reflectance/radiance, traceable to SI. In our instrument, LEDs are used both as radiation detectors and radiation reference sources. Each detector is coupled to its source counterpart, which is laboratory calibrated, so that a self-calibration could be performed before every reflectance measurement in the field. Measurements of the land reflectance in 4 spectral bands, from 350 nm to 900 nm are acquired. The instrument will be used as an in-situ sensor web, therefore it includes the ability to communicate through a wireless link. A master node (connected to a PC that runs LabVIEW control software) can send commands to sensor nodes, initiate a measurement sequence or a self-calibration procedure, and receives the data from individual sensors. Wireless communication between the master node and the prototype was successfully tested during its initial calibration. One prototype has been bench-tested and is now working outdoors together with an improved second instrument so that the long term reliability can be studied. At the same time, we are using the preliminary test results to build a sensor web composed of five improved radiometers that will be geographically distributed over hundreds of metres in the test site.

This paper provides information about the principle of operation, the design, and the realization of the multi-band radiometer. Special attention is given to the investigation of LED detection and emission properties and to LED temporal degradation tests, which are the basis of the self-calibration concept. Preliminary results are reported, together with some planned further improvements that are already starting to be implemented for the development of the full sensor web.

9639-46, Session 10

Vicarious calibration of KOMPSAT-3 AEISS

Ho Yong Ahn, Pukyong National Univ. (Korea, Republic of); Jinsoo Kim, Inje Univ. (Korea, Republic of); Cheonggil Jin, Korea Aerospace Research Institute (Korea, Republic of); Chuluong Choi, Pukyong National Univ. (Korea, Republic of)

A radiometric characterization of the Korea Multi-Purpose Satellite (KOMPSAT) Series multispectral imagery was performed by the Korea Aerospace Research Institute (KARI) and the Pukyong National University Remote Sensing Group (PKNU RSG). This paper presents a vicarious radiometric calibration performed by KARI and PKNU RSG in 2012 and 2014. Correlations between top-of-atmosphere (TOA) radiances and the spectral band responses of the KOMPSAT-3 sensors at the Zuunmod, Mongolia and Goheung, South Korea were significant for multispectral bands. KOMPSAT-3 calibration coefficients for all bands estimated in 2012 continued to agree well with calibration coefficients estimated in 2014 (within 1.5%). As a result of this study, KARI will update and publish the KOMPSAT-3 multispectral radiometric calibration coefficients as official values. The average difference in TOA reflectance between KOMPSAT-3 and Landsat-8 images over the Libya 4, Libya and Railroad Valley Playa, USA in the red-green-blue (RGB) region was under 3%, whereas in the NIR band, the TOA reflectance of KOMPSAT-3 was lower than the that of Landsat-8 due to the difference in the band passes of two sensors. The KOMPSAT-3 sensor includes a band pass near 940 nm that can be strongly absorbed by water vapor and therefore displayed low reflectance. To overcome this, we need to undertake a detailed analysis using rescale methods, such as the spectral bandwidth adjustment factor (SBAF).

9639-48, Session 11

The Traceable Radiometry Underpinning Terrestrial and Helio Studies (TRUTHS) mission

Paul Green, Nigel Fox, National Physical Lab. (United Kingdom); Daniel R. Lobb, Surrey Satellite Technology Ltd. (United Kingdom); Jonathan Friend, Surrey Satellite Technology Ltd (United Kingdom)

Our planet's climate is changing. Predicting the long term trend of this change, identifying the key processes and drivers and the manifestation of these changes on society rely upon the predictive capabilities of sophisticated, but highly complex simulation models. The output of these models is the cornerstone of international efforts to assess the magnitude of the foreseen changes and guides the policy decisions that select effective mitigation and adaptation strategies.

These model predictions need to be validated against an observational dataset. However, since the key indicators of climate change may only vary by a few percent per decade, the absolute accuracy of such an observational dataset also needs to be very small to allow detection and provide some means of validating, and discriminating between climate model predictions. The quality of currently available datasets (together with current strategies for creating long term datasets from multiple sensors) is not adequate to meet the requirements for climate benchmarking.

The only means of achieving robust data sets of sufficient quality and accuracy is through traceability to SI units, regularly re-established and guaranteed throughout the lifetime of a mission. The TRUTHS mission has been conceived to directly address this observational need; primarily through its own observations but also secondarily through improving the performance of other space assets through reference calibration from orbit.

TRUTHS will measure SI traceable spectrally-resolved Earth-reflected solar radiance, incoming solar spectral irradiance and total solar irradiance to an accuracy approximately 10 times higher than is available from current sensors - the optimum level needed to establish a robust climate benchmark. Climate model output is directly verified via the global top-of-atmosphere (TOA) Earth-reflected radiance. However, combined with the solar spectral irradiance measurement the TRUTHS data product will enable quantification of the wider climate system energetic drivers, particularly those effecting feedback mechanisms such as cloud and albedo.

The current status of the mission will be presented, including a review of the sensor design and calibration methods. A number of recent UKSA CEOI-funded studies have enabled significant development in a number of aspects of the mission, including:

• Evolution of the on-board calibration scheme to be evolved allowing some simplification, while retaining the robust SI-traceability critical to the mission,

• Development of the central hyperspectral imager sensor including performance evaluation.

• Reference cross-calibration method and uncertainty analysis

9639-49, Session 11

Creation and validation of Spectralon BRDF targets and standards

Christopher N. Durell, Labsphere, Inc. (United States)

Spectralon is an extremely stable, near-perfect lambertian reflecting diffuser and calibration standard material that has

been used by national labs, space, aerospace and commercial sectors for over two decades. New uncertainty targets of 2% on-orbit absolute validation in the Earth Observing Systems community have challenged the industry to improve is characterization and knowledge of almost every aspect of radiometric performance (space and ground). Assuming "near perfect" reflectance and BRDF performance is no longer going to suffice for many program needs. To ensure lowest possible uncertainty, Spectralon has NVLAP accreditation for total hemispherical spectral reflectance measurements. The hemispherical reflectance provides a good mark of general performance, but without the angular characterization critical data is missing from many applications and uncertainty budgets. Therefore, traceable BRDF measurement capability is needed to characterize Spectralon's "near perfect" angular response and provide a full uncertainty profile to many users. This paper presents an analysis of in-house instrument capability to determine a possible traceable (auditable) BRDF measurement capability for Spectralon materials. The analysis also includes the creation of potential BRDF standards that can be used for traceable inter-comparison or validation of BRDF measurements. Our internal capabilities and the new standards are tested against a round-robin cycle of traceable commercial, NIST and NASA instruments in an effort to develop an expected error profile for services and products when used in traceable measurements situations.

9639-50, Session 11

China radiometric calibration sites ground-based automatic observing systems for CAL/VAL

Yong Zhang, National Satellite Meteorological Ctr. (China); Xin Li, Anhui Institute of Optics and Fine Mechanical, Chinese Academy of Sciences (China); Zhiguo Rong, National Satellite Meteorological Ctr. (China); Lijun Zhang, National Satellite Meteorological Ctr (China); Xiuqing Hu, National Satellite Meteorological Ctr. (China); Xiutian Ba, Dunhuang Meteorological Bureau (China)

With the rapid development of remote sensing technology, a large number of satellites with a high-performance visible (VIS), near infrared (NIR) and thermal infrared (IR) detection capability have been launched into space. In China, the in-orbit field calibration is used to calibrate satellite instruments. Usually, this technique uses Gobi desert and plateau lake sites with a high altitude, a dry and clean atmosphere with few aerosol particulates, less human disturbance and uniform reflectance/temperature distribution and can reach high calibration accuracy. China has established two instrumented national radiometric calibration fields, called China Radiometric Calibration Sites (CRCS): a land surface site at Dunhuang Gobi and a water surface site at Lake Qinghai, for the absolute radiometric calibration of sensors. A number of instruments are deployed at these sites to gain accurate knowledge about atmospheric and earth surface conditions, which are needed to calibrate satellite instruments.

The CRCS Dunhuang site (40.1821°N, 94.3244°E) is located in the Gobi Desert in northwest China, about 35 km west of Dunhuang City, Gansu Province. Covering approximately 30 km ? 30 km, the entire site is formed on a stable alluvial fan of the Danghe River and its surface consists of cemented gravel without vegetation. This site was chosen as one CRCS site due to its extremely homogeneous surface conditions. The center area (600 m ? 600 m) of the site is designed for high spatial resolution visible/near-infrared (VIS/NIR) sensors such as the China-Brazil Earth Resources Satellite (CBERS) series. The extended large area (20 km ? 20 km) is used for low spatial resolution sensors such as the Multichannel Visible and Infrared Scanning Radiometer (MVISR), Visible and Infrared Radiometer (VIRR), and Medium Resolution Spectral Imager (MERSI) onboard the Fengyun-1 and 3 (FY-1/3) series of polar-orbiting satellites. It is also used for the field calibration of the VIS/NIR channels on Chinese geostationary weather satellites (Fengyun-2 or FY-2 series). The field calibration for the FY series of satellites has been conducted operationally since 2001 for only the VIS/NIR channels. Due to the lack of onboard VIS/NIR calibrators, the in-orbit field calibration based on the CRCS Dunhuang site is still the primary method for China's satellite sensors' VIS/NIR channels, such as the FY series satellites, Haiyang (HY) series of Ocean Satellites, Disaster and Environmental Monitoring Satellites (HJ) and CBERS series satellites. In recent years, the CRCS Dunhuang site has also been used for FY satellite IR channel field radiometric calibration.

Lake Qinghai, the largest saline lake in China, is located in the northeast of the Tibet Plateau and is the most important CRCS site for infrared sensors. The results from several sets of field experiments from 1994 to 2014 at Lake Qinghai indicated that the natural conditions, such as water surface radiative characteristics and local atmospheric conditions were suitable for the in-flight absolute radiometric calibration of the thermal channels of earth observation remote sensors. The lake's total area is 4473 km2 and its perimeter is 360 km. The shape of the lake is like an egg; it is 109 km long from east to west and 65 km wide from north to south. The average depth of the lake is 19 m, with a maximum depth of 32.8 m. The elevation of the water surface is 3196 m above sea level, and the volume of the lake is 105 Gm3. Lake Qinghai has a plateau continental climate with plentiful sunlight. Its climate has four distinct seasons. It has a windy spring, a short dry and hot summer, a clear and cool autumn and a long wet and freezing winter. The shortest and the longest recorded periods of ice cover on the lake are 76 days and 138 days, respectively. The depth of the ice layer is 40 cm on average and 90 cm at maximum. The water surface temperature tends to be spatially uniform, with a variation of less than 1 K. It is naturally a good infrared radiant point. There is a hilly island in the middle of the lake and the satellite-ground synchronous observation area on the lake is located in the southeast of the island, at 100°22?E - 100°30?E, and 36°41?N - 36°45?N.

In order to obtain the continuous, automatic and operational field observing data of CRSC ground features, upgrading and updating of the surface and atmospheric parameters observing systems were carried out at CRCS Dunhuang and Lake Qinghai, include construction field observing station at CRCS Duhuang Site and upgrading buoys at Lake Qinghai. The construction of Dunhuang field observing station include house, observing filed, instrument platforms, data transmission systems, power supply, tower crane, road, safeguard facilities and so on. Many new designed and developed instruments for the new field station had been tested during CRCS2014 field campaigns. This field observing station will be an open field test and exchange platform for sharing of observing data, research and infrastructure, promote exchanges and cooperation between the relevant disciplines and units.

9639-53, Session 12

Deployment simulation of a deployable reflector for earth science application

Xiaokai Wang, Houfei Fang, Bei Cai, Xiaofei Ma, Shanghai YS Information Technology Co., Ltd. (China)

Refers to the paper entitled "A Large and High Radio Frequency Deployable Reflector", a novel mission concept namely NEXRAD in Space has been developed for monitoring hurricanes, cyclones and other severe storms from a geostationary orbit. The proposed novel instrument concept requires a space-based 35-meter diameter and Ka-band (35 GHz) Doppler radar antenna. The system can measure hurricane precipitation intensity, dynamics and its life cycle, then providing temporal information critical for creating advanced warning systems and improving numerical model prediction of track, intensity, rain rate and hurricane-induced floods. To meet the requirements of the radar antenna system, a Membrane Shell Reflector Segment (MSRS) reflector technology has been developed and several technologies have been evaluated. However, the deployment analysis of this reflector with large size and high-precision has not been investigated. The ability to meet the surface accuracy

requirement of this large reflector is a major challenge. Deployment dynamics analysis of the 35-meter diameter antenna reflector has been performed using ADAMS. In our model, the basic building block of the reflector is a tetrahedral module and the surface accuracy was designed as 0.17 mm RMS. To provide the accuracy and repeatability during the deployment process of the reflector, the driving system of the reflector was used by a hybrid hinge composed of shape memory polymer composite components and polymer composite spring tapes. Considering the characteristics of the hybrid hinge, a stage joint was introduced to describe the driving hinge in the analytical model and there are two stages during the deployment process, i.e., before full deployed, the rods connected by the joint can rotate along its axis with an angle clearance; after full deployed, the hinge has a high structural stiffness and the two rods could not rotate. A deployment experiment of a tetrahedral module has been designed to study their deployment dynamic characteristics. Using a high-speed camera and a force transducer, we can obtain the spatial positions of the three freedom joints and the impact force along the gravity direction of the fixed joint, respectively. By using two objective functions, the parameter optimization was performed and the numerical results were compared well with the experimental results. The reliability of the analytical model to analyse this deployable truss structure has been proved. Considering all the hybrid hinge is a synchronous deployed process, the deployment process of the tetrahedral truss reflector with free boundary has three stages which include rapid deployment stage, slow deployment stage and rapid deployment impact stage. But for an asynchronous deployed process, the amplitude of the angle clearance affects the deployment of the tetrahedral truss reflector, the deployment analysis of the reflector with different angle clearance amplitudes were simulated and the geometrical compatibility was discussed. Besides, the driving torque of the hybrid hinge was optimized to ensure that the reflector not only deploys full but also has a high surface accuracy. The results provide an insight into the deployment mechanism of this deployable reflector and help to optimize the shape memory polymer composite hinge.

9639-54, Session 13

Radiometric uncertainty per pixel for the Sentinel-2 L1C products

Javier Gorroño, National Physical Lab. (United Kingdom); Ferran Gascon, European Space Agency (Italy); Nigel Fox, National Physical Lab. (United Kingdom)

In the framework of the European Copernicus programme, the European Space Agency (ESA) has launched the Sentinel-2 (S2) Earth Observation (EO) mission which provides optical high spatial -resolution imagery over land and coastal areas. Here is presented a tool (named S2-RUT, from Sentinel-2 Radiometric Uncertainty Tool) allowing estimating the radiometric uncertainties associated to each pixel using as input the top-of-atmosphere (TOA) reflectance images provided by ESA.

The Sentinel 2 radiometric analysis is centred in the review of the Instrument Calibration and Characterisation Database (ICCDB). This is used as a start point to follow up a top-down research. The final goal is specifying to uncertainty contributors at a pixel (or near) level. For example the detector noise can be specified (and updated after in-flight assessment) for each one of the detector modules of the S2 focal planes. Furthermore, the radiometric analysis proposes a change of approach for the uncertainty contributors' assessment where necessary. For example, the vibration and thermal cyclic pre-flight tests are under review in order to infer a probability distribution (type B uncertainty) rather than a worst case value selection.

The combined standard uncertainty relies on the propagation through a linearised radiometric model. The effect of higher-order components and covariance is assessed by comparing the results to a multivariate Monte Carlo Method (MCM). For example, the relative gains in the Visible and Near-Infrared (VNIR) are modelled by a cubic function. By using the MCM, the uncertainty propagation performs better than by using the combined standard uncertainty.

The TOA reflectance uncertainty per pixel implies that not only the radiometric calibration uncertainty and correction residual uncertainty (e.g. linearity model) must be provided but the interrelation with other effects at the L1 radiometry. For example, we are currently working in providing a framework (image processing and algorithm) in order to effectively evaluate the impact of the spectral response uncertainty and geometric uncertainty in the L1 radiometry.

Based on the previous theoretical framework description, the software implementation is a challenging task. This has been largely overcome by using the flexibility of the JPEG2000 (partial decoding) and the additional information provided in the product metadata and quality masks. The tool reads the images as blocks of 64 rows for 60m bands (x3 and x6 for 20m and 10m bands) and all columns. Using the detector footprint mask it is possible to reconstruct the focal plane ("synthetic" focal plane) and better account for uncertainty contributions dependent on the neighbouring pixels. This is the case of geometric or crosstalk effects. In addition, since the 13 bands are decoded at the same time, the spectral effects can be considered by linking (nearest neighbour method) to pre-calculated values in a Look-Up Table (LUT).

The tool directly modifies the L1C product. For each tile, it creates a subfolder where the 13 uncertainty images and the metadata are stored. The uncertainty values are coded just using 1 byte and providing values from 0-25.4% in steps of 0.1%. This, together with the partial decoding of the images reduces dramatically the system memory requirements.

9639-55, Session 13

G-MAP: a novel night vision system for satellites

Thomas Miletti, European Space Research and Technology Ctr. (Netherlands) and Univ. degli Studi di Trieste (Italy); Luca Maresi, Alessandro Zuccaro Marchi, European Space Research and Technology Ctr. (Netherlands); Giorgia Pontetti, G & A Engineering S.r.l. (Italy)

The recent developments of single photon counting array detectors opens the door to a novel type of systems that could be used on board of satellites in Low Earth Orbit (LEO). One of the possible applications is the detection of non cooperative vessels or illegal fishing activities. Currently only surveillance operations conducted by Navy or coast guard address this topic. But by nature these operations are costly and with limited coverage.

This paper aims to describe the architectural design of a system based on a novel Single Photon Counting Detector (SPCD). The SPCD works mainly in the visible range and it features a 256x256 matrix of 64 ?m-pixels, a fast readout and low noise. This detector is positioned in the focal plane of a fully aspherical reflective telescope, to guarantee state of the art performance, with f-number equal to 6. The combination of the two therefore grants optimal Ground Sampling Distance (GSD) and overall performance. In particular the GSD needs to be compatible with the average dimension of a fishing vessel.

A radiative analysis of the light transmitted from ground to the satellite is presented, starting from models of light bulbs used for attracting fishes and for illuminating the deck of the boats, and using a radiative transfer model to estimate the amount of photons emitted by such vessels reaching the detector. Since the novel SPCD features high frame rate and low noise, the system as it is envisaged is able to properly serve the proposed goal.

The paper shows the results of a trade-off between instrument parameters and spacecraft operations in order to maximize the detection probability and the covered sea surface. The status of development of both the SPCD and the selected telescope are also described.

9639-56, Session 13

Photonic front-end for the next-generation of space SAR applications

Miguel A. Piqueras, Teresa Mengual, DAS Photonics (Spain); Bartos Chmielak, AMO GmbH (Germany); Alfredo Catalani, Space Engineering S.p.A (Italy); Peter G. Huggard, RAL Space (United Kingdom); H. Wang, STFC Rutherford Appleton Lab. (United Kingdom); Rubén Ortuño, Univ. Politècnica de València (Spain)

The evolution of Synthetic Aperture Radar (SAR) space systems has shown a clear trend towards higher performance at lower cost, less mass, size and power consumption imposing strong requirements in the today's antenna technology since larger antennas means complex, bulky, difficult to route RF harness, and strong mechanical and thermal requirements for in-orbit deployable antennas. Larger bandwidths associated with larger antennas and scanning angles requires True-Time-Delay (TTD) beamforming, resulting in bulky and complex solutions.

The last SAR systems for satellite applications have been realized in C and X Bands. It is natural that a substantial step to an Antenna-SAR for the next future generation is the expected progress in increasing the operative bandwidth and in miniaturization of the SAR antenna. The miniaturization will drastically reduce the mass and volume of the antenna including the RF system down to 10 % of the today's value.

In this paper an array antenna system is reported, including the design of the antenna element, the optical beamformer and the optical harness suitable for large, deployable antennas and the development of an antenna array module in X band. The design is a modular antenna system with phase shifters and true-time-delay characteristics photonically controlled which will be the base of a large, deployable SAR antenna with a net gain in size, mass, complexity and cost when compared with the traditional implementations which will be measured in an anechoic chamber.

The use of photonic integrated circuits (PIC) technology in the beamforming is a clear key enabling technology due to TTD can be implemented by using integrated photonics achieving potentially order-of-magnitude improvements in size and mass, antenna system integration and reduction of the risks associated to the in-orbit antenna deployment.

A new optical monolithic technology capable of implementing ultra-low waveguide propagation losses and fibre coupling insertion losses has been developed based on Silicon Nitride. Waveguide losses lower than 0.1 dB/cm in high contrast technology has been developed in order to achieve low losses and a compact design for implementing the optical delays in the range of hundreds of picoseconds required for large antennas in a size of less than 20x20 millimeters. Integrated optical switching techniques have been implemented on-chip required for switchable optical delays designs (one for TX and other for RX). Electro-optical conversion components are included in the antenna in order to have the adequate RF interface from/to the antenna element as well as an broadband antenna tile based on a subarray of dual-polarization patch antennas with dual beamforming networks in microstrip technology with bandwidth of 600MHz in X-band.

A Tx/Rx antenna system for space SAR applications using photonic technology has been developed, including electro-optical conversion, fiber-optic antenna remoting and photonic integrated circuits (PIC) implementing switchable true-time delay lines with amplitude control. The compactness, broadband operation and easy routing and of optical fiber are suitable to address the requirements of the future space SAR missions.

9639-57, Session 13

Two conceptual designs for optical system of next-generation small satellites

Sayyed Ashkan Adibi, Shahid Bahonar Univ. of Kerman (Iran, Islamic Republic of); Azam Karami, Shahid Bahonar Univ. of Kerman (Iran, Islamic Republic of) and Univ. Antwerpen (Belgium)

In recent years, satellites are widely used in different practical applications such as communication systems, geology, agriculture, military applications, and etc. In this paper microsatellite (satellite weighing less than 100 kg) is investigated. This kind of satellite have lower cost of building and lunching due to their low weight. In this paper, two new techniques are proposed for manipulation of the microsatellite imaging structures and sensors. In order to show the importance of these techniques, TOP-SAT is investigated as one of the most significant microsatellites.

TOP-SAT can produce panchromatic images with the spatial resolution of 2.5m and multispectral images with the spatial resolution of 5m. This microsatellite weighs 120 kg, and has three mirrors. The weight of primary mirror, in this satellite, is 45kg. Therefore, it is very important to modify the optical part of this satellite in order to reduce the mirror weight, while preserving or even enhancing the image quality. For this purpose the following techniques are suggested:

First, replacing primary mirror by deformable mirror is suggested. Exploiting deformable mirror, enables the use of appropriate actuators in order to correct the optical aberrations and reduce the effects of atmospheric turbulences. Three conceptual deformable mirrors that can be used at this aim, are: segmented, microelectromechanical, and ferrofluid mirrors. Therefore, in this design, the primary mirror is replaced with deformable mirror, and the secondary mirror can be aligned in the cassegrain design, and tertiary mirror could be ignored. Utilizing deformable mirror, the optical system would occupy less space and the number of optical element could be reduced. In this paper the process of reshaping deformable mirror is also discussed.

Second, by changing the distance between the satellite sensors and focal plane, the image quality of different parts of an image can be changed. Normally, when the sensor is fixed, some parts of image might be blurred, noisy and distorted. Therefore, if the sensor was capable of changing its position, the quality of the distorted pixels would be improved, but other parts would become blurred. In this case the blurred pixels should be omitted and the improved pixels should be saved, and then concatenated to construct the final image.

In this paper a new concept of "local focusing" is introduced. This concept aims to process images at a variable distance of a sensor, which can cause the final image quality to become much better (higher signal to noise ratio) than the fixed sensor. Different parameters of mathematical functions of local focusing such as incident wavelength, manufacturing tolerances and testing process are discussed in paper.

The techniques that are suggested in this article, are meant to be implement on microsatellites like TOP-SAT, but generally they can be applied to all next- generation micro-satellites. It is noteworthy that the importance of applying these techniques is to reduce the weight and cost of building and launching the micro-satellites. In addition, they improve the image quality. Our future goal is to investigate applying these techniques to large satellites in order to improve their image quality.

9639-58, Session 14

Material choices and resulting dimensional stability of optical systems in orbit

Tony B. Hull, The Univ. of New Mexico (United States); Thomas Westerhoff, SCHOTT AG (Germany)

Various materials commonly used in orbit are considered. One class of material is ZERODUR®, offering very low thermal expansion over a long temperature range, yet also exhibits low thermal diffusivity. Another class of material is exemplified by beryllium or silicon carbide, which exhibit high thermal expansion and high thermal diffusivity. Unfortunately there is no optical material that offers both low thermal expansion and high diffusivity. Under soak conditions, a quasi-thermodynamic equilibrium exists, and relative figures of merit including CTE/k and k/rho*cp may express the relative stability. However under conditions where there is a modulating temperature gradient or a thermal transient changing faster than the thermal timescale, the stability conclusion changes. We will consider a surveillance telescope at low earth orbit.

9639-60, Session 14

Research on Dyson imaging spectrometer based on Fery prism

Linlin Pei Jr., Jianwei Wang, Qunbo Lv, Yangyang Liu, Weiyan Li, Academy of Opto-Electronics (China)

Rich feature information can be obtained through the imaging spectrometer. This kind of technology has a wide range of development. Now we focus on the high spectral resolution and its miniaturization. In this paper, we design a kind of Dyson imaging spectrometer based on Fery prism. Its average spectral resolution is 3nm. Its total length is just 225mm. The Fery prism is an modified optical element based on the conventional dispersion prism. Light through a prism into a spherical surface machining is obtained, the radius of curvature of the front and rear surfaces which can provide a certain degree of optical power, having an imaging function. Meanwhile, it is not in the front surface of the center of the sphere on the optical axis, the light beam after passing through the optical element will produce a dispersion effect. Fery prism does not need to be placed in the optical path parallel to simplify the prism dispersive spectrometer collimating lens and the imaging lens system that can get a compact spectrometer. Prism full spectral transmittance up to 94%, compared to the convex grating energy utilization is increased, and the free spectral range of the prism is wider, the dispersion will not bring higher order spectral aliasing problems. This design of compact hyperspectral instrument only two elements, simple structure, spectral range of 400nm ~ 1000nm, covering the near-ultraviolet to near-infrared spectral aberrations are each typically corrected spectrometer excellent performance.

9639-61, Session 14

Visible spectral imager for occultation and nightglow (VISION) for the PICASSO Mission

Heikki Saari, Antti Näsilä, Christer Holmlund, Rami Mannila, Ismo Näkki, Harri J. Ojanen, VTT Technical Research Ctr. of Finland Ltd. (Finland); Didier Fussen, Didier Pieroux, Philippe Demoulin, Emmanuel Dekemper, Filip Vanhellemont, Belgian Institute for Space Aeronomy (Belgium)

“PICASSO - A PICo-satellite for Atmospheric and Space Science Observations is an ESA In-Orbit-Demonstration (IOD) mission project led by the Belgian Institute for Space Aeronomy, in collaboration with VTT, Clyde Space Ltd. (UK) and Centre Spatial de Liège (BE). VTT Technical Research Centre of Finland Ltd. VTT will deliver the Visible Spectral Imager for Occultation and Nightglow (VISION) for the PICASSO mission. The VISION targets primarily the observation of the Earth’s atmospheric limb during orbital Sun occultation. By assessing the radiation absorption in the Chappuis band for different tangent altitudes, the vertical profile of the ozone is retrieved. A secondary objective is to measure the deformation of the solar disk so that stratospheric and mesospheric temperature profiles are retrieved by inversion of the refractive ray-tracing problem. Finally, occasional full spectral observations of polar auroras are also foreseen. The VISION design realized with commercial of the shelf (CoTS) parts is described. The VISION instrument is small, lightweight (ca. 500 g), Piezo-actuated Fabry-Perot Interferometer (PFPI) tunable spectral imager operating in the visible and near-infrared (430 – 800 nm). The spectral resolution over the whole wavelength range will be better than 10 nm @ FWHM. VISION has is 2.5 degrees x 2.5 degrees total field of view and it delivers maximum 2048 x 2048 pixel spectral images. The sun image size is around 0.5 i.e. ca. 500 pixels. To enable fast spectral data image acquisition VISION can be operated with programmable image sizes. VTT has previously developed PFPI tunable filter based AaSI Spectral Imager for the Aalto-1 Finnish CubeSat. In VISION the requirements of the spectral resolution and stability are tighter than in AaSI. Therefore the optimization of the of the PFPI gap control loop for the operating temperature range and vacuum conditions had to be improved. Calibration and characterization of the VISION engineering model in thermal vacuum is described.

9639-62, Session 14

The ESA RADGLASS activity: a radiation study of non rad-hard glasses

Ilias G. Manolis, Jean-Loup Bézy, European Space Research and Technology Ctr. (Netherlands); Alessandra Costantino, European Space Agency / ESTEC (Netherlands); Ramon J. Vink, Atul Deep, Munadi Ahmad, Emmanuel Amorim, European Space Research and Technology Ctr. (Netherlands); Micael D Miranda, European Space Agency / ESTEC (Netherlands); Roland Meynart, European Space Research and Technology Ctr. (Netherlands)

Traditionally, radiation hard optical glasses are primary candidates for optical instrumentation in space featuring dioptric optical designs. In that respect, SCHOTT has been a major supplier of optical glasses for optical space instrumentation. However, only very few radiation hardened optical glasses are currently supplied by Schott, which drastically limits the choice available to the optical designer at the early design phases of an instrument. In addition, availability of those glasses cannot be guaranteed by SCHOTT at the horizon of future space instrument development.

The effect of ionizing radiation at different doses of absorbed radiation has not been adequately measured yet on “new” arsenic and lead free Schott glasses (N-*). Furthermore, no radiation hardened colored glass filter are anymore supplied by Schott; Some older test results show significant sensitivity to high radiation levels but such levels are not necessarily representative of typical low Earth orbit (LEO) levels. These tests have also evidenced a rather fast curing process.

Similarly, radiation response data on optical materials from other key suppliers and in different grades are sparse and therefore their integration into space optical instruments is always subject to lengthy discussions in the early feasibility phases and to careful qualification later in the development phases.

Notably, the results of irradiation campaigns on the previous glasses of SCHOTT catalog suggest that the use of some standard glasses may be acceptable in low earth orbit or even in GEO orbits. The ESA RADGLASS activity aims at confirming and quantifying this statement. An extended pool of glass materials (about 50 different materials) has been selected based on the results of ongoing ESA studies for future (and under development) EO instrumentation, with the intention to test their response under ionizing radiation.

We are irradiating window samples in several consecutive step doses using the Co60 facility available at ESTEC and up to maximum doses of approximately 500 krad (dose in water). Traceability of the materials is guaranteed via the melt data provided and by sourcing the samples directly from the manufacturer.

Total transmission measurements are conducted in the spectral range 200nm to 2500nm immediately after each step dose to decouple from short term relaxation effects. Annealing is studied separately by monitoring the evolution of the spectral transmission in time after the completion of the irradiation campaign. Effects on the refractive index are also monitored by ellipsometric measurements before and after the campaign. This is necessary in order to derive in a reliable manner the effective change in the absorption coefficient of the materials from the measured total transmission.

In this paper we will present some first results from our campaigns for a handful of materials. Only raw spectral transmission data will be presented. Future work will include the analysis of these data together with empirical models previously developed (absorption peak decomposition) in order to estimate the evolution of the material in a representative space mission scenario (very low dose rate, log duration).

Eventually, we target to gather all results in an open database, for reference during early design phases of space optical instrumentation.

9639-64, Session 15

Design tradeoffs for a high-resolution, wide-field camera for a small-satellite Earth observation mission

Denis P. Naughton, CGS S.p.A. (Italy); Stefano Pieraccini, CGS S.p.A (Italy); Paolo Sandri, CGS S.p.A. (Italy)

Advances in CCD technology, optics manufacturing, spacecraft performance and the recent availability of low-cost launch vehicles capable of carrying multiple payloads into low-Earth-orbit have led to the deployment of small and agile Earth observation satellites. These systems provide lower cost imagery at modest resolution with reasonable radiometric sensitivity, while providing wide area coverage and repetitive monitoring capabilities. Small-satellite digital cameras were initially conceived to fill an image product gap as these capabilities are not usually achievable with the very-high resolution systems traditionally used for defense and commercial surveillance missions.

As the number of operational small-satellite systems has increased there has been a desire in the imagery user community for improved resolution while maintaining the area coverage and revisit capabilities. However, developing a remote sensing system with these characteristics is difficult to achieve since the capabilities impose conflicting design considerations for the optical system, focal plane and spacecraft.

This paper describes the design of a multi-spectral, high-resolution, wide-area coverage camera for a small-satellite Earth observation mission. The driving requirements for the system are assumed to be a resolution capability specified at a GSD < 4 m, a swath equal to ~ 40 km or larger, a revisit schedule at the Equator from 3.5 to 4.5 days, a modulation transfer function at Nyquist equal to at least ~ 0.1, a signal-to-noise ratio equal to or greater than ~80 and a radiometric sensitivity (noise equivalent delta reflectance) < 1% in all bands.

The fundamental interaction between detector sampling and the image formation process of the optical system is used to size the camera and establish derived performance parameters using the assumed mission requirements. A performance assessment in terms of achievable resolution, MTF, SNR and radiometric sensitivity was performed, and factored with an assessment of available manufacturing processes of the optics, provided a best design solution.

As a result, a prototype camera based on a Korsch optical form, commercially available CCD- focal planes, and low-noise, high-speed processing electronics is described. The camera is suitable for a small-satellite Earth observation mission in terms of estimated performance, mass, volume and power consumption. The results of the trade study, the validation of the prototype design and a comparison with operational and planned small satellite cameras are presented.

9639-65, Session 15

A new service support tool for COSMO-SkyMed: civil user coordination service and civil request management optimization

Maria Girolamo Daraio, Maria Libera Battagliere, Patrizia Sacco, Luca Fasano, Alessandro Coletta, Agenzia Spaziale Italiana (Italy)

COSMO-SkyMed is a dual-use program for both civilian and defense use resulting from an agreement between the Italian Space Agency(ASI), the Italian Ministry of Defense and the Italian Ministry of Research. The COSMO-SkyMed constellation is based on four mid-sized satellites equipped with Synthetic Aperture Radar (SAR) operating at X-band, fully operational starting from 2011. The main objective of the COSMO-SkyMed mission is to provide its user community (institutional and commercial) with SAR data in several applications such as agriculture monitoring, ship detection, interferometry, landslides monitoring, maritime surveillance, rapid mapping and security.

In the context of COSMO-SkyMed data and User management, one of the aspects carefully monitored is the user satisfaction level. An analysis of this parameter has clearly highlighted the need to reduce the rate of rejection among several acquisition requests submitted to the system by Civilian users. This is particularly true for some regions, such as Italy, where the concentration of requested orders is very high. Orders management is primarily based on the priority assigned at each user and the harmonization work of all the acquisition request lists performed by the Ranker Manager.

The operational experience of the first years of operational phase, and the consequent lessons learnt by the COSMO-SkyMed data and User management, have demonstrated that a lot of the acquisition rejections are due to conflicts (time conflicts or system conflicts) among two or more User Requests, and can be managed and solved implementing an improved coordination of the Users and their requests on a daily basis. With this aim a new Service Support Tool (SST) has been designed, developed, tested and is now operative. The SST supports the operators in the User Request coordination by analyzing conflicts among the Acquisition Requests (ARs) before the National Rankization phase and by elaborating proposals for conflict resolution. This tool is able to manage both periodic (requests that foresee regular time spaced acquisitions) and single requests (requests that foresee single acquisitions).

In this paper the most common causes of the occurred rejections will be showed, for example due to the impossibility to aggregate different orders, Spotlight orders with almost the same geometry, consecutive StripMap HIMAGE orders with the same geometry but with a too short transition time or consecutive orders with different geometry but a too short transition time, the inability to break orders, etc.. Before the submission of the request, a feasibility analysis is executed, based on specific requirements indicated in the user order and on the area of interest. Check conflict analysis aims to verify the presence of conflicts for the selected DTO (Data Take Opportunity) with other requests already submitted or still residing on the SST.

Once the conflicts for a specific AR have been analyzed, the SST tool propose automatized conflict solutions and if a request needs to be modified, the SST generates a “Request Modification Proposal”. SST also provides the functionality to calculate the service satisfaction parameter in term of number of solved conflicts despite the number of found conflict. All these SST functionalities will be described, in particular how it works to remove or minimize the conflicts among different orders.

9639-66, Session 15

The COSMO-SkyMed ground and ILS and ops segments upgrades for full civilian capacity exploitation

Luca Fasano, Giuseppe Francesco De Luca, Mauro Cardone, Rosa Loizzo, Patrizia Sacco, Maria Girolamo Daraio, Agenzia Spaziale Italiana (Italy)

COSMO-SkyMed (CSK), is an Earth Observation joint programme of Agenzia Spaziale Italiana (Italian Space Agency, ASI) and Italian Ministry of Defense (It-MoD).

The system is based on a co-planar constellation of 4 SAR satellites in Sun-synchronous Low Earth Orbit and is able to carry out accurate Earth observation over time, with parameters that ensure reliability, stability and continuity, relayed at intervals of a matter of hours, covering all changes and variations to the land and movements on both land and sea.

The CSK Ground Segment is composed by a worldwide assets including a Core Ground Segment (CGS), a Planning Centre (CPCM), the Italian Civilian User Ground Segment (I-CUGS), the Italian and French Defence User Ground Segments (I-DUGS and F-DUGS), two external stations (in Kiruna and Cordoba,), a Fiducial Network for GPS data accuracy augmentation with stations all around the world, and several transportable stations deployed in Italy and foreign countries. Furthermore, thanks to its native IEM (Interoperability, Expandability and Multi-Mission/ Multi Sensor) capabilities, COSMO-SkyMed is open to further expansions, both adding new COSMO-SkyMed user centres and other missions.

As part of a more complex and in-depth re-engineering process, aimed to fully exploit several system capabilities, manage the obsolescence and reduce the maintenance costs, a series of activities are planned to exploit all the constellation acquisition capability reserved for Civilian users. To reach this full capability of CSK system of programming, planning, acquiring, raw data processing and archiving, several upgrading have been necessary to the Ground Segment. More in depth, the following activities have been performed:

- H/W and S/W of I-CUGS Acquisition (ACQ) subsystem have been updated. ACQ has been fully refurbished from an H/W point of view. This need has required some S/W modifications.

- H/W and S/W of External Stations ACQ subsystems have been updated as for I-CUGS ACQ one.

- H/W and S/W of I-CUGS Production Manager (PM) subsystem have been updated. In order to guarantee a correct management of the increase of acquired images it had been necessary to upgrade the Tape Library archive. To better manage the library it had been necessary to upgrade also the PM Servers connected to the library.

- S/W of I-CUGS Interface Manager (IM) subsystem has been updated. The automatic feasibility has been introduced in order to speed up the order submission.

In particular it can be exploited for the background mission requests but is made available/configured for all the following services:

- Assisted mode for Standard Product Services from New Acquisitions and Archived Data;

- Assisted mode for High Level Product Services from New Acquisitions and Archived Data.

When these activities will be completed, it will be possible the programming, planning, acquiring, L0F processing and archiving all the images that the satellites can acquire, that are 1148 Civilian images per day in the maximum operative profile.

In this way all users will have more possibility to acquire on the desired area and some background programs, useful for example to populate a database with historical images for interferometric aims, can be easier planned.

9639-67, Session 15

OPTIMA: advanced methods for the analysis, integration and optimization of PRISMA mission products

Donatella Guzzi, Ivan Pippi, Bruno Aiazzi, Stefano Baronti, Roberto Carlà, Cinzia Lastri, Vanni Nardino, Valentina Raimondi, Leonardo Santurri, Massimo Selva, Istituto di Fisica Applicata Nello Carrara (Italy); Luciano Alparone, Istituto di Fisica Applicata Nello Carrara (Italy) and Univ. degli Studi di Firenze (Italy); Andrea Garzelli, Istituto di Fisica Applicata Nello Carrara (Italy) and Univ. degli Studi di Siena (Italy); Ettore Lopinto, Cristina Ananasso, Agenzia Spaziale Italiana (Italy); Alessandro Barducci, SOFASI S.R.L. (Italy)

PRISMA (PRecursore IperSpettrale della Missione Applicativa – Hyperspectral Precursor of the Application Mission) is an Earth observation system with an innovative electro-optical instrumentation that combines a hyperspectral sensor with a panchromatic, medium-resolution camera. Due to demanding requirements on the radiometric accuracy, an in-flight internal calibration unit (ICU) has been designed so as to allow operations of absolute and relative radiometric calibration and spectral calibration. PRISMA will primarily focus on the Euro-Mediterranean Regions; therefore, scientific applications will be aimed to study the most significant Earth processes in Europe and Mediterranean areas.

In the framework of the PRISMA mission, the Italian Space Agency has funded five independent scientific research projects for the development of added-value algorithms and advanced applications. OPTIMA (the acronym stands for “advanced methods for the analysis, integration and optimization of PRISMA mission level 1 and 2 products) is one of these projects.

The main goal of OPTIMA is to increase and to strengthen the applications of PRISMA mission through the implementation of advanced methodologies for the analysis, integration and optimization of level 1 and 2 products. The project is comprehensive of several working packages: data simulation, data quality, data optimization, data processing and integration and, finally, evaluation of some applications related to natural hazards. Several algorithms implemented during the project employ high-speed autonomous procedures for the elaboration of the upcoming images acquired by PRISMA.

To assess the performances of the developed algorithms and products, an end-to-end simulator of the instrument has been implemented. Inputs of the simulator are high-resolution aerial photographs and a database of reflectance spectra of typical targets. Atmospheric parameters and acquisition geometry are additional settings. Taking into account the instrumental characteristics, at-sensor radiance data are eventually converted into digital raw data. Furthermore, data quality analysis has been completed by introducing noise modeling and by evaluating, their spatial and spectral characteristics.

To improve the quality of the PRISMA data, stand-alone procedures of radiometric and atmospheric corrections have been developed, allowing for the retrieval of at-ground spectral reflectance maps. Moreover, specific studies about image enhancement, restoration and pan-sharpening have been carried out for providing added-value data to the future mission products.

Regarding the mission capability of monitoring environmental processes and disasters, different techniques for estimating surface humidity and for analyzing burned areas have been investigated. Finally, calibration and validation have been considered as future activities on the basis of the experience gained in previous space hyperspectral missions (HYPERION and CHRIS) utilizing the CAL/VAL test site managed by CNR-IFAC and located inside the Regional Park of San Rossore (Pisa), Italy.

9639-68, Session 16

Visible and near-infrared imaging spectrometer (VNIS) for in-situ lunar surface measurements

Zhiping He, Rui Xu, Chunlai Li, Gang Lv, Liyin Yuan, Binyong Wang, Rong Shu, Jianyu Wang, Shanghai Institute of Technical Physics (China)

The Visible and Near-Infrared Imaging Spectrometer (VNIS), is one of the main scientific instruments on Yutu. Using non-collinear acousto-optic tunable filters (AOTFs) as dispersive components, VNIS consists of a VIS/NIR imaging spectrometer (0.45–0.95 μm), a shortwave IR spectrometer (0.9–2.4 μm), and a calibration unit with dust-proofing functionality. And it has been designed to obtain mineralogical and compositional information for the lunar soil as the rover traverses the surface.

Change'E 3 entered into orbit around the Moon on 6 December 2013 and landed on 14 December 2013. After landing successfully on the moon, the VNIS performed several explorations and calibrations, and obtained several spectral images and spectral reflectance curves of the lunar soil in the Imbrium region.This paper describes the Instrument characteristics, lab calibration, on-orbit measurements and calibration.

9639-69, Session 16

Positioning accuracy improment of three-line mapping satellite after using laser altimeter

Qiang Dou, Qipeng Cao, Jun Zhu, Yan Li, Aerospace DongFangHong Satellite Co., Ltd. (China)

The laser altimeter associate with three-linear camera mapping is a kind of new space mapping system which is going to be used in next generation mapping satellites. Laser altimeter data is used to obtain the elevation information and digital elevation model, and then through the multi-source data fusion, the three-dimensional mapping can be achieved.

In this paper different mapping systems is analyzed. As a way of acquiring elevation with high accuracy and effectiveness, laser altimeter can improve the capability of 3- dimensional earth observation of satellite optical remote sensing imagery. Using high accuracy elevation observation of space-borne laser altimeter as control points accords with the trend of satellite photogrammetric without ground control points. The problems of satellite photogrammetric are firstly introduced, and then the method of space-borne laser altimeter supported aero triangulation is described, which can solve these problems due to the characteristics of laser altimeter. The bundle adjustment error equations are established according to the earth observation of satellite image and space-borne laser altimeter, as well as the relationship of their exterior orientation elements.

By the results of this paper, for 1:2.5 million scale surveying and mapping, before the use of laser altimeter, plane positioning precision without control point absolute positioning is 10.5m, which can satisfy the requirements 15m, but the elevation accuracy without laser control point is 8.98m, which can not meet the demand of the accuracy of elevation mapping 3m. With the combined adjustment of laser altimeter data, the height accuracy can get to 1.6m which is better than the requierment of 1:2.5 million scale mapping . The results shows that elevation observations supplied by laser altimeter can be used as elevation control points to improve the accuracy of aero triangulation and the positioning accuracy.

9639-71, Session 16

An on-orbit spectral calibration method for dispersive spectral imaging system

YU DAI, Jianwei Wang, Lin Zhang, Chinese Academy of Science (China)

In order to obtain accurate data for academic research and application, it is necessary for on-orbit spectrometer to obtain the spectrum information exactly and regularly. Most spectral calibration data are collected by atmospheric lines and absorption lines. In this paper, we described an on-orbit spectral calibration method for dispersive spectral imaging system, which is achieved by a series of light-emitting diodes (LED) target on the ground. The LED target consists of different narrow-band wavelengths LEDs, and each wavelength of LED target corresponds with a spectral channel of imaging spectrometer. The way of LED target laid down on the ground is analyzed and the energy emitted from the LED is calculated to ensure the detector of dispersive spectral imaging system receives enough energy when the satellite passes over the LED target location.

9640-36, Session PS

Influence of urban agglomerations on optical properties of aerosols based on remote sensing observations

Olga Zawadzka, Krzysztof M. Markowicz, Univ. of Warsaw (Poland)

Over the past few decades increasing urbanization resulted in large urban agglomerations around the world, which represent concentrated sources of anthropogenic emissions. The urban pollution sources are quite variable in space and time. Since the contribution of megacities to global pollutant emissions is of the order of 2-6% of the total global annual anthropogenic emission flux their impacts on the surrounding environment and the regional and global air quality have gained significant attention in the last decades. However, estimating urban polluted aerosol columnar properties, as well as the aerosol radiative forcing, and then distinguishing them from the typical background aerosol, is still a considerable problem.

We present study of the effect of the emmisions originated from urban agglomerations on optical properties of aerosols. As an example long-term observations of AOD and PM10 concentrations in the Warsaw extended area will be presented. We estimated the long-term effect of Warsaw urban emissions on the AOD, which is about 0.02 (at 500 nm) based on ground-based observations and 0.03 (at 550 nm) based on MODIS measurements. The impact of local emissions on the columnar aerosol optical properties is enhanced during smoke events which occur during specific weather conditions. Both, the PM10 concentrations and the AOD have a strong annual cycle with maxima in winter and summer, respectively. Long-term monthly mean values of the AOD and the PM10 concentrations measured in AERONET station in Belsk have a negative correlation coefficient (-0.33).

We also present study of the influence of population density on observed AOD. Information about population density was obtained from database „Gridded Population of the World". Based on MODIS data for Poland territory we analysed mean AOD for high populated (>300 os./km2) and low populated (<300 os./km2) areas. Calculated AOD difference was about 0,02. High variability of AOD observed for a given population density can be caused by an influence of some other factors, for instance by local sources of natural aerosol emissions (e.g. sea salt or dust). Similar relationship between AOD and population density is present in a results of analysis of data obtained in AERONET stations. We have taken into account all data from sites where time series of measurements is at least 5 years long. Annual mean of AOD increase with population density from 0,23 (for population density equaled 600 os./km2) to 0,35 (for population density equaled 4000 os./km2). In the case of Angstrom exponent there is no evident dependence on population density.

9640-37, Session PS

Geoinformation system for prediction of forest fire danger caused by solar radiation using remote sensing data

Nikolay V. Baranovskiy, Elena P. Yankovich, Tomsk Polytechnic Univ. (Russian Federation)

The reasons why the forest fires occur have a mixed characteristic. Such reasons include the possibility for the forest fuels to ignite because of a focused solar radiation effect. Earlier in theory and experiments we showed that the forest fuels can ignite in conditions of the solar energy concentration on the level of 15-17 times from the natural value. The energy concentrators can be the glass containers, their fragments and large drops of resin. We have developed a physically based method to estimate the forest fire danger in conditions of the focused solar radiation effect. At present, we must develop the technology that will answer the needs of forestry management. Its base should be this fire danger detection method of the forest areas.

This article reviews the project of subsystem that reflects the data of distance sounding of the Earth from the space in order to monitor the forest fire danger, caused by the focused solar radiation effect. This subsystem is based on the use of sounding data from the MODIS instrument aboard the Terra satellite. We consider the Timiryazevsky forestry of Tomsk region to be a typical territory of the boreal forest zone. To estimate the forest fire danger level, we use an original method to classify the forest areas according to their characteristics (the ground mensuration data) and the main meteorological parameters, namely, the cloud cover on this territory, obtained from the satellite data of the MODIS instrument.

The geographical information system planned to use the data of the distant sounding of the Earth from the space. The M?D14 product (Thermal Anomalies/Fire) is one of the real-time resources about the sites of possible thermal anomalies. It is obtained when processing the data from the MODIS sensor aboard the TERRA/AQUA satellites (the MOD14 and MYD14 products correspondingly). These products are made on the basis of the real-time data obtained in the ranges of 4 micrometers (the MODIS 21 and 22 channels) and 11 micrometers (the MODIS 31 channel). To mask the cloud cover, we use the 1 and 2 channels with resolution of 250 meters (ranges of 0.65 and 0.68 micrometers), as well as the 7 and 32 channels (the spatial resolution of the 7 channel is 500 meters, the range of 2.1 micrometers, the 32 channel has the spatial resolution of 1 km., the range is 12 micrometers). The product documentation and a number of articles describe the detection algorithm in detail. Besides, some fire products of the MODIS sensor have the products that inform about the fire location, the emitted energy, relation of ignition and smoldering, as well as some estimation of the outburned area.

The clouds are detected by a method, based on the technology, used when obtaining the global fire product with the help of AVHRR in the course of the International Geosphere Biosphere Program (IGBP).

With the MODIS products, we can have a probability estimate of the cloud cover parameters over the controlled territory. The cloud cover is characterized by four conditions: clear, may be clear, indefinitely and cloudy. In principle, it is enough to operatively monitor the forest fire danger in conditions of the focused solar radiation effect.

9640-38, Session PS

Quantitative interpretation of MODIS cloud mask: impact on cloud amount estimation

Andrzej Kotarba, Space Research Ctr. (Poland)

Cloud mask is the final product of cloud detection procedure. It comes in a form of the thematic map, which classifies image pixels into predefined groups. Moderate Resolution Imaging Spectroradiometer (MODIS) cloud mask covers four classes: "confident clear", "probably clear", "probably cloudy", and "confident cloudy". When one is interested in obtaining the quantitative information on the cloud amount, the qualitative classes have to be "translated" into the fractional cloud cover (0%-100%). That step is subjective in its nature and introduces the uncertainties into the final cloud amount estimation.

We evaluated this degree of uncertainty processing MODIS cloud mask with different interpretation scenarios. The base scenario is the approach used by NASA for producing MODIS L3 atmospheric products, i.e. the assumption that "confident clear", "probably clear" represents cloud fraction of 0%, while "probably cloudy" and "confident cloudy" cloud fraction

of 100%. We also investigated two extreme alternatives: 'optimistic' (only 'confident cloudy' IFOVs were 100% cloudy), and 'pessimistic' (only 'confident clear' IFOVs were 0% cloudy).

The first part of the analysis was conducted for Europe, and based on MODIS data covering years 2003-2013. We focusses on mean monthly cloud amount, computed with MODIS/Aqua and MODIS/Terra observations daytime and nighttime. Results showed that the range of uncertainty was 14.3% (the difference between optimistic and pessimistic estimation). To assess which cloud mask interpretation scenario is more accurate, or reliable, we compared MODIS data with surface-based observations (SYNOP). The analysis showed, that the best agreement was achieved for optimistic case: bias ?0.7%, RMSE 4.6%, standard deviation 6%, and correlation with SYNOP 0.935.

In order to evaluate the impact of the cloud mask interpretation globally, we calculated mean monthly cloud amount for January and July 2010, for the whole planed. The range of uncertainty reached 13%–15% on a global scale, but locally exceeded 30%–40% (e.g. in the tropics and at mid-latitudes, where the magnitude of the difference was controlled by the frequency of small convective clouds). Our results suggest that for climatological applications the 'optimistic' scenario should be considered as a more accurate 'best guess'.

9640-40, Session PS

The estimation of surface solar radiation considering the distortion of the cloud shadow on complex terrain

Bin Li, Xiaozhou Xin, Hailong Zhang, Lifeng Gong, Jichao Hu, Institute of Remote Sensing and Digital Earth (China)

Clouds and topography are the two most important factors that affect the surface radiation. On the one hand, clouds have influence on the radiation by absorbing, reflecting and scattering; on the other hand, cloud shadows are also an important influencing factor to estimate the surface radiation with remote sensing method. Cloud and its shadows under different observation angle and the angle of the sun will lead to 3-D geometry effect. Furthermore, the terrain also have influence on downward solar radiation, characterized by the redistribution of radiation, including direct radiation and scatter radiation and additional radiation from the surrounding terrain. At the same time, the shadow distortion of cloud on the complex terrain also should be taken into consideration in the estimation of downward radiation. So "coupling" the clouds, as well as its shadows, and the terrain under the certain condition has the vital significance on estimating the surface radiation values.

Cloud detection results of high resolution by HJ satellite data will be used, according to the height of the cloud and satellite observation angle information the position of cloud on the image will be corrected to get the true position of the cloud.

To more accurately describe the shadow distortion caused by the terrain, a geometrical method will be used to calculate the position of cloud shadow on complex terrain. On the basis of the result after the calculation, downward solar radiation of the corresponding position will be calculated based on the radiation look-up table with the radiation at the top of the atmosphere or reflectivity.

In the processing above we will take the heterogeneity of the cloud height, especially at the edge of the cloud, into account, as it will affect the calculated results.

Final cloud height will be determined by iteration of the cloud height from potential minimum to maximum, which will be determined by different adiabatic lapse rate, until the match similarity larger than a given threshold. The cloud height values will be calculated with thermal infrared data of HJ satellite, at the same time, an edge match method will be used to match the edge height from thermal infrared data to the edge of cloud from CCD, because of their different resolution.

Then, according to the mountain radiative transfer theory, DEM and albedo will be employed in the topographic correction model for the horizontal surface solar radiation (SSR) products. Several different types of radiation stations on The Tibetan plateau as study areas (Lhasa, Ganzi, Naqu, Golmud) will be selected to simulate the whole experiment process. Finally, the results will be used to verify with the ground observed data in the areas.

9640-41, Session PS

Detection of severe air pollution from multidirectional perspectives

Sonoyo Mukai, Kyoto College of Graduate Studies for Informatics (Japan); Itaru Sano, Makiko Nakata, Masayoshi Yasumoto, Kinki Univ. (Japan)

This work is aimed at developing efficient algorithms for aerosol remote sensing involving polarization information around urban areas in East Asia. Because the atmospheric aerosol distribution in East Asia is known to be complicated and not only yellow dust but also small anthropogenic aerosols dominate because of emissions from diesel vehicles and industrial activities in urban areas. On the other hand the satellite polarimetric sensor POLDER has shown that the spectro-photopolarimetry of the terrestrial atmosphere is very useful for the observation of the Earth, especially for atmospheric particles. JAXA has been developing the new Earth observing system, GCOM satellite. GCOM-C will board the polarimetric sensor SGLI in 2017. The SGLI has two polarization channels at near-infrared wavelengths of 670 and 870 nm. Furthermore EUMETSAT plans to collect polarization measurements with a POLDER follow on 3MI/EPS-SG in 2021. It is highly likely that large-scale air pollution will continue to occur because air pollution becomes severe due to both the increasing emissions of the anthropogenic aerosols and the complicated behavior of natural aerosols. At a time like this, the efficient algorithm for polarized radiation simulation in the optically thick atmosphere is expected.

It is natural to consider that incident solar light multiply interacts with the atmospheric aerosols due to dense radiation field in such a heavy haze. Accordingly efficient and practical algorithms for radiation simulation are indispensable to retrieve aerosol characteristics in a hazy atmosphere. Here the radiative transfer equation is described with the four dimensional vector representing the polarized radiation field. These four quantities represent the 'Stokes Parameters'. The method of successive order of scattering (named MSOS), which is available for the radiation simulation reflected from the optically semi-infinite atmosphere, has been examined in the scalar field [refer to S. Mukai, M. Yasumoto and M. Nakata, 2014: Estimation of biomass burning influence on air pollution around Beijing from an aerosol retrieval model. The Scientific World Journal, Article ID 649648.]. Now we intend to improve our MSOS-scalar code into more efficient and practical form, and further into MSOS-vector form. We show here that a dense aerosol episode can be well simulated by a semi-infinite radiation model. For an example, the biomass burning episode observed by Parasol/POLDER and Aqua/MODIS in the East China is treated. The retrieved results are evaluated with the ground measurements (NASA/AERONET and/or PM sampling) and numerical model simulations (MIROC5.0).

9640-42, Session PS

Air quality assessment from surface and space

Itaru Sano, Makiko Nakata, Kinki Univ. (Japan); Sonoyo Mukai, Kyoto College of Graduate Studies for Informatics (Japan)

Our air quality observation site is located in Osaka, which is known as 2nd large city in Japan. The population of the region is around 1.7 million that emit large amount of human related (industry origin's, local traffic, and so on) pollutants. Nowadays

large amount of pollutant is observed not only local emission but also Trans-boundary pollutants from the continent due to the weather condition. We have been taking the measurements of fine particulate matter (PM2.5) and total suspended particulate matter (TSP or PM10) by SPM-613D, and optical properties of aerosols by NASA/AERONET, and NIES/LIDAR system.

This work investigates seasonal variations of air quality in urban area based on the above mentioned ground measurements and also simultaneous usage of satellite data. Mass concentration of PM and spectral aerosol optical thickness AOT are the basic data.?At first, these data indicate high air pollutants during the spring and summer. The former must suggest dust events from China continent, and the latter photochemical events. Here we analyze the detail characteristics of air pollutants as follows:

1. The size and composition of PM with SEM-EDX analysis.

2. The obtained distributions are compared with AERONET data

3. The seasonal air pollution models are proposed based on LIDAR and satellite data.

9640-43, Session PS

Estimation of solar radiation by using modified Heliosat-II method and COMS-MI imagery

Wonseok Choi, Ahram Song, Yongil Kim, Seoul National Univ. (Korea, Republic of)

Estimation of solar radiation is very important basic research which can be used in solar energy resources estimation, prediction of crop yields, resource-related decision-making and so on. Accordingly, recently diverse researches for estimating solar radiation are performing in Korea. In this study modified Heliosat-II method and COMS-MI imagery were used in estimation radiation. Heliosat-II method is one of the widely used model to estimate solar irradiance, and it's accuracy has been demonstrated by many other studies. But Heliosat-II method cannot be applied directly for estimate solar irradiance around Korea. Because Heliosat-II method is optimized for estimating solar radiation of Europe. Basically Heliosat-II method estimate solar radiation by using Meteosat meteorological satellite imagery and statistical data which are taken around Europe. Because these data do not include Korea, Heliosat-II method must be modified for using in estimation solar radiation of Korea. In this study, Heliosat-II method was adjusted to the image of COMS-MI, weather satellite of Korea. And method of producing background albedo map which is used in Heliosat-II method is modified for getting more delicate one. Heliosat-II method estimated the background albedo map through statistical ways using satellite images between 1985 and 1997. However, COMS-MI data are not sufficient to make albedo map using statistical method. Because, COMS-MI have operated and taken image from 2011. Moreover such existing method is hard to reflect either the atmospheric and surface condition at the wanted moment of drawing solar radiation or a change occurring on ground. In this study, Solar radiation were estimated by using COMS-MI imagery which were taken during 2013.1.1~2013.12.31. And ground measurement data which were produced during same period also were used as reference data. Linke turbidity map, solar spectral model and sensor spectral response value also were used in estimation and all these data were performed pre-processing. Method of producing background albedo map was modified by using SSG method. As a results, background albedo map which is reflected current weather condition is produced. And imagery of hourly global solar radiation was produced. Finally accuracy of estimation was verified by using ground measurement value of radiation.

9640-44, Session PS

Exploiting the structure of microwave radiometer-derived temperature profile for stable boundary layer height estimation

Umar Saeed, Univ. Politècnica de Catalunya (Spain); Francesc Rocadenbosch, Univ. Politècnica de Catalunya (Spain) and Institut d'Estudis Espacials de Catalunya (Spain)

Continuous estimates of the atmospheric boundary-layer height are needed for several applications ranging from weather, meteorology, avionics and air-quality and dispersion models. While a lot of work has been done for the estimation of convective boundary layer height, only a few efforts have been made to estimate the night-time stable boundary-layer height (SBLH). SBLH is also one of the key uncertainties in the weather forecasting models.

In this work, we present a method for the estimation of SBLH using curvature of the curve within the potential temperature profiles retrieved by a microwave radiometer (MWR). The curve within the temperature profiles occurs at the inversion point and the fact that MWR retrieval introduces a smooth transition from the stable layer underneath to the residual layer above. However, the vertical resolution of the MWR-derived temperature profile decreases with the height. Therefore, as the first step, we use spline interpolation to come-up with a uniformly resolved temperature profile. Then first derivative of the interpolated temperature profile is calculated and smoothed to avoid sharp local transitions in the derivative. Finally, the second order derivative of the vertical potential temperature profile is calculated and a curvature parameter at each point in the vertical domain is obtained. The first minima of the curvature profile signifies the point where the temperature profile starts changing from the stable regime to the residual boundary layer.

We analyse the performance of the method by comparing it against the physically idealized models of the stable boundary-layer temperature profiles. There are five models which include stable-mixed, mixed-linear, linear, polynomial and exponential. For a given temperature profile these five models are fitted using the least-squares approach and the best fitting model is chosen as the one which fits with the minimum root-mean-square error.

The comparison of the SBLH estimates from curvature based method with the physically idealized models shows that the method works well in principle. Potential application of this approach is the situations where the given temperature profiles are more deviant from the idealized models and no models fits them well.

9640-45, Session PS

Synergy of remote sensing and UAV measurements in retrieval of vertical structure of the aerosol absorbing properties

Michal T. Chilinski, Krzysztof M. Markowicz, Univ. of Warsaw (Poland)

Absorbing aerosols vertical distribution is an important factor in radiative transfer processes, which influences energy budget and should be taken in account during atmospheric correction of remote sensing products. To determine real impact of those aerosols measurements of vertical profiles are necessary. Quantity which characterize how much of the radiation was absorbed by aerosols is called absorption coefficient. Most reliable methods of measuring absorption coefficient are measurements of filter attenuation and/or photo acoustic effect. Both methods are in-situ and need constant flow of air samples through measurement devices. Obtaining vertical profiles of aerosol absorption coefficient is much more

complicated due to lack of effective remote sensing methods. Most common remote sensing methods in atmosphere physics for acquiring profiles of aerosols optical properties are lidars. Lidars delivers range corrected profiles of backward scattering (backscatter coefficient), which in case of absorbing particles is hardly registered or negligible.

Single scattering albedo (SSA) is the ratio of scattering coefficient to the extinction coefficient, where extinction is the total amount of radiation absorbed or scattered in the atmosphere. SSA is very helpful in determining type of aerosols in airmass and their potential radiation feedback. Previously mentioned problems with remote sensing of absorption coefficient profiles, makes measurements of SSA profiles not a trivial task.

We propose method for obtaining profiles of SSA which is based on simultaneous measurements of profile of backscattering properties from lidar and profile of absorption coefficient measured by microaethalometer mounted on a remote piloted aerial system. Microaethalometer registers changes in a filter attenuation during the flight time, what allows retrieval of absorption coefficient profile in the range of flight. Combination of lidar retrievals and data from aethalometer lead to possibility of SSA profile estimation.

Proposed method delivers data, which then could be validated with radiative transfer models and additional measurement from radiometers. Main limitations are: endurance of used remote piloted aerial system, which allows measurements up to 1000 meters and sensitivity of microaethalometer, which limit measurements to cases with higher concentration of absorbing particles.

During our presentation concept and background for the method will be explained and most interesting cases measured during last field campaigns.

9640-47, Session PS

Time-series MODIS satellite and in-situ data for spatio-temporal distribution of aerosol pollution assessment over Bucharest metropolitan area

Maria A. Zoran, Roxana S. Savastru, Dan M. Savastru, National Institute of Research and Development for Optoelectronics (Romania)

Air quality has become one of the major environmental concerns in Bucharest, Romania due to the country's rapid development after 1989 year, particularly in transport, energy and building/road construction sectors. Emissions from road traffic, such as PM10 and PM2.5 (particles having aero-dynamic diameters less than 10?m) have become a threat to air quality, particularly in metropolitan areas. Very limited available information has indicated that these pollutants may present a challenge if future EU limits are to be met. The major mechanisms contributing to airborne particulate matter in the region (as elsewhere) are highly variable, including natural as well as pollution sources, chemical reactions in the atmosphere, long-range transport effects and meteorological conditions.

Air pollution estimates at high spatial-temporal scales are critically important for climate modeling and enforcing air quality standards in order to protect human health.

Atmospheric aerosols are one of the most important parameters affecting the Earth's energy balance and hydrological cycle, climate and human health. With the increasing industrialization and urbanization, especially in the metropolis regions, aerosol pollution has highly negative effects on environment. Urbanization is responsible of three major changes that may have impact on the urban atmosphere: replacement of the natural surfaces with buildings and impermeable pavements, heat of anthropogenic origin and air pollution. The importance of aerosols for radiative and atmospheric chemical processes is widely recognized. They can scatter and/or absorb solar radiation leading to changes of the radiation budget. Also, the so-called indirect effect of aerosols describes the cloud-aerosol interactions, which can modify the chemical and physical processes in the atmosphere. Their high spatial variability and short lifetime make spaceborne sensors especially well suited for their observation. Remote sensing is a key application in global-change science and urban climatology. Since the launch of the MODerate resolution Imaging Spectroradiometer (MODIS) there is detailed global aerosol information available, both over land and oceans The aerosol parameters can be measured directly in situ or derived from satellite remote sensing observations. All these methods are important and complementary. The objective of this work was to document the seasonal and inter-annual patterns of the aerosol pollution in two size fractions (PM10 and PM2.5) loading over the Bucharest metropolitan area in Romania based on in-situ and MODIS (Terra–Moderate Resolution Imaging Spectoradiometer) satellite time series data over 2010-2012 period. Accurate information of urban air pollution is required for environmental and health policy, but also to act as a basis for designing and stratifying future monitoring networks. Preliminary comparison, in the case of warm season (August month) and cold season (November month) between satellite-based and ground-based PM10 and PM2.5 measurements have shown a good agreement. As statistical approach, it is necessary a major number of samples for further validation. Despite the feature of high repetition cycle of 1 day of MODIS sensor, missing data is due to clouds 'presence. Furthermore, PM2.5 samplings at ground are not routinely performed.

9640-48, Session PS

Development of new shipborne aureolemeter to measure the intensities of direct and scattered solar radiation on rolling and pitching vessel

Hiroshi Kobayashi, Univ. of Yamanashi (Japan); Masataka Shiobara, National Institute of Polar Research (Japan)

Atmospheric aerosols play important role in the Earth's radiation budget through the scattering and absorption of solar radiation (direct effect) and modification of cloud properties (indirect effect). A global understanding of the spatial and temporal variations of aerosol optical thickness (AOT) and aerosol optical properties is necessary for assessment of it. Oceans cover about 70% of the Earth's surface and produce a large quantity of natural aerosols. Maritime aerosols mainly consist of sea salt; however, they also contain dust, particles from biomass burning, and anthropogenic aerosols that have been transported from land. Thus, aerosol optical properties over the ocean have significance for the radiation budget.

Japan Aerospace Exploration Agency (JAXA) plans to launch earth observation satellite as Global Change Observation Mission - Climate (GCOM-C). GCOM-C will mount Second generation Global Imager (SGLI). Aerosol optical thickness and properties over the ocean are required validations of products for atmosphere and ocean of GCOM-C / SGLI mission.

An earlier shipborne sky radiometer that automatically measured the direct sun and sky radiance distribution was developed. However, the sun tracking system of this sky radiometer could perform only direct solar radiation measurement. When this measures sky radiance distribution, the sensor direction is not decided precisely. Therefore, the new shipborne aureolemeter was developed to improve the sun-tracking performance for measurements of accurate direct and diffuse solar radiation, even with substantial vessel rolling and pitching.

Sun position or direction is determined with a CCD camera, which has 1236 X 1236 pixels. As the field of view of the CCD is 19.5˚, the angle resolution is 0.0157 ˚/pixel. To deduce solar radiation, ND filters are attached before the CCD camera lens. A round shape is extracted from a captured image with an image processing. In the case the area of the round shape corresponds to that of sun, it is recognized as sun. The position of the center of gravity of the round shape is used as the sun position. In the result, the sensitivity of the position determination is as fine as less than one pixel.

The radiometer is tracked the sun using feedback control

with the sun position derived from the CCD camera and image processing. In the case of the sky radiance distribution measurement, the control target position on the CCD camera image is shifted a pixel corresponding to a measuring scattering angle. On the other hand, in the case of larger scattering angle and the control target position becomes the out of the CCD camera's field of view, the radiometer's tracking is conducted with feed-forward control on the basis of the rolling and pitching angle detected with a gyroscope.

To decide the solid angle of the radiometer, the radiance around the sun was measured in the angle range between the sun and sensor directions from -1.5˚ to +1.5˚ with 0.1˚ resolution. The instrument constants were determined from Langley plot. In the future, we conduct a comparison observation between developed shipborne aureolemeter and an existing sky radiometer.

9640-1, Session 1

Aerosol properties from combined oxygen A band radiances and lidar *(Invited Paper)*

David Winker, NASA Langley Research Ctr. (United States); Pengwang Zhai, Univ. of Maryland, Baltimore County (United States); Yongxiang Hu, NASA Langley Research Ctr. (United States)

We have developed a new aerosol retrieval technique based on combing high-resolution A-band spectra with lidar profiles. Our goal is the development of a technique to retrieve aerosol absorption, one of the critical parameters affecting the global radiation budget and one which is currently poorly constrained by satellite measurements. Our approach relies on two key factors: 1) the use of high spectral resolution measurements which resolve the A-band line structure, and 2) the use of co-located lidar profile measurements to constrain the vertical distribution of scatterers in the forward model. This research was initiated early in the development of CALIPSO, when an A-band spectrometer was part of the payload. Initial retrieval simulations were promising but the spectrometer was later descoped from the CALIPSO payload. Launch of the OCO-2 satellite now offers the opportunity to test our retrieval approach.

The OCO-2 satellite was launched in July 2014 to provide global measurements of CO2 concentrations and is now flying in formation with the CALIPSO satellite. OCO-2 carries an oxygen A-band spectrometer with a spectral resolution of 21,000:1. This is sufficient to resolve the A-band line structure, which contains information on atmospheric photon path lengths. Combining channels with oxygen absorption ranging from weak to strong allows the separation of atmospheric and surface scattering. An optimal estimation algorithm for simultaneous retrieval of aerosol optical depth, aerosol absorption, and surface albedo has been developed. Lidar profile data is used for scene identification and to provide constraints on the vertical distribution of scatterers. The algorithm was developed using simulated OCO-2 spectra. The simulations show that AOD and surface albedo can be retrieved with high accuracy. The algorithm also shows skill at retrieving aerosol single scatter albedo when AOD is larger than about 0.15. Retrieval performance improves as the albedo of the underlying surface increases. Thus, the technique shows great promise for retrieving the absorption optical depth of aerosols located above clouds. This presentation will discuss the basis of the approach and results of initial tests using OCO-2 radiances.

9640-2, Session 1

The ESA-JAXA EarthCARE clouds, aerosol and radiation explorer mission: overview and development status

Dulce Lajas, European Space Research and Technology Ctr (Netherlands); Michael Eisinger, European Space Agency - European Centre for Space Applications and Telecommunications (ESA-ECSAT) (United Kingdom); Tobias Wehr, Robert Koopman, Alain Lefebvre, European Space Research and Technology Ctr (Netherlands)

EarthCARE, the Earth Clouds, Aerosol and Radiation Explorer, is a joint European-Japanese mission which has been defined with the objective of improving the understanding of cloud-aerosol-radiation interactions so as to include them correctly and reliably in climate and numerical weather prediction models. The EarthCARE Mission has been approved for implementation as ESA's third Earth Explorer Core Mission. It is currently in its Detailed Design Phase (phase C) with a launch scheduled for 2018.

The scientific objectives of EarthCARE are: - The observation of the vertical distributions of atmospheric liquid water and ice on a global scale, their transport by clouds and their radiative impact.

- The observation of cloud distribution, cloud-precipitation interactions and the characteristics of vertical motions within clouds.

- The observation of the vertical profiles of natural and anthropogenic aerosols on a global scale, their radiative properties and interaction with clouds.

- The retrieval of profiles of atmospheric radiative heating and cooling through the combination of the retrieved aerosol and cloud properties.

The EarthCARE payload comprises: an Atmospheric High Spectral Resolution (HSR) Lidar (ATLID) which operates at 355 nm and is equipped with a HSR receiver that will separate the back-scattered Mie and Rayleigh signals. The Cloud Profiling Radar (CPR), provided by JAXA and NICT is a highly sensitive 94GHz cloud radar with Doppler capability. The Lidar will provide the vertical profiles of aerosol and the synergy between the Lidar and the CPR will provide profiles of ice and liquid water content throughout clouds. Cloud vertical movements will be measured using the Doppler capability of the CPR. A Multi-Spectral Imager (MSI) will support the active instruments and consists of a push-broom imager with 7 channels in the visible, near-IR, short-wave IR and thermal IR, with a 500 m spatial resolution and a 150 km swath. Finally, a Broad-Band Radiometer (BBR) will measure the outgoing top-of-atmosphere radiances in a short wave channel and a total wave channel, from which the long wave contribution can be deduced.

This paper presents the EarthCARE programmatic status, the current instrument design and mission performance. The mission end-to-end simulator (E3SIM) and data processing up to level 2 (geophysical products) and related science activities will be discussed. The E3SIM supports end-to-end simulations from a scene definition to synergistic level 2 products. Level 2 retrieval algorithms can be tested in the full chain (provision of input data, algorithm performance tests by comparison of outputs with known inputs) by using a single framework with well-defined interfaces helping to harmonise algorithm developments.

9640-3, Session 1

94 GHz doppler wind radar satellite mission concept

Chung-Chi Lin, Björn Rommen, Christopher Buck, Dirk Schüttemeyer, European Space Research and Technology Ctr. (Netherlands)

Extreme weather such as storms, hurricanes and typhoons, also called 'high impact weather', is a high priority area of research for the atmospheric dynamics and meteorological science communities. Ground-based weather radars have extensively been used in order to gather data and to study the physical mechanisms involved in such weather phenomena, sometimes complemented by airborne in-situ measurements. ESA's ADM/Aeolus mission, presently planned to be launched in 2017, aims to observe large-scale wind profiles globally using an UV lidar technique. Due however to its active optical sensing technique, observations are restricted to cloud-free conditions and its spatial sampling rate is low (?250 km), thus unsuitable for the studies of convective or frontal systems with cloud cover.

A 94 GHz Doppler wind radar mission concept has been elaborated, which uses cloud and precipitation droplets/particles as tracers to measure 3-D wind fields. The so-called polarisation-diversity pulse-pair (PDPP) technique enables to derive line-of-sight wind speed with good accuracy (< 2-3 m/s) and large unambiguous dynamic range (e.g. 80 m/s). Two distinct system concepts have been elaborated: (1) a conically scanning radar concept with large coverage (> 800 km) and ?50 km along-track sampling, and; (2) a stereo viewing concept with high sampling resolution (< 4 km) within an inclined cut through the atmosphere. The former concept is adequate for studying large-scale severe/extreme weather systems, whereas the latter would be more suitable for understanding of small-scale convective phenomena.

For demonstrating the potential of the FDPP technique for deriving accurate Doppler observations, ground-based and airborne Doppler radar campaigns are in preparation.

9640-4, Session 1

Deriving aerosol properties from measurements of the Atmosphere-Surface Radiation Automatic Instrument (ASRAI)

Hua Xu, Donghui Li, Zhengqiang Li, Institute of Remote Sensing and Digital Earth (China); Xiaobing Zheng, Xin Li, Anhui Institute of Optics and Fine Mechanics (China); Yisong Xie, Enchao LIU, Institute of Remote Sensing and Digital Earth, Chinese Academy of Sciences (China)

The Atmosphere-Surface Radiation Automatic Instrument (ASRAI) by Anhui Institute of Optics and Fine Mechanics, Chinese Academy of Sciences, is a newly developed hyper-spectral apparatus which can measure both the atmosphere and territorial surface synchronously for the purpose of in-situ calibration of satellites. The ground-based instrument applies VIS-SWIR spectrum (0.4~2.4 ?m) and the averaged spectral resolution is 0.004 ?m. The automated hardware can measure the total spectral irradiance and diffuse spectral irradiance of the atmosphere together with the reflected radiance of land surface simultaneously, which are necessary inputs to 6S radiative transfer model for satellite TOA simulation. The goal of this paper is to describe a method which can derive both aerosol optical depth (AOD) and aerosol modes from atmospheric irradiance measurements under free cloudy conditions.

According to the Lambert-Beer Law, we get the total optical depth ?t of atmosphere from the directly transmitted solar irradiance by means of the total irradiance minus diffuse irradiance. From ?t we can determine the corresponding value of aerosol optical depth ?a. It is given by subtracting from ?t the contribution of Rayleigh optical depth ?r and gas absorption optical depth ?g. ?r is a function of surface pressure, while ?g is a function of absorptive gas content (atm-cm) multiplying absorption coefficients per centimeter of pure gas at STP. The absorption coefficients can be calculated by HITRAN at the spectral resolution of ASRAI. As for the contents of absorptive gas (such as water vapor, O3, NO2, etc.), we directly retrieve them from the spectral variation of ?t at absorbing wavelengths.

Moreover, we use the spectral dependency of AOD to obtain more information about aerosol modes. In the 6S model, the real aerosols are considered as an idea of "external mixing" of four basic components, dust-like, water-soluble, oceanic and soot, each of which has their inherent spectral extinction characteristics. Since the spectral dependency of AOD ?(?) varies the same as the spectral dependency of aerosol extinction coefficient, we can retrieve the percentage of volume concentration of each component from the shape of ?(?), with assumption that real aerosols only consist of four basic components. We use a spectrum matching technology based on an Euclidean-distance method to find the most probable mixing combination of four basic components.

It demonstrates that the method we use is reliable. We deployed ASRAI for continuous observation in Dunhuang Site and Hefei City in China. We successfully obtained the spectral AOD which is very close to the results of CE318 at discrete wavelengths. The volume concentration ratios of four basic components are in accordance with our priori knowledge of regional aerosol climatology. Also, another advantage to our method is that the retrievals would facilitate the TOA simulation when applying 6S model for satellite calibration.

9640-5, Session 1

Comparison of unfiltered Ceres radiances measured from the S-NPP and Aqua satellites over matched sites

Zbigniew P. Szewczyk, Science Systems and Applications, Inc. (United States); G. Louis Smith, Science Systems and Applications (United States); Kory J. Priestley, NASA Langley Research Ctr. (United States) and Science Systems and Applications (United States)

The main purpose of this paper is to present a comparison of unfiltered radiances measured by CERES instruments operating on two different platforms, namely the Suomi-NPP the Aqua satellite, when instruments scan over the matched sites. It is shown that using a nadir dwell elevation scan profile on FM5 and FM3, an unprecedented high precision dataset is collected for a more stringent test of the consistency between the two instruments on specific scene types. This mode is used in the "matched sites targeting" strategy, which a short description is provided below.

Matched sites targeting. A unique comparison opportunity is available when groundtracks of the S-NPP and Aqua satellites are within a 0.25o, and less than 5 minutes apart. These opportunities present themselves less than 10 times per months; however, they offer a comparison of very high precision data. Each opportunity lasts about 2 minutes, and the comparison is at a footprint level. Scanners on both satellites are operating in a nadir dwell scan profile that produces 330 footprints along their respective overlapping groundtracks.

A nadir dwell scan profile with 330 samples along a ground-track 330 measurements collected during each nadir dwell can be then averaged and compared between the two scanners. Sites for comparison are selected beforehand based on satellites groundtracks, and in the selection the time of overpass, solar zenith angle, and desired scene type are considered. In 2013 seven nadir dwell observations were carried out for several different scene types including snow/ice, ocean, and land. Another eight observations were carried out in 2014.

In the full paper, a detailed description of the strategy, and the data collection will be provided. Analyses will include detailed description of spatial match of each nadir well between FM5 and FM3 along with comparison of unfiltered radiances.

Nadir dwell observations are affected by a cloud cover, and therefore all radiance analyses are enhanced by using the SSF (single-scan-footprint) products. This product contains imager (MODIS) information about the clouds that is much more detailed to cloud information provided by an ERBE-like or ES8 data product.

9640-6, Session 1

Design and performances of microcameras and photometers instruments on TARANIS satellite for an advanced characterization of transient luminous event in the upper atmosphere

Fanny Le Mer-Dachard , Elodie Cansot, Philippe-Jean Hébert, Thomas Farges, Ctr. National d'Études Spatiales (France); Karen Ravel, SODERN (France); Stéphanie Gaillac, Bertin Technologies (France)

The general objective of the TARANIS mission is to study upper atmosphere coupling with a scientific nadir-pointing satellite. It is based on a CNES Myriade microsatellite family. The mission is planned for 2 years nominal life time at a low-altitude orbit (700 km). The satellite main mission is to study the occurrence of Transient Luminous Event (TLE) and Terrestrial Gamma-ray Flash (TGF), their emissions and trigger factors.

TARANIS instruments are currently in manufacturing, assembly, integration and testing phase. Among the eight instruments of TARANIS payload, the MicroCameras and Photometers instruments (MCP) are in charge of the remote sensing of the sprites and the lightning in optical wavelengths. MicroCameras instrument [MCP-MC] is an imager in the visible range and Photometers instrument [MCP-PH] is a radiometer with four bands from UV to NIR. This article will present the final design of these instruments and first measured performances.

The satellite will provide a complete survey of the atmosphere in low resolution together with a high resolution data of sites of interest automatically detected on board.

MCP-PH is a key instrument of the TARANIS payload as a triggering instrument for the whole payload thanks to its on-board detection of the TLEs.

Our paper will first shortly describe physical characteristics of TLEs, impulsive energetic optical phenomena generated by storms according to recently discovered process. They have been studied for only 20 years from ground and by few space missions. They last from less than 1 ms to more than hundreds of milliseconds and occur from 20 km height to 90 km height. Their vertical extension is from 10 km to 70 km while their horizontal extent is from 1 km to 300 km.

Then the MicroCameras design will be described. The results of the qualification and calibration of the optical unit (MC-U) developed by Sodern will be detailed. MicroCameras are dedicated to the spatial description of these phenomena: determination of absolute and relative position of lightning and TLEs and their horizontal extension. They are able to differentiate sprite and lightning thanks to two narrow bands ([757-767 nm] and [772-782 nm]) that provide pairs of images of an "event". The MCP-MC instrument's mass is 2.7 kg and its maximum consumption is 10.2W.

In the last part, the Photometers instrument final design will be exposed. MCP-PH shall cover a large field of view of 42°, same as the MicroCameras, (one band of 86°). It uses four spectral bands in the [170-260 nm], [332-342 nm], [757-767 nm] and [600-900 nm]. The signals captured by the optical unit (PH-U) developed by Bertin Technologies is temporally sampled at 20 kHz and digitized. The electronic board processes these signals in order to detect an event (TLE) and send an alert in real time to the central computer of the payload. Finally, Photometers will provide a temporal measurement and spectral characteristics of TLEs and lightning.

The Photometer unit mass is as low as 1.6 kg, and its consumption less that 3.5 W. Its analyser is a single PCB with only 6 W power.

9640-7, Session 1

Performance test of the synergetic use of simulated lidar and microwave radiometer observations for mixing-layer height detection

Umar Saeed, Univ. Politècnica de Catalunya (Spain); Francesc Rocadenbosch, Univ. Politècnica de Catalunya (Spain) and Institut d'Estudis Espacials de Catalunya (Spain); Susanne Crewell, Univ. zu Köln (Germany)

Mixing layer (ML) height is an important parameter for several applications ranging from weather, meteorology, avionics and air-quality and dispersion models. There are several instruments and methods to retrieve the ML height. However, none of these instruments or methods can measure the development of the ML height under all atmospheric conditions. For example, aerosol signatures measured by backscatter lidar can be used to determine the ML height but this approach works well only when the atmosphere is well-mixed. Also, in the presence of multiple transitions in the aerosol backscatter and low-level clouds ML estimates given by the lidar backscatter are not always physically consistent. Alternatively, Microwave Radiometer (MWR) measurements of brightness temperatures allow reconstruction of the thermodynamic structure of the atmosphere from which ML height can be determined directly. However, MWR-derived profiles have low vertical resolution and cannot resolve fine structures in the boundary layer, especially, at higher altitudes. Here we demonstrate a method which combines simulated data for a ground-based lidar and a MWR to overcome these limitations. The simulated data is obtained from the Dutch Atmospheric Large Eddy Simulation (DALES) model for boundary-layer studies. The method works by fitting an erf-like transition model function to the section of range-corrected lidar backscatter signal. The erf-like transition marks the change of aerosol concentration from the mixed-layer to the free troposphere. The section of the lidar backscatter signal for fitting the model function is obtained by incorporating the MWR estimates of ML height along with their uncertainties. The fitting is achieved by using an extended Kalman filter (EKF). The MWR, therefore, plays the role of layer attribution which is especially more pronounced in the multiple aerosol layers and cloudy conditions. The proposed approach, by exploiting the synergy between the two instruments, enables to detect ML height with original vertical and temporal resolutions. The use of MWR in conjunction with lidar provides physically consistent and meaningful estimates. Moreover, under noisy measurements (or observable), i.e. when the signal to noise ratio (SNR) is low, the use of Kalman filter permits continuous ML height estimates without the need of averaging the data. Test cases combining simulated data for a co-located lidar-ceilometer and a MWR at the measurement site Julich ObservatorY for Cloud Evolution (JOYCE) in Julich, Germany are presented. Doppler wind lidar data is used to assess the quality of the synergetic ML estimates.

9640-9, Session 2

Doppler capable FMCW cloud detection radar

Salih Coskun, Middle East Technical Univ. (Turkey) and ASELSAN Inc. (Turkey); Mert Celik, Middle East Technical Univ. (Turkey) and Meteksan Defense Ind. Inc. (Turkey); Ali Ozgur Yilmaz, Sencer Koc, Middle East Technical Univ. (Turkey)

The experimental FMCW weather radar system used in this study is constructed by using commercial on the shelf (COTS) test equipments at the tower of Ayasli Research Center at METU.

An X-band continuous wave whose frequency is modulated as a positive ramp is generated by using Agilent E8267D Signal generator. The bandwidth of the signal is adjusted as 30 MHz

and FM Rate is adjusted to 10 KHz. This signal is divided into two portions by a signal divider. While one of these portions is going to transmitter part, the other one merges with the received signal. Transmitted portion of the signal is strengthen with a TGA2502 Power Amplifier and then radiated from one of the horn or dish antennas with the chosen polarimetry with a power of 2 Watt.

Receiver part of the system proceeds from two edges. One of the edges starts from power divider with a duplicate of the transmitted signal. The other edge starts with the receiver antennas. Dish or horn antennas are used separately to catch the reflected signal. Then two cascaded Microsemi AML218L1502 Low Noise Amplifier are used to strengthen the echo of the transmitted signal by adding low amount of noise

Following the LNA step, the edges of the receiver system meet at the mixer. Both edges are mixed and the difference of the frequencies between the received and transmitted signal is obtained. After this deramping process, beat signal is obtained and passed to Agilent DSO 6102A oscilloscope. Oscilloscope is used as an analog to digital converter and memory of the system to store the captured data.

Captured data is taken from oscilloscope in binary format by either a USB flash memory or directly by the radar interface program from GPIB interface with the help of an Agilent GPIB to USB converter. When data is captured and stored to USB flash memory, it is processed offline. On the other hand, GPIB interface is used to take real time data with the intervals of 1 second and process it at the same time.

The last step of the system is handling the captured data. The program which is generated using Matlab takes the parameters from the Graphical User Interface, takes the offline or online data, process it and show the results on Graphical User Interface again. Some special techniques such as clipping, windowing, coherent data integration, and slow time signal processing are performed to the captured beat signal.

System parameters are adjusted to have maximum unambiguous range of 15.000 meters with the resolution of 5 meters and maximum speed measurement of 270 kmph with the resolution of 5.4 kmph.

Verification of the system is performed by buildings and cars whose range and velocities are known. The amount of water in the cloud is estimated by measuring the return power and calculating meteorological reflectivity.

9640-11, Session 2

Preventing the saturation phenomenon of detectors used in environmental remote sensing

Abdelkrim Kedadra, Mohammed Traïche, Ctr. de Développement des Téchnologies Avancées (Algeria)

The nowadays environmental issues motivated us to develop a mobile LiDAR system for two applications [1]: 1°/ the prevention against forest fires in the hilly and inaccessible continuous mountainous forests in north Algeria [2], where the risk factor of a forest fire is high in summer and 2°/ the study of the atmosphere by monitoring pollutant species [3-5] and sand aerosols emanating either from cement plants in the Algiers agglomeration and the Sahara. The system mobility enables measurements in different locations. For the first application, we use an eye safe laser wavelength at ?=1.57 ?m and an avalanche photodiode (APD) as a detector. For the second application, we use a Nd:YAG laser followed by a second harmonic generator that emits at ?=532 nm and a photomultiplier (PMT) as a detector. The LiDAR is an active technique [6] that often deals with weak return signals. The latter come with an intensity proportional to 1?R2, where R is the range from the target to the detector. The signal-to-noise ratio (SNR), as an effective detection criterion, needs to be optimized towards better performance [7]. That is, when the SNR is low, the detected signal is increased and vice versa.

In the case of forest fires detection, it may happen that strong signals from nearest objects lead the detector to a saturation status. We suggest a method to handle this issue that is base on the control of the detector gain by driving its applied voltage.

References

[1] M. Traïche and A. Kedadra, SPIENewsroom 4801 (21 June 2013). DOI: 10.1117/2.1201306.004801.

[2] M. Traïche et al., AIP Conf. Proc. 1047, 50–58 (2008).

[3] B. R. Clemesha, G. S. Kent, and R. W. H. Wright, J. Appl. Meteorol. 6(2), 386–395 (1967).

[4] V. Sivakumar et al., Atmos. Chem. Phys. 4(7), 1989–1996 (2004).

[5] P. M. Hamilton,Philos. Trans. R. Soc. Lond. A 265(1161), 153–172 (1969).

[6] A. Lavrov et al., Int. J. Therm. Sci. 45(09), 848–859 (2006).

[7] Abdelkrim Kedadra and Mohamed Traïche, J. Appl. Remote Sens. 8 (1), 083568 (August 14, 2014). DOI: 10.1117/1.JRS.8.083568.

9640-12, Session 3

Comparing different methods to retrieve cloud top height from Meteosat satellite data

Ilaria Tabone, Univ. degli Studi di Torino (Italy); Susana Briz, Univ. Carlos III de Madrid (Spain); Anna Anzalone, INAF - Istituto di Astrofisica Spaziale e Fisica Cosmica di Palermo (Italy); Antonio Jesus de Castro González, Univ. Carlos III de Madrid (Spain); Silvia Ferrarese, Univ. degli Studi di Torino (Italy); Francesco Isgrò, Univ. degli Studi di Napoli Federico II (Italy); Claudio Cassardo, Roberto Cremonini, Mario Bertaina, Univ. degli Studi di Torino (Italy); Fernando Lopez, Univ. Carlos III de Madrid (Spain)

Clouds play a fundamental role in weather and climate systems as they interact with short-wave solar and long-wave thermal radiation influencing the radiative balance and driving global climate changes. Water thick clouds are important for meteorological studies as their water content drives precipitation, while optically thin high level clouds, such as cirrus clouds, can impact on radiative processes. For this reason the monitoring of cloud parameters such as the Cloud Top Height (CTH), Cloud Top Temperature (CTT), cloud emissivity, cloud particle size and cloud optical depth have always been matter of interest for the atmospheric community. Particularly Cloud Top Height investigations provide informations on cloud vertical structure leading to better understand the cloud radiative effects. In this contribution we will describe three different methodologies to retrieve the CTH from IR images. The first technique is based on stereo-vision algorithms and requires two different views of the same scene. The height reconstruction relies on accurate image analysis, depends on the geometry of the system and does not need of extra atmospheric information. In the second one, brightness temperatures in IR spectral region are converted to real cloud temperature from which the CTH is estimated using temperature vertical profiles. As observed radiosounding data are rare, real-time atmospheric profiles can be reproduced using post-event simulations performed by NWP models, such as the mesoscale model WRF, which has been used in this work, also to retrieve the CTH based on the primary model output parameters. This article presents a preliminary work, in which the heights retrieved by the three methodologies are compared with the heights given by MODIS sensor installed on polar satellite TERRA. The two geostationary satellites Meteosat 9 and Meteosat 10 have been selected because they provide quasi synchronous images of the same scene from two different points of view, and for this reason they can be used in Stereo-Vision analysis. The radiative method (Split Window Algorithm) involves two spectral bands and is here applied to Channel 9 and 10 of Meteosat 10. This bi-spectral algorithm improves the temperature retrievals of a monoband

algorithm, expecially for low clouds. This work is a first step to validate a simplified version of CTH retrieval methodologies and to check the reliability of WRF model in CTH estimation. A cloudy scene, scanned simultaneously by the three considered satellites, has been selected to validate the methods. When applied to Meteosat images, the results revealed that the Split Window Algorithm is optimum for low clouds, while the Stereo-Vision Algorithm adopted in this work manages to recover high clouds. Regarding WRF, the choice of initial conditions, resolution and of opportune physical parametrizations is mandatory in order to get the optimal representation of cloudiness field. This promising results show that valuable information about CTH can be retrieved from Meteosats which provide high frequency and large scale data useful for weather and climate research.

9640-13, Session 3

On the reliability of geostationary satellite observations for diagnosing indirect aerosol effects

Daniel Merk, Hartwig Deneke, Leibniz Institut für Troposphärenforschung (Germany); Bernhard Pospichal, Univ. Leipzig (Germany); Patric Seifert, Leibniz-Institut für Atmosphärenphysik e.V. (Germany)

Indirect aerosol effects - changes in cloudiness due to variations in aerosol composition and concentration in the atmosphere - are still poorly understood and one of the main sources of uncertainty in climate projections. While reliable observational constraints on a global scale are a key pre-requisite for improving models, current methods for diagnosing aerosol effects from satellite observations are still highly uncertain. The goal of the present study is an investigation of the consistency of passive SEVIRI and MODIS satellite observations for diagnosing indirect aerosol effects, focusing on Central Europe due to the availability of complementary ground-based observations for a comparison. Ground-based observations are collected from a ceilometer network (~150 stations) in Germany and Cloudnet sites in Central Europe for the year 2013.

From the passive satellites datasets, we focus on retrieved cloud properties commonly used to diagnose indirect aerosol effects, in particular liquid water path and cloud droplet number concentration. One key assumption to retrieve such properties is that clouds behave adiabatically or sub-adiabatically, i.e. their liquid water content profile increases linearly, while the cloud droplet number concentration remains vertically constant. For the pure adiabatic assumption water vapour will be transformed into liquid water for a rising air parcel without entrainment of air outside the parcel. Many studies actually show a sub-adiabatic nature of clouds. In those, entrainment reduces the liquid water content, although a change in the cloud geometrical depth can lead to the same liquid water path as without entrainment. We examine the validity of the adiabatic assumption by means of satellite retrieved liquid water path and a synergistic estimate of cloud geometrical depth, obtained from satellite cloud top height and ground-based cloud base height. Cloud top heights obtained from MODIS and SEVIRI show a good correlation with radar-estimated cloud tops at the Cloudnet site LACROS (Leipzig) during summer months of 2013 for liquid clouds. We also investigate the uncertainty induced by the sub-adiabatic nature of those clouds in contrast to other uncertainty sources in the retrieval process of cloud key properties.

To explore if changes in aerosol composition and concentration lead to significant changes in cloud properties observed from passive satellites, we include aerosol mass concentration for different species as well as aerosol optical depth for different wavelengths from the MACC model. We apply common metrics used in the literature such as the relative change in effective radius or in cloud droplet number concentration, obtained from SEVIRI and MODIS independently, and check their robustness and consistency.

9640-15, Session 3

Clouds observations with high resolution FMCW cloud profiling radar FALCON-A at the arctic station in Ny-Alesund

Toshiaki Takano, Yohei Kawamura, Hiroyuki Nakata, Tamio Takamura, Chiba Univ. (Japan); Masataka Shiobara, National Institute of Polar Research (Japan)

Observation of clouds with radars in millimeter wave range is one of the most powerful methods to derive information on interior of clouds. We have developed a cloud profiling FMCW (Frequency Modulated Continuous Wave) Doppler radar named FALCON-A in W-band 94GHz and installed at the Arctic Station in Ny-Alesund, Svalbard, Norway, N79 deg. as a part of the project under GRENE Arctic Climate Change Research Project. It consists of two 1m-diameter antennas and has high spatial resolution of 0.18 degree FWHM. FALCON-A observes at zenith in regular observations, and can observes also a scanning mode, which sweep +-10 degrees from zenith. A high range resolution of 50m is realized with the FMCW type radar, which is about several times higher than that of normal pulse type radar. Output power of FALCON-A is as small as about 1W, and, therefore, it is realized with solid state components without any tubes. Although its small output power, FALCON-A has enough sensitivities to observe thin clouds at high altitude and has high resolution in Doppler measurements. We can observe +-3.2 m/s in Doppler measurements.

Using FALCON-A, we started regular observations in 2013 September at Ny-Alesund even in the winter days. We observed cirrocumuli on 2013 Sept. 16 at around 4 to 6 km in height, which consist of two layer. Upper layer of cirrocumuli having the thickness of around 1 km is quite stable and horizontal size is estimated to be 1-2 km, which is similar to the height thickness. Lower layer whose height thickness is around 1.5 km, contrary, has defuse structures and are falling down with 2-3 m/s. Lower layer would be larger snow particles produced in the upper cirrocumuli structures. Micro Pulse Lidar data operated in Ny-Alesund also suggest that the sizes of cloud particles in the lower layer should be larger because of the higher cross-polarization rate. These results would be useful to investigate characteristics of clouds in various cases in Arctic region and be useful for investigations of aerosol-cloud interactions.

9640-16, Session 3

Numerical modeling of polarization properties of the return signals in ground-based LIDAR cloud sensing

Evgeniya G. Kablukova, Institute of Computational Mathematics and Mathematical Geophysics (Russian Federation); Boris A. Kargin, Institute of Computational Mathematics and Mathematical Geophysics (Russian Federation) and Novosibirsk State Univ. (Russian Federation); Andrey A. Lisenko, V.E. Zuev Institute of Atmospheric Optics (Russian Federation) and National Research Tomsk State Univ. (Russian Federation)

The paper is devoted to comparing results of numerical statistical modeling of propagation and variation of polarization properties of a LIDAR returns from a ground-based sensing system in a cloudy atmosphere for various cloud models. The purpose of the calculations is researching the possibility of applying ground-based LIDARs in a broad wavelength spectrum to obtaining information about the structure of certain liquid-drop cloud microphysical parameters. As the presence of large drops in the medium exerts a considerable influence on absorption and scattering of radiation in the submillimeter spectrum, large drops of radius more than 20 μm are included in the model of drop size distribution. Water content in large drops is of the order of 0.1 g/m-3, may be

observed in marine as well as thick continental clouds of stratus form [1]. In the models, infrared and submillimeter radiation absorption by water vapor and the difference in vertical stratification of small drops of radius 1 - 20 μm [2] and large drops [3] are taken into account. Drop size distribution models from [4-6] are implemented. In the numerical models of the cloud layer the scattering and absorption coefficients as well as scattering matrices are calculated according to the Mie theory by W. Wiscombe's algorithm [7]. Modeling of radiation propagation is carried out by the Monte Carlo method using the local estimates method [8] on the ICM&MG calculation cluster [9].

The work was completed with financial support from the Program of fundamental research of the Board of RAS ? 43.

References

1. S. S. Yum and J.G. Hudson. Maritime/continental microphysical contrasts in stratus. – Tellus 2002, 54B, pp. 61–73.

2. Handbook of Cloud and Cloudy Atmosphere. Ed. by I.P. Mazin, A,Kh. Khrgian. – Gidrometeoizdat, 1989. p.648.

3. P. H. Daum, Y. Liu, R. L. McGraw, Y.-N. Lee, J. Wang, G. Senum, M. Miller, J. G. Hudson. Microphysical Properties Of Stratus/ Stratocumulus Clouds During The 2005 Marine Stratus/ Stratocumulus Experiment (MASE), 2007. Brookhaven National Laboratory.

4. G.M. Aivazyan. Propagation of millimeter and submillimeter waves in the clouds. - Gidrometeoizdat, 1991. p.480.

5. Wang, L., C. C. Li, Z. G. Yao, Z. L. Zhao, Z. G. Han, and Q. Wei. Application of aircraft observations over Beijing in cloud microphysical property retrievals from CloudSat. Adv. Atmos. Sci., 2014, 31(4), pp. 926–937, doi: 10.1007/s00376- 013-3156-2.

6. Miles N.L., Verlinde J., and Clothiaux E.E. Cloud Droplet Size Distributions in Low-Level Stratiform Clouds. // J. Atmos. Sci. 2000. V. 57, pp.295–311.

7. W. Wiscombe. Improved Mie Scattering Algorithms, Appl. Opt. 1980, 19 (9), pp. 1505-1509.

8. Marchuk G.I., et al. Monte Carlo methods in atmospheric optics // Springer-Verlag, New-York, Berlin, Heidelberg, 1980, p. 284.

9. http://www2.sscc.ru/

9640-17, Session 3

Analysis of heavy precipitation caused by the vortices in the lee of the Tibetan Plateau from TRMM (the Tropical Rainfall Measuring Mission) observations

Guoping Li, Lujun Jiang, Chengdu Univ. of Information Technology (China)

By using not only TRMM precipitation radar (TRMM PR) and microwave imager data, but also NCEP/NCAR reanalysis data, the paper compares and analyzes the two rainstorms caused by the southwest vortex (SWV) and eastwards Tibetan Plateau vortex (TPV) in Southwest China, respectively. It shows that the heavy rainfall systems of both two vortex rainstorms are consisted of a main rain band and several scattered precipitation clouds, with non-uniform distributed precipitation intensity. The horizontal scale of the main rain band and the intensive precipitation clouds of TPV rainstorm on 21st July, 2008 are larger than those of SWV on 17th July, 2007. The precipitation radar detects the stratiform precipitation which has large scale but weak intensity caused by the two kinds of precipitation. However, the convective precipitation contributes more to the total precipitation, with larger precipitation rate than the stratiform precipitation. The rainfall intensity spectrum of the convective precipitation is wider than that of the stratiform precipitation, which ranges from 1 to 50 mm/h. It also indicates that the height of the rain top increases along with the surface precipitation intensity in the two rainstorms. The highest height of the rain top reaches 16km. The SWV rainstorm is more intensive than TPV rainstorm, and the microwave brightness temperature varies inversely as the height of the rain top. The release of the precipitation latent heat, the increase of the raindrops and the change of the ice particles mainly occur below 8km. Moreover, mid- and low-level precipitation are the main source of the column precipitation. The convective precipitation and the stratiform precipitation caused by SWV release much more latent heat than those caused by TPV. This study used TRMM observations to describe two heavy rainfall cases associated with SWV and TPV, respectively. Comparisons of precipitation characteristics (e.g., precipitation intensity and type, rain top, etc.) for these two cases were the focus of this study. The results presented are generally interesting and may have a good potential to provide some useful implications of microphysical processes active within the convective systems induced by SWV and TPV.

9640-39, Session 3

Solar radiation environment study of near-space atmosphere in China area

Dongdong Fan, Aerospace DongFangHong Satellite Co., Ltd. (China); Xingfeng Chen, Zhengqiang Li, Institute of Remote Sensing and Digital Earth (China); Xiaodong Mei, Ocean Univ. of China (China)

With the development of aerospace technology, demands for aviation activities such as communications, remote sensing, and target surveillance in the near space increase rapidly. Studies on the high-altitude atmospheric environment, especially the hot environment, become key problem to guarantee normal aircraft flight performance and altitude resides. Near Space starts from the highest flight altitude of aircraft, and end at the minimum height of aircraft near-Earth orbit, usually refers to 20~100km altitude layer including stratosphere (11~55km), mesosphere (55~85km) and a small portion of thermosphere (85~800km). In this study we select the bottom layer (20~50km) of stratosphere.

The intensive solar radiation in near space, especially ultraviolet radiation (UV), affects some chemical and biological processes, which have potential hazard to aircraft material. Therefore, in this paper we studied the full band and ultraviolet solar radiation. Ozone has critical impacts on ultraviolet radiation, UV-B band (wavelength 280 ~ 315nm) is most affected by ozone, UV-A band (315 ~ 400nm) is also affected to some extent, UV-C band (200 ~ 280nm) is almost completely absorbed by stratospheric ozone and oxygen. Also intensive solar radiation and little heat convection make aircraft facing rather "too hot" or "too cold", so as to ensure long-time reliability, stability and control of aircraft, studies of radiation environment in near space is necessary. This basic research directly affects the aircraft's structural design, flight prediction and flight control. China's "High-Resolution Earth Observation System" major project deployed stratospheric airships, which environmental adaptability must be undertaken prior to engineering development. However, near space solar radiation lack of observation data because of its height restrictions, so selecting appropriate theoretical model to ensure that the output has certain reliability is necessary before carrying on the aircraft observation.

The near space (20~50km) in China area was divided into 5 regions except Tibet Plateau, because the NCEP-NCAR data are not reliable over there. According to underlying surface type, near space in China area is divided into over sea and over land two parts. According to climatic features of stratospheric air activities, denoting East Asian trough over Northeast region in winter, while prevailing westerly over other regions; in summer the southern region is under control of powerful South Asia High, pressure distribution helps divide mainland of China into 3 parts: North eastern, Central and Western regions. Considering latitudinal extent, China Sea is also divided to eastern South parts. SBDART (Santa Barbara DISORT Atmospheric Radiative Transfer) was used to modelling full-band solar radiation, ultraviolet radiation and also the ozone effect, to provide some guide for design and environmental adaptation of stratospheric aircraft.

Analysing the simulation results, we can conclude that the full-band solar radiation changes with latitude, season and the earth surface kind, and the ultraviolet radiation is affected

by ozone density spatial distribution in addition. We give the average and extreme values for the different regions. This research work supports the environmental suitability design of near space aircraft filling in research blanks, and it would be validated and reinforced by the future in-situ observations.

9640-19, Session 4

Characterization of optical properties, microphysical properties and vertical structure of aerosols using passive and active remote-sensing observations over the Mediterranean during the ChArMEx/ ADRIMED experiment *(Invited Paper)*

Marc Mallet, CNRS-Laboratoire d'Aérologie (France)

No Abstract Available

9640-20, Session 4

Estimation of aerosol direct radiative forcing in Lecce during the 2013 ADRIMED campaign

Rubén Barragan, Univ. Politècnica de Catalunya (Spain); Salvatore Romano, Univ. del Salento (Italy); Michaël Sicard, Univ. Politècnica de Catalunya (Spain); Pasquale Burlizzi, Maria-Rita Perrone, Univ. del Salento (Italy); Adolfo Comerón, Univ. Politècnica de Catalunya (Spain)

In the framework of the ChArMEx (Chemistry-Aerosol Mediterranean Experiment, http://charmex.lsce.ipsl.fr/) initiative, a field campaign took place in the western Mediterranean Basin between 10 June and 5 July 2013 within the ADRIMED (Aerosol Direct Radiative Impact on the regional climate in the MEDiterranean region) project. The scientific objectives of ADRIMED are the characterization of the typical "Mediterranean aerosol" and its direct radiative forcing (column closure and regional scale). This work is focused on the multi-intrusion Saharan dust transport period of moderate intensity that occurred over the western and central Mediterranean Basin during the period 14 – 27 June. The dust plumes were detected by the EARLINET/ACTRIS (European Aerosol Research Lidar Network / Aerosols, Clouds, and Trace gases Research InfraStructure Network, http://www.actris.net/) lidar stations of Barcelona (16 and 17 June) and Lecce (22 June). First, two well-known and robust radiative transfer models, parametrized by lidar profiles for the aerosol vertical distribution, are validated both in the shortwave and longwave spectral range 1) at the surface with downward and upward flux measurements from radiometers and 2) at the top of the atmosphere with upward flux measurements from the CERES (Clouds and the Earth's Radiant Energy System) radiometers on board the AQUA and TERRA satellites. The differences between models and their limitations are discussed. The instantaneous and clear-sky direct radiative forcing of mineral dust is then estimated using lidar data for parametrizing the particle vertical distribution at Barcelona and Lecce. The difference between the obtained forcings is discussed in regard to the mineralogy and vertical structure of the dust plume at both sites.

9640-21, Session 4

How well can we estimate areal-averaged spectral surface albedo from ground-based transmission in the Atlantic coastal area?

Evgueni I. Kassianov, Pacific Northwest National Lab. (United States); James Barnard, Univ. of Nevada, Reno (United States); Connor Flynn, Laura Riihimaki, Cristina Marinovici, Pacific Northwest National Lab. (United States)

The Department of Energy (DOE) Atmospheric Radiation Measurement (ARM) Mobile Facility (AMF) was deployed on Graciosa Island in the Azores, Portugal in June 2009 to provide continuous measurements of cloud, aerosol properties and precipitation. The multi-year (2009-2011) dataset collected by AMF includes spectral measurements of atmospheric transmission from the Multi-Filter Rotating Shadowband Radiometer (MFRSR) at five wavelengths (415, 500, 615, 675, and 870 nm). We apply the MFRSR-measured transmission and our recently developed approach (Kassianov et al., 2014) to retrieve the areal-averaged spectral surface albedo at five MFRSR wavelengths. We show examples of these MFRSR-based retrievals and discuss their reliability and potential accuracy using areal-averaged surface albedo from collocated and coincident Moderate Resolution Imaging Spectroradiometer (MODIS) observations.

Kassianov, E., J. Barnard, C. Flynn, L. Riihimaki, J. Michalsky, and G. Hodges, 2014: Areal-Averaged Spectral Surface Albedo from Ground-Based Transmission Data Alone: Toward an Operational Retrieval. Atmosphere, 5, 597-621.

9640-22, Session 4

Cloud radiative characteristic parameter calculation for space-based remote sensing sensors

Hongxia Wang, Xiaojian Xu, BeiHang Univ. (China)

Cloud coverage is not only a transmission factor but also a significant clutter source to space-based infrared remote sensing sensors through thermal emission as well as scattered solar radiation. In most existing works, cloud coverage was simply assumed to be a homogeneous medium with Lambertian cloud surface. However, real-world clouds are inhomogeneous. It is of great importance yet a big challenge to investigate the infrared radiative properties of inhomogeneous clouds.

In this paper, we focus on the studying of the thermal emission, reflection and transmission of solar radiation for inhomogeneous cloud coverage. Cloud particles are assumed to be spherical, and their size distribution follows a gamma function modified by Deirmendjian. Inhomogeneous cloud is divided into a number of parallel sub-layers along its height. These sub-layers are considered to be optically thin and uniform. In this way, the scattering characteristic parameters of cloud are first calculated using Mie scattering theory for follow-on radiative characteristic parameter calculation, including single-scattering albedo and phase function. The scattering calculation results are then used to calculate radiative characteristic parameters according to radiative transfer theory, including angular and spectral distribution functions of transmission and reflection for each layer. Both distribution function of transmission and reflection for a cloud of arbitrary thickness can be obtained recursively using the adding or doubling method, taking account of the multiple reflections of the light beam between layers.

To validate the proposed procedure, the scattering characteristic parameters, transmission and reflection spectral distribution functions within spectral band from 0.4?m to 14?m for stratocumulus cloud are calculated and compared with that of two-stream approximation method. Furthermore, the

variation of transmission and reflection with incident angle is calculated for given wavelength and outgoing angle.

9640-24, Session 4

The thermal infrared radiance properties of dust aerosol over ocean

Zengzhou Hao, Delu Pan, Qianguang Tu, Fang Gong, Jianyu Chen, The Second Institute of Oceanography, SOA (China)

Asian dust storms, which can long-range transport to ocean, often occur on spring. The present of Asian dust aerosols over ocean makes some difficult for other studies, such as cloud detection, and also take some advantage for ocean, such as take nutrition into the ocean by dry or wet deposition. Therefore, it is important to detect the dust and retrieve the properties of dust from satellite observations that is mainly from the thermal infrared radiance. The objective of this study is to analysis the thermal infrared radiation characteristics of Asian dust aerosols over ocean and to provide technical services for accurate monitoring dust aerosol region from satellite and retrieving the properties of dust aerosol. At first, Thermal infrared brightness temperature (BT) characteristics is firstly analyzed by combining some MODIS observations, which has 36 spectral channels including the 8.5 (Band29), 11 (Band31), 12?m (Band32) thermal infrared channels. And the Asian dust aerosol over ocean on 16th April, 2006 are selected as the general case for expressing its thermal infrared characteristics. It shows that the BT12 of Asian dust aerosol is always greater than BT11 and BT8.5, and BT8.5 is general greater than BT11, which exhibits some the different thermal infrared characteristics of other clouds. On the other hand, the thermal infrared brightness temperature (BT) characteristics under dust aerosol physical characteristics, such as optical thickness, particle effective radius, is also simulated and analyzed by Streamer model, which is a radiative transfer model based on plane-parallel theory, for reanalyzing the thermal infrared radiance properties of dust aerosol. At last, some theoretical explanation is done. The brightness temperature at 12?m for Asian dust aerosol is greatest due to that the dust aerosol particles extinction is stronger in 11?m than in 12?m and 8.5?m.

9640-25, Session 4

Modeling the adjacency effects in Earth observation data with different viewing geometry over mountainous area

Cheng Jiang, Hongyan He, Yunfei Bao, China Academy of Space Technology (China)

It is well known that the adjacency effects is a phenomenon of adding surrounding signals and atmospheric scattering signals at the sensor level, which can lead image blur. In addition to image blur, the effect contaminates the pixel spectrum when retrieving the surface reflectance from satellite imagery. As the resolution of earth observation sensors and the requirements of quantitative remote sensing increases, a precise modeling of the adjacency effects is necessary for the future remote sensing sensor. Atmospheric scattering, viewing geometry and reflectance contrast between a target pixel and its neighborhood are the significantly factors in the modeling. For an earth observation system, an increase in the off-nadir viewing angle leads to an increase in line of sight scattered radiance. Meanwhile, steep terrain over mountainous area induces changes in irradiance at ground level and then affects the top of atmosphere (TOA) signal.

In this paper, a methodology is presented to simulate and analyze the adjacency effects. In the second section of the paper, the radiative transfer equations are built separately for the nadir viewing geometry and the off-nadir viewing geometry over mountainous area. Furthermore, the topographic parameters and atmospheric parameters are introduced. The next section is devoted to the modeling the adjacency effects. The radiance items related to the adjacency effects are estimated. All the calculation methods depend on a physically-based model, in which atmospheric parameters are obtained by running MODTRAN4 for several times and topographic parameters are calculated based on DEM data and viewing geometry. During the procedure, the molecular/aerosol scattering phase functions, different viewing geometry, ground heterogeneity and topography are taken into account. The last section presents the validation experiments and results. Performance of this methodology is validated through simulating a set of space-borne data over mountainous areas for nadir viewing angles and off-nadir viewing angles. As expected, the results indicate that the contributions of adjacency effect at TOA are significantly different for the varying viewing geometry conditions. The proposed method proved to be useful in understanding the mechanisms of adjacency effects and it will be applied to atmospheric correction of remotely sensed data.

9640-26, Session 5

Mixing layer height measurements determines influence of meteorology on air pollutant concentrations in urban area

Klaus Schäfer, Thomas Blumenstock, Karlsruher Institut für Technologie (Germany); Boris Bonn, Institute for Advanced Sustainability Studies e.V. (Germany); Holger Gerwig, Umweltbundesamt (Germany); Frank Hase, Karlsruher Institut für Technologie (Germany); Christoph Münkel, Vaisala GmbH (Germany); Rainer Nothard, Senatsverwaltung für Stadtentwicklung und Umwelt (Germany); Erika von Schneidemesser, Institute for Advanced Sustainability Studies e.V. (Germany)

Mixing layer height (MLH) is a key parameter to determine the influence of meteorological parameters upon air pollutants such as trace gas species and particulate concentrations near the surface. Meteorology and MLH as a key parameter affect the budget of emission source strengths, deposition, and accumulation. However, greater possibilities for the application of MLH data have been identified in recent years. Here, the results of measurements in Berlin in 2014 are shown and discussed.

The concentrations of NO, NO2, O3, CO and about 70 volatile organic compounds (anthropogenic and biogenic of origin) as well as particle size distributions (PSD) were measured at the urban background station of the Berlin air quality network (BLUME) in Nansenstr./Framstr., Berlin-Neukölln. A Vaisala ceilometer CL51, which is a commercial mini-lidar system, was applied at that site to detect the layers of the lower atmosphere in real time. Special software for these ceilometers with MATLAB provided routine retrievals of MLH from vertical profiles of laser backscatter data.

Five portable Bruker EM27/SUN FTIR spectrometers were set up around Berlin to detect column averaged abundances of CO2 and CH4 by solar absorption spectrometry.

Correlation analyses were used to show the coupling of temporal variations of trace gas compounds and PSD with MLH. Significant influences of MLH upon NO2, PM2.5 and PM1 as well as PSD in the size modes 70 – 100 nm, 100 – 200 nm and 200 – 500 nm were found. A typical temporal shift of 6h between peak in traffic intensity at major roads close by and the urban background station was observed, which was related to the horizontal transport and vertical mixing characterized by the MLH.

Further, MLH was taken as important auxiliary information about the development of the boundary layer during each day of observations, which was required for the proper estimation of CO2 and CH4 source strengths from Berlin on the basis of atmospheric column density measurements.

9640-27, Session 5

Open-path quantum cascade laser-based system for simultaneous remote sensing of methane, nitrous oxide, and water vapor using chirped-pulse differential optical absorption spectroscopy

Fred Moshary, NOAA-CREST (United States); Paulo C. Castillo, Broohkaven National Lab. (United States); Adrian Diaz Fortich, NOAA-CREST (United States); Abdou S. Diba, The City College of New York (United States); Benjamin P. Thomas, NOAA-CREST (United States); Barry M. Gross, NOAA-CREST (United States) and The City College of New York (United States)

The advent of quantum cascade lasers have made mid-infrared trace gas sensing with differential optical absorption spectroscopy using compact and economical systems feasible. We report on a filed deployable open-path quantum cascade laser (QCL) based system for simultaneous remote detection of ambient methane, nitrous oxide, and water vapor gases with accuracies less than 1% at a path length of 250 meter using a retroreflector to fold the transmitter beam back into the receiver. The system is based on an 20 cm Newtonian telescope receiver with a TE cooled MCT detector, and a long pulse (280 nsec) TE cooled DFB QCL transmitter, which exhibits thermal intra-pulse chirp of the order of 2 cm-1 in the wavelength range of 7.7 microns. By temporally resolving the thermal chip of the laser with a Ge fabry-perot etalon, the time window can be converted to a frequency window. This pulse can be used to measure absorption signatures of atmospheric trace gases within the spectral window, which includes methane, nitrous oxide and water vapor. In this way, each pulse measures the entire absorption spectrum within the 2cm-1 window. The laser operates at 20 kHz repetition rate, which is the averaging rate for the experiment. The absorption spectrum can be then be fit via a multivariate least square technique to HITRAN data base of gas spectra for the target species, to obtain the concentration of each species. We have demonstrated that while the intensity can fluctuate, the TE cooled QCL chirp spectrum is extremely stable under varying environmental conditions and for long periods of time. We present result from unsupervised 32 hr ambient measurement of the target trace gases in New York City along a 250 meter path, and compare the result with a near-by methane sampler and nitrous oxide spectra obtained from an open-path FTIR system. We show that desired ambient measurement accuracies can be obtained within 10 msec. We also demonstrate that the system can operate in a true monostatic configuration using topographic backscatter at ranger approaching 45 meters. In this configuration, the system is well suited for applications in remote detection of fugitive gas emissions/leaks. Finally, we show that if the DFB QCL is replaced by a distributed brag reflector (DBR) QCL, the chirp pulse technique can be applied to a much broader spectral window using the electronic tuning properties of the laser, we demonstrate this at 4.5 micron range for ambient nitrous oxide measurements.

9640-28, Session 5

Impacts of surface albedo models on high-resolution AOD retrieval

Barry M. Gross, NOAA-CREST (United States)

In previous work, we have performed significant preliminary studies focused on the accuracy of the 10km MODIS aerosol retrievals over urban areas. In particular, we illustrated that there is a notable over-bias in NYC and Mexico City due to the under-estimation of surface albedo by the Collection 5.1 MODIS Operational 10km AOD product. In general, the underestimation of the surface albedo was due to the use of training data which focused globally on vegetation/soils and do not model urban/suburban domains very well. By using simultaneous AERONET / MODIS observations for fine mode dominated aerosols, we were able to estimate regional surface models and appropriate spectral albedo ratios.We found that if we modify the surface spectral ratio assumptions used in the operational model to those derived as above, a large part of the bias is removed.

In this presentation, we will present more recent studies with MODIS Collection 6. This product has been refined to some extent and produces an AOD product was produced 3km resolution. However, while this change may not be critical over dark surfaces such as forests, urban/suburban regions have the same bias issues as noted earlier. In this presentation, we show that the bias observed for the C005 10km product is even more enhanced for the 3km C006 MODIS product. This matchup was part of the intensive Dragon Network field campaign where > 40 AERONET Cimel sky-radiometers were deployed in the Maryland/DC area for 6 weeks in summer 2012. The use of simultaneous AERONET / MODIS observations allowed us to probe the surface reflection characteristics of the region and match them against MODIS derived land classes. In fact, we demonstrate that the surface albedos for different land classes and especially urban surfaces have very different surface spectral ratios that are not captured by the C006 algorithm. When these differences are taken into account, we show that bias is reduced by more than 50% and dispersion is slightly improved. Efforts to generalize this to a global scale using over 20 distributed aerosol sites with variable surface land class properties will be presented as well as preliminary results regarding VIIRS environmental data record AOD as well as the single pixel intermediate product retrieval performance and biases.

9640-29, Session 5

Inclusion of high resolution MODIS maps on a 3D tropospheric water vapor GPS tomography model

Pedro J. Benevides, João Catalão Fernandes, Univ. de Lisboa (Portugal); Giovanni Nico, Consiglio Nazionale delle Ricerche (Italy); Pedro M. A. Miranda, Univ. de Lisboa (Portugal)

The observation of the water vapour distribution on the troposphere remains a challenge and it poses difficulties on the weather forecast, particularly for the near real time models which are very dependent on the rapid water vapour variations. Better knowledge of the 3D water vapour state and its variability is therefore desirable. At the present, radiosondes provide precise water vapour profiles of the troposphere, but lack geographical coverage and generally are performed only a few launches per day, while satellite meteorological maps have good spatial resolution but even poorer temporal resolution (1 to 2 maps per day at best). GPS has proved its capacity to measure the integrated water vapour profile at a single station, in all weather conditions with high temporal sampling frequency and with a spatial resolution depending on the density of the GNSS network of stations. However these measurements lack a vertical discretization of the water vapour quantity along the profile. Reconstruction of the slant path GPS observation in the satellite line of view allows water vapour measurements in those oblique directions. Implementation of a 3D grid of voxels along the troposphere over an area where a dense GNSS network of stations is available enables the ray tracing of slant water vapour observations within that region, defining the GPS tomography technique. Each GPS slant observation is parametrized as an equation and collected during a short temporal interval, forming a system that is resolved by an inverse problem formulation, resulting in a water vapour solution for the defined tomographic model. Due to the GPS non optimal geometry, the lower levels are less traversed by observations leading to sparser distributions of the water vapour. This causes an ill-posed problem to the system inversion that usually can only be overcome with the inclusion of constraints to the system of equations.

Combination of high resolution precipitable water vapour (PWV) maps obtained for the Moderate Resolution Imaging Spectroradiometer (MODIS) satellite data with a GPS tomography model is performed in this work. The MODIS

PWV acquisitions have a pixel dimension of 1 or 5 km (near infrared and infrared products) covering a wide area (hundreds of kilometres) and can be obtained 2 times per day at most. In addition to the advantage of merging integrated water vapour measurements obtained from independent techniques, the inclusion of MODIS higher spatial resolution PWV maps provides an enhanced horizontal resolution for the tomographic solution and benefits the stability of the inversion problem, resulting in a better tropospheric water vapour representation.

A 3D tomographic grid was adjusted over an area of 60x60 km2 covering the Lisbon city, Portugal, and its surrounding area, where a GNSS network of 9 receivers is available. Each grid voxel has an 11 km2 horizontal size and a variable vertical dimension starting from 500 m up to 10 km. Radiosonde measurements within the model area were used to compare the 3D water vapour solution maps obtained from the inclusion of the PWV MODIS on the GPS tomography.

9640-30, Session 5

Intercomparison between MODIS 3km aerosol optical depth product and ground PM10 measurements over Athens-Greece

Adrianos Retalis, Dimitris Paronis, Dimitris Katsanos, National Observatory of Athens (Greece)

Satellite imagery has been considered as an add-on tool to air quality and pollution monitoring due to its extensive spatial and temporal coverage of the Earth's surface and atmosphere. The most widely used satellite parameter is the Aerosol Optical Depth (AOD), which is a measure of the extinction of electromagnetic radiation at a given wavelength due to the presence of aerosols in the atmospheric column. AOD has been extensively used to evaluate and enhance the satellite-based estimates of ground-level particulate matter (PM) as well as to reduce uncertainties in the studies of global health applications. The uncertainties in the estimation of PM levels from satellite AOD fields are due to time and spatial-varying parameters. The time-varying errors introduced by the variability in the vertical profile of the aerosol layer, the optical characteristics of particles, the vertical structure of the atmosphere and wind speed are related with the frequency of observations (e.g. hourly, daily, monthly measurements). Spatially varying effects such as differences between measurements errors in different ground stations, spatial changes in the type of particles, are directly linked to the extent of the area considered and the spatial resolution of the satellite measurements.

This study attempts to identify correlations between AOD values retrieved from the new MODIS/Aqua high resolution 3Km aerosol product and ground-based PM10 measurements obtained within a period of 10 years (2002-2012) in the area of Athens, Greece. In parallel, it attempts to assess the applicability of the so called mixed effects models (Lee et al., 2011; Yap and Hashim 2013) which take into account both the spatial and temporal variability of the underlying uncertainties in the estimation of PM10 levels from MODIS AOD measurements. The ground PM10 recordings were acquired from the archive of the in-situ operational air quality monitoring network of Athens. The PM10 measurements were collected from different types of sites such as urban/traffic, urban, rural/industrial and rural/background. Other meteorological parameters (e.g. wind speed and direction, vertical structure of the atmosphere) have been incorporated in the statistical analysis to further constrain the statistical models examined. In parallel, similar statistical analysis based on AERONET AOD values retrieved from the archive of the AERONET station in Athens were applied.

Correlation coefficients (R2) for the collocated AOD-PM10 data pairs and between the estimated versus measured PM10 values are to be presented for each ground station. Inter-comparison results will also be presented for various time-aggregation schemes (i.e. instantaneous values for the satellite overpass, daily averages, weekly and monthly averages). The paper, finally, will also attempt to conclude on recommendations regarding limitation and advantages of the use of the new released MODIS AOD product (3km) for the study area.

9640-31, Session 5

Remote sensing for studying atmospheric aerosols in Malaysia

Kasturi D. Kanniah, Hui Qi Lim, Nurul Amalin Fatihah Kamarul Zaman, Univ. Teknologi Malaysia (Malaysia)

The complex aerosol system of Southeast Asia (SEA) due to heterogeneity in land surface, meteorology and hydrology has made SEA as one of the most vulnerable regions to climate change. Poor air quality of this region is mainly contributed by sources from automobiles emissions, industrial activities, and trans-boundary pollutants as a consequent of biomass burning in Indonesia. Thus, observation, analysis and prediction of the atmospheric aerosols over this region are crucial for emergency management. Nevertheless, only a few studies have been carried out especially at large spatial extent and on a continuous basis to study atmospheric aerosols in Malaysia. Therefore, in this study we (i) review the use of remote sensing data to study atmospheric aerosols in Malaysia; and (ii) document gaps in aerosol research and recommend further studies to bridge the gaps. Satellite data notably AVHRR, MODIS and MERIS have been used to some extend to study the spatial and seasonal patterns of aerosol optical depth (AOD) in Malaysia. Satellite data combined with AERONET data were used to delineate different types and sizes of aerosols in different seasons and to identify the sources of aerosols in Peninsular Malaysia. Most of the aerosol studies performed in Malaysia was based on station-based PM10 data that have limited spatial coverage. Thus, satellite data have been used to extrapolate and retrieve PM data over large areas in a continuous manner. In the PM 10 estimation, remotely sensed AOD is correlated with ground-based PM 10. In some studies meteorological parameters that affect aerosol properties including surface temperature, relative humidity, and atmospheric stability were included in PM estimation. Realising the critical role of aerosols on radiative forcing numerous studies has been conducted worldwide to assess and quantify the aerosol radiative forcing (ARF). Such studies are yet to be conducted in Malaysia. The relationship between atmospheric pollutants and meteorological variables had been investigated in Malaysia and the result showed that the particulate matter concentration was positively correlated with ambient temperature but negatively correlated with humidity. One recent study found aerosols were to attenuate the total incoming solar radiation by 0.8% for a 0.1 increase in AOD. The aerosol studies in Malaysia are based on ground-based PM10 measurements, AERONET aerosol measurements and satellite remotely sensed observations. Ground-based PM10 data are found insufficient with only 73 stations measuring data nationwide and not well representative as most of the monitoring stations are located in urban, industrial and residential areas but less in rural areas. Currently there are only 3 AERONET stations operating in Malaysia to provide various aerosol data. So, only source of aerosol data covering large area is remote sensing but, satellite observations are having limitations such as cloud cover, orbital gaps of satellite track, etc. In addition, the studies on aerosol climatology are also limited. Remote sensing based aerosol data at high spatial resolution for urban studies are also not available for this region. Relatively less understanding were achieved on how the atmospheric aerosol interacts with the regional climate system at various temporal and spatial scales. These gaps can be bridged by conducting more studies associated with atmospheric aerosols using integrated approach of remote sensing, AERONET and ground based measurements.

9640-32, Session 5

Satellite and ground based seasonal variability of NO2 and SO2 over New Delhi, India

Alok K. Pandey, Ram P. Kumar, Jawaharlal Nehru Univ. (India); Krishan Kumar, Jawaharlal Nehru University (India)

Remote sensing technology application is emerged as a useful tool for exploring atmospheric pollution revelation in

the last two decade. In this study, we used Aura satellite Ozone Monitoring Instrument (OMI) tropospheric NO2 and pbl SO2 retrieval data (October 2004 – September 2013) to generate a composite spatial map of different seasons over New Delhi National Capital Region (NCR). For surface measurements we used Central Pollution Control Board (CPCB) NO2 and SO2 data (January 2005 – December 2013). Further we compared the satellite retrievals data to the surface measurements. A higher NO2 concentration in both OMI and CPCB stations measurements are obtained in winter season followed by summer and minimum in monsoon months. OMI SO2 concentration is higher in monsoon months and almost comparable in summer and winter seasons. We obtained a statistically significant correlation between OMI tropospheric NO2 and CPCB surface measurements.

9640-33, Session 5

Retrieval of aerosol optical depth from an airborne cross-track polarimeter in north China

Zhengqiang Li, Lili Qie, Institute of Remote Sensing and Digital Earth (China); Xiaobing Sun, Bin Sun, Anhui Institute of Optics and Fine Mechanics (China)

One of the most important advantages of polarimetric observations for retrieving aerosol properties is that the polarized surface reflectance is usually small and less spectrally dependent. The polarization measurements at near-infrared or short-wave infrared bands, where the atmospheric contribution is small or negligible, corrected for atmospheric effect can be used to derive the surface polarized reflectance at shorter bands. Then, the shorter bands can be used to estimate the aerosol loading and microphysical properties.

In this study, we present an aerosol optical depth (AOD) retrieval algorithm based on single-angular polarimetric measurements, which is obtained from cross-track scanning image of an airborne polarimeter flights over north China. Firstly, the surface polarized reflectance was studied to validate its spectral neutrality. The airborne polarized measurements at 670, 865 and 1640nm were corrected for molecular and aerosol scattering, based on AOD and microphysical model derived from the simultaneous ground-based Sun/Sky-radiometer measurements. They shows highly linear correlation with correlation coefficients larger than 0.91. The slope values (1.03 and 0.985) indicate that the average spectral variation of the surface polarized reflectance is not larger than ±3%.

A retrieval algorithm based on look-up table (LUT) approach is developed to obtain AOD over land, in which the 1640 nm observation is employed to estimate the surface polarized reflectance and the 670 and 865 nm bands measurements are used to derive the aerosol parameters. Six pre-defined aerosol models, which are clustered based on the Aerosol Robotic Network (AERONET) global aerosols observations (Omar et al., 2005), are employed to construct the LUT. An iteration procedure is then performed over all combinations of aerosol models and AODs, to search for the AOD that minimizes the least squares fitting residual between the measured and calculated polarized atmospheric reflectance. The retrieval results provide an optimization of the AOD and the atmospheric-corrected 1640 nm polarized surface reflectance simultaneously.

Several field experiments were conducted in north China from 2012 to 2014 to validate the AOD retrieval algorithm. Airborne cross-track polarimetric observations are acquired while the synchronously ground-based Sun/sky-radiometer measurements are collected including spectral AOD, aerosol complex refractive index and particle size distribution. The polarimeter retrieval algorithm is tested both for the relatively dirty condition and the clear condition, and the retrieved AOD agrees with the Sun/sky-radiometer measurements well. By ignoring AOD spatial changes between the flight track and the ground-based site, the results illustrates that the cross-track polarimetric measurements can retrieves AOD over land with an average uncertainty less than about 0.05 at 865 nm.

Further observations and investigations over various surface types (such as soil and urban) and highly polluted conditions (e.g. larger AOD), are expected to be performed soon to explore the robust of the aerosol retrieval using cross-track flights with the advantage of polarimetric scanning imagery.

9640-34, Session 5

Determination of nocturnal aerosol properties from a combination of lunar photometer and lidar observations

Donghui Li, Zhengqiang Li, Yang Lv, Ying Zhang, Kaitao Li, Hua Xu, Institute of Remote Sensing and Digital Earth (China)

Aerosol plays a key role in the assessment of global climate change and environmental health, while observation is one of important way to deepen the understanding of aerosol properties. Ground-based measurement is one of the most effective means to get aerosol properties, especially after the emergency of Aerosol Robotic Network(AERONET, Holben et al.,1998) measurement by sunphotometer in the day time. However, the lack of night aerosol observations introduces some uncertainties in the columnar aerosol properties estimations. For example, lidar measurements need aerosol optical depth(AOD) at night for constrain of lidar equation to retrieve aerosol concentration profile. What's more, some haze outbreaks occurred during night, which need to detect and investigate.

Recently, a newly lunar photometer was produced by CIMEL cooptation, France (namely CE318-U), designed to automatic track the moon and to perform lunar measurements which lead to get aerosol properties during possible(Barreto et al., 2013; Berkoff et al.,2011). This research is performed to retrieve nocturnal aerosol properties from a combination of lunar photometer and lidar observations. Firstly we applied Beer-Lambert-Bouguer law to get nocturnal column aerosol optical depth (AOD, ?) from lunar irradiance, which is calculated from the USGS ROLO lunar disk-equivalent reflectances(Kieffer and Stone,2005; Berkoff et al.,2011) and performed modified Langley calibration in clean and stable condition. The AOD algorithm is test and verified with sun photometer both in high and low aerosol loading, with the given precision 0.02 or 0.05AOD. Ångström exponent (?) and fine/coarse mode AOD (?f, ?c) (O'Neil, et al., 2003) is derived from spectral AOD. The column aerosol properties (?, ?, ?f, ?c) inferred from the lunar photometer is analyzed based on two month measurement in Beijing from various aerosol loadings.

Micro-pulse lidar has advantages in retrieval of aerosol vertical distribution, especially in night. However, the typical solution of lidar equation needs lidar ratio(ratio of aerosol backscatter and extinction coefficient) assumed in advance(Fernald et al., 1984), or constrained by AOD(Mortier et al.,2012). Yet lidar ratio is varied with aerosol type and not easy to fixed, and AOD is used of daylight measurement, which is not authentic when aerosol loading is different from day and night. In this paper, the nocturnal AOD measurement from lunar photometer combined with mie scattering lidar observations to inverse aerosol extinction coefficient(?) profile in Beijing is discussed and the accuracy is estimated.

In the conclusion, it will be provided more accurate nocturnal aerosol properties by combination of lunar photometer and

lidar measurements. For long-term night measurement, it's helpful to find phenomenon and reason of aerosol properties during night. Collocated with lidar observations, there is possibility to develop cloud screen algorithm to remove cloud-contaminated data.

9640-35, Session 5

Estimation of air pollution in Ulaanbaatar city, Mongolia using the satellite data

Bilguunmaa Myagmardulam, Mongolian Univ. of Science and Technology (Mongolia)

The air quality indicator approximated by satellite measurements is known as an atmospheric particulate loading, which is evaluated in terms of the columnar optical thickness of aerosol scattering. This paper is attempting and estimating PM10 concentration by using Landsat 5 satellite data and field sampling analyze results validating these with air pollution measurements in Ulaanbaatar, Mongolia. We have been used the empirical method which based on multispectral algorithm PM10 model and analyze result of interpolation in air pollution distribution map. After that, the relationship between estimation results and PM10 was analyzed. Different scenarios are used to evaluate the precision of result, and good consistency is found between the results and the ground monitoring data.

9641-1, Session 1

Overview of remote sensing activities at the Institute of Maritime Technology, South Africa *(Invited Paper)*

Willem H Gunter, IMT (South Africa)

The presentation is an overview of remote sensing activities at the Institute of Maritime Technology (Simon's Town, South Africa) conducted in the field of electro-optic in the last about 10 years. The presentation will contain a short overview of the institute followed by a brief discussion of remote sensing activities for the following purposes; infrared signature characterization (extended and point targets, grey-body and spectral emitters, ship wakes), persistent surveillance (harbours, on ships, panoramic systems), atmospheric and maritime environment characterization (sea surface temperature, atmospheric MTF, turbulence) and laser imaging/communications. This will be followed by a brief discussion of joint international trials conducted at the institute (in False Bay, South Africa) over the last 10 years. This includes a small targets trail (TNO- IMT- CSIR), the False Bay Atmospheric Experiment (FATMOSE, TNO-IMT) and the First European South African Transmission Experiment (FESTER, IOSB-TNO-IMT), which is currently underway. The small surface target trail focussed on the electro-optic signature characterization of small surface targets (including wakes) and sea, land and sky backgrounds. FATMOSE focussed mainly on characterization of atmospheric effects that influence electro-optic sensor performance, while FESTER will extend on above research efforts to also include the radio frequency spectrum (RF) and a significant oceanographic characterization effort in support of FESTER above water activities. The presentation will be concluded with a short discussion on the factors which make the False Bay location interesting for remote sensing electro-optic experiments and the interesting results that are expected from the FESTER experiment.

9641-2, Session 1

Estimation of the refraction index structure parameter Cn2 via image analysis of a point source

Leif Humbert, Ivo Buske, Deutsches Zentrum für Luft- und Raumfahrt e.V. (Germany)

In order to quantitatively determine the strength of atmospheric turbulence mostly scintillometers are used to evaluate the refraction index structure parameter Cn2 by probing a medium using a laser beam. The effect of the same atmospheric turbulence can also be seen when imaging an arbitrary object along the same line of sight. Within the regime of a Kolmogorov spectrum, e.g. weak fluctuations of the turbulence, simple expressions are valid to estimate the refraction index structure parameter Cn2 for plane and spherical waves.

Here we propose a method to determine an estimate for the refraction index structure parameter Cn2 when imaging an arbitrary scenario in weak turbulence. As long as an object in this scenario appears like for example a point source, it can be used to estimate the strength of the turbulence. At our test site we verify this method by imaging light of a far distant LED onto a standard CCD camera. Regarding the determination of the beam jitter and power fluctuation we analyze each frame by fitting a 2D-Gaussian distribution onto the column density and calculating the first and second order moments. From both methods we derive a value for refraction index structure parameter Cn2 and compare our results with an already operating scintillometer at our test site.

In general this method allows monitoring multiple point sources at the same time in order to measure a spatial profile of the refraction index structure parameter Cn2. Furthermore the estimation of the strength of the optical turbulence allows assessing the performance of an optical system for example developed for tracking objects over long distances.

9641-3, Session 1

Shortwave infrared for night vision applications: illumination levels and sensor performance

Uwe Adomeit, Jürgen Krieg, Fraunhofer-Institut für Optronik, Systemtechnik und Bildauswertung (Germany)

"Nightglow" is the name of an illumination phenomenon created by stimulation and recombination/deactivation of atoms and molecules in the higher earth atmosphere. It covers the spectral range from the ultraviolet up to the thermal infrared, with a maximum in the shortwave infrared (SWIR). For moonless nights, illumination in the SWIR exceeds the one in the visible spectral range by an order of magnitude. This makes nightglow an ideal candidate to be used for night vision applications. Although known for decades, with none of the SWIR sensor technologies available sensitive enough for this application, the nightglow was limited to be a disturbance in astronomic applications. Within the last years this changed. The SWIR sensor technology, especially the one based on InGaAs, improved and is nowadays at the threshold to practical night vision application. This necessitates understanding of the highly variable illumination levels created by the nightglow and the performance assessment of the SWIR detectors in comparison to the image intensifiers respectively Si focal plane array detectors.

IOSB started in 2013 to measure and compare visual and SWIR sensor performance. As figure of merit signal-to-noise ratio measured in dependence of illumination was selected. Whereas the night illumination levels for the visual are standardized with full moon / quarter moon / starlight / overcast illuminance values, corresponding levels for the SWIR are missing. Thus a parallel program began characterizing night illumination levels in both spectral ranges. This characterization is based on continuous illuminance and radiance measurements as well as recording imagery of reflectance reference targets with visual and SWIR cameras. One field trial in the Austrian Alps near Greifenburg proved extremely interesting. At three consecutive nights around new moon partially overcast conditions were found. Whereas the visual illumination behavior was roughly similar for all three nights, the SWIR levels were drastically different. They varied from night to night but also during one night. To date the number of IOSBs illumination measurements are not yet statistically sufficient to define the needed illumination levels, but at least allowed a first comparison of visual and SWIR detector technologies. With comparable F-number, integration time and frame rate for visual and SWIR systems presupposed, the characterized SWIR sensors performance were found to be inferior to the available visual technologies for good illumination conditions. This inferiority intensifies for adverse weather, with even the best of the characterized SWIR sensors unsuitable for such conditions.

Although currently the use of SWIR sensors at night seems to be no real alternative to visual based technologies like image intensifiers, it is highly probable that it becomes so in the near future. This makes it necessary to define corresponding SWIR and visual illumination levels for sensor performance assessment and modelling but also operation planning. As such definitions are only possible based on statistically confirmed data, long time observations are inevitable, with the most challenging part in finding areas undisturbed by urban lighting in Europe.

9641-4, Session 1

Ultimate turbulence experiment: simultaneous measurements of Cn2 near the ground using six devices and eight methods

Lydia I. Yatcheva, Rui Almeida de Sa Barros, Max Segel, Detlev Sprung, Erik Sucher, Christian Eisele, Szymon Gladysz, Fraunhofer-Institut für Optronik, Systemtechnik und Bildauswertung (Germany)

We have performed a series of experiments in order to simultaneously validate several devices and methods for measurement of the path-averaged refractive index structure constant (Cn2). The experiments were carried out along a horizontal path near the ground. Measuring turbulence in this layer is particularly important because of the prospect of using adaptive optics for free-space optical communications in an urban environment.

On one hand, several commercial sensors were used: SLS20, a laser scintillometer from Scintec AG; BLS900, a large-aperture scintillometer, also by Scintec AG, and a 3D sonic anemometer from Thies GmbH. On the other hand, we measured turbulence strength with new approaches and devices developed in-house. Firstly, an LED array combined with a high-speed camera allowed for measurement of Cn2 from raw- and differential image motion, and secondly a two-part system comprising a laser source, a Shack-Hartmann sensor and a PSF camera which enabled recording of turbulent modulation transfer functions, Zernike variances and angle-of-arrival structure functions, yielding three independent estimates of Cn2.

We compare the measured values yielded simultaneously by the commercial and the in-house developed devices and show very good agreement between Cn2 values for all the methods. Limitations of each experimental method are also discussed.

9641-5, Session 2

Influence of aerosols on atmospheric transmission at the Baltic Sea: comparison of experimental results with model simulations using MODTRAN

Silke Vogelbacher, Detlev Sprung, Fraunhofer-Institut für Optronik, Systemtechnik und Bildauswertung (Germany); Alexander M.J. Van Eijk, TNO (Netherlands); Karin Stein, Fraunhofer-Institut für Optronik, Systemtechnik und Bildauswertung (Germany)

Atmospheric transmission depending on wave length attaches great importance to its limitation of military electro-optical systems. In a field trial in the littoral area of the Baltic Sea at Northern Germany measurements of visibility, meteorological parameters, aerosol size distribution and optical turbulence were performed in October 2014 at a height of 3 m above the Baltic Sea. The results of the field trial were used to determine the transmission. The experimental results are compared to calculation using the MODTRAN (moderate resolution atmospheric transmission) model. The various offered aerosol models are applied for the propagation along a horizontal path of 1400 m. The differences of the use of the model assumptions are compared and discussed. The influence of the aerosol distribution and assumed composition is analyzed.

9641-6, Session 2

The shower curtain effect paradoxes

Gregoire Tremblay, AEREX avionique inc. (Canada); Robert Bernier, Les Instruments Optiques du St-Laurent Inc. (Canada); Gilles Roy, Defence Research and Development Canada, Valcartier (Canada)

It is generally admitted that the relative location of an aerosol between an observation device and the observed scene will have an influence on the detected image quality. These effects are usually classified under the label “shower curtain effect”. The name comes from an everyday life observation: someone standing away from a shower curtain can detect the presence of a person standing behind it; at the same time, the person hidden by the curtain cannot see this observer. In this situation, the light transmitted by the curtain is expected to be exclusively made of scattered radiation. The curtain also acts as a frequency low pass filter removing high frequencies from the observed scene by convoluting it to its transmission distribution function. The curtain is expected to be illuminated on both sides by an extended passive source (like broad day light or artificial illumination). Both observers are also illuminated by the same source. Extrapolating from this scheme, the quality of images produced when an aerosol is located close to a receiver should be lower than cases where the aerosol is close to the target. Doing such measurement using an active system, we found a paradoxical result where the image contrast was five times better when the aerosol was near the observer. To explain this apparent paradox, we first explored the measurement parameters to evaluate their impact. A passive illuminated scene differs considerable from a scene illuminated by a gated active imager. Previous experiments on the shower curtain effect were performed in the dark, using a source propagating through a turbid media and a camera to capture a none-gated signal. We evaluated the impact of this configuration change. The shower curtain effect for aerosol was first derived from the small angle approximation. We show the impact of an actual measurement made outside the SAA limited range of application. An actual shower curtain is expected to scatter all the light. This is not the case through an aerosol where an important proportion of the signal is expected to go through unscattered. Finally, we show the impact of the aerosol phase function on the results. In the end, the location of the aerosol in the system is only one of multiple elements to consider before inferring the relative quality of images: the scene illumination, the scatterer phase function, the receiver cut on and cut off frequencies play major roles in the image quality. The amount of scattered and unscattered light reaching the receiver is also critical. In the end, the apparent paradoxical results we found cannot be placed under the “shower curtain effect” denomination because: 1- the amount of unscattered light captured is higher than the amount of scattered light, and 2-) the receiver cut on frequency is much higher than the aerosol cut off frequency rendering most mechanisms of the shower curtain effect ineffective.

9641-7, Session 2

Polarimetric active imaging in dense fog

Robert Bernier, Les Instruments Optiques du St-Laurent Inc. (Canada); Xiaoying Cao, Lidar (Canada); Gregoire Tremblay, AEREX avionique inc. (Canada); Gilles Roy, Defence Research and Development Canada, Valcartier (Canada)

Operation under degraded visual environment (DVE) presents important strategic advantages. 3D mapping and active imaging have been performed under DVE. In these applications, the presence of fog clouds degrades the quality of the remotely sensed signal. In view of making the active imaging method more robust against dense fog, the use of polarimetry is herein studied.

Spherical particles do not depolarize incident polarized light in the backscattering (180o) direction. However strong depolarization occurs off 180o. The greater the ratio of size to wavelength, the closer to 180o will the depolarization occur. When the cloud optical depth is small, the major scattering event seen by an active camera is the backscattering event. However, when the optical depth of the cloud is higher than 1, multiple scattering becomes important and causes depolarization due to the backscattering off 180o. An increased in dazzling caused by dense aerosols is expected for active

imaging systems. The dazzling should be less important for systems operating using the secondary polarization because there is no contribution coming from single backscattering; higher image contrasts should result. The physics of this process will be discussed and experimental results supporting the analysis will be presented.

We present Monte Carlo (MC) simulations and experimental results obtained under controlled environment using DRDC Valcartier aerosol chamber. Analyses of image contrast were performed on both polarimetric and non-polarimetric lidar imaging systems. The targets were white-black or white-grey bar type targets of different spatial frequencies, observed through clouds (water or fog oil) of different optical depths. Comparison of experimental results with MC simulations showed that the image contrasts from the tests are close to those predicted by MC simulations.

The experimental method herein proposed is based upon the use of ICCD range gated cameras wherein gate width and gate location may be varied on the fly. The optimal conditions for the use of these devices in view of obtaining the best image contrast are experimentally studied and reported in this paper. Removing the effect of the background signal from the image is shown to be of utmost importance. The use of a narrow gate width in view of collecting ballistic photons only is also demonstrated to be of great strategic value. The location of the gate (front vs tail gating) is discussed from a theoretical standpoint and the conclusions reinforcing the choice of a front gating strategy are supported by experimental results.

9641-24, Session 2

Effect of geometrical focusing on femtosecond laser filamentation at high altitude

Haitao Wang, Chunhong Qiao, Honghua Huang, Chengyu Fan, Anhui Institute of Optics and Fine Mechanics (China)

The influence of geometrical focusing on the filamentation of femtosecond laser pulse under various low pressure (< 1 atm) corresponding to altitudes up to 10 km in air has been numerically demonstrated. The main peculiarities, such as filamentation dynamic, spatial-temporal evolution and super-continuum generation manipulated by external geometrical focusing in low atmospheric pressure regime, are analyzed by numerically solving a spatial-temporal equation for femtosecond laser pulse propagation in air. The results show that those important characteristics are more sensitive to the focal length rather than the variation of atmospheric pressure. By suitably design the optimum focal length, the compressed pulse should become further amplitude uniformity and the temporal aberration should be avoided at a certain extent, enabling the realization of delivering high energy laser pulse to kilometric high altitudes along a vertical axis in air.

9641-9, Session 3

Prediction of optical communication link availability: real-time observation of cloud patterns using a ground-based thermal infrared camera

Clément Bertin, IRT A. de Saint Exupéry (France) and Reuniwatt (France); Sylvain Cros, Reuniwatt (France); Laurent Saint-Antonin, IRT A. de Saint Exupéry (France); Nicolas Schmutz, Reuniwatt (France)

The growing demand for high-speed broadband communications with low orbital or geostationary satellites is a major challenge. Optical link at 1.55 μm are an advantageous solution avoiding complex Radio Frequency coordination.

Nevertheless, cloud cover is an obstacle for this optical frequency. Optically thick clouds passing through the links immediately break the communication between the satellite and the optical ground station (OGS). Laser links can also be scattered by thin cirrus which then decrease the quality of the optical communication. On the one hand, optical communications must be managed by developing an optimized distributed OGS network taking into account cloud presence occurrence over a continent. On the other hand, a coming cloud should be identified about 30 min. before it blocks the optical link. Then, another OGS under clear sky conditions can ensure the communication continuity. The optical link must be available 99.9 % of the communication time.

The Saint-Exupery Technological Research Institute of Toulouse (France) leads the project ALBS (French acronym for Broadband Satellite Access). This initiative involving small and medium enterprises, industrial groups and research institutions specialized in aeronautics and space industries, is currently developing various solutions to increase the telecommunication satellite bandwidth.

This paper presents the prediction system preventing a cloud blockage of the optical link. An uncooled microbolometer thermal infrared camera continuously (night and day) observes the entire sky vault above each OGS. The camera provides several images in the 7.5 - 13 μm band, corresponding to an atmospheric window, every one minute. Thermal emissions originating from clouds show a high radiometric contrast with the atmosphere.

Using these observations, two challenges appear. The first one is the assessment of the cloud optical depth and the determination of how it can significantly affect or not the optical link. The second one consists in forecasting the cloud patterns and in estimating the time before the next optical link interruption. A radiative transfer model (RTM) has been used to simulate the thermal infrared downward emission viewed by the camera for a diversity of detectable sky state situations. Radiance look-up tables have been established for a wide set of realistic values of atmospheric parameters significantly influencing the emission on this spectral band (temperature and water vapour profiles, aerosols optical depth and cloud microphysics properties). Then, a minimization algorithm between simulated and observed radiances provides the most likely cloud properties, permitting to retrieve presence of thick clouds and thin ice cloud optical depth at 1.55 μm.

The cloud pattern prediction algorithm consists in assessing the motion vectors from subsequent images. Cloud speed and trajectory are then derived and used to extrapolate the future pattern from a current image.

Finally, further improvements can be undertaken using spectral filters. Indeed, thin ice cloud microphysical properties have a significant influence on the differences between the thermal infrared emission's many narrow bands.

9641-10, Session 3

Laser beam propagation through turbulence and adaptive optics for beam delivery improvement

Stephane Nicolas, Norwegian Defence Research Establishment (Norway)

Laser-based systems have the intrinsic ability to produce small diffraction-limited beam spots at long distance. However, the performance of these systems is affected by the natural atmospheric turbulence, and any kind of turbulence induced by the carrier platform, as for example aircraft plume and aero-optical effects, and helicopter rotor downwash. In many cases, turbulence limits the operational range and capability, but may also result in system failure and temporary shutdown in strong turbulence conditions. Turbulence typically causes beam wander, beam broadening, and intensity fluctuations (so-called scintillations), which reduce the intensity or energy fluence at the target.

At FFI, a numerical simulation model for beam propagation has been developed, based on the split-step beam propagation method. This is a useful tool to study the impact of the diverse atmospheric and beam parameters in different applications,

and the results can be compared with results from analytic theory or experiments. In Figure 1, we show the irradiance at the target, simulated for a 2.7 km long propagation path in a case of strong turbulence (Cn2= 10-13 m-2/3). In this paper, we address several applications in some detail and investigate how the beam parameters can be optimized for different turbulence conditions and distances. We look at free space telecommunication, where 1.5 μm-wavelength laser beams are propagated over distances of more than 10 km and are subject to severe scintillation effects, ground-to-air 1 μm-laser weapons, which typically operate over ranges up to a few kilometers, and mid-infrared laser-based countermeasure systems, which may have to operate in harsh turbulence conditions due to high carrier speed, plumes, etc.

The effect of turbulence on the laser beam can be significantly reduced by adaptive optics (AO) techniques. We demonstrate this in an experiment at 0.63 μm laser wavelength, using a Shack-Hartmann sensor to measure the wave front distortion and a membrane deformable mirror that pre-corrects the outgoing laser beam for turbulence. A small retro-reflector is used as a target. Without AO the beam intensity profile is severely distorted and is changing rapidly. When AO is activated, the beam profile is much narrower with increased peak intensity, and the spot stays in a stable transverse position. The average energy inside an aperture whose size equals the diffraction limit of the laser beam is improved by a factor of 3, while the fluctuations are reduced by a factor of 10. Work is underway to extend the distance of the experiment to 600 m. So far, we are using a beacon located at the target to measure the turbulence and drive the AO correction loop. Under this condition, the average intensity and fluctuations are improved by a factor of about 2 and 3, respectively. An example of improved beam delivery at the target at 600 m distance is given in Figure 2.

9641-11, Session 3

Investigation of dual-wavelength laser beam propagation along the in-door atmospheric path

Alina V. Gorelaya, Elena V. Shubenkova, Saint Petersburg Electrotechnical Univ. “LETI” (Russian Federation); Dmitriy I Dmitriev, Scientific Research Institute for Optoelectronic Instrument Engineering (Russian Federation); Anna D Dmitrieva, St Petersburg State Electrotechnical Univ (Russian Federation); Alexis V. Kudryashov, Active Optics NightN Ltd (Russian Federation); Igor L Lovchiy, Scientific Research Institute for Optoelectronic Instrument Engineering (Russian Federation); Egor V Shalymov, St Petersburg State Electrotechnical Univ (Russian Federation); Yulia V Sheldakova, Active Optics NightN Ltd (Russian Federation); Arkadii D Tsvetkov, Scientific Research Institute for Optoelectronic Instrument Engineering (Russian Federation); Dmitriy V Venediktov, St.-Petersburg State University (Russian Federation); Vladimir Y. Venediktov, Saint Petersburg Electrotechnical Univ. “LETI” (Russian Federation)

The paper presents the results of measurement of dual-wavelength (0.53 and 1.06 mcm) collimated laser beam (diameter 50 mm) propagation along the calm in-door atmospheric beamlet with the length 80-360 m. Wavefront distortions, imposed by residual atmospheric turbulence, were measured synchronously at two wavelengths by two independent and mutually calibrated Shack-Hartman wavefront sensors.

9641-12, Session 3

Turbulent phase noise on asymmetric two-way ground-satellite coherent optical links

Clélia Robert, Jean-Marc Conan, ONERA (France); Peter Wolf, Observatoire de Paris (France)

Bidirectional ground-satellite laser links suffer from turbulence-induced scintillation and phase distortion. Driven by frequency transfer applications, we study how turbulence impacts on coherent detection capacity and on the associated phase noise that limits clock transfer precision. We thus evaluate not only the statistical properties of turbulence effects, but also their temporal evolution. We show an efficient two-way compensation of phase noise that is very promising for clock transfer, and to our knowledge not yet evaluated in the literature.

An efficient two-way cancellation of atmospheric effects in such time/frequency links requires reciprocity between up and downlink. This has been studied recently [1-4] on horizontal propagation paths and under conditions of perfect overlap between the two channels. To account for realistic turbulence and wind conditions, the asymmetry of the ground-satellite links, the point-ahead angle and the satellite cinematic, we use wave-optics propagation through turbulence for refined end-to-end simulations with the exact beam geometry. Monte-Carlo simulations allow characterizing the coherent detection in terms of heterodyne efficiency: mean value and statistical distribution. Temporal simulations provide time series and spectral density of the heterodyne efficiency and phase or frequency noises, thanks to translating phase screens following wind profiles and satellite cinematic.

The talk is twofold: first, we provide statistics on heterodyne efficiency for different turbulence strengths and system parameters. We show that to avoid large fluctuations in signal to noise ratio with frequent extinctions we need placing the ground station in altitude at a low turbulence site, using a small ground emission telescope diameter, and since ground reception diameter is rather large due to link budget, the downlink must be at least tip-tilt corrected. Second, we present examples of temporal phase noise evolution both for uplink and downlink. Finally, we quantify the two-way partial compensation of the phase noise and its impact on the frequency stability of space to ground clock comparisons in terms of Allan variance.

9641-13, Session 4

Analysis of perspective elongation for sodium laser guide star

Feng Wang, Wei Zhang, Tianjiang Chen, Wenchao Zhou, Hong Yan, China Academy of Engineering Physics (China)

In recent years, Laser Guide Star (LGS) Adaptive Optical systems become an established technique at the telescope facilities with large aperture. At these aperture diameters, such as 8m class telescope facilities, perspective elongation, arising from the finite distance and finite thickness of the artificial excited guide star can produce some error which could affect the performance of adaptive optical systems seriously. Because of formation reasons, the perspective elongation increases with the depth of the LGS and with the distance of the sub-aperture from the launch aperture of the LGS; and it decreases with LGS height. The perspective elongation impacts negatively wave-front detection and reconstruction, and varies in size over the sub-apertures and affects the gradient sensitivity of the sensor. To improve the LGS detection with perspective elongation, people is developing the algorithms in wave-front reconstruction and the polar coordinate CCD for use in a Shack Hartmann (SH) wave-front sensor. These techniques reduce negative effect of the perspective elongation, such as

the detection frequency, the accurate and efficient of centroid algorithms.

In this paper, we want to introduce and explain the effect of perspective elongation, and show some results of theoretical simulation and experiment. Nowadays, sodium LGS plays an important role in adaptive optical system, and our research of the perspective elongation based on the sodium LGS. The perspective elongation of sodium LGS is determined by the angular separation between launching and receiving, the altitude and thickness of sodium layer, the zenith angle of telescope facilities. First of all we analyzed how the elongation of sodium LGS change with these parameters, and give the results of simulation. The results give the relation between the perspective elongation and the parameters, and could be adopted in adaptive optical system design. The elongation not only affects the accurate of wave-front detection, but also produces some aberrations in the process of reconstruction. The aberrations were analyzed, and the possibility of aberration correction was discussed. With the results of the theoretical simulation, we designed an experiment to observe the perspective elongation. A Transmitting and receiving system has been set up. The system consists of a 300mJ sodium LGS laser, a telescope with an aperture of 450mm, a beam expander with an aperture of 200mm, a LGS detecting device, etc. As the light from the sodium LGS was dim, the system has been optimized to achieve a brighter sodium LGS, and some facilities and parameters of the system were introduced. Based on the pulsed laser and a mobile LGS projector, we operated the experiment at different distance between the telescope and the laser projector. According to the distance from 5m to 30m, a series of elongated images was obtained. With the experimental data, we deduced the aberration of wave-front at 30m separation. The analytic result of the image data agreed with the theoretical simulation.

By the theoretical simulation of the perspective elongation, the effects including the aberration of wave-front could be achieved, which has been verified in the experiment. It provides us with a possibility that one could improve the reconstruction accuracy at a sodium or Rayleigh LGS adaptive optical system by correcting the perspective elongation in advance.

9641-14, Session 4

Robust remote-pumping sodium laser for advanced LIDAR and guide star applications

Bernhard Ernstberger, Martin Enderlein, Axel Friedenauer, Robin Schwerdt, TOPTICA Photonics AG (Germany); Daoping Wei, Vladimir Karpov, MPB Communications Inc. (Canada); Patrick Leisching, TOPTICA Photonics AG (Germany); Wallace R. L. Clements, MPB Communications Inc. (Canada); Wilhelm Kaenders, TOPTICA Photonics AG (Germany)

Under a development contract with the European Southern Observatory (ESO), TOPTICA Photonics AG and partner MPB Communications Inc. have brought a next-generation sodium guide star laser system to production standard.

The laser is based on a narrow-band diode laser, polarization-maintaining Raman fiber amplifier (RFA) technology and resonant second-harmonic generation (SHG). With patented technology for the suppression of stimulated Brillouin scattering in the RFA, and SHG efficiencies > 80%, it emits > 22W of narrow-linewidth (≈ 5MHz) continuous-wave radiation at sodium resonance. Due to the SHG resonator acting as spatial mode filter and polarizer, the output is diffraction-limited with RMS wavefront error < 1/25? and a polarization extinction ratio > 20 dB.

Integrated is a repumping scheme generating a sodium D2b sideband for boosting guide star return flux. Being based on sum-frequency generation in the patented doubly-resonant SHG resonator, no additional optical wave front distortions are introduced.

A detuning option allows for measuring and subtracting the Rayleigh scattering background.

Apart from this unique optical design, a major effort has been dedicated to integrating all optical components into a ruggedized and reliable system, providing a maximum of convenience for telescope operators. With a cooling-water flow of less than 5l/min and an overall power consumption of only 700W, the infrastructure demands on site are minimal. Each system is built in a modular way, based on the concept of line-replaceable units (LRU). A comprehensive system software, as well as an intuitive service GUI, allow for remote control and error tracking down to at least the LRU level. In case of a failure, any LRU can be replaced within four hours. With the remote pumping option, the small 80-kg laser head consisting of RFA and second-harmonic generation stage can be separated by up to 27m from the larger (600kg) electronics cabinet. This minimizes the effort for integration with existing telescope infrastructure. The end result is a system designed throughout to provide convenient, turn-key operation in remote and harsh locations such as the Chilean Atacama desert or the summits of Hawaii.

In 2014 five laser systems have been delivered and each undergone long-term testing by the customer. The first telescope installations are scheduled for early 2015.

We present a comparison of characteristics and long-term test results of the first batch of systems, demonstrating the reproducibility of excellent optical characteristics and the robustness of the design. We propose the same or similar solution also for applications in laser satellite communication and space debris tracking and laser-based remediation by emphasizing the potential of this system.

9641-15, Session 4

Residual distortions caused by the size of a reference source

Vladimir P. Lukin, V.E. Zuev Institute of Atmospheric Optics (Russian Federation)

The problem of coherent optical radiation focusing through a turbulent medium—the atmosphere— arises in some practical applications, e.g., when energy is supplied to a distant object by use of laser radiation. Medium inhomogeneities and, first of all, atmospheric turbulence become a serious obstacle restricting ultimately achievable characteristics and possibilities of optoelectronic systems. It is well known that using adaptive optics allows one to significantly reduce these restrictions. However, the practical use of adaptive correction algorithms and systems needs an additional (reference) source providing the possibility to measure phase distortions in the radiation propagation channel. As a reference radiation of this kind, one can use, e.g., radiation reflected directly from the object on which it is necessary to focus the coherent laser radiation. A situation is possible when the operation of a wavefront sensor of an adaptive system is provided using a reference radiation created by “illumination” of the object by a radiation beam from an additional source. The approach considered here can be used both with coherent and incoherent illumination.

9641-16, Session 4

Enhanced monolithic diffraction gratings with high efficiency and reduced polarization sensitivity for remote sensing applications

Peter Triebel, Torsten Diehl, Tobias Moeller, Carl Zeiss Microscopy GmbH (Germany); Alexandre Gatto, Alexander Pesch, Lars Erdmann, Matthias Burkhardt, Alexander Kalies, Carl Zeiss Jena GmbH (Germany)

Spectral imaging systems lead to enhanced sensing properties when the sensing system provides sufficient spectral resolution to identify materials from its spectral reflectance signature.

The performance of diffraction gratings provide an initial way to improve instrumental resolution. Thus, subsequent manufacturing techniques of high quality gratings are essential to significantly improve the spectral performance.

The ZEISS unique technology of manufacturing real-blazed profiles comprising transparent substrates is well suited for the production of transmission gratings. In order to reduce high order aberrations, aspherical and free-form surfaces can be alternatively processed to allow more degrees of freedom in the optical design of spectroscopic instruments with less optical elements and therefore size and weight advantages. Prism substrates were used to manufacture monolithic GRISM elements for UV to IR spectral range. Many years of expertise in the research and development of optical coatings enable high transmission anti-reflection coatings from the DUV to the NIR. ZEISS has developed specially adapted coating processes (Ion beam sputtering, ion-assisted deposition and so on) for maintaining the micro-structure of blazed gratings in particular. Besides of transmission gratings, numerous spectrometer setups (e.g. Offner, Rowland circle, Czerny-Turner system layout) working on the optical design principles of reflection gratings. This technology steps can be applied to manufacture high quality reflection gratings from the EUV to the IR applications with an outstanding level of low stray light and ghost diffraction order by employing a combination of holography and reactive ion beam etching together with the in-house coating capabilities.

We report on results of transmission, reflection gratings on plane and curved substrates and GRISM elements with enhanced efficiency of the grating itself combined with low scattered light in the angular distribution. Focusing on the straylight characteristic a measurement of the actual straylight level, preferably with extremely high precision, was performed and will be discussed in this paper. Beside of the results of straylight measurement the actual results on improving efficiency for transmission and reflection gratings will be discussed on theoretical simulations compared to measured data over the entire wavelength range.

9641-17, Session 5

Fast PSF estimation under anisoplanatic conditions

Francisco de Asís Molina Martel, Fraunhofer-Institut für Optronik, Systemtechnik und Bildauswertung (Germany); Roberto Baena-Gallé, Real Academia de Ciencias y Artes de Barcelona (Spain); Szymon Gladysz, Fraunhofer-Institut für Optronik, Systemtechnik und Bildauswertung (Germany)

Correction of atmospheric turbulence effects on images involves mainly mitigation of distortion (“de-warping”) and removal of image blur. One of the approaches for correcting atmospheric blurring in images involves the use of deconvolution. The ill-posed nature of the problem and the number of unknowns makes this problem hard to solve. This is why methods like blind deconvolution can be too time-consuming for real-time application. Additionally, an optimal parameter input is also often required (which requires interaction from an operator).

Our ultimate goal is to perform an autonomous, software-based turbulence correction in real time. This requires both very fast point-spread function (PSF) estimation and a deconvolution method. Our research involves the study of deconvolution methods with the best quality-to-speed ratio. In this work we study new efficient ways to describe and estimate the PSF in anisoplanatic conditions. Describing the PSF efficiently with a small number of parameters allows us to accelerate PSF estimation by some orders of magnitude.

In order to maximize computational performance this work also includes the analysis of existing algorithms and the study of hardware architectures for an efficient implementation. In this paper we compare several hardware platforms (CPUs, GPUs and FPGAs) and discuss their pros and cons for solving this specific task.

9641-18, Session 5

Image enhancement methods for turbulence mitigation and the influence of different color spaces

Claudia S. Huebner, Fraunhofer-Institut für Optronik, Systemtechnik und Bildauswertung (Germany)

In mid- to long-range horizontal imaging applications it is quite often atmospheric turbulence which limits the performance of an electro-optical system rather than the design and quality of the system itself. Even weak or moderate turbulence conditions can suffice to cause significant image degradation, the predominant effects being image dancing and blurring. To mitigate these effects many different methods have been proposed, most of which use either a hardware approach, such as adaptive optics, or a software approach. A great number of these methods are highly specialized with regard to input data, e.g. aiming exclusively at very short exposure images or at infrared data. So far only a very limited number of these methods are concerned specifically with the restoration of RGB color video. Beside motion compensation and deblurring, contrast enhancement plays a vital part in many turbulence mitigation schemes. While most contrast enhancement techniques, such as Contrast Limited Adaptive Histogram Equalization (CLAHE) work quite well on monochrome data or single color frames, they tend to amplify noise in a color video stream disproportionately, especially in scenes with low contrast. Therefore, in this paper the impact of different color spaces (RGB, LAB, HSV) on the application of such typical image enhancement techniques is discussed and evaluated with regard to suppressing temporal noise as well as to their suitability for use in software-based turbulence mitigation algorithms.

9641-19, Session 5

The real-time atmospheric turbulence modeling and compensation with use of adaptive optics

Anna Lylova, Moscow State Univ. of Mechanical Enginnering (Russian Federation); Alexis Kudryashov, Moscow State Univ. of Mechanical Engineering (Russian Federation); Julia Sheldakova, Moscow State Univ. of Mechanical Engineering (Russian Federation)

Turbulent refractive index fluctuations lead to distortions of the light waves propagated throw the atmosphere. This phenomenon limits the telescopes resolution and disturbs the laser irradiance coherence that worsens the image quality and reducing the laser power. The problem of the wavefront distortions compensation is already solving by adaptive optics. The correction technique is rather well-developed but the experiments may be hard-implemented and very expensive. Thus, we suggested to design the real-time high-precision model of the atmospheric turbulence that is able to simplify the experiments and to reduce the outlays.

By now there is a lot of works devoted to representation of the sequence of the pre-generated phase screens. The described techniques may take into account the temporal characteristics of the atmosphere given by the Greenwood frequency. However any executive element has response time, and there are no models considering the reconstruction delays. Thus, the system work is slowing down and the phase screens cannot be reconstructed in real-time.

We suggest the model that takes into account the phase fluctuations dynamics and is able to recover the time-dependent phase screens by an executive element.

Every calculated phase screen presented in the sequence corresponds to defined time moment. But the executive device cannot represent the screens at exact moment because of some delays caused by calculations and response of the executive devise - that is the key problem associated with the

representation of a pre-generated sequence of phase screens. To overcome this problem let us suppose that our system delays are larger than the time increment. In this case every next generated phase screen of the sequence is reconstructed a little bit later than it would be required. To avoid the system delays we suggested supplementing our time-dependent phase screens sequence with missed elements using one of the following methods: to generate absolutely new phase screen according to the existing techniques or to interpolate the closest sequence elements.

We suggested to use the second way. We generated the phase-screens sequence (applying the FFT to the Wiener spectrum of the phase fluctuations) and interpolated them using Zernike polynomials. As soon as the phase screens were correlated to each other, we considered that Zernike coefficients are also non-independent. Thus, as we set the dependence of Zernike coefficients changing upon the time, we were able to calculate the voltage set that could be applied to the deformable mirror actuators to reproduce the phase screen. That technique allowed us to avoid the time-delays and to increase the frequency of the system.

The adaptive optical system for atmospheric turbulence generation consisted of the next elements: an executive element (in our case – bimorph deformable mirror), Shack–Hartmann wavefront sensor (to measure reproduced wavefront profile) and personal computer with an appropriate software (to generate the phase screens and calculate voltages to be applied to the electrodes of the mirror to reproduce the phase screens).

The modeled turbulence could be successfully compensated with the use of adaptive optical system that consists of deformable mirror, wavefront sensor and personal computer. The results of phase screens modeling and correction are presented at this work.

9641-25, Session 5

Bumps of the wave structure function in non-Kolmogorov turbulence

Chunhong Qiao, Lu Lu, Pengfei Zhang, Haitao Wang, Honghua Huang, Chengyu Fan, Anhui Institute of Optics and Fine Mechanics (China)

The analytical expressions for wave structure function of plane and spherical waves are derived both in the viscous dissipation and inertial range. Due topreviously research, there is a discrepancy between theoretical resultsand the experimental datum in viscous dissipation range.In this paper, only considering the inertial range, taking plane waves for example, we give a comparison of results of WSF calculated by the analytical formula obtained in this paper and the numerical calculations of the definition at the fixed parameter (i.e.,the generalized exponent?), it can be seen that the two results are in agreement with each other exactly. Based on non-Kolmogorov power spectrum, new characteristics for wave structure function (WSF) have been found for plane and spherical wave models when the different ratio of inner scale 0 l and outer scale of turbulence 0 L is obtained. In outer scale assumed finitecase (i.e., L0=1m), WSF obtains the maximum when? approximates to 3.3 both for plane and spherical wave models. In outer scale assumed infinite case (i.e., 0 L ? ?), the WSF can be sorted into three parts, including two rapid-rising regions (i.e., 3.0 ?? ? 3.3and 3.8 ?? ? 4.0) and one gently rising region (i.e., 3.3 ?? ? 3.8).Further, the changes of scaled WSF versus the ratio ofseparation distance and inner scale (0 ? / l) are investigated under mentioned above conditions for two models. In 0 L ?1m case, both for plane and spherical waves, the value of ? ?determines the bump position of WSF, and smaller ? has larger separation distance, which relates to a better coherence degradation of laser beams propagating through atmosphere induced by the strength of turbulence. In 0 L ? ? case, the bump of scaled WSF disappears when the generalized exponent has large values. The changings of scaled WSF monotonicallyincrease as ???increased when the generalized exponent is larger than 11/3 for two models. Besides, the properties of spherical waves are similar to plane waves, except which the values of WSF and the scaled WSF are smaller than plane ones.

9641-8, Session PS

New optical receiving system design for portable camera lidar

Laian Qin, Feng He, Xu Jing, Fengfu Tan, Anhui Institute of Optics and Fine Mechanics (China)

For its better spectral response characterization, higher quantum efficiency and signal-to-noise ratio, camera is more and more used in atmospheric parameters measurement lidar. Camera lidars retrieval atmospheric parameters by analyzing the light column images acquired by the cameras and objectives through gathering the backscatter light of the laser beam. Lidars of this kind usually have higher spatial resolution and better real time performance. However, because of its limited depth of field(DOF), the measurement accuracy of the area out of the DOF is influenced by optical defocus in different degree. In the meantime, it is also not suitable for portable equipments for using small relative aperture receiving objective. Based on improving the design of the receiving objective, a new design scheme is proposed in this paper about improving the optical receiving system of the camera lidar. This scheme can improve the measurement accuracy of the area out of the DOF in traditional structure by using large DOF ,large relative aperture off-axis objective and the special using mode of the camera . The optical receiving system designed according to this scheme is more compact and is specially suitable for portable instrument. Furthermore , the relation among the focus length, the distance between laser and objective and the installation angle is also analyzed in this paper. The formula is given at the same time. This scheme is carried out in camera lidar system in laboratory and the results is satisfactory.

9641-21, Session PS

Flipped mode's scintillation-expression for Kolmogorov turbulence under Rytov theory

Ángel M. Fernández Alvarez, Univ. d'Angers (France) and Univ. Técnica Federico Santa María (Chile) and Pontificia Univ. Católica de Valparaíso (Chile); Darío G. Pérez, Pontificia Univ. Católica de Valparaíso (Chile); Règis Barillé, Univ. d'Angers (France)

Most of Laser beam have a TEM00 Gaussian mode as standard output beam, these beams are affected when they propagate through a turbulent medium. We study another laser beam shape: a flipped mode obtained with a Sagnac-interferometer. With the Rytov theory we have obtained all the necessary statistical quantities describing the behavior of the flipped-mode when it propagates through optical turbulence. We will experience if this kind of beam shape has a better performance in optical communications, laser radar, imaging, adaptive optics, target designation, ranging, remote sensing, and among other areas.

9641-22, Session PS

Measurements of parabolic mirrors aberrations in hyperspectral microscope

Anna Lylova, Moscow State Univ. of Mechanical Enginnering (Russian Federation); Sergey Kalenkov, Moscow State Univ. of Mechanical Enginnering (Russian Federation); Alexander Shtanko, Moscow State Univ. of Mechanical Enginnering (Russian Federation); Julia Sheldakova, Moscow State Univ. of Mechanical

Engineering (Russian Federation)

Spectroscopic and microscopic imaging instruments are essential tools in biological and medical sciences. These techniques can further enhance the understanding of biological processes.

The main idea of our research is to design a new hyperspectral microscope which resolution could be as close as possible to the diffraction limit.

Nowadays to reconstruct the microobject image with use of holography method the holography microscope is used. One of the main part of any microscope is objective. However, our recent investigations have shown that the resolution of any microscope is not as high as required. Thus, we suggested a new method of spatial-spectral holographic imaging in white light with use of mirror optics. In our research, we considered to design a new holographic microscope equipped with parabolic mirrors, Shack-Hartmann wavefront sensor and high-resolution high-speed camera. The use of the wide-aperture parabolic mirrors allows us to increase the microscope resolution and to fix the high spatial frequencies.

However, it is wide known that the use of the parabolic mirrors lead to the significant aberrations of the wavefront that distort the image quality. Taking into account the aberration of the parabolic mirrors it is possible to increase the imaging quality. To estimate the parabolic mirror aberrations we constructed a mathematical model. This model described the light propagation from the point source that is placed randomly at the focal plane of the parabolic mirror as if it is a point on the object under test. The light beams optical path calculation allowed us to reconstruct the phase distribution at the observing plane. If our object is placed at the focus of the parabolic mirror, the phase of the registered wavefront was constant at the whole aperture. In case of the object shifting, we registered tilt and some high-order wavefront aberrations. Besides, our model showed that the dependence of these aberrations on the shift magnitude of the position of the focal spot was linear. Thus, we were able to represent the phase distribution at the observing plane.

The modeling results were confirmed by independent experiments. The system designed to measure the aberrations of the parabolic mirror consisted of a collimated laser beam, parabolic mirrors and Shack-Hartmann wavefront sensor. According to the Shack-Hartmann wavefront sensor principle, the incoming light beam is divided into a number of cells by two-dimensional sub-apertures of the lenslet array that form a set of focal spots. These spots captured by the camera's sensor are situated at the focal plane of the lenslet array. The local slope of the wavefront in each cell of the array is considered to be constant. The displacement of each focal spot from the ideal, reference, position is proportional to the wavefront local slope value. We can therefore reconstruct the wavefront structure by measuring the local slopes of the incoming beam.

Using described system we measured the phase error caused by non-ideal system adjustment. The main aberrations discovered in the system were astigmatism and coma. In fact by adjustment of these parabolic mirrors based on the information from the wavefront sensor it was possible to decrease the amplitude of aberrations by a factor of 3.

9641-23, Session PS

Airborne experiment results for spaceborne atmospheric synchronous correction system

Wenyu Cui, Weining Yi, Lili Du, Xiao Liu, Anhui Institute of Optics and Fine Mechanics, CAS (China)

The image quality of optical remote sensing satellite is affected by the atmosphere, thus the image needs to be corrected. Due to the spatial and temporal variability of atmospheric conditions, correction by using synchronous atmospheric parameters can effectively improve the remote sensing image quality. For this reason, a small light spaceborne instrument, the atmospheric synchronous correction device (airborne prototype), is developed by AIOFM of CAS(Anhui Institute of Optics and Fine Mechanics of Chinese Academy of Sciences). With this instrument, of which the detection mode is timing synchronization and spatial coverage, the atmospheric parameters consistent with the images to be corrected in time and space can be obtained, and then the correction is achieved by radiative transfer model. To test the correction effect for satellite and aviation images by atmospheric correction device, the experiment was implemented by the satellite-airborne-ground synchronous measuring method. On the one hand, within an hour when the satellite passed, the aircraft equipped with the atmospheric correction device flied above the satellite imaging area, by which atmospheric parameters synchronized with satellite images were obtained; on the other hand, an 0.4 meter resolution camera and the atmospheric correction device equipped on the plane observed the ground simultaneously, by which the atmospheric parameters synchronized with the aviation images were obtained. In addition, CE318 at ground observation sites were working during the experiment to get atmospheric data for results comparison and validation. Experimental results show that using the AOD and CWV of imagery area retrieved by the data obtained by the device to correct aviation and satellite images, can improve image definition and contrast by more than 30%, and increase MTF by more than 1 time, which means atmospheric correction for satellite images by using the data of spaceborne atmospheric synchronous correction device is accurate and effective.

9642-23, Session PS

A new MIMO SAR system based on Alamouti space-time coding scheme and OFDM-LFM waveform design

Xiaojin Shi, National Space Science Ctr. (China); Yunhua Zhang, National Space Science Center (China)

In recent years, multi-input and multi-output (MIMO) radar has attracted much attention of many researchers and institutions. In contrast with conventional phased array radar and SAR system, MIMO radar system has significant potential advantages for achieving higher system SNR?more accurate parameter estimation, or high resolution of radar image. In this paper, we propose a new MIMO SAR system based on Alamouti space-time coding scheme and orthogonal frequency division multiplexing linearly frequency modulated (OFDM-LFM) for obtaining higher system signal-to-noise ratio (SNR) and better range resolution of SAR image. Alamouti space-time coding scheme is commonly used in wireless communication area to decrease the probability of bit error. For MIMO SAR, we introduce Alamouti space-time code in transmitted waveform design to increase system SNR. Alamouti space-time code is suitable for MIMO radar system with two antennas. Two orthogonal signals are simultaneously transmitted from the two antennas at a given symbol period. During the next symbol period, the complex conjugated signals are transmitted through the cross over antennas. The received signals can be decoded by multiplying Alamouti space-time decoding matrix and additional 6dB gain can be acquired which is compared with conventional SAR matched filtering process. For decreasing interference of transmitted signals and improving range resolution of SAR image, we select OFDM-LFM as orthogonal waveforms. The signal of each subarray has the same frequency slope but different center frequency, just like stepped frequency signals. In the latter MIMO SAR processing, each receive subarray's signal can be separated through a group of matched filter. After spectrum synthesis process, the equivalent range resolution can be improved by M times (M is the number of transmit subarrays). The new MIMO SAR system is composed of 2n T/R subarrays and the transmitted signals are orthogonally designed which have the same bandwidth and increasing center frequency. Every two subarrays are designed as a group and Alamouti space-time encoding and decoding scheme is applied in every group. There are 4 steps in data process procedure for the new MIMO SAR system. Firstly, received data should be decoded by Alamouti decoding matrix. It is noticed that Alamouti decoding scheme is implemented in frequency-domain and the range compression has been accomplished in this step. Secondly, all of received data after Alamouti decoding should be realigned based on the center frequency of received signals. Thirdly, Inverse fast Fourier transform (IFFT) should be implemented to achieve higher range resolution. Finally, SAR image is generated through matched filter in the azimuth direction. The simulation results of 4 T/R subarrays indicate that Alamouti scheme provides additional 6dB gain in ideal compared with conventional SAR and range resolution of SAR image can be significantly improved by using OFDM-LFM as transmitted signals.

9642-24, Session PS

Automatic change detection in multitemporal X- and P-band SAR imagery using the difference between the digital elevation models

Rafael Rosa, Bradar Indústria S/A (Brazil) and Instituto Tecnológico de Aeronáutica (Brazil); David Fernandes, Instituto Tecnológico de Aeronáutica (Brazil); João B. Nogueira Jr., Santo Antônio Energia S/A (Brazil)

Forest monitoring is a major concern today due to climate changes, conservation of fauna and flora and to the lack of water. Therefore, several environmental monitoring techniques have been developed and used to detect changes in the scenes. However, the main techniques have limitations related to weather conditions and does not have the expected effect. The use of SAR (synthetic aperture radar) seems appropriate to detect changes due to its independence of atmospheric and lighting conditions. The SAR change detection is a process that uses SAR images acquired in the same geometric conditions but in different moment (multitemporal) to identify changes in the surface that occurred between two acquisitions. The purpose of this work is to create an efficient SAR change detection tool able to automatically identify regions where there was some kind of change, such as appearance of gaps in vegetation areas, trails, changes at forests borders, selective logging, growth of pastures, plantations and other dynamic land use. This paper will present a new method of change detection in multitemporal SAR imagery using the difference between the multitemporal digital elevation models of X-band (digital surface model) and P-band (digital terrain model) to calculate a change indicator image. The proposed change detection algorithm was implemented in IDL (Interactive Data Language) and experiments have been performed using multitemporal SAR digital elevation models acquired by the airborne sensor OrbiSAR-2 from Bradar. These multitemporal images were collected at the X- and P-band monthly since September 2012 in the Amazon Forest. The used orthoimages cover an area of 2,938.59km? and they were acquired with 1.0m planimetric resolution. The validation of the proposed method has been done by comparison with ground truth data. To measure the detection accuracy compared to the reference, one selected randomly 20 pairs of multitemporal SAR orthoimages with 0,25 km? (500 x 500 pixels) non-neighboring and non-intersecting each other from this area. The accuracy was calculated for all the selected regions and the average accuracy is 97.49%. Therefore, in this work, we got a new methodology that, without being complex or computationally onerous in terms of processing time, obtained great quality results as evidenced by the final accuracy value.

9642-26, Session PS

Refocusing of ground moving targets for range migration algorithm in FMCW SAR

Pu Cheng, Qin Xin, Jianwei Wan, Zhan Wang, National Univ. of Defense Technology (China)

Frequency-Modulated Continuous-Wave Synthetic Aperture Radar (FMCW SAR) is a compact, cost-effective and light-weight remote sensing radar system. Endowing FMCW SAR with simultaneous function of Ground Moving Targets Indication (GMTI) is an appealing and difficult work. In conventional pulse SAR, the moving target is presupposed not to move out a range cell in a coherent processing interval. However, in FMCW SAR whose longer sweep time producing wider bandwidth and higher range resolution, the moving target migrates several range cells easily even with a low radial velocity. What is worse, due to continuous transmitting and receiving at all time, the standard "stop-go-stop" approximation is not valid any more. The continuous motion during a sweep or pulse repetition interval should be taken into account and compensated. In order to overcome the aforementioned problems and discriminate moving target optimally, we propose a detection method based on the concept of relative motion to refocus the moving target. SAR formation is a scheme designed to form a high-resolution image of stationary targets. When required to process the moving target returns, the results will smear seriously with signal phase history mismatched. The proposed refocusing method changes the processing scheme to match the parameters with the kinematics of the moving target relative to the SAR. The moving target is considered as a stationary

target by changing the coordinates. Thus by searching only one parameter, the relative velocity, moving target can be focused accurately in the SAR formation process. The detection method by focusing has been developed in pulse SAR for back projection algorithm which costs too much time and frequency domain algorithm which is time saving. Range Migration Algorithm (RMA) is an accurate algorithm to reconstruct the image of large scenes at fine resolution. Here we expand this refocusing method for RMA to FMCW SAR considering the Doppler shift in one pulse. The signal processing and the performance of the method will be derived and presented in detail. To validate the efficiency and performance of the proposed method, key procedures are implemented using simulated FMCW SAR data. Initial simulation results shows that the ratio between the moving target and the stationary target is promoted about 10dB both in range and azimuth direction.

9642-27, Session PS

Classification accuracy of urban LULC map based on SAR dual ?polarimetric data

Ahmed I. Ramzi, National Authority for Remote Sensing and Space Sciences (Egypt)

High resolution space borne polarimetric Synthetic Aperture Radar data is less influenced by solar illumination and weather conditions, since more information could be obtained from it. So, PolSAR data can be used for urban land cover/land-use mapping. Land Use/Land Cover (LULC) map are essentials for many applications especially in the context of rapid urbanization. The study area is located in the Cairo District, Egypt covered with dual polarimetric SAR data. The objectives of this paper is to investigate and evaluate the classification accuracy of urban LULC map based on SAR dual polarimetric data and supervised algorithms. Methodology steps include: Collection of SAR gata, (dual polarimetric HH, HV); Image pre-Processing (to remove the speckle noise and geocoding); Multipolarized image (Layer stacking HH, HV and HH+HV); Collecting training samples for the classification and analysis; Feature extraction (Supervised classification); Classification accuracy assessment and producing Land Use/Land Cover (LULC) classification map. The results show that multipolarized image from SAR data and supervised algorithms achieved LULC classification map with high accuracy.

9642-28, Session PS

A comparison of feature extraction methods for Sentinel-1 images: Gabor and Weber transforms

Mihaela Stan, Anca-Andreea Popescu, Dan Alexandru Stoichescu, Univ. Politehnica of Bucharest (Romania)

The purpose of this paper is to compare the performance of two feature extraction methods applied on image patches in order to capture the spatial context. The tests are performed on Sentinel-1 satellites images. SENTINEL-1 (S-1) is an imaging radar mission providing continuous all-weather, day-and-night imagery at C-band. The main operational mode features a wide swath (250 km) with high geometric (typically 20 m Level-1 product resolution) and radiometric resolutions, suitable for most applications.

The feature extraction methods used in our experiments were previously tested on high and very high resolution SAR data (TerraSAR-X) and were reported to be able to discriminate between a relevant numbers of land cover classes (in the order of tens of classes). Based on the available resolution (20x22m) of S-1 Interferometric Wide Ground Range Detected images compared to the resolution of TerraSAR-X that can arrive up to 1m (in High Resolution Spotlight mode), the number of detected classes is expected to be much lower. Furthermore, our tests were aimed to determine the optimal size of the analysis window. Due the high resolution in TerraSAR-X images, the window sizes that were used for the computation of the descriptors were between 100x100 and 200x200 pixels as the retrievable information was very detailed. In our case, the image content has a lower degree of heterogeneity, so we choose a smaller window size used for our analysis: 30x30 and 50x50 pixels.

The Gabor and Weber descriptors were applied on image tiles obtained by applying a regular grid with the window size mentioned above. The impulse response of Gabor filters is defined by a sinusoidal wave multiplied by a Gaussian function. The Weber descriptor consists of two components: differential excitation and orientation. The differential excitation component is a function of the ratio between two terms: one is the relative intensity differences of a current pixel against its neighbors, the other is the intensity of the current pixel. The orientation component is the gradient orientation of the current pixel. After we obtained the patches, we applied a semi-automatic SVM (Support Vector Machine) classifier developed by DLR that helped us to label image patches with different classes.

The S-1 images that we use in our tests are covering the following European cities: Bucharest, Munich and Paris. The images were acquired in the Interferometric Wide Swath (IW) mode, which is the over-land pre-defined mode of S-1 with a resolution of 20x22 m, with 10 x ~10 m pixel spacing. Based on the information content in the test images we were able to distinguish between classes including vegetation, water, continuous and discontinuous urban fabric, and airport. Finally, we calculated the robustness by semantically annotating each class using as visual support optical data available in Google Earth and assigning each patch to the appropriate class. Test showed that better results are obtained using smaller window sizes and that generally the Weber descriptors outperform the Gabor features.

9642-29, Session PS

Estimation and characterization of physical and inorganic chemical indicators of water quality by using SAR images

Muntadher A. Shareef, Abdelmalek Toumi, Ali Khenchaf, Ecole Nationale Supérieure de Techniques Avancées Bretagne (France)

Recently, remote sensing is considering one of the most important tools in studies of water scattering and water characterization. Traditional methods for monitoring and estimating pollutants or Water Quality Parameters (WQP) depended on optical satellite data were relied on the spectral response, thermal or scattering reflected from water rather than Radar data. Thus, many of water quality parameters that can be determined from optical imagery are still limited.

In this paper, a new approach based on the exploitation of Synthetic Aperture Radar (SAR) images has been presented which it is used to map the region of interest and to estimate physical and chemical WQPs.

This approach is based on using the Small Perturbation Model (SPM) to estimate the reflectivity (backscatter coefficients) of the area of interest. This calculation of reflectivity is performed by modeling the surface of the river as a dielectric for which the permittivity is calculated from the Stogryn Debye formulation and the geometry of the surface is described by the Elfouhaily spectrum. Then, from SAR images, the backscatter coefficients were estimated for VV and HH polarizations. And by reversing the process, the temperature parameters and salinity were estimated. Inorganic Chemical parameters which are represented by Total Dissolved Salts (TDS) and the Electrical Conductivity (EC) are estimated directly from salinity.

A tow dataset of instu data have been used to validate this work. The validation included a comparison between parameters measured in situ and those estimated via Terra

SAR-X image. The validation also included fitting and confidence bounds models.

The results showed that there are a good statistical correlation between the in situ water quality and Terra SAR-X data. It demonstrates that Terra-SAR is helpful to improve the estimation of these four parameters for the practical use in the study area.

Finally, the results also demonstrated that the characteristics obtained by surface analysis are able to monitor and estimate the distribution of temperature, salinity, EC and TDS in large rivers with high accuracy. More details will be presenting in the final papers.

9642-30, Session PS

Speckle filtering in PolSAR images by bilateral distance

Souhila Boutarfa, National High School of Technology (ENST) (Algeria) and Univ. des Sciences et de la Technologie Houari Boumediene (Algeria); Youcef Smara, Lamia Bensalem, Univ. des Sciences et de la Technologie Houari Boumediene (Algeria)

The SAR and especially the polarimetric SAR radar (PolSAR) images are affected by a noise called speckle which deteriorates image quality. Its nature is multiplicative and corrupts both amplitude and phase data, which complicates image interpretation, degrades segmentation performance and reduces the detectability of targets. This is why polarimetric filtering is a necessary treatment prior to analysis that allows to reduce the undesirable effect of speckle, therefore, obtain an improved image quality and extract information in order to properly interpret the results.

In this paper, we present two speckle filtering methods in polarimetric SAR radar images. The first is the bilateral filter, is defined by the estimation of spatial and polarimetric distances which include all information in both spatial and polarimetric domains for better adaptation to the data structure and reducing speckle without destroying the information. A weighted average is calculated on a sliding window around the central pixel, in order to filter it. The main function of the filter is the definition of the weighting functions to filter the speckle with preserving the polarimetric information through the control of the weights sensitivity in the spatial and polarimetric domains. On the spatial domain the Euclidean distance is used. In the polarimetric domain two different parameters are estimated, one based on the diagonal of the polarimetric covariance matrix and the other based on the conical geometry of the positive definite Hermitian matrix. The second method is an improvement technique of the parameters calculated in the previous filter, since PolSAR images are highly affected by the noise speckle, the calculated parameters of the bilateral filter will also be affected by the resulting speckle of the noisy image. To reduce this undesirable effect, an iterative procedure for improving these parameters is performed using the filtered images to calculate a more reliable estimation of the weighting functions. At each iteration, the weights of the filter are calculated from the filtered images of the previous iteration. In this study, the Span and the polarimetric covariance matrix elements are taken into account.

The methods are applied to different polarisation data, the three polarimetric E-SAR images (HH, HV and VV) acquired on Oberpfaffenhofen area located in Munich, Germany, in P-band and the fully polarimetric RADARSAT-2 images (HH, HV, VH and VV) acquired on Algiers, Algeria, in C-band. These methods are compared with results obtained by the refined Lee filter.

To evaluate the performance of each filter, we based it on the following criteria: smoothing homogeneous areas, preserving structural characteristics of objects in the scene and maintaining the polarimetric information. Visual evaluation is included and statistical parameters are calculated by using the standard parameters for this type of treatment, such as mean, standard deviation and coefficient of variation, as well as other parameters necessary for the evaluation of PolSAR images to verify the requested criteria and an image classification is used to show the reduced speckle effect and also a comparative study is performed to validate the studied methods and determine the advantages and disadvantages of each filter.

9642-31, Session PS

Robust optical and SAR multi-sensor image registration

Yingdan Wu, Hubei Univ. of Technology (China); Yang Ming, CCCC Second Highway Consultants Co., Ltd. (China)

With the development of remote sensing technology, platforms for remote sensing have been diversely increasing, and taking advantage of multi-source SAR imagery to acquire three-dimensional spatial information has broad application prospects. Homologous feature point extraction is a key problem in the multi-source SAR image processing. In most cases, they are obtained by manual, and this is not only time consuming, but also cannot meet the requirements of fast processing massive data. The research on automatic conjugate point matching for multi-source satellite imagery is of great significance.

In this paper, a robust matching method for the multi-sensor imagery is proposed. Firstly, the SIFT feature matching and relaxation matching techniques are adopted for the matching in the highest pyramid level, to derive the approximate relationship between the reference image and the slave image. Then , the Normalized Mutual Information is taken as the similarity measure to find conjugate points, before the matching , the geometrical distortions such as scale difference, angular difference are compensated. After that, the multi-grid and multi-level RANSAC algorithm is used to delete the erroneous matching points automatically. Performing above steps iteratively until to the finest pyramid level, the facet-based transformation model is used to registration. To verify the effectiveness of the method, applications of proposed algorithm to different optical images as well as optical and synthetic aperture radar images are tested. One image pair consists of a Radarsat image and an ENVISAT image, which is from different SAR sensors. The other image pair includes a COSMO-SkyMed SAR image and CARTOSAT-1 image ,which is from SAR sensor and optical sensor. From the experimental results, it has found that this method can overcome the large rotation existing between the images and different radiation characteristics of images from different types of sensors. The matching points with even little error can be detected and eliminated automatically, and a large number of evenly distributed conjugate points can be delivered, which can realize the registration of multi-source remote sensing imagery accurately.

9642-32, Session PS

Modeling algorithm for SAR image based on fluctuations of echo signal of the Earth's surface

Vadim Nenashev, Alexander Shepeta, Saint-Petersburg State Univ. of Aerospace Instrumentation (Russian Federation)

During the mapping of the earth's surface to increase the resolution of radar are used the algorithms of synthetic aperture of antenna system. To synthesize the algorithms traditionally are used mathematical models of the Earth's surface, built on the principles of geometric optics. In this case the power of the echo signal from the element surface is calculated by the formulas radar which can calculate only the average power of the reflected signal. This signal fluctuations are not considered, and this can lead to inaccuracies in determining the characteristics of the aperture synthesis algorithms. In the study there is an extended mathematical

model of the reflected signal, which allows to take into account the statistical characteristics of the power fluctuations. This echo is much closer to the reality of the on-board radar. A special case of the proposed algorithm is a traditional simulation algorithm using the calculation according to the average power of the reflected signal. In the simulation of surveying the earth's surface is proposed to use a family of Weibull distributions, and for mapping the coastal edge of the complex law of distribution, which is a vector convolution of the lognormal law and the law of the Weibull distribution. The last is particularly important because with such are obtained distributions with convolution weighted tails, which may lead to inoperability synthesizing traditional algorithms. Excluding these fluctuations in the simulation of algorithms to detect non-functional synthetic aperture when working on certain types of surfaces is impossible. Therefore, these models can help developers avoid mistakes in the design of systems mapping.

9642-33, Session PS

Extraction of building areas from high-resolution SAR images based on tensor locality preserving projection

Bo Cheng, Institute of Remote Sensing and Digital Earth (China)

in this paper, we took Radarsat-2 images and TerraSAR-X images as the experimental data and employed Tensor Local Preserving Projection (TLPP) algorithm for feature extraction of high resolution SAR image to improve the ability to object recognition and achieve fast extraction of building areas. Firstly, a variety of texture features were calculated based on gray level co-occurrence matrix (GLCM). Secondly, TLPP algorithm was used for feature extraction of these texture features in order to reduce data redundancy and extract a new feature for recognition of building areas. Then, the new feature was used as input of Otsu method to extract building areas. Finally, the post-processing of image classification was performed. A comparison of the recognition result of building areas between TLPP algorithm and Local Preserving Projection (LPP) algorithm was made. It is concluded that TLPP algorithm has strong generalization ability; TLPP algorithm is applicable to feature extraction of high resolution SAR image, quickly and effectively extract building areas.

9642-34, Session PS

Effect of Faraday rotation angle and the orientation angle on the polarimetric decomposition

Houda Latrache, Mounira Ouarzeddine, Univ. des Sciences et de la Technologie Houari Boumediene (Algeria)

The data acquired by polarimetric synthetic aperture radar (PolSAR) does not only depend on the properties of the imaged scene but also the properties of the backscattered wave. The quality of POLSAR imagery depends on the accuracy of polarimetric observations of the SAR system and its calibration. In the case of PolSAR operating in the law frequency such as P and L band are significantly affected by Faraday rotation (FR). Faraday rotation angle (FRA) of the polarization vector produced when the Electromagnetic waves (EM) traveling through the ionosphere, this angle affect the balance between the polarization channels. The backscatter coefficient of the cross-polarization channel HV is most affected than the co-polarisation channels (HH and VV), this is a disadvantage for applications such as the extraction of forest biomass for which radiometry in the cross channel (HV) is used. An other parameter called the orientation Angle (OA), which affects also the surface backscattering; it is due to variations of terrain slope Changes in the azimuth direction, which induces a change in the backscattered wave. The data must be calibrated using FRA estimated and compensated with OA before further polarimetric applications such as terrain surface classification, geophysical parameters extraction (biomass, soil moister).

In this paper we investigate the effect of the Faraday rotation and the orientation angle on the scattering-model-based decompositions, for this we applied two decompositions model and H-alpha classification. The first one is Yamaguchi model which is incoherent decomposition, performed over the coherency matrix. It describes the total backscatter as sum of four types of basic scattering mechanisms surface, double bounce, volume and helix. The second model is a coherent decomposition called Krogager decomposition, performed over the coherent scattering matrix. This model factorizes the scattering matrix as the combination of the responses of a sphere, a diplane and a helix. The FRA displays a high response in cross polarization channel, which is characteristic of vegetation or canopy surface. This result overestimates the volume scattering power in vegetation area. In this paper the FRA was estimated using an estimator based on the off diagonal terms of the polarimetric covariance matrix PCM. The OA was derived using the circular polarization algorithm. The estimated FRA and OA were used to correct and compensate the data, after we decomposed the original and the corrected data. The ALOS PALSAR L bande fully polarimetric images (HH, HV ,VH and VV) acquired in a town in Indonesia, was utilized in this paper for the analysis of the results. The decomposition results obtained using the original data, the correct data using FRA and the compensate data using OA were compared. As expected the volume scattering from vegetation area were found to be increased.

To evaluate the results we selected small patches in vegetation area from the results using original data and the data corrected. The scattering contribution of each extracted scattering components of two decomposition model. The results were also evaluated by plots polarimetric signatures of targets selected from the original data and the corrected data.

9642-35, Session PS

A methodology for outperforming filtering results in the interferometric process

Arlinda Saqellari-Likoka, Vassilia Karathanassi, National Technical Univ. of Athens (Greece)

In this study, a method for reducing the filtering effects on the interferometric phase signal is proposed. Theoretical analysis showed that while noise reduction is maximized after filtering, the loose of interferometric phase signal is also maximized. This state has been also verified by observations on SAR interferometric data where pixels with high coherence value, which are assumed to contain a lot of information, presented lower coherence values after SAR image filtering.

The proposed method performs interferometric phase modeling. It inactivates the filtering of the interferometric phase for pixels with low noise i.e., high coherence value, or for pixels for which the coherence value is decreased after the filtering process. Since the second condition includes the first, the method does not need a threshold for defining pixels with high coherence value. The interferogram, which will serve as input in the next steps of the interferometric procedure, is created as a mosaic of the interferograms generated before and after filtering. For pixels presenting a decrease of the coherence value after filtering, the value of the unfiltered interferogram is selected when creating the mosaic. The method does not suggest the use of a specific filter. Any filter proposed in the literature as appropriate for interferometric applications can be chosen by the user.

Performance of the method depends on the performance of the used filter; however, it always improves the interferometric results. Since the phase signal is the basis for the DEM production, its preservation improves all the steps of the interferometric procedure, especially the phase unwapping. Consequently, effects of the method on the produced DEM are also evident.

The proposed method was evaluated using six Envisat images. Three different filters have been applied on the three interferometric pairs: Adaptive, Boxcar and Goldstein. It was observed that the maximum coherence value was reduced after the filtering, which means that a loss of information occurs. For evaluation purposes, two sub-images have been selected for every interferometric pair presenting low and relatively high mean coherence values, respectively. For these sub-images, the calculated mean coherence values were not increased after the filtering. After the application of the proposed method, it has been observed that independently of the filter used, all the sub-images presented pixels with increased coherence value.

In order to evaluate the method over the produced final results, the DEM of the six areas have been generated with and without the application of the proposed method. For each DEM, the Root Mean Square (RMS) Error in meters has been calculated using a reference DEM. The proposed method improved the accuracy of the estimated height in relation to the accuracy provided by simply filtering the images. Only for one area, when applying the proposed method in conjunction with the Adaptive filter, the RMS error of the produced DEM was higher than that resulted without the application of the proposed method. For all the other cases, the proposed method compensated the negative effects of the filtering and leaded to the improvement of the DEM accuracy.

9642-36, Session PS

Monitoring of “urban villages” in Shenzhen, China from high-resolution GF-1 and TerraSAR-X data

Chunzhu Wei, Thomas Blaschke, Univ. Salzburg (Austria); Hannes Taubenböck, German Aerospace Center (DLR), German Remote Sensing Data Center (Germany)

Shenzhen is part of the Pearl River Delta mega agglomeration in Southern China and one of the fastest growing cities in the world with a population of 12 to 15 million people. A unique phenomenon is the existence of so called ‘urban villages’. Urban villages comprise mainly low-rise and congested, often illegal buildings surrounded by new constructions and high-rise buildings whereby population structures can be very different from neighboring areas. Monitoring urban villages and analyzing their characteristics become crucial for urban development and sustainability research. Our objective is to develop an innovative method for an integrated analysis for urban villages monitoring. In this study we carry out a combined analysis of multispectral GaoFen-1 (GF-1) and high resolution TerraSAR-X radar (SAR) imagery. TerraSAR-X provides large amounts of high quality SAR data with up to sub-meter spatial resolution with which details of building and man-made structures can be analyzed. Such high resolution SAR image data bear a high potential but are difficult to handle: they are often corrupted by effects such as speckling shadowing, multisource, layover, or side lobes. Therefore, high resolution TerraSAR-X data are rarely employed for such detailed urban analyses. Also in the urban villages of Shenzhen man-made structures from numerous corner-reflectors which complicate the interpretation of high resolution SAR images. We therefore apply an integrated Object Based Image Analysis (OBIA) to reveal the spatial characteristics of urban villages. The GF-1 and TerraSAR-X data are jointly used for built-up area detection and height characteristic retrieval. The results demonstrate that urban villages and urban areas are clearly distinguishable through a particular combination of Normalized Difference Vegetation Index (NDVI), the spatial pattern of NDVI, and contextual parameters such as neighborhood distance features and digital surface features. Because of the side-looking nature of TerraSAR-X, high-rise buildings in the dense urban area are influenced by the severe layover problems. The integrated SAR/optical OBIA approach which includes GF-1 images can eliminate some layover and shadow effects. The height differences between the urban villages and surrounding high-rise buildings can be revealed with reasonable accuracy. We conclude that the particular combination of GF-1 and TerraSAR-X can effectively reveal the building characteristics of urban villages based while utilizing the spectral and spatial resolution advantages of GF-1 and the height retrieval capacity of TerraSAR-X. In addition, the fusion of SAR and optical imagery is an effective means to reduce the effects of layover, shadow and dominant scattering at building location. We are standardizing the OBIA-workflow in so called rulesets in the Cognition Network Language (CNL) programming environment within Trimble’s eCognition software suite. The transferability and repeatability of this workflow is analyzed with the aim to establish a standardized monitoring process for Urban Villages.

9642-38, Session PS

Comparison of SAR image segmentation by Gaussian and Rayleigh mixture models

Emre Akyilmaz, Middle East Technical Univ. (Turkey) and SDT Uzay & Savunma Teknolojileri (Turkey); Ugur M. Leloglu, Middle East Technical Univ. (Turkey)

Synthetic Aperture Radar(SAR) has the advantage of working in all weather conditions during day and night. This operational advantage is vital for acquiring images in any instant of time to be used for remote sensing applications where increase the quality and the quantity of the images are demanded. One essential step in the automatic analysis of SAR remote sensing data is segmenting the image so that it can be interpreted easily and can be used for the other imaging tasks such as change detection, automatic target detection and automatic target recognition.

The essence of image segmentation is to parcel an image into proper set of connected similar pixels according to their features such as intensities, colors or spatial attributes. Since speckle noise inherently exists in SAR images, the requirement of reliable partitioning of such images is essential for the achievement of satisfactory analysis of the SAR image. In terms of a reliable segmented image, modeling real data set with a probability distributions is not a trivial task. It is always possible that the distribution of the features cannot be well represented by those distributions with important analytical properties. This inconsistency between real data values and the probability distributions creates significant limitations. In order to overcome this problem, linear combinations of distributions known as finite mixture models have been developed.

The finite mixture model, which can be formulated by the weighted sum of various basic density components aims at providing a stable class of density models more representative than a single density model. In these models, each density component corresponds to a surface cover class. Gaussian mixture model which is the one of these basic distribution model is probably the most widely used one. Once the parameters of such a mixture model are estimated then the segmentation of the image can be performed. Expectation-Maximization(EM) algorithm is one of the most commonly used elaborate technique for estimating the mixture parameters. EM is not only used for the estimation of the mixture parameters but it is an excellent framework for segmenting the images.

It has been illustrated that SAR imaging data usually follows a Rayleigh distribution. However, some imaging data for those areas consisting of man-made structures follows a non-Rayleigh distribution. In this case, a Gaussian distribution can be an alternative. For such circumstances, it worths to know the merits of segmenting SAR images by both of the mixture models.

In this study, the SAR images first modeled using mixture of Gaussian and mixture of Rayleigh distributions with equal number of components. In two different mixture models, the mixture parameters are estimated using the EM algorithm. Since EM is sensitive to the initialized values of the parameters, the prior energies of the segmented images are iteratively minimized to eliminate the problem of those misplaced pixels due to the presence of speckles. The experimental results would demonstrate the performance of both mixture models in the segmentation process of SAR images. At this stage,

it seems that Rayleigh mixture model is also applicable for segmentation of SAR images as Gaussian model. Due to the heavy tail of Rayleigh distribution, its density component parameters probably would be low than those of the Gaussian distribution.

9642-1, Session 1

Multitemporal retrieval of soil moisture from SMAP radar data

Fabio Fascetti, Nazzareno Pierdicca, Sapienza Univ. di Roma (Italy); Luca Pulvirenti, CIMA Research Foundation (Italy) and Sapienza Univ. di Roma (Italy)

Remote sensing represents a very useful tool to monitor Soil Moisture Content (SMC) at difference spatial and temporal scales. In particular, SMC maps characterized by high spatial resolution can be obtained by Synthetic Aperture Radar (SAR) systems thanks to the sensitivity of radar return to soil permittivity. However, the surface roughness and the vegetation cover influence the radar return as well, so that the retrieval process is quite challenging. Nowadays, frequent coverage of SAR images becomes feasible thanks to the launch of the ESA Sentinel 1 (C-band) and especially of the NASA Soil Moisture Active and Passive (SMAP) satellites.

In this work, we apply a multitemporal algorithm (MLTA) to retrieve soil moisture from SMAP radar data, originally conceived for the C-band radar aboard the Sentinel-1 satellite ([1]). Such type of algorithm may deliver frequent and more accurate soil moisture maps mitigating the effect of roughness and vegetation changes, which are assumed to occur at longer temporal scales with respect to the soil moisture changes. Although SMAP radar resolution (1-3 km) is worse than the Sentinel 1 one, the operating frequency (L-band), polarization (HH, VV, HV) and shorter revisit time have been specifically designed for this application. Within the multitemporal inversion scheme based on the Bayesian Maximum A Priori (MAP) criterion, a dense time series of radar measurements are integrated (5 acquisitions) to invert a forward backscattering model which includes the contribution from vegetation ([2]).

The processing chain has been designed for local scale applications. It is then investigated how the exploitation of the full SMAP L1 product resolution (1 km) and a detailed description of the site of interest (e.g., detailed thematic maps) can improve the product to run hydrological models at local scale, i.e., to predict flood events.

The processor has been developed before launch thanks to the availability of the GLOSIM data set of simulated SMAP data. Then the calibration and validation tasks have been accomplished by using the data collected during the SMAP Validation Experiment 012. SMAPVEX012 consists of L-Band images collected by the UAVSAR sensor, in situ soil moisture and measurements of vegetation parameters. They have been used to update the forward model for bare soil scattering at L-band with respect to the Oh and Sarabandi model [3] previously used at C band. They have been also used to tune a simple vegetation scattering model which considers two different classes of vegetation, i.e., those producing mainly single scattering effects, and those characterized by a significant multiple scattering involving terrain surface and vegetation elements interaction.

The behaviour of the SMAPVEX012 data are presented and the capability to reproduce them by the proposed forward models are discussed. The results of the inversion algorithms are also presented, summarizing strength and weakness of the approach. Examples of the maps obtained at 1 km resolution are given using GLOSIM data and possibly and very preliminarily using real SMAP data after the commissioning phase that should end in July.

[1] N. Pierdicca, L. Pulvirenti, G. Pace: A Prototype Software Package to Retrieve Soil Moisture from Sentinel 1 Data by Using a Bayesian Multitemporal Algorithm, IEEE Journal of Selected Topics in Applied Earth Observations and Remote Sensing, vol. 7, no. 1, pp., 153-166, Jan. 2014.

[2] N. Pierdicca, L. Pulvirenti, C. Bignami: Soil moisture estimation over vegetated terrains using multitemporal remote sensing data, Remote Sensing of Environment, vol.114, pp. 440-448,2010

[3] Y. Oh, K. Sarabandi, F. T. Ulaby: Semi-empiricalmodel of the ensemble-averaged differential Mueller matrix for microwave backscattering from bare soil surfaces, IEEE Trans. Geosci. Remote Sens., vol. 40, 1348–1355, 2002.

9642-2, Session 1

Application of machine learning algorithms for soil moisture retrieval in view of the future EPS-SGA mission

Emanuele Santi, Simonetta Paloscia, Simone Pettinato, Istituto di Fisica Applicata Nello Carrara (Italy); Felix Greifeneder, Claudia Notarnicola, EURAC (Italy); Wolfgang Wagner, Sebastian Hahn, Mariette Vreugdenhil, Christoph Reimer, Technische Univ. Wien (Austria)

The EUMETSAT Polar System of second generation is currently under study to replace the current satellite system MetOp, and provide continuity of observations in the 2020 timeframe. Among other instruments, the satellites will carry the EPS-SG SCA scatterometer, heir of the current ASCAT instrument. For this instrument, the inclusion of a VH polarization channel on the mid-beam antenna is being evaluated.

In this study, different machine learning algorithms for soil moisture (SM) retrieval, namely, Artificial Neural Network (ANN) and Support Vector Regression (SVR), have been implemented. The objective was to investigate the potential of the VH channel for improving the SM retrieval accuracy, in respect to the existing ASCAT SM product, which relies on vertically polarized data. Tests of the proposed algorithms were carried out basing on real data from other radar sensor at L- and C- band (ENVISAT ASAR and Aquarius).

Additionally, waiting for the real SCA data, a simple scene simulator has been developed in order to provide synthetic data for testing the retrieval algorithms. The simulator is able to account for the topography and to calculate the Local Incidence Angle for each simulated pixel of the scene, accounting for the local topography observed by the SCA sensor at three different beams. Starting from the input Soil Moisture (SM) and vegetation biomass (PWC) products generated by the “Hydroalgo” algorithm, developed at IFAC for working with AMSR-E/AMSR2 spaceborne radiometers, scenes have been simulated at 12.5x12.5 and 25x25 km2 resolution. The simulated backscattering at the 3 beams in VV and VH polarizations was derived from these inputs trough a simple implementation of the Radiative Transfer Theory, obtained by coupling the Oh and the Vegetation Water Cloud (VWC) models. The simulator was validated considering Envisat ASAR GS data available at IFAC. The A and B semi-empirical parameters of the VWC were tuned on the available dataset, while the roughness parameter HSTD was treated as a random variable between 0.5 and 2.5 cm. The simulator outputs were used for implementing and testing the machine learning algorithms, which were based on a previous implementation for ASCAT that included backscatter acquired at the three beams and the corresponding incidence and azimuth angles. For this study, the VH polarized signal acquired in mid- beam by SCA was added as a further input.

The main aims of the work will be the understanding the potential of the VH channel in improving the SM retrieval accuracy, for example due to an improved compensation of vegetation dynamics, with respect to the existing ASCAT SM product, and in comparing the different retrieval approaches. The validation and comparison of the different estimation approaches will be based on modelled SMC from ERA-Land and with a focus on different parameters from the current ASCAT algorithm.

9642-3, Session 1

Large area robust identification of snow cover from multitemporal COSMO-SkyMed images

Simone Pettinato, Emanuele Santi, Simonetta Paloscia, Bruno Aiazzi, Stefano Baronti, Istituto di Fisica Applicata Nello Carrara (Italy); Enrico Palchetti, IFAC-CNR (Italy); Andrea Garzelli, Univ. degli Studi di Siena (Italy)

Quantitative snow-cover investigations can provide important information on global changes and water resource management, as well as flood and avalanche risk prevention. Continuous, cloud-insensitive monitoring is possibile through space-borne SAR imaging, while it is not possible by using optical sensors.. Even if X-band is not the most suitable frequency for snow detection, due to its scarce penetration power into snow cover, the availability of high-resolution SAR images from the COSMO-SkyMed (CSK) and TerraSAR-X constellations has fostered the research on the estimation of the snow water equivalent (SWE) also in the X-band. The backscattering coefficient in the case of dry snow is higher than the snow-free case for snow cover characterized by a relatively large snow depth. Therefore, accurate, high-resolution monitoring of dry-snow cover is made possible by CSK and TerraSAR-X data products.

The authors have recently proposed a nonparametric information-theoretic snow detection algorithm (ITSDA) for snow cover area identification from multitemporal CSK images [1]. The ITSDA method is based on the mean-shift information-theoretic change detection algorithm (MS-ITCD) [2], which is a non-parametric, unsupervised feature extraction method not requiring a preliminary despeckling procedure. Mean-shift clustering is applied on the estimated joint pdf of the SAR amplitude values acquired at two dates and can reliably detect the regions of change even for one-look amplitude SAR images. A possible drawback of this algorithm can be the high computational complexity for estimating and processing the joint pdf from the scatterplot of the two-date SAR amplitude values, which could be critical for large-scale monitoring applications.

The paper presents an improved version of ITSDA through a software optimization of the MS-ITCD algorithm that allows for processing large-size image data without reducing the algorithm sensitivity to backscattering changes, which is mainly related to the number of quantization levels for the estimation of the joint pdf of the SAR amplitude values at the two acquisition dates.

More recent bi-temporal (snow-free/snow) CSK acquisitions (2013) have been considered for testing and performance assessment. Full-frame (more than 20,000?20,000 pixels in slant range view) Himage CSK images in an Alpine scenario are processed and the results are compared with the available snow data. Landsat-7 imagery is considered as the reference data. Improved localization of the snow-covered areas and a reduced false alarm rate with respect to the classical LogRatio approach for change detection is attained also for large-scale monitoring.

[1] S. Pettinato, E. Santi, S. Paloscia, B. Aiazzi, S. Baronti, and A. Garzelli, “Snow cover area identification by using a change detection method applied to COSMO-SkyMed images,” SPIE Journal of Applied Remote Sensing, vol. 8, pp. 084684:1–14, August 2014.

[2] B. Aiazzi, L. Alparone, S. Baronti, A. Garzelli, and C. Zoppetti, “Non-parametric change detection in multitemporal SAR images based on mean-shift clustering,” IEEE Transactions on Geoscience and Remote Sensing, vol. 51, pp. 2022–2031, April 2013.

9642-4, Session 1

Land-cover classification in SAR Images using dictionary learning

Gizem Aktas, Çagdas Bak, Fatih Nar, Nigar Şen, SDT Uzay & Savunma Teknolojileri (Turkey)

Land-cover classification in Synthetic Aperture Radar (SAR) images has significance in various remote sensing applications. Accurate classification is considered as a challenging problem due to extreme variety of natural and man-made objects, seasonal changes due to acquistion time and differences caused by image reconstruction algorithms. Sliding window for feature extraction is widely used; however this approach has tradeoffs with respect to employed window size. In spite of the fact that small window has not enough pixels to obtain sufficient statistical power which leads to lower classification accuracy, it is computationally efficient. On the other hand, the use of large window does not necesserialy cause an increase in statistical power and classification accuracy. Classification accuracy can be decreased significantly since multiple class may exist in a large window especially in class boundaries. For remote sensing applications, land-cover classification algorithm is desired to be accurate and computationally efficient to deal with large images, different land-cover classes, variety within each class, differences occured during image reconstruction and differences occurred due to acquisition time. Images are despeckled and normalized as a pre-processing step in order to decrease differences caused by image reconstruction. The employed despeckling algorithm is Feature Preserving Despeckling (FPD) which is an edge preserving total variation (TV) based state-of-the art method. To handle the mentioned challenges, a novel feature extraction schema which is combined with a super-pixel segmentation algorithm and dictionary learning based classification is proposed. Our feature extraction approach uses an adaptive region of interest for determining statistical and textural features in salient locations. A dictionary is generated using extracted features for each class using a large data set containing sufficient variety. Large example set is modelled as a dictionary which can find a sparse representation to decrease space and time complexity during classification phase. Moreover, dictionary learning allows update of dictionaries for adding new images to training set. During classification, each salient location within a super-pixel cell is classified by using learned dictionaries and a voting mechanism is used for determining class of super-pixel cell. Since multiple dictionaries for each class can be used, proposed method can classify multiple land-cover types in single execution. This approach increases accuracy and computational efficiency of classification since all the pixels in super-pixel cell are classified at once. Computational complexity of the proposed method is linearly propotional to the size of the image because it does not require a sliding window and and a process for each pixel. Due to its computational efficiency and flexibility obtained by dictionaries, proposed method is applicable to both interactive land-cover classification and automatic land-cover classification scenarios. Accuracy and computational efficiency of the proposed method is validated on a large datasets which contain TerraSAR-X high resolutions spot mode SAR images.

9642-5, Session 2

Cosmo-SkyMed and RADARSAT image investigation for the monitoring of agricultural areas *(Invited Paper)*

Simonetta Paloscia, Simone Pettinato, Emanuele Santi, Istituto di Fisica Applicata Nello Carrara (Italy); Claudia Notarnicola, Felix Greifeneder, Giovanni Cuozzo, EURAC (Italy); Irene Nicolini, B. Demir, Lorenzo Bruzzone, Univ. degli Studi di Trento (Italy)

Agriculture is suffering for the progressive reduction of exploitable land due to increasing urbanization, urban waste, and industrial pollution. In the meantime human population is

increasing and its alimentary needs are necessarily increasing. As a consequence, there is an increasing interest in all the research efforts, focused on agriculture monitoring and development, which are devoted to the growth of resources, the protection of the environment, and the maximization of the final yield.

Remote sensing techniques can give a significant contribution to these topics, thanks also to the frequent revisit time and the enhanced ground resolution of the new generation SAR sensors, which allow a frequent and detailed monitoring of agricultural areas. The ground resolution of a few meters is very important for the Italian landscape, which is really heterogeneous with generally small agricultural fields. In agriculture, optical sensors are currently used mainly for classification purposes (e.g. CORINE), yield forecast, and disease monitoring thanks to the relationship between NDVI and green leaf area index. However, optical sensors have limitations in case of clouds and on the other hand microwave sensors are more related to the water content and the structure of vegetation, being also able to collect information on the underlying soil, according to observation frequency.

The monitoring of agricultural surfaces with SAR sensors, and in particular with COSMO-SkyMed (CSK, at X band) and RadarSAT2 (RS2, at C band) sensors, could exploit the synergy between these two frequencies and with optical sensors, making possible the collection of information on different types of vegetation, their biomass and water conditions. Moreover, in case of scarce vegetation cover, especially at C-band, the soil moisture conditions can also be investigated. The synergy between C and X band is essential for this purposes, since C band backscatter shows a noticeable sensitivity to the soil water content, even in case of vegetated surfaces, whereas X band signal shows an evident sensitivity to crop geometry and biomass.

By using multi-frequency, multi-polarization SAR images and adequate and innovative inversion algorithms, the estimate of plant water content and leaf area index of some crop types was carried out, along with the underlying moisture content of the first soil centimeters for low vegetated soils. Moreover, RS2 will enable the use of compact polarimetry data in wide swath imagery. Compared to current quad-pol modes, SAR systems with hybrid- polarity architecture offer some significant advantages like the increase of the swath width. This would mean shorter revisit times for a given location and therefore the possibility of improving the estimate of soil and vegetation parameters, similar to that of fully polarimetric SAR-imagery.

9642-7, Session 2

Multi-temporal intensity and coherence analysis of SAR images for land cover change detection on the Island of Crete

Elena Nikolaeva, Olga Sykioti, Panagiotis Elias, Charalambos C. Kontoes, National Observatory of Athens (Greece)

This study presents the use of multi-temporal Synthetic Aperture Radar (SAR) images for detection of land cover changes in the eastern part of the Island of Crete (Greece). For this purpose, fifteen Envisat ASAR acquisitions operating at C-band from July 2004 to December 2006 were calibrated and registered.

We applied a temporal filter and spatial averaging to the backscatter intensity to reduce the speckle noise. Futhermore, we used the concept that the changes between different backscatter intensity observations can show changes on the target dielectric properties. In order to detect changes due to geometrical characteristics of land cover types, we created coherence maps by using twenty-seven interferometric pairs with proper spatial and temporal baselines between acquisitions. In all calculations, layover and shadow effects, as well as the sea, were masked by using information from the digital elevation model of the area. The observed changes in the coherence values were analyzed with respect to different decorrelation factors that can contribute to the loss of coherence.

Our results present the different backscatter values for several land cover types (bare soil, farmland, olive groves, forests, etc.). In addition, some land cover types such as olive groves and forests show variations of backscatter signal due to the density and height of trees. Furthermore, olive groves show good coherence in interferograms with short time intervals (less than three months, in summer). However, all interferometric pairs have low coherence in farmland because of the rapid growth of plants. Finally, the maps of backscatter temporal changes and coherence changes were superimposed and merged. The resulted map was compared to other auxiliary data such as multi-temporal optical satellite imagery (i.e. Landsat/ETM, Terra/Aqua MODIS) and thematic land cover maps (i.e. Corinne 2000) in GIS environment. We found that changes are mostly due to both plant growth and man-made activity.

Our ongoing work has a prospect to monitor of land cover changes due to both dielectric and geometric properties by using backscatter intensity and phase. This study shows the potential of SAR in providing complementary information to optical data in land cover dynamics monitoring. SAR images likewise are less sensitive to weather conditions than optical data. In addition, the high temporal resolution of SAR images allows tracking changes with high time accuracy. The large areas cover and high special resolution are advantage to use SAR images for monitoring land cover changes.

9642-8, Session 2

MODIS VCF data (2000 - 2010) for deforestation and forest degradation hotspots detection and its validation with multi-temporal Landsat TM and ALOS PALSAR data

Yan Gao, Jean Francois Mas, Univ. Nacional Autónoma de México (Mexico); Kazuyo Hirose, Japan Space Systems (Japan); Mitsuru Osaki, Hokkaido Univ. (Japan)

In this paper, we assessed time-series MODIS Vegetation Continuous Fields (VCF) percent tree cover (PTC) data with 250 m spatial resolution for detection of vegetation dynamics for Central Kalimantan and validated the results with time series Landsat TM image with 30 m spatial resolution obtained for the years of 2000, 2004, and 2006, and ALOS Phased Array Synthetic Aperture Radar (PALSAR) data with 12.5 m spatial resolution for the year of 2007, 2008, 2009, and 2010. We applied a linear regression model to MODIS PTC data to test the spatial-temporal consistency. For each linear regression, we mapped slope and residual for each pixel to identify the regions where the PTC values are stable, or have a tendency of increasing or decreasing with time. The positive slope value indicates a tendency of increasing in percent tree cover through time, and a negative value indicates a tendency of losing forest cover over time. The residual map shows how well the linear model fits the data. Areas where the residual values are high could indicate that there are noises in the data, abrupt changes or changes that can be associated with a non-linear temporal profile. The calculated slope values are in the range of (-9 - 6). By grouping the slope values into 5 groups of (-9 - -5), (-4 - -1), 0, (1-3), (4-6), clear patterns of distribution of the hotspots of increasing, decreasing, and stable vegetation cover can be detected. We consider that areas with very high or very low slope values are hotspots of extreme vegetation change, either increasing or decreasing. We then extracted the areas with extremes slope values, and tested the tendency of vegetation dynamics with higher spatial resolution of both optical Landsat images and PALSAR data. For this, we extracted areas with slope values in the range of (-5 - -9), (3-6), and 0 and digitized those areas to form shape files of decreasing, increasing, and stable in vegetation dynamics. We then extracted multi-temporal optical and PALSAR data values for the areas indicated by the shape files. The preliminary results indicate that the multi-temporal images with higher spatial resolution have similar tendency as the multi-temporal MODIS PTC image data. This suggests that for the study area in Central Kalimantan, the MODIS percent tree cover data can

potentially be used to identify hotspots of deforestation and forest regeneration, especially those with very clear tendency of vegetation dynamics.

9642-9, Session 2

Canonical Huynen decomposition of radar targets

Dong Li, Yunhua Zhang, Ctr. for Space Science and Applied Research (China)

Polarimetric target decomposition concept was first formalized by Dr. J. R. Huynen in his dissertation. Pioneered by this work, a great deal of decompositions have been devised, which can be partitioned into three broad categories, i.e. the Huynen-type target dichotomies (such as Huynen decomposition, Holm-Barnes decomposition, and Yang decomposition), the eigenvector-based decompositions (such as Cloude decomposition and van Zyl decomposition), as well as the model-based decompositions (such as Freeman-Durden decomposition and Yamaguchi decomposition). These also promote the researches on coherent target decompositions (such as Krogager decomposition, Cameron decomposition, and Touzi decomposition). To classify the terrain by extracting helpful scattering information from polarimetric radar data via target decomposition has become one of the highly focused topics in geoscience and remote sensing research. It plays an important role in monitoring natural disasters like volcano eruption, landslide, earthquake, and tsunami, and inspecting human activity-related environmental changes such as deforestation and wetland degradation.

Although is of theoretical importance, however, Huynen decomposition has not received wide applications. A commonly-recognized reason is the non-uniqueness, because there may theoretically exist infinite target dichotomies if Huynen's restriction on roll-invariance is removed. Nevertheless, in this paper, we do not pay particular attention on such imperfection of Huynen decomposition, because it also exists in other decompositions. Take Cloude decomposition for example, as indicated by Cloude et al. recently, there are infinite ways to decompose a mixed target into the sum of three single targets, but orthogonality restricts the infinity to only Cloude's. Instead, our attention in this paper is paid to the incapability of Huynen decomposition on the analysis of irregular and non-symmetric scatterers. This has been independently validated by Barnes and Holm, Yang et al., and Paladini. Holm and Barnes first found this when they applied Huynen decomposition to decomposing a rotating diplane immersed in polarization noise. It was further validated by Yang et al. on a distributed dihedral scatterer (entropy is 0.08 and alpha angle is 88.93°). Paladini recently conducted the similar experiment on a mixed ship target dominated by even bounce scattering, and concluded that "the Huynen theory about the high-frequency noise nature of the N-target and the specular nature of the signal part is failed in practice for all such cases where a dominant dihedral scattering is observed".

This paper gives a revisitation to Huynen decomposition. Huynen's preference for symmetry and regularity is found to be the main reason that restricts the application of Huynen decomposition. From the physical realizability conditions of polarimetric scattering description, two other target dichotomies are devised, which prefer scattering irregularity and non-symmetry, respectively, and provide two competent supplements to Huynen decomposition. A canonical Huynen dichotomy is then proposed based on an adaptive selection among the two dichotomies and Huynen decomposition to provide us an adaptive extraction of the dominant scattering from mixed scattering. In virtue of a combination strategy, the canonical dichotomy is used in the characterization of mixed random scattering finally. Experiment on the real polarimetric radar data demonstrates its excellent discrimination of radar targets.

9642-10, Session JS2

Implementation of a fast time-domain processor for FMCW Synthetic Aperture Radar data

Max Frioud, Univ. of Zürich (Switzerland); Peter Wellig, Armasuisse (Switzerland); Stephan Stanko, Fraunhofer FHR (Germany); Erich H. Meier, Univ. of Zürich (Switzerland)

The use of Synthetic Aperture Radar (SAR) for the purpose of surveillance has the advantage of being weather-independent and the potential to provide sensitive information relevant to civil or military security. The development of compact millimeter-wave FMCW SAR systems with reduced size, weight and power consumption [1][2] allows these goals to be more safely achieved and at reduced cost, thanks to the use of unmanned light airborne platforms.

For extracting the best information from such systems, the SAR and navigational data need to be specially processed. Generally speaking, SAR processors fall into two classes, namely frequency-domain and time-domain. Frequency-domain processors are computationally the less intensive of the two, but they suffer several drawbacks: (a) they require a motion compensation step that performs ideally only as long as the sensor trajectory does not deviate too much from a straight line, (b) as they treat 2D collections of pixels as a whole, they are very demanding on RAM, and (c) strategies to properly deal with strong variations of the Doppler-Centroid in the range and/or in the azimuth dimensions further increase the demand on RAM and considerably reduce their efficiency.

In order to retain optimal quality also for highly non-linear trajectories as well as fast attitude variation, we developed a Time-Domain processor dedicated to the focusing of airborne FMCW SAR data. It outputs geocoded products in map geometry. The use of digital elevation models and dGPS for precise sensor trajectories contributes to the high focusing quality and geolocation accuracy. Despite the intense computational load, a high efficiency is reached thanks to (a) an efficient focusing algorithm [3], (b) process parallelization on a graphics processing unit using CUDA, (c) efficient partitioning of the dataset, and (d) efficient implementation of computationally heavy operations.

In addition to its robustness and efficiency, the processor already offers high precision relative radiometric calibration, single-look or multi-look processing modes as well as video-like processing.

The performance of the processor was assessed using real SAR data acquired by the Ka-band system MIRANDA35 [4][5][6] during measurement campaigns in Switzerland. Figure 1 presents an example of a SAR image from a curved trajectory, typically well suited for traffic monitoring along highways. Thanks to the radiometric calibration, the image intensity distribution is smooth and has a reduced dynamic range. The far range region in the curve has a poor SNR due to the combination of the platform banking and the use of a fixed antenna. Figure 2 presents the results from a point target analysis applied to the SAR signature of a corner reflector which was deployed on concrete. With resolutions close to the theoretical expectations, it demonstrates high focusing quality. Results from SAR processing efficiency tests are shown in Table 1. With 20 cm pixel spacing an areal processing rate as high as 6 km2/h can be achieved on a single Windows Workstation. Figure 3 is an example of the use of multi-looking for reducing speckle at the cost of reduced azimuth resolution.

9642-11, Session JS2

An object oriented approach to detect earthquake damage in urban area: application to Cosmo SkyMed imagery of L'Aquila earthquake

Roberta Anniballe, Sapienza Univ. di Roma (Italy); Marco

Chini, Luxembourg Institute of Science and Technology (Luxembourg); Nazzareno Pierdicca, Sapienza Univ. di Roma (Italy); Christian Bignami, Salvatore Stramondo, Istituto Nazionale di Geofisica e Vulcanologia (Italy); Fabrizio Noto, METIS S.r.l. (Italy); Tanya Scalia, D'Appolonia Rome (Italy); Antonio Martinelli, Antonio Mannella, CNR Istituto per le Tecnologie della Costruzione (Italy)

In this study we address the problem of the earthquake damage assessment at single building scale from Very High Resolution (VHR) SAR images by using an object oriented change detection technique.

In a VHR SAR image an isolated building is characterized by: a) a bright area corresponding to the backscatter from ground, wall and roof, which are integrated mostly in the same resolution cell (i.e., the layover area); b) a very bright stripe due to the double reflection from the ground to the wall facing the radar; c) the return from the roof; d) a dark shadow. When a building collapses the double bounce and the layover areas drastically decrease brightness. At the same time, an increase of backscattering is due to the presence of debris within the building footprint and to the return coming from the ground previously occluded by the shadow. Understanding these scattering mechanisms helps designing the procedure to recognize fully destroyed buildings. Due to the distinctive shape of these features (often elongated bright regions), a change detector based on a moving square window is less effective than an object oriented image analysis approach.

Based on these considerations a novel procedure is proposed and tested. The segmentation of the pre-event SAR image is performed in order to extract layover and double bounce areas. The mathematical morphology composition of opening and closing operations with different directions and lengths of a linear structural element is used to build a multiscale morphological profile. Then, this profile is used as input space of a K-means classifier to extract the objects. In order to identify the building footprint, other approaches are more effective, as for instance the classification of VHR optical images (Chini et al.) or simply the exploitation of available maps.

Several features can be computed within the objects in order to identify those changed across the earthquake event. In particular, the interferometric complex coherence, the correlation of image intensity and the Kullback-Leibler (KL) divergence are investigated. The first one is a change indicator particularly useful in urban areas, where anthropic structures show themselves coherent in time. Also the correlation of intensity has been also demonstrated to have complementary performances (Stramondo et al.) The KL divergence is a measure of similarity between two probability density functions.

For each changed segment, the mean backscattering value in the pre- and post-event image is computed in order to distinguish between objects characterized by a decreased backscattering from those with a backscattering increase. In the final step of our procedure, the regions of increased and decreased backscatter, associated to shadow and layover/foreshortening of the same building, respectively, are combined taking into account the SAR viewing geometry affecting their relative displacement.

We have tested our procedure using SAR images taken by COSMO-SkyMed in SPOTLIGHT mode before and after the earthquake that hit L'Aquila city (Italy) on April 6, 2009. A layer of polygons reporting the damage ground survey of the whole urban area of L'Aquila is used for validation purposes.

References

S. Stramondo, C. Bignami, M. Chini, N. Pierdicca, and A. Tertulliani, "Satellite radar and optical remote sensing for earthquake damage detection: results from different case studies," International Journal of Remote Sensing 27 (20), 4433–4447 (Oct. 2006).

M.Chini, N. Pierdicca, W. J. Emery, "Exploiting SAR and VHR optical images to quantify damage caused by the 2003 Bam earthquake". IEEE Trans. Geosci. Remote Sens,. 47(1),. 145 – 152 (2009).

9642-12, Session JS2

On the geolocation accuracy of COSMO-SkyMed products

Davide O. Nitti, Raffaele Nutricato, GAP S.r.l. (Italy); Rino Lorusso, Nunzia Lombardi, Agenzia Spaziale Italiana (Italy); Fabio Bovenga, CNR ISSIA (Italy); Maria F. Bruno, Maria T. Chiaradia, Politecnico di Bari (Italy); Giovanni Milillo, Agenzia Spaziale Italiana (Italy)

Many factors impact on the geolocation accuracy of Synthetic Aperture Radar (SAR) products. The improper Atmospheric Path Delay (APD), orbital errors and timing inaccuracies hinder sub-pixel geolocation accuracy, in particular for radar images acquired by the high resolution X-band side-looking SAR satellite constellations, TerraSAR-X (TSX) and COSMO-SkyMED (CSK).

Many scientific studies in the recent literature have demonstrated the suitability of TSX data for sub-decimetre level ranging accuracy without the use of ground control points (GCP, provided APD is properly estimated and corrected for. This is due to the high degree of orbital accuracy of the TSX satellites (the so-called science orbit is in an accuracy range of few centimetres and its very precise radar beam tracing.

On the contrary, no definitive results are reported yet in the scientific literature, concerning the best performances achievable by the CSK constellation in terms of geolocation accuracy. Preliminary studies have shown that sub-metric geolocation accuracies are hardly achievable with CSK data, and that APD compensation leads unexpectedly to a worsening of the results (with geolocation errors amounting even to several meters along the slant range direction). Two possible explanations were suggested: (1) a nominal, undocumented APD correction is incorporated into the CSK delivered timing annotations during sampling window start time (SWST) bias calibration, or (2) no APD correction has been implemented in the CSK delivered data, but the annotated range SWST bias is incorrect by several meters (implying the need for re-calibration). These results are in line with the conclusions of other independent studies.

The aim of the present work is to further invesigate the origin of the geolocation error sources in CSK products. The area surrounding Carlantino town in Daunia region (Southern Italy), has been selected for this study, thanks to the availability of six trihedral corner reflectors (CR) recently installed in the western slope, facing the Occhito lake. The geolocation of CR phase centers is surveyed with cm-level accuracy using differential GPS. A consistent number of CSK HIMAGE stripmap and enhanced spotlight data takes is available over the area of interest.

The experimental analysis includes the evaluation of the geolocation accuracy of both SCS and GTC products. Concerning SCS data, the performances of the official ASI processors are compared to those achievable by alternative promising focusing algorithms, for both stripmap and spotlight modes. APD compensation is performed by using the Regional Atmospheric Modelling System (RAMS), a Numerical Weather Prediction model already reliably used for this purpose in previous. The analysis is also extended to the cross-comparison of I-CUGS GTC products with those generated by internal geocoding tools.

--ACKNOWLEDGMENTS-- Project carried out using CSK® Products, © of the Italian Space Agency(ASI), delivered under a license to use by ASI.

9642-13, Session JS2

Visual analytics for semantic queries of TerraSAR-X image content

Daniela Espinoza-Molina, Kevin Alonso, Mihai P. Datcu, Deutsches Zentrum für Luft- und Raumfahrt e.V. (Germany)

With the continuous acquisition of satellite missions, the size of the image archives is considerably increasing every day as well as the variety and complexity of their content, surpassing the end-user capacity to analyze and to exploit them. Advances in the image retrieval field have contributed to the elaboration of tools for interactive exploration and extraction of the images from huge archives using different parameters like metadata, key words, and basic image descriptors. Even though we count on more powerful tools for automated image retrieval and data analysis, we still face the problem of understanding and analyzing the results. Thus, a systematic computational analysis of these results is required in order to provide to the end-user a summary of the archive content in comprehensible terms. In this context, visual analytics combines automated analysis with interactive visualizations analysis techniques for an effective understanding, reasoning and decision making on the basis of very large and complex datasets. Moreover, currently several researches are focused on associating the content of the images with semantic definitions for describing the data in a format to be easily understood by the end-user. In this paper, we present our approach for computing visual analytics and semantically querying the TerraSAR-X archive. Our approach is mainly composed of four steps: 1) the generation of a data model that explains the information contained in a TerraSAR-X product. The model is formed by primitive descriptors and metadata entries, 2) the storage of this model in a database system, 3) the semantic definition of the image content based on machine learning algorithms and relevance feedback, and 4) querying the image archive using semantic descriptors as query parameters and computing the statistical analysis of the query results. The experimental results shows that with the help of visual analytics and semantic definitions we are able to explain the image content using semantic terms and the relations between them answering questions such as what is the percentage of urban area in a region? or what is the distribution of water bodies in a city?

9642-15, Session 3

Detection of land subsidence at natural gas extraction sites using Persistent Scatterer Interferometry

Andre C. Kalia, Michaela Frei, Thomas Lege, Bundesanstalt für Geowissenschaften und Rohstoffe (Germany)

Natural gas extraction leads to a decrease in reservoir pressure which can cause land subsidence. This process can cause damage to buildings, infrastructure and may affect ecosystems by influencing the hydrogeological setting. Area-wide detection of this land subsidence is an important information for comprehensive geoscientific understanding of gas extraction impacts on the land surface and in time hazard mitigation. Using conventional measurement techniques (GNSS-, levelling-campaigns) remains a challenge due to limitations in spatial coverage and temporal resolution. Advanced multitemporal remote sensing techniques, e.g. Persistent Scatterer Interferometry (PSI), allows the detection of surface movements with large spatial coverage and high temporal resolution. The intention of this presentation is the illustration of the information content of PSI results and its benefits with respect to an optimized hazard mitigation approach.

Several studies, e.g. ESA´s Terrafirma project, demonstrated the capability of the PSI technique for the detection of surface movements and have proven the application potential. In order to assist the utilization of this technique for governmental tasks a national service-concept within the EU-ESA Program Copernicus is being prepared at the Federal Institute for Geosciences and Natural Resources (BGR), Germany. In collaboration with the State Authority for Mining, Energy and Geology (LBEG) a pilot study focusing on the application of the PSI technique for the detection of land subsidence at natural gas extraction sites is performed. The area of interest has a size of 15,730 km?, is located in the state of Lower Saxony and covers several natural gas extraction sites. The large extent of the area of interest requires robust algorithms for PS selection, network construction and inversion as well as atmospheric phase removal.

PSI processing is based on six partly overlapping stacks each with more than 60 ERS-1/2 scenes, covering the timespan from 1992 – 2000. The processing chain is characterized as being highly automated and capable of processing high quantity of data from neighboring acquisition tracks. Mean velocities, cumulated displacements, displacement time-series and superposition with existing geoscientific data (geological map, estimated zone of gas extraction caused influence, location of wells) are presented. Results show that land subsidence is concentrated at several gas extraction sites. This presentation highlights the usability of area-wide subsidence detection for optimized hazard mitigation. In the future, Sentinel-1 based PSI results seem to be a promising basic product within the context of a national Copernicus service for surface movement detection and monitoring since a good cost-benefit ratio is expected.

9642-16, Session 3

Sparsity-driven autofocus for multipass SAR tomography

Fiona Muirhead, Bernard Mulgrew, Iain H. Woodhouse, The Univ. of Edinburgh (United Kingdom); David Greig, Selex ES (United Kingdom)

Synthetic aperture radar (SAR) systems produce high resolution, 2-dimensional imaging of areas of interest. SAR tomography enables these techniques to extend to 3-dimensional imaging by producing aperture synthesis from multi-pass SAR data usually obtained by non-uniformly spaced acquisitions. Previous research has shown that compressive sensing approaches can be applied to reconstruct height distributions while reducing the number of SAR images required. This technique requires accurate phase information over multiple images. The data is extremely sensitive to deviations from the reference track; therefore, to enable tomography an accurate autofocus solution is required even after motion compensation has been carried out.

This paper investigates phase errors resulting from navigational uncertainties in multi-pass spotlight SAR imaging and uses the field of compressive sensing to achieve an autofocus solution. The proposed algorithm extends methods used by [1] to the multi-pass case and jointly recovers phase errors for all images. This is unlike conventional autofocus, which just works on an image-by-image basis. The tools of compressive sensing can be used to concurrently select pixels for bright image elements that are stable and coherent over all images, as these pixels are sparse in the image domain, and calculate the phase errors present in each pass. An Iterative Hard Thresholding technique as described in [2] is used for image construction, using a Fourier model, and phase error estimation. This algorithm differs from [1] in that it uses a complete phase history for phase error correction and determines the phase error for multiple images simultaneously. Contrary to conventional autofocus techniques such as phase gradient autofocus this algorithm can correct phase errors during image formation.

The performance of the algorithm is examined through numerical simulations and applications to real data. To analyse the effectiveness of the proposed algorithm we first consider simulated SAR data consisting of a small number of point targets with added Gaussian noise imaged over ten passes. Quadratic phase errors are applied to mimic platform navigational errors. The new algorithm is also applied to real data collected from Selex ES's airborne, X-band, experimental SAR system. A total of seven passes for a site of environmental interest was imaged. A reduction in sidelobes demonstrates that the algorithm effectively achieves an autofocus solution. The Muller Buffington sharpness metric [3] shows an increase in image sharpness after the multi-pass compressive sensing autofocus solution has been applied.

A computational comparison between this autofocus method and others such as phase gradient autofocus will be given. Additionally an approach to registration will be addressed as

this also plays a role in accounting for phase errors present between passes.

[1] Kelly, Shaun I., Mehrdad Yaghoobi, and Mike E. Davies. "Auto-focus for compressively sampled SAR." 1st International Workshop on Compressed Sensing Applied to Radar. 2012.

[2] Blumensath, Thomas, and Mike E. Davies. "Iterative hard thresholding for compressed sensing." Applied and Computational Harmonic Analysis 27.3 (2009): 265-274.

[3] Muller, Richard A., and Andrew Buffington. "Real-time correction of atmospherically degraded telescope images through image sharpening." JOSA 64.9 (1974): 1200-1210.

9642-17, Session 3

An integrated remote sensing approach for landslide susceptibly mapping at the volcanic islands of Vulcano and Lipari (Eolian Island, Italy)

Maria Marsella, Silvia Scifoni, Sapienza Univ. di Roma (Italy); José A. Palenzuela Baena, Univ. de Granada (Spain); Susi Pepe, Eugenio Sansosti, Giuseppe Solaro, Piero Tizzani, Istituto per il Rilevamento Elettromagnetico dell'Ambiente (Italy)

Volcanic Island can be affected by instability phenomena such as landslide and partial collapse events also in quiescent period.

Starting from the evaluation of the effects of critical historical instability events and from the analysis of morphological, geological and monitoring data (from in-situ, aerial and satellite techniques), a classification of areas potentially affected by debris avalanches/flows and rock falls can be carried out. The activity started from consolidated methodologies (aerial laser scanning and digital photogrammetry) for the acquisition of accurate (cm-level accuracy) topographical data. The collected data was used to detect and map the morphological features and the discontinuities useful to evaluate the geometry of the potential deep-seated failure. These data were integrated with Differential Synthetic Aperture Radar Interferometry (DinSAR) data to identify the on-going deformation processes.

The analysis was focused on the Aeolian island in particular on the active volcanic edifice of Vulcano island (La Fossa Cone and La Forgia Vecchia) and some areas of Lipari island.

A dataset formed by digital terrain models (from Airborne Laser Scanning, Terrestrial Laser Scanning and Aerial Photogrammetry) and DinSAR time series was collected and analysed in a GIS environment, with the aim to obtain useful information for a preliminary hazard map compilation. The DinSAR data was obtained applying the Small BAseline Subsets (SBAS) approach to COSMO SkyMed data both from ascending and descending orbits, generating time series of displacements extending from 2009 to 2013. Furthermore, combining ascending and descending data, the vertical and horizontal components of the deformation velocity were extracted.

The geometrical and DinSAR data were combined with the geo-engineering information in order to implement a preliminary stability analysis. Numerical models were adopted to define the areas that may be potentially interested by the instability phenomena.

The results of the study, allowed a better comprehension of the potential instability processes on Vulcano and Lipari island, contributing to the evaluation of the vulnerability of the different areas and providing insights on the improvement of the monitoring system on the implementation of mitigation actions.

9642-18, Session 3

The PSIG procedure to Persistent Scatterer Interferometry (PSI) using X-band and C-band Sentinel-1 data

María Cuevas-González, Núria Devanthéry, Michele Crosetto, Oriol Monserrat, Ctr. Tecnològic de Telecomunicacions de Catalunya (Spain); Bruno Crippa, Univ. degli Studi di Milano (Italy)

A new approach to Persistent Scatterer Interferometry (PSI) data processing and analysis implemented in the PSI chain of the Geomatics (PSIG) Division of CTTC is described. The performance of the PSIG procedure will be illustrated using X-band data and C-band Sentinel-1 data and the results will be shown.

A stack of N co-registered SAR images, the amplitude dispersion (DA) and M wrapped interferograms, with M>>N, are the main inputs of the PSIG. The PSIG chain is composed of three main processing blocks. In the first block, correctly unwrapped and temporally ordered phases are derived for Persistent Scatterers (PSs) that homogeneously cover the area of interest. In fact, a set of Cousin PSs (CPSs), which are PSs characterized by a moderate spatial phase variation that ensures a correct phase unwrapping, are exploited. Flexible tools are employed in this block to check the consistency of phase unwrapping and guarantee a uniform CPS coverage. The second block is dedicated to estimate the atmospheric phase screen (APS) by exploiting the phases estimated in the first block. Finally, the deformation velocity and time series of deformation of the selected CPSs are derived in the third block. A new 2+1D phase unwrapping algorithm is exploited in this final stage of the PSIG procedure.

The main PSIG processing steps are as follows: (1) Candidate Cousin PS (CPS) selection. A set of PSs with phases characterized by a moderate spatial variation is sought in this step, in which at least a seed PS is required to initiate a search for its "cousins", i.e. PSs with similar characteristics; (2) 2D phase unwrapping. 2D phase unwrapping is performed on the candidate CPSs using a redundant set of M interferograms; (3) Phase unwrapping consistency check. This check is based on a least squares estimation followed by the analysis of the so-called residuals. The final set of CPSs is selected at this stage; (4) APS estimation and removal. The APS is estimated using the selected CPSs and subsequently removed from the original interferograms, thus obtaining a set of M APS-free interferograms; (5) Estimation of deformation velocity and residual topographic error (RTE). The M wrapped APS-free interferograms are used to estimate the deformation velocity and RTE over a dense set of PSs (much denser than the selected CPSs) using the method of the periodogram. Optionally, an extension of the two-parameter model can be used to account for the thermal expansion; (6) RTE removal. The RTE phase component is removed from the wrapped APS-free interferograms. The linear deformation component can optionally also be removed and then, in a later stage, added back to the deformation time series. The same procedure can be applied to the thermal expansion component; and (7) 2+1D phase unwrapping. A 2+1D phase unwrapping is performed on the set of M APS- and RTE-free interferograms in order to obtain the final deformation phase time series, a quality index for each time series and other parameters related to the detection and correction of unwrapping errors.

9642-20, Session 4

Multitemporal SAR interferometry for landslide analysis: requirements and prospects from recent satellite missions

Fabio Bovenga, Alberto Refice, Guido Pasquariello, CNR ISSIA (Italy); Raffaele Nutricato, Davide O. Nitti, GAP S.r.l. (Italy); Janusz Wasowski, Consiglio Nazionale delle Ricerche (Italy)

Thanks to the all-weather, day-night capability to detect and measure small ground surface deformations, multi-temporal Synthetic Aperture Radar (SAR) Interferometry (InSAR) techniques are attractive for landslide investigations.

This Multi-temporal InSAR (MTI) application poses challenges related to the limited spatial extent of the phenomenon, the complexity of the ground deformations, and the occurrence in mountainous and vegetated areas that cause visibility problems. Nowadays, several satellite missions are available providing interferometric SAR data at different wavelengths, spatial resolutions, and revisit time.

High-resolution X-Band SAR sensors, such as the COSMO-SkyMed constellation, have recently provided data with spatial resolution reaching metric values, and revisit time up to few days leading to increase the density of the measurable targets as well as to improve the detection of non linear movement. Medium resolution C-band SAR data have been thoroughly exploited in the last two decades thanks to the ERS-1/2 and ENVISAT-ASAR missions. A new interesting opportunity is recently provided by Sentinel-1 mission, which has just started to deliver data to the user community. Although the spatial resolution is comparable to previous ESA C-band missions the revisit time is reduced to 12 and 6 days, by considering, respectively, one or two satellites.

It is envisioned that by offering regular globe-scale coverage, improved temporal resolution and freely available imagery, Sentinel-1 will guarantee an increasing use of MTI in landslide investigations. These background missions are necessary for long-term, systematic mapping of unstable unstable slopes and regional scale assessment of landslide processes.

According to these different SAR space-borne missions, the present work discusses current and future opportunities of MTI applications to slope instability monitoring. Issues related to slope visibility, sensitivity to ground displacement, modeling of slope instability process, coherent target detection, mean velocity precision, and MTI processing will be addressed through a simple theoretical model supported by numerical simulations. In particular a comparative analysis will be carried out aimed at address specific advantages of different satellite missions with respect to slope instability investigations.

Examples of multi-sensor and multi-scale slope instability investigations are also presented coming from processing both C-band medium resolution and X-band high resolution SAR data.

-- ACKNOWLEDGMENTS--

Work supported by the project “APULIA SPACE” (PON03PE_00067_6), PON Ricerca e competitività 2007-2013.

-- REFERENCES--

[1] F. Bovenga, J. Wasowski, D.O. Nitti, R. Nutricato, M.T. Chiaradia, “Using COSMO/SkyMed X-band and ENVISAT C-band SAR interferometry for landslides analysis”, Remote Sensing of Environment, Volume 119, 16 April 2012, Pages 272-285, 10.1016/j.rse.2011.12.013.

[2] Wasowski J., Bovenga F. 2014a. “Investigating landslides and unstable slopes with satellite Multi Temporal Interferometry: Current issues and future perspectives”. Engineering Geology 174: 103–138.

9642-21, Session 4

Advanced DInSAR analysis for building damage assessment in large urban areas: an application to the city of Roma, Italy

Maria Marsella, Peppe J. V. D’Aranno, Silvia Scifoni, Marianna Scutti, Alberico Sonnessa, Sapienza Univ. di Roma (Italy); Stefania Arangio, Stronger S.r.l. (Italy); Manuela Bonano, Istituto per il Rilevamento Elettromagnetico dell’Ambiente (Italy)

Remote sensing data play an important role for the environmental monitoring because they allow to provide systematic information on very large areas and for a long period of time. Such information must be analyzed, validated and incorporated into proper modeling tools in order to become useful for performing risk assessment analysis. These approachs has been already applied in the field of natural hazard evaluation (i.e. for monitoring seismic, volcanic areas and landslides). However, not enough attention has been devoted to the development of validated methods for implementing quantitative analysis on civil structures.

Therefore, in this work a downstream service was presented to provide reliable information satisfying the requirement for civil engineering applications.

More specifically, the Differential Synthetic Aperture Radar Interferometry (DInSAR) technology, applied to an archive of satellite data that covering several years of observations (from 1992) allows to analyze the evolution of the deformation of structures and infrastructures, by providing information useful to the quantitative assessment of critical phenomena and contributing to the definition of the risk associated. Currently, the availability of high-resolution images from the Cosmo Sky-Med constellation, developed by the Italian Space Agency (ASI), provides new perspectives in terms of spatial and temporal resolution for monitoring sensible areas such as the historical center of large town. In the historical centers of large cities with high urbanization, the historical buildings and monuments are subject to various factors that cause deterioration of structures with different degrees of damage (cracking, sagging, etc..) up to irreversible situations. In addition, this technology can be applied to monitor also recent structures in urban areas affected by ground settlements and large infrastructure (roads, bridges, railways).

This work is dedicated to the comprehensive utilization of ERS / ENVISAT data store ESA SAR used to detect deformation trends and perform back-analysis of the investigated structures useful to calibrate the damage assessment models. After this preliminary analysis, SAR data of the new satellite mission (ie Cosmo SkyMed) were adopted to monitor the evolution of existent surface deformation processes and to detect new occurrence. The specific objective was to set up a data processing and data analysis chain tailored on a service that sustains the safe maintenance of the built-up environment, including critical construction such as public (schools, hospital, etc), strategic (dam, highways, etc) and also the cultural heritage sites.

We focused on the Torrino area, in the south-eastern sector of Roma, where independent studies had already revealed that significant deformation signals were present, testified by the serious damages which have affected many buildings in the area.

The analysis of this area has provided three different levels and sub-levels of products from metropolitan area scale (territorial analysis), settlement scale (aggregated analysis) to single structure scale (damage degree associated to the structure).

9642-22, Session 4

Interferometric SAR imaging by transmitting stepped frequency chaotic noise signals

Yunhua Zhang, Xiang Gu, Wenshuai Zhai, Xiao Dong, Xiaojin Shi, Xueyan Kang, Ctr. for Space Science and Applied Research (China)

Noise radars have been applied in many fields since they were proposed more than 50 years ago, such as SAR/ISAR imaging, surveillance, tracking, collision warning, through-wall imaging, foliage penetration imaging, and so on. This is because noise radars transmit random, noise-like, and uncorrelated waveforms, they are of low probability of detection (LPD) / low probability of interception (LPI) characteristics as well as are immune to deceiving interference. We have developed an experimental noise radar system at Ka band with 4GHz bandwidth by using stepped-frequency noise signal and high-resolution imaging experiments have been conducted.

However, noise radars have not been applied for interferometric SAR imaging yet as far as we know. This paper introduces our recent work on interferometric noise radar. An interferometric SAR system was developed which can transmit both chirp signal and chaotic noise signal (CNS) with stepped carrier frequencies. An airborne experiment with this system by transmitting both signals was carried out, and the data were processed to show the capability of interferometric SAR imaging with CNS. The interferometric images of different carrier frequencies agree with each other very well. The results shows that although the interferometric phase quality of CNS is degraded due to the SNR is lower compared with that of chirp signal, we still can get satisfied DEM after multi-looking processing. By using multi-carrier frequencies, the quality of interferometric phase can be remarkably improved.

Another work of this paper is to apply compressive sensing (CS) theory to the interferometric SAR imaging with CNS. CS theory was emerged nearly ten years ago, which has been extensively applied to almost all aspects of radars since then. This theory states that if a signal is sparse, then it can be accurately reconstructed with much less sampled data than that regularly required according to Nyquist Sampling Theory. One of the major key steps of CS reconstruction of sparse signal is to form the sensing matrix. There are mainly three random matrices which can act as a sensing matrix, i.e. random matrix, deterministic matrix and structured random matrix, among them the third one is of much better property. To form a structured random matrix, if the transmitted signal is of fixed waveform, then random sampling is needed. However, if the transmitted signal is of random waveform, then only uniform subsampling is needed. It is to say, when random noise signal is used for transmitted signal, if CS is applied to reconstruct sparse signals, the sampling process can be greatly simplified. This is another advantage of noise signal.

Both interferometric phase images and DEMs by regular method and by CS method are processed with results compared. It is shown that the degradation of interferometric phases due to subsampling is larger than that of amplitude image.

9643-6, Session 1

Bulk processing of the Landsat MSS/TM/ETM+ archive of the European Space Agency

Ferran Gascon, Roberto Biasutti, European Space Agency (Italy); R. Ferrara, Advanced Computer Systems s.P.a. (Italy); Peggy Fischer, European Space Agency (Italy); Luca Galli, Advanced Computer Systems S.p.A. (Italy); Bianca Hoersch, European Space Agency (Italy); Samantha Lavender, Telespazio Vega UK (United Kingdom); Marco Meloni, Serco SpA (Italy); Sergio Mica, Advanced Computer Systems S.p.A. (Italy); Amy Northrop, Telespazio Vega UK (United Kingdom); Alessandra Paciucci, Serco SpA (Italy); Sébastien Saunier, Magellium (France)

Landsat is a joint USGS and NASA space program for Earth Observation, which represents the world's longest running system of satellites for moderate-resolution.

The European Space Agency (ESA) has acquired Landsat data over Europe during the last 40 years starting with Landsat-1 satellite.

A new ESA Landsat Multi-Spectral Scanner (MSS), Thematic Mapper (TM) and Enhanced Thematic Mapper Plus (ETM+) processor has been developed. This enhanced processor aligns historical Landsat products to the highest quality standards that can be achieved with the current knowledge of the instruments. The updated processor is mainly based on the USGS algorithm; however it has some different features that are detailed in this paper.

Using this upgraded processor, ESA is currently performing for the first time a bulk-processing of its entire Landsat series MSS/TM/ETM+ historical consolidated archives to make all products available to users. One of the most important improvements was the usage of the full acquisition contact information and processes it in one unique flow: this allowed processing many scenes for the first time making benefit of the adjacent ones. Quality pre-analysis of the raw data, metadata enrichment, new corrections, accurate systematic quality control after production allowed to introduce many improvement in respect a processing chain consolidated since more than 15 years.

Current achievements include the processing and online distribution of approximately 700,000 new TM/ETM+ high-quality products from Kiruna (S), Maspalomas (E) and Matera (I) archives (including from the Fucino (I), Neustrelitz (D), O'Higgins (Antarctica), Malindi (Kenya), Libreville (Gabon) and Bishkek (Kyrgyzstan) ground stations) between 1983 and 2011. The products are available for immediate download to the users through a very fast and simple dissemination service (at: https://landsat-ds.eo.esa.int/app/) and through ESA's browsing systems. The remaining of the ESA's Landsat data, dating back more than 40 years, will gradually become available during 2015.

The ESA Landsat processor algorithm enhancement, together with the results of the ESA archive bulk-processing data regarding production, quality control and data validation are herein presented.

9643-7, Session 1

Star-based defocus computing technique for PLEIADES-HR satellites

Virginie Amberg, Ctr. National d'Études Spatiales (France); Laurent Bernard, Magellium (France); Christophe Latry, Ctr. National d'Études Spatiales (France)

This paper deals with the problem of MTF (Modulation Transfer Function) and focus measurement of earth-observing optical satellites. This operation is mandatory for refocusing the telescope. Thanks to the high steering ability of satellites such as PLEIADES-HR satellites, it is now possible to observe stars. Assuming that this celestial object is a punctual object, it is possible to access directly the point spread function of the instrument from a star acquisition. The advantages of stars acquisitions are that firstly, all acquisitions are exploitable (no weather constraints) and secondly, they can be acquired during the night side of orbits avoiding any conflict with the operational mission on the sunny side.

Stars can be also exploited to compute the defocus of the telescope. During the commissioning period of PLEIADES-HR satellites, such a method has been developed. This latter exploits further images of stars acquired with differential defocus of the telescope. More precisely, given several images of stars whose relative focus is known, the minimization of residuals in the least squares equation with regard to the mean focus provides the best focus point with a great accuracy. This method was based on the hypothesis that the defocus consists in a low-pass filter defined by the Steel approximation to be multiplied by the MTF in the Fourier transform domain.

This method presents three disadvantages. Firstly the telescope focus course must be sufficiently dimensioned in order to be able to focus the telescope on both sides of the focus position to infinity. Secondly, a high number of defocus (typically 8) and of star images (about 8 images per defocus) are necessary to assure the high accuracy of the focus measurement. Given that the PLEIADES-HR focus system is a thermal system, it takes time to change the focus between each defocus position. Thus this calibration operation takes 8 orbits period during which the telescope is not well-focused, also on the sunny side of the orbits where operational images are acquired. Thirdly, the defocus modelling is not adapted in presence of optical aberrations.

In this article, significant evolutions are proposed in order to relieve those disadvantages. We consider the problem as a phase diversity inverse problem: using only a couple of images with known differential defocus and a decomposition of optical aberrations on a finite set of Zernike polynomials, it is possible to identify these aberrations including defocus. This modelling allows taking into account not only the defocus effect on MTF but also the whole set of optical aberrations effects on MTF. It is more accurate than the Steel approximation. This new method has been tested on real PLEIADES-HR images and the results have been compared with the previous method. It has been proved that thanks to this accurate modelling of PSF, it is not necessary to acquire images from both sides of the focus position to infinity and that it is possible to greatly reduce the number of defocus. Finally, we retrieve not only the best focus but also the whole set of optical aberrations.

9643-8, Session 1

ScaRaB: first results of absolute and cross calibration

Thierry L. Trémas, Ctr. National d'Études Spatiales (France); Ouahid Aznay, CS Systèmes d'information (France); Michel Dejus, Ctr. National d'Études Spatiales (France); Olivier Chomette, Lab. de Météorologie Dynamique (France)

ScaRaB (SCAnner for RAdiation Budget) is the name of three radiometers whose two first flight models have been launched in 1994 and 1997. The instruments were mounted on-board Russian satellites, METEOR and RESURS. On October 12th 2011, a last model has been launched from the Indian site of

Sriharikota. ScaRaB is a passenger of MEGHA-TROPIQUES, an Indo-French joint Satellite Mission for studying the water cycle and energy exchanges in the tropics. ScaRaB is composed of four parallel and independent channels. Channel-2 and channel-3 are considered as the main ones. Channel-1 is dedicated to measure solar radiance (0.5 to 0.7 ?m) while channel-4 (10 to 13 ?m) is an infrared window. The absolute calibration of ScaRab is assured by internal calibration sources (black bodies and a lamp for channel-1). However, during the commissioning phase, the lamp used for the absolute calibration of channel-1 revealed to be inaccurate. We propose here an alternative calibration method based on terrestrial targets. Due to the spectral range of channel-1, only calibration over desert sites (temporal monitoring) and clouds (cross band) is suitable.

Desert sites have been widely used for sensor calibration since they have a stable spectral response over time. Because of their high reflectances, the atmospheric effect on the upward radiance is relatively minimal. In addition, they are spatially uniform. Their temporal instability without atmospheric correction has been determined to be less than 1-2 % over a year. Very-high-altitude (10 km) bright clouds are good validation targets in the visible and near-infrared spectra because of their high spectrally consistent reflectance. If the clouds are very high, there is no need to correct aerosol scattering and water vapor absorption as both aerosol and water vapor are distributed near the surface. Only Rayleigh scattering and ozone absorption need to be considered. This method has been found to give a 4 % uncertainty.

Radiometric cross calibration of Earth observation sensors is a crucial need to guarantee or quantify the consistency of measurements from different sensors. ScaRaB is compatible with CERES mission. Two main spectral bands are measured by the radiometer: A short-wave channel (0.2 to 4 μm) dedicated to solar fluxes and a Total channel (0.2 to 200 μm) for fluxes combining the infrared earth radiance and the albedo. The earth long-wave radiance is isolated by subtracting the short-wave channel to the Total channel.

Both Earth Radiation Budget missions (CERES and ScaRaB) have the same specification: to provide an accuracy of ~1 % in the measurement of short-wave and long-wave radiances and an estimation of the short-wave and long-wave fluxes less than 10 W/m2. We use the CERES PAPS and Cross-Track SSF datasets for direct radiances and fluxes comparisons during two validation phases. The first one occurred during April 17th to June 8th (51 days) in 2012 and the second one is scheduled between March 22th and May 31st 2015. The first validation campaign has been held with the CERES team using the Terra FM2 data. The CERES PAPS mode was used to align the swath scan, in order to increase the collocated pixels between the two instruments. This campaign allows us to validate the ScaRaB radiances and to refine the error budget. The second validation campaign aims to provide a temporal monitoring of ScaRab calibration.

9643-9, Session 1

End-to-end performance analysis using engineering confidence models and a ground processor prototype

Klaus Kruse, Maximilian Sauer, Thomas Jäger, Airbus Defence and Space (Germany); Alexandra Herzog, Airbus Defence & Space (Germany); Michael Schmitt, Markus Huchler, Airbus Defence and Space (Germany); Kotska Wallace, Michael Eisinger, Arnaud Heliere, Alain Lefebvre, European Space Agency (Netherlands); Mat Maher, Mark Chang, Traqcy Phillips, Steve Knight, Surrey Satellite Technology Ltd. (United Kingdom); Bryan T. G. de Goeij, Frits van der Knaap, Adriaan Van't Hof, TNO (Netherlands)

The European Space Agency (ESA) and the Japan Aerospace Exploration Agency (JAXA) are co-operating to develop the EarthCARE satellite mission with the fundamental objective of improving the understanding of the processes involving clouds, aerosols and radiation in the Earth's atmosphere.

A Cloud Profiling RADAR (CPR), an Atmospheric LIDAR (ATLID), a Broadband Radiometer (BBR) and a Multi-Spectral Imager (MSI), the last being the subject of this paper, constitute the payload complement of the EarthCARE satellite. By acquiring images of the clouds and aerosol distribution, the MSI instrument will provide important contextual information in support of the RADAR and LIDAR data processing.

The EarthCARE MSI is relatively compact for a space borne imager. As a consequence, the immediate point-spread function (PSF) of the instrument will be mainly determined by the diffraction caused by the relatively small optical aperture. In order to still achieve a high contrast image, de-convolution processing is applied to remove the impact of diffraction on the PSF. A Lucy-Richardson algorithm has been chosen for this purpose.

The correction efficiency of an iterative de-convolution algorithm depends on several performance aspects of the raw data, such as signal-to-noise ratio, spatial sampling frequency and additional variations of the point-spread function due to stray light, motion blur etc. The radiometric quality of the product may also be affected due to de-convolution of noise and processing artefacts at the edges of the field-of-view.

The overall impact of the de-convolution is not trivial to assess in an analytical manner. Therefore we have devised an end-to-end test of the instrument and processor performance:

- SSTL and TNO have assembled and tested engineering confidence models (ECM) of the thermal infrared (TIR) and visible, near infrared & short-wave infrared (VNS) cameras of the MSI respectively.

- Airbus DS has used a prototype implementation of the EarthCARE ground processor (ECGP) to process selected test data sets from the ECM characterization campaigns.

The Level 1 data sets generated in this way are representative for the end-to-end chain including the flight hardware and the operational processor, and provide a direct measure of the geometrical and radiometric (SNR, MTF) performance that will be achieved. This paper will describe the system setup and the necessary data pre-processing and post-processing steps applied in order to compare the end-to-end image quality with the L1b performance required by the science community.

9643-1, Session 2

Sentinel-2 geometric image quality commissioning: first results

Florie Languille, Cécile Dechoz, Angélique Gaudel, Daniel Greslou, Françoise de Lussy, Thierry Trémas, Ctr. National d'Études Spatiales (France); Claudia Isola, Philippe Martimort, European Space Research and Technology Ctr. (Netherlands); Vincent Poulain, Thales Services (France)

In the frame of the Copernicus program of the European Comission, Sentinel-2 will offer multispectral high-spatial-resolution optical images over global terrestrial surfaces. In cooperation with ESA, the Centre National d'Etudes Spatiales (CNES) is in charge of the image quality of the project, and will so ensure the CAL/VAL commissioning phase during the months following the launch.

Sentinel-2 is a constellation of 2 satellites on a polar sun-synchronous orbit with a revisit time of 5 days (with both satellites), a high field of view - 290km, 13 spectral bands in visible and shortwave infrared, and high spatial resolution - 10m, 20m and60m. The Sentinel-2 mission offers a global coverage over terrestrial surfaces. The satellites acquire systematically terrestrial surfaces under the same viewing conditions in order to have temporal images stacks. The first satellite will be launched in June 2015. Following the launch, the CAL/VAL commissioning phase will then last during 6 months for geometrical calibration.

This paper first provides explanations about Sentinel-2

products delivered with geometric corrections. Then this paper details calibration sites, and the methods used for geometrical parameters calibration and presents the first linked results. The following topics are presented: viewing frames orientation assessment, focal plane mapping for all spectral bands, first results on geolocation assessment, and multispectral registration. There is a systematic images recalibration over a same reference which will be a set of S2 images produced during the 6 months of CAL/VAL. As it takes time to have all needed images, the geolocation performance with ground control points and the multitemporal performance are only first results and will be improved during the last phase of the CAL/VAL. So this paper mainly shows the system performances, the preliminary product performances and the way to perform them.

9643-2, Session 2

MACCS : Multi-Mission Atmospheric Correction and Cloud Screening tool for high-frequency revisit data processing

Beatrice Petrucci, Mireille Huc, Ctr. National d'Études Spatiales (France); Thomas Feuvrier, Caroline Ruffel, CS Systèmes d'information (France); Olivier Hagolle, Vincent Lonjou, Camille Desjardins, Ctr. National d'Études Spatiales (France)

For the production of Level2A products during Sentinel-2 commissioning in the Technical Expertise Center Sentinel-2 in CNES, CESBIO proposed to adapt the Venus Level-2 and 3 processor, taking advantage of the similarities between the two missions: image acquisition at high frequency (2 days for Venus, 5 days with the two Sentinel-2), high resolution (5m for Venus, 10, 20 and 60m for Sentinel-2), images acquisition under constant viewing conditions.

The Multi-Mission Atmospheric Correction and Cloud Screening (MACCS) tool was born: based on CNES Orfeo Toolbox Library, Venus processor which was already able to process Formosat2 and VENμS data, was adapted to process Sentinel-2 and Landsat5-7 data; since then, a great effort has been made reviewing MACCS software architecture in order to ease the add-on of new missions that have also the peculiarity of acquiring images at high resolution, high revisit and under constant viewing angles, such as Spot4/Take5 and Landsat8.

The recursive and multi-temporal algorithm is implemented in a core that is the same for all the sensors and that combines several processing steps: estimation of cloud cover, cloud shadow, water, snow and shadows masks, of water vapor content, aerosol optical thickness, atmospheric correction. This core is accessed via a number of plug-ins where the specificity of the sensor and of the user project are taken into account: products format, algorithmic processing chaining and parameters.

After a presentation of MACCS architecture and functionalities, the paper will give an overview of the production facilities integrating MACCS and the associated specifities: the interest for this tool has grown worldwide and MACCS will be used for extensive production within the THEIA land data center and Agri-S2 project.

Finally the paper will zoom on the use of MACCS during Sentinel-2 In Orbit Test phase showing, if already available, the first Level-2A products.

9643-3, Session 2

The ground prototype processor: Level-1 production during Sentinel-2 in-orbit acceptance

Beatrice Petrucci, Cécile Dechoz, Sophie Lachérade, Céline L'Helguen, Ctr. National d'Études Spatiales (France); Cécile Picard, Thales Services (France); Jean-Louis Raynaud, Julien Nosavan, Ctr. National d'Études Spatiales (France); Amandine Rolland, Thales Services (France); Thierry L. Trémas, Ctr. National d'Études Spatiales (France); Claudia Isola, Philippe Martimort, François Spoto, European Space Research and Technology Ctr. (Netherlands)

Jointly with the European Commission, the Sentinel-2 earth observation optical mission is developed by the European Space Agency (ESA).

Relying on a constellation of satellites put in orbit starting mid-2015, Sentinel-2 will be devoted to the monitoring of land and coastal areas worldwide thanks to an imagery at high revisit (5 days with two satellites), high resolution (10m, 20m and 60m) with large swath (290km), and multi-spectral imagery (13 bands in visible and shortwave infra-red).

In this framework, the French Space Agency (CNES: Centre National d'Etudes Spatiales) supports ESA on the activities related to Image Quality, defining the image products and prototyping the processing techniques.

Scope of this paper is to present the Ground Prototype Processor (GPP) that will be in charge of Level-1 production during Sentinel-2 In Orbit Acceptance phase.

GPP has been developed by a European industrial consortium composed of Advanced Computer Systems (ACS), Magellium and DLR on the basis of CNES technical specification of Sentinel-2 data processing and under the joint management of ESA-ESTEC and CNES.

It will assure the generation of the products used for Calibration and Validation activities and it will provide the reference data for Sentinel-2 Payload Data Ground Segment Validation.

At first, Sentinel-2 end-users products definition is recalled with the associated radiometric and geometric performances; secondly the methods implemented will be presented with an overview of the Ground Image Processing Parameters that need to be tuned during the In Orbit Acceptance phase to assure the required performance of the products.

Finally, the complexity of the processing having been showed, the challenges of the production in terms of data volume and processing time will be highlighted.

If already available, the first Sentinel-2 Level-1 products will be shown.

9643-4, Session 2

Sentinel-2A: presentation of the CAL/VAL commissioning phase, first images

Thierry L. Trémas, Cécile Dechoz, Sophie Lachérade, Julien Nosavan, Beatrice Petrucci, Ctr. National d'Études Spatiales (France); Claudia Isola, Philippe Martimort, European Space Research and Technology Ctr. (Netherlands)

In partnership with the European Commission and in the frame of the Copernicus program, the European Space Agency (ESA) has developped the Sentinel-2 optical imaging mission devoted to the operational monitoring of land and coastal areas.

The Sentinel-2 mission is based on a satellites constellation deployed in polar sun-synchronous orbit. Sentinel-2 will offer a unique combination of global coverage with a wide field of view (290km), a high revisit (5 days with two satellites), a high resolution (10m, 20m and 60m) and multi-spectral imagery (13 spectral bands in visible and shortwave infra-red domains). The first satellite is planned to be launched in late 2014. The first sentinel 2A satellite is planned to be launched on June 12th, 2015.

In this context, the Centre National d'Etudes Spatiales (CNES) supports ESA to insure the cal/val commissioning phase.

This paper provides first, an overview of the Sentinel-2 system after the launch.

Then the articles focuses on the means implemented and

activated in CNES to perform the In Orbit Commissioning, the availability and performances of the different devices involved in the ground segment : the GPP in charge of producing the level 1 files, the “radiometric unit” that processes sensitivity parameters, the “geometric unit” in charge of fitting the images on a reference map, MACCS that will produce Level 2A files (computing reflectances at the Bottom of Atmosphere) and the TEC-S2 that will coordinate all the previous software and drive a database in which will be gather the incoming Level 0 files and the processed Level 1 files.

Finally are presented some examples of products, images processed by the evoked means

9643-5, Session 2

Sentinel-2 global reference image

Cécile Dechoz, Florie Languille, Ctr. National d’Études Spatiales (France); Stéphane Massera, Institut Géographique National (France); Angélique Gaudel, Ctr. National d’Études Spatiales (France); Vincent Poulain, Thales Services (France); Céline L’Helguen, Ctr. National d’Études Spatiales (France); Cécile Picard, Thales Services (France); Philippe Martimort, Claudia Isola, European Space Agency (Netherlands); Thierry Trémas, Ctr. National d’Études Spatiales (France)

Sentinel-2 is a multispectral, high-resolution, optical imaging mission, developed by the European Space Agency (ESA) in the frame of the Copernicus program of the European Commission. In cooperation with ESA, the Centre National d’Etudes Spatiales (CNES) is responsible for the image quality of the project, and will ensure the CAL/VAL commissioning phase.

Sentinel-2 mission is devoted the operational monitoring of land and coastal areas, and will provide a continuity of SPOT- and Landsat-type data. Sentinel-2 will also deliver information for emergency services. Launched in 2015 and 2016, there will be a constellation of 2 satellites on a polar sun-synchronous orbit, imaging systematically terrestrial surfaces with a revisit time of 5 days, in 13 spectral bands in visible and shortwave infra-red. Therefore, multi-temporal series of images, taken under the same viewing conditions, will be available.

So as to ensure for the multi-temporal registration of the products, specified to be better than 0.3 pixels at 2?, a Global Reference Image (GRI) will be produced during the CAL/VAL period. This GRI is composed of a set of Sentinel-2 acquisitions, which geometry has been corrected by bundle block adjustment. During L1B processing, Ground Control Points will be taken between this reference image and the sentinel-2 acquisition processed and the geometric model of the image corrected, so as to ensure the good multi-temporal registration.

This paper first details the production of the reference during the CALVAL period, then details the qualification and geolocation performance assessment of the GRI. It finally presents its use in the Level-1 processing chain and gives a first assessment of the multi-temporal registration.

9643-11, Session 3

Multiscale statistical image destriping algorithm

Vincent Martin, Ctr. National d’Études Spatiales (France); Arnaud Kelbert, Thales Services (France)

Most satellite imaging systems rely on scanning detection units comprised of limited sets of individual detectors, allowing generating large images while restraining the detection unit size. For instance, in the push-broom design, one-dimensional CCD arrays are arranged across-track while the along-track dimension is imaged through the satellite motion along its orbit. In this case, each raw image column corresponds to successive acquisitions by the same individual detector. In whisk-broom sensors such as MODIS, where collection of a series of lines in the across-track direction is ensured by a rotating mirror, each raw image line corresponds to successive acquisitions by the same detector. Individual detectors of a multi-detector sensor yet present inhomogeneous responses: for instance depending on input integrated radiances or on observed scene spectral profiles. This results in striping patterns corrupting the image, oriented along the scanning direction.

Individual detectors response can be independently calibrated then compensated in order to remove stripes off raw images. This inter-detector normalization process must be performed periodically in order to compensate for sensitivities temporal fluctuation. Residual striping noise is often perceptible on uniform landscape zones, mostly due to temporal fluctuation, non-linearities and spectral sensitivity differences. Classically, calibration relies on comparing detectors viewing similar targets, using specific acquisitions of supposedly homogeneous natural sites or in-flight internal calibration systems.

Statistical destriping consists in estimating normalization coefficients on the very image to correct, achieving self-calibration of any operational image. This principle adapts ideally to temporal fluctuation and at least partially to mean radiance or spectral characteristics of the processed image zone. The mathematical difficulty relies in separating the sensor contribution from the operational ideal image corresponding to an unknown landscape of any sort which can include linear patterns oriented in the instrument striping direction.

Many statistical destriping algorithms are based on the hypothesis of statistically independent detector response residuals. While this property is often verified concerning detectors, optical elements contributing to the acquisition can be in practice associated to defects spread over several neighboring lines/columns.

In this paper, a multi-scale algorithm is proposed, performing a statistical destriping that addresses high and low frequency stripe patterns. The proposed algorithm consists in successively processing under-sampled versions of the image with a core statistical destriping algorithm, starting from the full resolution image. At each zoom level, normalization coefficients are stored and the image is corrected before being used as an input for the next zoom level. Finally, normalization coefficients of different levels are combined thanks to an interpolation process. This principle has for instance been combined to a state-of-the-art algorithm based on MAP criterion minimization, Markov random field perfect data model and independent linear responses assumptions.

The proposed method is generic: it can be applied to any image (satellite imagery or not) including unidirectional structured noise, e.g. vertically or horizontally. Although it applies easily to multi-channel imagery, only a single channel is required. It is an unsupervised method, which is essential to process any acquisition in an operational ground segment. An application to real PLEIADES satellite imagery is presented.

9643-12, Session 3

Noise correlation-based adaptive polarimetric image representation for contrast enhancement of a polarized beacon in fog

Swapnesh Panigrahi, Julien Fade, Mehdi Alouini, Institut de Physique de Rennes (France)

Estimation and detection of active light sources embedded in turbid media has many applications in various fields like medical imaging, navigation and machine vision. Polarimetric imaging is one of the techniques that has been used in imaging through turbid media for contrast enhancement. In general, polarimetric imaging provides a multidimensional image that needs to be reduced to a single image for interpretation or automatic detection. The final image is produced such that the contrast of the polarimetric non-uniformities in the imaged scene are maximized. In this work, we present the contrast

enhancement of polarized light source through fog by using an image representation that is shown to be optimal and differs from the standard image representations that are widely used.

We have setup a long distance imaging experiment that spans over a distance of more than a kilometer. A polarized source of incoherent light is placed on a nearby telecommunication tower and is imaged in two orthogonal polarization directions using a Wollaston prism based snapshot polarimetric camera. A suitable linear combination of the two images is sought such that the contrast of the polarized source is maximized in the resulting image.

We use contrast-to-noise ratio (CNR) as a local measure of contrast of the source with respect to its immediate neighbouring pixels. Using this statistical contrast measure we quantify and compare the contrast performance of various standard polarimetric image representations and computationally find an optimally weighted linear combination that maximize the contrast measure of the polarized beacon. To identify the parameter influencing the linear weights, we analytically maximize the the expression for CNR using a correlated Gaussian noise model. Consequently, we identify the background noise correlation in polarimetric channels as the parameter that influences the weights of the optimal linear combination. Further, we show that the resulting polarimetric representation corresponds to a minimum variance estimator of the mean source intensity in the Maximum likelihood sense.

Further, using the mentioned noise model, we compute the optimal gain in source contrast that can be obtained when using polarization sensitive imaging as against using a simple intensity imager. We conclude that the gain in performance in using a polarimetric imager is a function of correlation in background noise fluctuation in the two polarimetric channels. Finally, we compare the experimentally obtained contrast gain as a function of estimated background correlation and compare it with theoretical predictions and find that they agree well.

The contrast maximizing polarimetric representations has a simple form and is easily implemented under real-time processing constraints. The study of a such a system in real fog has potential applications in navigation and can serve as an intermediate image for automatic detection or as direct visual aide. Thus, enhancing visibility in obscured weather conditions.

9643-13, Session 3

Performance prediction for 3D filtering of multichannel images

Oleksii S. Rubel, Ruslan A. Kozhemiakin, Sergey K. Abramov, Vladimir V. Lukin, National Aerospace Univ. (Ukraine); Benoit Vozel, Kacem Chehdi, Univ. de Rennes 1 (France)

Quite often, multichannel (multi-polarization radar, multi- or hyperspectral) images acquired by remote sensing (RS) systems are noisy. This makes desirable to remove the noise in all or some channels (sub-bands) by image pre-filtering [1]. Efficiency of pre-filtering depends upon many factors as noise type and intensity, image complexity and dynamic range, filter type, availability of a priori information on noise properties and its accuracy, etc. It might be so that filtering does not bring obvious benefits for further processing of data. This might happen for component-wise processing of images that are textural and/or if noise relative intensity is not high [2, 3]. Then, it might be good to predict filtering efficiency in order to apply filtering only if it is predicted that denoising will be efficient enough.

Such prediction mechanisms for the cases of additive and signal-dependent noises in grayscale images have been developed recently for filters based on discrete cosine transform (DCT) [2, 4]. The prediction mechanisms are fast and based on estimating simple statistics of DCT coefficients in 8x8 pixel blocks. It is usually enough to have about 500 blocks to estimate statistics with accuracy necessary for appropriate prediction.

Meanwhile, it is known that the use of 3D (vector) filtering of multichannel images instead of their component-wise denoising is able to provide considerable improvement due to possibility to exploit inter-channel correlation of component images inherent for multichannel data [1, 5]. Recall that 3D DCT-based filtering is carried out in 3D blocks of size Kx8x8 where K denotes the number of channels combined together (this number can be smaller than the total number of channels in multichannel data). If noise in different channels has different properties (type, variance values, etc.), proper homomorphic (variance stabilizing) transforms have to be applied before starting efficiency prediction and filtering [5].

Our experiments have shown that filtering efficiency prediction can be performed for 3D DCT based denoising similarly to component-wise (single-channel) processing. For this purpose, it is enough to consider about 500 3D blocks of multichannel data (after transformations described above), to carry out 3D DCT for them and to estimate certain statistics of DCT coefficients. This can be, for example, mean probability that amplitudes of DCT coefficients do not exceed 2*sigma or 0.5*sigma where sigma is noise standard deviation after homomorphic transforms applied component-wise in advance (here we suppose that noise properties in original images are known in advance or pre-estimated with appropriate accuracy).

It is possible to predict such quantitative criteria as improvement of PSNR (IPSNR) or the ratio of mean square error after filtering to noise equivalent variance before filtering. Prediction is carried out using simple functions (e.g., exponential or power) with two or three parameters. These functions are obtained by fitting them into corresponding scatter-plots (e.g., IPSNR vs considered mean probability) carried out off-line (at research stage in advance) using a set of multichannel set images.

An interesting observation is that 3D filtering provides by 1...3 dB better IPSNR compared to component-wise processing. Due to this, it occurs that it is almost always expedient to apply 3D denoising to improve multichannel RS images. Moreover, the proposed prediction approach allows forecasting what channels have to be jointly processed (filtered) to provide a larger benefit. This will be shown in the final paper for real-life hyperspectral images.

[1] Zhong P., Wang R., Multiple-Spectral-Band CRFs for Denoising Junk Bands of Hyperspectral Imagery, IEEE Transactions on Geoscience and Remote Sensing. – 2013. – vol. 51. – no. 4. – P. 2260-2275.

[2] Abramov S., Krivenko S., Roenko A., Lukin V., Djurovic I., Chobanu M., Prediction of Filtering Efficiency for DCT-based Image Denoising, Proceedings of MECO, Budva, Montenegro. – June 2013. – P. 97-100.

[3] Rubel A., Lukin V., Pogrebniak O., Efficiency of DCT-based denoising techniques applied to texture images, Proceedings of MCPR, Cancun, Mexico. – June 2014. – P. 111-120.

[4] Krivenko S., Lukin V., Vozel B., Chehdi K., Prediction of DCT-based Denoising Eficiency for Images Corrupted by Signal-Dependent Noise, Proceedings of IEEE 34th International Scientific Conference Electronics and Nanotechnology, Kiev, Ukraine. – 2014. – P. 254-258.

[5] N.N. Ponomarenko, V.V. Lukin, A.A. Zelensky, P.T. Koivisto, K.O. Egiazarian, 3D DCT Based Filtering of Color and Multichannel Images, Telecommunications and Radio Engineering, No 15, 2008, pp. 1369-1392.

9643-14, Session 3

Advanced signal processing based on support vector regression for lidar applications

Michela Gelfusa, Univ. degli Studi di Roma “Tor Vergata” (Italy); Andrea Murari, Consorzio RFX-Association EURATOM-ENEA (Italy); Andrea Malizia, Michele Lungaroni, Emmanuele Peluso, Stefano Parracino, Univ. degli Studi di Roma “Tor Vergata” (Italy); Saeed Talebzadeh, Univ degli Studi di Roma Tor Vergata (Italy); Jesus Vega, Ctr. de Investigaciones Energéticas, Medioambientales y Tecnológicas (Spain); Pasqualino

Gaudio, Univ. degli Studi di Roma “Tor Vergata” (Italy)

The LIDAR technique has recently found many applications in atmospheric physics and remote sensing. One of the main issues, in the deployment of systems based on LIDAR, is the filtering of the backscattered signal to alleviate the problems generated by noise. Improvement in the signal to noise ratio is typically achieved by averaging a quite large number (of the order of hundreds) of successive laser pulses. This approach can be effective but presents significant limitations. First of all, it implies a great stress on the laser source, particularly in the case of systems for automatic monitoring of areas for long periods. Secondly, this solution can become difficult to implement in applications characterised by rapid variations of the atmosphere or in general of the source of noise. In this contribution, a new method for the software filtering and denoising of LIDAR signals is presented. The technique is based on support vector regression. The proposed new method is insensitive to the statistics of the noise and is therefore fully general and quite robust. The developed numerical tool has been systematically compared with the most powerful techniques available, using both synthetic and experimental data. Its performances have been tested for noise of various statistics and also for other disturbances of the acquired signal such as outliers. The competitive advantages of the proposed method are fully documented. The potential of the proposed approach to widen the capability of the LIDAR technique, particularly in the detection of widespread smoke, is discussed in detail.

9643-15, Session 3

An improved mutual information similarity measure for registration of multi-modal remote sensing images

Maha Shadaydeh, Tamás Szirányi, Hungarian Academy of Sciences (Hungary)

Registration of multi-modal remote sensing images is an essential and challenging task in different remote sensing applications such as image fusion and multi-temporal change detection.

Mutual Information (MI) has shown to be successful similarity measure for multi-modal image registration applications in medical as well as remote sensing imagery. MI measures the strength of the statistical relationship between two data-sets using their joint probability density function (PDF). The maximum value of MI is expected to be achieved when the data-sets are geometrically aligned. In spite of its effectiveness, MI measure has some drawbacks. 1. MI surface is highly non-convex with many local minima, 2. Spatial information is completely lost in the calculation of the global intensity joint PDF. These MI-based registration problems have been approached so far either by combining other image features and MI measure, or with appropriate joint PDF estimation methods.

In this paper we present an improved MI similarity measure based on a new concept in integrating other image features as well as spatial information in the estimation of the joint intensity histogram which is used here as an estimate of the joint PDF. The proposed method is based on the idea that each pixel in the reference image is assigned a weight; each pixel contribute to the calculation of joint histogram according to its weight only. That is, each bin in proposed joint histogram is calculated as the summations of the weights of the pixels corresponding to that bin. The weight w(s) given to each pixel s in the reference image is chosen to be an exponential function defined by $w(s) = \exp(-K\, d(s)/g(s))$; where d(s) and g(s) are respectively the values of the distance image and normalized gradient image; and K is a positive constant. The gradient image g(s) is calculated using the Laplacian of Gaussian (LoG) filter. The distance d(s) is defined as the Euclidean coordinate distance of pixel s from the closest key-point among set of one or more key-points in the reference image. These key-points can be defined either arbitrarily by the user or automatically using for example Harris or Scale-Invariant Feature Transform. The constant K is used to control the slope of the exponential function.

We have compared the proposed method with the standard normalized MI algorithm for registration of multi-spectral remote sensing images as well as pairs of multi-sensor optical images taken at two different dates. We observed that the proposed method produces better registration function containing fewer erroneous maxima and leading to higher registration success rate.

The advantages of the proposed methods are summarized in the following points:

1. Reduction of the peaks in the joint histogram due to background or large homogenous areas by giving more weights to pixels with high gradient value which contain more relevant information for registration.

2. Integration of spatial information through the distance parameter d(s).

3. Possibility of multi-scale analysis based on different values of the LoG filter parameters.

4. The gradient and distance images depend on the reference image only and are calculated once for all geometric transformations of the floating image; hence no considerable additional computational load is required.

5. Extension to integration of image features other than gradient image and/or different distance definition is straight forward.

6. Extension to other multi-modal images, e.g. registration of LIDAR and optical images, is in progress.

9643-16, Session 4

Estimation of noise model parameters for images taken by a full-frame hyperspectral camera

Can Demirkesen, TÜBITAK UZAY (Turkey); Ugur M. Leloglu, Middle East Technical Univ. (Turkey)

Noise estimation is a critical stage in the processing of hyperspectral images (HSI). Noise has to be taken into account in the algorithms of classification, target detection and anomaly detection. Recent studies indicate that noise estimation is also crucial in subspace identification of HSI. Several techniques were proposed for noise estimation including: multiple linear regression based techniques, spectral unmixing and remixing etc.

The noise in HSI is widely accepted to be a spatially stationary random process. But the variance of the noise varies from one wavelength to another. Two types of noise are considered: the first one is the circuitry noise (thermal noise) which is signal independent. The second one is the photonic noise (shot noise) which is signal dependent. The latter is considered to be the dominant one.

A reliable way to accurately estimate the noise requires the identification of a large uniform surface in the image. To this end, we propose a probabilistic region growing technique. The algorithm starts from random seed points and tries to grow the seeds consecutively until no more pixels left unreached. For inclusion of a new pixel into region a threshold on the Mahalanobis distance is checked.

At the end of this process, a certain number of regions with different sizes and uniformities are obtained. The next step consists of identifying the most uniform region having the largest area. This step can be considered as an optimization problem where the objective function is a weighted sum of uniformity and size. This function is to be maximized and the maximizer is the region that we search. The uniformity is measured in terms of standard deviations normalized by the maximum standard deviation of all regions.

Once the most uniform and largest region of the scene is identified the next step is to apply an ideal low pass filter to this region. This yields an estimate of the noise-free data, hence the noise itself by calculating the difference.

It is also possible to apply the well-known scatter plot technique. According to this approach, pixels belonging to a uniform region exhibit scatter-points clustered along a straight line. The slope of this line measures the noise power of the signal-dependent noise component. While the intercept measures the signal-independent component of the noise.

Experiments conducted on space-borne Hyperion data and airborne AVIRIS data suggest that the proposed scheme produces comparable results to its competitors. A major advantage of the technique is the automated identification of an homogenous region.

9643-17, Session 4

Using hyperspectral image enhancement method for small size object detection on the sea surface

Lu Yan, Tokyo Institute of Technology (Japan); Naoki Noro, Yohei Takara, Fuminori Ando, EBA Japan Co., Ltd. (Japan); Masahiro YAMAGUCHI, Tokyo Institute of Technology (Japan)

Small size object detection in vast ocean plays an important role in rescues after accident or disaster. Nowadays many different approaches have been applied in such purpose: acoustic sensors, radar, photography etc. One of the promising approach is a hyperspectral imaging system (HIS), since HIS can collect a lot of information in a single pixel. However, due to the limitation of HIS sensor's resolution, interested target might occupy only several pixels or less in the image, it's difficult to detect small object, moreover the sun glint of the sea surface make it even more difficult. In this paper, we propose an image analysis technique suitable for the computer aided detection of small objects on the sea surface, especially humans.

We firstly separate objects from background by adapting a previously proposed image enhancement method and then apply classification method to detect a specific kind of object. The enhancement technique employs the principal component analysis (PCA), and the most significant components obtained by PCA usually contain large part of information of imagery, however, the small targets' information exist in the insignificant components. Therefore, the most significant component are removed while the less significant components are not changed. The residuals part then applied multi-wavelength-enhancement technology with a defined target spectrum that need to be enhanced. Various unknown target objects, which have different spectral features can be enhanced in this method, and enhancement result is visualized as a color image.

Moreover, for the purpose of automated alert system of human detection, a specific human detection technique based on the spectral signature of human reflectance is applied for further detection of specific object. As human radiance spectrum shows particular features: from 600nm to 650nm there is a significant single augmentation area which might due to the Oxygenated Hemoglobin absorption changes, therefore, the discriminant function is derived in this wavelength range in our study.

The proposed system provides the following results for supporting the detection of humans and other small objects on the sea surface; an image with spectral color enhancement, alerts of various objects, and the human detection results. This multilayered approach is expected to reduce the oversight, i.e., false negative error.

In the experiment, hyperspectral images of sea surface with small-size objects that obtained from aircraft have been studied. Results of the proposed technique have been compared with existent methods, and our method has successfully enhance the hyperspectral image, and detect small object from the sea surface with low false detection rate, shows the ability to further detection of Human in this study). The result are less influenced by the sun glint effects. This study helps recognizing small objects on the sea surface, and it leads to advances in the rescuing system using aircraft equipped HIS technology.

9643-18, Session 4

A new method for spatial resolution enhancement of hyperspectral images using sparse coding and linear spectral unmixing

Zahra Hashemi, Shahid Bahonar Univ. of Kerman (Iran, Islamic Republic of); Azam Karami, Shahid Bahonar Univ. of Kerman (Iran, Islamic Republic of) and Univ. Antwerp (Belgium)

Recently, hyperspectral images (HSI) have been widely used in different practical applications such as in detecting earth surface, agriculture, forest monitoring, environmental studies and military issues. HSI have high spectral and low spatial resolutions. However, multispectral images (MSI) usually have low spectral and high spatial resolutions. In various applications HSI with high spectral and spatial resolutions are required. In this paper, a new method for spatial resolution enhancement of hyperspectral images using high resolution MSI based on sparse coding and linear spectral unmixing (SCLSU) is introduced.

In the proposed method (SCLSU), high spectral resolution features of HSI and high spatial resolution features of MSI are fused. In this case, the sparse representation of MSI and linear spectral unmixing (LSU) model of HSI is used in order to construct high resolution HSI (HRHSI). The fusion process of HSI and MSI are formulated as an ill-posed inverse problem which requires regularization term or prior information. In the following paragraphs, the SCLSU algorithm is briefly explained.

First, in order to maintain the spectral consistency and reduce the dimension of HSI, LSU algorithm is applied. In this case, the spectral information of HSI is represented by its endmembers while the spatial information is represented by its abundance fractions. In addition, both HSI and MSI which were acquired from the same scene, has the same endmembers. Therefore, endmembers are extracted from HSI which have high spectral resolution, using vertex component analysis (VCA).

Second, the sparse representation is considered as a regularization term in an ill-posed inverse problem by constructing proper dictionary using K-SVD algorithm. For constructing the dictionary, several MSI is used and they are divided to small patches. They can be obtained from an arbitrary set of natural images with high spatial resolution. In fact, they include a lot of edges and rich textures. After that, small patches of HRHSI represented as weighted linear combinations of small number of atoms in the dictionary with sparse coding.

Third, the optimization problem is defined by three terms. The first and second terms are related to the LSU of HSI and MSI respectively and the third term depends on the sparse coding. This optimization problem is solved by optimizing alternatively with respect to the projected abundance fractions and the sparse code.

In this paper, the abundance fractions is calculated by the Split Augmented Lagrangian Shrinkage Algorithm (SALSA) and sparse code is solved using an orthogonal matching pursuit (OMP) algorithm.

Finally the HRHSI is constructed by multiplying the abundance fractions and endmembers.

The proposed algorithm is applied to real datasets (Hyperion and ALI sensors images). Compared with the other state-of-the-art algorithms such as Coupled Nonnegative Matrix Factorization (CNMF) and local spectral unmixing, the SCLSU achieves smaller Spectral Angle Mapper (SAM), smaller Error Relative Global Dimensional Synthesis (ERGAS) and higher Peak Signal to Noise Ratio (PSNR). Therefore, the proposed method has significantly increased the spatial resolution and in addition it highly preserves the spectral content of HSI.

9643-19, Session 4

Development of Bayesian-based transformation method of Landsat imagery into pseudo-hyperspectral imagery

Nguyen Tien Hoang, Kyoto Univ. Graduate School of Engineering (Japan) and Hue Univ. (Viet Nam); Katsuaki Koike, Kyoto Univ. Graduate School of Engineering (Japan)

It is generally accepted that hyperspectral remote sensing is more effective and provides greater accuracy than multispectral remote sensing in many application fields. For example, hyperspectral sensors have a greater potential to identify differences among endmembers of surface materials. EO-1 Hyperion, a representative hyperspectral sensor, has much more spectral bands, while Landsat data has much wider image scene and longer continuous space-based record of Earth's land. To date, there has not been any method to simulate Hyperion bands from a Landsat ETM+ image. This study aims to develop a transformation method of Landsat imagery into pseudo- hyperspectral imagery using the correlation between Landsat and EO-1 Hyperion data. The pseudo-hyperspectral imagery has the number of bands as same as the number of high-quality Hyperion bands, and promises to be the same swath width as Landsat scene. For a case study, we selected an area of 6 km ? 7.1 km in the southwestern Nevada volcanic field in America, which is located about 10 km northwest of Gold Mountain and 30 km southwest of Cuprite alteration zones. At first Hyperion scene was precisely pre-processed and co-registered to Landsat scene, and both data were corrected for atmospheric effects. Assuming that there are good multivariate linear regression models between each of Hyperion bands and Landsat bands, Bayesian model averaging method (BMA) was applied to select the best model from a class of several possible models. Subsequently, this best model is utilised to calculate pseudo-hyperspectral data by R programming. The results are verified by magnitude of Pearson's coefficient and Root Mean Square Error (RMSE) between the pseudo- and original bands. Based on the selection results by BMA, we transform Landsat imagery into 155 bands of pseudo-hyperspectral imagery. Band 5 of Landsat imagery appears the most frequently (152 times), while Band 7 is less frequently observed (105 times) in the models. Most models have multiple R-squared values that are higher than 90%, which assures high accuracy of the models. There are no clear differences between the pseudo- and original data. The pattern, texture, tone, shape, and border of objects in both natural color composite images look similar. Most bands have Pearson's coefficients > 0.95, and a small fraction have the coefficients < 0.93 like outliers in the data sets. Band 220 has the lowest correlation coefficient of 0.87. In a similar manner, RMSE values are mostly smaller than 0.014, which is considerably low. Spectral reflectance curves for each of example patterns have equivalent behaviors in both pseudo- and original data, but that curve in the pseudo-data is slightly smoother. These observations strongly highlight that our proposed method is valid for transforming Landsat data into pseudo-hyperspectral data from the outlook of statistics. The resultant pseudo-hyperspectral data will contribute to detailed identification of surface materials related to mineral mapping than the traditional satellite imagery. Our next step is to compare the pseudo- and original imagery by classification application and mineral mapping, and improve the method by finding the best model of each feature at every band.

9643-20, Session 4

Striping noise mitigation: performance evaluation on real and simulated hyperspectral images

Donatella Guzzi, Cinzia Lastri, Vanni Nardino, Ivan Pippi, Valentina Raimondi, Istituto di Fisica Applicata Nello Carrara (Italy); Alessandro Barducci, SOFASI S.R.L. (Italy)

Coherent noise, also known as "striping noise", is a well-known phenomenon that is intrinsic to the process of image acquisition by means of scanning or pushbroom spaceborne systems. Whereas in scanning system coherent noise exhibits a periodic pattern, in pushbroom sensors the striping effect is not periodic, but can be seen as vertical stripes of different intensity.

The striping effect has different characteristics, depending on the instrument scanning of the scene and on the number of detection elements. The main cause is a difference in the response of the single photosensitive elements of the sensors.

In hyperspectral systems, stripe disturbance can be seen as a spatially and spectrally coherent noise, which would affect each pixel spectrum as well as the intensity distribution of each monochromatic image.

Even if pre-launch radiometric calibration phase is always performed, such measurements become obsolete with sensor aging. Presently, most systems have in-flight calibration facilities, that should guarantee accurate radiometric calibration during the entire life of a sensor. Residual coherent noise after calibration, however, may still perturb the quantitative analysis of images and the extraction of physical parameters.

Many destriping methods have been proposed in the literature and they can be classified in three main groups: statistical-based approach, digital-filtering methods and radiometric-equalization procedures. The performance of each algorithm depends both on the scene under investigation and on the type and intensity of noise to be treated: for example, some algorithms that provide good results for almost homogeneous images could become not suitable for textured scene. In this context, the availability of simulated data at each step of the digital image formation process, including that one before the introduction of the striping effect, is particularly useful since it offers the opportunity to test and adjust a variety of image processing and calibration algorithms.

In this paper we present the performance of a statistical-based destriping method applied to a set of simulated and real hyperspectral data representing a wide area around Florence, Italy. These images contain different environments, such as urban areas, forests, agricultural land and water bodies.

The set of real data are images acquired by the EO-1 Hyperion hyperspectral sensor, while the set of simulated data were generated using an image simulator implemented for the PRISMA hyperspectral mission in the frame of the OPTIMA project funded by the Italian Space Agency (ASI).

The simulated images have been generated using different intensities of coherent and random noise in order to extensively test the destriping algorithm. In order to assess the algorithm performance, the quality indexes most commonly used for the evaluation of these pre-processing algorithms have been computed. In addition, a statistical evaluation based on image difference and ratios between the corrected and ideal images has been carried out for the same purpose. Finally, the results of the statistical analysis were compared with the outcome of the quality indexes-based analysis.

9643-21, Session 5

Low-dimensional representations of hyperspectral data for use in CRF-based classification

Yang Hu, Nathan D. Cahill, Sildomar T. Monteiro, Eli Saber, David W. Messinger, Rochester Institute of Technology (United States)

Rapid developments in satellite and sensor technologies have led to a significant increase in the availability of remotely sensed images. Consequently, image analysis techniques are urgently needed to extract meaningful information in an efficient and timely manner. Hyperspectral image classification with the aid of probabilistic graphical models is one of the

most promising study areas. Conditional Random Field (CRF) models are extensively investigated due to their distinct advantages: no independence assumption must be made over the observations, and local and pairwise potential features can be defined with flexibility.

The selection of feature potentials is crucial for superior CRF-based classification performance. Conventional methods utilize all spectral bands and assign the corresponding raw intensity values into the feature functions in CRFs. However, these methods require significant computational effort and yield an ambiguous summary of data. Therefore, instead of processing all bands from hyperspectral imagery, we propose performing nonlinear dimensionality reduction as a pre-processing step to removes the redundant spectral information while preserving essential properties of the data. Hence, classifiers execute low dimensional but compactly informed representations of hyperspectral data thanks to dimensionality reduction techniques. In this paper, we compare three types of graph-based dimensionality reduction algorithms by assessing their impact on subsequent CRF-based classification: Laplacian Eigenmaps (LE), which retains the intrinsic geometry of the data by exploiting spectral characteristics of the graph Laplacian operator, Schroedinger Eigenmaps (SE), which extends Laplacian Eigenmaps to incorporate a potential matrix capable of encoding expert knowledge about the manifold structure, and Local Linear Embedding (LLE), which guarantees invariance to data rotation, scale and translation.

To illustrate and compare the different dimensionality reduction algorithms, we incorporate them into CRF-based classification, and assess classification results within the N folds cross-validation scheme. Extensive quantitative (accuracy, precision, sensitivity and specificity measurements) and qualitative evaluations are performed on publicly available hyperspectral image datasets with expert-labeled ground truth (AVIRIS Indian Pines and HYDICE DC Mall).

9643-22, Session 5

Unsupervised hierarchical partitioning of hyperspectral images: application to marine algae identification

Baiyang Chen, EDF Recherche & Développement (France) and Univ. de Rennes 1 (France); Kacem Chehdi, Univ. de Rennes 1 (France); Eric De Oliveria, EDF Recherche & Développement (France); Claude Cariou, Univ. de Rennes 1 (France); Bruno Charbonnier, EDF Recherche & Développement (France)

In this paper a new unsupervised top-down hierarchical classification method to partition airborne hyperspectral images is proposed. The unsupervised approach is preferred because the difficulty of area access and the human and financial resources required to obtain ground truth data, constitute serious handicaps especially in the case of airborne or satellite images covering large areas.

The developed classification approach allows i) a successive partitioning of data into several levels or partitions in which the main classes are first identified, ii) an estimation of the number of classes automatically at each level without any end user help, iii) a nonsystematic subdivision of all classes of a partition Pj to form a partition Pj+1, iv) a stable partitioning result of the same data set from one run of the method to another.

The principle of the proposed approach to classify N pixels, where each pixel is characterized by B features (spectral signature) into M partitions is the following:

For the first partition P1, the set of N pixels is divided into several classes, the number of which is estimated automatically, and each class of the partition P1 is either divided again or not, to get the partition P2, and so on, until the optimal partition is obtained.

The partitioning process is stopped when the evaluation criterion applied to Pj+1 is greater than the one corresponding to Pj. Hence, Pj is retained as the optimal partition and its classes are those obtained by the division of classes of Pj-1 and those from Pj-1 which are not divided. This criterion combines the dispersion of classes and the minimal distance between classes.

This criterion is also used to validate or stop the partition of a class.

To provide a stable partitioning result of each class of Pj , (j=2,..., M-1), we used the Fuzzy C-Means method (FCM) where the centres of subclasses are initialized by the Linde-Buzo-Gray method (LBG).

The choice of the FCM method in this scheme is justified by its effectiveness compared to similar methods (e.g. k-means, SOM, affinity propagation). However, this algorithm has two major drawbacks: it requires the a priori knowledge of the number of classes and it is unstable (sensitive to the random initialization of the centres of classes).

To overcome these two drawbacks, the proposed class partitioning process of Pj introduces incrementally initial centres of subclasses of the FCM algorithm, calculated by the LBG algorithm (the number of subclasses k = 2, 3, ..., NKC, with NKC the number of pixels of the candidate class to split). The estimated number of subclasses (stop the incrementing of k), is performed according to a criterion which combines dispersions of subclasses, the average of these dispersions and the minimum distance between subclasses.

The proposed approach was validated on synthetic and on real hyperspectral images related to the identification of several marine algae species. In addition to highly accurate and consistent results (correct classification rate over 99%), this approach is completely unsupervised. It estimates the optimal final partition without any end user intervention.

9643-23, Session 5

Hyperspectral anomaly detection method based on auto-encoder

Emrecan Bati, Akın Çalıskan, Alper Koz, Aydin A. Alatan, Middle East Technical Univ. (Turkey)

Hyperspectral target detection studies until now can be classified in two categories. In anomaly detection, which can be considered as the first category, a hyperspectral image is analysed by considering the spectral difference between the hyperspectral pixels and their surrounding. In the second category, namely spectral signature based target detection, a previously available spectral signature is compared with each pixel of the hyperspectral image according to a spectral distance measure to detect the target location. Among these two categories, anomaly detection methods have found a wider range of applications as they do not require a prior information about the desired target.

Anomaly can be defined as the data or observation which does not fit into the general characteristics of a given data set. Among these methods, Reed-Xiaoli (RX) method has taken a significant attention in the literature with its pioneer aspect and simplicity. The algorithm stands as a benchmark as an anomaly detector, on which several modifications have been implemented so far. The method produces Mahalanobis metrics to describe the similarity between the target pixel and the background to differentiate the abnormal objects.

In this paper, a novel approach based on autoencoder is proposed to detect anomalies in a hyperspectral image as an alternative to conventional RX based anomaly detection. The proposed anomaly method is based on the adaptation of the Predictive Sparse Decomposition Autoencoder (PSDAE) to hyperspectral images due to its efficient joint learning for the encoding and decoding functions. The proposed method first encodes the spectral signature of a hyperspectral pixel into a sparse code with a learned function and computes the code prediction error which is defined as the difference between the optimal sparse code and the calculated code. The algorithm then decodes the encoded pixel and computes the reconstruction error between the decoded pixel and the original pixel. The prediction error, reconstruction error, together with the code sparsity defined as the L1 norm of the code, form the total energy that should be optimized for the

autoencoder. The parameters of the encoding and decoding functions are tuned to minimize the defined total energy of all spectral pixels in the learning phase. Finally, the obtained reconstruction error at each pixel with the learned parameters is assigned to that pixel as a measure of being anomaly.

For the experimental procedure different fabrics and construction supplies are placed on a rural area and their hyperspectral image is acquired from a height of 500 meter. A visible-near infrared (VNIR) camera having a spectral range of 400-1000 nm with 4.9 nm spectral resolution is utilized for the acquisition. The proposed method is compared with the conventional anomaly detection method, namely Reed-Xiaoli (RX) detector. The experiments has verified the superiority of the proposed anomaly detection method in terms of receiver operating characteristics (ROC) performance.

(The figures regarding the utilized hyperspectral image, the outputs of RX detector and the proposed anomaly detector, and the resulting ROC curves are given in the attachment.)

9643-24, Session 5

Post-processing for improving hyperspectral anomaly detection accuracy

Jee-Cheng Wu, Chi-Ming Jiang, Chen-Liang Huang, National Ilan Univ. (Taiwan)

Anomaly detection (AD) has become an important topic for hyperspectral target applications, because it can detect the small targets whose spectral characteristics are differently from their surroundings without any prior knowledge and atmospheric correction, particularly when the interested targets are of low probabilities of occurrence.

Over the past three decades, many AD algorithms have been proposed. Depending on the global or local strategies used, different anomalies can be detected. A benchmark anomaly detector for multi/hyperspectral images is the Reed-Xiaoli (RX) detector. Nevertheless, RX-based detector is limited by two main problems. The first problem is assuming the data are uncorrelated and homogeneous; however, the assumptions are not existed in hyperspectral image. The second problem is that RX-based detector involves estimation and inversion of a high-dimensional covariance matrix, frequently under a small sample size.

To overcome the above two problems, many improved/modified versions of the RX detector have been explored. The main difference between the various modified RX-based approaches lies in the manner in which the background is characterized; however, some errors always remain. In this paper, a two-stage post-process to improve RX-based anomaly detection accuracy in hyperspectral image was proposed.

At the first stage, assign the weight value of each pixel based on the distance between each of pixel spectra and mean spectrum using spectral angle mapper (SAM). At the second stage, detect those pixels around high score anomalous pixels using morphological operator. The morphology operator used to process an image is based on shape (i.e. structural elements). In this research, the dilation operator is used to process the RX-scored image, and the transfer pixels will assign new spectrum by multiple weight value.

Tests were conducted using two real hyperspectral images with ground truth information. Based on receiver operating characteristic (ROC) curves and the area under the curve (AUC), the results demonstrate that the proposed method reduced the false alarm rates of the RX-based detector.

9643-25, Session 5

Hyperspectral classification with reduced bands by using HMM and entropy

Samir Y. W. Arabi, Instituto Federal de Educação, Ciência e Tecnologia de Goiás (Brazil) and Insituto Tecnológico de Aeronáutica (Brazil); David Fernandes, Instituto Tecnológico de Aeronáutica (Brazil); Marco A. Pizarro, Instituto Nacional de Pesquisas Espaciais (Brazil)

The Hyperspectral images due to its good spectral resolution are extensively used in scenes classification, but its high number of bands requires a high bandwidth in the transmission data equipment, a higher data storage capability and a high computational cost in processing systems. This work presents a new methodology for hyperspectral data classification that can work with a reduced number of spectral bands and achieve good results, comparable with processing methods that require all hyperspectral bands.

The proposed method for hyperspectral spectra classification is based on the Hidden Markov Model (HMM) associated to each Endmember (EM) of a scene and in the set of conditional probabilities of a spectrum belongs to each HMM of each EM. The original spectrum is decomposed in four orthogonal functions using the Discrete Wavelet Transform (DWT) and the HMM parameters and the conditional probabilities are calculated using the Baum-Welch procedure.

The methodology has three main steps. In the first, the learning procedure, each EM spectrum is represented by a HMM and then each EM spectrum has its conditional probability to belongs to each HMM calculated. This set of conditional probabilities is transformed in an EM entropy vector that has its entropies elements calculated directly from the conditional probabilities set. The EM entropy vectors will be the reference vectors related to each class associated to each EM.

In the second step, the measurement procedure, each spectrum to be classified generates a set of conditional probabilities of this spectrum belongs to each HMM associated to each EM. The set of conditional probabilities is then transformed in a spectrum entropy vector that will be compared with the EM entropy vectors in the next step.

In the thirty step, the classification procedure, it is calculated the Euclidean Distance (ED) among each spectrum entropy vector, to be classified, and each EM entropy vector. The minimum ED identifies the class to be attributed to the spectrum.

The method is tested with AVIRIS spectra of a scene with its 209 original bands and also with reduced number of bands of 128, 64 and 32 randomly, with the assurance of having samples throughout the space of bands, take from the original spectrum. It is choose 13 EM to classify 117 spectra samples and 5 EM to classify 45 spectra samples, the samples are taking in a neighborhood of 3x3 of each EM. The choose EM are types of Green Vegetation, Nonphotosynthetic Vegetation, Red Soil Latossolo Vermelho (LV), Neossolo Quartzarênico Órtico (RQo) and Water.

It is shown that the method compared with classical classification methods as SAM (Spectral Angle Map), SID (Spectral Information Divergence) and ED among spectra has a better performance with reduced number of bands. The comparison is made by the confusion matrix and its Kappa coefficient evaluation.

The methodology take the advantage of the knowledge acquire by the HMM of each EM to performer a classification using a reduced number of band.

9643-26, Session 6

Deep learning for multi-label land cover classification

Konstantinos T. Karalas, Technical Univ. of Crete (Greece) and Foundation for Research & Technology-Hellas (Greece); Grigorios Tsagkatakis, Foundation for Research and Technology-Hellas (Greece); Michalis Zervakis, Technical Univ. of Crete (Greece); Panagiotis Tsakalides, Foundation for Research and Technology-Hellas (Greece) and Univ. of Crete (Greece)

Satellite remote sensing is an essential tool for the

quantification of land cover change, allowing for a greater understanding of large-scale climate and biodiversity dynamics. The significance of land cover has been acknowledged by the community and investigation of related classification tasks is a highly active topic. While land cover classification is typically treated as a single-label problem, where a remote sensed pixel is associated with a particular label or class, in real-life scenarios, the pixels of the sensed images encode a mix of materials, due both to instrumentation and physical interactions of light. The situation where a specific example is associated with multiple labels is a well-known machine learning approach, the multi-label classification problem, with numerous applications in text, image, audio and bioinformatics classification. In this work, we consider the introduction of a multi-label learning scheme, adapted to a remote sensing application, where we combine real satellite data from MODIS sensor and high spatial resolution ground data from the CORINE land cover project.

In general, the performance of machine learning methods is heavily dependent on the choice of data representation on which they are applied. The goal of this study is to learn generic, robust and more useful features as part of a representation learning system and thus support subsequent classification algorithms. We consider the binary relevance transformation, a state-of-the-art multi-label classification technique and apply representational learning as a preprocessing step. In particular, we investigate unsupervised feature learning by utilizing the framework of sparse autoencoders, a type of artificial neural network which employs nonlinear codes for representing the original data. By imposing constraints on the network (e.g. sparsity and number of hidden units), a sparse autoencoder can reveal interesting structures in the data, i.e. correlations between the features. We also examine "deep learning" architectures, employing multiple levels of representation e.g. two and three layers, where the sparse autoencoders are ''stacked'' in a greedy layer-wise fashion such that the outputs of each layer are wired to the inputs of the successive layer (feed-forward pass). Although training deep architectures is a challenging and time consuming task, these architectures are more expressive and can extract more sophisticated features from input data. At the top layer of our implementations, we use two types of classifiers, namely the SVM and the Softmax classifiers, and measure the performance with respect to the number of hidden layers, the use of the top-layer classifier and the activation function. Experimental results suggest that even such shallow architectures with a sparse overcomplete layer can efficiently represent the training data, while deep architectures generate more abstract, and hence more invariant, higher-level features, leading to greater classification performance.

9643-27, Session 6

Compressed histogram attribute profiles for the classification of VHR remote sensing images

Romano Battiti, Begüm Demir, Lorenzo Bruzzone, Univ. degli Studi di Trento (Italy)

No Abstract Available

9643-28, Session 6

Multipath sparse coding for scene classification in very high resolution satellite imagery

Jiayuan Fan, Hui Li Tan, Shijian Lu, Institute for Infocomm Research (Singapore)

With the rapid development of various satellite sensors, very high resolution satellite imagery (better than 5m spatial resolution) that contains rich spectral and geographic information has becoming available nowadays. In order to process the huge amount of satellite image data, automatic and advanced scene classification technique for very high resolution satellite imagery is urgently needed. Efficient scene representation from raw satellite image data becomes more demanding, specifically for complex urban satellite imagery.

Bag-of-Visual-Words (BoVW) [1] has been widely used for scene classification. Its performance depends greatly on the extracted local feature representation and the used k-means clustering algorithm. Recently, a few systems [2, 3] implant the sparse coding for feature learning in aerial scene classification. In [2], orthogonal matching pursuit (OMP) as a variant of sparse coding is applied for efficient aerial scene recognition and its performance is highly related with multiple low-level features, including raw pixel intensities, orientated filter responses, and scale-invariant feature transform (SIFT). Later, the work in [3] utilizes sparse autoencoder for unsupervised feature learning based on saliency. In addition, both works [2, 3] use the single-layer sparse coding.

Motivated by the importance of feature learning through multiple layers [4], we propose an unsupervised feature learning approach for scene classification on very high resolution satellite imagery. The scheme of the proposed unsupervised feature learning utilizes multipath sparse coding architecture in order to capture multiple aspects of discriminative structures within complex satellite scene images. The dense low-level features are simply extracted from the raw satellite data by using different image patches with varying size at different layers, and this approach is not limited to a particularly designed feature descriptors compared with the other related works [1, 2, 3]. The proposed technique has been evaluated on two challenging high-resolution datasets, including the UC Merced dataset containing 21 different aerial scene categories with a 1 foot resolution and the Singapore dataset containing 5 land-use categories with a 0.5m spatial resolution. Experimental results show that it outperforms the state-of-the-art that uses the single-layer sparse coding.

The major contributions of this proposed technique include (1) a new unsupervised feature learning approach to generate feature representation for very high-resolution satellite imagery, (2) the first to apply multipath sparse coding for scene classification in very high resolution satellite imagery, (3) a simple low-level feature descriptor instead of many particularly designed low-level descriptors, such as SIFT, (4) evaluation on two satellite image datasets that come from different sources.

[1]. S. Lazebnik, C. Schmid, and J. Ponce, "Beyond bags of features: Spatial pyramid matching for recognizing natural scene categories," CVPR, vol. 2, pp. 2169-2178, 2006.

[2]. A. M. Cheriyadat, "Unsupervised feature learning for aerial scene classification," IEEE TGRS, vol. 52, no. 1, pp. 439-451, Jan. 2014.

[3]. F. Zhang, B. Du and L. Zhang, "Saliency-Guided Unsupervised Feature Learning for Scene Classification," IEEE TGRS, vol.53, no.4, pp.2175-2184, April 2015.

[4]. L. Bo, X. Ren and D. Fox, "Multipath Sparse Coding Using Hierarchical Matching Pursuit," CVPR, pp.660-667, June 2013.

9643-29, Session 6

Impact of spatial resolution on correlation between segmentation evaluation metrics and forest classification accuracy

Andreja Švab Lenarčič, Slovenian Ctr. of Excellence for Space Sciences and Technologies (Slovenia); Klemen Ritlop, Univ. of Ljubljana (Slovenia); Nataša Đurić, Klemen Čotar, Slovenian Ctr. of Excellence for Space Sciences and Technologies (Slovenia); Krištof Oštir, Research Ctr. of the Slovenian Academy of the Sciences and Arts (Slovenia) and Slovenian Ctr. of Excellence for Space Sciences and Technologies (Slovenia)

Slovenia is one of the most forested countries in Europe. Slovenian forest management authorities have to perform

national forest inventories at regular intervals and to observe the degree and impact of forest degradation. Remote sensing data and appropriate remote sensing based mapping methods represent essential tool for an effective and sustainable forest management.

Due to the exceptional increase of satellite imagery over the last decade and the forthcoming Sentinel-2 data, availability of remote sensing data is no longer a problem. On the other hand, suitable mapping methods present bigger challenge. Methods should enable frequent mapping, therefore they should be fast. However, their speed should not be affected by huge amount of data. Thus, the input satellite images should have as low spatial resolution as possible, but still meet the desired classification quality criteria. In order to find out which spatial resolution is still suitable for forest classification, we compared forest classification accuracies obtained by using different spatial resolution imagery.

Since we used both high and very high spatial resolution imagery, an object?based classification was applied in this study. The speed of the classification method could be maximised, if each of the step in object-based classification was automated. However, automation is hard to achieve, since segmentation requires choosing optimum parameters for optimum classification results. It is known that the final land cover classification depends on a number of different factors, where the quality of the segmentation is of fundamental significance. Many scientists continue to design and develop more sophisticated image segmentation algorithms suitable for a wide range of applications, and new methods have been designed to test their quality. Because of real-time segmentation evaluation tendency some authors have proposed procedures for automatic selection of segmentation parameters. However, they are describing selection of optimal parameters for the best segmentation quality, which is according to the test performed by us and others not necessarily the best classification quality.

The main aim of our study was to answer the following questions: Which spatial resolution is still suitable for forest object-based classification? If and which segmentation evaluation metrics can indicate forest classification accuracy most efficiently? Is over-segmentation really a drawback for forest classification? Does the correlation between segmentation evaluation metrics and forest classification accuracy differ for input imagery with different spatial resolution? Which are the optimal segmentation parameters for forest classification at different spatial resolution imagery?

In our test we calculated seven different segmentation quality measures and seven corresponding classification accuracy measures for a hundred combinations of segmentation parameters scale and merge and for four different spatial resolution satellite images. All the segmentation evaluation results were compared to all the classification accuracy results. We used R, G, B and NIR bands of aerial ortophoto, WorldView2 and RapidEye images and R, G, NIR bands of SPOT5 image as input for segmentation, merging and classification process. A reference layer has been produced to generate classification training sample selection and segmentation/classification evaluation. Evaluation was performed for forest land cover class.

9643-30, Session 6

SMV: Simplex of maximal volume based upon the Gram-Schmidt process

Jairo Salazar, Ctr. de Investigación y de Estudios Avanzados del Instituto Politécnico Nacional (Mexico); Andres Mendez, Investigación y de Estudios Avanzados del Instituto Politécnico Nacional (Mexico)

I. Introduction

The present work explores the idea of building a deterministic method to estimate the simplex in R^n using a bottom-up approach, Orthogonal Complements and the Gram-Schmith process. The SMV⊥ algorithm is introduced and it has been compared against N-FINDR, ATGP and OBA because they are the algorithms that show a grater similitude with the propose algorithm.

II. Theoretical framework

Among the literature, the concept of hyperspectral image and spectral pixel are extensively used. In this paper is introduced a formal definition for these two important concepts.

Let X be a hyperspectral image with N spectral pixels and L dimensions. Suppose that it is required to extract k endmembers from X. Let ξ = { E_1 , E_2 , ..., E_n } be the set of all subsets (E_i ⊂ X) of cardinality equal to (k + 1), where (1 ≤ i ≤ n).

Due to the geometric nature of the hyperspectral image: endmember extraction is equivalent to finding the set (E ∈ξ) that inscribe the Simplex in R^k of maximum volume (SMV^k), according to the Linear Mixing Models. In this paper is proposed a method to find the SMV^k using Linear Algebra.

Unlike to N-FINDR, the propose of this paper does not require to guaranty the determinant existence or band removal.

III. The algorithm

A. Description

Extracting e_0 : SMV⊥ considers that the endmeber e_0 is the vertex (x∈X) with maximum magnitude and define the orthogonal base ($\hat{E}^0$ = { e_0 }) because the fact that any vector is orthogonal to the null space.

Extracting e_j : SMV⊥ considers at iteration j that the endmember e_j is that vertex (x∈X) with the maximum orthogonal complement x^⊥ in reference to the orthogonal base (Ê^(j-1)). SMV⊥ adds e_j to the set E of endmembers extracted and creates a new orthogonal base (ÊÎ= E^(j − 1) ∪ x^⊥). This process is repeated (k-1) times until all endmembers are extracted. The resultant set (E = { e_0 , e_1 , ..., e_(k-1) }) contains the list of endmembers and it is considered as the Simplex of Maximal Volume (SMV^k).

IV. Unmixing

This paper uses the unmixing method explained in (N-FINDR, 1999) that uses the following equation:

A = [((E^T) E) ^(− 1)] (E^T) X, (Eq. 1)

where all (A_j ∈ A) is a image that represent the j-th (0 ≤ j < k) endmember distribution in the original hyperspectral image; non-negatively constrained (Rawlings, 1998).

V. Hyperspectral imagery used in experiments

(Fig. 1) shows the six synthetic hyperspectral images while (Fig. 2) shows the real AVIRIS hyperspectral image.

VI. Results

r1) SMV⊥ requires to perform the fewest number of arithmetic operation.

r2) SMV⊥ is faster than N-FINDR, ATGP and OBA. This result is congruent with what we can infer in r1.

r3) The simplex calculated by SMV⊥ is bigger than the simplex calculated by N-FINDR, ATGP and OBA. Therefore, SMV⊥ provide the best performance for Linear Mixing Models.

VII. Conclusions

This paper proposes a novel idea to calculate the Simplex of Maximum Volume in R^n used for fast member extraction bounded by O(n). The propose provide a well performance because it calculates a bigger volume, and has lower computational time complexity than N-FINDR, ATGP, and OBA algorithms on synthetic and real scenarios.

9643-31, Session 7

Are spectral or spatial methods better for pansharpening? An evaluation for four sample methods based on spatial modulation of pixel spectra

Andrea Garzelli, Univ. degli Studi di Siena (Italy); Luciano Alparone, Univ. degli Studi di Firenze (Italy); Gemine Vivone, STO-CMRE (Italy)

The majority of pansharpening methods follows a general protocol that can be summarized in two points:

1) extract high-resolution geometrical information of the scene, not present in the MS image, from Pan;

2) incorporate such spatial details into the low-resolution MS bands, interpolated to the spatial scale of Pan.

Pansharpening methods can be further divided into two classes depending on how the spatial details are extracted:

a) techniques exploiting a spectral transformation of the MS data, replacement of one transformed component with Pan and reverse transformation to yield the sharpened MS bands;

b) techniques employing spatial filtering to extract the geometrical information from Pan.

Methods of the first class are known as component substitution (CS), or "spectral", methods even though the computation of the forward and backward spectral transformation is generally not required. Methods of the second class are "spatial" methods and are referred to as based on multiresolution analysis (MRA), even though a unique lowpass filter is sufficient in most cases. The CS and MRA strategies may be mixed together to yield hybrid methods, whose most notable example is AWLP. However, hybrid methods always belong to a unique class. Spectral methods are those for which the injected detail is given by Pan–I, where I is the intensity component calculated as a linear combination of the interpolated MS bands, with or without the explicit calculation of the whole spectral transformation. Spatial methods are those for which the injected detail is given by Pan–Pan_low, where Pan_low is a smooth approximation of Pan achieved by means of a lowpass filter. In AWLP the injected detail is Pan–Pan_low, multiplied by an injection gain equal to (MS_int)/I, in order to achieve proportionality between fused and interpolated pixel vectors. Thus, AWLP belong to the class of spatial methods.

Another spatial method is the optimized version of HPM. The optimization consists of replacing the boxcar filter with a Gaussian filter matching the MTF of the multispectral instrument. The injection model is (MS_int)/Pan_low, as for the original HPM. The two spectral methods analyzed are Brovey/SVR with optimized intensity achieved from a multivariate regression of MS to Pan_low, and the dual of AWLP, obtained by exchanging I with Pan_low. In principle, if I = Pan_low, all four methods turn out to be identical to one another. Goal of this paper is to demonstrate how optimized spectral and spatial methods behave if an ideal spectral matching does not occur.

Through experiments on IKONOS, WorldView-2 and simulated Pléiades datasets, we demonstrate that the performances of spectral methods depend on the extent of matching between MS and Pan, measured by the regression coefficient of determination (CD). For simulated data, CD is closest to one and all methods perform almost identically. For WorldView-2 and IKONOS data the CD is two to three percent lower and spatial methods (HPM, AWLP) are always more performing than spectral methods (Brovey, AWLP_DUAL). Spatial methods are unaffected by the spectral matching and are preferable whenever such an issue is critical, e.g., for hyperspectral pansharpening.

9643-32, Session 7

Potential accuracy of translation estimation between radar and optical images

Mikhail L. Uss, National Aerospace Univ. (Ukraine); Benoit Vozel, Univ. de Rennes 1 (France); Vladimir V. Lukin, National Aerospace Univ. (Ukraine); Kacem Chehdi, Univ. de Rennes 1 (France)

Precise registration of radar to optical images is one of the most challenging problems of remote sensing image fusion. Different modalities of radar and optical images and intensive speckle noise inherent for radar images add to the problem complexity [1].

A number of approaches were proposed and quite successfully applied to co-register radar to optical images. Among them, area-based methods utilizing such similarity measures as mutual information and normalized correlation coefficient have gained the main interest [2]. Despite a large number of experimental studies of radar to optical images registration, this problem lacks theoretical analysis of potential registration accuracy reachable by area-based methods. Few papers dealing with lower bound on translation estimation accuracy are available in the literature [3, 4] but none of them is suitable for both multimodal registration and complex properties of speckle noise.

In this paper, we propose a Cramér–Rao Lower Bound on translation between radar and optical image estimation accuracy. This bound is based on our previous work [4] but extends it to take into account specific characteristics of speckle noise in radar images. Firstly, we use a more complex spatially-correlated noise model instead of spatially uncorrelated one. Secondly, we consider signal-dependent noise model even within small image control fragments (CF) instead of approximating noise as additive with fixed variance (but different for each CF).

Signal-dependent noise model is crucial for radar data. Indeed, speckle noise can be approximated as multiplicative noise with variance being proportional to squared image intensity. For a single CF, the ratio between the highest and lowest speckle noise variance is therefore proportional to squared ratio between the highest and lowest image intensities. Even within small CF with high contrast, ratio between the highest and lowest image intensities can take values up to 2...10 and the ratio between the highest and lowest speckle noise variance can be as high as 100. To cope with this problem, we propose to set noise variance for each pixel individually. As noise variance is a function of unknown image intensity, radar image prefiltering is used to obtain estimates of the true image intensity for each pixel.

For each pair of CF, we characterize registration problem by the following set of parameters: the reference and template image amplitude; the roughness of image texture (assumed the same for both radar and optical image); correlation between reference and template images; characteristics of noise affecting both registered images. The distribution of the parameter vector defined above has been obtained using real radar and optical images. As our test data, we considered the pair of SIR-C radar data and Landsat8 optical data covering urban, rural, forestry and agricultural areas. These images were registered with accuracy better than one pixel using images metadata and manually selected control points. Noise parameters for both Landsat8 and SIR-C images were estimated based on automatic approach described in [5].

The proposed CRLB on translation estimation accuracy is derived in closed-form as a function of the described above set of parameters and allows studying influence of their desired combination on the registration accuracy.

[1] S. Suri and P. Reinartz, "Mutual-Information-Based Registration of TerraSAR-X and Ikonos Imagery in Urban Areas," Geoscience and Remote Sensing, IEEE Transactions on, vol. 48, pp. 939-949, 2010.

[2] J. Inglada and A. Giros, "On the possibility of automatic multisensor image registration," Geoscience and Remote Sensing, IEEE Transactions on, vol. 42, pp. 2104-2120, 2004.

[3] D. Robinson and P. Milanfar, "Fundamental performance limits in image registration," IEEE Trans Image Process, vol. 13, pp. 1185-99, Sep 2004.

[4] M. L. Uss, B. Vozel, V. A. Dushepa, V. A. Komjak, and K. Chehdi, "A Precise Lower Bound on Image Subpixel Registration Accuracy," Geoscience and Remote Sensing, IEEE Transactions on, vol. 52, pp. 3333-3345, 2014.

[5] M. L. Uss, B. Vozel, V. V. Lukin, and K. Chehdi, "Maximum likelihood estimation of spatially correlated signal-dependent noise in hyperspectral images," Optical Engineering, vol. 51, pp. 111712-1-111712-11, 2012.

9643-33, Session 7

Multiresolution fusion of radar sounder and altimeter data for the generation of high resolution DEMs of ice sheets

Ana-Maria Ilisei, Lorenzo Bruzzone, Univ. degli Studi di Trento (Italy)

No Abstract Available

9643-34, Session 7

Local hyperspectral data multisharpening based on linear/linear-quadratic nonnegative matrix factorization by integrating lidar data

Fatima Zohra F. Benhalouche , Univ. Des Sciences et de la Technologie d'Oran Mohamed Boudiaf (Algeria) and Institut de Recherche en Astrophysique et Planétologie (France); Moussa Sofiane Karoui, Univ. Des Sciences et de la Technologie d'Oran Mohamed Boudiaf (Algeria) and Ctr. National des Techniques Spatiales (Algeria) and Institut de Recherche en Astrophysique et Planétologie (France); Yannick Deville, Institut de Recherche en Astrophysique et Planétologie (France); Abdelaziz Ouamri, Univ. Des Sciences et de la Technologie d'Oran Mohamed Boudiaf (Algeria)

Hyperspectral sensors are characterized by their high spectral resolution, but their spatial resolution is often lower than for multispectral sensors with low spectral resolution. The multi-sharpening process is one way to improve the spatial resolution of hyperspectral data.

Various approaches to hyperspectral data multi-sharpening have been designed by using Spectral Unmixing (SU) techniques based on Nonnegative Matrix Factorization (NMF). SU techniques consist in extracting a collection of endmember spectra and their abundance coefficients, from remote sensing data.

Generally, when the objects on Earth's surface (land) have approximately the same elevations (i.e., the landscape is flat so that there are no multi-reflections between the considered objects), the mixing model involved in SU techniques is linear and Linear Spectral Unmixing (LSU) techniques are appropriate. Otherwise (i.e., when the objects have different elevations generating multi-reflections between these objects), the mixing model is linear-quadratic in the usual configuration, and Linear-Quadratic Spectral Unmixing (LQSU) techniques should be used.

When the mixing model is not known in advance, it is difficult to choose between LSU and LQSU techniques. In this work, a new NMF-based approach is proposed to locally multi-sharpen hyperspectral data by integrating a Digital Surface Model (DSM) obtained from LIDAR data. These DSM data may inform one about the local mixing model (linear or linear-quadratic) since they can be used for determining the object elevations.

The proposed approach detects the local mixing model by using the variance of the object elevations obtained from the DSM data. The hyper/multispectral images are explored using small zones. In each zone, the variance of the object elevations is calculated from the DSM data in this zone. This variance is compared to a threshold value and the adequate spectral unmixing technique is used in the considered zone to independently unmix hyperspectral and multispectral data, using an adequate NMF-based approach. More precisely, when the calculated variance is lower than the fixed threshold (i.e., the considered objects have approximately the same elevations), the mixing model is considered to be linear. Otherwise, it is linear-quadratic. The obtained spectral and spatial information thus respectively extracted from the hyper/multispectral images are then recombined in the considered zone, according to the selected mixing model.

Experiments based on synthetic hyper/multispectral data are performed to evaluate the performance of (i) the proposed multi-sharpening approach and (ii) approaches only based on the linear or linear-quadratic mixing model, used on the whole hyper/multispectral data (i.e., not locally). These synthetic data are generated as follows from a real hyperspectral image classification and associated ground truth. Averaging classification results in small spatial zones yield linear abundance coefficients. In addition, only in zones where the real DSM data exhibit high-variance elevations, Fan's model is used to create quadratic abundance coefficients. The ground truth is also used to generate the hyper/multispectral pure spectra, by averaging spectra in each class. Then, when performing multi-sharpening, the DSM data are also used for locally detecting the mixing model in the proposed approach. Globally, the proposed approach yields good spatial and spectral fidelities for the multi-sharpened data.

9643-35, Session 7

An approach for combining aerial lidar and high-resolution imagery using Gaussian processes

Yansong Liu, Sildomar T. Monteiro, Eli Saber, Rochester Institute of Technology (United States)

Airborne Light Detection and Ranging (LiDAR) system has been used for generating high density 3D point clouds for decades. It is used for a variety of applications including 3D building reconstruction, urban planning and disaster assessments. However, some of the applications are limited due to the lack of spatial and spectral information if only using LiDAR data. Therefore combining the LiDAR data with a high-resolution aerial optical imagery intrigues more and more researches due to its more complete description for the scene. Fusion of these two data also helps us explore other applications like complex land cover classification, small object detection and recognition. The challenge is how to avoid false classification/detection caused by combining the features derived from two different image modalities. In this paper, we propose an approach of handling the uncertainties of both interpolation and classification using Gaussian Processes (GP). We classify the land cover in an urban area into buildings, roads, trees, grass, waterway and vehicles using Gaussian Processes. The LiDAR system used in this paper provides a very high density of point clouds (around 65 points/m^2), which is related to point spacing of approximately 10cm. Each point has the information of latitude, longitude, elevation and LiDAR intensity (wavelength of 1064 nm). A georeferenced color image with a spatial resolution of approximate 5 cm is provided along with the LiDAR data. We post processing the 3D LiDAR points to derive the LiDAR features. We calculate the mean of elevation value, variance of the elevations and the mean of the LiDAR intensity. In the meantime, RGB image is converted into CIE L*a*b* space for extracting color features. Since the resolution for LiDAR data and color image is different and two images are not perfectly registered, a GP based interpolation method is performed on LiDAR data so that each point in the RGB image now is assigned a 6 dimensional feature vector that will be used for classification. Approximately 20% of the RGB image is labeled as the ground truth for training purposes while the rest will be used for cross validation. GP is a powerful tool for handling uncertainties, measuring errors and providing probabilistic estimates. In this paper, we apply the Laplacian approximation for GP binary classifier on the new combined feature space. The multiclass classification has been implemented by using the pair wise binary classification strategy. In order to tackle the issue of computational burden for GP classification, a sparse approximation method is also implemented to speed up the classification process. The result of using support vector machine (SVM) classifier is also given in this paper for comparison. Our experiments show that the GP classification can compete with SVM, which is considered as state-of-the-art method, in terms of accuracy as well as provide probabilistic estimate for each class that can be interpreted as

a confidence map. The advantages and disadvantages of both classifiers will be thoroughly discussed in the end.

9643-10, Session PS

Enhancement on spotlight COSMO-SkyMed SAR products

Rino Lorusso, Agenzia Spaziale Italiana (Italy) and Univ. degli Studi della Basilicata (Italy); Giovanni Milillo, Agenzia Spaziale Italiana (Italy)

INTRODUCTION:

Spotlight SAR data processing is already an established topic; efficient and accurate solutions have been proposed over the last years. The ?-k algorithm provides the highest precision among the frequency-domain imaging algorithms. However, it provides an effective solution to the SAR inverse problem when the sensor trajectory is a straight line; satellite-borne sensors do not fit this scheme. The assumption of a hyperbolic range history is no longer accurate for sub-metric spatial resolutions due to the satellite curved orbit. Furthermore getting close to decimeter resolution (at X-band) other several effects appear; in particular the motion of the satellite during the transmission and reception of the chirp signal deteriorate the impulse response function (IRF), if not properly considered (so called stop-and-go approximation). In this work new aspects are considered for high precision processing of COSMO-SkyMed (CSK) spotlight SAR data with a resolution in the meter range. The ?-k algorithm is used to focus CSK spotlight data and a new data processing chain, also including curved orbit handling and stop-and-go correction, is proposed.

CURVED ORBIT HANDLING:

When the sensor moves along a curved path, the hyperbolas generated by point targets vary with ranges differently from the ones that would be experienced with a sensor flying along a straight line. One possible solution is to achieve the exact correspondence at predefined range values, so that the error can be kept very small at all ranges of interest. This procedure defines an effective rectilinear flight path that will be used in the ?-k algorithm in order to minimize errors at all range swaths. We define a constant velocity veff that is a relative velocity but takes into account the rectilinear orbit. The range of the closest approach range r0 is evaluated starting from this rectilinear orbit, which is not the original one. A nonlinear equations system could be formulated in order to evaluate veff and r0, forcing the true Doppler rate and centroid values to be equal to those that would be obtained on the effective rectilinear orbit on predefined range values. The system solution is obtained by the numerical Newton method and the effective parameters (veff, r0) are used in the ?-k and allows CSK spotlight SAR data to be accurately focused in the azimuth direction.

STOP AND GO APPROXIMATION:

In conventional spaceborne SAR systems the stop-and-go approximation is usually assumed. We show that a residual phase history migration is induced by the stop-and-go approximation on CSK SL focused products. This anomaly has been observed in a very large analyzed CSK SL dataset. The effect is space invariant and it can be easily corrected in the two dimensional frequency domain, simultaneously with the wavenumber focusing step. Results with real CSK SL data validates the suggested methodology. The stop-and-go approximation removal improves the IRF quality of CSK SL SCS products, due to the residual phase history migration correction. With the stop-and-go correction the resolution enhancements are 3.0% in azimuth and 2.2% in range direction.

9643-52, Session PS

Designing an efficient LT-code with unequal error protection for image transmission

Fabio da Silva Marques, Ctr. Federal de Educação Tecnológica de Goiás (Brazil) and Instituto Tecnológico de Aeronáutica (Brazil); Christofer Schwartz, Marcelo S. da Silva Pinho, Instituto Tecnológico de Aeronáutica (Brazil); Weiler A. Finamore, UFJF (Brazil)

The use of images from earth observation satellites is spread over different applications, such as a car navigation system and a disaster monitoring. In general, those images are captured by on board imaging devices and must be transmitted to the earth using a communication system. Even though a high resolution image can produce a better quality of service, it leads to transmitters with high bit rate which require a large bandwidth and expend a large amount of energy. Therefore it is very important to design efficient communication systems. From communication theory, it is well known that a source encoder is crucial in an efficient system. In a remote sensing satellite image transmission, this efficiency is achieved by the use of an image compressor, reducing the amount of data which must be transmitted. The Consultative Committee for Space Data Systems (CCSDS), a multi-national forum for the development of communications and data systems standards for spaceflight, establishes a recommended standard for a data compression algorithm for images from space systems. Unfortunately, in the satellite communication channel, the transmitted signal is corrupted by the presence of noise, interference signals, etc. Therefore, the receiver of a digital communication system may fail to recover the transmitted bit. Actually, to reduce the effect of this failure, a channel code can be used. In 2002, the Luby Transform code (LT-code) was introduced and it was shown that it was very efficient when the binary erasure channel model is used. Since the effect of the bit recovery failure depends on the position of the bit in the compressed image stream, in the last decade many efforts were done to develop LT-code with unequal error protection. In 2012, Arslan et al. showed improvements when the LT-code with unequal error protection is used in images compressed by SPIHT algorithm. Recently, we propose the use of a LT-code based on the weighted approach to protect the transmission of images encoded by the algorithm for image compression recommended by CCSDS. The performance was measured using two figure of merits: (a) the probability of achieve a minimum acceptable PSNR, and (b) the mean of PSNR, given that the minimum acceptable PSNR was achieved. To design a LT-code with an unequal error protection, in our recent work, the bit stream produced by the algorithm recommended by CCSDS is partitioned in M disjoint sets of bits. Using the weighted approach, the LT-code produces M different failure probabilities for each set of bits, p1,..., pM leading to a total probability of failure, p which is an average of p1,..., pM. In our previous work, the parameters of the LT-code with unequal error protection were set using a heuristic procedure. In this work, we analyze the problem of choosing the LT-code parameters to maximize the mean of PSNR, given that the minimum acceptable PSNR was achieved. The main contribution of this work is a set of equations that p1,..., pM must meet to optimize the performance of the image transmission.

9643-54, Session PS

Unsupervised and stable LBG algorithm for data classification: application to aerial multicomponent images

Akar Taher, Koya Univ. (Iraq) and Univ. de Rennes 1 (France); Kacem Chehdi, Claude Cariou, Univ. de Rennes 1 (France)

Classification is an important machine learning tool for

discovering hidden patterns, structures and relationships between data objects, which is in its turn is an ill-posed problem, and the choice of an optimal method is not obvious.

In this paper a stable and unsupervised Linde-Buzo-Gray (LBG) algorithm named optimized LBG (OLBG) is presented. The originality of the proposed algorithm relies: i) on the usage of an adaptive incremental technique to initialize the class centres that calls into question the intermediate initializations; this technique renders the algorithm stable and deterministic, and the classification results do not vary from a run to another, and ii) on the unsupervised evaluation criteria of the intermediate classification result to estimate the optimal number of classes; this makes the algorithm completely unsupervised.

To develop a robust classification method giving the best classification of a dataset X where each element is characterized by a vector of features, we propose an optimized version of LBG that meets the properties cited above. For this, the following important steps are required:

Step 1: Choice of the class to be subdivided (to obtain k+1 classes): at the beginning (K=1), the class to be divided is the whole dataset X. When K>1, choose the most expanded class.

Step 2: Choice of the initial class centres: after choosing the class to be subdivided into two subclasses, we need to identify their centres. The first subclass centre will be the centre of gravity of the chosen class, and the other subclass centre is a random element within the selected class to be subdivided.

Step 3: Classification with class centre fine-tuning: we classify the dataset using LBG. To make the approach independent of the initial class centres a removal-insertion fine-tuning process.

Step 4: Evaluation of the obtained intermediate classification results using a completely unsupervised criterion: if this criterion is satisfied the classification result into K+1 classes is validated, then go to step 1. If the criterion is not satisfied go to step 1 and change the class to be subdivided, choosing the next most expanded. The algorithm stops in case none of the classes satisfy the criterion, in other words if none of the classes in the current result is divisible, hence the current number of classes is considered as optimal.

The efficiency of this optimized version of LBG is shown through some experimental results. More precisely we have tested our proposed unsupervised classification approach OLBG regarding four aspects: firstly for its stability, secondly for its correct classification rate, and thirdly for the correct estimation of number of classes, and lastly for its computation time complexity.

OLBG was also used to partition multicomponent aerial images for two real applications (classification of different types of vegetation, and detection of a specific type of trees). In both applications the algorithm detects the exact number of classes with a correct classification rate of more than 91% and 94% for each application respectively. While, by using LBG algorithm these rates drop to 71% and 84% respectively for each application.

9643-55, Session PS

Lossy compression of hyperspectral images using shearlet transform and 3D SPECK

Azam Karami, Shahid Bahonar Univ. of Kerman (Iran, Islamic Republic of)

In recent years, compression of hyperspectral images (HSI) has gained particular attention to reduce the cost of equipment storage and bandwidth interests. There are two types of redundancy in HSI: spatial and spectral redundancies. These redundancies allow for development of effective compression algorithms. Some compression methods currently consider HSI as 3D dataset, two spatial dimensions and one spectral dimension. These methods try to take into account the spatial and spectral correlation of hyperspectral data simultaneously. For example, several 3D wavelet-based techniques such as Set Partitioning in Hierarchical Trees (SPIHT) and Set Partitioned Embedded bloCK (SPECK) algorithms for HSI compression have been proposed. But Wavelets are known to successfully represent 1D signals with high sparsity. However, 2D wavelet representation is not highly sparse. In recent years, multidirectional representations based on contourlets, curvelets etc. have been introduced in order to efficiently handle the geometrical features of multidimensional signals. Recently, the shearlet transformation was introduced and was shown that it has a superior directional selectivity which makes it an optimal sparse representation of images. For this reason, in this paper a new lossy compression method for HSI is introduced based on 3D discrete shearlet transform. In the proposed method, first the 3D HSI are efficiently decorrelated by shearlet transform. Second, soft thresholding is used to reduce the precision of the transformed coefficients and in addition it caused to reduce the number bits required to represent the images. Third, the output of threshold step is encoded by one of the efficient wavelet coder, 3D- SPECK. It includes a block splitting algorithm in order to to sort the significant pixels. If a code block contains significant coefficients it splits it into smaller sub-blocks. This technique can find the areas with high energy and code them first this process continued until a certain bit rate is achieved. Finally, the compressed dataset is transmitted in to the receiver, then the SPIHT decoding is performed and the inverse 3D shearlet transform is applied to the decoded values in order to obtain the reconstructed HSI. The proposed algorithm is applied on the real HSI (AVIRIS datasets: Cuprite and Moffett Field), simulation results show that the proposed method, in comparison with well-known approaches such as 3D-SPECK (using 3D wavelet) and combined PCA and JPEG2000 algorithms, provides a higher SNR (signal to noise ratio) for any given compression ratio (CR). It is noteworthy to mention that the superiority of proposed method is distinguishable as the value of CR grows especially when the target CR is selected higher than 160, in this case the performance of the proposed algorithm is significantly better than the other techniques. In addition, the effect of proposed method on the spectral umixing analysis is evaluated.

9643-56, Session PS

An image matching method based on closed edges incorporated with vertex angles

Baoming Zhang, Xiaowei Chen, Jun Lu, Zhihui Gong, Haitao Guo, Zhengzhou Institute of Surveying and Mapping (China)

Robust and adaptable, feature-based matching has become a focus and hotspot in image matching research field. With the development of edge detection and image segmentation techniques, edge-based matching method has got wide interests from researchers. Obtaining edge features through hysteresis thresholding of edge intensity and confidence, Edison operator makes full use of the pixel gradient phase information and detect weak edges efficiently. Based on edge detection results by Edison operator, we select closed edges and vertex angles in free-form line features as conjugate entities. The seven invariant moments which have an invariance for rotation, translation and scale change constructed by Hu are chosen as the matching entities for closed edges. On the other hand, the angle of two sides of edges for vertex angles are selected as matching entities, and the vertex angles are extracted by the difference of the sum of absolute chain-code algorithm which have not only a good performance in feature point extracting but also a good capacity in information compressing and anti-interference. It should be noted that the vertex angle with consistent direction of two sides of edges and large enough distance with its adjacent vertex angles can be saved. After extracting closed edges and vertex angles and their matching entities, there are three main steps to determine the conjugate features and transformation parameters between the matching images. Firstly, conjugate feature candidates are determined by matching entities based on the similarity measurement. Next, combining conjugate feature candidates in pair-wise and eliminating mismatching candidates. In remote sensing image processing, many 2D (or 3D) transformations can be approximated by the 2D (or 3D)

similarity transformation. Additionally, composed of scaling, rotation and translation parameter, parameters in similarity transformation are comparatively less, and can be solved independently. Therefore, 2D similarity transformation is chosen as the transformation model to eliminate mismatching pairs. Each pair of conjugate feature candidates can determine a group of parameters, and they can be viewed as a point in high-dimensional space(R4). The points determined by real conjugate features are relative concentrated. In other words, the points far away from their nearest point are determined by mismatching features. Through this way, most of pairs containing mismatching can be eliminated. Finally, K-means space clustering method is used to further eliminate pairs containing mismatching features. Taking these steps, conjugate features can be determined. In order to verify the stability and precision of this method, two group of experiments have been designed. The first experiment is between real image and its simulate image generated through affine transformation, and the second is between space stereo images. Experimental results turn out that the extracted features are even distributed and comparatively stable and reliable, and the image matching method shows a stable performance and can achieve a high matching accuracy with a small number of homogenous features.

9643-57, Session PS

Fast geometric processing for unmanned aerial vehicle images of large area

Haitao Guo, Baoming Zhang, Jun Lu, Junfeng Xv, Chunxue Jiang, Zhengzhou Institute of Surveying and Mapping (China)

The fast geometric processing of remote sensing image from unmanned aerial vehicle (UAV) has been widely used in lash-up detection and evaluation for disaster, military reconnaissance, topographic mapping, environmental monitoring, and so on. Aiming at the problem of how to improve the data processing speed for remote sensing image from unmanned aerial vehicle, the procedures of unmanned aerial vehicle image matching, bundle triangulation, orthophoto generation and image mosaic are analyzed in this paper. Image connection point matching algorithm of geometric constraint condition is proposed. Various optimization strategies are used to improve the matching speed. On the one hand, SURF matching method is used to resist rotation and scale change. At the other hand, hierarchical pyramid matching strategy from coarse to fine is introduced to improve the matching efficiency. Sparse matrix technique is introduced, completing block adjustment rapidly under the POS data aided. Firstly, relative orientation, bridging of model and block adjustment of strip method are done while elements of exterior orientation of image are obtained from POS data is as initial value. Secondly bundle block adjustment is done while the result of block adjustment of strip method is as initial value. Sparse matrix technique is introduced while bundle block adjustment is done. Image mosaic method based on Voronoi diagram is adopted. The method realizes seamline network generated automatically and a wide range of image mosaic and reduces the data redundancy of overlap zone. The operation speed of the algorithm is improved by the above improvement and optimization for processing algorithm. The parallel processing algorithms of matching, geometry rectification and mosaic of unmanned aerial vehicle images on multi-core CPU are introduced to improve the efficiency of data processing. These algorithms take full advantage of the computer resources and don't need to enhance computer configuration. A fast processing process for unmanned aerial vehicle images is provided. Extensive tests for unmanned aerial vehicle images indicate that the method significantly improves the efficiency of UAV images processing, especially for large area UAV images processing. At the same time, the precision of relative positioning and the effect of image mosaic of the method are excellent to meet the requirements of the fast geometric processing for UAV images.

9643-58, Session PS

Size-varying small target detection for infrared image processing

Miao Li, Ran Zhu, YunLi Long, Wei An, Yiyu Zhou, National Univ. of Defense Technology (China)

IRST (Infrared Search and Track) has been applied to many military or civil fields such as precise guidance, aerospace, early warning. As a key technique, small target detection based on infrared image plays an important role. The small target is defined as having a total spatial extent of less than 80 pixels (9?9) by SPIE. However, infrared targets have their own characteristics, such as target size variation, which make the detection work quite difficult. In practical application, the target size may vary due to many reasons, such as optic angle of sensors, imaging distance, environment and so on. For conventional detection methods, it is difficult to detect such size-varying targets, because they are size-fixed methods. In fact, the performance of them may become worse, when the backgrounds have strong clutters.

This paper presents a novel method to detect size-varying infrared targets in a cluttered background. It is easy to find that the target region is salient in infrared images. It means that target region have a signature of discontinuity with its neighboring regions and concentrates in a relatively small region, which can be considered as a homogeneous compact region, and the background is consistent with its neighboring regions. Motivated by the saliency feature and gradient feature, we introduce minimum target intensity (MTI) to measure the dissimilarity between different scales, and use mean gradient to restrict the target scale in a reasonable range. They are integrated to be multiscale MTI filter. The basic concept of the MTI is introduced first time in our paper, and it means the valid target intensity after rejecting the estimated max background. To calculate MTI, the local image patch is divided into 3?3 cells, and the central cell is the target cell, where the signals of target could appear. The surrounding cells are background cells and used to estimate max background value. Only when the size of target cell is suitable for true target size, the MTI reach the maximum. Besides, gradient feature of target boundary is helpful to decide when to stop scale search. The proposed detection method is designed based on multiscale MTI filter. Firstly, salient region is got by morphological low-pass filtering, where the potential target exists in. It can provide saliency map effectively and quickly, then speed up extraction of candidate targets. Secondly, the candidate target regions are extracted by multiscale minimum target intensity filter, which can effectively give the optimal target size. At last, signal-to-clutter ratio (SCR) is used to segment targets, which is computed based on optimal scale of candidate targets. To evaluate the detection performance of the presented method, an experimental system is set up. The proposed method based on multiscale MTI filter is tested and also compared with two state-of-the-art methods. In order to obtain an objective evaluation, the infrared images belonging to two scenes, low-level clutter scene and high-level clutter scene, are used. The experimental results indicate that the proposed method outperforms other methods by achieving both higher detection precision and robustness.

9643-60, Session PS

Semi-auto assessment system on building damage caused by landslide disaster with high-resolution satellite and aerial images

Bo Sun, Qihua Xu, Jun He, Fengxiang Ge, Ying Wang, Beijing Normal Univ. (China)

In recent years, earthquake and heavy rain have triggered more and more landslides, which have caused serious economic losses. Detecting the disaster area and assessing the hazard timely are necessary and primary for disaster mitigation and relief. As high-resolution satellite and aerial images have been widely used in the field of environmental monitoring and

disaster management, the damage assessment by processing satellite and aerial images has become a hot spot of research work. While, the rapid assessment of building damage caused by landslides with high-resolution satellite or aerial Images is just the focus of this article.

In this paper, after analyzing the characteristics of the landslide disaster, we proposed a set of standard for rating building damage caused by landslides, according to which a semi-automatic evaluation system has been designed. The system is a kind of practical application of satellite and aerial images processing, it first classifies landslide area from other surface changes with SVM method. Then, combining with the hand-annotated outline vector of each building's roof, the relative position and distance between the building and the landslide area are available. Additionally, some texture features and geometrical dimensions of the roof are also calculated. Thus, the system can grade the building damage semi-automatically. Finally, to validate the performance of the proposed system, we have performed extensive experiments on the landslide-images of Longtou Mountain in Yunnan Province of China in 2014. Compared with visual interpretation results, the system has got an overall accuracy of 79 percent, which has shown the system is effective. In the paper, detailed scheme, experiments and analysis of the system have been introduced. What's more, in order to meet the requirement for practical application, some ideas of further improvement and optimization of the system have been also brought out.

This research was primarily supported by the National Key Technology R & D Program of the Twelfth Five-Year of China (No. 2012BAK10B03).

9643-61, Session PS

The research of land covers classification based on waveform features correction of full-waveform LiDAR

Mei Zhou, Academy of Opto-Electronics (China); Meng H. Liu, Zheng Zhang, Lian Ma, Hui Jing Zhang, Academy of Opto-Electronics (China) and Chinese Academy of Sciences (China)

LiDAR is an advanced active remote sensing technology that can quickly obtain the 3D information of the targets, has been widely applied in many fields of remote sensing, such as land resource investigation, environment monitoring, disaster assessment, land covers classification and so on. According to land covers classification, the traditional discrete LiDAR usually uses three-dimensional coordinate information of the targets since it can only record several echoes and obtain limited information about the targets. Thus it usually resulted in insufficient classification types and low classification accuracy. Relative to the discrete LiDAR system, full waveform LiDAR system can record the entire waveform of the targets. And the waveform features reflecting the inherent characteristics of the targets can be also obtained after waveform processing, which can improve the classification accuracy when used for land covers classification. In this paper, the waveform features of small footprint airborne Full-waveform LiDAR were analyzed and corrected to be used for land covers classification. Firstly, the waveforms of different targets were processed, including waveform preprocessing, waveform decomposition and feature extraction. Then classification ability of extracted waveform features that are distance, amplitude, waveform width and the scattering cross-section were clearly analyzed using the measured full waveform LiDAR data with different characteristics. The pseudo color maps reflecting the values of extracted feature were also given and clearly showed the certain ability of each feature to distinguish different kinds of land covers. In order to decrease the differences of features of the same land cover type, weaken the influence of different factors such as emission pulse, incident angle and atmospheric attenuation on the features, and further improve the effectiveness of the extracted features for the land covers classification, this paper has made comprehensive correction on the extracted features considering about these factors. The features of waveform data obtained in Zhangye were extracted and corrected. It showed that the variance of the corrected waveform feature can be reduced by about 20% compared to original features. In order to verify whether the corrected features can improve the classification accuracy, this paper has respectively classified typical land covers of Zhangye based on the original features and corrected features. Since the features of the land covers have independently Gaussian distribution, the Gaussian mixture density model (GMDE) was put forward to be the classification model to classify the targets as road, trees, buildings and farmland in this paper. For each land cover type, typical samples were selected to train the classification model. Then relevant parameters were obtained through the training and used for land cover classification. The classification results of these five land cover types were obtained according to the ground truth information gotten from CCD image data of the targets region. It showed that the classification accuracy can be improved by about 8% when the corrected features were used for land covers classification.

9643-62, Session PS

Mapping the urban area extent with a nighttime imagery of OLS and ISS

Andrzej Z. Kotarba, Sebastian R. Aleksandrowicz, Space Research Ctr. (Poland)

The human activity constantly transforms the natural environment into a more comfortable and suitable for man's live and prosperity. As a consequence, the natural surfaces are being turned into artificial: housing, industrial facilities, transportation, etc. The soil becomes sealed (less pervious for water), resulting in a change in the energy budget and hydrological budget of the environment. Simultaneously, impervious surfaces are the predominant land use type occupied by the humans.

Mapping the extend of artificial impervious areas becomes the essential issue for the monitoring human activity and its impact on the environment. The most effective method for such monitoring is the satellite remote sensing. A number of methods have been developed for the discrimination between artificial surfaces and other land use/land cover types. The optical remote sensing focuses on the visible and short infrared range of the electromagnetic spectrum, which is usable daytime, when the Sun serves as a source of the radiation. However, Earth's surface can be also imaged nighttime, with detectors sensitive enough to register the lights emitted by a human-related installation (e.g. street lighting). Since "artificial" nocturnal light is attributed to the urban areas, it comes as a proxy for detecting the impervious surfaces. For decades the only nighttime data were available with the Operational Linescan System. However, the data have a coarse resolution (~2.5 km/pixel), feature no radiometry, and are overexposed. We propose to use high-resolution ISS photography, instead of the OLS imagery.

We estimated the spatial extent of the impervious surfaces in the city of Berlin using the nighttime photography taken by an astronaut onboard the International Space Station. The photography was took with Nikon D3S digital still camera equipped with a 400-mm AF-I Nikkor lens. After pre-processing, the spatial resolution of the image was found to be 16.95 m/pixel. Image was converted into 16-bit TIFF file and classified into two classes: "impervious surfaces" and "other surfaces". Accuracy of the classification was assessed with standard products of the EU Copernicus program: High Resolution Layer-Imperviousness (HRL-I), Urban Atlas, and CORINE Land Cover. Both the user and producer accuracy exceeded 85%. The misclassified were transit roads and airport runways (omission error), and green areas, water bodies within the city (commission error).

Results based on the ISS photography were compared with the map produced with the OLS. We used OLS data in a form of the imperviousness degree, and assumed that impervious were those areas with the imperviousness greater than zero. That assumption resulted in a significant disagreement: ISS indicated that 55.7% of the study area was impervious, while OLS suggested as much as 99.5%. The true value was calculated

with HRL-I dataset: 59.6%. OLS become to agree with HRL-I only when assumed that surfaces with imperviousness lower than 10% (according to OLS) were pervious. Our results demonstrated that ISS is more accurate in detecting the impervious surfaces than OLS.

9643-63, Session PS

A PSF equalization technique for the Multi-Order Solar Extreme-ultraviolet Spectrograph (MOSES)

Shane Atwood, Charles C. Kankelborg, Montana State Univ. (United States)

The Multi-Order Solar Extreme Ultraviolet Spectrograph (MOSES) is a rocket borne slitless imaging spectrometer, designed to observe He II (30.4 nm) emission in the solar transition region. This instrument forms three simultaneous images at spectral orders m=-1, 0, +1 over an extended field of view. A multi-layer coating on the grating and thin film filters in front of the detectors define the instrument passband. Each image contains a unique combination of spectral and spatial information. Our overarching goal in analyzing these data is to estimate a spectral line profile at every point in the field of view (FOV).

Each spectral order has a different image geometry, and therefore different aberrations. Since the PSF differs between any two images, systematic errors are introduced when we use all three images together to invert for spectral line profiles. To combat this source of systematic error, we have developed a PSF equalization scheme.

Determination of the image PSFs is impractical for several reasons, including changes that may occur due to vibration during both launch and recovery operations. We have therefore developed a strategy using only the solar images obtained during flight to generate digital filters that modify each image so that they have the same effective PSF. Generation of the PSF equalization filters does not require that the PSFs themselves be known. Our approach begins with the assumption that there are only two things that cause the power spectra of our images to differ:

(1) aberrations; and

(2) the FOV average spectral line profile, which is known in principle from an abundance of historical data.

To validate our technique, we generate three synthetic images with three different PSFs. We compare PSF equalizations performed without knowledge of the PSF to corrections performed with that knowledge. Finally, we apply PSF equalization to solar images obtained in the 2006 flight MOSES and demonstrate the removal of artifacts.

9643-64, Session PS

A novel scheme for automatic nonrigid image registration using deformation invariant feature and geometric constraint

Zhipeng Deng, Lin Lei, Shilin Zhou, National Univ. of Defense Technology (China)

Automatic image registration is a vital yet challenging task and most classic algorithms for image registration problems center around the rigid deformation. However, there is a widespread and growing need of the non-rigid image registration which is more complicated and common in remote sensing images, such as distorted UAV(Unmanned Aerial Vehicle) images or scanning imaging images caused by flutter. Traditional non-rigid image registration methods are based on the correctly matched corresponding landmarks, which usually needs artificial markers. It is a rather challenging task to locate the accurate position of the points and get accurate homonymy point sets. In this paper, we proposed an automatic non-rigid image registration algorithm which mainly consists of three steps: uniform distributed point feature detection, point sets matching using deformation invariant feature descriptor and geometric constraint, image registration based on non-rigid geometry deformation model.

In point feature detection, for demands of non-rigid image registration, a point detection method based on non-linear scale space and uniform distribution strategy are proposed, in order to extract the point set which is uniform distributed along the edge of the image. This method uses bilateral filter instead of Gaussian filter to build the non-linear scale space, and then extract a specified number of feature points based on uniform distribution strategy in both scale space and image space.

In terms of point sets matching, inspired by the thought of object recognition which model the target as a feature point set and search the best matched point set in the scene point set, we propose a hybrid point matching algorithm based on local features and geometric constraints in order to get more correctly matched points. This method uses DaLI(Deformation and Light Invariant) deformation invariant descriptor which is constructed in terms of HKS(Heat Kernel Signature) in the embed 3D image space, and built the local affine invariant geometric constraint based on triangulation which is constructed by K-nearest neighbor algorithm. Based on the utilization of local descriptor and geometric constraints, an objective function is constructed and the corresponding match matrix is solved. Based on the accurate homonymy point sets, the two images are registrated by the model of TPS(Thin Plate Spline).

The proposed algorithm is tested on deliberately designed synthetic data set and real data set by three experiments. The first experiment is designed to evaluate the distribution of point set. Compared with SIFT(Scale-Invariant Feature Transform),BFSIFT(Bilateral Filter-SIFT) and UDSIFT(Uniform Distributed-SIFT), the point set detected by our method is uniform distributed along the edge of the image which is useful to be the CPs(Control Points) for on-rigid image registration and the number of the point set can be assigned beforehand. The second experiment is designed to evaluate the correctly matching rate. Compared with SIFT, GIH (Geodesic Intensity Histogram),DaLI, our method can better improve the registration accuracy and limit the wrong matching points' effect. The last experiment is designed on the non-rigid deformation remote sensing images and the successful use of our algorithm achieved good results compared with SIFT. The three experimental results demonstrate the accuracy, robustness, and efficiency of the proposed algorithm.

9643-65, Session PS

A fast sparse unmixing method for hyperspectral images using iterative detection and estimation

Mohammad Saleh Hasani, Azam Karami, Shahid Bahonar Univ. of Kerman (Iran, Islamic Republic of)

The main objective of spectral unmixing is to extract pure spectral signatures (endmembers) and estimat abundance map of each endmember. Recently, linear spectral unmixing (LSU) is highly used due to a simple model. In this model, it is assumed that spectrum of each pixel of hyperspectral image is a linear combination of various endmembers. Different methods for LSU have been proposed for example efficient methods based on sparse regression are highly considered.

In fact, sparse unmixing is the solution of X=A?S equation. Each column of matrix X is related to spectrum of each pixel of hyperspectral image. Columns of matrix A represent endmembers and rows of matrix S consist of abundance map corresponding to each endmember. In this paper, it is assumed that matrix A is known and available in a library, it can be constructed from the U.S. Geological Survey. A new Sparse Unmixing method using Iterative Detection and Estimation (SUIDE) is proposed in this paper in order to identify matrix S.

SUIDE is an iterative algorithm with small number of iterations compared to the other existing iterative sparse unmixing

methods (e.g. SUnSAL and CLSUnSAL). Each iteration of the proposed algorithm includes two following steps:

First, detection: in this step active and inactive rows of matrix S should be detected. In fact, a few endmembers of library A exist in real hyperspectral images, this means that not many rows of matrix S consist nonzero values (i.e. active rows), implying sparsity, and the rest are called inactive rows. In this case, matrix S is considered as a Gaussian mixture model. Elements of active and inactive rows of S are assumed zero-mean Gaussian with high and low variances, respectively. Indeed, the goal of this step is to find the active rows of S and it can easily be solved using detection algorithms. In order to solve it, Neyman-Pearson (NP) test is used. However, because of matrix S being unknown, sub-optimal NP test is applied. In fact, instead of S, its estimation is used. Finally, this step ends with active rows of S being detected and consequently their corresponding endmembers existing in hyperspectral image are distinguished from columns of A.

Second, estimation: using obtained endmembers from the previous step and existing X, active rows of fractional abundance matrix S is calculated utilizing Least-Squares method. After that, inactive rows of S will be set to zero.

Finally, SUIDE algorithm is applied to the synthetic and real hyperspectral datasets. Simulation results show that the proposed method achieves a higher Signal to Reconstruction Error (SRE), and also lower Root Mean-Squared Error (RMSE), compared to the state of the art algorithms such as SUnSAL and CLSUnSAL. It is noteworthy to mention that an important advantage of the proposed algorithm is fast implementation because it requires small numbers of iterations (normally less than 10 iterations) in order to solve the spectral unmixing problem. In future works, Non-Gaussian distributions in detection step, and also novel approaches for estimating of fractional abundances matrix will be investigated.

9643-66, Session PS

A new polarimetric active radar calibrator and calibration technique

Jianguo Tang, Xiaojian Xu, BeiHang Univ. (China)

Polarimetric active radar calibration techniques attracted quite a few researchers in recent years. Polarimetric active radar calibrator (PARC) using a single antenna was designed, manufactured and applied to polarimetric calibration with acceptable performance. However, single antenna PARC usually uses a square horn with waveguide orthomode transducers (OMT), where electromagnetic polarization filter cannot be applied to decrease the cross polarization which severely degrades the calibration accuracy. Besides, single antenna PARC also restricts the variety of forms for polarimetric scattering matrices (PSM) available. In addition, conventional approach for polarimetric active calibration relies on the measured scattering matrices of a PARC for a few special rotation angles about the incidence direction, such that the parameters of a polarimetric radar system are obtained by solving a set of equations that associate the theoretical PSMs with the measured PSMs data through the RST model, which is always sensitive to noise and clutter.

As an ideal calibrator, it is necessary for a PARC to possess excellent cross polarization isolation so that accurate radar system parameters can be obtained through the polarimetric calibration measurement. To this end, a new PARC consisting of two separate antennas is preferred, where the two antennas serve as the receiving and transmitting antenna independently. Each antenna of the PARC is equipped with a wideband electromagnetic polarization filter to achieve lower cross-polarization electromagnetic field transmission and reception levels. By rotating the two antennas about the incidence direction with different combinations, a variety of PSM forms will be available. Moreover, the measured data also contain noise and background clutter including the scattering from the PARC itself. The contribution of the PARC's scattering usually can be separated in down range by using a delay line in its RF loop. However, other noise and clutter cannot be simply eliminated, which impacts on the calibration accuracy as well. With the rotation about the incidence direction of each antenna in the double-antenna PARC (DPARC), the four elements of its PSM varies sinusoidally. This suggests that a Fourier analysis may be utilized in the calibration process to improve the robustness of the process when the measured data contain noise and clutter interference.

The overall process for polarmetric calibration using the currently proposed DPARC is as follows: First, set the polarization of the receiving and transmitting antennas of the DPARC to be the same, simultaneously rotate the two antennas about the incidence direction from 0 to 180 degrees(or an integer multiple of 180 degrees), record returned signals at different rotation angles from the DPARC; Second, the RST model is used to establish a set of equations which define quantitative relations between the theoretical PSM and the measured polarimetric data of the DPARC; Last, Fourier analysis is applied to derive the polarimetric radar system parameters according to the set of equations.

Numerical simulation results show that the Fourier analysis technique can estimate radar parameters more accurate than conventional techniques, suggesting that the DPARC is an ideal calibrator for its excellent polarization isolation as well as its variety of PSM forms.

9643-67, Session PS

A landmark matching algorithm using the improved generalised Hough transform

Binbin Chen, Xin-Pu Deng, National Univ. of Defense Technology (China)

The paper addresses the issue on landmark matching of images from Geosynchronous Earth Orbit (GEO) satellites. In general, satellite images are matched against the base image. The base image is defined in advance. If the satellite images are rotated, the accuracy of many landmark matching algorithms deteriorates. To overcome this problem, an improved generalised Hough transform (GHT) is proposed to apply for landmark matching.

In recent years, many efficient GHT algorithms have been proposed for shape analysis. However, a weakness of many algorithms is using the point spread function (PSF), which replaces the R-table used in the conventional GHT. It means that all entries in the PSF are employed to compute possible locations of reference points for each boundary point of satellite images. Therefore, it is feasible to propose a more efficient GHT algorithm by constructing a modified R-table. Using the R-table instead of the PSF not only reduces computation load, but also increases the algorithm reliability. The improved GHT algorithm is described as follows.

In this paper, the modified R-table is defined by the base image using the curvature, the displacement vector model |?| and the relative angle ? between its gradient and displacement vectors. Where, the displacement vector is defined that points from the reference point to the boundary point, the reference point is the centroid. The index of the modified R-table is the curvature, and the entry in the R-table is (?,|?|). Furthermore, if more than one boundary points have the same curvature, their respective (?,|?|) of these points are placed in the same entry in the R-table.

For landmark matching, the boundary is the coastline. Through all the boundary points from the base image, the R-table is complete.

For the satellite image, the curvature k and thus the index of the R-table are obtained from each edge point. So the respective entries in the R-table are obtained through looking up the R-table. Next, the certain rule is used to compute possible locations of reference points in the satellite image. And a matrix called the accumulator matrix, which has the same size with the satellite image, is set up to count frequencies of each possible reference point. The reference point is retrieved and the appropriate cell in the accumulator matrix is incremented. The cell with maximum "votes" in the accumulator matrix can be a possible point of existence of the object in the satellite image.

Another factor to consider is curvature. In order to ensure that the modified R-table is orientation-invariant, the curvature must remain unchanged or change in an acceptable extent when the boundary from the satellite image is rotated. In this paper, U-chord method is used to calculate curvature. The slight change in curvature occurs due to satellite images rotation, which hardly affects the performance of matching using nearly equal approach to look up the R-table.

The invariance to rotation, different level of noise, and occlusion are conducted to assess the performance of the proposed algorithm. The simulation results show that the improved GHT algorithm performs well on matching satellite images that are rotated.

9643-68, Session PS

A hyperspectral imagery anomaly detection algorithm based on local three-dimensional orthogonal subspace projection

Xing Zhang, Gongjian Wen, National Univ. of Defense Technology (China)

Anomaly detection (AD) becomes increasingly important in hyperspectral imagery analysis with many practical applications. In hyperspectral domain, anomalies refer to pixels that have distinct spectral differences with regard to the surrounding background pixels. Therefore, most of the interference affecting anomalies derives from the background materials in which they are inserted. Such background interference lies in a subspace that is more likely spanned by the spectra of the pixels in the target neighborhood, rather than by the endmembers/eigenvectors extracted from the whole image. Accordingly, a number of local AD algorithms have been carried out in the past few years including the local orthogonal subspace projection (LOSP) detector which is based on geometric model avoiding estimating the background characteristic in a statistic way. LOSP exploits local endmembers/eigenvectors around the pixel under test (PUT) to construct background subspace. However, this subspace only takes advantage of the spectral information, but the spatial correlation of the background clutter is neglected, which leads to the anomaly detection result sensitive to the accuracy of the estimated subspace. In this paper, a local three dimensional orthogonal subspace projection (3D-LOSP) algorithm is proposed. Firstly, under the jointly use of both spectral and spatial information, three directional background subspaces are created along the image height direction, the image width direction and the spectral direction, respectively. Then, the three corresponding orthogonal subspaces are calculated. After that, each vector along three direction of the local cube is projected onto the corresponding orthogonal subspace. Finally, a composite score is given through the three direction operators. In 3D-LOSP, the anomalies are redefined as the target not only spectrally different to background, but also spatially distinct. Thanks to the addition of the spatial information, the robustness of the anomaly detection result has been improved greatly by the proposed 3D-LOSP algorithm. It is noteworthy that the proposed algorithm is an expansion of LOSP and this ideology can inspire many other spectral-based anomaly detection methods. Experiments with real hyperspectral images have proved the stability of the detection result.

9643-69, Session PS

Lossy compression of hyperspectral images using block coordinate descent search and compress sensing methods

Shirin Hassanzadeh, Shahid Bahonar Univ. of Kerman (Iran, Islamic Republic of); Azam Karami, Shahid Bahonar Univ. of Kerman (Iran, Islamic Republic of) and Univ. Antwerp (Belgium)

Nowadays lossy compression of hyperspectral images (HSI) has gained particular attention. There are two types of correlation in HSI: spatial and spectral correlations. Recent compression methods consider HSI as a 3D dataset: two spatial dimensions and one spectral dimension. In fact, these methods simultaneously consider spectral and spatial correlations. For example, one of the efficient methods is Non-Negative tucker decomposition (NTD). In this method, the original 3D dataset is decomposed to a smaller 3D dataset (core tensor) and three matrices. In this case, if the size of core tensor is selected lower, the compression ratio (CR) will become higher. There are different methods for solving the NTD problem. One of the popular methods is Block Coordinate Descent Search (BCDS). In this method, first three initial values for size of core tensor are manually selected and the initial values for elements of three matrices and core tensor are randomly generated. However this method is very sensitive to these selected values. Therefore, in this paper a new compression method is introduced in order to increase the performance of BCDS. The two simultaneous following modifications are proposed:

First, in the existing BCDS, the size of core tensor is manually selected. In this paper, these values are automatically defined which helps the performance of BCDS for compression to significantly increase. In this case, the objective function of BCDS is modified. The existing objective function is to minimize the difference norm between the original and reconstructed datasets. In the proposed method, a penalty term is added in order to find the optimum values for core tensor size. In fact, it assumes the sum of core tensor size values is constant and this constraint is added to the objective function.

Second, compressed sensing (CS) algorithm is applied to the original dataset. For this purpose, three Gaussian matrices are multiplied in three directions to the original 3D dataset. After that, three tensors (Compressive Measurements) are obtained. Using these tensors, three initial matrices and core tensor for BCDS algorithm could be calculated. Applying these two modifications, the optimum values of core tensor size and the elements of three matrices and core tensor, are obtained.

One of the important applications of HSI is target detection in military applications. Due to the effect of lossy compression on all voxels in the proposed method, first, targets are detected using Uniformly Most Powerful test. After that, targets and their locations are coded using JPEG2000-LS. Then, the whole compressed dataset is transmitted. In the receiver the compressed dataset is reconstructed then the targets are replaced.

The proposed algorithm is applied to the real HSI datasets. Simulation results show that the proposed method, in comparison with the-state-of-the-art algorithms such as PCA+JPEG2000, Kronecker CS and ALS-NTD achieves a higher signal to noise ratio for any given CR. Finally, it is noteworthy to mention that the superiority of the proposed compression method is to achieve good compression performance and preserve the targets unchanged.

9643-70, Session PS

Fusion of multispectral satellite images by using IHS and local fractal dimension

Mohamed Khider, Soumya Ourabia, Youcef Smara, Univ. des Sciences et de la Technologie Houari Boumediene (Algeria)

In this work, we have implemented a Pansharpening fusion method based on Intensity Hue Saturation (IHS) and the local fractal dimension. The up-sampled pixels from the multispectral image are generated by the random midpoint displacement method. Indeed, several fusion algorithms for satellite images have been developed in various applications. Because of the variation in the reflectivity due to the different characteristics of the environment to be treated, the use of a non suitable fusion algorithm can introduce spatial and spectral distortions, e.g. the processing of an image which represent an urban area/ city requires an algorithm which keeps the edges, also the observation of agricultural surfaces require the preservation of low frequencies information. Other applications that concern

humanitarian crisis, e.g. refugees camps, have a rather complex texture structure, in this case we must consider the presence of a heterogeneous texture, to preserve the details of structures in fine scales. To respond to these requirements, we propose the improvement of the IHS algorithm, by introducing into the up-sampling operation of the multispectral image (MSP), the random midpoint displacement technique (RMD), using as parameter the local fractal dimension to generate the new pixels. The local fractal dimension is calculated by introducing the continuous wavelet transform with the first order derivative of Gaussian, and applied to the panchromatic image (PAN). This procedure is based on the use of the exponent of singularity, which is estimated using the theorem of Mallat and Hwang 1992, then for each pixel, the local fractal dimension is determined, related by definition to the singularity exponent also called local Hurst exponent, using a relationship outcome from the study of 2D fractional Brownian motion (2D-fBm) that connects fractal dimension and Hurst exponent. Thus, we use such calculations to deduce locally the Hölder exponent or the local fractal dimension, and consequently determine the nature of the texture for each PAN pixel position (e.g. Dirac structures, edges, smooth surfaces).

We resume the method as follows: in the step of up-sampling of the multispectral image, the new pixels are generated with RMD, this technique is originally designed to generate 2D-fBm synthetic surfaces. In our case, it is used in the up-sampling operation with the Hölder exponent calculated from the PAN image. This exponent changes according to the position of the up-sampling pixel in the image. With Alsat-2A images, we need two iterations with the RMD techniques to quadruple the size of the MSP. So according to the degree of the local singularity, the change introduced by the RMD is more or less important, for example less important in the case of smooth surfaces, and more important in the case of heterogeneous texture. After the up-sampling operation, the relations of the IHS method are then used to find the fused image. The results show an improvement in our fusion method compared to the conventional IHS, based on the opinion of an expert and the calculation results obtained by the spatial and spectral quality metrics, using correlation coefficient and the Wang and Bovic factor.

9643-71, Session PS

Local correlation tracking to recover doppler shifts from solar observations with an EUV slitless spectrograph

Hans T. Courrier, Charles C. Kankelborg, Montana State Univ. (United States)

The Multi-Order Solar EUV Spectrograph (MOSES) is a sounding rocket instrument that utilizes a concave spherical diffraction grating to form simultaneous solar images in the diffraction orders m = 0, +1, and -1. The large 2D field of view allows a single exposure to capture spatial and spectral information for large, complex solar features in their entirety.

Most of the solar emission within the instrument passband comes from a single bright emission line. The m = 0 image is simply an intensity as a function of position, integrated over the passband of the instrument. Dispersion in the images at m = +/- 1 leads to a field-dependent displacement that is proportional to Doppler shift. Our goal is to estimate the Doppler shift as a function of position for every exposure. However, the interpretation of the data is not straightforward. Imaging an extended object such as the Sun without an entrance slit results in the overlapping of spectral and spatial information in the two dispersed images.

We demonstrate the use of local correlation tracking as a means to quantify the differences between the m = 0 image and either one of the dispersed images. The result is a vector displacement field that may be interpreted as a measurement of the Doppler shift. Since two dispersed images are available, we can generate two independent Doppler maps from the same exposure. We compare these to produce an error estimate.

9643-72, Session PS

Colored coded-apertures for spectral image unmixing

Hector M. Vargas, Henry Arguello, Univ. Industrial de Santander (Colombia)

Hyperspectral remote sensing technology provides detailed spectral information from every pixel in an image. Due to the low spatial resolution of hyperspectral image sensors, and the presence of multiple materials in a scene, each pixel can be a combination of pure spectral constituents (endmembers). Therefore, endmember extraction is used to determine the pure spectral signature of the mixed materials and its corresponding abundance fractions in a remotely sensed hyperspectral scene. Advanced endmember extraction algorithms have been proposed to solve this linear problem called spectral unmixing which assumes linear interactions between endmembers. However, such techniques require the acquisition of the complete hyperspectral data cube to perform the unmixing procedure and the linear mixture model does not include spatial information, which is an important source of information to solve the unmixing problem. Compressive Spectral imaging (CSI) systems have been proposed under compressive sensing theory (CS), which states that it is possible to reconstruct a signal (N-dimensional) from a small set of random projections solving an optimization problem. En CSI, the projections are performing through the use block-unblock coded apertures that permit or block the light path to an array detector. Recently, the use of colored coded apertures (optical filter arrays) has been extended to CSI systems, where a block-unblock coded is replacing by optical filter. This paper aims at developing a compressive supervised spectral unmixing algorithm to estimate the endmembers and its corresponding abundance fractions in a spectral scene from compressive measurements. For this, a sparse model has been proposed for the representation of spectral pixels such that a spectral pixel in the scene is represented as a linear combination of a few endmembers of the entire spectral library. Then a numerical procedure estimates the sparse vector in the proposed basis representation by solving a sparsity-constrained optimization problem. The basis is a 3-D dictionary formed by a 2-D wavelet basis and a known endmembers spectral library, where the Wavelet basis is used to exploit the spatial information. The performance of the proposed spectral unmixing method is improved by taking optimal compressive measurements obtained when optimal colored coded-apertures are used in the optical system. The colored coded-apertures are designed such that the sensing matrix satisfies the restricted isometry property with high probability which characterizes matrices as nearly orthonormal. The performance discriminator used to measure the quality of the estimated abundance planes is the signal-to-reconstruction error (SRE, in decibels) and compared when the full spectral image cube is available. Simulations show that the proposed scheme attains comparable results to the full data cube unmixing technique, but using fewer measurements.

9643-73, Session PS

Calibration of mirror angle error for hyper spectral imagery with motion compensation model

Zhiwen Liu, Hei Baoqing, Chinese Academy of Sciences (China)

As hyper spectral image has become more widely used, hyper spectral imager obtained the rapid development. In order to get that image with higher signal to-noise ratio, motion compensation technology is widely used for Imaging Spectrometer. The technology is adopted by increasing the integration time of a pixel by using pointing mirror. Due to the hyper spectral imager with motion compensation is not a simple linear array CCD scanning imaging system, a new rigorous geometric processing model needs to be established. And the system geometric correction precision is strongly

relevant to exterior orientation. The exterior orientation, such as the satellite orbit, has to be further improved with suitable time-dependent functions and estimates in a bundle adjustment. However, the quality of the mirror angle acquired by pointing mirror is still difficult to satisfy the requirement of direction location. And the calibration model of mirror angle error is not the same to the other exterior orientation model. Therefore, in order to obtain high accuracy system geometric correction products, the mirror angle error model needs to be established and the mirror angle needs to be corrected.

First, a rigorous geometric processing model of hyper spectral imagery with motion compensation is established. The imaging characteristics are analyzed and a geometric equation between mirror angle position and the observation vector is established. The independent variable in this equation is the mirror angle, the dependent variable is the observation vector. A rigorous geometric processing model of this kind of imager is established on the collinearity equations.

Secondly, a calibration model of mirror angle error is established based on hyper spectral imagery with motion compensation. According to the analysis of the pointing mirror designer, the mirror angle error change by the sine rule. So the specific form of the calibration model is sine function. The independent variable in this model is the measured mirror angle, the dependent variable is mirror angle error.

Finally, a calibration model of mirror angle error with motion compensation is solved by few ground control points(GCP). The parameters in the calibration model are solved by normal iteration method The mirror angle error is added to enhance mirror angle precision. Then the high precision mirror angle are obtained. The images are geometric corrected by The calibration model and the rigorous geometric processing model.

The calibration model and the rigorous geometric processing model are tested on Tiangong-1 imageries and have been proved its practicality and efficiency. After compensating the mirror angle error of images, an object positioning accuracy of 1 pixels was achieved in flat surface. The test results indicate that the rigorous geometric processing model is correct, and the calibration model of mirror angle error is valid , and high-precision imaging products can be obtained.

9643-75, Session PS

Small target detection based on human visual system utilizing distance information

Linna Yang, Wei An, Zai-ping Lin, An-dong Li, National Univ. of Defense Technology (China); Jundu Ye, Xi'an satellite control center (China)

Many researchers have paid attention to simulate the mechanisms of human visual system (HVS) for small target detection. HVS perceived target brightness according to the contrast between target and background. The existing small target algorithms based on HVS can improve the signal-to-noise ratio and detection rate simultaneously. However, they also have the problems of a high false alarm rate and the algorithms can be easily affected by noise.

Researchers exploited local contrast measure (LCM) to suppress the background clutter and enhance the target intensity simultaneously inspired by the contrast mechanism of HVS. Then the algorithm of LCM detects small targets through the local contrast map of the original image, but LCM made an excessive enhancement on noises with high brightness, which results in a high false alarm rate. Subsequently, the improved LCM (ILCM) was proposed to improve detection rate and reduce false alarm rate, as well as the HVS size-adaptation process and attention shift mechanism are adopted in pre-detection stage and threshold operation with traversal mechanism.

However, the gray level of each pixel is not fully used in both LCM and ILCM. Moreover, distance information which is one of the most important factors in human visual system is not considered in the definition of the contrast map. In this letter, an algorithm for small target detection which is based on human visual system utilizing distance information is proposed to pursuit a good performance in detection rate and false alarm rate simultaneously. First, local region of each pixel is divided into target block and background block; second, gray average of the target block is calculated; third, distance information is weighted to each pixel of the background block to get a weighted sum, the distance information is calculated using Euclidean distance between each pixel of background block and the target pixel. To be more specific, the longer the distance is, the smaller the weighted value is; finally, the ratio of gray average of the target block and weighted sum of background block is weighed to the gray value of the central pixel to get a contrast map, then a threshold is used to get the target.

Experiments on two Infrared images have showed many properties of the proposed method. The signal-to-noise ratio (SNR) of the original image and that of the contrast map showed that the proposed method can improved the SNR of the image significantly. Moreover, the comparison of receiver operating characteristic (ROC) curves of four algorithms (Middle, LCM, ILCM and the proposed) have validated the detection capability of the proposed target detection method, in other word, the proposed can improve detection rate and reduce false alarm rate.

Although the experiments confirm that the proposed method is robust and provide empirical evidence supporting the claim that it is fit for small target detection, we can improve it from different directions in the future work. For example, the existing algorithm based on HVS comparing with the real HVS is simplified in calculation part, many factors are not considered in the algorithm.

9643-76, Session PS

Self-adaptive infrared small target detection in compressive domain

An-dong Li, Zai-ping Lin, Wei An, Linna Yang, National Univ. of Defense Technology (China)

The detection of small targets is one of the key techniques in infrared search and tracking applications,and infrared small target detection in compressive domain is a hot topic in research nowadays. Recently, infrared small target detection methods using matrix decomposition were proposed. Motivated by cat-eye effect target identification using compressed sensing, a compressive low-rank and sparse decomposition method (CLSDM) for detecting infrared small target was presented, in which the constant r and K denote the low-rank of background and sparse of target,respectively, and then Walsh Hadamard matrix was chosen as the measurement matrix. The existing infrared target detection algorithm in compressive domain achieves good performance with low required data storage. But there is one shortcoming existing algorithm:it is difficult to estimate background parameters in the algorithm, the constant r and K, which are sensitive to noise and complex background with low compressive ratio.

Considering the shortcoming, an infrared small target detection algorithm in compressive domain based on self-adaptive parameter configuration is proposed in this letter. Initially, the original infrared image is projected on a sensing matrix to obtain the measurement vector. Then, because of the slowly changing property of the infrared background image, infrared small target image is regarded as low-rank background matrix corrupted by sparse target and noise matrices. The sparse target matrix and the low-rank background matrix can be recovered and separated simultaneously from the measurements, based on low-rank and sparse matrix decomposition in compressive domain with self-adaptive parameter configuration. For the sparsity parameter K, reference to the CLSDM algorithm, there is an upper limit of target component, whose size is less than 0.15% of the whole image. For the low-rank parameter r, an adaptive estimate method is presented based on the estimation error of image reconstruction.The recovered image sequence and variation trend of estimation error sequence are get by traversing the

parameter. And the target and background clutters can be effectively distinguished in an adaptive chosen range, where the reconstruction error trend is smooth.Finally, the infrared small target detection is realized by threshold segmentation of occurrences and maximum local energy. Considering the sparsity of rebuilt target matrix, in which the recovered target pixels are directly affected by zero errors, the target energy is a weighted average prediction based on occurrences. The uncertain target is judged as the error to the reconstruction, when the occurrence number is less than the threshold of occurrences, or the weighted mean energy is less than the threshold of the product of maximum local energy and threshold coefficient.

Experiments are done with test images synthesized by using infrared background images and targets. The background images are chosen from real infrared image sequences with different clutters and the targets are obtained by using the cubic interpolation method to resize real targets. Experimental results indicate that the proposed method outperforms the previous method in both subjective and objective qualities under different complex infrared backgrounds with less data storage.

9643-77, Session PS

Accurate multisource forest species mapping using the multiple spectral–spatial classification approach

Dimitris G. Stavrakoudis, Ioannis Z. Gitas, Christos G. Karydas, Aristotle Univ. of Thessaloniki (Greece); Polychronis Kolokoussis, Vassilia Karathanassi, National Technical Univ. of Athens (Greece)

This paper proposes an efficient methodology for combining multiple remotely sensed imagery, in order to increase the classification accuracy of complex forest species mapping tasks. The proposed scheme is based on the so-called multiple spectral–spatial classifier (MSSC), which constitutes an effective post-regularization procedure for enhancing the result of an initial pixel-based classification. More specifically, three simple segmentation algorithms are used to mark some pixels of a pixel-based classification. The rest of the pixels are subsequently classified through a graph-theoretic algorithm (namely, minimum spanning forest, MSF), grown from the automatically selected markers. In the present study, we extend MSSC-MSF in order to handle multiple images. Each image is first separately classified through a pixel-based Fuzzy-Output Support Vector Machine (FO-SVM) classifier. The fuzzy outputs are fused and used to grow the MSF, whereas the markers are also determined considering both classifications.

The proposed methodology has been tested on a challenging classification task, defined in a complex Mediterranean forest mosaic in northern Greece. The classification scheme comprises seven classes, namely, Oak, Beech, Pinus brutia, Pinus nigra, Pinus halepensis, Maquis, and Other, with the later describing non-vegetated and agricultural areas. A GeoEye multispectral satellite image has been acquired on April 2013, exhibiting a spatial resolution of 2m. Approximately three months later, a hyperspectral image of the study area was acquired using the Compact Airborne Spectrographic Imager (CASI-550) airborne sensor. The spatial resolution of the CASI image was also 2m. Due to the irregular weather patterns that are characteristic of the study area, a portion of the CASI image is covered with shadows from clouds. These areas have not considered during the respective pixel-based classification. Nevertheless, the whole study area is classified by the proposed scheme, since it is fully covered by the GeoEye image. This fact highlights an additional merit of the multi-source fusion approaches. Using a large set of auxiliary data and after careful photointerpretation, almost 37% of the study area has been digitized and assigned to one of the seven classes, thus obtaining a rich testing set for the purposes of the comparative analysis.

The results obtained highlight the effectiveness of the proposed approach. The pixel-based classifications resulted in overall accuracies (OA) of 65.63% for the GeoEye and 66.60% for the CASI images, respectively. The latter is underestimated due to the existence of the areas covered by shadows (which are treated as unclassified and hence erroneous by definition). If we omit the parts of the reference areas in those areas, the CASI's OA reaches 78%. Nevertheless, both pixel-based classifications are strongly affected by the salt-and-pepper phenomenon. Applying the MSSC-MSF approach to each pixel-based classification, the OA climbs to 82.04% for the GeoEye and 75.24% for the CASI images, respectively. Finally, the proposed multi-source MSSC-MSF approach yields an OA of 90.07%. This increase is primarily attributed to the fact that the fusion approach exploits the relative advantages of both the GeoEye classification (better discrimination between Oak and Beech) and the CASI (effective discrimination between the three pine species) one.

9643-78, Session PS

Introduction of a generic INR architecture and its ultimate form

Handol Kim, Korea Aerospace Research Institute (Korea, Republic of)

INR (Image Navigation and Registration) system is an essential part of geostationary remote sensing satellites for their on-board instrument payloads to maximally fulfil their expected missions and utility, which basically provides the knowledge and control of the geo-location of each image pixel relative to a fixed reference frame, where the navigation pertains to the knowledge and the registration pertains to the control, or stabilization, respectively. INR is also a difficult subject because it should deal with many relevant subsystems and interfaces and because its requirements are expressed in the order of micro-radians which in turn require thorough system analysis, careful space and ground segments design and testing as well as on-orbit fine tuning to meet these tight requirements.

After analysing the diverse INR systems of the past, the current and in the foreseeable future, in terms of their commonalities and distinctions, we have tried to systemize their characteristics in large and the differences in contrast, to come up with a generic architecture of INR systems, in an effort to provide a general framework for a standardized and systematic approach to the design and implementation of diverse INR systems both for the current and the future.

In this paper, we introduce and report such a generic INR architecture in its current form. In this trial, we also provide a synthetic estimation of the current state of fidelity in each building block of the generic architecture with the focus on identifying the areas of further potential improvement. And lastly, we provide a projected sketch of this generic INR architecture in its ultimate form in the long run, which we believe will eventually take shape with the continuous advancement, evolution and revolution of the computer and other subsidiary technologies.

9643-79, Session PS

Space-based infrared scanning sensor LOS determination and calibration using star observation

Jun Chen, Zhan Xu, Wei An, Xin-Pu Deng, Jun-Gang Yang, National Univ. of Defense Technology (China)

The conventional sensor's line of sight (LOS) determination and calibration process is widely used before the start of the tracking process. The subsequent changes of sensor bias are not usually token into account in the conventional LOS determination and calibration process. Space based infrared (IR) tracking system uses the LOS of target for target location. LOS determination and calibration is the key precondition of accurate location and tracking of target in Space based IR tracking system and the LOS calibration of scanning sensor is one of the difficulties?

This paper provides a novel methodology for removing sensor bias from a space based infrared tracking system through the use of stars detected in the background field of the sensor. Based on the analysis of the imaging process of scanning sensor, a theoretical model based on the estimation of bias angles using star observation is proposed. By establishing the process model of the bias angles and the observation model of stars, this paper utilizes an extended Kalman filter (EKF) to estimate the bias angles from star observation. The detailed derivation of the EKF using quaternion formulation is given in the paper. Once stars are detected during the target tracking, the bias angles can be estimated with using star residuals (the differences between the measured star azimuth/elevation angles and the true star azimuth/elevation angles), and simultaneously the accurate LOS of target can be figured out.

Time domain simulations results indicate that the proposed algorithm has a high precision and smooth performance for sensor LOS determination and calibration. The timeliness and precision of target tracking process in the space based infrared tracking system could be met with the proposed algorithm?

9643-80, Session PS

A study of selected textural features usefulness for impervious surface coverage estimation using Landsat images

Katarzyna K. Bernat, Wojciech Drzewiecki, AGH Univ. of Science and Technology (Poland)

Texture is considered one of the most crucial digital image feature used commonly in computer science and it constitutes significant source of references about image content. Texture has been widely used for panchromatic images description but in recent years textural features for multispectral images classification have been applied as well. Some studies have shown that textural descriptors improve accuracy of medium resolution satellite images subpixel classification [1].

Following the previous tests, the aim of our research is to examine and compare the accuracy of impervious surface coverage estimation with the particular focus on determining usefulness of several textural features groups combined with spectral features based on multispectral Landsat TM images derived from summer 2009 and 2010. The study was conducted in respect to pixel- and sub-pixel level but also the two-stage approach to impervious surface coverage estimation was tested on the research area, which cover the part of southern Poland for the immediate catchment of the Dobczyce Reservoir. The land use in the catchment is dominated by agriculture and forest with numerous villages of dispersed development.

Impervious surface coverage estimation was done using machine learning methods based on decision and regression trees (C5.0 and Cubist algorithm). At the stage of hard classification the study area was divided into two categories: a) completely permeable (imperviousness index less than 1%) and b) fully or partially impervious areas. At the regression stage percentage impervious surface coverage within a single Landsat pixel was calculated. Two-stage procedure based on initial hard classification and then sub-pixel estimation, was used only for pixels classified as impervious.

Decision and regression trees using various sets of textural attributes calculated for Landsat TM images with 5x5 window size were built. In this study groups of histogram-based characteristics, co-occurrence matrix-based parameters, run length matrix-based features, absolute gradient-based characteristics and autoregressive model parameters were chosen. Textural features were obtained using MaZda software.

Decision and regression trees model construction was based on training data set derived from reference fragments of Landsat images. In order to obtain the most accurate impervious surface coverage estimation 5-folds cross-validation using training set for C5.0 and Cubist algorithm was performed. For C5.0 method several approaches, with changing global pruning parameter, were checked. In some cases fuzzy thresholds were added. In the Cubist algorithm over a dozen settings were tested using various number of nearest neighbors and number of committee members.

Based on the results of 5-fold cross-validation carried out using C5.0 and Cubist algorithms approaches, guaranteeing the lowest means errors in terms of training set, were selected. Accuracy of the imperviousness index estimation was checked based on validation data set, which was not used for learning classifiers. The average error of hard classification using spectral features only was 6.2% and about 5.5% for spectral features combining with textural characteristics. The root mean square error (RMS) of determination of the percentage of the impervious surfaces within a single pixel was about 9.7%-9.9% for all tested combinations of spectral and textural parameters. Similar accuracy levels were achieved for the two-stage procedure. The research has shown usefulness of selected textural features groups for pixel level impervious surface classification. Our work has proved, that textural features do not improve sub-pixel impervious surface coverage estimation in conditions of southern Poland using Landsat images.

[1] Youjing, Zhang, Chen Liang, and He Chuan. “Estimating urban impervious surfaces using LS-SVM with multi-scale texture.” Urban Remote Sensing Event, 2009 Joint. IEEE, 2009.

9643-81, Session PS

Unsupervised change detection from multitemporal SAR images based on a detail preserving approach and a robust threshold estimation

Boulerbah Chabira, Takieddine Skanderi, Aichouche Belhadj Aissa, Univ. des Sciences et de la Technologie Houari Boumediene (Algeria)

Monitoring environment and managing disasters have received a great deal of attention in recent years due to the fact that satellite sensors have known tremendous advances in all aspects. They can provide multidate imagery at short times on a global scale. One application that is subjected to a lot of studies recently is to detect changes between multitemporal satellite images. Optical images have been proven to present a good discrimination between changed and non-changed areas. However, they are affected by sun illumination and the atmospheric conditions. This renders the problem of detecting the changes very hard and in the most cases nearly impossible especially in frequently overcast countries. On the other hand, synthetic aperture radars (SARs) are active sensors, they emit radio waves and receives the scattered ones, and are independent to such issues because they operate in the microwave region. Due to the reason that SAR images are corrupted by the presence of speckle which renders the classification accuracy of changed and non-changed areas very difficult, SAR-based change detection need a preprocessing step, which is reducing the effect of speckle, before any further analysis.

In this paper, we propose an unsupervised technique for the change detection from multitemporal single-channel SAR images that does not require any speckle filtering. This technique is based on: i) generating a multiresolution set of the single-channel log ratio image using stationary wavelet transform (SWT); ii) applying the T-point algorithm for all the images of the multiresolution set; and iii) fusing the obtained images at the optimum reliable scale to generate the change map. In the first step, a multiresolution set of the log ratio image is generated using the stationary wavelet. For each pixel of the single-channel SAR image, we must identify a reliable scale in the multiresolution set. Reliable scale is selected to whether the considered pixel belongs to a border or a homogeneous area at different scales. These reliable scales represent a trade-off between speckle reduction and geometrical detail preservation and they are identified using multiscale local coefficient of variation. In the second step, a robust threshold estimation which is based on the T-point algorithm is used to threshold each image of the multiresolution set. This robust threshold estimator has been

chosen because it has shown its robustness when dealing with multiresolution transformations. A set of multiresolution change maps are derived from the obtained thresholded images. In the final step, the fusion is conducted through the use of an optimum reliable scale. The final change map is then generated.

The proposed technique was experimentally validated using semisimulated and real HH images acquired by RADARSAT-2 satellite in the region of Algiers. Tests have been conducted using two-look HH semisimulated datasets consisting of 455 ? 540 pixels. Results show that, out of 4365 simulated change pixels, the detection accuracy reaches 96.56% with minimum overall error rate equals to 0.799%. For the HH real datasets, the assessment is performed visually and good change detection is obtained.

9643-82, Session PS

Method for infrared image background suppression based on sparse decomposition

Lihua Wu, Weidong Sheng, National Univ. of Defense Technology (China)

Remote infrared detected target is usually manifested as punctuates and lack of effective shape information , since the detection distance is far and the reflection and scattering of sun from the atmosphere and clouds forms very strong background clutter.

Background suppression methods based on single frame image mainly utilizes the local correlation characteristics of clutter and background in spatial area, using the local neighborhood data to estimate the current background, and realizing the background suppression by difference. Recent years, neural network, wavelet analysis and Markov random field theory are introduced in infrared image background suppression, which has made great progresses. In this paper, based on the latest development of image signal processing and signal representation theory, we introduce image sparse representation theory to research suppression problem to solve single frame infrared image background suppression.

For the infrared image, the image signal can be expressed as a linear superposition of target, background and noise. A large number of background signal in the infrared image are mainly in the low frequency area, while the target and noise signals are mainly in the high frequency area. In this paper, we regard image background information as the effective information, and utilize sparse decomposition algorithm to sparsely decompose image. The residual information decreases in the decomposition process, and then the background information of the image can be totally extracted, with the remained component of target and noise. It is easier to interpret the relationship between background and target, when studying infrared image background suppression from the point of sparse decomposition.

The progress for the proposed infrared image background suppression method based on sparse decomposition is as follows: firstly, constructing the over complete dictionary of atoms, which directly influence the sparsity of the infrared image sparse decomposition and have a significant effect on the infrared image background suppression. Then, sparsely decompose images, utilizing decomposition algorithm to sparsely decompose the infrared image in the area of over complete dictionary. In this step, the residual ratio based threshold is used to distinguish the background and the target, which can extract the background information as much as possible when considering the sparisity of the images. The last step is to reconstruct the background image. We utilize sparse matrix and the effective atomic sets to reconstruct image to obtain the background information of infrared image, and then suppress the infrared background by means of difference method.

9643-83, Session PS

Applied noncentral Chi-squared distribution in CFAR detection of hyperspectral projected images

Zhiyong Li, Dong Chen, Gongtao Shi, National Univ. of Defense Technology (China); Guopeng Yang, Wuhan Univ. (China); Gang Wang, National Univ. of Defense Technology (China)

A Constant False Alarm Rate (CFAR) detection based on the noncentral chi-squared distribution is presented in this paper. It has been applied to detect the anomaly points in hyperspectral projected images. Usually, the process of many hyperspectral detectors can be considered as a linear projection, such as the benchmark detectors RX algorithm. The operators of them are a kind of linear transforms, and the results after the projection are quadratic form. It means that every pixel of the projected image is a quadratic form which comes from the transform of spectral vectors. Anomaly targets will be brighter than background in the projected image. Then, the CFAR detector can be used to segment the image into the foreground and the background. More generally, multivariate normal distribution is the appropriate model for describing the statistic characteristics of hyperspectral image data. Chi-squared distribution could be the best choice to describe the projected image. Because every pixel in the projected image which is quadratic form could be considered as the quadratic sum of many normal random variables.

However, the standard chi-squared distribution often cannot be applied to describe the real hyperspectral projected images. Because the statistic characteristics of real hyperspectral image are very complicate. On one hand, it is inaccurate to use the standard normal distribution to describe the image data. Sometimes there are the different means and variances in different bands. On the other hand, taking into consideration the nonlinear mixture of spectra in real environment, there is strong nonlinear correlation among the band images. Therefore, the band number cannot be used as the number of degrees of freedom in central chi-squared distribution, because these normal random variables are not independent.

In this paper, the noncentral chi-squared distribution has been applied to describe the hyperspectral projected image and used to estimate the threshold value of CFAR detection. In general, there are two important parameters in noncentral chi-squared distribution model. One is the number of degrees of freedom and the other is noncentrality parameter. The degrees of freedom plays key role in accurate approximation of the statistic distribution of projected image data. However, this value is hard to be estimated due to the nonlinear correlation among the band image. In fact, the independence of hyperspectral band images is associated with the intrinsic dimension of datasets. If the intrinsic dimension can be calculated accurately, then the number of degrees of freedom can be estimated according to it. In this paper, we firstly considered the dataset as a linear manifold in spectral space and estimate the intrinsic dimension; then the means vector and the covariance matrix are used to calculate the noncentrality parameter; thirdly, the value of intrinsic dimension was increased gradually and the approximation between the new noncentral chi-squared distribution and data statistic model was checked automatically, the best value of degrees of freedom was determined when the mean square error between them was least. We applied the method in the real aerial hyperspectral images. The results demonstrate effectiveness of the proposed method in tightly modeling the projected image statistic distribution and improving CFAR detection.

9643-84, Session PS

A comparative study of Landsat TM and RapidEye imagery for two-stage impervious surface coverage estimation

Katarzyna K. Bernat, Wojciech Drzewiecki, AGH Univ. of Science and Technology (Poland)

The paper presents accuracy comparison of subpixel classification based on medium resolution Landsat and RapidEye satellite image, performed using machine learning algorithm built on decision and regression trees method (C.5.0 and Cubist). The research was conducted in southern Poland for the immediate catchment of the Dobczyce Reservoir along with an adjacent area of towns (My?lenice and Dobczyce). The research area is hilly and the land use in the catchment is dominated by agriculture with numerous villages of dispersed development. The southern part of the study area is covered mainly by forests. The aim of the study was to obtain image of percentage impervious surface coverage, valid for the period of 2009-2011.

Imperviousness index map generation was a two-stage procedure. The first step was classification using C.5.0 algorithm, which divided the study area into two categories: a) completely permeable (imperviousness index less than 1%) and b) fully or partially impervious areas. For pixels classified as impervious, the percentage of impervious surface coverage within a single pixel area was estimated using Cubist algorithm.

Decision and regression trees model construction was done twice based on training data set derived from Landsat TM pixels or fragments of RapidEye images corresponding to the same Landsat TM training pixels. RapidEye training data set division into learning and test pixels was also corresponding to the Landsat training data set distribution.

In order to obtain Landsat imperviousness index map with the minimum possible error, estimation of the accuracy of models based on the results of 5-folds cross-validation using training set for C5.0 and Cubist algorithm was performed. In RapidEye study 10-folds cross-validation, using analogous settings for C5.0 and Cubist algorithm, was done. For C5.0 method six approaches changing global pruning parameter were checked and also in some cases fuzzy thresholds were used. In the Cubist algorithm thirteen setting options were tested using various number of nearest neighbors and number of committee members.

Based on the results of cross-validation carried out using C5.0 and Cubist algorithm for Landsat and Rapid images, approaches guaranteeing the lowest means errors in terms of training set were selected.

Accuracy of the final imperviousness index maps was checked based on validation data sets, which were not used for classifiers learning. The root mean square error (RMS) of determination of the percentage of the impervious surfaces within a single Landsat pixel was ±9.9% and within a single RapidEye pixel was ±16.5% for C.5.0/Cubist method. However, the root mean square error specified for RapidEye test data aggregated to 30m x 30m areas corresponding to Landsat test pixels was ±7.2%.

The study has shown that better results of two-stage imperiousness index map estimation using RapidEye satellite images can be obtained. The two-stage procedure for tested approached has given similar errors to only regression procedure but it also has been proved that only regression method caused higher error in agriculture and forestry areas.

9643-85, Session PS

Modified wavelet kernel methods for hyperspectral image classification

Pai-Hui Hsu, Xiu-Man Huang, National Taiwan Univ. (Taiwan)

Compared with multispectral images, hyperspectral images have the capability of acquiring images of earth surface with several hundred of spectral bands. For example, the Hyperion instrument of EO-1 is capable of collecting 220 spectral channels with a complete spectrum covering 400-2500nm. Providing such abundant spectral data should increase the abilities in classifying land use/cover type. However, due to the high dimensionality of hyperspectral data, traditional statistical classification methods are not suitable for hyperspectral data classification. This problem has been termed the “curse of dimensionality.” The common method to solve this problem is a two-stage method which reduces the data dimensionality firstly by feature extraction, and then the traditional statistics-based classifier can be directly applied to the extracted features.

Kernel methods such as support vector machine (SVM) and multiple kernel learning (MKL) have been successfully applied to hyperspectral images classification. In contrast with above mentioned two-stage method, these methods can be considered as one-stage methods, which perform the feature extraction and classification simultaneously. In kernel methods applications, the selection of kernel function plays an important role. The most common kernels include linear, polynomial, and radial basis function; in addition, it has been proposed that wavelet kernel, which use wavelet transform as the mapping function, is also an admissible support vector kernel. The wavelet kernel with multidimensional wavelet functions can find the optimal approximation of data in feature space for classification. The SVM with wavelet kernels, called wavelet support vector machine (WSVM), has also been applied to hyperspectral data and improve classification accuracy successfully. In this study, a modified WSVM algorithm is proposed and implemented on hyperspectral images. The modified WSVMs considered not only the approximation but also the detail information of hyperspectral data in wavelet kernels, and the parameters of wavelet kernels are determined by the data property and structure of the hyperspectral image.

Furthermore, wavelet kernel method combined multiple kernel learning algorithm and wavelet kernels was also proposed for hyperspectral image classification in this study. After the appropriate selection of a linear combination of kernel functions, the hyperspectral data will be transformed to the wavelet feature space, which should has the optimal data distribution for kernel learning and classification. Finally, the proposed methods were compared with the existing two-stage or one stage methods. A real hyperspectral data set was used to analyze the performance and test the effectiveness of the classification using the wavelet kernel method. According to the experimental results the proposed wavelet kernel methods in this study have well performance, and would be an appropriate tool for hyperspectral image classification.

9643-86, Session PS

Inshore ship detection in high-resolution satellite images: approximation of harbors using sea-land segmentation

Beril Besbinar, Aydin A. Alatan, Middle East Technical Univ. (Turkey) and Ctr. for Image Analysis (OGAM) (Turkey)

Inshore ship detection is a challenging yet important issue in remote sensing with many applications, such as maritime surveillance, fishery activity monitoring, illegal border crossing and naval warfare. The problem arises from the high similarity between ships and harbor background in terms of color and texture. To overcome this problem, a novel inshore ship detection method that mainly depends on a very fine sea-land segmentation is proposed in this paper. Satellite images consisting of red, green, blue (RGB) and near infrared channels (NIR) in 0.5m spatial resolution are used to show the performance of the algorithm.

Available global 30m elevation data is used to obtain plenty of sea samples from images covering large areas. The distribution of normalized difference water index (NDWI) of these sea samples is observed to exhibit similar characteristics to a normal distribution. Considering the possible pixels of islands

or ships taken as sea samples, median and median absolute deviation of the distribution are used to threshold the index for the initial segmentation result.

This initial mask is further enhanced using graph-cut algorithm as the second step. For this purpose, spectral characteristics of sea and land areas are modelled with Kernel Density Estimation using the samples quite close to the segmentation mask boundary. Pixels around the boundary are represented as nodes and link weights between each node and source (land) and sink (sea) nodes are determined according to the consistency with sea and land models. The spatial relationship between pixels is also taken into consideration as the link weights between pixel nodes and they correspond to the similarity with the neighboring pixels. As a result of solving this energy minimization problem via min-cut max-low algorithm, each pixel is labelled as either sea or land. Final morphological operations result in a sea-land mask with fine details which can be used to approximate the harbor area with piecewise linear line segments.

Line Segment Detection (LSD) algorithm results in many small line segments with high accuracy and speed when ran over the land area close to the sea boundary. Our aim is to merge LSD segments and realize an elimination step to generate long line segments that fit to the man-made boundaries of an harbor. Perpendicular and parallel distances between each line segment pair are defined in order to combine two segments if they lie along the same direction with small parallel and even smaller perpendicular distance. Pairwise comparison of segments are made in a grid structure in order to narrow the search area and all segments are compared hierarchically in a few iterations. Extended line segments which lie on the very thin boundary of sea-land segmentation mask are chosen to extract the harbor area. Remaining connected components are regarded as ship candidates and false alarm removal is realized via a Support Vector Machine (SVM) that discriminates the shape features obtained by Angular Radial Transform (ART). The machine is trained using a variety of binary ship masks of different types and dimensions. Test results has shown that provided a good land segmentation mask, approximation of harbors with piecewise linear lines leads inshore ship detection with a high success rate.

9643-87, Session PS

A new method to obtain uniform distribution of ground control points based on regional statistical information

Chao Ma, Wei An, Xin-Pu Deng, National Univ. of Defense Technology (China)

The Ground Control Points (GCPs) is an important source of fundamental data in geometric correction for remote sensing imagery. The quantity, accuracy and distribution of GCPs are three factors, which may affect the accuracy of geometric correction. In particular, the spatial distribution of GCPs has a great influence on the Geometric Correction's accuracy of the remote sensing image. It is generally required that the distribution of GCP should be uniform, so they can fully control the accuracy of mapping regions. In this paper, we establish an objective standard of evaluating the uniformity of the distribution of GCPs based on regional statistical information, and get an optimal distribution of GCPs based on this standard. The image is divided into blocks in accordance with the upper and lower, the left and right, the upper left and lower right, the upper right and lower left, the center and periphery, etc. The number of GCPs of the block in each direction is counted, which comprises a regional statistical information distribution vector, then variance of the distribution vector indicates the degree of number divergence of GCPs in different direction of image. The distribution of GCPs that have the minimum variance of the distribution vector, which means the deviation of data in the samples is small, is relatively uniform in five directions, then GCPs in the image are distributed relatively uniform. In this paper, the simulation annealing is employed to search the optimal distribution of GCPs that have the minimum variance of the distribution vector of regional statistical information. Experiments are carried out to test the method proposed in this paper, and sampling designs compared are simple random sampling, and universal kriging model-based sampling. The experiments indicate that this method is highly recommended as a new GCPs sampling design method for geometric correction of remotely sensed imagery.

9643-88, Session PS

Fuzzy ontologies for semantic interpretation of remotely sensed images

Khelifa Djerriri, Ctr. National des Techniques Spatiales (Algeria); Mimoun Malki, Univ. de Sidi-Bel-Abbes (Algeria)

In order to perform a land cover mapping, the remote sensing expert uses its experience and personal knowledge, which is rarely formalized and thus cannot be reused in an automatic process. Ontologies have been proposed as solution to capture, represent and store domain knowledge agreed by domain experts in a formal and machine readable language, which can be easily shared and integrated in various software environments. Over the last decades, Ontologies has attracted the interest of researchers in the remote sensing field. Therefore, we believe the use of ontologies can contribute to improve the exploitation of satellite images and computerized reasoning.

Ontology includes a vocabulary of terms together with the specification of their meaning. From the explicitly declared facts, an inference mechanism allows to elicit additional implicit knowledge. Such a mechanism is implemented by means of ontology reasoners.

In the current paper, we propose an approach for generating land cover maps from Landsat-8 Operational Land Imager (OLI) Images by integrating object-based image analysis and ontologies. The images objects are selected as main processing units instead of pixels to reduce the number of calls to reasoner and to use more characteristics.

The used Land-cover ontology is written in Ontology Web Language (OWL-2), which is nowadays one of the most popular languages for authoring ontologies. It has been originally intended to build semantic webs. But eventually, it has attracted strong academic interest. OWL is endorsed by the World Wide Web Consortium (W3C).

Remote sensing domain elements whose nature is imprecise cannot be represented by classic crisp ontology, since they can only model relations between entities that may be either true or false. For example the rule "Vegetated objects have High Vegetation Index Value" does not have to be precise in practice. Thus classical ontology languages are not appropriate to deal with vagueness in knowledge. Fortunately, Description Logics for the semantic web has been enhanced by various approaches to handle such knowledge. Contrary to classical set theory, where elements either belong to a set or not, in the fuzzy set theory, elements can belong to a set with some degree.

Among different approaches available for fuzzifying an ontology, we find Fuzzy OWL-2 mappings or value discretization approaches. To fuzzify the crisp ontology, it needs to be translated into a language supported by a fuzzy ontology reasoner. Fuzzy OWL-2 parsers convert Fuzzy OWL-2 ontologies into DeLorean and fuzzyDL reasoners syntax. However, we consider fuzzyDL to be the most convenient existing tool for ontological reasoning with uncertainty.

The proposed approach was applied to two study areas. The first step is consists in partitioning the image into homogeneous objects by means of segmentation algorithm. Once the objects are created, a fuzzy ontology that represents main classes in Landsat8-OLI scenes (vegetation, built-up areas, water bodies, shadow, clouds, forest) is used to classify image objects. A good overall classification accuracy was obtained. Results highlight the potential of the method to be replicated in time and space in the perspective of a cost–efficient transferability of the procedure.

9643-91, Session PS

Nonlinear sparse separation and semantic source identification

Hela Elmannai, Ecole Supérieure des Communications de Tunis (Tunisia); Mohamed Anis Loghmari, Mohamed Saber Naceur, Ecole Nationale d'Ingenieurs de Tunis (Tunisia)

Geosciences application's are based on converting remote sensed image to maps. Many approaches have been developed for land classification and end-member identification. Source separation works have interested recent research due to their efficient contribution in land characterization. Many mixing model have been implemented to approach the natural observation phenomenon.

This paper presents a nonlinear mixing model for multispectral image observation. Pixels reflectance are nonlinear function of unknown spectral component. Observation are also contaminated by noise. Mixing model distribution's are considered as gaussians.

1-Separation process

Based on the real assumption of nonlinear mixture, sparse source and semantic source identification is a new approach in remote sensed image analysis. Nonlinear source separation is based on sparse transform.

The separation procedure processes the image through their sparse representation. The nonlinear un-mixing task is performed by neuron networks. Bayesian algorithm and optimization methods are proposed for model parameter's estimation. Latent Factor are independent and have gaussian distribution. Unknown parameter are estimated from their priors through two Layer Perceptron.

2- Source separation for land classification

The separation technique aims to provide more suitable presentation for data, feature extraction and land classification. The approach has the advantage of integrating the sparse separation and simulating the natural non linear mixing process. Another merit is the physical source identification. For this task, source separation is determined by both: the Kullback-Leibler cost function measuring the mutual information , and the classification quality. Separation process will ovoid observation correlation and fit the classification task.

3- Source semantic attribution

Physical identification is challenging for separated source. Provided sparse sources present a sparse morphological presentation for land and we aim to determine a physical signification for the underlying dictionary. Source separation space is therefore a feature presentation for observation. Ones each source is classified separately a merging step will perform the land truth identification taking advantage from the source space additional character.

4- Experiments

Studying source space in term of mutual independency and land characterization will interest the experiment part.

The performance of the strategy is evaluated by simulation conducted on synthetic and real data. Source de-correlation is inherently a statically differentiating for data.

Classification effectiveness for the approach is demonstrated in real multispectral image and compared to classification in band representation and linear sparse source separation. The approach presents a reliable tool when there is limited or unsure information about ground truth. The source image have too lower correlation coefficients. For the classification accuracy, source provide the best accuracy compared to band and other separation approach namely sparse separation, SOBI and JADE. The semantic source identification for the experiment scene show that every sources presents some land items in a complementary way which encouraged further works in this axe.

9643-92, Session PS

Comparison of ARSIS concept with Fourier domain methods for VHR images

Alper Akoguz, Melih Hayirsever, Ahmet H. Kayran, Sedef Kent Pinar, Istanbul Technical Univ. (Turkey)

Recent high level studies based on remote sensing are pioneered among the technical developments of the earth observation satellites in the modern era. Despite of the developments so far, technological and physical parameters, even for new generation satellite sensors, cause tradeoffs between higher spatial resolution and higher spectral resolution. In order to deal about this currently mentioned constraint for the optical satellite imagery, the merging operations performed over lower spatial resolution multi-spectral (MS) image of a specific area with higher spatial resolution Panchromatic (Pan) image with lower spectral information is called image fusion, or pansharpening, which is a sub discipline of data fusion process. Pansharpening leads MS images to carry not only higher spectral, but also higher spatial information where to be used as an input for geographical information systems, remote sensing, various civil (like urbanization, change detection, agriculture, meteorology, etc.) and military applications.

Over thirty years of research on pansharpening held by the remote sensing community, there are made several contributions and novel approaches on pansharpening methods which are mostly categorized in generic subsections. The traditional methods, which are based on applying transformation to the original data without any filtering operation of the Pan image, are called as component substitution (CS) methods which consist of Intensity-Hue-Saturation (IHS), Principal Component Analysis (PCA) and Gram-Schmidt Orthogonalization (GS) based algorithms. The methods based on spatial details injection from the Pan image into MS image which is performed by filtering are defined as multiresolution analysis (MRA) fusion methods which consist of Smoothing Filter based Intensity Modulation (SFIM), and Discrete Wavelet Transform (DWT) based algorithms, including Amélioration de la Résolution Spatiale par Injection de Structures (ARSIS) concept developed by Ranchin and Wald (2000), which is an improvement on spatial information via statistical MRA.

In this study, there has been examined ARSIS pansharpening concept for Very High Resolution (VHR) images and compared with Fourier based filtering methods which performs Fourier domain filtering, using several 2D Finite Impulse Response (FIR) filters in Fourier domain (rather than using DWT kernels as in MRA) which implies that the filters were applied after taking 2D Discrete Fourier Transform (DFT) of both multispectral and panchromatic image and after the pansharpening process in Fourier domain, the resulting pansharpened image was obtained with an inverse 2D DFT.

The algorithms were applied to Pléiades (Airbus Defence & Space) VHR coregistered satellite image couples that were acquired simultaneously. Couples were chosen for different regions of Turkey in order to analyze the methods in different regional characteristics. In addition, the methods were compared by the fusion quality assessment methods that are mostly used by the community which are Spectral Angle Mapper (SAM), Root Mean Square Error (RMSE), Relative Average Spectral Error (RASE), Erreur Relative Adimensionelle de Synthése (ERGAS), Correlation Coefficient (CC), Universal Image Quality Index (UIQI) and Hybrid Quality with No Reference (HQNR). Under each metric, each algorithm was ranked and the best competitors were identified. The results of these quality assessments shows ARSIS based methods had the best scores among the traditional methods and remaining MRA methods.

9643-93, Session PS

The use of extreme learning machines in land changes classification: a case study of Novo Progresso, Brazil

Helder A. Louzada, Ana C. Quintão Siravenha, Evaldo Goncalves Pelaes, Univ. Federal do Pará (Brazil)

Through the years the availability of remote sensory data and the development of machinery able to process large amount of information allow the dissemination of methods directed to detect the land use, as well as, the land cover and analyse their pattern of occurrence around the globe. The municipality of Novo Progresso, in Brazil, over the years was common theme in discussions about environmental issues, mainly because it has one of the highest deforestation rates in the Brazilian Amazon. These high rates of deforestation are directly related to the development of national public policies directed to the Amazon region from the decade of 1970, and years later (in 1984), by the discovery of a large deposit of gold. Both events attracted thousands of people to the region and nowadays, most of the local economy revolves around wood industry, cattle breeding, agriculture and factory mining. In this context, the objective of this work is to develop a supervised architecture of remote sensing image classification by Artificial Neural Network, using the algorithm extreme learning machines (ELM), due to its remarkable advantages such as fast operation, straightforward solution, and strong generalization. The application of neural networks for remote sensing data classification is a promising approach to image classification. The learning phase represents the bottleneck of a neural network implementation when taking into account how fast it can learn a pattern from the input data. The main reasons can be the use of slow gradient-based learning algorithms, and/or all the parameters to be tuned iteratively during this phase. The ELM is developed for single-hidden layer feedforward neural networks where not only the input weights, but also the hidden bases are tuned randomly. This feature tends to provide good generalization performance at extremely fast learning speed. The set of ELM parameters are then capable of identifying deforestation characteristics of the acquired images and, consequently, the use of different features and land cover in images acquired by sensors. The scenes acquired for this work, from the Landsat-5 TM satellite, represent part of Novo Progresso municipality, during the period of 1984-2011. They were geometric corrected and it was applied a contrast enhancement technique, as a pre-processing step. 90 samples were extracted to training the network, and confusion matrices, where the coefficients quantify the correctness of the classes, evaluated the tests. The Kappa index and the index of overall accuracy, beyond the Mean Square Error were also considered during the evaluation. A post-classification process was applied for residual misclassification correction. To do this, it was implemented a Gaussian filtering, a 2-D smoothing operator commonly used to blur images, removing details and noise. The idea is to use this distribution as a point-spread function, achieved by convolution. Its behaviour is similar to the low-pass filter and the standardizes ranked themes. Although the effectiveness of the proposed methodology, there are some features to be considered in future work, such as, which the best bands composition to form the image and which contrast enhancement technique can result in a better classification.

9643-94, Session PS

A research of selected textural features for detection of asbestos-cement roofing sheets using orthoimages

Judyta Ksiazek, AGH Univ. of Science and Technology (Poland)

At present, there has been a great interest in the development of texture based image classification methods in many different areas. The current studies using remote sensing detection of asbestos-cement roofs present various methodological approaches. In most cases researchers focus on multispectral and hyperspectral imaging but availability to these data is often quite difficult. In contrast, orthoimages are more widely available but they are rarely used. This work presents the results of research carried out to assess the usefulness of selected textural features for detection of asbestos-cement roofs in orthophotos classification.

The study was conducted in two areas of southern Poland. Data for the first study area (Krzczonow, village near Myslenice) was analysed on 25 cm ground resolution orthoimages. The second region (Bochnia, small town near Krakow) was imaged on 5 cm ground resolution orthophotos. RGB orthoimages were transformed using Principal Component Analysis (PCA). From the first component of PCA from both orthophotos, there were selected representative panchromatic samples for two classes: asbestos-cement roofing sheets and other roofing materials.

Estimation of usefulness was conducted using machine learning methods based on decision trees (C5.0 algorithm). Various sets of textural attributes (using 5x5 window) was calculated in MaZda software for this purpose. In this study, several texture parameters were used: group of histogram-based characteristics, co-occurrence matrix-based parameters, run length matrix-based features, absolute gradient-based characteristics and autoregressive model parameters. Decision trees model was constructed based on training data - textural features from roofing samples set. In order to obtain the best settings for decision trees model, 4-folds cross-validation was performed with training set for C5.0 algorithm. Eight rounds of 4-folds cross-validation with changes in global pruning parameter and fuzzy threshold were done. After analyzing of the results of 4-fold cross-validation carried out using C5.0 there were selected the decision trees models which guaranteeing the lowest mean classification error.

The accuracy of the classification was held based on validation data sets, which were not used for the classifiers learning. Used data sets were divided in relation: 70% - learning data, 30% - validation data. For 5 cm ground resolution roofing samples set, the lowest mean classification error on the level 15.6% was obtained (with 99 boosting iterations). While using a smaller number of boosting iterations the final mean classification error was increased. For 10 boosting trials it was 20.0% and without any boosting option mean error has risen up to 31.1%. Respectively, for roofing samples set with 25 cm ground resolution, mean classification error with 99 boosting iterations was 24.4%. For 10 boosting trials average classification error on the level 28.9% was obtained and without any boosting mean error increased to 33.3%.

Literature review on accuracy in methods using hyperspectral imaging shows its high level around 90%. When the study is based on multispectral satellite data accuracy is between 70-90%. The level of obtained results in comparison with other research confirm potential usefulness of the textural features image processing for detection of asbestos-cement roofing sheets in orthophotos classification. In order to improve the accuracy another extended study should be considered in which additional textural features as well as spectral characteristics should be analyzed.

9643-95, Session PS

Statistical and structural pattern recognition techniques for single pulse detection of fire smoke by lidar

Cherifa Sabrina Amrouche, Basma El Amel Boussaha, Ecole Nationale Supérieue d'Informatique (Algeria); Mohammed Traïche, Ctr. de Développement des Téchnologies Avancées (Algeria); Karima Benatchba, Ecole Nationale Supérieue d'Informatique (Algeria); Riad Guehaz, Abdelkrim Kedadra, Ctr. de Développement des Téchnologies Avancées (Algeria)

Light Detection And Ranging (LiDAR) is a remote sensing technique largely used for atmospheric [1,2] and environment

[3,4] analysis. As an active technique, the LiDAR emits optical pulses with powers ranging from kilowatts to tens of megawatts which sense different species in the environment and return to the detector, delivering information on those species. Depending on the application purpose, this information may be the nature of those species, their size and spatial distribution, their position, their dynamic behaviour during short times or extended periods, etc. The useful signal always is defined by the purpose assigned to the application. The analysis of the return signal is a powerful way to retrieve all kind of sought information on the targeted species. As well, the LiDAR is used for forest fires detection owing to its unique performances: rapid and accurate localization along with wide scanned areas [5,6]. The laser beam is shined toward the smoke emanating from the fire (Fig.1). Then, by means of a time of flight detection, a large number of return signals is accumulated so as to enhance the signal to noise ratio [6,7]. The latter is the criterion of the detection effectiveness.

In this contribution, we utilize a breadboard LiDAR system to remotely sense the fire smoke. Rather than accumulating return pulses, we perform the detection based on a single return pulse long of 5 to 50 nanoseconds (Fig. 2). We present a preprocessing method of the return signal optimized for better precision and least processing time. Several features are then defined to selectively characterize the smoke signature on the nanosecond return pulse. Furthermore, an automatic classification of features is proposed. New signals are being classified according to their features and final decision is based on hybrid machine learning models to adaptively recognize forest fire smoke in the scanned area.

References

1. B. R. Clemesha, G. S. Kent, and R. W. H. Wright, “A laser radar for atmospheric studies,” J. Appl. Meteorol.6, 386–395 (1967)

2. V. Sivakumar, M. Tesfaye, W. Alemu, A. Sharma, C. Bollig and G. Mengistu: “Aerosol measurements over South Africa using Satellite, Sun Photometer, and LIDAR in World Scientific books, Advances in geosciences 16, Atmospheric Science, Chapter 22 253-62 (2010)

3. Y. Bhavani Kumar, “Development of LIDAR Techniques for Environmental Remote Sensing,” International Journal of Engineering Science and Technology 2(10), 5872-5881 (2010)

4. M. Traïche and A. Kedadra, “A Dual LiDAR System for Environmental Studies.” SPIE Newsroom 4801, (21 June 2013)

5. F. Andreucci and M. V. Arbolino, “A Study Of Forest Fire Automatic Detection Systems. Ii. - Smoke Plume Detection Performance,” Il Nuovo Cimento 16c, 51-65 (1993)

6. A.B. Utkin et al., “Detection of small forest fires by lidar.” Appl. Phys. B 73, 77-83 (2001)

7. A.Kedadra and M.Traïche: “Photomultiplier and avalanche photodiode detection performance for LiDAR application to environmentstudies,” J. Appl. Remote Sens., 8(1), 083568 (2014).

9643-96, Session PS

Unsupervised methodology for change detection and analysis: a comparison of classifier models

Ana C. Quintão Siravenha, Evaldo Goncalves Pelaes, Univ. Federal do Pará (Brazil)

The existence of remote sensing image databases allows a sort of studies about the land use and land coverage. The understanding of human occupation patterns through remote sensing data can assist the development of planning public politics in order to avoid, for example, dramatic sanitary problems. The identification of multiple changes in remote sensory images requires great effort to perform the high heterogeneity inherent of these data. This proposal aims to identify changes in land use and land coverage in multispectral images obtained by the Thematic Mapper sensor. The images correspond to the municipalities of Canaa dos Carajas and Parauapebas (Brazil), in which there is a huge mining project in activity since the 60’s, which caused intense migratory movement to the region. It is used the technique called Compressed Change Vector Analysis (C2VA), a method based on concepts of change vector analysis (CVA), a well know change detection technique. This approach comprises all spectral information available into two vectors of features, which represent (a) the magnitude of changes (about the presence or absence of changes) and (b) the direction of changes (about the kind of occurrence). Both magnitude and direction are similar to the CVA ones, but the compressed form is not affected by the ambiguity in magnitude space and does not require any a priori information about the analysed data, once does not select two bands to process each time. The magnitude ambiguity is overcome by the use of the direction information, and occurs by the information compression in a simplified two-dimensional representation. The discrimination between changed and unchanged pixels is made by an automatic k-means implementation. In this methodology, the user does not define the number of k clusters and the groups’ formation observes the distance between a pixel and an initial random centroid. The space of groups is partitioned according to this distance and when there is not larger enough distances computed the algorithm stops the centroids creation. The Euclidean distance is used at this phase and this automatic approach presents fast and very accurate discrimination. After definition of changed and unchanged pixels, three decision models are applied over the vector containing only the changed pixels in order to analyse the best classification approach to deal with the C2VA data: expectation maximization, k-means and ISODATA. The objective of use unsupervised methods is to present a user independent, still efficient, framework for change detection and analysis. Still, the k-means approach can be used in both way: with k defined manually or automatically. Four dates are analysed to validate this proposal: 1989, 1998, 2005 and 2014, and the classification assessment is based on confusion matrices and kappa index. The scenes were chose in order to avoid the presence of clouds.

9643-97, Session PS

Object detection in rural areas using hyperspectral imaging

Safak Ozturk, Yunus Emre Esin, Yusuf Artan, HAVELSAN A.S. (Turkey)

Object detection in rural areas has gained considerable interest in remote sensing with various applications including the remote monitoring of building development in rural areas. Many of the earlier studies on this task typically performed their analysis using either multispectral satellite imagery or color (RGB) images obtained via an aerial vehicle. In recent years, hyperspectral imaging (HSI) has emerged as an alternative technique for remote monitoring of building developments. Unlike other imaging techniques, HSI provides a continous spectral signature of the objects in the field of view (FOV) which facilitates the separation among different objects. However, most of HSI based object detection studies perform a pixel-wise spectral classification to localize the object of interest. Drawbacks of the pixel wise classification is well-known in remote sensing community. In general, spectral signature similarity between different objects often causes a significant amount of false alarm (FA) rate that adversely effects the overall accuracy of these systems. In order to reduce the FA rate posed by the pixel-wise classification, many region based object detection algorithms proposed in recent years. However, most of the existing methods are developed for a specific application that typically fails when the image acquisition parameters varies. In this study, we propose a novel rural building detection method that utilizes spatial information as well as the spectral signature of the pixels. Proposed technique consists of three parts; a spectral signature classifier, watershed based superixel map and a man-made object detector. While spectral signature classifier provides us with a class probability value corresponding to each pixel, watershed based superpixel map allows us to determine large homogeneous regions that can not be buildings. Similarly, man-made objects typically have a geometric structure (e.g.,

rectangle, square) that can be easily separated from a non man-made region. In our analysis, we heuristically determined a set of bands to generate our watershed superpixel map and derived a set of filters to localize man-made objects. Integration of a spectral signature classifier, watershed based superpixel-map and man made object detector yields the final building detection output. In our analysis, we have evaluated the performance of the proposed approach using hyperspectral image dataset obtained at various elevation levels, namely 500 meters and 3000 meters. NEO HySpex VNIR – 1800 camera is used for 182 band (between 400 nm-1000nm) hyperspectral data acqusition. First 155 band is used due to the atmospheric effects on the last bands. Radiance to reflectance conversion is done by using a white- tyvek. Performance comparison between the proposed technique and the pixel-wise spectral classifier indicates a reduction insensitivity rate but a notable increase in specificity and accuracy rates. Proposed method yields sensitivity, specificity, accuracy rate of 0.690, 0.997 and 0.992, respectively, whereas pixel-wise classification yields sensitivity, specificity, and accuracy rate of 0.758, 0.983, and 0.977, respectively. Note that the sensitivity reduction is due to the sparseness of buildings in rural areas, however, increase in overall accuracy is considered more important in this study. In summary, we proposed an HSI based building detection system in rural areas that reduces false alarm rates compared to existing systems while preserving similar sensitivity rate.

9643-98, Session PS

Utilizing hyperspectral remote sensing imagery for afforestation planning of partially covered areas

Fatih Omruuzun, Didem Ozisik Baskurt, Middle East Technical Univ. (Turkey); Hazan Daglayan, Atilim Üniv. (Turkey); Yasemin Yardimci Cetin, Middle East Technical Univ. (Turkey)

Areas dedicated for forestation may remain partially covered due to natural disasters such as landslide, fire etc. and unauthorized cutting or it may have never been planted. Reforestation with similar species of trees is a widely used technique that is essential to promote the growth and preservation of healthy forests, and this enrichment process requires an effective afforestation planning management. However, three important issues affect the accuracy of planning: estimation of area to be afforested, amount of trees required, and the locations of trees to be planted. Challenges of on-site evaluation include accessibility and size of the area to be investigated. Therefore, remote sensing algorithms are widely used for this purpose. In this study, a supportive method for afforestation planning process of partially forested areas using hyperspectral remote sensing imagery has been proposed. The main contribution of this study to the literature is segmentation of partially forested regions with a semi-supervised classification of specific tree species based on chlorophyll content quantified in hyperspectral scenes. In addition, the proposed method makes use of various hyperspectral image processing algorithms to improve identification accuracy of image regions to be planted.

The proposed method begins with selection of a pixel belonging to central point of a specific mature tree from a sparsely planted region by the user. Using this supportive pixel, two critical features of the tree species are extracted from the image. The first feature to be extracted is canopy area that is calculated by using hyperspectral unmixing and region growing methods. The canopy area is calculated in both meter square and pixel units using flight data recorded by GPS/IMU data. Moreover, minimum plant spacing for a specific tree species can also be obtained from an expert user. The second feature is the vegetation index (NDVI) value of this tree species to be used in classification process of the method.

In the upcoming part of the algorithm, a semi-supervised learning method classifies the image to detect the area that has already been afforested. At this point, NDVI provides further verification to improve the accuracy of classification process. Subsequently, a morphology based region growing algorithm highlights the pre-afforested area utilizing the tree canopy area computed in first step.

The third part of the proposed method tries to identify pixels that are suitable for afforestation process. To do that, Reed-Xiaoli (RX) hyperspectral anomaly detection algorithm is applied to determine the areas that should not be forested. In this way, roads, urban facilities and other man-made objects are excluded from the image. Proposed algorithm also eliminates shaded regions that are labeled by the anomaly detection algorithm using both normalized Shadow Index (nSI) and the spectral Shadow Index (sSI).

Experiments conducted on a hyperspectral image acquired by Visible + NIR sensor during a flight held on 22nd of October 2014 over METU Ankara campus shows that proposed algorithm produces promising results for utilizing hyperspectral images in afforestation planning management.

9643-99, Session PS

An effective band selection approach for classification in remote sensing imagery

Huseyin Cukur, Hamidullah Binol, Faruk S. Uslu, Abdullah Bal, Yildiz Technical Univ. (Turkey)

Hyperspectral imagery (HSI) is a special imaging form that is characterized by high spectral resolution with up to hundreds of very narrow and contiguous bands which is ranging from the visible to the infrared region. Since HSI contains more distinctive features than conventional images, its computation cost of processing is very high. That's why; band reduction is significant for classification performance. Variable Neighborhood Search (VNS) is a method that aims to quickly investigate search space to find the best or near optimal solutions. This method is based on systematic change of neighborhood used in the search. It becomes prominent method because of the success in achieving optimum results by exploring search space in a short time especially with the large size of the data. In this study, dimension reduction has been achieved via VNS based band selection method on hyperspectral images. The selected bands have been utilized for classification purpose using Support Vector Machine (SVM) to evaluate the performance of the proposed band selection technique. In order to improve the band selection performance, we have designed clustering technique based on mutual information (MI) which measures how much similar each of two random variables. While the mutual information is high for similar two variables, it becomes less by decreasing similarity. After MI based band clustering, the VNS is applied for band selection. Thus, MI-VNS combination presents better results due to clustering of similar bands. The experimental results show that MI-VNS approach has increased the classification performance compare to without band selection and only VNS based band selection.

Brief Information About Experimental Results:

In this experiment, we have chosen NASA AVIRIS HSI data captured over Kennedy Space Center (KSC) in 1996. All 13 classes for HSI have been tested via proposed methods, and the results of 5 classes are given in Table 1 to see the performance. According to Table 1, both VNS and MI-VNS band selection techniques present better classification results compare to full number of bands case (without band selection).

9643-36, Session 8

Analysis on the effectiveness of multitemporal COSMO-SkyMed images for crop classification

Rocchina Guarini, Agenzia Spaziale Italiana (Italy); Lorenzo Bruzzone, Massimo Santoni, Univ. degli Studi di Trento (Italy); Luigi Dini, Agenzia Spaziale Italiana (Italy)

Satellite synthetic aperture radar (SAR) systems, thanks to their almost independence from weather conditions, have an

important relevance in agricultural research and management, at regional scale.

Previous studies have demonstrated the better capability of multi-temporal than mono-temporal image classification to discriminate different annual crop types at X-band, C- and L-band. At X-band, only few images, acquired at the beginning of the growing season, are needed to accurately identify corn and soybean. In particular, at HV polarization X-band SAR response provides more accurate classification than at HH polarization. Increases in discrimination between ploughed fields and sugarcane fields in vegetation were also shown, in large crops at X-band.

The main objectives of this paper are: i) to test the performance of COSMO-SkyMed® (CSK®) X-band system for identifying different crop types over an agricultural site; ii) to assess the effectiveness of multi-temporal features for the discrimination of different crops; iii) to assess the importance of the polarization (VV, HH, VH) for crop classification. These objectives are addressed by developing a classification architecture based on a supervised Support Vector Machine (SVM) classifier.

COSMO-SkyMed® (X-band, frequency 9.6 GHz, wavelength 3.1 cm) system offers the opportunity to acquire images with a very short revisit time. This characteristic can provide useful information for monitoring changes of annual crops. In this study, CSK® images are collected from April 1st to October 30th 2014, in Stripmap Himage acquisition mode, at HH, VV and VH polarizations, at approximately 40° incidence angle.

The study site is located in the Austrian region of Marchfeld, a flat area near the city of Wien. This region has been chosen as an interesting test site thanks to its heterogeneous varieties of crop types.

The crop mix in Marchfeld includes ten classes namely: alpha alpha, carrot, corn, cucurbit, pea, potato, soybean, sugar beet, summer crops, winter crops.

The CSK® data are co-registered and multi-temporal and spatial filtered.

The temporal variability of backscattering is analyzed in multi-temporal CSK® imagery for all species and the related information is extracted by computing specific features. Moreover, texture features are extracted for modeling the different crops structures.

A SVM Machine technique is then used for the classification and the differentiation of agricultural crops within their phenological cycles.

Ground truth data were collected and divided into a training and a test subset of equal size. There is no overlap between the training fields and testing fields.

In order to assess the classification accuracy of SVM result, the overall accuracy, the user's accuracy, the producer's accuracy and the Kappa statistics are evaluated on the basis of the confusion matrix (error matrix) approach.

In the final paper results of the crop classification using multi-temporal COSMO-SkyMed® data at different polarizations (VV, HH, VH) will be shown. In order to evaluate the possibility to monitor crops at the start of crop growth stage, the results of the CSK® classification carried out on the whole season dataset will be compared to the CSK® classification conducted on few scenes acquired at the beginning of the season.

9643-37, Session 8

A fast and reliable change detection feature from bi-temporal amplitude SAR images

Andrea Garzelli, Claudia Zoppetti, Univ. degli Studi di Siena (Italy)

The discrimination between changed and unchanged pixels is particularly difficult in SAR imagery for the presence of speckle noise. A preprocessing step is usually recommended to reduce the speckle originated by a multiplicative fading term and, due to the nature of the SAR signal, using the ratio (R) or the Log-Ratio (LR) appears more suitable for detecting changes.

Information-theoretic (IT) concepts have been introduced for SAR change detection in the past decade. The information-theoretic change detection (ITCD) feature extraction method is unsupervised, non-parametric, and does not require a preliminary despeckling procedure. A further improvement adopts mean-shift clustering of the estimated joint pdf of the SAR amplitude values acquired at two dates (MS-ITCD). MS-ITCD can reliably detect the regions of change even for one-look amplitude SAR images. However, a possible drawback of this algorithm can be the high computational complexity for estimating and processing the joint pdf from the scatterplot of the two-date SAR amplitude values. Another issue concerns the detection of changes in small areas: this is possible only when the extraction of the local modes of the joint pdf is extremely accurate and reliable.

A modified version of MS-ITCD, namely LR-ITCD, is capable of capturing small-area structural changes between the two images, by maintaining at the same time the capability of rejecting statistical changes due to speckle patterns or co-registration inaccuracies. LR-ITCD is obtained by bootstrapping the IT-based change detection algorithm by means of an adaptive preliminary selection of potentially changed pixels extracted from the LR image. LR-ITCD has introduced two main advantages with respect to MS-ITCD: it reduces the computational complexity by eliminating the mean-shift clustering; it is capable of detecting small percentage of changed pixels. The first advantage is obtained by replacing the mode-seeking clustering step with an empirical modification of the underlying joint pdf (second date vs first date). The second advantage is possible thanks to the preservation of the scatterplot regions corresponding the most likely changed pixels.

This paper introduces two significant improvements in the general ITCD scheme. It preliminary partitions the image pixels according to a constant false alarm rate decision based on the probabilistic model of the ratio image R. This step segments the scatterplot into two regions: region A of the unchanged pixels (whose extension is determined by the CFAR criterion) and region B of the changed pixels. Secondly, it adaptively quantizes the 2-D scatterplot instead of applying clustering, as in MS-ITCD, or empirically modulating the change feature, as in LR-ITCD. Region A is quantized with a lower number of levels with respect to region B. The effect of this adaptive quantization of the scatterplot is equivalent to mean-shift clustering on region A only, thus preserving small structural changes in region B.

Experimental results have been carried out with simulated changes applied to synthetically-generated 1-look SAR images produced from an optical remote sensing image and independent Nakagami-distributed speckle patterns. True Cosmo-SkyMed SAR images will be also considered on a damage assessment scenario.

9643-38, Session 8

Fully polarimetric high-resolution airborne SAR image change detection with morphological component analysis

Elias Mendez Dominguez, Univ. Zürich (Switzerland); Daniel Henke, Univ. Zurich (Switzerland); David Small, Erich H. Meier, Univ. Zürich (Switzerland)

Change detection techniques interrogate a test image with respect to a reference image to obtain a binary map with information of the changes. SAR sensors can operate in unfavorable weather and daylight conditions, and can collect time series data. Previous studies showed great potential for SAR-based image change detection [1-3]. However, the inherent complexity of SAR data imposes multiple challenges that need to be tackled. To overcome some limitations, in particular with high resolution airborne SAR imagery, we exploit shape-based decomposition techniques combined with polarimetric layers to provide physically meaningful features to the change detector. In this manner, we exploit six image

features (three scattering mechanisms decomposed in two shapes) to remove false alarms introduced by clutter, diverse focusing errors (sidelobes, moving targets…), and differences caused by non-uniform acquisition geometries, e.g. migration of the Point Spread Functions (PSFs) of the same target to different image pixels.

The images were acquired within a single week with the DLR F-SAR sensor at X-band [4] over the region of Memmingen (Germany) from two quasi-identical flight paths. The SAR imagery has a range and azimuth resolution of 0.23 m and 0.15 m respectively. To detect changes, first the power of the scattering mechanisms (single-bounce, double-bounce and volume) was computed with a suitable decomposition for each set [5]. To suppress noise-induced errors, each RGB composite was denoised with C-BM3D [6]. Subsequently, the power of each mechanism was extracted and decomposed into two image shapes using a wavelet- and a curvelet-based Morphological Component Analysis [7]. The wavelet component was suitable to retain uniform areas and point-like targets, whereas the curvelet component was used to retain edges and contours. To extract the changes we applied a subtraction of the different scattering mechanisms and combine their corresponding binary maps. This combination allowed us to retain detected changes of interest while discarding the rest.

Figure 1 illustrates some preliminary results of the method, where the binary maps are overlaid on the total scatter power of the reference image: pixels marked in red/green indicate appearing/disappearing objects. Figure 1(d) shows the binary map computed with all the scattering mechanisms and shapes. Figure 1(e) shows the results after removing the changes of the curvelet component of the single and double bounce mechanisms, as those changes can be related to clutter zones and sidelobes of man-made objects. For comparison purposes, Figure 1(f) shows the removed false alarms in red; e.g. moving cars on the parking lot north-west of the airport terminal.

From the preliminary results, we observed that the method's detection performance expedites human interpretation of the changes themselves as well as their possible origin. By exploiting the power of the scattering mechanisms and their corresponding shape factor, we can significantly improve the performance of the detector for some errors introduced by clutter zones, sidelobes and PSF migrations. Currently we are analyzing the additional information provided with the H/A/? decomposition [5] and diverse techniques to combine the multiple features, as well as considering the extension of other morphological components.

[1] Brunner, D., Lemone, G. and Bruzzone, L., "Earthquake damage assessment of buildings using VHR optical and SAR imagery," IEEE Transactions on Geoscience and Remote Sensing, 48(5), 2403-2420 (2010).

[2] Schmitt, A., Wessel, B. and Roth, A., "Curvelet approach for SAR image denoising, structure enhancement, and change detection," The International Archives of the Photogrammetry, Remote Sensing and Spatial Information Sciences, 38(3/W4), 151-156 (2009).

[3] Schmitt, A. and Wessel, B., "Introducing Partial Polarimetric Layers into a Curvelet-based Change Detection," 8th European Conference on Synthetic Aperture Radar (Aachen, Germany), 1-4, (2010).

[4] Reigber, A., Scheiber, R., Jager, M., Prats-Iraola, P., Hajnsek, I., Jagdhuber, T., Papathanassiou, K.P., Nannini, M., Aguilera, E., Baumgartner, S., Horn, R., Nottensteiner, A. and Moreira, A., "Very-High-Resolution Airborne Synthetic Aperture Radar Imaging: Signal Processing and Applications," Proceedings of the IEEE, 101(3), 759-783 (2013).

[5] Lee, J. and Pottier, E., [Polarimetric radar imaging: from basics to applications], CRC press, 179-264 (2009).

[6] Dabov, K., Foi, A., Katkovnik, V. and Egiazarian, K., "Image Denoising by Sparse 3-D Transform-Domain Collaborative Filtering," IEEE Transactions on Image Processing, 16(8), 2080-2095, (2007).

[7] Starck, J. L., [Sparse Image and Signal Processing: Wavelets, Curvelets and Morphological Diversity], Cambridge University Press, 190-196 (2010).

9643-39, Session 8

Change detection in quad and dual pol, single- and bi-frequency SAR data

Allan A. Nielsen, Knut Conradsen, Henning Skriver, Technical Univ. of Denmark (Denmark)

In 2003 we introduced a new test statistic for equality of two variance-covariance matrices following the complex Wishart distribution with an associated probability of observing a smaller value of the test statistic [1]. We also demonstrated its use to change detection in both quad and dual polarimetric SAR data. We also mentioned the possibility of application of the test statistic and the associated probability to block-structured covariance SAR data such as the azimuthal symmetric and diagonal-only cases. This feature was further described in [2] where we also showed the application of the test statistic and the associated probability to edge detection in polarimetric SAR data. In [3] we introduced multi-frequency applications. Application of the Hotelling-Lawley trace statistic to the change detection problem is described in [4].

In the early 2000s, not many workers had access to polarimetric SAR data. With the advent of several spaceborne polarimetric SAR instruments this situation has improved. These instruments include

- the Japanese ALOS (a.k.a. DAICHI), L-band with single, dual and full polarization,

- the Canadian Radarsat-2, C-band with single, dual and full polarization,

- the German TerraSAR-X, X-band with single, dual and full polarization,

- the Italian COSMO-SkyMed, X-band with single and dual polarization,

- the European (ESA) Sentinel-1, C-band with single and dual polarization.

For power supply and coverage reasons some of the instruments among the above which have full polarization capability are often operated in (either single or) dual polarization modes, i.e., they transmit one polarization only and receive (either one or) both polarizations. We therefore think that a revisit to the methods described and sketched in [1,2] with emphasis on dual polarization and multi-frequency SAR data is timely.

[1] Conradsen, K., Nielsen, A. A., Schou, J., and Skriver, H., "A test statistic in the complex Wishart distribution and its application to change detection in polarimetric SAR data," IEEE Transactions on Geoscience and Remote Sensing 41, 4-19, Jan. 2003. http://www.imm.dtu.dk/pubdb/p.php?1219.

[2] Schou, J., Skriver, H., Nielsen, A. A., and Conradsen, K., "CFAR edge detector for polarimetric SAR images," EEE Transactions on Geoscience and Remote Sensing 41, 20-32, Jan. 2003. http://www.imm.dtu.dk/pubdb/p.php?1224.

[3] Nielsen, A. A., Conradsen, K., and Skriver, H., "Change detection in full and dual polarization, single- and multi-frequency SAR data," Accepted for IEEE Journal of Selected Topics in Applied Earth Observations and Remote Sensing, Mar. 2015. http://www.imm.dtu.dk/pubdb/p.php?6827.

[4] Akbari, V., Anfinsen, S. N., Doulgeris, A. P., and Eltoft, T., "The Hotelling-Lawley trace statistic for change detection in polarimetric SAR data under the complex Wishart distribution," in IEEE IGARSS, 4162-4165, Melbourne, Australia, 21-26 July 2013.

9643-40, Session 8

Change detection in UAV video mosaics combining a feature-based approach and extended image differencing

Günter Saur, Wolfagang Krüger, Fraunhofer-Institut für Optronik, Systemtechnik und Bildauswertung (Germany)

Change detection is one of the most important tasks

when applying unmanned aerial vehicles (UAV) for video reconnaissance and surveillance. Here we address changes of short time scale, i. e. the observations are taken in time distances from several minutes up to few hours. Each observation is a short video sequence corresponding to the near-nadir overflight of the UAV over the interesting area and the relevant changes are e. g. recently parked or moved vehicles. The change detection algorithm has to distinguish between relevant and non-relevant changes. Examples for non-relevant changes are 3D structures of the scene and compression or transmission artifacts.

A precise image-to-image registration combined with a robust matching approach is needed to stitch the video frames together to a mosaic.

Additionally this matching algorithm is applied to mosaic pairs in order to align them to a common geometry. The resulting registered video mosaic pairs are the input of the change detection procedures.

In this paper we present:

1. a new feature based approach to change detection

2. combination with extended image differencing (Saur et al. 2014)

In the feature based approach, information about local image features, e.g. corners (Shi and Tomasi 1994), is extracted in both images. The label “new object” is generated at image points, where features occur in the first image and no or weaker features are present in the second image. The label “vanished object” corresponds to missing or weaker features in first image and present features in the second image. This leads to two “directed” change masks and differs from image differencing where only one “undirected” change mask is extracted which combines both label types to the single label “changed object”.

Extended image differencing is based on intensity and gradient changes (Saur et al. 2014). Compared to corner features, this gives additional independent information about changes in the image pair. We investigate and discuss the different characteristics of both approaches using UAV video mosaics. The extended image differencing approach emphasizes slight changes in intensity which may have smooth borders. The feature based approach is less sensitive to registration errors and small 3D parallax. By fusing the results of both algorithms we intend to benefit from their different characteristics. In a first realization, the fusion was performed using color channels for the three resulting change masks. The color mask is used for visual inspection by a human photo interpreter, see Fig. 1.

References:

Günter Saur, Wolfgang Krüger, and Arne Schumann “Extended image differencing for change detection in UAV video mosaics”, Proc. SPIE 9026, Video Surveillance and Transportation Imaging Applications 2014, 90260L (March 5, 2014); doi:10.1117/12.2043209; http://dx.doi.org/10.1117/12.2043209

J. Shi; C. Tomasi “Good Features to Track”, Proceedings of the IEEE Conference on Computer Vision and Pattern Recognition, pages 593-600, June 1994.

9643-41, Session 9

A game-theoretic tree matching approach for object detection in high-resolution remotely sensed images

Yilong Liang, Nathan D. Cahill, Eli Saber, David W. Messinger, Rochester Institute of Technology (United States)

Generally speaking, object-based methods for analyzing high-resolution (HR) remotely sensed images are more favored than pixel-based approaches. A variety of research has shown that object-based methods have superior performance to pixel-based approaches in applications such as classification and change detection.

In this paper, we propose an object-based game-theoretic approach to address the problem of object detection in HR remotely sensed images. We employ a scale tree structure to represent the images, where each level of the scale tree denotes a segmentation of the image at a specific scale. The nodes in the tree represent regions in the segmentations, and the edges denote the relative containment relationships between segments at different scales. Given the tree representations of the scene and object images, we formulate the task of object detection as a tree-matching problem. We propose a game-theoretic technique to search for node correspondences between pairs of trees. This involves defining a non-cooperative matching game, where strategies denote the possible matching between regions, and payoffs determine the compatibilities between different strategies. The tree-matching problem is solved by searching for the evolutionary stable states (ESS) of the game.

The game-theoretic tree matching algorithm comprises the following steps: 1) Determine candidate matches for all the nodes in the object image tree. These matches correspond to all available strategies in the game. This step aims at selecting moderate size strategies in a matching game. 2) Construct a payoff matrix based on strategies derived in the first step. Each entry in the payoff matrix corresponds to the compatibility between a pair of nodes from the object tree and another pair from the scene tree. These compatibilities encode the spectrum similarity properties, as well as the spatial consistency properties, between different pairs of matching nodes. 3) Carry out a game dynamic by evolving an initial population iteratively until evolutionary stable states (ESS) of the game are reached. The surviving strategies in the ESS correspond to the matching results, which in turn correspond to detected objects.

In order to validate the effectiveness of the proposed algorithm, we have carried out experiments on both synthetic and HR remotely sensed images. Our results demonstrate the robustness of the tree representation methodology and the effectiveness of detecting objects in the presence of spectrum variations and spatial variations, including translation and rotation.

9643-42, Session 9

Object-based detection of vehicles in airborne data

Hendrik Schilling, Dimitri Bulatov, Wolfgang Middelmann, Fraunhofer-Institut für Optronik, Systemtechnik und Bildauswertung (Germany)

Robust detection of vehicles in airborne data is a challenging task since a high variation in the object signatures – depending on data resolution - and often a small contrast between objects and background lead to high false classification rates and missed detections. Despite these facts, many applications require reliable results which can be obtained in a short time.

In this paper, an object-based approach for vehicle detection in airborne laser scans (ALS) and photogrammetrically reconstructed 2.5 D data is described. The focus of this paper lies on a robust object segmentation algorithm as well as the identification of features for a reliable separation between vehicles and background (all none-vehicle objects) on different scenes. The described method is based on three consecutive steps, namely, object segmentation, feature extraction and supervised classification.

Despite the fact that the initial segmentation can cause additional errors, an object-based approach has certain advantages on contrast to a pixel-based. First, the initial segmentation allows using object-based features like area or shape. Furthermore, the computational effort for feature extraction and classification is dramatically reduced due to the fact that not each pixel in the image but only a limited amount of objects needs to be classified. This allows utilization of more complex features and classifiers without losing near real-time capability.

In the first step, the 2.5 data is segmented and possible targets are identified. This segmentation process should be designed

in a way which achieves high detection rates, possibly at cost of a high false alarm rate. The segmentation progress is based on the morphological top-hat filtering, which leaves objects that are smaller than a given filter size and higher (brighter) than their surroundings. The approach is chosen due to the low computational effort of this filter, which allows a fast computation even for large areas. The morphological top-hat filtering works local, therefore no digital terrain model for the separation between high and low objects is needed.

The next step is feature extraction. Based on the initial segmentation, features for every identified object are extracted. In addition to frequently used features like height above ground, object area, or point distribution, more complex features like object planarity, entropy in the intensity image, and lineness measures are used.

The last step contains classification of each object. For this purpose, a support vector machine (SVM) using the normalized features extracted in the previous step is chosen. SVMs are suitable for high dimensional and nonlinear problems. In contrast to stochastic approaches (e.g. maximum likelihood classifier), SVMs achieves good results even with relatively small training samples.

Two scores will be evaluated for each scene, the correctness of the classification in relation to the used features as well as the completeness of detected vehicles. High resolution images, which are available for each scene, are used to generate the ground truth. Therefore, partially occluded or otherwise hardly detectable targets will be included in the evaluation procedure.

9643-43, Session 9

A GUI visualization system for airborne lidar image data to reconstruct 3D city model

Yoshiyuki Kawata, Kohei Koizumi, Kanazawa Institute of Technology (Japan)

The demand of 3D urban model has been increasing in many applications such as urban planing, computer gaming with realistic city environment, virtual city tourism inviting future visitors and others. However, while accurate 3D positional data are available with the advancement of LiDAR technology, the processing of 3D LiDAR point cloud data is not readily done and it is still one of hot research topics in remote sensing and photogrammetry fields.

A visualization toolbox system with a graphical user interface (GUI) was developed for LiDAR point cloud data, as a compound object oriented widget application in IDL (Interractive Data Language). The main features in our toolbox include an input and output file handling capability, a data conversion capability from raw LiDAR data to a gray scale LiDAR image in which each pixel's gray level value is assigned to a corresponding altitude measured by LiDAR, a visualization capability of 2D/3D images in various processing steps and a reconstruction capability of 3D city model. Different kinds of image processing operations for LiDAR image data are invoked by either pressing buttons or inputting necessary numerical values in our textbox. They are a noise removal process, a masking operation to generate altitude masked binary images, an extruding process of the connected regions extracted from the altitude masked binary image and a final integration process to reconstruct a 3D city model from all connected regions with different altitude values.

Finally, the reconstruction of a 3D city model was successfully demonstrated by applying our GUI toolbox system to the actual airborne LiDAR point cloud data.

9643-44, Session 9

L-shaped corner detector for rooftop extraction from satellite/aerial imagery

Hui Li Tan, Jiayuan Fan, Shijian Lu, Institute for Infocomm Research (Singapore)

Rooftop extraction from satellite/aerial imagery is an important geospatial problem with many practical applications such as urban planning, military simulation, and geo-mapping. However, rooftop extraction remains a challenging problem due to the diverse characteristics (size, shape) and appearances (illumination, viewing angle) of the buildings, as well as the quality (resolution, contrast, and visibility) of the satellite/aerial images.

Different rooftop extraction approaches have been reported in the literature [1] [2]. One typical approach uses edges to detect corners for quadrilateral footprint extraction [3]. Nonetheless, detecting corners from edges can lead to many miss detections, as the detected edges are often fragmented due to the line extraction process and occlusion. Another approach uses corners for level set evolution [4], in which the corners are extracted using generic corner detectors. Nonetheless, as generic corner detectors are designed to identify corners of arbitrary shape and scale, they can introduce many false alarms.

Based on the observation that rooftop corners are typically of L-shape, we propose an L-shaped corner detector for rooftop extraction. The proposed detector considers information in a spatial circle around each pixel to construct a feature map which captures the probability of L-shaped corner at every pixel. By employing equal-distance and equal-length rays that radiate from each pixel, the proposed detector computes the L-shape structural strength of the pixel. The L-shape structural strength of the pixel is computed based on the goodness-of-fit of any pair of rays to the rooftop edges and the goodness-of-fit of the pair of rays to a 90-degree structure. The corners can then be easily extracted by non-maximum suppressing the feature map.

Our experimental results on a rooftop dataset [5] of over 200 buildings demonstrate the effectiveness of the proposed detector for rooftop corner detection. In particular, the proposed detector produces much fewer false alarms when compared to the widely used Harris detector [6] (refer to figure), and gives a higher F-measure over the dataset. The good results can be attributed to the effective use of spatial instead of very local information around each pixel. Furthermore, the proposed detector is complementary to many existing rooftop extraction approaches which require reliable corners as their inputs. For instance, it can be used in the quadrilateral footprint methods [3] or in driving level set evolution based techniques [4].

References:

[1] Mayer, "Automatic object extraction from aerial imagery - a survey focusing on buildings," CVIU, vol. 74, no. 2, pp.138-149, 1999.

[2] Baltsavias, "Object extraction and revision by image analysis using existing geodata and knowledge: current status and steps towards operational systems," Journal of Photogrammetry and Remote Sensing, vol. 58, pp.129-151, 2004.

[3] Nosrati and Saeedi, "A novel approach for polygonal rooftop detection in satellite/aerial imageries," ICIP, pp.1709-1712, 2009.

[4] Cote and Saeedi, "Automatic rooftop extraction in nadir aerial imagery of suburban regions using corners and variational level set evolution," IEEE Trans. Geoscience and Remote Sensing, vol. 51, no. 1, pp.313-328, 2013.

[5] Rooftop dataset, "http://cvlab.epfl.ch/data/polygonalobjectdataset".

[6] Harris and Stephens, "A combined corner and edge detector," 4th Alvey Vision Conference, pp.147-151, 1988.

9643-45, Session 9

Information theoretic SAR boundary detection with user interaction

Can Demirkesen, TÜBITAK UZAY (Turkey); Ugur M. Leloglu, Middle East Technical Univ. (Turkey)

Fully automated detection of object boundaries is a very challenging task especially in low resolution or low signal-to-noise ratio images such as synthetic aperture radar images or hyperspectral images. There exist several very sophisticated edge detection techniques such as ratio of averages for SAR images for instance or very advanced segmentation techniques such as graph cuts. However there is still room for improvement in this field of research both in theoretic plane and in terms of performance.

In this work, we propose a user interaction based boundary detection technique which makes use of a very well-known concept of information theory: the Kullback-Leibler divergence (KLD) and cubic splines which is a powerful tool.

The architecture consists of the following four main steps:

1. The user selects points inside and outside of a region (an object)

2. Profiles that link these inside and outside points are extracted

3. Boundary points that lie on the profile are located using KLD.

4. Boundary points are connected with cubic splines.

The only user interaction required in this scheme is at the stage of point selection. Once the interior and exterior points are available, the pixel intensity values along each line connecting a pair of points are collected. Since one end point is inside a region while the other end point is outside the region, there must a point between the two end points that lays on the boundary i.e. a boundary point.

In order to find the exact location of the aforementioned boundary point KLD is used. Starting from one end point, the profile is divided into two until reaching the other end. At each location, the KLD is calculated and stored in an array called J. We assume that if a point belongs to the boundary then for this point, the KLD of the two portions of the profile is larger than any other point on that profile. Under this assumption, the point that corresponds to the maximum value of the array J is identified as a boundary point. The principle of divergence is applicable because there are two sets of data generated from different probability mass functions, in other words, pixels belonging to two different regions are samples of different probability distributions.

Finally, the cubic splines that provide both elasticity and smoothness are used connect boundary points together to obtain an accurate estimate of the actual boundary.

This generic boundary detection approach has proven itself to be robust to the speckle phenomenon that exists in SAR images. Experiments were conducted using Sentinel-1, TerraSAR-X and COSMO SkyMed SAR images as well as hyperspectral images acquired by Hyperion sensor on board EO-1 satellite.

9643-46, Session JS1

Understanding target delineation using simple probabilistic modelling

Christopher J. Willis, BAE Systems (United Kingdom)

Target delineation is recognised to be the critical step in Automatic Target Recognition methods from image and signal data. Here the signal or image elements upon which the recognition decision is to be made are identified, and those not to be included in the decision are eliminated. Clearly, if too many actual target elements are missed, then the candidate target region presented for recognition processing will be compromised. Likewise, if too many background elements are included then ATR performance will also be limited through the incorporation of non-informative signal. A good delineation approach must trade-off the two sources of error to select an ensemble of elements suitable for recognition across the range of potential target types, sizes and clutter backgrounds that might be presented to the ATR system. It follows that gaining an understanding of the performance of target delineation processes is key to understanding the ATR step as a whole. A modelling-based process for delineation understanding might also be used to make parameterisation recommendations so that the ATR has the best opportunity in achieving a high performance in the follow-on recognition steps.

The paper examines a simple target delineation method and uses the information contained in Receiver Operating Characteristic curves, along with basic observations regarding target sizes and shapes, to generate assessments of delineation performance. Performance is gauged by considering the delineations that might result from having particular arrangements of detected pixels within the vicinity of a hypothesized target. In particular, the method considers the qualities of delineations generated when having various combinations of detected pixels at a number of locations around the inner and outer boundaries of the underlying object. Several distinct types of arrangement for pixels on the inner target boundary are proposed. Each has the potential to lead to good delineations in a thresholding and shape fitting scheme. The compromising effect of false alarms within the surrounding local region is also taken into account. The resulting ensembles of detected pixels are treated using familiar rules for combination to form probabilities for the delineations as a whole. The methods derived may be applied to imagery from a range of sensor types, simply using Receiver Operating Characteristic curves as a driver. Results are derived for hypothesized targets in idealized Synthetic Aperture Radar imagery. They are presented as performance estimates varying with a thresholding parameter for a range of target sizes, shapes, contrast settings and pixel scattering types. The target pixels treated are taken from the Swerling model set whilst those for the background are taken from standard SAR clutter representations, including exponential and various parameterisations of the K-distribution.

9643-47, Session JS1

Reducing scalloping in synthetic aperture radar images using a composite image transform

Knut Landmark, Norwegian Defence Research Establishment (Norway); Anne H. S. Solberg, Univ. I Oslo (Norway)

In burst mode synthetic aperture radar (SAR) imaging, a point target is illuminated for only a part of the time it lies within the radar beam footprint. Consequently, the received echo intensity depends on the azimuth (along-track) antennae pattern and the target's azimuth angles relative to the beam centre, during the burst. This azimuth dependence may cause artefacts in SAR imagery, including azimuth scalloping, a periodic modulation of the image intensity in the azimuth direction. Standard SAR image formation includes descalloping corrections. In particular, if several adjacent looks overlap, weighting functions may be applied when summing the contributions of each look to reduce the azimuth dependence. However, this requires accurate estimates of the Doppler centroid, otherwise a residual scalloping remains. Residual scalloping has been seen in particular in wide-swath ScanSAR images of ocean areas and may interfere with e.g. surface wind field mapping and other image recognition tasks.

A new image restoration method was recently developed for reducing track line artefacts and motion-induced errors in multibeam echo sounder bathymetry. We demonstrate that the method can be successfully applied to remove residual scalloping in processed ScanSAR images. The method is system independent and applied at the image level. It is analogous to a filter in the Fourier or wavelet transform domains, with no assumptions about noise periodicity or orientation. The forward transform consists of a modified Laplacian spatial filter composed with a discrete Radon transform (DRT). The Laplacian operator, which is linear, rotation-invariant, edge sensitive, and noise sensitive, accentuates fine-scale intensity changes; the DRT focuses linear features because each DRT value is the sum of pixel intensities along a straight line. To avoid boundary effects, a Chebyshev approximation (trend) is temporarily subtracted from the image. A descalloping filter can be implemented in the DRT domain by zeroing values at the across-track angle.

The restored image is obtained by inverting the DRT and Laplacian. The former means solving an overdetermined linear system; we find a rapidly converging, iterative pseudo-inverse solution. Filtered backprojection, by comparison, may cause unwanted distortion of fine features. The standard Laplacian operator is not invertible due to a zero in the transfer function. A modified point spread function for the Laplacian is therefore introduced such that the operator becomes invertible.

The method was tested on ocean scene images from the ENVISAT Advanced Synthetic Aperture Radar.The scalloping effect was significantly reduced, while there was no apparent distortion or smoothing effect in the filtered images.

While the example data used in this work were obtained with the now inoperative ENVISAT satellite, scalloping is still a concern for existing SAR systems. Even the Terrain Observation by Progressive Scans (TOPS) imaging mode, whose design promises to eliminate the azimuth dependence problem, may exhibit some scalloping caused by electronic beam steering. The simplicity of filter design in the DRT domain is in our view an advantage; the denoised images shown in this work were obtained directly without experimentation and parameter tuning. The method may also be useful for reducing e.g. stripe noise caused by detector-to-detector variations in optical pushbroom-type systems.

9643-48, Session JS1

Curvelet-based compressive sensing for InSAR raw data

Marcello G. Costa, Marcelo S. da Silva Pinho, David Fernandes, Instituto Tecnológico de Aeronáutica (Brazil)

Synthetic Aperture Radar (SAR) is an active ground imaging system based on coherent processing of multiple radar echoes acquired along the path of a moving platform (Airborne or satellite), providing informations for civil and military applications. InSAR is an interferometric configuration of SAR to generate digital elevation models and measurement of centimetric surface deformations of the terrain. The increasing demand for high resolution have resulted in high sample rates and large amount of collected data which represent constraints in the operation of SAR to transmit the data to ground station or to store data onboard. Therefore, an efficient compression can be essential to reduce storage costs and providing real-time transmission. The conventional techniques for compression of raw SAR signal are based on scalar, vectorial and transform domain which exploit the redundancy inherent in the Nyquist rate sampled signal to achieve compact representation and efficient transmission of the information. However, a sampling at a higher rate requires the processing of a large amount of data to eliminate redundancy. Thus, the compression process become inefficient in terms of sampling rate and computational complexity. To solve this problem, Compressed sensing (CS) is a technique that offers a framework for the detection and allocation of sparse signals with a reduced number of samples, below the Nyquist rate, allowing to reduce data size, complexity, weight, power consumption and costs of radar systems. This theory was proposed by Donoho in 2006, as a combined method of data acquisition and compression for reconstruction from incomplete sets of linear measurements by a nonlinear recovery algorithm. There are three main steps for CS: 1. sparsity expression of the original signal; 2. Low dimension measures to the original signal; and 3. Application of an effective reconstruction algorithm to recover the original signal. In this work is evaluated the compression and recover performance of InSAR raw data using the compressive sensing. SAR raw data was made available by airbone from BRADAR (Brazilian InSAR radar, operating in X and P bands). Each scene contents a 2048 x 256 data with 2 m of resolution in X and P bands to generate the inSAR processed image. To achieve the compression for reduce onboard storage and bandwidth required for transmission was proposed a CS scheme in each band. Firstly, SAR signal was transformed in a curvelet basis to do it sparse and to achieve better results under multiplicative speckle noise effect than the wavelets transforms. The sparse representation was compressed using random measurements matrices to achieve 25% and 50% of compression ratio, and, finally, for recover the signal, a greedy algorithm for CS reconstruction - IST (Iterative Soft Threshold) was applied, improving the quality of reconstruction by adjust of threshold parameter. Measurements of performance were obtained by means of PSNR (Peak Signal-Noise Ratio) between the generated image from original signal and the generated image from the recovered signal. Preliminary results have shown that the recovered data in each band applied to the radar processing achieved very low distortion in both compression ratio with low effort of coding and presented more efficiency than the quantization based method for storage raw data.

9643-49, Session JS1

Modelling backscattering of adjacent buildings in VHR SAR images for complex urban area analysis

Davide Pirrone, Francesca Bovolo, Fondazione Bruno Kessler (Italy); Lorenzo Bruzzone, Univ. degli Studi di Trento (Italy)

No Abstract Available

9643-50, Session JS1

Azimuth sidelobe suppression technique for near-field MIMO radar imaging

Yongze Liu, Xiaojian Xu, BeiHang Univ. (China)

Multiple input multiple output (MIMO) radar imaging system is getting more and more applications over the last years. However, the high azimuth sidelobes result in small dynamic ranges which in turn leads to severe image degradation. This is especially true in near field MIMO radar imaging. The paper focuses on the development of an azimuth sidelobe suppression technique for near field MIMO radar imaging based on convex optimization.

The sidelobes in near field MIMO radar image are not aligned in down range and cross range as in most far field images and spread out especially in azimuth dimension. In this work, an azimuth sidelobe suppression technique is proposed where apodization or amplitude weighting is applied to the multiple channel data prior to azimuth focusing. For best suppression of sidelobes, optimal channel weights are obtained through mathematical optimization. To this end, the paper formulates the problem of finding optimal weights as a convex optimization problem, which is the minimization of a convex function over a convex set and any local minimum of a convex function is a global minimum. The overall process of finding mainly includes three steps as follows: Firstly, the expression of the point spread function (PSF) in azimuth, , is defined by the azimuth focusing process; Secondly, based on the fact that, for an idea PSF the maximum value of the mainlobe should be one and the values of sidelobes should be zeros, the problem of finding is formulated as a convex optimization problem; Lastly, by setting a proper mainlobe width and sidelobe suppression level, the optimal weights can be found using a convex optimization algorithm.

A linear MIMO array is taken as an example to validate the proposed technique and analyze the performance, which consists of M transmitters and N receivers with uniform spaces. The array synthesizes MN virtual elements (or data channels) which are nonuniform in terms of azimuth sampling for near field imaging geometry. A modified filtered back projection (FBP) algorithm adapted to MIMO radar imaging is developed and used for image reconstruction. Simulation results demonstrate that the azimuth sidelobe level can be suppressed to be below -40dB in near field MIMO radar images.

Conference 9644: Earth Resources and Environmental Remote Sensing/GIS Applications

SPIE. REMOTE SENSING

Tuesday - Thursday 22–24 September 2015

Part of Proceedings of SPIE Vol. 9644 Earth Resources and Environmental Remote Sensing/GIS Applications VI

9644-1, Session 1

Solar diffusers in Earth observation instruments with an illumination angle of up to 70 degrees: design and verification of performance in BSDF

Bilgehan Gür, Hans Bol, TNO Technical Sciences (Netherlands) and SINO Holland Optical Joint Lab. (China); Pengmei Xu, Bicen Li, Beijing Institute of Space Mechanics and Electricity (China) and SINO Holland Optical Joint Lab. (China)

An important part of an earth observation instrument is the onboard calibration unit. This unit ensures through its calibrating and monitoring functionality accurate performances and thus accurate scientific observations of an instrument during its lifetime in orbit. One critical optical element in this unit is the so-called solar diffuser, which is illuminated by the sun as an irradiance source. The diffusers performance is expressed through its scattering properties, the Bi-Directional Scattering Function BSDF. The BSDF depends on several parameters, such as surface properties, angle of incidence and detection and further. This paper describes the challenging diffuser design and verification activities of TNO under contract of a customer for an earth observation instrument with observation conditions that require feasible BSDF under large angles of incidence of up to 70° with respect to the surface normal. Not only the design though but also the verification of the diffuser performance under such angles including “out-of-plane”, i.e. angle theta detection of the scattered light, was an essential activity to be executed. A representative measurement set-up was realized in the “Absolute Radiometric Calibration Facility ARCF” at TNO Delft in the Netherlands, a unique facility for the characterization and calibration of optical components for space applications. In this paper we will summarize the R&D activities with respect to diffuser design and verification that were recently carried out at TNO and present its applicability to current and future earth observation missions with challenging observation conditions and thus challenging diffuser requirements under high illumination angles.

9644-2, Session 1

Analysis of spectral data and images for assessing state of vegetables

Denitsa Borisova, Valentin Atanassov, Georgi Jelev, Space Research and Technology Institute (Bulgaria); Kiril Alexiev, Petia Koprinkova-Hristova, Institute of Information and Communication Technologies (Bulgaria)

New applications for monitoring have become possible with the advent of new high-spatial and spectral resolution imagery. The data processing methodologies such as spectral analytic approaches have been applied in different practical fields.

In this work we are discussed important applications of remote sensing spectrometric measurements for assessing quality parameters of selected representative samples of agricultural products /fruits and vegetables/.

Principles of obtaining spectral data and images are described and possibilities of using the spectral characteristics for the evaluation of the quality indicators of the tested samples are discussed. Special attention is paid to the methods of pre-processing and to the applied mathematical methods for segmentation and classification of the observed objects. Also important problems for device calibration and for verification of the received data are indicated.

9644-3, Session 1

A comparative study between Landsat-8 OLI and Landsat-7 ETM+, for sensor signal-to-noise performance, spectral distortion, spectral signature matching and land surface temperature: a study in the Iraq landscape

Shaheen M. Alhirmizei, Kirkuk Univ. (Iraq)

After two successful years of working with landsat8 images there is a need to assess differences between Landsat8 and lansat7 in practice, this comparative study using imagery from the area of interest presents a large scale study of the differences between ETM+ and OLI and the Thermal band of Landsat 7 with lansat8 TIR in the Iraq landscape. the analysis is carried out in terms sensor signal-to-noise performance (Image quality) caused by dynamic range of the digital number (DNs) output from the sensors and the Spectral Distortion(color distortion) caused by The character of the panchromatic band And also the spectral signature matching differences result from the passbands for Landsat 8 bands 5, 6 and 7 are narrower than the corresponding Landsat 7 bands and finally the Land Surface Temperature differences between two narrower TIR bands of landsat8 in place of the single Landsat 7 TIR band . The paper attempts to measure the signal-to-noise performance, Spectral Distortion and quality of multispectral images of a region that has a variety of artificial and natural patterns for both landsat7 and landsat8 using some well known image quality assessment metrics(PSNR,SSIM) the assessment is performed in both visual and statistical manner and The derived remotely sensed land surface temperatures from both satellites are compared to ground-based remote sensing observations Of land surface temperature .The results show obvious differences between the sensors in multispectral signature matching for example The signal to noise ratio is much better as well IN LANDSAT8 , also color distortions resulting from pan sharpening , but perhaps not quite so severe as Landsat 7 , the passbands for narrower Landsat 8 bands 5, 6 and 7 are (more discriminating) than the corresponding Landsat 7 bands This will benefit spectral signature matching and other target discrimination techniques. Although the spatial resolution of TIRS is degraded to 100 m, in comparison with the 60 m resolution of the Landsat-7 ETM+ thermal band, BESIDE the on-board calibration ERROR OF LANDSAT8 the added value of having two bands is more accurate LST estimations with TIRS than with its predecessor. THE lessons to be learned from both Landsat-8 and lansat7 data for better forward planning and what kind of new technologies should The future Landsat platforms (landsat9,landsat10) leverage to improve data and quality

9644-4, Session 2

Flood mapping from Sentinel-1 and Landsat-8 data: a case study from river Evros, Greece

Aggeliki Kyriou, Konstantinos G. Nikolakopoulos, Univ. of Patras (Greece)

Floods are suddenly and temporary natural events, affecting areas which are not normally covered by water. The influence of floods plays a significant role both in society and the natural environment, therefore flood mapping is crucial. Remote sensing data can be used to develop flood map in an efficient and effective way. This work is focused on expansion of water bodies overtopping natural levees of the river Evros, invading the surroundings areas and converting them in flooded.

Different techniques of flood mapping were used using data from active and passive remote sensing sensors like Sentinlel-1 and Landsat-8 respectively. Space borne pairs obtained from Sentinel-1 were processed in this study. Each pair included an image during the flood, which is called "crisis image" and another one before the event, which is called "archived image". Both images covering the same area were processed producing a map, which shows the spread of the flood. In addition statistics, such as mean, median were evaluated and were compared with the respective values of the others pairs. Multispectral data From Landsat-8 were also processed in order to detect and map the flooded areas. Different image processing techniques were applied and the results were compared to the respective results of the radar data processing.

9644-5, Session 2

Seasonal effects on the estimation of height of boreal and deciduous forests from interferometric TanDEM-X coherence data

Aire Olesk, Regio, Ltd. (Estonia); Kaupo Voormansik, Tanel Tamm, Mart Noorma, Univ. of Tartu (Estonia); Jaan Praks, Aalto Univ. School of Science and Technology (Finland)

1. INTRODUCTION:

This study demonstrates the use of X-band SAR interferometric data for retrieving tree height of coniferous and deciduous forests during leaf-off season in spring and leaf-on period in summer. The volume decorrelation analysis of bistatic single-baseline TanDEM-X coherence data provided an insight into how the accuracy of SAR-based forest height estimation depends on different seasonal and environmental factors.

Single-pass X-band coherence has shown good sensitivity to forest height and structure and can provide estimates of height, especially for boreal forests [1]. Cloude et al. [2] have proposed that coherence images may be suitable for height estimation of boreal forests using only single channel (HH or VV) data. The limitations of this method are reportedly sensitivity to the variations in forest vertical structure and density [3]. The height estimation results were influenced by the penetration of X-band into different forest types, the density of different tree layers and the weather conditions. Also further tests were carried out to analyse the effect of incidence angle and baseline differences to the forest height estimation accuracy. According to Kugler et al. [4], short baselines can reduce the sensitivity to forest height and large baselines can lead to low coherence levels that are limiting to the height mapping range.

2. DATA AND METHODS:

TanDEM-X HH and VV polarization channel coherence images were studied over large forested areas in Estonia and compared against LiDAR and inventory data from Estonian Forest Registry. Correlation coefficients (r2) and standard deviations (?) were calculated for all the plots, differentiating tree species into three groups (pine, spruce and mixed deciduous forest stands). The chosen method relies on single-polarization data and homogeneous forested areas which provide a strong relationship in regression analysis between X-band SAR coherence and LiDAR derived forest stand height.

3. CONCLUSIONS AND OUTLOOK:

The selected homogeneous forests provided a strong relationship in regression analysis between SAR coherence and LiDAR derived forest stand height and demonstrate the feasibility of this method for estimating canopy height for boreal and deciduous forests. The results indicate that single-polarized (both HH and VV) images are suitable for height estimations, but the accuracy of the results depend on the season, tree species, forest density and structure, flooding and amount of rainfall prior to the satellite data take. The regression models show the strongest correlation between pine stand heights and single-polarization interferometric coherence where the correlation coefficients (r2) range between 0.75 and 0.97. The best performance for mixed deciduous tree stands was found during leaf-off period with r2 ranging from 0.87 to 0.94, whereas leaf-on period resulted in r2 from 0.58 to 0.75. The VV channel is less sensitive to floods than the HH channel and is thus more suitable for forest height estimation in wet conditions. Under Northern-European conditions, seasonal changes have a significant effect on height estimation of deciduous stands and require leaf-off conditions for accurate coherence-based height retrieval. Further research is being carried out to investigate the relation between SAR interferometric coherence and tree species, tree water content, forest density and structure.

REFERENCES:

[1] A. T. Caicoya, F. Kugler, I. Hajnsek, and K. Papathanassiou, "Boreal forest biomass classification with TanDEM-X," in Geoscience and Remote Sensing Symp. (IGARSS), 2012 IEEE Int., pp. 3439-3442.

[2] S. R. Cloude, H. Chen, and D. G. Goodenough, "Forest Height Estimation and Validation Using Tandem-X Polinsar," in Geoscience and Remote Sensing Symp. (IGARSS), Melbourne, 2013 IEEE Int., pp. 1889 – 1892.

[3] M. Schlund, F. von Poncet, D. H. Hoekman, S. Kuntz, and C. Schmullius, "Importance of bistatic SAR features from TanDEM-X for forest mapping and monitoring," Remote Sensing of Environment, 2013.

[4] F. Kugler, D. Schulze, I. Hajnsek, H. Pretzsch, and K. P. Papathanassiou, "TanDEM-X PolInSAR Performance for Forest Height Estimation," IEEE Trans. Geoscience and Remote Sensing, vol.52 (10), pp. 6404-6422, 2013.

9644-6, Session 2

Aboveground forest biomass estimation combining information from optical and SAR remotely sensed imagery

Dimitris G. Stavrakoudis, Aristotle Univ. of Thessaloniki (Greece); Kleanthis Karamvasis, National Technical Univ. of Athens (Greece); Dimitris Zianis, National Agricultural Research Foundation (Greece); Ioannis Z. Gitas, Aristotle Univ. of Thessaloniki (Greece); Vassilia Karathanassi, National Technical Univ. of Athens (Greece); Gavriil Spyroglou, National Agricultural Research Foundation (Greece); Vassilis Andronis, National Technical Univ. of Athens (Greece); Kalliopi Radoglou, Democritus Univ. of Thrace (Greece)

This paper proposes a methodology for estimating aboveground forest biomass through remotely sensed data, acquired from both active and passive sensors. As a study area we have selected the Taxiarchis, Chalkidiki experimental forest (40° 25'N, 23° 31'E), a typical Mediterranean forest which is located on the central, mountainous part of Chalkidiki peninsula approximately 70 km southeast of the city of Thessaloniki. It consists of deciduous Hungarian oaks (Quercus frainetto) and European beech (Fagus sylvatica s.l.) natural stands in upper elevations and evergreen broadleaved (marquis) vegetation in lower elevations, planted black pines (Pinus nigra), Calabrian pines (Pinus brutia) and firs (Abies cephalonica, Abies borisii regis) are also included in the tree species composition. Our analysis concentrates on the four dominant forest species (Hungarian oak, European beech, black pine, and Calabrian pine). A multispectral GeoEye and a hyperspectral image acquired from the Compact Airborne Spectrographic Imager (CASI-550) airborne sensor have been used for forest species mapping, using a supervised classifier within an efficient fusion approach. The average classification accuracy for those four species exceeded 92%. The CASI image was also used for calculating a large number of vegetation and chlorophyll content indices, out of which three were deemed to be more sensitive with respect to vegetation cover, namely, TRDVI, TCI2, and TCARI/OSAVI. These indices have been considered as an easy to obtain proxy of vegetation density. Moreover, L-band SAR images (ALOS-PALSAR) and X-band ones (COSMO-

SkyMed) were used to derive a digital terrain model (DTM) and a digital surface model (DSM), respectively. The tree height has been subsequently estimated through their difference.

The specific study area is characterized by a special conservation status and a detailed management plan is being devised every 10 years. The most recent one (2012) provided us detailed information for a relative dense grid of sampling plots within the forest. Within each 300 m2 circular sample plot the species and breast height diameter for all trees above 6 cm were registered, tree height was measured randomly on 3 dominant and 2 dominated individuals. This information has been used for deriving the average biomass of each plot (in tn/ha) through allometric equations. Specifically for Hungarian oak, allometric equations have been devised through field measurements (25 trees have been destructively sampled and an allometric model for total above ground biomass was calibrated). For the other three species we employed the respective allometric equations found in the literature.

All remotely sensed data have been resampled to the finest resolution of 2m, which was the native resolution of the GeoEye and CASI images. All pixels within each sampling plot have been assigned the plot's average biomass value, as calculated by the application of the allometric equations. Half of the reference data have been used as training and the rest as testing. For each one of the four species, a separate Classification and Regression Tree (CART) model has been learned, using the three density measures (indices) and the tree height estimation as inputs. Considering each pixel individually, the average absolute normalized error has been 18.45% (16.83% for oak, 23.96% for beech, 18.50% for Calabrian pine, and 14.52% for black pine). These values represent the relative error of the methodology in a per-pixel basis. Nevertheless, the respective aggregate error for each class (i.e., comparing the sum of all pixels' outputs and references for each class) was only 6.20%, which represents the average relative error in terms of total estimated biomass per species. Finally, the total biomass estimation error (irrespective of class) was 3.76%.

9644-7, Session 2

Results of long-term oil spill monitoring in the Black Sea and the Caspian Sea with synthetic aperture radars

Andrei Y. Ivanov, P.P. Shirshov Institute of Oceanology (Russian Federation); Alexey A. Kucheiko, RISKSAT (Russian Federation); Natalia Evtushenko, ScanEx Research and Development Ctr. (Russian Federation); Nadezhda Terleeva, P.P. Shirshov Institute of Oceanology (Russian Federation)

The results of routine satellite oil spill monitoring of the Eastern Black Sea (2011-2013) and the Northern & Middle Caspian Sea (2009-2014) are presented and discussed. Monitoring was performed by using the synthetic aperture radar (SAR) images acquired by spaceborne SARs onboard the Envisat, Radarsat-1 and Radarast-2 satellites. The focus of operational monitoring is on providing information that assists in adequate responses as well as further investigation into problem of recent oil pollution of these seas. For this the web-GIS technology/application developed by Scanex and named Geomixer has been used. Geomixer allows integration and combination of all information needed for analysis, such as offshore and onshore oil-&-gas infrastructure, ship tracks, boundaries of territorial waters, EEZs and license blocks, bathymetry, locations of known oil seeps, etc. By integrating all detected spills, by combining annual oil spill distribution maps and comparing them, it is shown that distributions of oil spills in the Black Sea and in the Caspian Sea are quite different, i.e. quite different their spatial patterns. For the Black Sea the most important source of oil pollution is the tank washing in the open sea (20 -= 100 and more km2) and illegal discharges. For the Caspian Sea the most of detected oil spills in the northern and middle parts are little ship-made discharges (< 10 km2) related to freight traffic and fishery. In spite the oil exploration and production (Lukoil and others) in the northern Caspian, there is no oil spills related to oil production have been detected. Other ill-estimated source is natural oil seeping, mainly in its southern part. It is concluded therefore that the distribution of oil spills in a particular sea may depend strong on a number of reasons among them is ship and tanker traffic.

9644-8, Session 2

Factors influencing the detectability of oil pollution using vegetation indices in the Niger Delta mangrove region

Bashir Adamu, Univ. of Leicester (United Kingdom)

Hydrocarbons found in polluted environment are as a result of spills from oil facilities. Monitoring these hydrocarbon polluted sites using spectral indices (e.g. BMVIs) has proved to be great potentials from many researches. In previous works factors such as volume of oil spill, time and spatial distance that characterised the spill sites. These factors were not taken into account which could influence the detection of oil pollution in vegetated areas using vegetation spectral indices. This study analysis the influence of these factors on detecting the spill sites using the vegetation spectral indices (BMVIs). Twenty eight sample sites were used to extract the BMVIs and quantitative analysis was carried out on volume of oil spill <200 and >200 Barrels (bbl). We found that oil spill sites with <200 bbl have weak relationship with the BMVIs (R2=0.000006 for NDVI and R2=0.1245 for NDWI), and >200 bbl have relatively strong relationship (R2=0.019 for NDVI and R2=0.016 for NDWI). The results showed that the relationship between the BMVIs and volume of oil spill at 19 spill sites with >200 bbl have strongly improved from R2=0.019 to R2=0.33 for NDVI and R2=0.016 to R2=0.073 for NDWI as the volume increases the BMVIs values decreases. Similarly, results between the BMVIs and number of days less than 365 days (oil spill and image date) indicated relatively strong relationship R2= 0.29 for NDVI and R2=0.14 for NDWI as days increases the BMVIs values also increases at 11 spill sites. Both results inferred that large volume of oil spill could have effect on vegetation health and that number of days between the spill event and image acquisition date may influence disappearance of oil spill and provide opportunity for vegetation recovery at these spill sites. The spatial distance analysis did not show any difference between the polluted pixels and the two neighbouring pixels suggesting migration of oil spill did not go beyond the polluted point.

9644-9, Session 2

Application of remote sensing in wetland monitoring: case study Hamoun wetland

Saeideh Maleki, Alireza Soffianian, Isfahan Univ. of Technology (Iran, Islamic Republic of); Saeid Soltani, Isfahan University of Technology (Iran, Islamic Republic of); Sassan Saatchi, Jet Propulsion Lab. (United States)

Since wetlands are among the most important part of global ecosystem, monitoring these valuable ecosystems is essential for conservational goals. But, access to in situ data is often limited by their highly dynamic characteristics, the remote locations, complex terrain, and large areas. Extensive and time-consuming field surveys are insufficient to document wetlands changes at a landscape scale. Remote sensing techniques, which can acquire the information in a periodic manner, provide a cost effective means to monitor the seasonal changes and hydrological patterns of wetlands at different scale.

Hamoun wetland, located on the boundary of Iran and Afghanistan (lat 30 25 to 31 27N – long 60 56 to 61 43 E), is a globally important breeding and stop-over site for many migratory bird species. Hamoun have a natural annual hydro period: each year the water level rises in the spring and falls from April to August and large parts of the wetlands dry out regularly. However, it has a fragile ecosystem and is facing severe impacts from drought and human activities. Land use-land cover change detection during water inundation period

were investigated in order to demonstrate change trend in this wetland. Demonstrating this trend is important for decision makers and for bird's habitat investigations. Thus, remote sensing data were used to obtain enough accuracy. Landsat data and field study were combined to create land use- land cover maps. Validation showed that estimated land use- land cover agreed well with in-situ measurements (R2 from 0.95 to 0.99) and the root mean square error (RMSE) was within 4.6 to 13.1% of the mean Volumes of in-situ measurements. After that, change detection method were used to show parts that have changed. Finally, these parts were compared to bird's habitat suitability map with GIS techniques. Results have shown, a large part of suitable habitats are in area with minimum changes but there are some parts that are suitable for birds but water dried out very quickly. So, it is essential to have conservational plane in these area in order to protect birds.

9644-10, Session 2

Rangeland mapping and monitoring for Bayankhongor aimag of Mongolia case study:Buutsagaan, Khureemaral and Dzag soums

Sanjaa Tuya, Mongolian Univ. of Science and Technology (Mongolia); Doljinsuren Naymdorj, Establishment of Climate Resilient Rural Livelihoods Project (JFPR9164-MON) (Mongolia)

Rangeland monitoring is observing or measuring changes in the health of the land over space and time. Over one-third of Mongolia's 3 million people depend directly on livestock production and rangelands for their livelihood. Overgrazing is widespread in some areas. They are subjected to intensive use (overgrazing, human activity) and severe climatic conditions. Rangeland monitoring study areas were selected in each of the tree ecological zones dominated by rangeland. This study conducted under the scope of actions for defining the geographical location's coordinates and mapping to be provided with respect to the herdsmen groups' pasture boundaries, herdsmen's winter, spring, summer and autumn camp sites and water points for Bayankhongor province's 3 soums Buutsagaan, Khureemaral and Dzag covered by the project. Pastureland units of study were customary grazing areas used by groups of herders in bag administrative units. Rangeland monitoring sites were established in the tree study areas to monitor status and trend of rangeland ecological condition. The resulting overgrazing associated with socio-economic conditions in rural areas indicates the need for rangeland management and monitoring. A geographical information system (GIS) was used for rangeland monitoring maps and positioning of the field measurement data.

9644-40, Session PS

Study of spatial-temporal variation of evapotranspiration estimation in urban green area using high-resolution remote sensing technology

Ning Zhang, Ministry of Housing and Urban-Rural Development of the People's Republic of China (China); Liuzhong Yang, Ministry of Housing and Urban-Rural Development of the People's Republic of China (China); Jing Yu, Ministry of Housing and Urban-Rural Development of the People's Republic of China (China); Liqiao Guo, Ministry of Housing and Urban-Rural Development of the People's Republic of China (China)

Evapotranspiration is one of the major components of the ecological processes and hydrological processes for land surface and is arguably the most important component of the water cycle and regional water resource management. Remotely sensed data methods provides a powerful means to compute regional evapotranspiration. Urban green, which uses transpiration to increase CO2 absorption and O2 release, becomes a significant factor for improving urban microclimate environment and regulating temperature. The spacial distribution of urban green is ecologically related to urban environment. This study includes two parts about evapotranspiration estimation and analysis of spatial-temporal variation.

In the first part, we employ Surface Energy Balance Algorithm for Land (SEBAL) model, which has been proved to perform well in supporting high resolution remote sensing approach by comparing with other models, to calculate evapotranspiration in urban green area. Based on high resolution remote sensing imagery, the parameters are necessary in the inversion process of SEBAL model. The land cover map, which includesbasic elements of vegetation, water and impervious surfaces, and the land use cover map in urban green area, which is used to classify public park, productive plantation area, green buffer and attached green space, are extracted from 0.5m Quickbird imagery as shown below (Picture 1: Land cover and land use map). The GF-1 Wide Field View(WFV) data with 16m observation capabilities is used for the inversion of NDVI, LAI and albedo. By the synthetic process, we get monthly GF-1 WFV data from September 2013 to April 2014. Supposing that in one month the land surface condition does not have significant changes in our study area on China's southern coast, we acquire thermal infrared band from Landsat-8 TIRS to match with GF-1 WFV spatially and temporally. The resolution of Landsat-8 TIRS is 100m, but it has to be resampled to be 16m that we can adopt a more effective approach--pixel decomposition based on LST-NDVI relationship. Urban DEM data is produced by ASTER Stereo pair data. The average height of vegetation is estimated by combining the land cover map and field experiments. Besides, meteorological department provides daily atmospheric temperature, wind speed, precipitation, etc.

In the second part, we analysis the relationship of evapotranspiration and heat island in the respect of temporal changes and also study on the correlation between evapotranspiration and urban green space system layout in the respect of spatial variation. In months of time series analysis, we find that comparing with green land, the impervious surfaces help heat island phenomenon involve by preventing water vapor from transporting upward and going against heat diffusion, because of their higher value of surface roughness. We also find unbalanced spatial distribution in urban green. The city carries out high-density green in waterfront, where the dominant green classification is public park.. The attached green space, which is more closely related to human living, is apparently different in blocks.

9644-43, Session PS

Remote sensing technology in combination with geographic information system (GIS) for rare vegetation conservation in Azerbaijan

Yelena M. Gambarova, Adil Gambarov, R.I.S.K. Co. (Azerbaijan)

This paper investigates the spatial change of rare vegetation cover of Gobustan, Azerbaijan. The Gobustan State National Park (Conservation Area) is a nationally important desert/ semi-desert located west and south-west of Baku, Azerbaijan. In 2007 Gobustan was declared a UNESCO World Heritage Site considered being of "outstanding universal value" for the quality and density of its rock art engravings. The Study Area at Gobustan contains a wealth of historical and archaeological sites and is also known for its rare vegetation.

These investigates include monitoring of existing threats to rare vegetation (Global Climate Change, oil and gas exploration, overgrazing of winter and summer pastures by domestic sheep, goats and cattle, pollution, etc.) as well the processing

of remote sensing data to produce "measured" vegetation indicators. Remote sensing technology in combination with geographic information system (GIS) can render reliable information on rare vegetation cover. The analysis of the spatial extent and temporal change of rare vegetation cover using remotely sensed data is of critical importance to rare vegetation monitoring.

For this study, out of various change detection techniques, spectral change analysis method with special emphasis on vegetation indices was selected because of its acceptable accuracy and ability to detect the green vegetation.

The Geographical Data Base and Specialized GIS Environment were created. The main pasture types, summer and winter pastures were distinguished.

Map of current pasture usage was created to provide data on the extent of pasturelands in Gobustan National Park for rare vegetation conservation.

This study has shown that oil and gas infrastructure, in an ecologically important semi-arid region, has a negative effect on species abundance and cover of vegetation.

Rare vegetation classification within a buffer zone indicates:

Plant cover has decreased in the buffer zone and is higher than the Sensitive Area. Bare ground has increased dramatically in the buffer zone whereas in the Sensitive Area it has decreased slightly.

The results indicates that major changes in the study area from 2004 to 2012 years involved decrease in vegetation cover types including Alhagi pseudoalhagi (-0.7%), Salsola Nodulosa/ Artemisia Lerchiana/Salsola Dendroides communities (-18.7 %) and Suaeda Dendroides (-5.24 %); and increase in Tamarix (+21.7 %) and Bare ground (+3.6 %).

9644-44, Session PS

A scale-up method for reference data for validation of global land cover maps using ALOS/AVNIR-2 satellite data

Noriko Soyama, Tenri Univ. (Japan); Kanako Muramatsu, Nara Women's Univ. (Japan); Itsuko Ohashi, Japan Aerospace Exploration Agency (Japan); Motomasa Daigo, Doshisha Univ. (Japan); Fumio Ochiai, Nara Women's Univ. (Japan); Takeo Tadono, Kenlo Nasahara, Japan Aerospace Exploration Agency (Japan)

The data used in this study were ALOS/AVNIR-2 data of Nara Prefecture, Japan observed from 2008 to 2011. ALNIR-2 sensor has four bands (460, 560, 650 and 830 nm) with 10-m spatial resolution. To examine features of each land cover type, three coefficients and vegetation index (MVIUPD) calculated using the Universal Pattern Decomposition Method (UPDM) were used. The three coefficients correspond almost directly to actual objects on the ground, i.e., the water coefficient, vegetation coefficient, soil coefficient.

Firstly, suitable representative values of land surface feature for each land cover class type were derived from three coefficients and MVIUPD values. Secondly, condition of each representative value was determined from probability distribution of 100 pixels centered around the target point, in order to examine if a pixel has the same feature as the target position.

In this study, scale size of reference data is spatial resolution of 250m. The occurrence ratio is the ratio of pixels satisfying the condition of representative value to 625 pixels: 25pixels times 25 pixels of AVNIR-2 on 10-m spatial resolution. The ground truth reference is available as scale-up reference data when the occurrence ratio of the target position is larger than 80%.

9644-45, Session PS

Diachronic analysis of the occupation of the steppe area of the Wilaya of Sidi Bel'Abbès (Western Algeria)

Abbassia Ayache, Univ. Djillali Liabes (Algeria)

Modes of occupation of the soil of the steppe area of the wilaya of sidi bel'abbès (Western Algeria) know lots of mutations during the period 1987/2013; compromising the future of pastoral activity. This dissection based on supervised classification TSAVI values (Transformed Soil Adjusted Vegetation Index) using images of remote sensing of average spatial resolution of type Landsat-TM 5 and 8. The determination of the state of occupation of the ground and validation of remote sensing map with confusion matrix shows that the status of the halophytic/pasammophitic steppes and the Matorrals are detected in 38.38% and 55.71% of cases, respectively. On the other hand, the steppes chamaephytic mark -9,81% regression only, agricultural land -24,51% ,and -46,24% dense vegetation are correctly mapped. The sensing medium resolution is therefore, in the light of these figures, a management tool of the steppe field relevant and effective, which, in addition, allows enriching the field for a proper plan for the fight against desertification.

9644-46, Session PS

Development of the Philippine Hydrologic Dataset (PHD) from LiDAR and other remotely-sensed data

Anjillyn Mae C. Perez, Melanie C. Gaspa, Dominic S. Aloc, Univ. of the Philippines, Diliman (Philippines); Margarita Andrea P Mahor, Kevin Angelo C Gonzalez, Phil-LiDAR 2 Program, Training Center for Applied Geodesy and Photogrammetry (Philippines); Noel Jerome B. Borlongan, Roel M. De la Cruz, Nestor T. Olfindo Jr., Ariel C. Blanco, Univ. of the Philippines, Diliman (Philippines)

The Philippines, being an archipelagic nation, is composed of a wide variety of natural and man-made water bodies including lakes, ponds, marshes, wetlands, dams, reservoirs, water impounds, and river networks stretching to hundreds of kilometers throughout the land. Having such vast amount of resources, the first step in proper water management is to have an accurate and updated water resource inventory in the form of multi-scale maps showing the location, extent, and characteristics of all significant hydrologic features in the country. With the recently available large coverage of Light Detection and Ranging (LiDAR) and other remotely-sensed datasets in the Philippines from various research efforts of government agencies and academic institutions, the extraction and mapping of water resources becomes more feasible. This paper discusses the general development framework of the Philippine Hydrologic Dataset (PHD), from data gathering, pre-processing, feature extraction workflows, data models, data integration and geodatabasing, up to data sharing and information dissemination.

Various methodologies for the extraction of stream network, inland bodies of water, and agricultural ditches were developed and implemented by integrating Remote Sensing (RS), Geographic Object-based Image Analysis (GEOBIA), and Geographic Information Systems (GIS). The primary datasets used in the different feature extraction workflows include 1-meter resolution Digital Terrain Model (DTM) and Digital Surface Model (DSM) derived from LiDAR point cloud data obtained using Optech Gemini and Pegasus Airborne Laser Terrain Mapper (ALTM) systems. Since the available LiDAR data does not usually cover whole river basins which is the required extent for watershed modeling and stream extraction, 10-meter Radarsat-2 Synthetic Aperture Radar (SAR) DTM image for the whole country was also used as a supplement. Some orthophotos obtained during LiDAR data gathering and available WorldView-2 multispectral satellite imagery were also

integrated in the developed methods. To ensure the quality of the results, all the datasets were subjected to pre-processing, such as reprojection and proper georeferencing, hydrologic conditioning, and clipping, before performing the different feature extraction workflows that mostly involve watershed modeling, integration and fusion of multi-scale imageries, multi-resolution segmentation, classification, post-processing, and accuracy assessment.

Aside from hydrologic data extraction, another major objective of this research project is to produce a geodatabase into which the multi-scale hydrologic features are integrated and then tied to relevant ancillary information collected from different agencies and from the results of previous research efforts. Ultimately, data sharing and access for target end-users and stakeholders will be facilitated through a Web-based GIS which will serve as the online repository of all hydrologic datasets where users, with different levels of access, may edit or download data for needed for applications requiring updated national hydrologic datasets, such as flood control planning, discharge and runoff researches, sedimentation and erosion studies, power generation, and groundwater monitoring, among others.

9644-47, Session PS

Detecting of soil salinization dynamics in irrigated Tadla Plain using Landsat TM/ OLI imagery

Abderrazak El Harti, Rachid Lhissou, Faculty of Science and Technology Beni Mellal (Morocco); Karem Chokmani, Centre Eau Terre Environnement, Institut National de la Recherche Scientifique (Canada); Asma Dakir, Basma Naouil, Jamal-eddine Ouzemou, El Mostafa Bachaoui, Abderrahmène El Ghmari, Faculty of Science and Technology Beni Mellal (Morocco); Mohammed Hassouna, Office Régional de Mise en Valeur Agricole du Tadla (Morocco)

Soil salinization is an environmental problem that is getting amplified by both irrigation practices and changes in temperature and precipitation. The use of conventional methods for salinization monitoring is insufficient and limited by the high spatiotemporal variability of this phenomenon. The aim of this work is the spatiotemporal monitoring of soil salinization in the Tadla plain in central Morocco using spectral indices derived from Thematic Mapper (TM) and Operational Land Imager (OLI) data. Six Landsat TM/OLI satellite images taken during 13 years (2000?2013) coupled with field measurements of electrical conductivity (EC) were used as the basic data sources. After radiometric and atmospheric correction of images data, two spectral indices were calculated and calibrated by the EC measurements. The results indicate that the OLI-SI index provides better characterization of saline lands than the SI index. The change matrix of mapped salinity classes demonstrated that soil salinity has slightly decreased in intensity and progressively increased in spatial extent. In addition, obtained maps and vegetation trend statistics show a loss of agricultural activities in the south-western lands located in the hydraulic downgradient; this is due to sterilization of agricultural lands. Moreover, other lands are threatened to be sterile from downstream to the north. The results of this study show the usefulness of spectral indices for soil salinity monitoring and suggest a help for optimal management of irrigation water resource and salinization control in the irrigated Tadla Plain.

9644-48, Session PS

Headward erosion and deep erosion estimations in the wider area of Nemea, Greece, using GIS and freely available DSM

Konstantina K. Mexia, Univ. of Patras (Greece)

The objective of the present paper is to study and compare the headward erosion and deep erosion rates in the river systems of Asopos, Nemeas and Raizanis, which are in the wider area of the Nemea archaeological site, in the Peloponnese, Greece. The study area is a section of the NE part of the Peloponnese, specifically the zone between the villages of Velo and Vrachati. In the study area terraces appear, which have been mapped in detail and which correspond to isotopic stages of interglacial periods of the Pleistocene. The basic processes that act in our study area and have shaped the current relief is headward erosion and deep erosion, which are favored by the dominant lithology and fault tectonic. The northern parts of the three river networks intersect sea at terraced levels, where the local terrace front backward retreat indicates the rate of headward erosion and the depth of the valleys at the terrace front indicates the rate of deep erosion . Thus we tried to calculate the rate of these two factors for each river system in order to understand the course of the phenomenon in time. In order to achieve our goal, we used geological and topographical maps of the area at a 1/50.000 scale. Mapinfo GIS software was used in order to make the necessary measurements. The results from the analysis of the topographic maps were compared with the results from freely available DSMs such as ASTER GDEM and SRTM DEM.

9644-49, Session PS

Study of the climate change of Northeast China over hundred years and its Influence

Nanping Xu, Meteorological Bureau of Heilongjiang (China)

The research shows that the first eigenvector of the annual and quarterly temperature EOF of Heilongjiang Province accounts for over 77% of the total variance. The temperature change in the province has the feature of uniformity. For the annual average temperature series of 1881~2000, 10 years' moving average and 30 years' average were applied for comparison. The result indicates that the average temperature of the recent 30 years (1971~2000) in Heilongjiang Province was 1.4? higher than that of the 30 years (1881~1910) from the end of 19th century to the beginning of 20th century. In 1897, there was a strong warming and around 1990, there was another strong warming. The temperature rises in both cases were more than significant. Particularly, the temperature of the warming around 1990 was 1.7? higher than the annual average temperature of 1897. Abrupt winter temperature change happened in 1990, the same time with the abrupt annual temperature change, indicating that the temperature rise after 1990 was greater.

The calculation of D-value between the annual average temperatures of 1981~2000 and 1951~1980 reveals that the province-wide annual average temperature in the recent 20 years was 1.0? higher than that of the 30 years before 1981.

The result also shows that compared with the 26 years before 1981, the annual average extreme maximum temperature of the 20 years after 1981 (post-warming) rose slightly at an average rise of 0.54?. However, the the annual average extreme minimum temperature of the 20 years after 1981 rose remarkably at an average rise of 1.7?, which was much higher than the rises of the annual average extreme maximum temperature and annual average temperature.

Model calculation indicates that the future temperatures of 2030 and 2050 will rise greatly. For the year 2030, the annual average temperature may rise by 1.94?, the spring temperature by 2.06?, the summer temperature by 1.26?, the autumn

temperature by 1.79? and the winter temperature by 2.66?.

Climate warming has a significant influence on agricultural environment and crops production. To be specific, climate warming increases the occurrence of extreme weather, extreme climate and disasters, which bring great loss to the national economy. Climate warming affects agroecological environment, leading to more heavy rainfalls and serious loss of water and soil. Climate warming may result in water shortage, larger drought area, smaller wetland area, decrease of organic content in soil, decline of soil fertility, more serious soil pollution and greater damage by disease and insect.

Another influence of climate warming on crops production is that it leads to 3 remarkable changes of agricultural heat resources: ?Northward movement of the accumulated temperature zone and increase of active accumulated temperature for crops growth; ?Temperature rise in spring and autumn, extended crops growth period and larger number of growing days; ?reduced chilling damage. Thanks to the climate warming in the 1980s, the crops production of Heilongjiang Province has increased stably. It is estimated that climate warming over the recent 15 years has contributed to 10-13% growth of national crops production. The curve of food development since 1990s clearly reflects this.

9644-50, Session PS

Diachronic analysis of salt-affected areas using remote sensing techniques: the case study of Biskra area (Algeria)

Gabriela M. Afrasinei, Maria T. Melis, Cristina Buttau, Univ. degli Studi di Cagliari (Italy); John M. Bradd, Univ. of Wollongong (Australia); Claudio Arras, Giorgio Ghiglieri, University of Cagliari (Italy) and University of Sassari (Italy)

In the Wadi Biskra area, one of the most important date palm production region of Algeria, the bio – physical setting defines it as an environmentally fragile area that faces water scarcity, being highly exposed to desertification processes. Diachronic analyses of changes in vegetation and land use, as well as other land degradation - indicating features, i.e. salt - affected soils, are widely used to assess and monitor desertification processes. This study is part of the WADIS-MAR Demonstration Project, funded by the European Commission through the Sustainable Water Integrated Management (SWIM) Programme, mainly aimed at implementing sustainable water and agriculture management system in two study areas of the Maghreb region, including the Wadi Biskra area, which represents the object of this paper. In such arid and semi-arid areas, sustainable development require the understanding of the dynamics of these processes and their underlying forces. Apart from primary salinization, secondary salinization increases the menace on sustainable agriculture, given the increasing population and economic demand. In this study, an assessment of valid methods for the identification and change detection of salt-affected soils over three decades has been set up based on image interpretation and image processing techniques with the use of Landsat series. Special emphasis is laid on targets such as salt-affected soils, hydro - saline areas and halophyte vegetation. In this paper we put forward and try to validate a framework of an off – site analysis and mapping of salt – affected soils, given the socio – political context of such areas, which have restricted access. Thus, various types of remote sensing data may provide provisional solutions, given the lack of other means. This was carried out using both ancillary data, conducting a preliminary study of land cover through visual interpretation and an automated classification that we proposed for this specific study: a decision tree classifier and principal components (PC) analysis of Knepper ratios (Langford, 2015). Vegetation, salinity indices and specific band ratios were combined and tested within the decision tree (Allbed & Kumar, 2013; Fares & Philip, 2008). A supervised classification was applied on the three principal components of specific band ratios proposed by Knepper (D.H. Jr, 1989) was used to extract the salt – affected areas. The results of the 1984, 1999, 2002, 2007 and 2014 annual and inter - seasonal analysis of salt – affected soils distribution and variation were integrated in a GIS with the interpreted 34 – class land cover map for accuracy assessment. Auxiliary data, partly provided by the Algerian Ministry of Hydraulic resources, and free high resolution imagery (online ArcGIS BING base map and Google Earth imagery) were also included for discussion and accuracy assessment. Connecting the outputs with auxiliary bio-geographical and socio-economic data, comprehensive results are argued, contributing to the understanding of land degradation dynamics and vulnerability to desertification. In the study area, one of the two scenarios that emerged from the diachronic series analyses is that the expansion of agricultural land in the last three decades may have led and continue to contribute to a secondary salinization of soils.

Refrences

Allbed, A., & Kumar, L. (2013). Soil Salinity Mapping and Monitoring in Arid and Semi-Arid Regions Using Remote Sensing Technology: A Review. Advances in Remote Sensing, 02(04), 373-385. doi: 10.4236/ars.2013.24040

Fares, M. H., & Philip, C. G. (2008). Characterization of Salt-Crust Build-Up and Soil Salinization in the United Arab Emirates by Means of Field and Remote Sensing Techniques Remote Sensing of Soil Salinization: CRC Press.

Langford, R. L. (2015). Temporal merging of remote sensing data to enhance spectral regolith, lithological and alteration patterns for regional mineral exploration. Ore Geology Reviews, 68(0), 14-29. doi: http://dx.doi.org/10.1016/j.oregeorev.2015.01.005

9644-51, Session PS

MODIS dust detection on the Mediterranean area: a web application for data sharing

Maria T. Melis, Univ. degli Studi di Cagliari (Italy); Francesco Dessì, Istituto di Scienze dell'Atmosfera e del Clima (Italy); Paolo Loddo, Paolo Loddo (Italy); Luca Naitza, Luca Naitza (Italy)

In the framework of the Italian Project I-AMICA a web system for the publication of classified maps of dust in the atmosphere has been developed. This system is integrated in the SHARE-GeoNetwork , a web GIS service for data and metadata management, collected by the Italian atmospheric and climate stations I –AMICA. These data, acquired during the project, provide tools and information that should be used by stakeholders to better monitor the Mediterranean area and then to support appropriate environmental policies. Moreover, I-AMICA promotes links to national reference laboratories and to European projects and programs and international network in climate practices such ACTRIS, WMO-GAW, EARLINET, ICOS, AIQUA, SHARE, NEXT-DATA. In particular, the network of infrastructure built in I-AMICA wants to become a node of a European Research Infrastructure and globally for the Mediterranean Basin. Here we present the new system based on an automatic processing of MODIS data acquired from the specific NASA service, where available datasets are accessible and downloadable. The implementation of the mapping service and its integration in the web platform SHARE-GeoNetwork dedicated to I-AMICA project is shown. The interest of this service is the possibility to access to different -but integrated- data on climate and atmospheric conditions at the same time and to compare directly the MODIS maps with the specific data from the stations. The system developed for the project I- Amica utilizes a procedure of automatic MODIS data processing, which consists, schematically, of three modules: data acquisition, georeferencing and spectral processing of the data. The entire procedure, developed on Linux , using open source code components is assembled by the use of the programming language Python. The procedure is exportable and its use is also allowed with other components for different data processing and analysis.

The MODIS data processing is based on the parameterization of specific radiometric thresholds applied to the index BDT

- "Brightnes Difference Temperature", chosen for the Dust Detection. The BDT index allows to highlight the elements of the atmosphere characterized by higher temperature than the surrounding ones. In order to improve the quality of images in terms of contrast, the index BDT has been modified by applying the normalization of the difference between the emissivity values expressed.

The classification algorithm defined in this procedure is a Decision tree and relates the thermal bands of the infrared spectrum (TIR) of the MODIS sensor. In particular, the algorithm processes, into four steps of calculation, the normalized differences between the MODIS bands 29, 30, 31 and 32. The final classification is a map with five classes: cloud, no dust, low, medium and strong dust. The procedure was implemented using the Python bindings libraries open source GDAL (Geospatial Data Abstraction Library) for image management. The command gdal_rasterize was instead used for superimposing on the final borders between countries in order to provide consultation in a geographical context.

The system is accessible at http://sharegeonetwork.i-amica.it.

9644-53, Session PS

A disparity between erosional hazard and accretion of the sundarbans with its adjacent east coast, Bangladesh: a remote sensing and GIS approach

Ershad U. D. Pahlowan, A.T.M. Shakhawat Hossain, Jahangirnagar Univ. (Bangladesh)

The Sundarbans, UNESCO affiliated world heritage site and world largest mangrove forest covering with (~10000) km2 along the coastal areas of Bangladesh and India. Bangladesh is one of the most vulnerable countries due to sea level rise caused by global warming. In the present situation world mangrove forest are declining at alarming rate. The extensions of this mangrove forest continuously changing with the nature of Bay of Bengal coast. This paper represents the contrast result of erosional hazard and accretion of Sundarbans with its adjacent east coast of Bangladesh. This study based on images of Thematic Mapper (TM), Enhanced Thematic Mapper (ETM), and Operational Land Imager (OLI) from Landsat 8. Landsat images from 1980 to 2014 were analyzed by supervised classification. The result shows the net erosion rate of Sundarbans is higher than its adjacent east coast. The study area has been divided into two portions - Phase I and Phase II. Phase I represent only Sundarbans and Phase II represents adjacent east coast. These two phases has equal longitudinal distance. Many small channels and river supply water and sediment into the Sundarbans. The adjacent east coast of Sundarbans lies on the Meghana estuary that experienced with huge amount of sediment flow. The Sundarbans has been facing erosional stage with a rate of net erosion about 3 km2y-1 whereas the adjacent east coast facing an accretional stage with rate of accretion about 1 km2y-1. The highest erosion rate of Phase I (Sundarbans) was 10.61 km2y-1 and highest erosion of Phase II adjacent east coast) was 18-km2 y-1 in the period of 1989-1999. The highest accretion rate in the Sundarbans was 6.48 km2y-1 in the period of 1999-2006 and in the Phase II, accretion rate was 16.43 km2y-1 in the period of 1980-1989. The lowest erosion rate was 3 km2y-1 in Phase I and 2.11 km2y-1 in Phase II in the period of 1999-2006. The reworking area in phase I is about 37 km2 and phase II is about 51 Km2.So, water is highly active in adjacent west coast than Sundarbans. Though the mean sea level is increasing at a same rate in two different phases but the accretion and erosion rate are not same. From the result, Sundarbans has lost 113.31 km2 of its land in the 34 years of study period whereas adjacent east coast has gain about 35 km2 land. The rate of water discharges and sediment supply are not same in two different phases that plays a vital role in erosion and accretion. Therefore, Sundarbans declining at frightening rate than its adjacent east coast.

9644-54, Session PS

Spatio-temporal pattern of eco-environmental parameters in Jharia coalfield, India

Varinder Saini, R. P. Gupta, Indian Institute of Technology Roorkee (India); Manoj K. Arora, PEC Univ. of Technology (India)

Eco-environment of an area is composed of ecology and environment of the area. Jharia coal-field (JCF) lies in Jharkhand state of India and has a long history of mining. It holds unequivocal importance in the Indian context as it is the only source of prime coking coal in the country. The coalfield is also known for its infamous coal mine fires which have been burning since last more than a century. Haphazard mining over a century has led to eco-environmental changes to a large extent such as changes in vegetation distribution and widespread development of surface and subsurface fires. The remote sensing data has great operational potential for monitoring and surveillance of eco-environmental parameters. The present study aims at studying eco-environmental parameters derived using remote sensing data such as normalized difference vegetation index (NDVI), tasseled cap transformation (TCT) and temperature in two subsets of JCF and their spatio-temporal pattern so as to find out the changes that have occurred over the years. Multi-temporal Landsat (MSS, TM, ETM+, OLI) data ranging from 1972 to 2013 have been used for this study. NDVI, TCT and at-sensor brightness temperature have been calculated following the well defined procedures outlined in the literature. Upon analysis, the following results have been observed:

- The NDVI images belonging to 1972 (MSS), 1992 (TM), 1999 (ETM+) and 2013 (OLI) have been density sliced and the area has been divided into two classes namely, non-vegetated area and vegetated area which further comprises of sparse vegetation and moderate to dense vegetation. It has been observed that the dense vegetation has drastically decreased from 1972 to 2013.

- TC brightness and greenness images of 1992 and 2013 have been subtracted to generate difference images (BRdiff and GRdiff respectively) for both the subsets. A colour composite has been generated (R : BRdiff ; G : GRdiff; B : BRdiff) to show the changes that have occurred in both the subsets over 21 years. In the colour, composite, white colour represents increase in brightness and decrease in vegetation while single colour purple or green show change in brightness or greenness correspondingly.

- For temperature based study, the entire dataset has been divided into four classes based on the acquisition dates namely, Early November, Late November to early December, Mid December and Mid January. The purpose of dividing the data in the above stated classes is to avoid any change in temperature due to seasonal effect. On comparison, it has been observed that the temperature is increasing in each class over the years in both the subsets which indicates that the fire has increased over the years in these subsets.

Thus, it could be concluded that the eco-environment is highly disturbed in JCF and repetitive satellite data is extremely useful for studying the changes in eco-environment.

9644-55, Session PS

Water quality assessment using satellite remote sensing

Saad Ul Haque, Institute of Space Technology (Pakistan)

The two main global issues related to water are its declining quality and quantity. Population growth, industrialization, increase in agriculture land and urbanization are the main causes upon which the inland water bodies are confronted with the increasing water demand. The quality of surface water has also been degraded in many countries over the past few decades due to the inputs of nutrients and sediments

especially in the lakes and reservoirs. Since water is essential for not only meeting the human needs but also to maintain natural ecosystem health and integrity, there are efforts worldwide to assess and restore quality of surface waters. Remote sensing techniques provide a tool for continuous water quality information in order to identify and minimize sources of pollutants that are harmful for human and aquatic life. The proposed methodology is focused on assessing quality of water at selected lakes in Pakistan (Sindh); namely, HUBDAM, KEENJHAR LAKE, HALEEJI and HADEERO. These lakes are drinking water sources for several major cities of Pakistan including Karachi. Satellite imagery of Landsat 7 (ETM+) is used to identify the variation in water quality of these lakes in terms of their optical properties. All bands of Landsat 7 (ETM+) image are analyzed to select only those that may be correlated with some water quality parameters (e.g. suspended solids, chlorophyll a). The Optimum Index Factor (OIF) developed by Chavez et al. (1982) is used for selection of the optimum combination of bands. The OIF is calculated by dividing the sum of standard deviations of any three bands with the sum of their respective correlation coefficients (absolute values). It is assumed that the band with the higher standard deviation contains the higher amount of 'information' than other bands. Therefore, OIF values are ranked and three bands with the highest OIF are selected for the visual interpretation. A color composite image is created using these three bands. The water quality of these lakes are assessed by comparing their reflectance values with the spectral signatures of distilled water. The layout water quality maps of these lakes are prepared in terms of these deviations. The results of the study can be utilized for preliminary water quality monitoring of the selected lakes.

9644-57, Session PS

Automatic landslide and mudflow detection method via multichannel sparse representation

Chen Chao, Jianjun Zhou, Beijing Normal Univ. (China) and Naval Academy of Armament (China); Zhuo Hao, Bo Sun, Jun He, Fengxiang Ge, Beijing Normal Univ. (China)

Landslide and mudflow detection is an important application of aerial images and high resolution remote sensing images, which is crucial for national security and disaster relief. Since the high resolution images are often large in size, it's necessary to develop an efficient algorithm for landslide and mudflow detection. Considering that the district of landslide and mudflow is often irregular-shaped and of changeful topographical features, it is difficult to extract features of it with lower computational-complexity. To deal with the problem, we first analyzed the characteristics of the high-resolution images of landslide and mudflow in this paper. Then, based on the theory of sparse representation, we proposed a novel automatic landslide and mudflow detection method via multi-channel sparse representation.

In this paper, after introducing the principle theory of sparse representation based classification method, we bring out the detailed thinking and process of the proposed method. Firstly, we build up an over-complete dictionary with sample images of typical landslide and mudflow. Each sample is decomposed into R,G,B tri-channel images, each of which is segmented into many overlapped blocks. With those blocks, tri-channel dictionaries are built up through the normalization and vectorization. With the similar operations, test–blocks of tri-channel can be achieved from a test image. It should be note that the position of each test block on the whole test image is retained. Then we represent each test block with the responding channel dictionary by convex optimization, and achieve the representation residual. With a residual threshold, we may decide and label whether it belongs to the mudslide area or not. After traversing the whole image with the same operation iteratively, we can find the possible landslide and mudflow on each channel image by combining the labeled blocks. Thus, we can get tri-channel temporary images. Always, those three are not the same for some wrong labeled blocks, which may cause false-alarm or discontinuity. After further analyzing, we propose a channel-weighting method to filter a part of wrong detected label so that the false alarm rate is reduced. Meanwhile, considering the continuity of landslide and mudflow, we propose a label combination method based on eight neighbor judgment. Finally, we may get continuous landslide and mudflow area on the image. For test the performance of the proposed method, We make the experiment on high resolution image of ZhouQu district of Gansu province in China on August, 2010, which has a serious landslide and mudflow. With the proposed method, we achieve a 75% correct rate by comparing with the reference image labeled by the experts of The Chinese National Disaster Reduction Center. Furthermore, owing to the over-complete dictionary we built, the process of the detection is totally automatic which brings great convenience. This is a promising result which proved the effective of using sparse representation on landslide and mudflow detection.

9644-58, Session PS

Continuum removed band depth analysis for waste detection in the north of Tunisia

Faten Alayet, Nouha Mezned, Saadi Abdeljaoued, Faculté des Sciences de Tunis (Tunisia)

The north of Tunisia holds fifty metal deposits which were exploited during the last century for the extraction of lead and zinc. Despite the economic importance of mining, it is considered as a major factor of pollution. Indeed, the mining extraction left over large amounts of wastes, stored as dikes and threatens soils, vegetation, aquatic environments and above all harmful effects on human health. To evaluate these impacts, several techniques based on sampling and laboratory analysis were applied. Studies results give valuable informations but discontinuous, punctual and expensive. In this study, we used remote sensing techniques for waste distribution mapping.

In particular, we focused on the district of Jebel (Hill) el Ressas which is considered as a pilot mine site, located at 30 kilometers south-east of the city of Tunis with an area of about 4 km2. The Jebel el Ressas is one of the last of the Tunisian Dorsal, towards the sea, between Zaghouan and boukernine. Around the mine, wastes are distributed in three large dumps, located near the village and olive groves. These wastes, estimated between 56,000 and 310,000 m3 and charged with Pb, Zn and Cd, threaten soils, environment and human health.

In this study, we investigated the possibility of estimating the concentration of heavy metals within wastes using measured spectral reflectance. The methodology is based on waste spectral measurement with respect to the field truth for the indirect heavy metal detection. Indeed, our contribution consists on detailed mapping of wastes around Jebel el Ressas mine site. Waste spectral measurements in the visible and near infrared (VNIR 400 - 1200 nm) and mid-infrared (SWIR 1200-2500) were taken in the field using an ASD Field spec Pro FR spectroradiometer considering grain sizes. Qualitative and quantitative interpretation of measured spectra was performed using continuum removed derivative reflectance (CRDR), band depth (BD), band depth ratio (BDR) derived from continuum removed absorption features and second derivatives methods. An accurate mineral versus heavy metal identification was than operated.

9644-59, Session PS

Remote sensing and GIS for monitoring the progress of national housing program

Bouhadjar Meguenni, Khelifa Djerriri, Ctr. National des Techniques Spatiales (Algeria)

Urban planning assumes having access to reliable, accurate and up-to-date data. In developing countries like Algeria, such

kind of data are rarely available because traditional means of collecting are tedious task, expensive and often beyond the financial possibilities of planners. In other hand, the high growth rate (6 to 10% per year) may involve an uncontrolled spatial extensions.

In addition to previously cited issues and during the last decade, Algeria has launched many national housing programs. Such programs accelerate the rate of urban growth and thus need an alternative tool to be monitored in efficient way.

With the advent of high spatial resolution satellites, the frequency and quality of urban data have been widely enhanced in comparison to previous more costly aerial photography. Also, space-borne remote sensing provides large-scale images. This makes remote sensing imagery a suitable tool for surveying efficiently under-construction sites and their progress.

In current work we present a methodology to detect change in areas dedicated to national housing programs by using multi-date high spatial resolution satellite images.

The ENVI feature extraction tool was used to automatically digitize building objects from multi-spectral recent QuickBird images. Such tool adopts object-based image analysis approach, which starts by segmenting the images into homogeneous objects. Once these objects are created, a set of spectral, spatial and textural attributes is computed for each one. The last step consists in classifying the obtained objects into multiple classes. In our case these classes may include achieved buildings and remaining under-construction buildings with different degrees of progress. The classification is done in supervised fashion using training samples selected by an expert. The results are in the form of vector format, which can be easily exported to any Geographical information system (GIS) software. Only the polygons of the building class is extracted with their related attributes.

The aforementioned procedure was applied for each available single-date image, which result in multi-date vector layers that contains various attributes such as: achievement status, areas, type. These layers are used within a GIS software to quantify automatically the advancement of housing program in the study area. Processing of the vector data is needed to correct the imperfections in shapes of polygons issued from the feature extraction step.

Finally, the rate of progress of construction is estimated for each building and for the whole site, then compared to the progress expected by the planner. Also, the obtained results of automatic extraction are compared to those obtained from manual digitizing by domain experts.

9644-60, Session PS

Application of remote senisng technique and development of optical algorithms suitable for inland water in Korea

JongCheol Pyo, KyungHwa Cho, Ulsan National Institute of Science and Technology (Korea, Republic of)

The objectives of this study were to apply remote sensing technique to estimate algae and the other water quality constituents in inland water body of Korea. After optical and water quality sampling, empirical optical algorithms which could estimate algae and water quality constituents were developed and modified to improve the results. In aspect of a performance of the algorithms, finding a relationship between the performance and the interferences which are colored dissolve organic matter and suspended solid was a key part. By calibrating and validating this model with checking accuracy which is evaluated by R square, NSE, and RMSE values, the results will be a fundamental data of application to airborne or satellite remote sensing methods in Korea

9644-61, Session PS

Ground truth and mapping capability of urban areas in large scale ?using GE images

Ahmed I. Ramzi V, National Authority for Remote Sensing and Space Sciences (Egypt)

Monitoring and mapping complex urban features (e.g. roads and buildings) from remotely sensed data multispectral and hyperspectral has gained enormous research interest. Accurate ground truth allows for high quality assessment of classified images and to verify the produced map. Ground truth can be acquired from: field using the handheld Global Positioning System (GPS) device and from Images with high resolution extracted from Google earth in additional to field. Ground truth or training samples could be achieved from VHR satellite images such as QuickBird, Ikonos, Geoeye-1 and Wordview images. Archived images are costly for researchers in developing countries. Images from GE with high spatial resolution are free for public and can be used directly producing large scale maps, in producing LULC mapping and training samples. Google Earth (GE) provides free access to high resolution satellite imagery, but is the quality good enough to map urban areas. costal of the Red sea, Marsa Alam, could be mapped using GE images. The main objective of this research is exploring the accuracy assessment of producing large scale maps from free Google Earth imagery and to collect ground truth or training samples in limited geographical extend. This research will be performed on Marsa Alam city or located on the western shore of the Red Sea, Red sea Governorate, Egypt. Marsa Alam is located 274 km south of Hurghada. The methodology involved image collection taken into consideration the resultion of collected photographs which depend on the height of view. After that, image rectification using suitable rectification methods with different number and distributions of GCPs and CPs. Database and Geographic information systems (GIS) layers were created by on-screen vectorization based on the requirement 6f large scale maps. Attribute data have been collected from the field. In this research the obtained results show that the planimetric accuracy of the rectified Google Earth Image met map 10,000 according to (National Map Accuracy Standards). The collect ground truth or training samples from GE images and field help in accuracy assessment of classification process.

9644-62, Session PS

Assessing coastline exploitation from multitemporal medium-high resolution images: Jintang Island, China

Xiaoping Zhang, Hunan Univ. of Science and Technology (China); Delu Pan, Jianyu Chen, State Key Lab. of Satellite Ocean Environment Dynamics (China); Hao Chen, Shifeng Jia, Hunan Univ. of Science and Technology (China)

Jintang Island, located in Zhoushan archipelago New Area, China, covers an area of ~76.4 km2. As the closest island to connecting the continental shore of Zhejiang Province and the eastern Zhoushan Island after the project of Zhoushan Tran-Oceanic Bridges, it has experienced great changes during the past four decades, and however little attention was paid to discuss the coastline changes of Jintang Island. In this paper coastline positions were mainly extracted by combining histogram thresholding and band ratio techniques with visual interpretation supplemented, based on Landsat multi-spectral imagery in 1975, 1995 and 2015. And then the coastline exploitation degree for different periods was quantified from three index, coastline tortuosity, coastline artificial intensity and coastline dominant use type. The results showed that the position of coastline accreted seaward since 1975. As the natural coastline was straightened, the proportion of artificial coastline has surpassed the natural coastline after

1995. Until 2015, the dominant coastline type has been changed as artificial coastline, mainly covering urban/ industrial and port coast. Using the linear weighted sum of the scores for the above three index, the total coastline exploitation degree was derived and further divided into four grades: extremely high exploitation intensity (EHEI), high exploitation intensity (HEI), median exploitation intensity (MEI) and low exploitation intensity (LEI). From the total coastline exploitation degree maps, we found Jintang Island got the LEI for 1975, the MEI for 1995 and the HEI for 2015. This indicates that it is facing increasing human intervention for reclaiming more coastal land to develop the marine economy.

9644-63, Session PS

Limestone distribution based on spectral reflectance value of multispectral satellite imagery, in Timor-Leste area

Sung Soon Lee, Sung-Ja Choi, Korea Institute of Geoscience & Mineral Resources (Korea, Republic of)

This paper presents a possibility of rock-type classification based on spectral reflectance of multi spectral satellite image. First, FLAASH atmospheric collection is performed to convert from brightness value to spectral reflectance value of ASTER satellite image and masking method is performed to remove abnormal cover area caused by dense vegetation, artificial features, clouds, shadows and etc. As for image based end-member extraction, SMACC method is performed about whole area to extract end-members of individual land cover features. In addition, spectral reflectance values, of field sampled limestone, was observed to verification limestone cover area. Spectral reflectance of real limestone was compared with end-members of random land cover features extracted from ASTER satellite image. Finally, to estimate classification possibility of certain rock type, SAM method is used in case study area. A case study with limestone sediment compositions in East Timor is carried out to illustrate the possibility of the rock-type classification using multi-spectral reflectance. SAM result well presented the deposit area of limestone sediment composition. Through limestone rock-type classification based on satellite image with multi spectral reflectance, the possibility of rock-type classification was obtained instead of a conventional geological survey and a geochemical analysis. Therefore, it is expected that the rock-type can be effectively classified using geological ground truth and hyper-spectral reflectance data.

9644-65, Session PS

Urban green spatio- temporal changes assessment through time-series satellite data

Maria A. Zoran, Roxana S. Savastru, Dan M. Savastru, Marina N. Tautan, Laurentiu V. Baschir, National Institute of Research and Development for Optoelectronics (Romania)

Understanding spatio-temporal changes of urban environments is essential for regional and local planning and environmental management. Remotely sensed data because of its synoptic view and repeat coverage over large geographic areas are useful tools for monitoring and analyzing urban ecosystems. Through reducing air pollution effects and improving urban air quality with positive impacts on human health, green spaces play important functions in urban environments.The spatial distribution and abundance of urban vegetation (forests, parks, gardens, green open spaces) is recognized as a key factor influencing numerous biophysical processes of the urban environment, including air and water quality, temperature, moisture, and precipitation regimes as well as people's health and welfares. Detailed vegetation characteristics, such as the structure of plant canopies and their physiological condition also exert a strong influence on more complex processes such as urban wind flow and rates of transpiration. With the rapid change of urban area in Bucharest city during the past decades, green spaces have been fragmented and dispersed causing impairment and dysfunction of these important urban elements Urban vegetation land cover change is a direct measure of quantitative increase or decrease in sources of urban pollution and the dimension of extreme climate events and changes that determine environment quality. The main goal of this study is to address these tasks in synergy with in-situ data and new analytical methods. Spatio- temporal monitoring of urban vegetation land cover changes is important for policy decisions, regulatory actions and subsequent land use activities. This study explored the use of time-series MODIS Terra/Aqua Normalized Difference Vegetation Index (NDVI) and Leaf Area Index (LAI), data to provide vegetation change detection information for metropolitan area of Bucharest in Romania. Training and validation are based on a reference dataset collected from IKONOS high resolution remote sensing data. The mean detection accuracy for period 2002- 2014 was assessed to be of 87%, with a reasonable balance between change commission errors (20.24%), change omission errors (25.65%), and Kappa coefficient of 0.72. Annual change detection rates across the urban/periurban areas over the study period (2002–2014) were estimated at 0.79% per annum in the range of 0.46% (2002) to 0.77% (2014).Vegetation dynamics in urban areas at seasonal and longer timescales reflect large-scale interactions between the terrestrial biosphere and the climate system. Extracted green space areas were further analyzed quantitatively in relation with air quality data and extreme climate events. The results have been analyzed in terms of environmental impacts and future climate trends. This study provides valuable insights for city planners and decision makers in their endeavors for future development planning. The information on the urban green changes is of great use to land managers and decision makers in order to act effectively to mitigate the risks and preserve the urban green space resources and enhance urban life quality through sustaining a healthy environment.Urban greening is often proposed as an effective way to mitigate urban environmental problems such as air pollution, noise, and urban heat islands which pose serious risks to urban residents' health.

9644-66, Session PS

An Integrated Geospatial System for earthquake precursors assessment in Vrancea tectonic active zone in Romania

Maria A. Zoran, Roxana S. Savastru, Dan M. Savastru, National Institute of Research and Development for Optoelectronics (Romania)

Remote sensing and geospatial information tools and techniques, including numerical modeling, have advanced considerably in recent years, enabling a greater understanding of the Earth as a complex system of geophysical phenomena. Cumulative stress energy in tectonic active regions manifests various earthquakes' precursors. According to classical earthquake theory, small earthquakes should continue to grow into large earthquakes until they spread all along the fault line. The mechanical processes of earthquake preparation are always accompanied by deformations, afterwards complex short- or long term precursory phenomena can appear .Seismic events are associated with ongoing deformation along the main active geologic faults. Macro-fracturing processes are preceding by micro-fracturing phenomena which amplify strain field, with a resulting radon and other gas precursors (He, CH4, NO, Ne, Ar, and N2) anomalies in soil-gas and groundwater, geomagnetic and geoelectric fields anomalies, ionospheric perturbations, thermic land surface anomalies, sudden water-level change in some wells, abnormality of behaviour in some animals, etc.These precursors anomalies are strong indicators of the physical basis of earthquake prediction for tectonically active areas, being correlated with seismic events. Space-time anomalies of Earth's emitted radiation (thermal infrared in spectral range measured from satellite months to weeks before the occurrence of earthquakes, radon in underground water and soil, etc.), and electromagnetic anomalies are considered

as pre-seismic signals. Multispectral and multisensor time-series satellite remote sensing data and space-based geodetic measurements in synergy with ground-based geophysical/geochemical measurements bring a significantly contribution to survey pre-earthquake signals in the areas of strong tectonic activity. With the development of space-based technologies to measure surface geophysical parameters and deformation at the boundaries of tectonic plates and large faults, earthquake science has entered a new era. Using time series satellite data for earthquake prediction, it is possible to pursue the behaviours of earthquake precursors in the future and to announce early warnings when the differences between the predicted value and the observed value exceed the pre-define threshold value. Starting with almost one week prior to a moderate or strong earthquake a transient thermal infrared rise in LST of several Celsius degrees and the increased OLR values higher than the normal have been recorded around epicentral areas, function of the magnitude and focal depth, which disappeared after the main shock. Also are recorded associated geomagnetic and ionospheric distrurbances. Vrancea tectonic active zone in Romania is characterized by a high seismic hazard in European- Mediterranean region, being responsible of strong or moderate intermediate depth and normal earthquakes generation on a confined epicentral area. Based on recorded geophysical parameters anomalies was developed an integrated geospatial system for earthquake precursors in assessment in Vrancea zone. This system integrates derived from time series MODIS Terra/Aqua, NOAA-AVHRR , ASTER , Landsat TM/ETM satellite data multi geophysical parameters (land surface temperature -LST, outgoing long-wave radiation- OLR, net surface latent heat flux (LHF) and mean air temperature- AT as well as geomagnetic and ionospheric data in synergy with in-situ data for surveillance and forecasting of seismic events.

9644-67, Session PS

Impact of climate and anthropogenic changes on urban surface albedo assessed from time-series MODIS satellite data

Maria A. Zoran, National Institute of Research and Development for Optoelectronics (Romania); Adrian I. Dida, Transilvania Univ. of Brasov (Romania); Liviu-Florin V. Zoran, Univ. Politehnica of Bucharest (Romania)

Urbanization may be considered the most significant anthropogenic force that has brought about fundamental changes in urban land cover and landscape pattern around the globe, being one of the crucial issues of global change in the 21st century affecting urban ecosystem. Urban areas and mostly agglomerated towns are so called “environment pollution hot spots” due to activities and processes at city surface responsible for emissions in the form of gases and particulate matter that either directly, or through secondary processes (i.e., chemical reaction, phase change, dissolution, etc.) can affect human health. The pollutants of concern in the urban atmosphere are nitrogen oxides, sulfur dioxide, volatile organic compounds (as precursors to ozone), carbon monoxide, lead, ozone and particulate matter PM (PM10 and PM2.5). Long-range transport of ozone and particulate matter (PM) influences air quality and climate in regions far from their sources. The influence of aerosol particles on climate, and how their properties are perturbed by anthropogenic activity, is one of the key uncertainties in climate change assessments. In the physical climate system, land surface albedo determines the radiation balance of the surface and affects the surface temperature and boundary-layer structure of the atmosphere. Due to anthropogenic and natural factors, urban land covers changes result is the land surfaces albedo changes. The main aim of this paper is to investigate the albedo patterns dynamics due to the impact of atmospheric pollution and climate variations on land cover of Bucharest metropolitan area, Romania based on satellite remote sensing MODIS Terra/Aqua (Moderate Imaging Spectroradiometer) data over 2000–2014 time period. This study is based on MODIS derived biogeophysical parameters land surface BRDF/albedo , LST (land surface temperature) and NDVI products and in-situ monitoring ground data (as air temperature, aerosols distribution, relative humidity, etc.). For urban land cover changes over the same investigated period have been used also Landsat TM/ETM and IKONOS satellite data. Have been analyzed also other biogeophysical effects of urban land cover change in addition to surface albedo, particularly changes in the surface moisture budget leading to shifts in the ratio of latent and sensible heat fluxes and changes in rate of air surface temperature, aerosol and precipitation. Due to deforestation in the periurban areas albedo change appears to be the most significant biogeophysical effect in temperate forests. Satellite data and climate station observations show that surface albedo changes of a forested zone placed close to a large urban area highly respond to atmospheric pollution influence and climate variations. As the physical climate system is very sensitive to surface albedo, urban/periurban vegetation systems could significantly feedback to the projected climate change modeling scenarios through albedo changes.

9644-68, Session PS

Radiometric cross-calibration of KOMPSAT-3 AEISS with Landsat-8

Dong Yoon Shin, Pukyong National Univ. (Korea, Republic of); Cheong-Gil Jin, Korea Aerospace Research Institute (Korea, Republic of); Ho Yong Ahn, Chuluong Choi, Pukyong National Univ. (Korea, Republic of)

Around the Earth, there are a lot of EOS(Earth Observation Satellite)s that are doing their own duties. As each of the EOS is designed to function according to its own purpose, the spectral bandwidth that they measure is different from one another. Thus, it is fairly hard to compare the data directly. However, the spectral bandwidth being used for the purpose of a satellite is similar to one another in general. This can be very often found in optical satellites using the visible band. Therefore, this study examines whether it is possible to normalize the radiance measured by the optical EOS equipped with a similar spectral bandwidth in the visible band and then compares the results of radiance that has been normalized. The normalization is conducted by converting the digital number into the TOA radiance then applying Cosine Correction and the SBAF (Spectral Band Adjustment Factor).

The purpose of this study is to perform the Cross Radiometric Calibration for KOMPSAT-3 AEISS (Advanced Earth Imaging Sensor System) using satellite imagery taken by Landsat-8 OLI and EO-1 Hyperion. Converted DN value from each band of Landsat-8 sensor represent spectral radiance at wavelength. Therefore, the Cross Calibration can be performed applying the Relative Response Function of KOMPSAT-3 to interpolated radiance from EO-1. The problem according to the different spatial resolution is solve by using average DN value from large area have uniformly surface like the Cal/Val site. The Cal/Val site is Libya-4 in Africa. In order to estimate tolerance, calculate the DN to Radiance Conversion Coefficients for Min, Max and Mean DN. This study will improve spectroscopic reliability of KOMPSAT-3 through compare with KOMPSAT-3 Absolute Radiometric Calibration Result. Furthermore, the result can be apply to the Radiometric Calibration/Validation study on KOMPSAT-3A, in a future.

9644-69, Session PS

Case study: mapping mangroves and coastal wetlands

Christopher Dubia, Kent Lewis, Andy Long, MapWorks Learning (United States)

Mapping the Mangroves (MTM), a project of MapWorks Learning, provides formal and informal education, and gives citizen scientists and the larger scientific community the ability

to engage with and explore mangroves and their ecosystems. Mangroves are a cornerstone species and play important roles in habitat formation, stabilization of coastal environments, and carbon sequestration. The MTM open curricula and GIS tool provide opportunities for anyone to learn about authentic applications of GIS in the field, explore mangroves and their ecosystems, and share their findings. Learners develop an understanding and appreciation for the role mangroves play in a healthy environment and how GIS can aid in conservation.

9644-70, Session PS

Evaluation of satellite-based precipitation using APHRODITE and observed station over diverse topography of Pakistan

Muhammad Farooq Iqbal, COMSATS Institute of Information Technology (Pakistan)

Satellites offer effective, efficient and economical means for calculating areal precipitation estimates in sparsely gauged regions. Satellite based precipitation play a vital role for hydrological applications due to the unavailability of ground based data. Absence of real time ground-based gauge observations during high intensity precipitation over diverse topography of Pakistan and unreliable flood forecasting leads to infrastructure and agricultural land damages. In the current study the accuracy of remote sensing based Tropical Rainfall Measuring Mission (TRMM) Satellite Precipitation (TSP) data was assessed using Asian Precipitation Highly Resolved Observational Data Integration Towards Evaluation of Water Resources (APHRODITE) Gridded Precipitation (AGP) data and Ground Station Precipitation (GSP). TSP and AGP data were acquired on same spatial and temporal resolution and mean monthly data of selected grid cells were derived from these two datasets. Advanced Spaceborne Thermal Emission and Reflection Radiometer (ASTER) Global Digital Elevation Model (GDEM) data was used for topographic extraction of the selected grid cells. Grid cells were selected from sufficiently large number of stations observed for validation areas. Results of the study revealed that strong positive linear relationship was observed between TSP, AGP and GSP on mean annual and monthly time scale. TSP overestimated from AGP on mean annual and mean monthly time scale, whereas no biased was observed between TSP and GSP and magnitude of error was also very trivial. Strong positive linear relationship was also observed in all the four seasons including pre-monsoon, monsoon, post-monsoon and winter season, whereas, perfect correlation was observed between GSP and AGP in winter season. Mean daily comparison show moderate relationship and error magnitude was high as compared to mean monthly and mean annual time scale. Station to station comparison on daily scale resulted in strong correlation in low topographic areas like Rohri, Jacobabad and Khuzdar and error magnitude was less in plain areas like Jiwani. Whereas maximum magnitude of error was observed in high topographic areas like Balakot, Muzaffarabad and Risalpur. It is evident that TSP overestimate in some seasons, areas and time scale but also underestimates on some seasons, areas and time scale. It is concluded from current study that TSP gives better results on annual and monthly time scale as compared to daily time scale over different topographic regions. Less magnitude of error was observed in all the four seasons expect monsoon season with having high error as compared to rest of seasons. Therefore, TSP can be used in all the four seasons including pre-monsoon, monsoon, post-monsoon and winter season, however it overestimates in monsoon season. TSP underestimates in high topographic areas, whereas, in plain and mid topographic areas gives better results.

9644-71, Session PS

Slope adjustment of runoff curve number (CN) using Advanced Spaceborne Thermal Emission and Reflection Radiometer (ASTER) Global Digital Elevation Model (GDEM) for Kuantan River Basin

Abolghasem Akbari, University Malaysia Pahang (Malaysia)

The Natural Resources Conservation Service Curve Number (NRCS-CN) method is widely used for predicting direct runoff from rainfall. It employs the hydrologic soil groups and landuse information along with period soil moisture conditions to derive NRCS-CN. This method has been well documented and available in popular rainfall-runoff models such as HEC-HMS, SWAT, SWMM and many more. The Sharply-Williams and Hank methods was used to adjust CN values provided in standard table of TR-55. The Advanced Spaceborne Thermal Emission and Reflection Radiometer (ASTER) Global Digital Elevation Model (GDEM) is used to derive slope map with spatial resolution of 30 m for Kuantan River Bsin (KRB). The two investigated method stretches the conventional CN domain to the lower values. The study shows a successful application of remote sensing data and GIS tools in hydrological studies. The result of this work can be used for rainfall-runoff simulation and flood modeling in KRB.

9644-11, Session 3

Modelling prehistoric terrain Models using LiDAR-data: a geomorphological approach

Veit Höfler, Christine Wessollek, Pierre Karrasch, Technische Univ. Dresden (Germany)

Terrain surfaces conserve human activities in terms of textures and structures. With reference to archaeological questions, the geological archive is investigated by means of models regarding anthropogenic traces. In doing so, the high-resolution digital terrain model is of inestimable value for the decoding of the archive. The evaluation of these terrain models and the reconstruction of historical surfaces is still a challenging issue. Due to the data collection by means of LiDAR systems (light detection and ranging) and despite their subsequent pre-processing and filtering, recently anthropogenic artefacts are still present in the digital terrain model.

Currently, there are different filter algorithms available for removing these structures [e.g. Vosselman2000]. From the geomorphological process understanding, the landscape-genetic patterns of a relief can often only be modelled insufficiently with these methods, because they only consider local surface structures and only process them in terms of mathematical aspects. Recent structures of the surface, such as crop lands and settlements, have been preserved in some cases, and not only recently anthropogenic artefacts are eliminated. Thus, investigations in an area with different slope inclinations do not show a significant change of recent build-up areas when applying the mentioned filter procedure.

It must be the objective of a filter working from a geomorphological perspective to distinguish between anthropogenically undisturbed and disturbed surfaces. Analysis have shown that elements, such as contour lines and channels, can well be extracted from a high-resolution digital terrain model. This way, channels in settlement areas show a clear anthropogenic character. This fact can also be observed for contour lines. Some contour lines representing a possibly natural ground surface and avoid anthropogenic artefacts. Comparable to channels, noticeable patterns of contour lines become visible in areas with anthropogenic artefacts.

The presented workflow uses functionalities of ArcGIS and the programming language R [RCoreTeam2013]. The method

starts with the extraction of contour lines from the digital terrain model. Through macroscopic analyses based on geomorphological expert knowledge, contour lines are selected representing the natural geomorphological character of the surface. These selected contour lines pass through a two-stage process.

In a first step, points are determined along each contour line in regular intervals. This points and the corresponding height information which is taken from an original digital terrain model is saved as a point cloud. Using the programme library gstat (cf. Pebesma [Pebesma2004683] [Pebesma2014]), a variographic analysis and the use of a Kriging-procedure based on this ([Akin1988]) follow. The result is a digital terrain model filtered considering geomorphological expert knowledge showing no human degradation in terms of artefacts, preserving the landscape-genetic character and can be called a prehistoric terrain model.

For archaeology, this method offers an excellent approach to reconstruct ground surfaces. Areas with a dense building development in the original terrain model can be illustrated under prehistorical conditions and in the absence of human activities.

This method seems equally helpful for all scientific areas, which utilize the relief as a research object and which rely on context-based processes of filtering. The method allows both, the removal of disturbing factors, as well as the inclusion of simulated disturbances as required for risk analysis.

9644-12, Session 3

An integrated multimedial approach to cultural heritage conservation and documentation: from remotely-sensed lidar imaging to historical archive data

Valentina Raimondi, Lorenzo Palombi, Istituto di Fisica Applicata Nello Carrara (Italy); Annalisa Morelli, SO.IN.G Strutture e Ambiente S.r.l (Italy); Massimo Chimenti, Culturanuova s.r.l. (Italy); Sara Penoni, FABERestauro s.n.c. (Italy); Ute Dercks, Kunsthistorisches Institut in Florenz (Italy); Alessia Andreotti, Univ. di Pisa (Italy); Giovanni Bartolozzi, Istituto di Fisica Applicata Nello Carrara (Italy); Marco Bini, ELab Scientific s.r.l. (Italy); Ilaria Bonaduce, Univ. di Pisa (Italy); Susanna Bracci, Emma Cantisani, Maria Perla Colombini, CNR-Istituto per la Conservazione e la Valorizzazione dei Beni Culturali (Italy); Costanza Cucci, Istituto di Fisica Applicata Nello Carrara (Italy); Laura Fenelli, Kunsthistorisches Institut in Florenz (Italy); Monica Galeotti, Opificio delle Pietre Dure (Italy); Irene Malesci, CNR-Istituto per la Conservazione e la Valorizzazione dei Beni Culturali (Italy); Alessandra Malquori, Scuola di Studi Umanistici e della Formazione (Italy); Emanuela Massa, Art-Test s.a.s. (Italy); Marco Montanelli, AK Innovation s.r.l. (Italy); Roberto Olmi, Marcello Picollo, Istituto di Fisica Applicata Nello Carrara (Italy); Louis D. Pierelli, NIKE Restauro Opere D'Arte Snc (Italy); Daniela Pinna, Opificio delle Pietre Dure (Italy); Cristiano Riminesi, CNR-Istituto per la Conservazione e la Valorizzazione dei Beni Culturali (Italy); Sara Rutigliano, Culturanuova s.r.l. (Italy); Barbara Sacchi, CNR-Istituto per la Conservazione e la Valorizzazione dei Beni Culturali (Italy); Sergio Stella, Bel Chimica S.r.l (Italy); Gabriella Tonini, NIKE Restauro Opere D Arte Snc (Italy)

Fluorescence lidar imaging has been already proposed in several studies as a valuable technique for the remote diagnostics and documentation of the monumental surfaces, with main applications referring to the detection and classification of biodeteriogens, the caracterisation of lithotypes, the detection and characterisation protective coatings and also of some types of pigments. However, the conservation and documentation of the cultural heritage is an application field where a highly multi-disciplinary, integrated approach is typically required. In this respect, the fluorescence lidar technique can be particularly useful to provide an overall assessment of the whole investigated surface, which can be profitably used to identify those specific areas in which further analytical measurements or sampling for laboratory analysis are needed.

This paper presents the research carried out within the PRIMARTE project, funded by the Region of Tuscany, with the aim to develop an integrated methodology for the combined use of data by using diverse techniques: from fluorescence lidar remote sensing to UV fluorescence and IR imaging, from IR thermography, georadar, 3D electric tomography to microwave reflectometry, from analytical techniques (FORS, FT-IR, GC-MS) to high resolution photo-documentation and historical archive studies. In particular, this paper presents the results of the use of this methodology applied to a 'pilot site', a chapel dating back to the fourteenth century, situated at 'Le Campora' site in the vicinity of Florence. The chapel is actually the remnant of a much larger structure, a major church and the adjacent monastery, which were destroyed in the past. The site was also chosen because it had both mural paintings and stone artifacts and buried structures, which offered a broad-spectrum test-bench for the project's team.

Finally, all data were made available in a multi-medial tool – implemented in the frame of the same project - for the archiving, management, exploitation and dissemination of the collected information, which can be performed at different levels of complexity, starting from a low level where all scientific data are available as a tool for restorers and conservators to a level suitable for the dissemination to the general public.

9644-13, Session 3

Remote sensing modelling of cellulose, lignin and wax content of Pistacia for phylogenetic analysis

Giorgi Kozhoridze, Nikolai Orlovsky, Leah Orlovsky, Dan G. Blumberg, Avi Golan-Goldhirsh, Ben-Gurion Univ. of the Negev (Israel)

Remote sensing analysis of vegetation is based on measurements of the reflected electromagnetic radiation, which "carries information" about the shape, size, pattern and chemical composition of the plants. We have hypothesized that biochemicals i.e., cellulose, lignin and wax, which are involved in cell wall structure, leaf surface and bark properties, affect the reflected spectra, in the range between 400 nm – 2500 nm, in a species related manner.

A germplasm collection of trees of the Pistacia genus, at BIDR, was used as a model system for analysis. Laboratory and field spectrometry measurements were carried-out and the data was analyzed and tested for modelling species-specificity of reflectance. Development of species-specific spectral signature is indeed a big challenge, since different plants may have similar spectral properties. The measurements are even more complicated in field spectroscopy due to soil background, and atmospheric noise that cannot be avoided. Furthermore, daily timing and seasonal variation of measurements are critical factors in the resulting reflectance values. Various plant species have different life cycles that add complexity to the spectral results, which can be turned into an advantage in development of a model for identification of the species. As a result, we have added seasonal reflectance data series measurements in order to improve the models based on the reflected spectrum and first derivative of reflectance (FDR), in correlation to the content of cellulose, lignin and wax of leaf and bark of the tress, determined chemically.

It was shown that Near InfraRed (NIR) and Short Wave InfraRed (SWIR) ranges of reflectance and the FDR contain most of the information about the biochemicals studied. The models were improved from R2 = 35%-81% to R2 = 69%-84%, by

normalization against the visible spectrum bands, Blue/Green/Red/Red Edge, for each biochemical. Furthermore, a wider range of biochemicals: chlorophyll, carotenoids, anthocyanins, cellulose, wax and lignin of leaf and bark of the trees, was used for Pistacia phylogenetic analysis. It should be noted that seasonal variations appeared to play a significant role in classification of species, when scaling-up the data from hyper-spectral to multispectral resolution.

Biogeographic phylogeny of Pistacia species based on Global Biodiversity Information Facility database (GBIF) coordinates was related to climate, landscape and soil parameters. Geostatistical, spatial and climate analyses showed specific distribution centers of the genus, between 4 ° S - 50 ° N latitudinal belt. The predicted and probability distributions showed phylogenetic relationship among the Pistacia species that correlated to the remote-sensing-based classification and the molecular phylogeny.

9644-14, Session 4

Active landslide monitoring using remote sensing data, GPS measurements and cameras on board UAV

Konstantinos G. Nikolakopoulos, Katerina Kavoura, Nikolaos Depountis, Nikolaos Argyropoulos, Ioannis Koukouvelas, Nikolaos Sabatakakis, Univ. of Patras (Greece)

An active landslide can be monitored using many different methods: Classical geotechnical measurements like inclinometer, topographical survey measurements with total stations or GPS and photogrammetric techniques using airphotos or high resolution satellite images. As the cost of the aerial photo campaign and the acquisition of very high resolution satellite data is quite expensive the use of cameras on board UAV could be an identical solution. Small UAVs (Unmanned Aerial Vehicles) have started their development as expensive toys but they currently became a very valuable tool in remote sensing monitoring of small areas. The purpose of this work is to demonstrate a cheap but effective solution for an active landslide monitoring. We present the first experimental results of the synergistic use of UAV, GPS measurements and remote sensing data. A six-rotor aircraft with a total weight of 6 kg carrying two small cameras has been used. Very accurate digital airphotos, high accuracy DSM, DGPS measurements and the data captured from the UAV are combined and the results are presented in the current study.

9644-15, Session 4

Lithological mapping of igneous and metamorphic rocks in the Central Eastern Desert of Egypt using remote sensing data

Mohamed Fouad Sadek, National Authority for Remote Sensing and Space Sciences (Egypt)

The central Eastern Desert of Egypt is composed mainly of Precambrian metamorphic and intrusive assemblages including serpentinites-talc carbonate rocks and metavolcanics which are intruded by syn to late to post orogenic granitoids. This study is focused on the Um Gheig area which comprises El- Sibai-Um Gheig and Kadabora-Suwaqat areas.

The integrated remotely sensed processed data together with the field study have been used to discriminate the exposed metamorphic and magmatic basement rock assemblages as well as modifying the previously geological mapping for the study area. These rocks have been successfully discriminated on Landsat-8 images including, Minimum Noise Fraction MNF (4, 3, 7), Principal component analysis PCA (PC6, PC2, PC7) and various band ratios (b6/b2, b6/b7 b6/b5xb4b5) and (b7/b6, b7/b5, b5/b3). ASTER TIR data with various ASTER indices e.g. clay index (5x7/6) and silica index (10/13) successfully discriminated the varieties of granitoid rocks, while the serpentinite-talc carbonate and metavolcanics (particularly banded iron bearing varieties) are clearly distinguished on the ASTER images of amphibole index (6+9/7+8) and (6/8). Comparing the results of the investigated study with the previously published geological maps for the study area, the present study produced geological maps which are the best in lithological discrimination and lithological boundaries.

9644-16, Session 4

WebGIS for calculation of main geomagnetic field parameters on the basis of ESRI ArcGIS API

Andrei V. Vorobev, Gulnara R. Shakirova, Ufa State Aviation Technical Univ. (Russian Federation)

Today the specialists in many scientific and applied spheres (such as biology, medicine, geophysics, geology, technics, sociology, psychology, ecology and many others) consider a wide range of parameters of geomagnetic field and its variations as one of the key factors, which can significantly influence on systems and objects of various origins and structure. The estimation of the influence requires an effective approach to analyze the principles of distribution of geomagnetic field parameters on the Earth's surface, its subsoil and in circumterrestrial space. The approach causes a complicated problem to be solved, which is concerned with modeling, analysis and visualization of geomagnetic field and its variations parameters. The most effective and obvious solution to this problem is supposed to be a geographic information system, because of the data-centric character of the problem itself. In spite of wide variety of approaches for mathematical modeling, analysis and graphical visualization of various data (including spatial data) a problem of modeling, automated analyzing and 2D/3D-visualization of geomagnetic field and its variations is still not solved. In this paper the authors suggest the solution, which is based on modern geoinformation (ESRI ArcGIS API) and web (Ajax, XML, Web Script Languages) technologies and provides the mechanisms to calculate, analyze and visualize parameters of geomagnetic field (North, East, Down components, total intensity, magnetic inclination and declination, etc.) and its variations. It is WebGIS "GIMS-Calculator", which provides the complex calculation, analysis and 2D/3D-visualization of geomagnetic field and its variations parameters. The system "GIMS-Calculator" provides effective and reliable calculation and analysis of parameters of normal (or undisturbed) GMF by the spatiotemporal coordinates with error value no more than 0.1%. Geomagnetic field and its variations models, which are represented and described by "GIMS-Calculator", meet the requirements of specialists in various areas. They effectively provide formatting and structuring the data about the Earth magnetosphere parameters and their further analysis.

9644-18, Session 5

Concept of an advanced hyperspectral remote sensing system for pipeline monitoring

Göksu Keskin, Caroline Teutsch, Andreas Lenz, Wolfgang Middelmann, Fraunhofer-Institut für Optronik, Systemtechnik und Bildauswertung (Germany)

Areas occupied by oil pipelines are prone to severe contamination by leakages occurring for reasons such as poor maintenance, accidents or illegal extraction. Allowing rapid identification of hazards, regular monitoring of oil pipelines and refineries for possible leaks is a critical task. Airborne monitoring is a favored approach considering the pipeline structures and their broad land coverage. However, it is usually carried out by visual inspection from a flight platform, which could make it erroneous, inefficient and expensive. In this work,

as an efficient alternative, an airborne hyperspectral remote sensing system for pipeline monitoring is presented and its feasibility will be evaluated.

The suggested system includes the airborne hyperspectral multisensor platform developed at Fraunhofer IOSB for data acquisition, pre-processing, fusion and analysis with near real-time processing capability. This work aims to utilize this system in environmental protection, with a primary emphasis on pipeline monitoring.

The airborne multisensor platform consists of a preferred hyperspectral sensor complemented with an inertial navigation system (INS) for georectification and georeferencing of the sensor data, as well as an embedded high-performance computer for required sensor interfaces and data acquisition. The components are flexibly integrated in a lightweight flight platform. According to application requirements, adding supplementary imaging sensors is practicable. There are two operation modes available: In offline-mode, the data acquired by the sensors is stored on-board and can be processed after flight, whereas the online-mode provides the possibility of in-flight reporting by transmitting the processing results to a remote operator. This application mode could be required in time-critical operational purposes such as disaster management. For pipeline monitoring activities, both operation modes are considered to be useful: For scheduled inspection, the offline-mode would be sufficient, while the online-mode could support on-site examination in emergencies. Furthermore, the system can be connected to an OGC standard GIS in order to allow interoperable access to the hyperspectral detection results.

To employ this system, a post-processing step for oil detection in hyperspectral data is suggested. Due to their well-studied performance, the Hydrocarbon Index (HI) and Hydrocarbon Detection Index (HDI) are used for hydrocarbon detection. Both methods are based on features of hydrocarbon spectra, which are calculated from specific reflectance bands in SWIR wavelengths. The advantage of these methods is that they do not require reference spectra, which could be dangerous to obtain in a contaminated area by ground measurements. The detection results would indicate the possible oil leaks around pipelines.

Another aspect in data analysis is to determine the limiting performance with respect to size of the contaminated area due to the lower spatial resolution of hyperspectral sensors compared to multispectral cameras. For this work a field study is costly, therefore the analysis will be based on simulated data including different sizes of contamination in airborne-acquired hyperspectral data.

The hyperspectral sensor type of choice for this application is an SWIR pushbroom sensor with a spectral resolution around 6 nm and suitable SNR, covering the required spectral wavelength regions for HI and HDI calculation. In this paper, the hyperspectral data acquired from Ettlingen, Germany will be used in feasibility and robustness evaluation of oil detection.

9644-19, Session 5

Hydrocarbon microseepage mapping using signature based target detection techniques

Hilal Soydan, Alper Koz, Sebnem Düzgün, Aydin A. Alatan, Middle East Technical Univ. (Turkey)

Micro- and macro-seepages of oil and gas reservoirs stand as a valuable source for exploration purposes. Alterations because of long term in situ seeps or along the mitigation pathways cause anomalies in the near surface sediments overlying the gas or oil reservoirs, which provide a potential opportunity for gas/oil exploration (Shi et al., 2010). Several studies exploit remote sensing techniques to detect hydrocarbon induced anomalies for oil exploration with multispectral and hyperspectral images, emphasizing the fact that hydrocarbon bearing materials have specified absorption features on electromagnetic spectrum. The spectral signature of the target region with micro/macro seeps are expected to have different characteristics from the surrounding, with its absorption characteristics at 1.73 and 2.31 μm (Kühn et al., 2004). The studies with multispectral images for hydrocarbon microseepage mapping until now mainly utilize the band ratio images of specified altered minerals, feature oriented principal components, or false color composites with original bands or band ratios (He et al., 2014). A main characteristics of these methods is to make use of only few specific bands to describe the features of the searched mineral during the image analysis. However, considering the multi-dimensional nature of the spectral data, the use of the all spectral bands for image analysis as in signature based target detection methods can be expected to be more resourceful to identify the mineral in interest.

In this paper, we compare the conventional methods in hydrocarbon seepage anomalies with the signature based detection algorithms. The CROSTA technique is selected as a basement in the experimental comparisons for the conventional approach. The CROSTA technique utilizes the characteristic bands of the searched target for principal component transformation in order to determine the components characterizing the target in interest. Desired Target Detection and Classification Algorithm (DTDCA), Spectral Matched Filter (SMF), and Normalized Correlation (NC) are employed for signature based target detection. Signature based target detection algorithms are applied to the whole data set benefiting from the information stored in all spectral bands of the image.

The selected methods are applied to a multispectral Advanced SpaceBorne Thermal Emmission and Radiometer (ASTER) image of the study region, with an atmospheric correction prior to the realization of the algorithms. ASTER provides multispectral bands covering visible, short wave and thermal infrared region that serve as a useful tool for the interpretation of the areas with hydrocarbon anomalies. The exploration area is selected as Gemrik Anticline which is located in South East Anatolia, Adiyaman, Bozova Oil Field, where micro seeps can be observed with almost no vegetation cover. The spectral signatures collected with Analytical Spectral Devices Inc. (ASD) spectrometer from the reference valley (Avcıo?lu, 2010) have been utilized as an input to the signature based detection algorithms.

The experiments have indicated that DTDCA and MF outperforms the CROSTA technique by locating the microseepage patterns along the mitigation pathways with a better contrast. On the other hand, NC has not been able to map the searched target with a visible distinction. It is concluded that the signature based algorithms can be more effective than the conventional methods for the detection of microseepage induced anomalies.

9644-20, Session 5

Quarry monitoring using GPS measurements and UAV photogrammetry

Konstantinos G. Nikolakopoulos, Ioannis Koukouvelas, Nikolaos Argyropoulos, Vasileios Megalooikonomou, Univ. of Patras (Greece)

Active quarries near to urban centers are at the same time a necessity but also a source of pollution. Necessity as they supply to the construction companies the necessary aggregates and source of pollution as they affect biodiversity, vegetation cover and threaten water resources. The objective of this work is to indicate a monitoring methodology in order to survey the present state of the quarry sites and their evolution in time, which are the basic data needed to implement an adequate land reclamation project. The land monitoring has been realised by UAV photogrammetry and GPS measurements supported by a Geographic Information System. A six-rotor aircraft with a total weight of 6 kg carrying two small cameras has been used. Very accurate digital airphotos have been used in order to create orthophotos mosaic and DSM from the quarry planes. DGPS measurements and the data captured from the UAV are combined in GIS and the results are presented in the current study.

9644-21, Session 5

Soil volume estimation in debris flow areas using lidar data in the 2014 Hiroshima, Japan rainstorm

Hiroyuki Miura, Hiroshima Univ. (Japan)

Debris flows triggered by the rainstorm in Hiroshima, Japan on August 20th, 2014 produced extensive damage to the built-up areas in the northern part of Hiroshima city. The number of deaths was 74 and more than 4,500 buildings were damaged or inundated by the debris flows. In order to consider various emergency response activities and early-stage recovery planning, it is important to evaluate the distribution of the soil volumes in the debris flow areas immediately after the disaster. Light Detection and Ranging (LiDAR) technique is useful to quickly capture the post-disaster terrain. The Digital Elevation Model (DEM) with the spatial resolution of 1 m was constructed from LiDAR data observed after the rainstorm. Pre-disaster DEM with the spatial resolution of 5 m constructed from LiDAR data was officially prepared by the Geospatial Information Authority of Japan (GSI). The spatial distortions and location errors, however, are observed in the data and they may produce large errors of the soil volume estimation.

In this study, nonlinear mapping technique proposed in the digital image processing field is applied to the pre- and post-disaster DEMs in order to precisely superpose them and to evaluate the terrain change. The nonlinear mapping technique is based on local exploration process and selective smoothing. The transfer vectors in a small window area are explored to correct the local geometric distortions and the vectors are selectively smoothed by using the neighboring vectors. The result shows that the errors of the elevations between the data are significantly reduced by the nonlinear mapping compared to the traditional geometric correction technique.

The difference of the elevation are calculated from the DEMs corrected in this study. The terrains are dramatically eroded in the upper streams of the debris flow areas and are accumulated in the down streams. The maximum erosion and sediment heights are approximately 4 m and 3 m, respectively. These values almost correspond to the results of the field surveys. The eroded and accumulated soil volumes are calculated by aggregating the differences of the elevation in each debris flow area. The soils with about 30,000 cubic meters are flowed in a channel at a maximum. The total volumes of the erosion and sediment are approximately 700,000 and 350,000 cubic meters, respectively. The sediment volume is remarkably smaller than the erosion volume because the runoff soils were flowed into rivers and houses in the down streams, and the soils in the built-up areas were removed immediately after the disaster for the emergency rescue operation and early recovery activity.

9644-23, Session 5

Lithological mapping using multispectral ASTER and Landsat 8 data in the Bas Drâa inlier, Moroccan Anti Atlas

Zakaria Adiri, Abderrazak El Harti, Amine Jellouli, Faculty of Science and Technology Beni Mellal (Morocco); Lhou Maacha, MANAGEM Group (Morocco); El Mostafa Bachaoui, Faculty of Science and Technology Beni Mellal (Morocco)

Lithological mapping is one of the fundamental steps in the various mineral prospecting studies, because it forms the basis of the interpretation and validation of retrieved results. Therefore, this study exploited the multispectral ASTER (Advanced Spaceborne Thermal Emission and Reflection Radiometer) and Landsat 8 data in order to map lithological units in the Bas Drâa inlier, at the Moroccan Anti Atlas. Surface reflectance was retrieved using FLAASH model for VNIR and SWIR ASTER data and Dark Object Subtraction Method for Landsat 8 data. Otherwise, the Emissivity was calculated using the Emissivity Normalization algorithm implemented in ENVI software. Then, lithological units were discriminated by using the Principal Component Analysis (PCA), Band Ratios (BR) and Support Vector Machine (SVM) classification. According to the overall accuracy and the Kappa coefficient based on ground truth image, SVM shows good precision. In addition, the results of PCA and BR show an excellent correlation with the existing geological maps and previous works on the study area. Consequently, the methodology proposed demonstrates a high potential of ASTER and Landsat 8 data in lithological units discrimination.

9644-24, Session 6

Introducing a rain-adjusted vegetation index (RAVI) for improvement of long-term trend analyses in vegetation dynamics

Christine Wessollek, Pierre Karrasch, Babatunde A. Osunmadewa, Technische Univ. Dresden (Germany)

Vegetation is one of the most important intrinsic parts of an ecosystem. An extensive knowledge about vegetation dynamics plays a key role especially in developing countries on the African continent. For this reason detailed analyses of trends in vegetation dynamics are an obligatory precondition for the general development of the analysed regions and also to decision makers particularly in the chosen study area of Kogi state, a semiarid region of Nigeria.

Currently, the analyses of vegetation dynamics using the Normalized Vegetation Index (NDVI) in Kogi state is often performed by time series analyses using constant seasonality. It is obvious and also proven [1] that an annual cycle presents the strongest frequency in vegetation dynamics. Nevertheless, considering this annual seasonality, it is evident from the analyses of the remaining residuals that further research on vegetation modelling is needed. This is also the case if structural break points in the trend component of an original NDVI signal are considered [2]. Detailed analyses of the mean annual seasonality shows their variability over a period of about three decades. Small temporal events of e.g. a dry summer or a comparatively wet dry-season have an impact on the estimated trend component of the original NDVI time series (GIMMS) and also on the linear, segmented-linear or non-linear trend model. This applies particular in regions with strong distinctions in availability of water. It seems to be obvious that precipitation has a major impact on greening during the rainy season in semiarid regions. First results [1] implies a strong dependence of NDVI on rainfall. Therefore it will be necessary to consider specific rainfall events besides the known ordinary annual cycle. Based on this fundamental idea, the paper will introduce the development of a rain adjusted vegetation index (RAVI). The index is based on the enhancement of the well-known normalized difference vegetation index (NDVI [3]) by means of TAMSAT rainfall data and includes a 3-step procedure of determining RAVI. Within the first step both time series were analysed over a period of 29 years to find best cross correlation values between TAMSAT rainfall and NDVI signal itself. The results indicate the strongest correlation for a weighted mean rainfall for a period of three months before the corresponding NDVI value. Based on these results different mathematical models (linear, logarithmic, arc tangent, etc.) are tested to find a functional relation between the NDVI value and the 3-months rainfall period before (0.8). Finally, the resulting NDVI-Rain-Model can be used to determine a spatially individual correction factor to transform every NDVI-value into an appropriate rain adjusted vegetation index (RAVI).

The resulting RAVI time series is the basis for a comparative long term trend analyses with the original NDVI time series. The results are used to assess the added value of including additional meteorological data (like precipitation) into the process of analysing long term vegetation dynamics.

[1] Osunmadewa, Babatunde A. ; Wessollek, Christine ; Karrasch, Pierre: Identification of long term trends in vegetation dynamics in the guinea savannah region of Nigeria. Proc.

SPIE 9239, Remote Sensing for Agriculture, Ecosystems, and Hydrology XVI, 92390F (October 21, 2014).

[2] Osunmadewa, Babatunde A. ; Wessollek, Christine ; Karrasch, Pierre: Linear and Segmented Linear Trend Detection for Vegetation Cover using GIMMS NDVI data in Semiarid Regions of Nigeria. Journal of applied Remote Sensing (Status: under Review)

[3] Rouse, J. W. ; Haas; R. H. ; Schell, J. A and. Deering, D. W (1973) Monitoring vegetation systems in the Great Plains with ERTS, Third ERTS Symposium, NASA SP-351 I, 309-317.

9644-25, Session 6

The use of UAV to document sloping landscapes to produce digital elevation models to examine environmental degradation

Kyriacos Themistocleous, Athos Agapiou, Cyprus Univ. of Technology (Cyprus); George Papadavid, Michalis Christoforou, Cyprus Univ of Technology (Cyprus); Diofantos G. Hadjimitsis, Cyprus Univ. of Technology (Cyprus)

This paper focuses on the use of Unmanned Aerial Vehicles (UAVs) over the study area of Pissouri in Cyprus to document the sloping landscapes of the area. The study area has been affected by overgrazing, which has led to shifts in the vegetation patterns and changing microtopography of the soil. The UAV images were used to generate digital elevation models (DEMs) to examine the changes in microtopography. Next to that orthophotos were used to detect changes in vegetation patterns. The combined data of the digital elevation models and the orthophotos will be used to detect the occurrence of catastrophic shifts and mechanisms for desertification in the study area due to overgrazing. This study is part of the "CASCADE- Catastrophic shifts in dryland" project.

9644-26, Session 6

Evaluation of multitemporal percent tree cover data for detection of deforestation and forest degradation

Yan Gao, Jean F. Mas, Jaime Paneque-Galvez, Margaret Skutsch, Univ. Nacional Autónoma de México (Mexico)

We evaluated time-series MODIS Vegetation Continuous Fields (VCF) percent tree cover data for the detection of deforestation and forest degradation. The MODIS Vegetation Continuous Field Product (VCF) collection 5 was developed by the University of Maryland. It contains four data sets: percentage tree cover (PTC), quality of the data, percent tree cover standard deviation, and presence/absence of clouds. The VCF PTC is a primary layer which describes the percent of a pixel covered by tree canopy (Townshend et al. 2011). This layer can be used to identify forested areas. To produce the MODIS VCF product, data inputs are a 16 – day surface reflectance composite including MODIS bands 1 – 7 and brightness temperature from MODIS bands 20, 31, 32; the training data; and the MODIS Global 250m Land/Water Map (Townshend et al. 2011). The version 5 MODIS VCF data have spatial resolution of 250m. The detailed description of the algorithm is in Townshend et al. (2011). Until now the data are available from 2000 – 2010 as annual data.

We evaluated the spatial-temporal consistency of MOD44B data for the period of 2000-2010 by a linear regression analysis for each pixel between the tree cover value and the time. Before the analysis, the time series MODIS data were pre-processed by applying quality data layer, from which the pixels with doubtful quality were removed. And then we mapped the correlation coefficient r2, the slope, and the residual of each regression model in order to identify the regions where the percent tree cover value is stable, or has a tendency of increasing or decreasing in a stable way through time.

The map of the correlation coefficient r2 shows that there is poor correlation between forest cover data and the time. In the North of the country, there are some areas with high coefficient values indicating a good fit of both variables with linear regression. On the other hand, the poor correlation could indicate that the data have more variation due to noises making it difficult to detect areas of degradation or vegetation recovery, or the linear regression model is not suitable to represent the change profiles. As for the slope map, the majority of the areas have values close to 0 meaning that there is no important forest cover change during 2000-2010. The west Sierra Madre mountain range has negative slope values indicating that there is a tendency of losing forest cover through time. The same situation is also in parts of the Yucatan Peninsula. There are few areas with high positive slope values, which are mainly concentrated tin eastern Sierra Madre mountain range, some are in western Sierre Madre mountain range, and some are in Yucatan Peninsula. Those areas have clear tendency of increasing in forest cover through time. However, it is important to take into account that this interpretation is valid only for areas with also high correlation coefficient value, since in regression model, the slope map with correlation coefficient close to 0 can indicate abrupt value or not accurate change tendency. The residual map also shows the information of the linear regression. The areas with high residual values could indicate non-linear temporal profile, or noisy data in which the time series data have abrupt values.

9644-27, Session 6

Hazard zone mapping of Kedarnath region using remote sensing and FR method

Hrishabh Gupta, Shashank Bhushan, Jigyasu Agrawal, Indian School of Mines (India)

1. Introduction

Landslides are major mass-wasting processes and landscape building factors in mountainous terrains. They are primarily triggered by earthquake, rainfall, or road construction and cause enormous destruction to properties and lives in those areas.

In study of Landslides, the surface along which the landslide has taken place is banded by well-defined and continuous cracks. This surface is the characteristic feature which can be detected by Landsat imagery and other Remote Sensing sensor.

2. Objectives:

This study aims to use Remote Sensing and Geotechnical soil surveys to prepare a revised landslide hazard zonation map.

3. Study Area:

The area lie within Uttarakhand state. Geographically, the area is situated in the foothills of Siwaliks. The study area falls in the survey of India topographic sheet No. 53 N/2.The study area is located between the latitudes 30° 35? to 30° 45? N, and between longitudes 79° 00?to 79° 10?E.

4. DATA TO BE USED:

- LISS IV
- Topographical Sheet
- Geological Maps
- Landsat Imagery

5. Methodology

1). PREPERATION OF CARTOSAT-1 DEM :

2). PREPERATION OF THEMATIC LAYERS:

1. Geology
2. Land use and Land cover
3. Slope
4. Aspect

5. Relief
6. Soil
7. Rainfall
8. Drainage density
9. NDVI
10. Lineament Density
11. Distance to Roads

3). Preperation of Landslide Inventory Map

Base Map
Slope Map
Aspect map
NDVI Map
Soil Map
Geology Map
Rainfall
Relief Map
Land use and Land Cover Map
Drainage density Map
Lineament Density
Distance from Roads

Database for GIS Analysis:

A digital database for the entire watershed will be generated on 1:25,000 scale. Ten parameters will be mapped in GIS environment, which have been identified for the occurrence of landslide. Those factors will be used to calculate Landslide Susceptibility Index by Frequency Ratio Method (Probability Method) for the whole study area.

Frequency Ratio Method:

The purpose of this study is to produce the landslide susceptibility mapping using the method of frequency ratio (FR). Landslide susceptibility maps will be produced from the frequency ratio.

In general, to predict landslides, it is necessary to assume that landslide occurrence is determined by landslide-related factors, and that future landslides will occur under the same conditions as past landslides (Lee and Talib, 2005).

The frequency ratio is the ratio of the area where landslides occurred in the total study area, and also is the ratio of the probabilities of a landslide occurrence to a non-occurrence for a given attribute.

First the frequency ratio was calculated for each range or type of factor, the frequency ratios were than summed to calculate the landslide susceptibility index (LSI).

$LSI=\sum FR$

The frequency ratio method is very easy to apply, and results obtained by Lee and Talib (2005), are very intelligible. The susceptibility map will be drawn to include a classification which will be divided into several categories. The higher the LSI (Landslide Susceptibility Index), the more susceptible is the corresponding combination of factors to landslide.

9644-28, Session 6

Developing a sustainable satellite-based environmental monitoring system In Nigeria

Joseph O. Akinyede, The Federal Univ. of Technology, Akure (Niger); K. A. Adepoju, Obafemi Awolowo Univ. (Nigeria); Francis O. Akinluyi, A. Y. B. Anifowose, Federal Univ. of Technology, Owerri (Nigeria)

Increased anthropogenic activities over the year have remained a major factor of the Earth changing environment. This phenomenon has given rise to a number of environmental degraded sites that characterize the Nigeria's landscape. The human-induced elements include gully erosion, mangrove ecosystems degradation, desertification and deforestation, particularly in the south east, Niger Delta, north east and south west of Nigeria respectively, as well as river flooding/ flood plain inundation and land degradation around Kainji lake area. Because of little or no effective management measures, the attendant environmental hazards have been extremely damaging to the infrastructures and socio-economic development of the affected area. Hence, a concerted effort, through integrated and space-based research, is being intensified to manage and monitor the environment in order to restore the stability, goods and services of the environment.

This has justified Nigeria's investment in its space programm, especially the launch of NigeriaSat-1, an Earth observation micro-satellite in constellation with five (5) other similar satellites, Alsat-1, China DMC, Bilsat-1, DEMOS and UK DMC belonging to Algeria, China, Turkey, Spain and United Kingdom respectively. The use of data from these satellites, particularly NigeriaSat-1, in conjunction with associated technologies such as Geographic Information System (GIS) and Global Positioning System (GPS) has proved to be very useful in understanding the influence of both natural and human activities on the Nigeria's ecosystems and environment. The ability to obtain bulk and timely data over extensive areas with short repetitive cycles and comparative analysis with Landsat data has made NigeriaSat-1 particularly versatile and useful for these studies and for geoinformation-based environmental monitoring in Nigeria. The results of the researches on predictive modeling of gully erosion in south eastern Nigeria, deforestation and its implications on biodiversity, mangrove ecosystems degradation in the Niger delta, development of models for desertification early warning in north eastern Nigeria and water resources management and ecosystems degradation around Kainji lake area are presented in this paper. Appropriate sustainable land and water resources management in the affected areas, based on Nigeria's satellite data capture and integration, are also discussed.

9644-29, Session 6

Estimation of evapotranspiration in Mongolian steppe area of Mongolia combining satellite and ground data

Sanjaa Tuya, Nas-Urt Tugjsuren, Mongolian Univ. of Science and Technology (Mongolia); Jadamba Batbayar, National Agency of Meteorology and Environmental Monitoring (Mongolia); Battumur Azzaya, Mongolian Univ. of Science and Technology (Mongolia)

This Evapotranspiration (ET) is one of the most important elements in water cycle, especially in arid and semi arid area. In order to research the water cycle, it is important to quantify the amount evapotranspiration. In this study, we proposed MODIS and weather station data for seasonal changes of evapotranspiration in year 2008- 2013 was investigated. The remote sensing estimated ET was imported into geographic information systems (GIS) for further spatial analysis and mapping, in combination with land use and other ancillary data. Ancillary GIS data were also used in the quality control process to ensure accepted accuracy. It is expected that this technique and the resulting ET maps will assist us to monitor the effects of ground water management on the water uses and the indicative health of these terrestrial groundwater ecosystems.

9644-30, Session 7

The use of UAVs for remote sensing applications: case studies in Cyprus

Kyriacos Themistocleous, Cyprus Univ. of Technology (Cyprus); Athos Agapiou, Vasiliki Lysandrou, Cyprus Univ of Technology (Cyprus); Diofantos G. Hadjimitsis, Cyprus Univ. of Technology (Cyprus)

Unmanned aerial vehicles (UAVs) for use in remote sensing offer simple and affordable observation from the air. Due to

the decreasing size of the sensors, receivers and antennas, it is now possible to create an integration in a low-altitude airborne system. Remote sensing technologies on a UAV platform are an efficient, non-evasive and low cost resource for the detection and monitoring of environmental features. Different remote sensing techniques can be used with UAVs, such as field spectroscopy, multi-spectral cameras, infrared cameras and thermal cameras. A variety of sensors can be added to the basic UAV unit. Among the types of camera sensors that can be used with the UAVs are visible spectrum cameras, multi-spectral cameras and hyperspectral cameras. These cameras can extract more detailed information as an entire spectrum is acquired in each pixel in the image.

In this paper, various UAVs, including gliders, quadcopters, octocopters and balloons, were used for remote sensing applications in different areas of Cyprus. The UAVs used in this study were equipped with sensors, including cameras and spectroradiometers. The paper examines the benefits and limitation of each type of UAV platform used.

9644-32, Session 7

Estimation of regional-scale forest resources using ICESat/GLAS spaceborne lidar

Masato Hayashi, Nobuko Saigusa, Habura Borjigin, Yoshito Sawada, Yoshiki Yamagata, National Institute for Environmental Studies (Japan); Takashi Hirano, Hokkaido Univ. (Japan); Kazuhito Ichii, Japan Agency for Marine-Earth Science and Technology (Japan) and National Institute for Environmental Studies (Japan)

The demand of forest resources monitoring technology for understanding the carbon cycle processes on a large scale, namely, from regional to global scale, is growing recently. Spaceborne LiDAR can observe vertical structure of forests, therefore, it is expected to provide a means for accurate monitoring. This study aims to clarify the potential of ICESat/GLAS, which had been the only spaceborne LiDAR up to now, for forest resources monitoring on a regional scale. The study areas were two islands: Hokkaido Island in Japan (cool-temperate forest) and Borneo Island (tropical forest). Firstly, we conducted field measurements at 106 points in Hokkaido and 37 points in Borneo, which were coincident with the GLAS footprints. We measured tree height and diameter at breast height (DBH) for each tree chosen by the Bitterlich sampling method, then, calculated the average canopy height (Lorey's height) and the above-ground biomass (AGB) for each footprint. Next, we developed some models to estimate canopy height and AGB from the GLAS waveform parameters for each of Hokkaido and Borneo based on the field measurement data. As a result of cross-validation, the root-mean-square error (RMSE) of the canopy height estimation model was 3.8 m for both study areas, and the RMSE of the AGB estimation models was 41.2 Mg ha-1 for Hokkaido, and 38.7 Mg ha-1 for Borneo. Next, we applied the developed models to the GLAS data which were 13,774 points in Hokkaido, and 127,862 points in Borneo, to estimate canopy height and AGB on a regional scale. The average canopy height (± standard deviations) was 17.8 ± 4.3 m in Hokkaido, and 16.2 ± 8.5 m in Borneo. The average AGB was 119.4 ± 49.5 Mg ha-1 in Hokkaido, and 190.2 ± 131.6 Mg ha-1 in Borneo. These results suggest that the tropical forest in Borneo have a higher biomass and a greater dynamic range of forest resources than the cool-temperate forest in Hokkaido. Furthermore, we calculated the average canopy height and AGB for each forest type. In the Hokkaido forest, the difference in canopy heights among forest types was small, however, there was a large difference in AGBs, and the evergreen coniferous forest had the highest biomass. In the Borneo forest, there were large differences in both canopy height and AGB among forest types, and they were correlated. The evergreen broad-leaved forest had the highest biomass, which was almost twice as large as that of the mangrove forest. This study showed that spaceborne LiDAR had an ability of forest resources monitoring on a regional scale for both cool-temperate and tropical forests. Additionally, we apply the methodology of this study to the entire region of Siberia, and estimate the forest resources using GLAS data. In Siberia, the vegetation index of satellite imagery has shown an increasing trend in recent years. The GLAS data analysis will reveal the causes of this trend, as to whether the forest biomass or the undergrowth area increases.

9644-33, Session 8

Quality evaluation of different fusion techniques applied on Worldview-2 data

Aristides D. Vaiopoulos, National Technical Univ. of Athens (Greece); Konstantinos G. Nikolakopoulos, Univ. of Patras (Greece)

In the current study a Worldview-2 image was used for the fusion quality assessment. The bundle image was collected on July 2014 over Araxos area in Western Peloponnese. Worldview-2 is the first satellite that collects at the same time a panchromatic (Pan) band and 8 multispectral (MS) band. The Pan data have a spatial resolution of 0.46m while the MS data have a spatial resolution of 1.84m. In contrary to the respective Pan band of Ikonos and Quickbird that range between 0.45 and 0.90 micrometers the Worldview Pan band is narrower and ranges between 0.45 and 0.8 micrometers. The MS bands include four conventional visible and near-infrared bands common to multispectral satellites like Ikonos Quickbird, Geoeye Landsat-7 etc., and four new bands. Thus, it is quite interesting to investigate the assessment of the common used fusion algorithms with Worldview-2 data. Twelve fusion techniques and more especially the Ehlers, Gram-Schmidt, Color Normalized, High Pass Filter, Hyperspherical Color Space, Local Mean Matching (LMM), Local Mean and Variance Matching (LMVM), Modified IHS (ModIHS), Pansharp, Pansharp2, PCA and Wavelet were used for the fusion of Worldview-2 panchromatic and multispectral data. The optical result, the statistical parameters and different quality indexes such as ERGAS, Q and entropy were examined and the results are presented. The quality control was performed both in spectral and spatial domain.

9644-34, Session 8

Superpixel-based active learning classification of endemic species of Teide National Park

Angel M. García-Pedrero, Consuelo Gonzalo Martín, Univ. Politécnica de Madrid (Spain); Dionisio Rodriguez Esparragón, Univ. de Las Palmas de Gran Canaria (Spain); Mario F. Lillo-Saavedra, Univ. de Concepción (Chile); Francisco Javier Marcello Ruiz, Univ. de Las Palmas de Gran Canaria (Spain)

The Teide National Park (TNP), located in the island of Tenerife (Canary Islands, Spain), presents not only an outstanding geological value but also an extraordinary biodiversity formed by unique species of invertebrates and a large number of endemic plants, adapted to the extreme altitude conditions of the park (a volcanic caldera at 2,000 meters altitude and above, with its 3,718-meters summit). These exceptional natural values led the Spanish government to protect this area (18,990 ha.) under National Park considerations in 1954.

58 endemic plants have been described in the park, including Pino Canario (Pinus canariensis), Rosalillo de Cumbre (Pterocephalus lasiospermus), Retama del Teide (Cytisus supranubius), and Hierba Pajonera (Descurainia bourgaena). All of them are of great importance for sustainability of the flora and fauna in the park. This is the reason why the identification and tracking of the evolution of the population of these species becomes a relevant issue for those responsible for the management and conservation of the park.

Currently, experts identify these vegetative species through

field campaigns. During this process, the area of the park is divided into a grid and each square (4 ha.) is labeled according to the prevalent specie in the area. This process is unreliable because it suffers from subjectivity, and is highly time-consuming; moreover the repeatability of the labeling is not ensured. Since high-resolution satellite images provide information on the spatial distribution of the species at a suitable spatial resolution, they seem to be a good source of data; which in combination with the usual remote sensing approaches may be able to avoid the aforementioned problems.

However, preliminary studies point out that current classification methods, both pixel-based and object-based, tend to fail due to the small size and highly sparse spatial distribution of the species under analysis. Another problem is that most of the time two species can coexist in the same area, one over the other, generating mixed classes. Therefore, alternative remote sensing methods should be investigated.

In this work, the potential of superpixels combined with active learning (AL) is exploited to analyze a WorldView-2 image of the TNP. First, superpixels are able to provide an image representation (segmentation) similar to the grid used by TNP managers, but its shape is adjusted according to the spectral similarity of the surrounding pixels. The superpixels technique is capable of decreasing the number of noisy pixels, which reduce classification performance, as well as the total number of instances to process. Second, AL allows interaction between the expert and the classifier: the first provides labeled information and knowledge about the desired classes, while the latter provides both its own interpretation of the distribution of the classes and the most relevant observations that are needed in order to solve the discrepancies encountered. This reduces the uncertainty in areas where it is not possible to automatically distinguish one class from another, as happens in areas where two species coexist. To facilitate the AL process an interactive GIS tool has been developed to support the labor of the TNP managers.

9644-35, Session 8

Karst features detection and mapping using airphotos, DSMs and GIS techniques

Maria Kakavas, Konstantinos G. Nikolakopoulos, Helen Zagana, Univ. of Patras (Greece)

Remote sensing data has been used in karst studies to identify limestone terrain, describe exokarst features, analyze karst depressions, and detect geological structures important to karst development. The aim of this work is to detect and qualify natural karst depressions in the Aitoloakarnania Prefecture, Western Greece, using remote sensing in conjunction with the Geographical Information Systems - GIS. The study area is a part of the Ionian geotectonic zone, and its geological background consists of the Triassic Evaporates. The Triassic carbonate breccias where formed as a result of the tectonic and orogenetic setting of the external Hellenides and the diaper phenomena of the Triassic Evaporates. The landscape characterized by exokarst features closed depressions in the Triassic carbonate breccias. At the threshold of this study, an in situ observation was performed in order to identify dolines and swallow holes, many of which contain standing water. The creation of sinkholes, in general, is based on the collapse of the surface layer due to chemical dissolution of carbonate rocks. In the current study airphotos stereopairs, DSMs and GIS were combined in order to detect and map the karst features. Thirty seven airphotos were imported in Leica Photogrammetry Suite and a stereo model of the study area was created. Then in 3D view possible karst features were detected and digitized. Those sites were verified during the in situ survey. ASTER GDEM and SRTM DEM were also evaluated in GIS environment for the automatic detection of the karst depressions. The results are presented in this study.

9644-36, Session 8

High-spatial resolution multispectral and panchromatic satellite imagery for mapping perennial desert plants

Saad Alsharrah, David Bruce, Univ. of South Australia (Australia); Rachid Bouabid, Ecole Nationale d'Agriculture de Meknès (Morocco); Sekhar Somenahalli, Univ. of South Australia (Australia); Paul Corcoran, University of South Australia (Australia)

The use of remote sensing techniques to extract vegetation cover information used in the assessment and monitoring of land degradation in arid and semi-arid environments has gained increased interest in recent years. However, such a task can be challenging, especially for medium spatial resolution satellite sensors, due to soil background effects, the distribution and structure of perennial desert vegetation. Perennial vegetation cover in desert environments is typically small in size and sparse in distribution; this leads to small contributions of vegetation reflectance in the total pixel reflectance relative to the other more dominant materials such as soils. Many methods in remote sensing are insensitive to non-photosynthetic xerophytic vegetation and most classification techniques are applied to low to medium resolution multispectral imagery. This is possibly satisfactory for regional or global level assessment. However, such approaches struggle to provide reliable information at the local scale. In our study, we utilised Pleiades high-resolution multispectral (2m) and panchromatic (0.5m) imagery and focused on three classification techniques: 1) vegetation index (VI) threshold analysis, 2) object oriented classification, and 3) contextual reclassification. We calculated and analysed different thresholds for six vegetation indices (NDVI, SAVI, MSAVI-2, TSAVI, PVI-3 and PD-54) and evaluated their success using a RMS error algorithm, which incorporated field data as control. Four error measures were introduced relating to commonality, omission, percent cover and plant density. The algorithm was used to assess the performance of the VIs across two study sites in the southern Atlas Mountains in Morocco. Results showed that MSAVI2 performed best out of the six VIs. However, the threshold analysis for all VIs lead to errors of commission and omission. Optimum performers returned good vegetation cover estimates at certain thresholds, but failed to accurately map the distribution of the desert plants. Using an object oriented classification approach, we improved the vegetation distribution mapping accuracy, but this came at the cost of a higher error of commission, similar to results of lowering VI thresholds. Associating vegetation shadow with the object oriented classification approach improved the results slightly, but failed to map smaller shrubs with shadows hard to detect in the multispectral pixels. We further introduced a contextual reclassification approach where the panchromatic image was integrated with our optimum vegetation classification to further refine the accuracy. The approach involved classifying shadow from the panchromatic image using an object oriented approach and resampling the vegetation cover layer derived from the multispectral image to match the panchromatic resolution. We then implemented a filter that returned each vegetation pixel that was associated with a shadow pixel from the panchromatic image. The results showed significant improvements in vegetation cover and distribution accuracy compared to the other techniques. We argue that a contextual reclassification approach using higher spatial resolution imagery provides a more accurate representation of the desert landscape and should be considered in assessments for land degradation. Although, the current economic feasibility might be a limiting factor, high resolution images can act as accuracy assessors for land degradation studies using low to medium resolution satellite imagery.

9644-37, Session 9

Feature extraction for change analysis in SAR time series

Markus Boldt, Fraunhofer-Institut für Optronik, Systemtechnik und Bildauswertung (Germany); Antje Thiele, Fraunhofer-Institut für Optronik, Systemtechnik und Bildauswertung (Germany) and Karlsruher Institut für Technologie (Germany); Karsten Schulz, Fraunhofer-Institut für Optronik, Systemtechnik und Bildauswertung (Germany); Stefan Hinz, Karlsruher Institut für Technologie (Germany)

In remote sensing, the change detection topic represents a broad field of research. If time series data is available, change detection can be used for monitoring applications. These applications require regular image acquisitions at identical time of day along a defined period. Focusing on remote sensing sensors, radar is especially well-capable for applications requiring regularity. In contrast to sensor systems operating in the visual part of the electromagnetic spectrum and due to its active sensing character, radar combines some significant advantages. Since radar uses microwaves operating with a wavelength much longer than the visible light, it is independent from most weather and atmospheric influences (fog, dust, clouds etc.). Furthermore, for planning the image acquisitions, the time of day does not matter.

Since 2007, the German SAR (Synthetic Aperture Radar) satellite TerraSAR-X (TSX) permits the acquisition of high resolution (HR) images. The high resolution SpotLight mode (HS300), for example, delivers imagery with a pixel spacing of 0.45 m (range) and 0.86 m (azimuth) which is useable for applications analyzing dense built-up areas.

In our former study, the change analysis of the Stuttgart (Germany) airport area using a time series of HS300 TSX images covering a period of approximately on year has been presented [1]. The aim of this study is given by the categorization of detected changes. The categorization is motivated by the fact that it is a poor statement only to describe where and when a specific area has changed. For a comprehensive interpretation of the detected changes, it is important to describe what has caused the change event.

In this paper, the focus is set on the analysis of so-called high activity areas (HAA) representing areas changing at least three times along the investigated period. Examples for HAAs are parking areas or parking slots, construction sites and embark points. As a first step for categorizing these HAAs, the matching HAA changes (blobs) have to be identified. Afterwards, operating in this object-based blob level, several features are extracted for each high activity (HA) blob. These features comprise shape-based, radiometric, statistic and morphological values as well as spatial context. The context feature bases on the segmentation of the HAAs. This segmentation [2] builds on the pixelwise calculation of morphological differential attribute profiles (DAPs) in the HAAs. As DAP attributes, the SAR specific parameters normalized radar cross section (NRCS) “sigma nought” and the coefficient of variation (Cov) are used.

Five classes for describing the spatial context are established: Forest, urban, infrastructure, rural and water. The specific HA blob is assigned to one of these classes analyzing the CovAmCoh [3] time series signature of the surrounding segments. In combination, also surrounding GIS information is included to verify the CovAmCoh based context assignment. In the presented case, OpenStreetMap (OSM) layers are used, comprising for example landuse, natural, roads and waterways.

In summary, in this paper, the features and their blob-based extraction are explained. Here, the focus is set on the segmentation-based context feature and the assignment of HA blobs to the five pre-defined classes.

[1] Boldt, M., Thiele, A., Cadario, E., Schulz, K., Hinz, S.: “Change Analysis at Stuttgart Airport using TerraSAR-X Imagery”, Proceedings of SPIE Vol. 9245, Earth Resources and Environmental Remote Sensing/GIS Applications V, pp. 924502-1 – 924502-8, 2014.

[2] Boldt, M., Thiele, A., Schulz, K., Hinz, S.: “SAR Image Segmentation Using Morphological Attribute Profiles“, The International Archives of the Photogrammetry, Remote Sensing and Spatial Information Sciences, Vol. XL-3, ISPRS Technical Commission III Symposium, pp. 39 – 44, 2014.

[3] Schulz, K., Boldt, M., Even, M.: “Generalization of the CovAmCoh Analysis for the Interpretation of Arbitrary InSAR Images”, Proceedings of the International Geoscience and Remote Sensing Symposium IGARSS 2012, Munich (Germany), pp. 7444 – 7447, 2012.

9644-38, Session 9

Updating road databases from shape-files using aerial images

Gisela Häufel, Dimitri Bulatov, Melanie Pohl, Fraunhofer-Institut für Optronik, Systemtechnik und Bildauswertung (Germany)

Road databases are an important part of geo data infrastructure. The knowledge about their characteristics and course is essential for urban planning, navigation or evacuation tasks.

Due to the progress of sensor technology, there is a huge amount of sensor data of urban terrain. All over the world, mapping organizations use various sensor types for urban terrain reconstruction, and, in particular, for road data extraction.

To improve existing street maps, we introduce an algorithm to enrich the available road maps by results obtained from evaluation of sensor data. As an example, we use free vector data distributed by the OpenStreetMap (OSM) community and the proposed workflow is tested with data covering the area of a village Bonnland in Southern Germany. Depending on the environment, these shape-files sometimes do not contain minor roads, such as dead-end streets or narrow passages. With road networks generated from aerial images or LIDAR data by means of classification, skeletonization and filtering algorithms [1], the original geodatabase can be updated. While the case of two equally or arbitrarily weighted data sets will be considered in our future work, in this paper, we consider a hierarchical case: road segments from the shape-file are supposed to be error-free.

Road segments are given as 2D polylines with additional attributes, such as length, width, main direction, and others. Within preprocessing, road segments obtained by our sensor data processing algorithm are straightened by a modified generalization algorithm. Due to the thinning of the segmentation results, road segments bordering trees, buildings, or vehicles cause a roughly frayed roadside and therewith a wriggled street course that shall be adjusted.

The main procedure consists of three steps. After transformation of the roads from the geodatabase and from our procedure into a common coordinate system, in the first step, we check whether the bounding boxes formed by road segments from different data sets overlap. This allows a subdivision of the entire data into three categories:

- Road segments in the shape-file that are not detected in our procedure.

- Road segments that are detected by our procedure but are not given in the shape-files.

- Road segments that are given in both data sets with a similar but not identical course.

Secondly, since road segments from the shape-file are considered as error-free, those road segments acquired from sensor data which belong to the third category can be deleted. In the third step, we care about the neighbors of the deleted street, where neighborhood is defined by common junctions. These junctions now have to lie on the road segments belonging to the shape- file. Their exact position is given by the street attributes and the results of the classification. The procedure generating the junctions leads to prolongations or cuttings of neighbored roads. Roads which were not connected during the process are attached. The output is the updated

road course and the updated shape-file.

[1] D. Bulatov, M. Ziems, F. Rottensteiner, M. Pohl," Very fast road database verification using textured 3D city models obtained from airborne imagery", Proc. SPIE 9244, Image and Signal Processing for Remote Sensing XX, 92440T (October 23, 2014) pp. 92440T-1 - 92440T-11

9644-39, Session 9

Future prediction of urban growth in OMR (IT expressway of Chennai) by using Markov Chain approach

Kiran N. S., Anna Univ. (India)

The spatial planning is a challenging task when it comes to mega cities like Chennai due to rapid population shifts that has occurred over the recent years and is still in the run. This study approach involves the urban modelling of the IT Expressway of Chennai city (OMR) using Markov-Chain model for predicting the future urban expansion. This OMR is a 27 kilometre stretch starting from Madhya Kailash to Kelambakkam and it was considered because we have experienced unprecedented growth over the past years. The study aims to foresee the pattern of urban growth after detecting the landuse/landcover changes with the help of Remote Sensing and Geographic Information System. Moreover, urban infill developments are expected to emerge in the southern regions, and these developments are expected to increase urban pressure. Markov-Chain is one of the most accepted method for modelling the urban growth using current trends. The probabilities are generated from past changes and then applied to predict future change. The landuse maps have been prepared for the years2006, 2009, 2014 and the expected transition for OMR by 2020 is generated.The urban map prepared is useful for the references by state administrations involved in urban planning and management.

9644-41, Session 9

Effect of land cover and green space on land surface temperature of a fast growing economic region in Malaysia

Afsaneh Sheikhi, Kasturi D. Kanniah, Univ. Teknologi Malaysia (Malaysia); Chin Siong Ho, Univ Teknologi Malaysia (Malaysia)

Development of cities has led to various environmental problems, such as increased air temperature, air pollution, and global climate change. In order to make cities as a livable environment, green space must be increased in the development of new cities. Among the services provided by green space include sequestrating and storing excessive CO2 from the atmosphere and moderating high temperature in the cities. The objective of this study was to estimate the land surface temperature (LST), examine the spatial pattern of land-covers and establish relationships between LST and land cover and various vegetation and urban surface indices in the Iskandar Malaysia (IM) region. IM is one of the emerging economic gateways of Malaysia, and is envisaged to transform into a metropolis by 2025. This change may result the region to expose to higher temperature and other environmental problems. To accomplish the goal of this study, several scenes of Landsat images covering the study region (2,217km2) for years 2000, 2005, 2007, and 2013 were used to estimate LST, classify different land cover/land use classes (using maximum likelihood (MLC) and support vector machine (SVM) classification techniques)) and vegetation/urban surface indices (Normalized Difference Vegetation Index (NDVI), Normalized Difference Water Index (NDWI) and normalized difference built-up Index (NDBI)). Results of classification shows that MLC performed better than SVM and therefore six land cover classes obtained using MLC were used to establish relationships between LST and land cover types in IM. A clear relationship between the land cover/land use patterns and LST was obtained where higher mean temperatures were obtained for urban surface (24.0 to 26.8°C) in all years investigated in this study. The lowest temperature was recorded in water bodies, mangroves and forest ecosystems (20.8 to 24.1 °C). Rubber and oil palm areas showed intermediate values (21.1 to 24.6°C). An increase in LST was found for urban surface from 24.0°C in 2000 to 26.8 °C in 2013. A similar patterns in LST was also found for other land cover classes and the increase was between 1.73 °C (rubber) and 3.53 °C (oil palm). Higher temperature recorded in built areas can be attributed to the presence of materials that absorb solar radiation and absence of dense vegetated areas and water bodies. We further investigated the relationship between vegetation and build up densities with temperature. We extracted 100 collocated pure pixels of NDVI, NDWI, NDBI and LST in the study area. Results show a strong and significant ($p<0.001$) negative correlation ($R2= 0.71$) between NDVI and NDWI and LST respectively. Meanwhile a strong positive correlation ($R2=0.52$) exists between NDBI and LST. These results indicate that increasing vegetation density can decrease the LST, while increasing built up areas could lead to increasing temperatures. These results show the importance of increasing green cover in urban environment to combat any adverse effects of climate change. In our future study we aim to predict the future LST in IM in 2025 based on land cover changes.

9644-42, Session 9

Integrated method of water column correction technique for satellite-based benthic habitats mapping

Pramaditya Wicaksono, Projo Danoedoro, Hartono Hartono, Univ. Gadjah Mada (Indonesia)

The issue of benthic habitats mapping is the environmental restriction, which limits the ability of remote sensing data to properly map these habitats. We presented an integrated method to minimize the effect of water column on spectral values of benthic habitats during the mapping. The proposed method integrated the depth of each pixel, the water column attenuation coefficient for each band (k), and the reflectance of pure optically deep water, to model the bottom reflectance. Kemujan Island was selected as the study area and Quickbird image was used to test the method. These parameters were derived empirically by integrating field measurement data and image pixel values. The water column corrected bands were then used to classify benthic habitats at three levels of benthic habitats classification schemes based on ecological and spectral perspective, to test the effectiveness of the method as the level of class complexity increases. Per-pixel classification algorithm with knowledge-based image segmentation was used to classify benthic habitats. In addition, we compared the benthic habitats classification accuracy from the integrated method with the accuracy from water depth invariant bottom index (DII) and Principle Component Analysis (PCA). The results showed that the integrated method managed to minimize major noises due to water column effect up to the maximum depth of penetration (DOP) of each band. Bands produced by integrated method produced 52.04%, 47.36%, and 33.68% overall accuracy for 5, 7, and 13 benthic habitats class complexity respectively. These accuracies were slightly lower than the accuracy from DII or PC bands due to the sensitivity of the method to the accuracy of the modelled bathymetry data and water column attenuation coefficient. Nevertheless, the integrated method performed well on the most detailed and complex classification scheme.

Conference 9645: Lidar Technologies, Techniques, and Measurements for Atmospheric Remote Sensing

SPIE. REMOTE SENSING

Tuesday - Wednesday 22–23 September 2015

Part of Proceedings of SPIE Vol. 9645 Lidar Technologies, Techniques, and Measurements for Atmospheric Remote Sensing XI

9645-1, Session 1

Double-pulsed 2-micron IPDA lidar validation for atmospheric CO2 measurements *(Invited Paper)*

Upendra N. Singh, Tamer F. Refaat, Jirong Yu, Mulugeta Petros, Ruben G. Remus, NASA Langley Research Ctr. (United States)

A double-pulsed, 2-μm Integrated Path Differential Absorption (IPDA) lidar instrument for atmospheric carbon dioxide (CO2) measurements is successfully developed at NASA Langley Research Center (LaRC). Based on direct detection technique, the instrument can be operated on ground or onboard a small aircraft. Key features of this compact, rugged and reliable IPDA lidar includes high transmitted laser energy, wavelength tuning, switching and locking, and sensitive detection. As a proof of concept, the IPDA ground and airborne CO2 measurement and validation will be presented. IPDA lidar CO2 measurements ground validation were conducted at NASA LaRC using hard targets and a calibrated in-situ sensor. Airborne validation, conducted onboard the NASA B-200 aircraft, included CO2 plum detection from power stations incinerators, comparison to in-flight CO2 in-situ sensor and comparison to air sampling at different altitude conducted by NOAA at the same site. Airborne measurements, spanning for 20 hours, were obtained from different target conditions. Ground targets included soil, vegetation, sand, snow and ocean. In addition, cloud slicing was examined over the ocean. These flight validations were conducted at different altitudes, up to 7 km, with different wavelength controlled weighing functions. CO2 measurement results agree with modeling conducted through the different sensors, as will be discussed.

9645-2, Session 1

Atmospheric CO2 remote sensing system based on high brightness semiconductor lasers and single photon counting detection

Antonio Perez-Serrano, Maria Fernanda Vilera Suárez, Ignacio Esquivias, Univ. Politécnica de Madrid (Spain); Mickael Faugeron, Michel Krakowski, Frédéric van Dijk, III-V Lab. (France); Gerd Kochem, Martin Traub, Fraunhofer-Institut für Lasertechnik (Germany); Pawel Adamiec, Juan Barbero, Alter Technology (Spain); Xiao Ai, John G. Rarity, Univ. of Bristol (United Kingdom); Mathieu Quatrevalet, Gerhard Ehret, Deutsches Zentrum für Luft- und Raumfahrt e.V. (Germany)

The availability of suitable laser sources is one of the main challenges in future space missions for accurate measurement of atmospheric CO2. We propose an all-semiconductor laser source for an Integrated Path Differential Absorption (IPDA) lidar system for column-averaged measurements of atmospheric CO2 in future satellite missions. Standard IPDA systems use high peak power optical pulses at two sounding frequencies to calculate the column averaged gas concentration. Semiconductor lasers are superior to other types of lasers in terms of reliability, compactness and efficiency, but they cannot provide the high peak power required by the application. In consequence, the complete system architecture has to be adapted to the particular emission properties of these devices.

The Random Modulated Continuous Wave (RM-CW) approach has been selected as the best suited to semiconductor lasers. In a RM-CW lidar, a Pseudo-Random Binary Sequence (PRBS) is transmitted to the atmosphere. The received signal from the target correlated with the original PRBS gives a range resolved response with a non-ambiguous range determined by the number of PRBS bits (repetition rate) which can be extended further than the trip time corresponding to the atmosphere thickness. The auto-correlation property of the PRBS and the temporal shifting of the codes can be used to transmit both wavelengths simultaneously, which avoids the beam misalignment problem. The ratio between the cross-correlation intensities of the reference output and received signals provides information about the differential absorption optical depth and hence on the dry air mixing ratio of CO2.

The transmitter design is based on two monolithic Master Oscillator Power Amplifiers (MOPAs), providing the ON and OFF wavelengths close to the selected CO2 absorption line around 1.57 μm. Each MOPA consists of three sections: a frequency stabilized Distributed Feedback (DFB) master oscillator, a bent modulator section and a tapered amplifier. The use of this original structure aims to fulfill the performances required by the IPDA system in terms of high power, frequency stability and good beam quality. The DFB section is accurately frequency stabilized by an external opto-electrical feedback loop through the frequency stabilization unit. The modulator section is introduced for implementation of the RM-CW technique in the proposed IPDA system. Finally, the geometry of the tapered SOA is optimized in order to provide high brightness output beam with sufficient power and beam quality. More than 400 mW ouput power with a SMSR higher than 45 dB and stable emission have been demonstrated.

On the side of the receiver, our modeling and simulations indicate that the major noise contribution comes from the ambient light. For this reason narrow band optical filters are used in the detection together with high sensitivity and low noise single photon counting techniques. The receiver is composed of a Cassegrain telescope, a negative feedback avalanche detector, a short wave infrared camera for alignment and an integrating sphere for beam homogenization.

In this contribution, we present the latest progresses regarding the design, modelling and characterization of the transmitter, the receiver, the frequency stabilization unit and the system.

9645-3, Session 1

Advanced intensity-modulation continuous-wave lidar techniques for ASCENDS CO2 column measurements

Joel F. Campbell, Bing Lin, Amin R. Nehrir, Fenton W. Harrison, Michael D. Obland, Byron L. Meadows, NASA Langley Research Ctr. (United States)

Global atmospheric carbon dioxide (CO2) measurements for the NASA Active Sensing of CO2 Emissions over Nights, Days, and Seasons (ASCENDS) space mission are critical for improving our understanding of global CO2 sources and sinks. Advanced Intensity- Modulated Continuous-Wave (IM-CW) lidar techniques are investigated as a means of facilitating CO2 measurements from space to meet the ASCENDS measurement requirements. In recent numerical, laboratory and flight experiments we have successfully used the Binary Phase Shift Keying (BPSK) modulation technique to uniquely discriminate surface lidar returns from intermediate aerosol and cloud contamination. We demonstrate the utility of BPSK to eliminate sidelobes in the range profile as a means of making Integrated Path Differential Absorption (IPDA) column CO2 measurements in the presence of optically thin clouds, thereby eliminating the need to correct for sidelobe bias errors caused by the clouds. Furthermore, high accuracy and precision ranging to the surface as well as to the top of intermediate cloud layers, which is a requirement for the inversion of column CO2 number density measurements to column CO2 mixing ratios, has been

demonstrated using new hyperfine interpolation techniques that takes advantage of the periodicity of the modulation waveforms. This approach works well for both BPSK and linear swept-frequency modulation techniques. The BPSK technique under investigation has excellent auto-correlation properties while possessing a finite bandwidth. A comparison of BPSK and linear swept-frequency is also discussed in this paper. These results are extended to include Richardson-Lucy deconvolution techniques to extend the resolution of the lidar beyond that implied by limit of the bandwidth of the modulation, where it is shown useful for making tree canopy measurements.

9645-4, Session 1

Developing the CO2 Sounder Lidar as a candidate for the ASCENDS Mission: an update

James B. Abshire, NASA Goddard Space Flight Ctr. (United States); Anand K. Ramanathan, Univ. of Maryland, College Park (United States); Haris Riris, NASA Goddard Space Flight Ctr. (United States); Graham R. Allan, Sigma Space (United States); Jeffrey R. Chen, Anthony W. Yu, Xiaoli Sun, NASA Goddard Space Flight Ctr. (United States)

The CO2 lidar on NASA's ASCENDS mission will measure atmospheric CO2 column absorption and range, allowing calculation of the atmospheric CO2 mixing ratio needed for flux estimates. The ASCENDS mission will permit, for the first time, accurate atmospheric CO2 concentration measurements to be made globally over a wide range of conditions. These include at those night, at high latitudes during all seasons, through hazy and thin cloud conditions and to cloud tops.

The CO2 Sounder is one candidate lidar approach for the ASCENDS mission. The CO2 Sounder team has demonstrated their airborne lidar on flights since 2008, including ones onboard the NASA DC-8 during 2011, 2013 and 2014. The results show that airborne measurements made in 2011 and 2013 were accurate to ~1 ppm for airborne altitudes between 6 and 12 km. Analysis also highlighted a new capability to measure CO2 column absorption and range both to cloud tops and the ground. Differencing the retrievals allows estimating the CO2 in the column between the ground and cloud top, which allows a direct estimate of the CO2 concentrations in the boundary layer. For the 2014 airborne campaign, the CO2 Sounder team incorporated several new capabilities into the airborne lidar, including a step-locked laser source and sensitive HgCdTe APD detector. Airborne measurements of column CO2 concentration and range were made over the California Central Valley, the redwood forests along the northern California coast, and above growing agriculture in Iowa.

The CO2 Sounder team has also made significant progress in developing of the CO2 Sounder approach and laser technologies for the space-based ASCENDS lidar. An important capability is using wavelength distributed sampling the CO2 absorption line near 1572 nm using 8 or more wavelengths, which allows for control of potential biases, accurate retrievals, and solving for CO2 vertical gradients. The project has also demonstrated most key technology elements needed for the space lidar, including a new step-locked laser diode source and a high power fiber laser amplifier stage. The high power fiber amplifier is based on an EDFA and has demonstrated over 350 uJ/pulse energies at 1572 nm. Work is underway to demonstrate a rugged packaged laser that emits the space-required energy of > 2 mJ/pulse. The new HgCdTe APD detector was also developed in collaboration with DRS RSTA. Laboratory tests and the 2014 flight campaign showed it has highly linear analog response with wide dynamic range and more sensitivity than the IR-PMT used previously. A summary of all these results will be presented.

9645-5, Session 1

Signal to noise ratio estimation of the ASCENDS CarbonHawk Experiment Simulator (ACES) for Atmospheric CO2 Measurement

Songsheng Chen, Amin R. Nehrir, Larry B. Petway, NASA Langley Research Ctr. (United States); Yingxin Bai, Science Systems and Applications, Inc. (United States); Fenton W. Harrison, Joel F. Campbell, Byron L. Meadows, Bing Lin, Michael D. Obland, NASA Langley Research Ctr. (United States); Edward V. Browell, Science, Technology, and Research Support Services (United States)

The ASCENDS CarbonHawk Experiment Simulator (ACES) for an airborne platform has been developed at NASA Langley Research Center to advance technologies in support of the NASA Active Sensing of CO2 Emissions over Nights, Days, and Seasons (ASCENDS) mission. With a fiber-amplifier-based multiple Swept-Frequency Intensity-Modulated Continuous-Wave (SF-IM-CW) laser transmitter, the ACES system promises a precise and simultaneous measurement of the range between the transmitter and target and the differential optical depth in the 1571-nm CO2 absorption line on an airborne platform. The precise measurement of the range and the differential optical depth, together with the temperature, pressure, and water vapor information at the same location, make it possible to retrieve the column-averaged CO2 dry air mixing ratio (XCO2) precisely. Advancing the technologies of the active precise CO2 measurement and the retrieval algorithm of the XCO2 from the airborne platform to a spaceborne platform in the future, global precise measurements of atmospheric CO2 during both day and night times and for all seasons are expected. This will enable the quantitative study of atmospheric CO2 sources, sinks, and transports, which will significantly improve the predictions of future climates.

The precision of the range and the differential optical depth measurements as well as the retrieval of XCO2 from the airborne platform are directly affected by the Signal to Noise Ratio (SNR) of the ACES remote sensing system. To perform the precise measurement and retrieval, we have studied the SNR of the ACES system on an airborne platform at different altitudes by using Maximum Likelihood Estimator (MLE). In this paper, both ranges and signal amplitudes of three simultaneously received linear swept-frequency continuous wave signals in an additive high Gaussian-distributed noise with a constant variance have been simulated with MLE. This is a good approximation for the detector-noise-limited system or the solar background shot-noise dominated continuous-wave systems for both airborne platforms and a future spaceborne platform. The signal-dependent Gaussian-distributed shot noise has also be simulated for the high-power (~30W) ACES system on an airborne platform at different altitudes. The simulations indicate that the SNR, signal amplitude divided by the square-root of the amplitude variance, increases as the square-root of the total sampling numbers or integration time from 0.1ms to 1.0s. The relative error of less than 0.2-0.5% can be achieved for the CO2 column density measurement from airborne platforms over the ocean/vegetation areas.

9645-6, Session 2

Multispecies transmitter for DIAL sensing of atmospheric water vapour, methane and carbon dioxide in the 2 μm region

Dominique Mammez, Erwan Cadiou, Jean-Baptiste Dherbecourt, Myriam Raybaut, Jean-Michel Melkonian, Antoine Godard, Guillaume Gorju, ONERA (France); Jacques R. Pelon, Univ. Pierre et Marie Curie (France); Michel Lefebvre, ONERA (France)

For the purpose of active sensing of the global distribution of greenhouse gases , differential absorption lidar (DIAL) instruments are being developed to measure atmospheric CO2, H2O, or CH4 concentrations with unprecedented precision. For integrated-path DIAL (IP-DIAL) measurements from space, suitable absorption lines have been identified as good candidates around 2.05 μm for CO2, 2.29 μm for CH4, and 2.06 μm for H2O [1].

In this context and in the frame of ground based validation experiments, we have developed a high energy transmitter around 2 μm based on frequency conversion in a nested cavity doubly resonant optical parametric oscillator (NesCOPO) followed by high energy parametric amplification. This master oscillator power amplifier (MOPA) architecture enables the generation of tunable single-frequency high energy (tens of mJ) pulses suitable for atmospheric DIAL applications. Moreover taking advantage of the wide spectral coverage capability of the NesCOPO, we demonstrate the potential for this single emitter to address the aforementioned spectral lines.

In the experimental set-up, we use a commercial 100 mJ single-frequency Nd:YAG laser pump laser providing 12 ns pulses at a 30 Hz repetition rate. The NesCOPO master oscillator is based on a narrow gain bandwidth type II 16 mm-long periodically poled lithium niobate (PPLN) nonlinear crystal. Single-frequency emission is obtained by adequately adjusting the dissociation of the two cavity lengths in order to allow the parametric oscillation for a single pair of signal and idler modes [2]. The OPO is pumped with 500 μJ from the primary laser, and 30 μJ of idler radiation are typically extracted from the cavity for further parametric amplification. The power scaling is then realized in a two-step amplifier architecture. The first stage is composed of a 25 mm-long 2 mm-thick type 0 PPLN crystal and the second stage is composed of three high aperture (5 x 5 mm? section) 25 mm-long bulk KTP crystals.

By tuning the phase matching conditions of these different stages the emitter can be tuned at 2051 nm, then at 2057 nm for the signal wave, and then at 2290 nm for the idler wave. After filtering out the depleted pump, 20 mJ for the signal and 16 mJ for the idler can be extracted for each operating point, corresponding to an overall conversion efficiency of 36 %. By measuring the optical frequency with a wavemeter and actively controlling the OPO cavity mirrors, long term frequency drifts of the signal wave can be corrected at a level better than 1 MHz rms (100 s time averaging). Additionally, by mixing the parametric source output with a stabilized laser diode, optical heterodyne analysis enables to assess the linewidth of the emitter, which has been measured to be less than 60 MHz (FWHM of the line).

References:

[1] G. Ehret, et al. “Space-borne remote sensing of CO2, CH4, and N2O by integrated path differential absorption lidar: a sensitivity analysis”, Appl. Physics B, pp. 593-608 (2008)

[2] B. Hardy, et al., “Compact, single-frequency, doubly resonant optical parametric oscillator pumped in an achromatic phase-adapted double-pass geometry”, Opt. Lett. 36(5), 678-680 (2011)

9645-8, Session 2

Langley Mobile Ozone Lidar (LMOL) results from the Denver, CO DISCOVER-AQ campaign

Russell J. De Young, NASA Langley Research Ctr. (United States); William Carrion, Coherent Applications, Inc. (United States); Denis Pliutau, Rene Ganoe, Science Systems and Applications, Inc. (United States)

The Langley Mobile Ozone Lidar is a compact mobile differential absorption lidar (DIAL) system that was developed at NASA Langley Research Center to provide ozone, aerosol and cloud atmospheric measurements in a mobile trailer for ground-based atmospheric air quality campaigns. This lidar is part of the Tropopheric Ozone Lidar Network (TOLNet) currently made up of four other ozone lidars across the U.S.

The lidar system consists of a UV and green laser transmitter, a telescope and an optical signal receiver with associated Licel photon counting and analog channels. The laser transmitter consist of a Coherent Evolution 30 TEM00 1-kHz diode pumped Q-switched Nd:YLF inter-cavity doubled laser pumping a Ce:LiCAF tunable UV laser. A custom-designed Ce:LiCAF tunable UV laser has a wavelength range of 282 to 300-nm that is selectable between two wavelengths. The current wavelengths are online 286 nm and offline 293 nm. The 527-nm visible beam is transmitted into the atmosphere for aerosol measurements.The system has been configured to enable mobile operation from a trailer and was deployed to Denver, CO July 15-August 15, 2014 for the DISCOVER-AQ air quality campaign. Ozone and aerosol profiles were taken showing the influence of emissions from the Denver region. Results of ozone concentration, aerosol scattering ratio, boundary layer height and clouds will be presented.

9645-9, Session 2

LED mini-Raman lidar for hydrogen gas detection

Tatsuo Shiina, Chiba Univ. (Japan); Kazuo Noguchi, Kenji Tsuji, Chiba Institute of Technology (Japan)

Hydrogen gas is not only used for energy, but also becomes by-product from nuclear facility. It becomes so important to monitor its leakage. Some chemical sensors such as combustible material, catalyst materials (Pt or Pd), and semiconductor type (SnO2) can detect hydrogen gas with a high-sensitive of the order of a few tens ppm, while it is hard to get the gas distribution in whole of monitoring site. As hydrogen gas does not have any clear absorption lines in visible light – near infrared ray spectrum, it cannot be detected with any differential absorption spectroscopy.

Here, we focused on Raman scattering light from hydrogen gas. Raman scattering shifts wavelength form the incident light due to material composition. Raman lidar is ideal to detect the leaked gas remotely and safely. In this study of initial stage, a compact Raman lidar with a DPSS laser has been developed for leaked hydrogen gas detection. The minimal detection limit of hydrogen gas concentration is 1% at the observation range of 0 – 50m. We aimed to utilize this system at hydrogen gas station for fuel cell car.

After the hydrogen explosion in nuclear facility at Great East Japan Earthquake, the dangerousness of leaked hydrogen gas is recognized and its remote sensing is desired once more. In such an emergency case, it is hard to use the commercial electric power, and the monitoring device should be act with buttery power. We focused to rebuild the Raman lidar system to be easy-to-use and to be easy-to-install. LED based mini-lidar is developed for this purpose. Its gas detection optics is as same as the laser based Raman lidar, while the LED module is installed into the system. Its transmitting power is 0.75W(=7.5nJ/10ns@365nm). It is quite eye-safe. The pulse repetition frequency is about 500kHz to increase signal-to-noise ratio with the tiny output optical power. We install several optical filters into lidar optics to monitor atmospheric nitrogen gas, hydrogen gas, and water Raman scattering echoes. Nitrogen gas echo is utilized to estimate the quantitative concentration of hydrogen gas. Liquid water and water vapor Raman scattering echoes will be used as the purpose of the atmosphere monitoring under nuclear environment. LED mini-Raman lidar is so compact, simple construction, and low power-consumption. It can be utilize with a small buttery.

As the result of the experiment, the LED mini-Raman lidar could detect the atmospheric nitrogen Raman echo in the distance of 30m, the water vapor Raman echo in 40m, and liquid water Raman echo in 25m under a rain day. Those results were good performance in comparison with the DPSS laser used Raman lidar. The experiment of hydrogen gas detection was conducted with a big gas chamber, which was 200mm? x 500mm. The linear relationship between the hydrogen Raman echo and its gas concentration was confirmed.

LED mini-Raman lidar is not a device for precise estimation of lower concentration gas. It has a concept for easy-to-use and

easy-to-install. It will become one of the solutions to detect the leakage hydrogen gas in the emergency case of no electrical power.

9645-11, Session 3

Design study for an airborne multi-wavelength, multi-depolarization high-spectral resolution lidar *(Invited Paper)*

Ilya Serikov, Max-Planck-Institut für Meteorologie (Germany); Doina N. Nicolae, National Institute of Research and Development for Optoelectronics (Romania); Vasilis Amiridis, National Observatory of Athens (Greece); Holger Linné, Björn Brügmann, Max-Planck-Institut für Meteorologie (Germany)

Multi-wavelength HSRL capabilities do not presently exist at European level to validate current missions in the implementation or operational phase or to support new EO missions and science studies. ADM/Aeolus, EarthCARE and Sentinel-3/-4/-5/-5p, as well as a number of future EO mission concepts such as the EE8 mission candidates CarbonSat and FLEX will include products related to atmospheric aerosols. In support of these missions, ESA kicked-off the development of an airborne lidar to be used as reference for aerosol profile observations.

This paper presents the design study for an airborne multi-wavelength, multi-depolarization high spectral resolution lidar, to be installed on board of a Hawker Beechcraft King Air C90-GTx aircraft. The system is meant to deliver the aerosol extinction, backscatter and depolarization profile distributions in IR, VIS and UV, with accuracy better than 10% and a maximum vertical resolution of 100 m. The horizontal resolution is estimated to be 500 m for backscatter and particle depolarization, and 5 km for extinction, considering a cruise speed of 80 m/s. Challenges in designing of this system refer primarily to the development of a high spectral resolution filter for UV range also capable of maintaining the high performance required when operated on board of aircraft. The interferometer based filtering technique is identified as the only feasible approach to be considered for UV range. The main restriction introduced by selecting this solution, which also adds to the system complexity, is the necessity of limiting the field-of-view of receiving telescopes. This is required to allow sufficiently small divergence of the beam entering interferometer, to achieve a high contrast of interferometer transmission function. Eye-safety at ground level, aerosol suppression requirements, in-cabin space, vibrations and power reserve are also taken into consideration in the lidar design.

The working concept of HSRL channels assumes a combination of three sequentially coupled Fabry-Pérot Interferometers exposed to on-axial beam. The aerosol signal penetrating into molecular channel will be suppressed approximately by three orders of magnitude, while the total efficiency for molecular signal will be kept at about 30% (interferometers only). Narrow band single frequency emission of He-Ne laser is foreseen to be used as a reference when monitoring the interferometer alignment, which is to be done by analysing the interference pattern observed for the He-Ne light. The radius and the width of interference fringe characterize, respectively, the mirror spacing and parallelism. Thermal stability is addressed by keeping a low pressure environment in the interferometer's cavity. Pressure tuning is foreseen to adjust the interferometer free spectral range.

The receiving telescope assembly is designed as a combination of five separate telescopes placed as close as possible to the outgoing laser beam to allow the better lidar overlap function. Parabolic mirror with clear aperture of 0.2 m and 0.5 m focal length will be used for the far range measurement. "Near range" telescope is foreseen to measure extinction within the ncomplete overlap region of "far range" telescope. Three more telescopes with nearly identical lens-based design will be built in for depolarization measurements.

9645-12, Session 3

Long range wind lidars based on novel high spectral brilliance all-fibered sources

Laurent Lombard, Agnès Dolfi-Bouteyre, Claudine Besson, Béatrice Augère, Pierre Bourdon, Anne Durecu, Didier Goular, Julien Le Gouët, Christophe Planchat, William Renard, Matthieu Valla, Guillaume Canat, Onera (France)

New Lidar applications related to aircraft safety in the area of an airport include mapping wind velocity and monitoring turbulences within a radius longer than 8km in a short acquisition time (360° map in 1 minute). During landing and take-off, a minimal distance separation between aircrafts is set by referring to wake turbulence categories. However, it was shown that wake vortices can dissipate quicker because of atmospheric turbulence (characterized by eddy dissipation rate - EDR) or can be transported out of the way on oncoming traffic by cross-winds. Long range scanning Lidars provide radial wind data that can be used to calculate EDR.

To reach long range within a short acquisition time, coherent wind Lidars require high power (~kW), narrow linewidth (few MHz) pulsed laser sources with nearly TF limited pulse duration (~1µs). Eyesafe, all-fiber laser sources based on MOPFA (master oscillator, power fiber amplifier) architecture offer many advantages over bulk sources such as low sensitivity to vibrations, efficiency and versatility. However, narrow linewidth pulsed fiber lasers and amplifiers are usually limited by nonlinear effects. In particular, stimulated Brillouin scattering (SBS) threshold usually limits output peak power of fiber amplifiers to ~100W. This limit can be overcome without degrading the beam quality by increasing the fundamental mode effective area with large mode area (LMA) fibers. Commercial LMA fibers can be used to produce 300W. We investigated various solutions to push this limit further.

SBS can be mitigated by applying a strain gradient along the fiber. This translates into the fiber into an acoustic velocity gradient along the fiber, and thus into an inhomogeneous broadening of the Brillouin gain spectrum. Thanks to this method, we raised the peak power and energy of our laser source up to 600 W and 500 µJ respectively, which represented a gain of more than 3 dB compared to the same fiber source without strain gradient. We integrated the laser source in a Lidar system in the UFO EU project, and its improved long range sensitivity allowed a campaign of comparison between Radar and Lidar for turbulence detection in the vicinity of an airport.

We have also investigated a new fiber composition that allows the use of short fibers with reduced SBS and good beam quality in the framework of FEYMOUS project. One of these fibers was used in an all-fiber MOPA configuration and yielded a peak power of 1120W for 650ns pulse duration with excellent beam quality. This source has been tested in a Lidar configuration and a record range of 16km has been obtained in 0.1s averaging time.

During this talk, we will present some recent results obtained with our wind Lidars based on these high power sources with record ranges. EDR measurement using the developed algorithm based on structure function calculation will also be presented, as well as its validation with simulations and measurements campaign results.

9645-13, Session 3

CW Lidar for wind sensing featuring numerical range scanning and strong inherent suppression of disturbing reflections

Ernst Brinkmeyer, Technische Univ. Hamburg-Harburg (Germany)

Lidar systems with small footprint, based on fiber-optic components and operating in a forward-looking mode are in use for measuring the wind speed ahead of wind turbines. In that way a real-time velocity forecast can be implemented with a leadtime of 10 seconds or more so that better turbine efficiencies can be obtained and damage to the gear units can be avoided. Beside technical aspects low cost is an indispensable precondition for becoming a widely used product in wind-energy industry. In that latter respect CW Lidars are advantageous, their weak points, however, as compared to pulsed systems are related to range resolution: the spatial resolution is given by the length of the focal zone, the resolution zone is only moderately defined so that conventional CW Lidars suffer if stronger signal contributions from outside the target zone are present, the resolution depends on the aperture of the transmitting lens/telescope, it deteriorates roughly quadratically with range, and refocussing is required for changing the location of the target zone. To remove these limitations we recommend the use of a standard CW wind-sensing Lidar with two add-ons: (i) an optical phase modulator (after a narrowband laser source) and (ii) a slightly modified electronic data processing. The phase modulator has to be driven by a staircase signal – calculated in advance – with the property that the optical spectrum after the modulator has a Gaussian shape with a predetermined bandwidth. Appropriate phase modulations are found by a special iterative algorithm and stored in an electronic memory. The Gaussian power spectral density distribution of our synthetic broadband source (i.e. laser + phase modulator) yields a coherence function which is also Gaussian and excellently defines the target zone (e.g. with a 1/e2 width of 5m). That way a special kind of low coherence reflectometry OLCR can be realized where the spatial resolution is given by the coherence length and the optical bandwidth, respectively. What is of utmost importance is the unique fact that the values of the optical phase as a function of time are numerically known in our system and can be used in the detection process and the data processing. As a result the spatial resolution is electronically adjustable, signal contributions from different locations are strongly discriminated, no moving parts are necessary, spurious reflections – in particular the unavoidable reflections from inside the setup which are many orders of magnitude above the quantum limit – can be effectively suppressed or even eliminated, and refocussing and measurement repetition is not necessary since each measurement already contains the full information along the line of sight. That information can be revealed by a simple and time-efficient numerical procedure, by far fast enough to evaluate ten or more resolution zones and to perform hundreds of averages for noise reduction and to approach the quantum limit.

9645-14, Session 3

An innovative rotational Raman lidar to measure the temperature profile from the surface to 30 km altitude

Alain Hauchecorne, Philippe L. Keckhut, Jean Francois Mariscal, Eric D'Almeida, Pierre-Richard Dahoo, Jacques Porteneuve, LATMOS (France)

The temperature is a fundamental parameter for meteorology and climatology. It is measured firstly twice a day using radiosondes with good vertical resolution but in a limited number of stations in the world and secondly from space but often with a vertical resolution limited by the weighting function of the instrument. Lidars provide a good vertical resolution and continuity of measurements. Currently the temperature is measured by lidar Rayeigh from NDACC ground stations but only above 30 km due to the presence of aerosols below this altitude. There is currently no space lidar in flight or in project measuring the temperature. The rotational Raman lidar technology allows access to the evolution of the temperature profile in the troposphere and lower stratosphere. It requires developing an efficient optical system with separation between the Rayleigh and the rotational Raman signal, the first being 2 to 3 orders of magnitude stronger than the second. It requires acquiring the full Stokes and anti-Stokes rotational Raman spectrum of molecular nitrogen using a 1-D detector array operated in photon counting mode. The temperature is deduced from the evolution of the relationship between the Raman spectral lines, the lines close to the Rayleigh line having an amplitude decreasing with increasing temperature and the line far from the Rayleigh line having an amplitude increasing with increasing temperature.

We are developing at LATMOS a prototype rotational Raman lidar with daylight measurement capability that will be implemented in the NDACC station at Haute-Provence Observatory to benefit from the facilities available on site (laser source, telescopes, ...). The Rayleigh line is attenuated using a Fabry-Pérot etalon with a line spacing exactly equal to the line spacing of the N2 rotational Raman spectrum. The Raman lines are equally spaced in wave number and the Rayleigh-Mie line is exactly at half-interval of the Raman comb. Using a Fabry-Pérot with finesse 30, the Rayleigh-Mie line is attenuated by a factor 160, preventing a saturation of the detector. Such a system will perform a continuous survey of the temperature profile from the surface to the middle stratosphere and could serve as a reference to define a future space lidar for measuring the temperature in the troposphere and lower stratosphere. The total intensity of the N2 rotational Raman spectrum represents about 2% of the Rayleigh line. This is sufficient to expect a signal from a space-lidar strong enough to derive useful information on the temperature profile.

9645-15, Session 3

ALART: a novel lidar system for vegetation height retrieval from space

Pierluigi Foglia Manzillo, Chris van Dijk, Simon S. Conticello, Marco Esposito, cosine Research B.V. (Netherlands); Rudi Lussana, Federica Villa, Davide Tamborini, Franco Zappa, Alberto Tosi, Politecnico di Milano, Dipartimento di Elettronica, Informazione e Bioingegneria (Italy); Andreas Roncat, Norbert Pfeifer, TU Wien, Department of Geodesy and Geoinformation (Austria); Dimitris Lampridis, Logikon Labs (Greece); Thomas Entner, Entner Electronics KG (Austria)

Laser altimeters are employed in space since the early Seventies. Current developments in laser and detector technologies are enabling novel LIDAR applications, among which special interest is raised by vegetation height retrieval from space.

Traditional LIDARs, based on the analogue Full Waveform (FW) approach, use high energy laser pulses with low repetition frequencies. The analysis of the return pulse shape allows the height retrieval. A complementary technique is based on Single Photon Counting (SPC) detectors, producing a digital output when triggered by a single photon. The delay of the triggering photon with respect to the laser pulse (time of flight -TOF) provides the information on the height. Yet, SP detectors suffer from long dead-times and are prone to unwanted triggering events due to background photons.

In this work, we propose a multi-kHz Single-Photon Counting (SPC) LIDAR, exploiting low energy laser pulses with high repetition frequency (PRF). This approach perfectly fits space operations. Reduced power consumption is achieved through the limited pulse energy. Moreover, the high PRF is the key to overcome the low signal intensity limitations, as many return shots can be collected from nearly the same scattering area, while the platform is orbiting. The ALART space instrument exhibits a multi-beam design, providing the possibility of performing height retrieval over a wide area, as well as the measurement of terrain slope. This novel ranging technique, working with low SNRs, allows the use of a single laser to generate multiple beams, limiting the instrument mass and power consumption.

The vegetation height and shape are retrieved, as the receiver has a certain probability to detect photons from different levels of canopy. As multiple photons can be acquired, thanks to the high PRF, a histogram (analogous to the FW signal) is

constructed and used to obtain the properties of the target tree, by means of a modal decomposition of the reconstructed waveform.

A field demonstrator of the ALART space instrument is currently being developed by a European consortium led by cosine | measurement systems and funded by ESA under the TRP program. The demonstrator requirements have been derived to be representative of the target instrument. For its performance evaluation, two different test facilities have been identified in the Netherlands, providing equipped towers in woodland areas.

The employed detectors are state-of-the-art CMOS Single-Photon Avalanche Diode (SPAD) matrices, developed in a custom process by Politecnico di Milano. Each pixel is independently equipped with an integrated Time-to-Digital Converter (TDC), achieving a timing accuracy that is much lower than the SPAD dead time, resulting in a distance resolution in the centimeter range.

The system is equipped with a micro-chip green laser, emitting nanosecond pulses with energy in the order of several mJ, at a PRF of ~ 10 kHz, and projects on ground a three-beams pattern, generated with a state-of-the-art optical system.

An extensive field measurement campaign will validate the employed technologies and different algorithms for vegetation height retrieval. The demonstrator can be also interfaced with a Skyarrow aircraft for future airborne tests.

9645-17, Session 4

Detecting the planetary boundary layer height from low-level jet with Doppler lidar measurements

Gregori de Arruda Moreira, Márcia Talita Amorim Marques, Walter Nakaema, Instituto de Pesquisas Energéticas e Nucleares (Brazil); Andréia C. de C. A. Moreira, Petrobrás (Brazil); Eduardo Landulfo, Instituto de Pesquisas Energéticas e Nucleares (Brazil)

The Planetary Boundary Layer (PBL) is an important object of study, meant to: Micrometeorology, Modeling, Forecast, Air Quality and etc. However, It is not simple to obtain this value and/or mapping along the day, the main reason is that the direct measurement device more indicated for this study, the radiosounding, that we have available, has low temporal and spatial resolution. In order two solve this problem, in last decades remote sensing devices has been applied in these studies, and the Doppler Wind LIDAR system has been appointed by many authors as one of the best tools to obtain these information.

The main objective of this paper is to obtain the PBL height from data of a Doppler Wind LIDAR system. The data were collected in a measurement campaign carried in December 2014, at Ressacada's Farm (-27.68; -43.50) – Santa Catarina State – Brazil. It was used a Leosphere Doppler Wind LIDAR, model WLS70, with a range from 100 to 1.500 meters, accumulation time of 7 seconds, data output frequency of 0.1Hz, probed length of 50 meters, 15º scanning cone angle, speed accuracy of 0.3 m/s, speed range from 0 to 100 m/s, direction accuracy of 1.5º and data availability higher than 95% up to 500 meters.

The PBL height was obtained from low-level jet (LLJ) method, which consists in detecting the PBL height through the height of LLJ. The results obtained were validated by bulk Richardson number (BRN), which was obtained from radiosounding data and from Hybrid Single-Particle Lagrangian Integrated Trajectory model (HYSPLIT).

The LLJ method shows high correlation with PBL heights obtained from BRN in unstable and neutral situations, but in stable situations, the correlation between them is lower. The main problem in stable situations is the difficult to detect the LLJ or absence of them.

This study gave us background for further improvements of the algorithm used in order to obtain more accurate results. As a next step, it is expected to use a wide variety of algorithms and models, comparing their results to understand and elect the most appropriate method to estimate the PBL height, considering each limitation.

9645-18, Session 4

Use of lidar water vapor retrieval for assessment of model capability to simulate water vapor profiles

Lev Labzovskii, National Institute of Research and Development for Optoelectronics (Romania) and Univ. of Bucharest (Romania); Ioannis Binietoglou, National Institute for Research and Development for Optoelectronics (Romania); Alexandros D. Papayannis, National Technical Univ. of Athens (Greece); Robert F. Banks, José Maria Baldasano, Barcelona Supercomputing Ctr. - Ctr. Nacional de Supercomputación (Spain)

Atmospheric water vapor can affect important components of the atmosphere such as aerosols and clouds by alteration their optical and microphysical properties. This alteration can be caused by changing humidity conditions and it is still assessed with relatively high uncertainties. Humidity effects on aerosols are estimated in aerosols hygroscopicity studies and atmospheric water vapor content can be taken from measurements or from model simulations for these studies. Systematic observations of water vapor profiles are widely performed by means of remote sensing and insitu instruments, but there is still a lack of experimental data. Lack of data is caused by different instrumental limitations. In most lidars the water vapor retrieval works only during the nighttime when Raman channels are operated. Radiosoundings do not provide continuous measurements as well; they are usually launched no more than 1-2 times per day. Microwave radiometer provides continuous measurements but it has lower resolution and shows significant uncertainties in high layers of the troposphere. Because of these limitations, model-simulated water vapor profiles can be used as input data for aerosol hygroscopicity studies. Hence, the capability of models to simulate water vapor parameters has to be assessed using experimental data from measurements with further estimations of uncertainties given by simulations. This work is devoted to the intercomparison of water vapor profiles measured by lidar and other instruments; experimental data is used for further model evaluation. For this work water vapor parameters are measured by Raman lidar, microwave radiometer, sun photometer and radiosounding. The experimental data presented is acquired during the HygrA-CD campaign held in Athens from May to June 2014. Modeled water vapor profiles were simulated using the WRF model (Weather Research and Forecasting Model). The Raman lidar was calibrated by radiosoundings launched during the campaign. Lidar capability to measure water vapor parameters was validated by the intercomparison with sun photometer and microwave radiometer data. A final comparison between the lidar experimental and model-simulated water vapor profiles is presented for model evaluation. The uncertainties associated to both experimental and modeled data are assessed in the final step of this work.

9645-19, Session 4

A comparison and evaluation between ICESat/GLAS altimetry and mean sea level in Thailand

Didsaphan Naksen, Royal Thai Survey Dept (Thailand) and Beihang Univ. (China); Dong Kai YANG, Beihang Univ. (China)

GIS is Stage of the Art and leading technology to represent,

visualize, analyze and process the real Erath in mathematic way. Surface elevation is one of the importance information, this data also have efficient to generate Digital Elevation Model: DEM quite accurately. Usually surface elevation can acquired from many sources such as satellite imageries, aerial photograph, SAR data or LiDAR by photogrammetry, remote sensing methodology. However the most trust information describe the actual surface elevation is Leveling from terrestrial survey. Leveling is giving the highest accuracy but in the other hand is also long period process spending a lot of budget and resources, moreover the LiDAR technology is new era to measure surface elevation. ICESat/GLAS is spaceborne LiDAR platform, a scientific satellite lunched by NASA in 2003. One of the ICESat/GLAS ability that can be evaluated surface elevation by extracted from waveform. The study area was located at the middle part of Thailand between 12. ° -14° North and 98° -100° East Latitude and Longitude, approximately 48,500 km2 cover Bangkok: capital city of Thailand, and another 15 provinces nearby

This study idea is compared and evaluated elevation between ICESat/GLAS Altimetry and mean sea level of Thailand. The data collection from various places, first the ICESat/GLAS altimetry data product (Product GLA14, GLA06 release 34). Next is mean sea level (1st Layer National Leveling Reference Network) from Royal Thai Survey Department: RTSD is government organization under supervised of Royal Thai armed force. Last one is EGM 96(Erath Gravitational Model 1996) from National Imageries Mapping Agency: NIMA and National Aeronautics and Space Administration: NASA. Methodology of this study first is transformation ICESat GLA14 and GLA06 from TOPX/Poseidon-Jason ellipsoid to WGS84 ellipsoid, subtraction of geoid undulation values was aware because of the difference between WGS84 and TOPX ellipsoids around 0.7 m. Next is compare and evaluate the elevation form mean sea level and ICESat/GLAS altimetry that extracted form footprint center coordinate. Calculate and evaluated find the significant relevant information between ICESat/GLAS and mean sea level.

Evaluation elevation between two data set show that ICESat/GLAS and mean sea level due to the potential complexity of surface slope and roughness (including vegetation of tree height). ICESat/GLAS center coordinate which samples footprint were located near 1st Layer National Leveling Reference Network, surface slope not high and low relief area. The difference distributions are associated elevation show that range of differences wildly from 0. 8 until 25 meters in general overall the study area but in the southern part of Thailand the differences were increasing 18 – 35 meters. The biggest impact has been on a steep slope.

9645-20, Session 5

EARLINET quality assurance efforts building up to the ACTRIS Lidar Calibration centre *(Invited Paper)*

Volker Freudenthaler, Ludwig-Maximilians-Univ. München (Germany)

Light scattering measurements of aerosols are widely used together with model calculations and inversion algorithms deduced there-from to determine micro-physical parameters of the aerosols and to estimate other scattering parameters, which are not originally measured, for use in radiative balance calculations.

The principle constraints of this technique are both on the experimental and theoretical side. Apart from the measuring accuracies, the limited number of measurable scattering parameters limits the number of retrieved micro-physical parameters. On the model side, the few calculable aerosol shapes, like homogeneous ellipsoids, cannot fully represent the huge natural variability of aerosol morphology.

Mixtures of the few calculable model aerosols are chosen to reproduce the light scattering measurements. In order to determine mixtures, which are compatible with the measurements, and to evaluate the variability of their properties, the uncertainty ranges of the measured light parameters have to be known. The smaller the uncertainty ranges are, the smaller is the variability of the compatible mixtures, thus the uncertainty of the inversion. But realistic uncertainty ranges, including statistical as well as systematic uncertainties, are difficult to determine for most remote sensing systems.

Advanced lidar systems measure linear depolarisation ratios and backscatter coefficients at three, and extinction coefficients at two wavelengths. Such complex systems exhibit complex systematic uncertainties. A direct, relative calibration is only possible at the molecular backscatter in aerosol free ranges in the far range, but most aerosols are accumulated in the planetary boundary layer, i.e. in the near range of the lidars, where systematic errors increase.

In EARLINET (European Aerosol Research Lidar NETwork) we developed quality assurance (QA) tools to better characterise the performance and to improve the lidar systems, like the Rayleigh fit (far range), the telecover- (near range), trigger delay-, and dark-measurements. We are working on the retrieval of quantitative, systematic error bars from those qualitative QA measurements.

A recent progress is the detailed theoretical description of the polarisation sensitivity and of calibration techniques for all sorts of lidar systems, which enables to design and analyse special measurements for each lidar system to characterise and calibrate the polarisation sensitivity and to perform error calculations.

On the experimental side the ACTRIS (Aerosols, Clouds and Trace gases Research Infrastructure Network) Lidar Calibration centre (LiCal) has been established in a cooperation between the National Institute of R&D for Optoelectronics (INOE, Bucharest), the Consiglio Nazionale delle Ricerche (CNR, Potenza), and the Meteorological Institute of the Ludwig-Maximilians-University (LMU-MIM, Munich). LiCal enables to support lidar groups worldwide with specialised QA measurements and lidar system analysis techniques, which they cannot afford by their own.

9645-21, Session 5

Aerosol variability in Romania from combined remote sensing data

Doina N. Nicolae, Anca V. Nemuc, Simona Andrei, National Institute of Research and Development for Optoelectronics (Romania); Alexandru Dandocsi, National Institute of Research and Development for Optoelectronics (Romania) and Univ. Politehnica of Bucharest (Romania); Horatiu Stefanie, National Institute of Research and Development for Optoelectronics (Romania) and Univ. Babes-Bolyai (Romania)

Determination of the spatial-temporal variability of chemical, optical and microphysical properties of atmospheric aerosols is still needed in order to reduce the uncertainties of their effects on the radiative forcing. The effects can be very different in the polluted boundary layer (dominated by local and regional aerosols) and in the free troposphere (controlled by long-range aerosol transport).

There are several methods for the observation and measurement of aerosol particles to assess information about their optical, and radiative properties. Our analysis is based on ground-based lidar measurements performed in Bucharest between 2012 - 2014 following the EARLINET climatology schedule, and co-located AERONET (AErosol RObotic NETwork) sun photometer observations.

The multi-wavelength Raman lidar is a YAG:Nd based system which provides aerosol backscatter and extinction profiles in VIS and UV within a typical range of 0.8 – 15 km. It also has depolarization capabilities, allowing to distinguish between spherical and non-spherical aerosol layers. Measurements are performed three times per week, Monday at noon and Thursday at noon and sunset, following EARLINET standard operation procedures.

The climate in the observation area is characterized as

temperate–continental, with four seasons, hot and dry summers and cold and wet winters. Proximity of the Carpathians mountains and of the Black Sea generates specific regional features, with an important influence from the main pressure systems activating in Europe. Permanent advection of humid air masses by the Icelandic Lows and Azores Highs affects western and central Romania, while the cold and dry air masses brought by Siberian Highs and warm and humid air masses brought by Mediterranean Lows influence eastern and southern regions.

The aerosol optical depth (AOD) is characterized by daily mean values ranging from 0.03 to 1.07 (referenced to 500 nm wavelength). The analysis of seasonal dynamics of aerosol loading has revealed two AOD high value peaks. The spring peak observed in April-May is the result of solitary transportation of Saharan dust in the atmosphere over Eastern Europe, and frequent agricultural fires. The summer peak in July–August is associated with forest and peat wildfires, and the presence of soil dust aerosols due to traffic and agricultural activity. The maximum values of AOD are observed in August 2013 (0.298 monthly mean value, and the minimum values in November 2013 (0.131 monthly mean value).

The occurrence of strong, elevated aerosol layers can best be seen in the lidar profiles measured during spring and summer. Large extinction coefficients occur frequently up to 5 km, and are generally associated with long-range transport of polluted dust from desert regions (spring) and biomass burning from Ukraine and Greece (summer). In contrast, the winter profiles mostly show aerosol below 1.2 km, generally from local sources.

The three years analysis showed that long-range transport in the free troposphere contributes significantly to the column AOD especially during the warm season, while local sources are predominant during the cold season.

9645-22, Session 5

Spatial mapping of greenhouse gases using laser absorption spectrometers at local scales of interest

Jeremy T Dobler, Harris Corporation (United States); T. S Zaccheo, Atmospheric and Environmental Research, Inc. (United States); Nathan Blume, Michael Braun, Harris Corporation (United States); Christopher Botos, Timothy Pernini, Atmospheric and Environmental Research, Inc. (United States)

Over the past two years a new system capable of measuring the 2D spatial distribution of atmospheric CO2 over areas on the order of 1 km2 and time scales of a few minutes, has been developed and demonstrated. The Greenhouse gas Laser Imaging Tomography Experiment (GreenLITE) was developed under a cooperative agreement with the National Energy Technology Laboratory of the U.S. Department of Energy, with the focus of improving monitoring capabilities of Ground Carbon Sequestration (GCS) sites. GreenLITE sensors are based on an Intensity Modulated Continuous Wave (IM-CW) approach developed at Exelis in 2004. At the time of this abstract, the GreenLITE system has been operating continuously and remotely for more than 2000 hours at a GCS site in Illinois. It has been providing real time spatial distribution maps of CO2 via an open-web-based interface and is planned to continue 24/7operation at this site until July 2015. In early 2015 we began work on a new implementation of GreenLITE capable of providing similar measurements over a 25 km2 area and are planning to test the system over a 5 km range late summer 2015. If successful the system will be deployed in an urban environment late 2015, demonstrating the utility of real time 2D spatial mapping of CO2 concentrations at this scale. This paper will review the concept for this new measurement capability, including results from both the 1 km system and the 5 km system. Ultimately, the measurement concept can be adapted to other greenhouse gases of interest such as CH4 and NO2.

9645-23, Session 5

Aerosol classification study by lidar

Nianwen Cao, Nanjing Univ. of Information Science & Technology (China)

This paper presents a new method about how to classify different types of aerosols by lidar measurements. Two lidar equations containing the optic parameters (backscatter coefficient, extinction coefficient) about two different types of aerosols, background aerosol and cloud, were built. The solutions about the two lidar equations, optic parameters inversion, were given to classify the background aerosol and cloud. The lidar signals generated from backscatter of two different types of aerosols, with two different extinction to backscatter coefficient ratio (,), were simulated, and the optic parameters inversion from the two simulated lidar signals were almost identical to the simulation parameters for different types of aerosols. Two types of aerosols, the background aerosol and cloud, were simultaneously measured by lidar, and were obviously discriminated by using this new method. The simulations and measurements results verified the new method for aerosols classifications.

9645-24, Session 5

One-year monitoring of the atmosphere over Penang Island using a ground-based lidar

Wei Ying Khor, Mohamad Zubir Mat Jafri, Hwee San Lim, Wan Shen Hee, Univ. Sains Malaysia (Malaysia); Lolli Simone, NASA/GSFC (United States)

The atmosphere over Penang Island is monitored for one year using a ground based Lidar. It is observed that there are two main haze events which occur throughout the year. The haze events occur during the South-East monsoon season and during the North-West monsoon season. The origins of the aerosols are also identified through the Hysplit backward trajectory. The atmosphere over Penang Island consists of a mixture of marine particles and fine particles.

9645-16, Session PS

Aerosol cloud interaction: a multiplatform-scenario-based methodology

Eduardo Landulfo, Instituto de Pesquisas Energéticas e Nucleares (Brazil); Fabio Juliano S. da Silva Lopes, Univ. de São Paulo (Brazil); Juan Luis Guerrero-Rascado, Lucas Alados-Arboledas, Univ. de Granada (Spain)

Suspended atmospheric particles and aerosols go through many chemical and physical processes, and those interactions and transformations may cause particle change in size, structure and composition, regulated by mechanisms, which are also present in clouds. These interactions play a great role in the radiation transfer in the atmosphere and are not completely understood, as competing effects might occur which are known as indirect aerosol effects. Using remote sensing to improve the knowledge of these processes is also a challenge. In face of that we propose a multi-platform approach based lidar, sun photometry and satellite observations that should be characterized under a scenario perspective. Thus, given the cloud height, geometric and optical properties in a diurnal/nocturnal basis will make possible to apply different analytical tools using a set of products that specify the aerosol present in the vicinity of clouds, their optical and physical properties. These scenarios will aid in tagging the expected products and help in creating a robust database to systematically study the aerosol-cloud interaction.

In total we will present 6 scenarios: 3 under daylight conditions,

3 under at nighttime. Each scenario and their counterpart should be able to provide the cloud base/top height, aerosol backscattering profile and cloud optical/geometric thickness. In each instance we should count on a 5 wavelength Raman lidar system measurement (5 nighttime wavelengths, 3 daytime wavelengths), a collocated sun photometer and CALIPSO/ MODIS observation from AQUA/TERRA platforms. To further improve the aerosol cloud interaction the Raman lidar system should have a water vapor channel or moreover a liquid water channel. In our study we will present a two-day case study to show the methodology feasibility and its potential application.

9645-26, Session PS

Estimation of particle mass concentration from eight-year lidar measurements in Seoul, Korea and its application to Asian dust and pollution events

Sang-Woo Kim, Man-Hae Kim, Huidong Yeo, Seoul National Univ. (Korea, Republic of); Nobuo Sugimoto, National Institute for Environmental Studies (Japan)

We estimate vertical distribution of particle mass concentrations from 8-year continuous elastic-backscatter lidar, sky radiometer, and ground-level particulate matter concentrations in Seoul, Korea. Lidar ratio and mass extinction efficiency are firstly determined from aerosol optical depth (AOD) and ground-level PM10 concentrations, which are used as constraints to estimate particle mass concentration. The mean lidar ratio (with standard deviation) and mass extinction efficiency for the entire 8-year study period are 60.44±23.17 sr and 3.69±3.00 m2 g-1, respectively. The lidar ratio did not vary significantly with the Ångström exponent (less than ±10%); however, the mass extinction efficiency decreases to 1.82±1.67 m2 g-1 (i.e., about 51% less than the mean value) when the Ångström exponent is less than 0.5. This result implies that the particle mass concentration from lidar measurements can be underestimated for dust events. Seasonal variation of the particle mass concentration estimated from lidar measurements for the atmospheric boundary layer is quite different from ground-level PM10 measurements. This can be attributable to an inhomogeneous vertical distribution of aerosol in the atmospheric boundary layer. We also estimate vertically resolved aerosol mass concentration for severe Asian dust and pollution events by classifying aerosol subtypes and validate the results with ground-based measurements. We found that pollution-dominant airmass preceded by the appearance of a major mineral dust plume with about 6-12h time-lag.

9645-27, Session PS

DIAL measurements of the vertical ozone distribution at the Siberian lidar station

Oleg A. Romanovskii, V.E. Zuev Institute of Atmospheric Optics (Russian Federation) and Tomsk State Univ. (Russian Federation); Vladimir D. Burlakov, Sergei S. I. Dolgii, V.E. Zuev Institute of Atmospheric Optics (Russian Federation); Olga V. Kharchenko, VE Zuev Institute of Atmospheric Optics (Russian Federation); Alexey A. Nevzorov, Alexey A. Nevzorov, V.E. Zuev Institute of Atmospheric Optics (Russian Federation)

The paper presents the results of DIAL measurements of the vertical ozone distribution at the Siberian lidar station. Sensing is performed according to the method of differential absorption and scattering at wavelength pair of 299/341 nm, which are, respectively, the first and second Stokes components of SRS conversion of 4th harmonic of Nd:YAG laser (266 nm) in hydrogen. Lidar with receiving mirror 0.5 m in diameter is used to implement sensing of vertical ozone distribution in altitude range of 6-16 km. The temperature correction of zone absorption coefficients is introduced in the software to reduce the retrieval errors.

9645-29, Session PS

A portable imaging lidar for lower boundary layer atmospheric measurement

Xiaoqin Liu, Zaihong Hou, Laian Qin, Ningquan Weng, Anhui Institute of Optics and Fine Mechanics (China)

Atmospheric environment is the basis of human survival, which is related to people's physical and mental healthy. It is very important for human health and climate change measuring on aerosol with high vertical resolution in the lower boundary layer. Aerosols are mainly present in the layer which is lower than 0.5km, serious haze also occurs in this layer. However, the traditional aerosol Mie Lidar in the near ground to hundreds of meters height has the blind area or overlapping region. Mie Lidar cannot receive signal in the blind area, and has low precision in the overlapped region.

A portable imaging Lidar using continuous wave(cw) laser is built for the remote sensing of aerosol, fog and haze. It has high spatial resolution for aerosol measurements in the boundary layer. The output beam from a simple, stable power, cw laser no modulated is transmitted into the atmosphere, and backscattered light from along the visible beam path is imaged onto a charge-coupled-device(CCD) camera. It can be used to scan atmosphere from different angles (ranging from 0 to 90 degrees). Principle of measuring using of cw Lidar and CCD are reported in the paper. Configuration and parameters of the Lidar was described in detail. The horizontal measurements are obtained and compared with those obtained by the America Belfort model 6230A visibility meter. The horizontal results show that the average relative error below 10%. The 2-d scanning and temporal-spatial variations of aerosol profiles in low boundary layer are presented.

9645-30, Session PS

Calibrated depolarization retrievals using lidar

Livio Belegante, National Institute of Research and Development for Optoelectronics (Romania); Volker Freudenthaler, Ludwig-Maximilians-Univ. München (Germany); Anca V. Nemuc, Jeni G. Vasilescu, National Institute of Research and Development for Optoelectronics (Romania); Ioannis Binietoglou, National Institute of Research and Development for Optoelectronics (Romania); Cristian M. Radu, Valentin F. Benciu, Doina N. Nicolae, National Institute of Research and Development for Optoelectronics (Romania)

Particle linear depolarization ratio profiles are important for aerosol typing studies and mass concentration retrievals from lidar instruments. The accuracy and associated uncertainties depend strongly on the calibration applied. For lidar systems using the molecular calibration technique in aerosol-free ranges, the associated uncertainties for both aerosol studies and mass concentration retrievals are significantly high. Much lower uncertainties can be obtained if the channels are calibrated and the calibration function is measured.

This study presents the influence of lidar parameters contributing to systematic instrumental errors which lead to high uncertainty of the lidar depolarization ratio, experimental methods to reduce the effects of these parameters, and results of calibrated lidar depolarization profiles. The analysis is based on simulations performed for the Bucharest multi-wavelength Raman depolarization lidar - RALI, a system that is part of the European Aerosol Research Lidar Network - (EARLINET).

We used the Mueller-Stokes formalism applied to a typical lidar

set-up in order to describe how light is altered when interacting with different optics in the lidar emission and receiving modules - e.g. laser optics, mirrors in the emission module, beam expanders, dichroic beam splitters, and the polarizing beam splitter (PBS) in the receiving unit.

According to the simulations, critical parameters that alter the lidar depolarization products (the volume and particle linear depolarization ratios) are the rotation of the plane of polarization of the laser, the receiving optics diattenuation, the calibration factor - including the electronic amplification and the optical diattenuation of the polarizing beam splitter - and the elliptical polarization caused by the optics rotation in respect to the plane of polarization of the laser.

Calibration modules designed to correct for this parameters are analyzed with respect to the type of calibrator and it's placement inside the optical chain. Different experimental methods for assessing and reducing the effects of all parameters using the calibrator modules are presented and discussed.

The depolarization results obtained for RALI at 532nm show significant improvements in the aerosol free region when performing a complete calibration, correcting for the rotation of the plane of polarization of the laser and for the diattenuation of the receiving optics. The volume linear depolarization values retrieved from calibrated data in the aerosol free region agree with the theory for the molecular contribution.

9645-31, Session PS

A method of precision airborne laser scanning and collaborative design in expressway reconstruction

Fei Yu, Chujiang Chen, YANG MING, Shaohuai Yu, Liyuan Wang, Xiao Zhang, CCCC Second Highway Consultant Co. Ltd, (China)

This paper presents the method of automatic surveying and collaborative design of airborne laser scanning and expressway reconstruction in Expressway Reconstruction. First, the organization and management of the mass density of laser radar data was realized, and the large scale 3D digital products and road characteristic information needed for production were fast generated. Then, through the design of collaborative and CAD, the various section ground line data which design required was rapid automaticly generated. Finally, with the coordination and automatic interaction of flat, vertical, transverse data, the road alignment elements was restored and expansion engineering design of road engineering was optimized. The application shows that the result accuracy can satisfy the requirements of detailed survey and construction drawing design of highway reconstruction and extension with economy, safety and high—efficiency?

9645-32, Session PS

Remote sensing solutions using GIS with mobile or land laser scanning

Ahmet Erdoğdu, Engineer (Turkey)

No Abstract Available

Conference 9646: High-Performance Computing in Remote Sensing

Monday - Tuesday 21–22 September 2015

Part of Proceedings of SPIE Vol. 9646 High-Performance Computing in Remote Sensing V

9646-1, Session 1

The implementation of multiple objects tracking algorithm based on partition of bipartite graph in FPGA-based onboard vision systems

Boris A. Alpatov, Ryazan State Radio Engineering Univ. (Russian Federation); Pavel V Babayan, Ryazan State Radio Engineering University (Russian Federation); Valeriy V. Strotov, Ryazan State Radio Engineering Univ. (Russian Federation)

FPGA-based onboard vision systems are widely used for different tasks including image registration, enhancement and recognition, aircraft and spacecraft video-based navigation. These systems have some distinctive features including high performance, small sizes and relatively moderate energy consumption. The unique nature of FPGA allows performing sophisticated video processing in real time with high frame rate. The main disadvantage of such computation architecture is that some algorithms (e.g., recursive or strong branching algorithms) cannot be effectively implemented.

In this paper, we consider the multiple target tracking algorithm based on bipartite graph partitioning. The suggested algorithm solves such tasks as multiple object identification in several sequential video frames and building the object trajectories. The initial data for this algorithm consist of lists of unidentified image segments. As a result, we get a list of objects which contains information about objects' speeds and sizes. The considered algorithm takes into account such situations as object appearance and disappearance, splitting and merging.

The described algorithm has some problematical stages in terms of implementation in FPGA-based systems. First, on the graph preparation stage, we must make a selection of incoming segments when the total segment number exceeds the segment memory size. Second, the most time-consuming procedure of the algorithm is a graph partitioning. This procedure can not be implemented in FPGA because of its recursive behavior.

In this work, we suggest the way to implement the described multiple object tracking algorithm in FPGA-based onboard systems. The algorithm modification includes the procedure of segment preselection that can be executed while incoming data are prepared. Also, the graph description tables were supplemented with additional node data. This form of description allows performing a graph partitioning into two stages: table sorting and one-passed node link disconnection.

The described algorithm is designed for a family of onboard vision systems with common architecture. The structure of the particular system depends on a vehicle type and the list of solving tasks. Typically, the system consists of top-level TI DSP (320 series) and 1-4 FPGAs (Xilinx Virtex, Virtex II, Spartan or Virtex 5). The FPGAs are used to perform the most of time-consuming operations such as spatial and temporal image filtering, geometric and spectral transformations, template matching and thresholding, binary image marking and SLAE solving. The DSP is used to execute unique operations with small amount of data, FPGA dispatching and internal control.

The onboard system model has been designed with Xilinx Virtex 7 evaluation kit. This system model includes Xilinx MicroBlaze soft processor and several FPGA-based computation blocks on the same chip. The model can be adjusted to fit its architecture and performance to any onboard system from the described family. It allows estimating the computation costs of each stage of the suggested algorithm.

The results of the proposed multiple object algorithm examination have shown that it can be implemented in the most of real-time FPGA-based systems.

9646-3, Session 1

Connected Component Labeling algorithm for very complex and high-resolution images on an FPGA platform

Kurt Schwenk, Felix Huber, Deutsches Zentrum für Luft- und Raumfahrt e.V. (Germany)

Connected Component Labeling (CCL) is a basic algorithm in image processing and an essential step in nearly every application dealing with object detection. It groups together pixels belonging to the same connected component (e.g. object) [fig. 1,2]. In the past 30 years many different CCL algorithms and implementations for various hardware architectures were presented in literature. Architectures as ASICs, FPGAs and GPUs were utilised for achieving high data throughput, primarily for video processing.

This work originated from a project for performing image data analysis, primarily for remote sensing applications, on board of a satellite [1,2]. Big data should be processed in realtime, despite the relatively low processing power of common onboard computers. To overcome this limitation, it was intended to implement computationally intensive image processing tasks directly on an FPGA.

In this articel, the FPGA implementation of CCL method is presented, which was specially designed to for the processing of high resolution images with complex structure at high speed [fig. 2,3]. The input of this implementation is a (local) connectivty map, the output a label mask.

In general, CCL is a dynamic task and therefore not well suited for parallelisation, which is needed to achieve high processing speed with an FPGA. To overcome this issue, most of the FPGA CCL implementations are restricted to low resolution images and a maximal number of objects. Furthermore, in many cases, instead of a label map only object data, such as the framebox, the size or the centre coordinates are extracted. In this manner, a very high processing speed can be achieved on an FPGA platform with low hardware ressource usage [3]. This perfectly suffices for most of the video processing applications. But in the present case, these restrictions are incompatible with the requirements to label high resolution images with high complex structure. Therefore a new approach was required.

The CCL method presented in this work is based on a two-pass CCL algorithm, which was modified with respect to low memory consumption and suitability for a FPGA implementation.

Nevertheless, union-find data structures were required, which are hard to implement efficiently on an FPGA, because their dynamic character. Due to the potential large size of the union-find data structures, the union-find data structures could not be buffered in the Block RAM of the available FPGA. This is a showstopper for efficient parallelisation and especially for pipeline processing. However, a thorough analysis of the algorithm revealed that most computation steps can be handled in a pipeline mode. Based on this fact, a stop-and-go high-performance pipeline processing CCL module was designed.

The algorithm, the performance and hardware requirements of a prototype implementation are prestented. Furthermore, a clock-accurate runtime analysis is shown, which illustrates the dependency between processing speed and image complexity in detail [fig.5] . This is a issue concerning all CCL methods, but is in particular a question of matter when high resolution images with high complexity have to be processed. At last, the performance of FPGA implementations is compared with that of a software implementations on a modern embedded platform (rasperry pi, xilix zynq 7000).

9646-4, Session 1

Dimensionality reduction and endmember extraction for hyperspectral imaging using an RVC-CAL library

Daniel Madroñal, Raquel Lazcano, Eduardo Juárez, César Sanz, Univ. Politécnica de Madrid (Spain)

Hyperspectral Imaging (HI) collects high resolution spectral information consisting of hundred of bands raging from the infrared to the ultraviolet wave lengths. In the medical field, specifically, in the cancer tissue identification at the operating room, the potential of HI is huge. However, given the data volume of HI and the computational complexity and cost of identification algorithms, real-time processing is the key, differential feature that brings value to surgeons. In order to achieve real-time implementations, the parallelism available in a specification needs to be explicitly highlighted. Data-flow programming languages, like RVC-CAL, are able to accomplish this goal.

In this paper, a RVC-CAL library to implement dimensionality reduction and endmenber extraction is presented. The results obtained show some improvements that the use of the library give to us: speedups of 30% using the complete processing chain and, in particular, a speedup of 5% have been achieve in the dimensionality reduction step compared with a functional software that already exists. This dimensionality reduction takes ten of the thirteen seconds that the whole system needs to analyze one of the images. The library also allows a simplification of the implementation process of this kind of algorithms. During the experimental test, the potential of the RVC – CAL library for processing hyperspectral images have achieve great results in real-time analysis. It also give us the possibility of testing the system performance and the possible bottlenecks present in the processing chain.

The paper is structured as follows. Section 1 introduces the motivation of the research and the main objectives to achieve. After that, the state of the art of the technologies related with the development of the RVC – CAL library has been studied. This section contains concepts like the definition and characteristics of an hyperspectral image and the way to process it. Once the theoretical bases have been exposed, in the third section the followed methodology to implement the library and to compose the processing chain have been explained. This chain will be tested in order to analyze the correct behavior of the implemented algorithms and the time required to process one of these images. This analysis include the execution in one and several cores in order to cross-compare their advantages . The results obtained in the previous section will be analyzed following these steps: first of all, the results of each stage – dimensionality reduction and endmember extraction – will be studied and, after that, the results obtained from the complete chain will be analyzed. To finish the analysis of the system and the library behavior, some conclusions related with algorithm behavior, time processing and system performance have been drawn. At last, the paper concludes with some possible future research lines.

9646-5, Session 1

Revisiting Intel Xeon Phi optimization of Thompson cloud microphysics scheme in Weather Research and Forecasting (WRF) model

Jarno Mielikainen, Bormin Huang, Hung-Lung A. Huang, Univ. of Wisconsin-Madison (United States)

The Thompson cloud microphysics scheme is a sophisticated cloud microphysics scheme in the Weather Research and Forecasting (WRF) model. The scheme is very suitable for massively parallel computation as there are no interactions among horizontal grid points. Compared to the earlier microphysics schemes, the Thompson scheme incorporates a large number of improvements. Thus, we have optimized the speed of this important part of WRF. Intel Many Integrated Core (MIC) ushers in a new era of supercomputing speed, performance, and compatibility. It allows the developers to run code at trillions of calculations per second using the familiar programming model. In this paper, we present our results of optimizing the Thompson microphysics scheme on Intel Many Integrated Core Architecture (MIC) hardware. The Intel Xeon Phi coprocessor is the first product based on Intel MIC architecture, and it consists of up to 61 cores connected by a high performance on-die bidirectional interconnect. The coprocessor supports all important Intel development tools. Thus, the development environment is familiar one to a vast number of CPU developers. Although, getting a maximum performance out of MICs will require using some novel optimization techniques. New optimizations for an updated Thompson scheme are discusses in this paper.

9646-6, Session 2

GPU-based ray tracing algorithm for high-speed propagation prediction in typical indoor environments

Lixin Guo, Xiaowei Guan, Zhongyu Liu, Xidian University (China)

As the demand for mobile communications increases dramatically, research on indoor radio propagation prediction has attracted more and more attention in recent years. A fast 3-D ray tracing propagation prediction model based on virtual source tree is presented in this paper, whose theoretical foundations are geometrical optics(GO) and the uniform theory of diffraction(UTD). Based on the assumption that the frequencies of electromagnetic waves are high enough, the ray tracing algorithm fully applies the concept of ray in geometric optics to computational electromagnetics and thus can achieve good accuracy. In terms of typical single room indoor scene, taking the geometrical and electromagnetic information into account, some acceleration techniques (such as multiple space partition method, z-buffer method, etc.) are adopted to raise the efficiency of the ray tracing algorithm. The simulation results indicate that the runtime of the ray tracing algorithm will sharply increase when the number of the objects in the single room is large enough. Therefore, GPU acceleration technology is used to solve that problem. Compared with CPU, GPU is good at calculation operation rather than logical judgment, so that tens of thousands of threads in CUDA programs are able to calculate at the same time, in order to achieve massively parallel acceleration. Finally, a typical single room with several objects is simulated by using the serial ray tracing algorithm and the parallel one respectively. It can be found easily from the results that compared with the serial algorithm, the GPU-based one can achieve greater efficiency.

9646-7, Session 2

GPU implementation of the simplex identification via split augmented Lagrangian

Jorge Sevilla Cedillo, Jose M. Nascimento, Instituto de Telecomunicações (Portugal)

Hyperspectral imaging is a fast growing area in remote sensing applications. Hyperspectral sensors collect hundred or even thousands of spectral bands at different wavelength of the same area on the surface Earth. For instance, the NASA Jet Propulsion Laboratory's Airborne Visible Infra-Red Imaging Spectrometer (AVIRIS) is able to record the visible and near-infrared spectrum of the reflected light of an area of several kilometers long (depending on the duration of the flight) using 224 spectral bands, which generates large data volumes comprising several GBs per flight. This high spectral resolution can be used for object detection and for discriminating between different objects based on their spectral characteristics.

One of the main problems of hyperspectral data analysis is the presence of mixed pixels, due to the low spatial resolution of such images. In AVIRIS case a pixel cover an area of approximately 20 meters diameter on the ground. This means that several spectrally pure signatures (endmembers) are combined into the same mixed pixel. Linear spectral unmixing follows an unsupervised approach which aims at inferring pure spectral signatures and their material fractions at each pixel of the scene. Hyperspectral linear unmixing approaches can be mainly classified as either statistical or geometrical, the last sub-class is based on the fact that hyperspectral vectors belong to a simplex set whose vertices correspond to the endmembers.

Simplex identification via split augmented Lagrangian} (SISAL) is an efficient method that finds the smallest simplex that contain the dataset. The non-convex optimization problem is solved as a sequence of nonsmooth

convex subproblems using variable splitting to obtain a constraint formulation, and then applying an augmented Lagrangian technique.

In recent years, graphics processing units (GPUs) have evolved into highly parallel and programmable systems. Specifically, several hyperspectral imaging algorithms have shown to be able to benefit from this hardware taking advantage of the extremely high floating-point processing performance, compact size, huge memory bandwidth, and relatively low cost of these units, which make them appealing for onboard data processing.

This paper proposes an efficient implementation of SISAL algorithm for unsupervised hyperspectral linear unmixing on GPUs using CUDA. SISAL aims to identify the endmembers that compose the scene, i.e., is able to unmix hyperspectral data sets in which the pure pixel assumption is violated. The parallel implementation of SISAL presented in this work exploits the GPU architecture at low level, using shared memory and coalesced accesses to memory.

Our preliminary results conducted using synthetic hyperspectral images generated from spectral signatures randomly selected from the United States Geological Survey (USGS) using 224 bands, show that for an image composed of 20 spectral signatures mixed in 10^5 pixels the speedup is up to five times. The experiments were conducted on a NVidia GeForce GTX 590, and on one core of the Intel i7-2600 CPU (3.4GHz), with 16 Gbyte memory, for the proposed GPU optimized version and for sequential version, respectively.

The results herein presented indicate that the GPU implementation can significantly accelerate the execution of SISAL over big datasets, when compared with the sequential version which has been carefully optimized for one CPU core. It s noteworthy to mention that both methods have the same accuracy regarding the extracted signatures from the scene.

9646-8, Session 2

Embedded GPU implementation of anomaly detection for hyperspectral images

Yuanfeng Wu, Lianru Gao, Bing Zhang, Institute of Remote Sensing and Digital Earth (China); Bin Yang, Central South Univ. (China); Zhengchao Chen, Institute of Remote Sensing and Digital Earth (China)

Anomaly detection is one of the most important techniques for remotely sensed hyperspectral data interpretation. Due to the high dimensionality of hyperspectral images and the large computational complexity associated to processing algorithms, developing fast techniques for anomaly detection has received considerable attention in recent years.

The utilization of high performance computing infrastructure in hyperspectral imaging applications has become more widespread. According to the specific timely responses for swift decisions, hyperspectral image processing algorithms implemented on clusters, field programmable gate arrays (FPGAs), and graphics processing units (GPUs), have been made available. In particular, GPUs are quickly evolving as a standardized architecture in hyperspectral imaging due to their low cost, portability, and high computational power.

In this paper, we develop a novel embedded GPU based technique for efficient anomaly detection in hyperspectral images. The proposed method uses a streaming background statistics (SBS) approach for optimizing the Reed-Xiaoli (RX) algorithm, which is one of the most widely used technique of anomaly detection for hyperspectral images. Specifically, this algorithm is implemented in streaming fashion on NVIDIA Jetson TK1. The NVIDIA Jetson TK1 development kit built around the NVIDIA Tegra K1 SOC and uses the NVIDIA Kepler GPU with 192 CUDA cores.

Our experiments, conducted with several well-known hyperspectral scenes, indicate the effectiveness of the proposed implementations. This work gives a promising solution for high-performance with low power consumption hyperspectral image applications.

9646-9, Session 2

RVC-CAL library for endmember and abundance estimation in hyperspectral image analysis

Raquel Lazcano, Daniel Madroñal, Eduardo Juárez, César Sanz, Univ. Politécnica de Madrid (Spain)

Hyperspectral imaging (HI) collects information from across the electromagnetic spectrum, covering a wide range of wavelengths. Although this technology was initially developed for remote sensing and earth observation, its multiple advantages - such as high spectral resolution - led to its application in other fields, as cancer detection. However, this new field has shown specific requirements; for instance, it needs to accomplish strong time specifications, since all the potential applications - like surgical guidance or in vivo tumor detection - imply real-time requisites. Achieving this time requirements is a great challenge, as hyperspectral images generate extremely high volumes of data to process. Thus, some new research lines are studying new processing techniques, and the most relevant ones are related to system parallelization.

In that line, this paper describes the construction of a new hyperspectral processing library for RVC - CAL language, which is specifically designed for multimedia applications and allows multithreading compilation and system parallelization. This paper presents the development of the required library functions to implement two of the four stages of the hyperspectral imaging processing chain – endmember and abundances estimation –. The results obtained show that the library achieves speedups of 30%, approximately, comparing to an existing software of hyperspectral images analysis; concretely, the endmember estimation step reaches an average speedup of 27.6%, which saves almost 8 seconds in the execution time. It also shows the existence of some bottlenecks, as the communication interfaces among the different actors due to the volume of data to transfer. Finally, it is shown that the library considerably simplifies the implementation process. Thus, experimental results show the potential of a RVC – CAL library for analyzing hyperspectral images in real-time, as it provides enough resources to study the system performance.

The document is organized as follows: firstly, it introduces the motivations that have inspired this research work and the main objectives to achieve. After that, it studies the state of the art of the technologies related to the development of the library. Thirdly, it explains the methodology of the library implementation, as well as the construction of a complete processing chain in RVC - CAL applying the mentioned library. This chain will test both the correct behavior of the library and the time requirements for the complete analysis of one hyperspectral image, either executing the chain in one processor or in several ones. Afterwards, the collected results will be carefully analyzed: first of all, individual results -from endmember and abundance estimations stages - will be

discussed and, after that, complete results will be studied; this results will be obtained from the complete processing chain, so they will analyze the effects of multithreading and system parallelization on the mentioned processing chain. Finally, as a result of this discussion, some conclusions will be gathered regarding some relevant aspects, such as algorithm behavior, execution times and processing performance. Likewise, this document will conclude with the proposal of some future research lines that could continue the research work described in this document.

9646-10, Session 2

Robust hyperspectral vegetation indices to estimate leaf chlorophyll content

Shan Lu, Northeast Normal Univ. (China)

Hyperspetral vegetation indices are always applied for the assessment of leaf chemicals, especially chlorophyll content. But most vegetation indices were developed based on the spectral information from the upper leaf surface. In fact, the abaxial leaf surfaces can have impact on reflectance spectra due to the canopy structure or the inclination of leaves. In this study, we measured the reflectance spectra of both upper and lower leaf surfaces of Populus alba. The results showed that structural differences between the leaf upper and lower surfaces may lead to obvious differences in reflectance and hyperspectral vegetation indices calculation. Among more than thirty vegetation indices tested, only R672/(R550 ? R708) had no significant difference between upper and lower surfaces of the same leaf. However, the results of linear regression analysis showed that the vegetation indices, (R850–R710)/(R850–R680), VOG2, D730, and D740, had high better relationshipe with the chlorophyll content (R2 > 0.8) and varied little between the two leaf surfaces of Populus alba.. This manifested that these four vegetation indices had relatively robust accuracy for estimating leaf chlorophyll content insensitive to the upper and lower surfaces of leaf. The coefficients of determination (R2) for the calibration P. alba leaves were 0.92, 0.98, 0.93 and 0.95 on the upper surfaces, and 0.88, 0.87, 0.88 and 0.92 on the lower surfaces.

9646-11, Session 3

Fault-tolerant NAND-flash memory module for next-generation scientific instruments

Tobias Lange, Holger Michel, Björn Fiethe, Harald Michalik, Technische Univ. Braunschweig (Germany); Dietmar Walter, DSI GmbH (Germany)

State-of-the-art remote sensing instruments deliver vast amounts of high-resolution data. For classical earth-observation missions, this data is typically evaluated after reception on ground. Due to the limited telemetry rate on deep space missions the increasing amount of data requires the scientific evaluation and thereby a reduction of data volume to take place at instrument level already on-board the spacecraft. In most cases observation time is limited and scheduled to specific time slots with idle periods in between. Thus, instead of high-power real-time processing using high-performance Field-Programmable Gate Arrays (FPGAs) or many-core processors, an offline processing in between the observation slots is an efficient method to process and finally reduce the volume of the collected data. The offline processing not only requires the needed processing capabilities inside the instrument's DPU, but also pushes the need for a compact non-volatile memory to store data on instrument level.

A demanding example for this kind of processing is the data processing unit (DPU) for the Polarimetric and Helioseismic Imager (PHI) instrument on Solar Orbiter. The PHI instrument will provide maps of the continuum intensity, the magnetic-field vector, and the line-of-sight velocity in the solar photosphere. The data processing is done using reconfigurable SRAM based FPGAs. These devices allow a hardware accelerated processing, which can be reconfigured in-flight. The data-flow of the instrument can be divided into two phases, allowing the computing resources to be shared over time.

(i) During acquisition phase, images of different wavelength and polarization modes are accumulated and finally stored into an internal non-volatile memory module. A dedicated image stabilization system is running in parallel, to reduce the influence of residual spacecraft jitter.

(ii) Each observation period is subsequently followed by an offline processing. During this step, previously stored data is recalled from the memory and passed to a pre-processing core which consists of different submodules (e.g. flat/-darkfield correction, convolution, arithmetical operations). This is followed by a computation intensive inversion of the Radiative Transfer Equation (RTE), which finally provides the desired data of reduced size. As a last step the reduced data sets are compressed by a standard compression and stored on spacecraft level until transmission to ground.

For an efficient offline processing a lightweight but reliable memory module with a net capacity of 4 Tbit is needed on instrument level. The module is based on commercial NAND-Flash memory technology, packaged and screened to required quality. The module is organized in two redundant partitions, which can be powered individually.

To provide required fault tolerance, the memory is protected by a Reed-Solomon code enabling to correct double block errors. This results in a gross memory word size of 96 bit (64 bit without EDAC). Because every device is 8 bit wide, this involves 12 NAND-Flash devices to be addressed individually. While the memory devices are on a seperate board, the NAND-Flash controller is placed on a radiation-hardened RTAX2000 FPGA inside the DPU. In the full paper the data-flow and architecture together with the advantages of the system will be presented, including details of the offline processing in combination with the operation of the NAND-Flash memory module.

9646-12, Session 3

APES-based procedure for super-resolution SAR imagery with GPU parallel computing

Weiwei Jia, Xiaojian Xu, Guangyao Xu, BeiHang Univ. (China)

The amplitude and phase estimation (APES) algorithm is widely used in modern spectral analysis, which simultaneously estimates the amplitude and phase of a complex sinusoidal signal. Compared with conventional Fourier transform, APES results in much lower sidelobes and narrower spectral peaks. However, in synthetic aperture radar(SAR) imaging with large scene, without parallel computation, it is difficult for APES to be applied for super-resolution radar image processing due to its great amount of calculation.

In this paper, a procedure is developed to achieve target extraction and parallel computing of APES in super-resolution SAR imaging. The overall process of the current procedure mainly includes three steps as follows: Firstly, an image chip for specific target region of interest is segmented from the large scene SAR image with coarse resolution. Secondly, the automatic censoring based cell averaging-constant false alarm rate(ACCA-CFAR) is used to obtain the minimum bounding rectangle of the target. Based on the length, width and squint angle of the rectangle, a two-dimensional(2D) filter is designed to extract target from the image chip, while the clutter is greatly suppressed. Finally, the filtered image is transformed back to 2D data domain and a GPU parallelized APES is implemented to obtain super-resolved target image.

Numerical tests are made on Tesla K40C with 745 MHz GPU clock rate and 2880 CUDA cores. Results on different SAR images demonstrate that the computational speed of proposed procedure is remarkably faster than the CPU-based APES with the same finely resolved images.

9646-13, Session 3

FAPEC-based lossless and lossy hyperspectral data compression

Jordi Portell de Mora, Univ. de Barcelona (Spain); Gabriel Artigues, Institut de Ciències de l'Espai (Spain); Riccardo Iudica, Univ. de Barcelona (Spain); Enrique García-Berro, Univ. Politècnica de Catalunya (Spain)

Data compression is essential for remote sensing based on hyperspectral sensors owing to the increasing amount of data generated by modern instrumentation. CCSDS issued the 123.0 standard for lossless hyperspectral compression, and a new lossy hyperspectral compression recommendation is being prepared. We have developed two multispectral and hyperspectral pre-processing stages for FAPEC, a data compression algorithm based on an entropy coder. We can select a prediction-based lossless stage that offers excellent results and speed. Alternatively, a DWT-based lossless and lossy stage can be selected, which offers excellent results yet obviously requiring more compression time. Here we present the overall design of these data compression systems and the results obtained on a variety of real data, including ratios, speed and quality.

9646-14, Session 3

GPU-accelerated computation of faced-based investigation on electromagnetic scattering from the dynamic ocean surface with volume scattering

Longxiang Ling-Hu, Xidian Univ (China)

In this paper we develop a graphics processing unit (GPU)-based massively parallel approach for efficient simulation of dynamic ocean model and computation of electromagnetic scattering with the volume scattering. The ocean is envisaged as a two-scale profile on which the long waves are locally approximated by planar facets. The microscopic profile within a facet is assumed to be represented by a set of sinusoidal ripple patches. The complex reflective function of each modified facet is evaluated by a modified formula of the original Bass and Fuks two-scale model, in which the phase factor of each facet is with the capillary wave modification. On this basis, with the oceanic whitecap coverage taken into account, a composite model for predicting the ocean surface backscattering coefficient is constructed tentatively with the proposed vector radiative transfer (VRT) model employed. In the original CPU-based sequential code, the ocean surface simulation and the electromagnetic scattering calculation of dynamic ocean takes up 99% of the total execution time. In this paper we take advantage of the massively parallel compute capability of NVIDIA Kepler k40 with the compute Unified Device Architecture (CUDA) to simulate the ocean surface and compute the backscattering coefficient of the dynamic ocean surface. Our parallel design includes the registers for faster memory access, the shared memory for parallel reduction, the pipelined multiple-stream asynchronous transfer and the CPU-GPU heterogeneous computation. By using these techniques, we achieved speedup of 318-fold for the simulation of the ocean surface and 288-fold for the computation of the dynamic surface as compared with its single-code CPU counterpart.

9646-15, Session 3

Application of Intel Many Integrated Core (MIC) accelerators to the Pleim-Xiu land surface scheme

Melin Huang, Bormin Huang, Hung-Lung A. Huang, Univ. of Wisconsin-Madison (United States)

The land-surface model (LSM) is one physics process in the weather research and forecast (WRF) model. The LSM includes atmospheric information from the surface layer scheme, radiative forcing from the radiation scheme, and precipitation forcing from the microphysics and convective schemes, together with internal information on the land's state variables and land-surface properties. The LSM is to provide heat and moisture fluxes over land points and sea-ice points. The Pleim-Xiu (PX) scheme is one LSM. The PX LSM features three pathways for moisture fluxes: evapotranspiration, soil evaporation, and evaporation from wet canopies. To accelerate the computation process of this scheme, we employ Intel Xeon Phi Many Integrated Core (MIC) Architecture as it is a multiprocessor computer structure with merits of efficient parallelization and vectorization essentials. The accelerating results of this scheme using Intel MIC architecture will be delivered.

9646-16, Session 4

GPU-based ray tracing algorithm for high-speed propagation prediction in multiroom indoor environments

Xiaowei Guan, Lixin Guo, Zhongyu Liu, Xidian University (China)

As the demand for mobile communications increases dramatically, research on indoor radio propagation prediction has attracted more and more attention in recent years. A novel ray tracing algorithm for high-speed propagation prediction in multi-room indoor environments is proposed in this paper, whose theoretical foundations are geometrical optics(GO) and the uniform theory of diffraction(UTD). Based on the assumption that the frequencies of electromagnetic waves are high enough, the ray tracing algorithm fully applies the concept of ray in geometric optics to computational electromagnetics and thus can achieve good accuracy. Taking the geometrical and electromagnetic information of the complex indoor scene into account, some acceleration techniques (such as multiple space partition method, z-buffer method, etc.) are adopted to raise the efficiency of the ray tracing algorithm. The simulation results indicate that the runtime of the ray tracing algorithm will sharply increase when the number of the objects in multi-room buildings is large enough. Therefore, GPU acceleration technology is used to solve that problem. Compared with CPU, GPU is good at calculation operation rather than logical judgment, so that tens of thousands of threads in CUDA programs are able to calculate at the same time, in order to achieve massively parallel acceleration. Finally, a typical multi-room indoor environment with several objects in each room is simulated by using the serial ray tracing algorithm and the parallel one respectively. It can be found easily from the results that compared with the serial algorithm, the GPU-based one can achieve greater efficiency.

9646-17, Session 4

Performance tuning Weather Research and Forecasting (WRF) Goddard longwave radiative transfer scheme on Intel Xeon Phi

Jarno Mielikainen, Bormin Huang, Hung-Lung A. Huang, Univ. of Wisconsin-Madison (United States)

Next-generation mesoscale numerical weather prediction system, the Weather Research and Forecasting (WRF) model, is a designed for dual use for forecasting and research. WRF offers multiple physics options that can be combined in any way. One of the physics options is radiance computation. The major source for energy for the earth's climate is solar radiation. Thus, it is imperative to accurately model horizontal and vertical distribution of the heating. Goddard solar radiative transfer model includes the absorption duo to water vapor,ozone, ozygen, carbon dioxide, clouds and

aerosols. The model computes the interactions among the absorption and scattering by clouds, aerosols, molecules and surface. Finally, fluxes are integrated over the entire longwave spectrum.In this paper, we present our results of optimizing the Goddard longwave radiative transfer scheme on Intel Many Integrated Core Architecture (MIC) hardware. The Intel Xeon Phi coprocessor is the first product based on Intel MIC architecture, and it consists of up to 61 cores connected by a high performance on-die bidirectional interconnect. The coprocessor supports all important Intel development tools. Thus, the development environment is familiar one to a vast number of CPU developers. Although, getting a maximum performance out of MICs will require using some novel optimization techniques. Those optimization techniques are discusses in this paper.

9646-18, Session 4

A novel hardware-friendly algorithm for hyperspectral linear unmixing

Raúl Guerra, Lucana Santos, Sebastián López, Roberto Sarmiento, Univ. de Las Palmas de Gran Canaria (Spain)

Linear unmixing of hyperspectral images has rapidly become one of the most widely utilized tools for analyzing the content of hyperspectral images captured by state-of-the-art remote hyperspectral sensors. The aforementioned unmixing process consists of the following three sequential steps: dimensionality estimation, endmember extraction and abundances computation. Within this procedure, the first two steps are by far the most demanding from a computational point of view, since they involve a large amount of matrix operations. Moreover, the complex nature of these operations seriously difficult the hardware implementation of these two unmixing steps, leading to non-optimized implementations which are not able to satisfy the strict delay requirements imposed by those applications under real-time or near real-time requirements. This paper uncovers a new algorithm which is capable of estimating the number of endmembers and extracting them from a given hyperspectral image with at least the same accuracy than state-of-the-art approaches while demanding a much lower computational effort, with independence of the characteristics of the image under analysis. In particular, the proposed algorithm is based on the concept of orthogonal projections and allows performing the estimation of the number of endmembers and their extraction simultaneously, using simple operations, which can be also easily parallelized. In this sense, it is worth to mention that our algorithm does not perform complex matrix operations, such as the inverse of a matrix or the extraction of eigenvalues and eigenvectors, which makes easier its ulterior hardware. The experimental results obtained with synthetic and real hyperspectral images demonstrate that the accuracy obtained with the proposed algorithm when estimating the number of endmembers and extracting them is similar or better than the one provided by well-known state-of-the-art algorithms, while the complexity of the overall process is significantly reduced.

9646-20, Session 4

Parallel implementation of the multiple endmember spectral mixture analysis algorithm for hyperspectral unmixing

Sergio Bernabé García, Francisco D. Igual, Guillermo Botella, Manuel Prieto-Matías, Univ. Complutense de Madrid (Spain); Antonio J. Plaza Miguel, Univ. de Extremadura (Spain)

Spectral unmixing is an important technique for remotely sensed hyperspectral data exploitation. It amounts at identifying pure spectral components (called endmembers) and their abundance fractions in each (possibly mixed) pixel of the scene. In the last decade, the issue of endmember variability has received considerable attention, particularly when each pixel is modeled as a linear combination of endmembers or pure materials. This is because it is difficult to characterize a complex class (e.g., vegetation) using just one spectral signature. As a result, several models and algorithms have been developed for considering the effect of endmember variability in spectral unmixing and possibly include multiple endmembers in the spectral unmixing stage. Perhaps the most popular approach for this purpose is the multiple endmember spectral mixture analysis (MESMA) algorithm.

The procedure executed by MESMA can be summarized as follows: (i) First, a standard linear spectral unmixing (LSU) or fully constrained linear spectral unmixing (FCLSU) algorithm is run in iterative fashion; (ii) Then, we use different endmember combinations, randomly selected from a spectral library, to decompose each mixed pixel; (iii) Finally, the model with the best fit, i.e., with the lowest root mean square error (RMSE) in the reconstruction of the original pixel, is adopted. However, this procedure can be computationally very expensive due to the fact that several endmember combinations need to be tested and several abundance estimation steps need to be conducted, a fact that compromises the use of MESMA in application under real-time constraints.

In this paper we develop (for the first time in the literature) an efficient implementation of MESA on different platforms using OpenCL, an open standard for parallel programing on heterogeneous systems, which includes a wide variety of devices, from dense multicore systems from major manufactures such as Intel or ARM to new accelerators such as graphics processing units (GPUs), field programmable gate arrays (FPGAs), the Intel Xeon Phi and other custom devices. Our proposed implementation of MESMA significantly reduces its computational complexity. Our experiments have been conducted using a hyperspectral data set collected by NASA´s Airborne Visible Infra-red Imaging Spectrometer (AVIRIS) over the Cuprite mining district in Nevada. This kind of implementations with the same descriptive language on different architectures are very important in order to really calibrate the possibility of using heterogeneous platforms for efficient hyperspectral imaging processing in real remote sensing missions.

9646-21, Session 5

MESMA based on collaborative sparse unmixing

Xiang Xu, Jun Li, Sun Yat-Sen Univ. (China)

Multiple endmember spectral mixture analysis(MESMA) is a widely used spectral unmixing methods which considers the endmember variability in unmixing, and can give different number and type of endmembers for per pixel. In order to solve the MESMA problem, often needs to iteratively enumerate all possible composition of endmembers, which is a very huge computation burden. In recent years, a new method called sparse unmixing was proposed to solve these problems, and people found that all pixels in a hyperspectral image share a small number of endmembers support compared to the whole endmember library, so a type of constraint called Collaborative sparse was add to the sparse equation. In this paper, we proposed a new framework for solving the MESMA problem by using collaborative sparse unmixing.

9646-23, Session 5

Region of interest detection in remote sensing images based on integer wavelet transform and color opponent mechanism

Libao Zhang, Jie Chen, Jue Zhang, Beijing Normal Univ. (China)

With the overwhelming number of remote sensing images available today, it is necessary to provide automatic algorithms

for region of interest (ROI) detection in remote sensing images. Traditional approaches for detecting regions of interest include classification and segmentation procedures. However, most classification methods require prior knowledge that is inherently difficult to generate and involve time-consuming global searches. To solve these problems, this paper proposes a more efficient region of interest detection model in remote sensing images, which is constructed by saliency analysis based on integer wavelet transform (IWT) and color opponent mechanism (COM). The IWT is used to extract the orientation feature of the remote sensing image and to generate the orientation saliency feature map. The color opponent mechanism is used to extract the color features to generate the color saliency feature map of the remote sensing image. Color opponent mechanisms is an important tool used to simulate the color opponent channels in HSV, which are regarded as the building blocks for various color perception tasks such as boundary detection and saliency region detection. The difference of Gaussian (DoG) template is employed to compute the intensity saliency feature map. In addition, a new feature competition strategy is proposed to add different weights to each saliency feature map. Thus, the details of the saliency maps can be detected in this process. Finally, an effective adaptive thresholding is used to acquire the accurate regions of interest from the saliency map of the remote sensing image. Compared with existing models, our method can not only effectively extract detail of the salient region but also effectively remove mistaken detection of the inner parts of the saliency region.

9646-24, Session 5

Performance portability study of an automatic target detection and classification algorithm for hyperspectral image analysis using OpenCL

Sergio Bernabé García, Francisco D. Igual, Guillermo Botella, Carlos E. Garcia Gonzalez, Manuel Prieto-Matías, Univ. Complutense de Madrid (Spain); Antonio J. Plaza Miguel, Univ. de Extremadura (Spain)

Recent advances in heterogeneous high performance computing (HPC) have opened new avenues for demanding remote sensing applications, such as target detection and identification for military purposes, biological threat detection, monitoring of oil spills and other types of chemical contamination, wildfire tracking, and so on.

Previous research studies have shown that the ever-growing computational demands of these applications, which often require real- or near real-time responses, can fully benefit from these emerging computing platforms. Unfortunately, programing heterogeneous systems is a laborious task that often involves a deep knowledge of the underlying architecture. In fact, programmers are usually forced to concentrate on implementation details and learning new APIs rather than on other important issues related to the application. Furthermore, the lack of standardization in the first generation products from IBM (Cell BE) or NVIDIA resulted in most applications being too specific to a given architecture, eliminating or at least making extremely difficult the possibility of reusing code across different platforms.

The necessity to improve portability led to the development of OpenCL, an open and royalty-free standard based on C99 for parallel programing on heterogeneous systems. Its first specification was released in late 2008. Since then, it has been adopted by many vendors for all sort of computing devices, from dense multicore systems to new accelerators such as graphics processing units (GPUs), digital signal processors (DSPs), field programmable gate arrays (FPGAs), the Intel Xeon Phi and other custom devices. However, OpenCL makes no guarantee of performance portability. Portability is important for application and library developers, but performance is what really matters to application users. Our focus in this work is on analyzing and studying this emerging problem using as a benchmark the automatic target detection and classification algorithm (ATDCA), a well-known algorithm that has been widely used for the detection of (moving or static) targets in remotely sensed hyperspectral images.

Previous research has already investigated the mapping of ATDCA on GPUs and FPGAs, showing impressive speedup factors that allow its exploitation in time-critical scenarios. Based on these studies, our work explores the performance portability of a tuned OpenCL implementation across a range of processing devices including low-power multicore processors, GPUs and FPGAs. This approach differs from previous papers, which focused on achieving the optimal performance on each platform. Here, we are more interested in the following issues: (1) evaluating if a single code written in OpenCL allows us to achieve acceptable performance across all of them, and (2) assessing the gap between our portable OpenCL code and those hand-tuned versions previously investigated. Our study includes the analysis of different tuning techniques that expose data parallelism as well as enable an efficient exploitation of the complex memory hierarchies found in these new heterogeneous devices.

Experiments have been conducted using hyperspectral data sets collected by NASA's Airborne Visible Infra-red Imaging Spectrometer (AVIRIS) and the Hyperspectral Digital Imagery Collection Experiment (HYDICE) sensors. To the best of our knowledge, this kind of analysis has not been previously conducted in the hyperspectral imaging processing literature, and in our opinion it is very important in order to really calibrate the possibility of using heterogeneous platforms for efficient hyperspectral imaging processing in real remote sensing missions.

9646-25, Session 5

Accelerating the prediction-based lower triangular transform for data compression using Intel MIC

Shih-Chieh Wei, Tamkang Univ. (Taiwan); Bormin Huang, University of Wisconsin-Madison (United States)

With its decorrelation and coding gain capabilities as the Karhunen-Loeve transform, the prediction-based lower triangular transform can apply its perfect reconstruction property for lossless compression of ultraspectral sounder data. As the compression process requires computation of the covariance matrix, the LDU decomposition, and the transform kernel and coefficient matrices, it will be beneficial to introduce parallel processing technology in implementation. In this work, the recent Intel Many Integrated Core (MIC) architecture will be used which can exploit up to 60 CPU cores with 4 hardware threads per core. Both threading and vectorization techniques will be explored for performance improvement.

9646-26, Session 6

Optimizing the Betts-Miller-Janjic cumulus parameterization on the Intel Xeon Phi Many-Core coprocessor

Melin Huang, Bormin Huang, Hung-Lung A. Huang, Univ. of Wisconsin-Madison (United States)

The schemes of cumulus parameterization are responsible for the sub-grid-scale effects of convective and/or shallow clouds, and intended to represent vertical fluxes due to unresolved updrafts and downdrafts and compensating motion outside the clouds. Some schemes additionally provide cloud and precipitation field tendencies in the convective column, and momentum tendencies due to convective transport of momentum. The schemes all provide the convective component of surface rainfall. Betts-Miller-Janjic (BMJ) is one scheme to fulfill such purposes in the weather research and forecast (WRF) model. National Centers for Environmental Prediction (NCEP) has tried to optimized the BMJ scheme for operational application. As there are no interactions

among horizontal grid points, this scheme is very suitable for parallel computation. With the advantage of Intel Xeon Phi Many Integrated Core (MIC) architecture, efficient parallelization and vectorization essentials, it allows us to optimize the BMJ scheme. We will present the results of the computing performance on this scheme with Intel Xeon Phi MIC architecture.

9646-27, Session 6

Parallel hyperspectral compressive sensing method on GPU

Sergio Bernabé García, Gabriel Martín Hernández, Jose M. Nascimento, Instituto de Telecomunicações (Portugal)

Remote hyperspectral sensors collect hundreds of images within their ground instantaneous field of view corresponding to nearly contiguous spectral channels of high spectral resolution. This technology provides enough spectral resolution for material identification, facilitating an enormous number of civilian and military applications. Due to the generally low spatial resolution provided by these devices and due to natural composition of terrestrial surface, each pixel is generally a mixture of several spectrally distinct materials (also called (endmembers).

Hyperspectral unmixing is a source separation problem which amounts to estimating the number of endmembers, their spectral signatures and their abundance fractions (i.e., the percentage of each endmember). The linear mixture model has been the most popular tool used to unmix remotely sensed hyperspectral data. In recent years, several approaches have been proposed to solve the aforementioned problem using high performance computing systems: commodity clusters, field programmable gate arrays (FPGAs), multi-core processors and commodity graphics processing units (GPUs). The last two alternatives offer highly relevant computational power at low cost, thus offering the opportunity to bridge the gap towards real-time analysis of remotely sensed hyperspectral data. Usually the bandwidth connection between the satellite/airborne platform and the ground station is reduced, which limits the amount of data that can be transmitted. As a result, there is a clear need for (either lossless or lossy) hyperspectral data compression techniques that can be applied onboard the imaging instrument.

In contrast, the application of compressive sensing (CS) to hyperspectral images is an active area of research, where the acquisition of the data in an already compressed form is involved. In Gabriel work, a hyperspectral coded aperture (HYCA) method is proposed, which combines the ideas of spectral unmixing and compressive sensing. It takes advantage of two main properties of hyperspectral data, namely the high correlation existing among the spectral bands of the hyperspectral data sets and the generally low number of endmembers needed to explain the data, which largely reduces the number of measurements necessary to correctly reconstruct the original data. Until now, there has been no effort to accelerate coded aperture algorithms for hyperspectral images using parallel techniques in the open literature.

In this paper, a parallel implementation of HYCA algorithm for compressive sensing on GPUs using the compute unified device architecture (CUDA) is proposed. The parallel hyperspectral coded aperture (P-HYCA) implementation exploits the GPU architecture at low level, using shared memory and coalesced accesses to memory. Preliminary results conducted using real hyperspectral data set collected by the AVIRIS instrument on two different GPU architectures by NVIDIA: GeForce GTX 590 and GeForce GTX TITAN, reveal that the use of GPUs can provide real-time compressive sensing performance. The speedup achieve is up to 20 times when compared with the processing time of HYCA running on one core of the Intel i7-2600 CPU (3.4GHz), with 16 Gbyte memory.

9646-28, Session 6

Bistatic scattering characteristics of the vegetation base on the second-order vector radiative transfer theory

Yuanyuan Zhang, Xidian Univ (China); Zhensen Wu, Xidian Univ. (China); Kaiyuan Fu, Xidian Univ (China)

The bistatic scattering from the vegetation is a subject of increasing interest. Compared to the backscattering coefficient, bistatic scattering echo contains multi-dimension information about the vegetation. Based on the second-order vector radiative transfer theory (VRT), the bistatic scattering returns in co-polarization and cross-polarization from wheat and soybean in L band and C band are investigated in this paper. The main effect characterizing of the bistatic scattering from vegetations are shown that: for the VV polarization and HH polarization, the bistatic scattering from the ground, vegetations and the vegetations-ground are the three dominant scattering mechanisms in L band, while the second order scattering from vegetations has a little effect, and it increases fast with the incident angle increasing. At C band, the second order near field interaction is profound in VV polarization and cross polarization, and it is dominate with the vegetations scattering. The data simulated by the second-order VRT increase the value of coefficients predicted by the first-order VRT in co-polarization and the cross polarization, and it is more obvious in the high frequency band. The simulated data by the first-order and second-order VRT summation are in good agreement with the backscattering data measured, improved the results by the single first-order VRT in high frequency. Because the bistatic scattering echo and backscattering echo are sensitive to the vegetation parameters in C band and higher frequency, and are sensitive to the soil parameters in L band and lower frequency, this high fidelity scattering model will be helpful for inversion of the vegetation parameters and the soil moisture in a high precision.

9646-29, Session 6

GPU-based parallel clustered differential pulse code modulation

Jiaji Wu, Wenze Li, Wanqiu Kong, Xidian Univ (China)

Hyperspectral remote sensing technology is widely used in marine remote sensing, geological exploration, atmospheric and environmental remote sensing and other exploration purpose. It not only contains a wealth of feature information, but also contains a large number of spectral information. Owing to the rapid development of hyperspectral remote sensing technology, the resolution of hyperspectral image has got a huge boost. Thus, the data size of hyperspectral image is becoming larger. In order to reduce their saving and transmission costs, lossless compression for hyperspectral image have become an important research topic.

According to the strong correlation between the spectra in a hyperspectral image, large numbers of algorithms have been proposed using the linear regression to train the relationship between different spectra, and reduce the redundancy between different spectra. Among of them, the most classical and high expansibility algorithm is the Clustered Different Pulse Code Modulation (C-DPCM) algorithm. This algorithm contains three parts: clustering, prediction and coding. It first uses k-means clustering algorithm to cluster all the spectral lines, then trains linear predictors for each band. Second, use these predictors to predict pixels, and we get the residual image by subtraction between original image and predicted image. Finally, use arithmetic coding to encode the residual image.

However, the process of calculating predictors is time-costing. Especially, prediction order is usually set particularly high for better compression ratio. In order to improve the processing speed, we propose a parallel C-DPCM based on CUDA (Compute Unified Device Architecture) with GPU.

Recently, general-purpose computing based on GPUs has been greatly developed, with current GPUs having hundreds

of cores and abundant bandwidth. The capacity of GPU improves rapidly by increasing the number of processing units and storage control units. CUDA is a parallel computing platform and programming model created by NVIDIA. It gives developers direct access to the virtual instruction set and memory of the parallel computational elements in GPUs.

Our core idea is to achieve the calculation of predictors in parallel. By respectively adopting global memory, shared memory and register memory, we finally get a decent speedup.

9646-30, Session 6

Hyperspectral unmixing based on local collaborative sparse regression

Shaoquan Zhang, Jun Li, Sun Yat-Sen Univ. (China); José M. Bioucas-Dias, Univ. de Lisboa (Portugal); Antonio J. Plaza Miguel, Univ. de Extremadura (Spain)

Spectral unmixing is an important technique for hyperspectral data exploitation. In order to solve the unmixing problem using a collection of previously available spectral signatures, sparse unmixing has been developed under the assumption that each mixed pixel can be expressed in the form of linear combinations of a limited number of pure spectral signatures that are known in advance and available in a database. Collaborative sparse unmixing exploits the fact that the number of endmembers participating in a given mixture is generally low. However, the classic collaborative formulation globally assumes that all pixels in a hyperspectral scene share the same active set of endmembers. This global assumption rarely holds in practice, as endmembers tend to appear concentrated in local spatial regions rather than spread over the whole image. To address this limitation, in this work we introduce a new strategy to preserve local collaborativity for sparse hyperspectral unmixing. The proposed approach, called local collaborative sparse unmixing (LCSU), by taking advantage from the neighborhood information, also considers the fact that endmember signatures generally appear distributed in local spatial regions instead of uniformly distributed throughout the scene. It is computationally expensive due to the high dimensionality of the data. In order to improve the computational efficiency of the algorithm, this work develops a new parallel implementation on graphics processing units (GPUs). The presented optimizations are tested in different analysis scenarios (using both simulated and real hyperspectral data) and shown to provide state-of-the-art results from the viewpoint of unmixing accuracy and computational performance.

9646-31, Session 7

Differential evolution algorithm-based kernel parameter selection for Fukunaga-Koontz Transform subspaces construction

Hamidullah Binol, Yildiz Technical Univ. (Turkey); Abdullah Bal, Huseyin Cukur, Yildiz Technical Univ (Turkey)

In this study, we propose an automatic technique to select the appropriate parameter of the RBF kernel for KFKT. An objective function is defined to evaluate the discrimination ability of KFKT, and then the optimal values of the kernel parameters are obtained by a DEA-based optimization algorithm.

The test data is a widely used hyperspectral image, namely the Indian Pine data which was captured by AVIRIS sensor over northwest Indiana in June 1992. Original data has 16 labeled classes and has 145 lines/scene and 145 pixels/line with 220 spectral bands. After discarding the water absorption 200 spectral bands are used in the experiments. In this study, challenging two classes are selected and the number of samples of each test class is listed in Table I.

To investigate the effects of the number of the learning sets belong to the target class, we have tested for three different number of sample data cases which are {10, 20, 30}. It is not necessary to employ crossover operation in DE algorithm since KFKT has only one parameter, i.e. ?, to be optimized. The other parameters, NP and F, are assigned as 25 and 0.3 for 0<?<0.5, respectively. Table II gives the parameter selection results for the RBF kernel with the area under ROC curves (AUCs) in percentage.

The experimental results show that the proposed algorithm can find optimum kernel parameters for KFKT, successfully.

9646-32, Session 7

Accelerated ray tracing algorithm under urban macro cell

Zhongyu Liu, Lixin Guo, Xiaowei Guan, Xidian Univ. (China)

The rising demand for mobile communications, particularly in urban macro cell, has led to the adoption of macrocellular systems to accommodate an influx of users despite limited frequency resources. The successful implementation of these systems requires a fast and accurate propagation prediction model for system deployment. In this study, an ray tracing propagation prediction model, which is based on creating a virtual source tree in which the relationship between neighbor nodes is a left-son-and-right-brother one, is used because of their high efficiency and reliable prediction accuracy. In addition, the usage of threshold control of each ray path and the handling of visible grid points for reflection and diffraction sources are also adopted, resulting in an improved efficiency of ray-tracing-based prediction over large areas. However, in the process of employing the ray tracing method for coverage zone prediction, runtime is linearly proportional to the total number of prediction points, leading to large and sometimes prohibitive computation time requirements under complex geographical environments. In order to overcome this bottleneck, the compute unified device architecture (CUDA), which provides fine-grained data parallelism and thread parallelism, is implemented to accelerate the calculation. Taking full advantage of tens of thousands of threads in CUDA program, the decomposition of the coverage prediction problem is firstly conducted by partitioning the image tree and the visible prediction points to different sources. Then, we make every thread calculate the electromagnetic field of one propagation path and then collect these results. Comparing this parallel algorithm with the traditional sequential algorithm, it can be found that computational efficiency has been improved.

9646-33, Session 7

Region of saliency detection based on low-level contrast features for remote sensing images

Libao Zhang, Shuang Wang, Beijing Normal Univ. (China)

Region of saliency detection (ROS) of an image is useful for many applications like object recognition, image compression, image retrieval, and image segmentation. It has been introduced into the remote sensing image analysis and has become an important technical approach for improving target detection accuracy in remote sensing image processing.
In recent years, salient region detection has got a great of development, but it is still a profound challenge. Many saliency detection algorithms have been proposed recently, but the detection results in remote sensing images are inaccurate.
The goal of region of saliency detection is retaining salient regions and eliminating background information effectively. In this letter, a new computational model is proposed to improve computational accuracy in ROS detection of remote sensing images. For the high-spatial-resolution remote sensing images,

the structure, shape, and texture information is abundant and complicated. Considering the characteristics of remote sensing image, low-level contrast features are extracted for ROS analysis. We first use directional integer wavelet transform (DIWT) to obtain multi-scale approximate and detail coefficients. The detail coefficients are used to extract orientation contrast information. The approximate coefficients are utilized to extract local and global contrast information. Across-scale feature fusion is used to integrate multi-scale contrast features for generating a saliency map. Finally, an adaptive threshold segmentation algorithm is employed to obtain accurate ROS. In experiments, eight state-of-the-art saliency extraction algorithms are utilized to compare the subjective and objective performance. Our model outperforms these models both on the qualitative and quantitative evaluation. Moreover, our model not only can obtain highlighted and integrated salient regions with well-defined boundaries, but also can eliminate the shadow interference in remote sensing image.

9646-19, Session PS

The scale effects of anisotropic land surface reflectance: an analysis with Landsat and MODIS imagery

Lu Bai, Xun Huang, Zhensen Wu, Lixin Guo, Xidian Univ (China)

Scale is a key issue in the spatial and environmental sciences. It is widely recognized that the data conversion of different resolutions is vital important. In a recent study, it is emphasized that upscaling of reflectance and albedo products from 30m resolution to the 1000m resolution is highly linear, while other non-vegetated heterogeneous cover types, such as snow, soil and water, need further experiments.

In this paper, we first retrieved the sun-view geometry for each slope element of Badain Jaran Desert using ASTER GDEM data. Combined with the 30m resolution of Landsat-TM/ETM+ data, the characteristic of anisotropic of land surface reflectance was then discussed. Considering the anisotropy of the surface reflectance, we derived the land surface reflectance of spatial resolutions from 30m to 500m and 1000m using Landsat-TM/ETM+ data assuming that the main radiation source of land surface is direct solar radiation, which is compared with the result calculated by MODIS BRDF model parameters products in given sun-view geometry respectively. Then we simulate the upscaling of surface reflectance from 30m resolution to the 500m and 1000m resolution for several scenes of different Landsat-TM/ETM+ images and analyse scale characteristics by performing linear-regression analyses. The result shows that we cannot linearly average the Landsat-TM/ETM+ reflectance of 30m to the MODIS products of 1000m because of the adjacent effect. Moreover, somes factors, such as zenith angle and the relative azimuth angle, are take into account for its fitting precision. As MODIS BRDF model parameters products have a limited ability of characterizing the directional reflectance in other viewing directions when the viewing zenith angle increases and the relative azimuth angle is in the near principal plane, which indicated us that we should select Landsat-TM/ETM+ data with proper viewing zenith angles and relative azimuth angles for the accuracy of the reflectance calculated from MODIS BRDF model parameters products.

9646-22, Session PS

Semi-supervised classification tool for DubaiSat-2 multispectral images

Saeed H. Al-Mansoori, Emirates Institution for Advanced Science and Technology (United Arab Emirates)

Remote sensing is a way of measuring object properties on the earth's surface without physical contact with the object through recording electromagnetic radiation that reflected or emitted from the Earth's surface. The source of acquired data can be either from satellites or aircrafts. The rich amount of information gained from high spectral-spatial resolution leads to increase the area of applications such as environmental assessment and monitoring, military surveillance, agriculture, etc. Most of these applications are based on image processing techniques; segmentation and classification. This paper presents an efficient technique to classify four bands DubaiSat-2 images into a number of classes using an artificial neural network. These classes include urban areas, vegetation, roads, buildings and extensive tracts of water.

9646-34, Session PS

Parallel algorithm of real-time infrared image restoration based on total variation theory

Ran Zhu, Miao Li, YunLi Long, Yaoyuan Zeng, Wei An, National Univ. of Defense Technology (China)

Image restoration is a necessary preprocessing step for infrared remote sensing applications due to the environment sensitivity and inherent thermal noise of an infrared imaging system. Traditional methods allow us to remove the noise but penalize too much the gradients corresponding to edges. Since only local image structures are concerned during the whole process, they fail to diminish the effects of such degradation. Image restoration techniques based on variational approaches can solve this over-smoothing problem for the merits of their well-defined mathematical modeling of the restore procedure. However, the major disadvantage of such methods is that the numerical implementation involves massive computation, which impedes further application in real-time systems.

A commonly used model with white additive Gaussian noise is discussed by applying the probability theory. From the viewpoint of maximum a posteriori (MAP) estimation, we analyze the restoration procedure and interpret it as an inverse problem. To overcome this ill-posed minimization problem, the total variation (TV) of infrared image is introduced as a regularization term added to the objective energy functional. This concept depicts the smoothness of background image, which can be regarded as prior information. It converts the restoration process to an optimization problem of functional involving a fidelity term to the image data plus a regularization term. In other word, we search for an estimation of original image that best fits the data while its gradient is low, which means noise is removed. Infrared image restoration technology with TV-L1 model exploits the remote sensing data obtained sufficiently and preserves information at edges caused by clouds. Numerical implementation algorithm is presented in detail.

Analysis indicates that the structure of this algorithm can be easily implemented in parallelization. Therefore a parallel implementation of the TV-L1 filter based on multicore architecture with shared memory is proposed for infrared real-time remote sensing systems. The search procedure needs to perform a large amount of consecutive numerical calculations until the termination condition is satisfied. However, the gradient terms and divergence terms in the algorithm can be calculated separately in a parallel way. At the beginning of each numerical iterative step, the master thread creates a team of threads. Then massive computation of image data is performed in parallel by cooperating threads running simultaneously on multiple cores. When the parallel region is finished there is a synchronization of data, and the master thread will calculates some global terms and decides whether to start the next iteration. OpenMP standard provides appropriate library routines for synchronization mechanisms to avoid thread conflict, race conditions and deadlocks, which enabled us to achieve a substantial speedup for parallel implementation of the TV-L1 filter.

Several groups of synthesized infrared image data are used to validate the feasibility and effectiveness of the proposed parallel algorithm. Quantitative analysis of measuring the restored image quality compared to input image is presented. Experiment results show that the TV-L1 filter can restore the varying background image reasonably, and that its

performance can achieve the requirement of real-time image processing. Furthermore, the proposed parallel algorithm for image restoration can be easily modified for implementation on other parallel architectures such as general purpose graphics processing units (GPGPUs) and Intel Many Integrated Core (MIC).

9646-35, Session PS

GPU implementation of the discrete artificial bee colony for hyperspectral unmixing

Yuanchao Su, Sun Yat-Sen Univ. (China); Sun Xu, Institute of Remote Sensing and Digital Earth (China); Jun Li, Sun Yat-Sen Univ. (China); Lianru Gao, Institute of Remote Sensing and Digital Earth (China)

Spectral Unmixing is an important topic in hyperspectural image exploitation. It comprises of extraction of a set of pure spectral signatures and their corresponding fractional abundance in each pixel. The key step of unmixing is endmember extraction. In the past years, many algorithms for endmember extraction have been developed based on swarm intelligence techniques, such as, DPSO, ACO, etc.

The basic model of spectral unmixing is that the geometry description follows a Linear Mixture Model (LMM). According to our experience, we have found out there are some inevitable disadvantages in the umixing process. First and foremost, the error accumulates due to the fact that there is noinformation from a feedback mechanism. Also some maladjustments may appear when dealing with images having big errors or strong noises for simple evaluation of endmembers.

In this paper, we present a new optimal model for endmember extraction, namely, a new swarm intelligent method based on discrete artificial bee colony algorithm for endmember extraction (DABC). This method could resolve the aforementioned issues and lead to good estimation of the endmembers. Furthermore, in order to improve the low efficiency of DABC, which is typical for swarm intelligence algorithms, in this work, we use graphics processing units (GPUs) to effectively solve (in parallel) the optimization problem involved in the computation of DABC.

9646-36, Session PS

Fault tolerance of SVM algorithm for hyperspectral image

Yabo Cui, Institute of Remote Sensing and Digital Earth (China); Zhengwu Yuan, College of Computer Science and Technology, Chongqing Univ. of Posts and Telecommunications (China); Yuanfeng Wu, Lianru Gao, Hao Zhang, Key laboratory of Digital Earth Science, Institute of Remote Sensing and Digital Earth (China)

One of the important tasks in analyzing hyperspectral image data is the classification process[1]. In general, in order to enhance the classification accuracy, the data to classify should be exact data by pre-processing. But for the time-sensitive applications, we hope that even the data contains noise the classifier can still appear to execute correctly from the user's perspective, such as risk prevention and response. As the most popular classifier, Support Vector Machine (SVM) has been widely used for hyperspectral image classification and proved to be a very promising technique in supervised classification[2]. Two experiments are performed in this paper to demonstrate that for the hyperspectral data with noise, if the noise of the data is within a certain range, SVM algorithm is still able to execute correctly from the user's perspective.

9646-37, Session PS

A lossless compression algorithm for aurora spectral data using online regression prediction

Wanqiu Kong, Jiaji Wu, Xidian University (China)

Aurora spectral image, which adds spectral information to two-dimensional spatial images, is a kind of spectral image. In Chinese Antarctic Zhongshan Station, aurora spectral data produced every day is required to be transmitted to Polar Research Institute of China in read-time. Considering that transmission speed between these two places is less than 10KB/s and transmission distance is as long as 11785 km, massive data size of each aurora spectral image and continuity of producing a frame image every 15 seconds cause transmission difficult to be in time. To solve the tough problem, this paper proposes a lossless compression algorithm for aurora spectral data using online linear prediction, dedicated to break the limitation of transmission bandwidth.

As known, the correlation of traditional spectral images consists of inter-spectral and intra-spectral correlation. Aurora spectral image essentially has the same features with spectral image, and redundancy reduction is critical for data compression. In our proposed algorithm, we first utilize prediction-based methods to remove the redundancy by using a linear regression model. Choosing pixels of original aurora spectral image in two directions to be the reference pixels for prediction, the algorithm is able to make full use of inter-spectral and intra-spectral correlation. However, the process uses multiple regression model and least square method to predict, meaning that all pixels of the image is required during the computation. Additionally, side information also necessitate to be transmitted to the decoder involves prediction coefficients of all bands, which increases in proportion to prediction order.

Hence then we presents online linear prediction method opposed to the above mentioned algorithm. The online linear prediction method utilizes pixels encoded to predict the pixels have not been encoded, correspondingly while decoding, decoded pixels are utilized to predict the pixels have not been decoded. Nevertheless, to avoid time-consuming matrix inversion computation of least square algorithm, we adopt recursive least square (RLS) algorithm in the process of researching. By gradually correcting prediction coefficients using encoded pixels, the coefficients need not to be transmitted, from which the name of "online prediction" derives. However, our proposed algorithm adaptively decide whether least square algorithm or RLS algorithm is chosen to do the prediction.

For lossless compression, entropy-encoded differences between actual values and predicted value of the pixels, called residuals, are also transmitted after prediction. We employ the same entropy encoding method called range encoding. Then we experimented these two algorithms both on whole-sky aurora images in the direction of magnetic field line, indeed aurora spectral images, of Chinese Antarctic Zhongshan Station. The experiment results show that compression performance of the online one seems to be better and the performance difference becomes greater while prediction order increases. Besides, for four-day 16-bit aurora spectral images, the online one gains improvement over JPEG-LS.

9646-38, Session PS

An empirical model for the prediction of the bistatic scattering characteristics from soil surface in microwave band

Zhensen Wu, Yuanyuan Zhang, Xidian Univ (China);
Yunhua Cao, Xidian Univ. (China)

Bistatic scattering from the land surface has an advantage in the targets anti-stealth, anti-radiation and low altitude defense, which is a subject of increasing interest. But a method with high precision and widely used as the surface scattering model, the advanced integral equation (AIEM), is time-consuming in the multi-angle calculations for soil surface scattering and the composite scattering between the soil and targets. In this paper, an empirical model for bistatic scattering prediction from soil surface, called as B-SCDF, for roughness less than 3 , and the slope less than 0.3 , is proposed, For the little outdoor bistatic data, the bistatic scattering database is simulated by the AIEM method, using the equivalent parameters (permittivity and roughness) of the soil measured in L and X band. The unknowns of the B-SCDF are retrieved by the Genetic Algorithms (GA) with AIEM database. And then the bistatic scattering coefficient in other directions, not included in the retrieval, can be predicted. A comparison between AIEM and B-SCDF for the bistatic scattering coefficient prediction is performed. The absolute error is in the range of [-2, 2] and the time cost by empirical model is much shorter than that cost by AIEM, suggesting that the empirical model is a good representative of the original AIEM, and it can dramatically decrease the complexity of the AIEM.

Conference 9647A: Unmanned/Unattended Sensors and Sensor Networks

SPIE. SECURITY+ DEFENCE

Wednesday 23 September 2015

Part of Proceedings of SPIE Vol. 9647 Unmanned/Unattended Sensors and Sensor Networks XI; and Advanced Free-Space Optical Communication Techniques and Applications

9647-1, Session 1

Next-generation sensors and sensor networks *(Keynote Presentation)*

George C. McNamara, Naval Undersea Warfare Ctr. (United States)

No Abstract Available

9647-19, Session 1

Recent development of high power, widely tunable THz quantum cascade laser sources based on difference-frequency generation *(Keynote Presentation)*

Manijeh Razeghi, Northwestern Univ. (United States)

No Abstract Available

9647-2, Session 2

Chemical detection using IR quantum cascade lasers

Panos G Datskos, Marissa E. Morales-Rodríguez, Lawrence R Senesac, Oak Ridge National Lab (United States)

We report on a spectroscopic technique for identifying chemicals and chemical residues on surfaces. A wavelength tunable mid-IR quantum cascade laser (QCL) was used to acquire spectral signatures and compared withreference spectra.

9647-3, Session 2

Preprocessing and compression of Hyperspectral images captured onboard UAVs

Rolando R. Herrero, Northeastern Univ. (United States); Martin Cadirola, Ecotronics Ventures, LLC (United States); Vinay K. Ingle, Northeastern Univ. (United States)

The recent improvements and advancements in image sensors and signal processing have enabled the development of lightweight hyperspectral imaging systems. These systems are instrumental to the successful deployment of Photometry and Remote Sensing (PaRS) capabilities in unmanned aerial vehicles (UAVs). Typically, hyperspectral images are data cubes including a few dozens of spectral bands that are useful for remote sensing applications ranging from detection of land vegetation to monitoring of atmospheric products derived from the processing of lower level radiance images. Since these images are captured in the marginal environment of a UAV, where storage and transmission resources are limited, source encoding by means of compression is a fundamental component that considerably improves the overall system performance. In this paper, we focus on the hyperspectral images captured by a state-of-the-art commercial hyperspectral camera that provides around forty 1024x1024 spectral bands in the 500 nm to 900 nm wavelength range of the visible and near infrared spectral region. In normal conditions a single hyperspectral image accounts for well over 80 MB, and as mentioned before, their storage and transmission is a critical problem that can be solved by means of compression. First, we show the results of adapting an ultraspectral data compression architecture to the hyperspectral data set captured by the aforementioned camera as both type of images exhibit strong interband correlation even for those that are not contiguous. Specifically the compression scheme we introduce integrates two stages; (1) preprocessing and (2) compression itself. For the preprocessing stage, the encoder applies a reversible procedure that generates side information beforehand. The decoder reverses the process and applies the same side information to recover the data processed by the encoder. In this case as part of preprocessing, the spectral bands are normalized and reordered resulting in a transformed cube with spectral bands that are spatially segmented and scanned to generate a unidimensional signal. For the compression stage the encoder applies a lossy image compression technique and based on the desired rate-distortion it determines the compression parameters. The decoder uses the compression side information as well as the compressed data to reconstruct the original image. Since distortion is introduced in the decompressed data the process is not fully reversible. In this case, at the compression stage, the preprocessed unidimensional signal is modeled as an autoregressive (AR) process and subjected to linear prediction (LP) such that a valid filter order is obtained by analyzing the prediction gain of the filter. The outcomes of this procedure are linear prediction coefficients and an error signal that, when encoded, results in a compressed version of the original image. Second, these preprocessing and compression algorithms are optimized and have their time complexity analyzed to guarantee their successful deployment using low power ARM based embedded processors in the context of UAVs. Lastly, we compare the proposed architecture against other well known compression schemes and show how the new compression scheme presented in this paper outperforms all of them by providing substantial improvement and delivering both lower compression rates and lower distortion.

9647-4, Session 2

Anomaly detection and situation assessment in indoor location using symbolic pattern recognition

Pristley Sathyaraj Selvakumar Samraj, Univ. of Calgary (Canada)

Anomaly detection and situation assessment is quite important while monitoring indoor locations. Recently it has become a hot research topic in computer vision and artificial intelligence. Objects in the real world exhibit complex interactions with each other. When captured in a video signal, these interactions manifest themselves as intertwining motions, occlusion and pose changes. These complex interactions can be modelled into different situations which can be benign or harmful to the containing environment. It has its applications in many areas like home surveillance, airport threat detection and monitoring closed circuit television in contained units like prison and bank vaults. Situation assessment techniques allow the system to dynamically learn the difference between normal situations and anomalies. It can be used as a complete monitoring in low priority surveillances and aid humans in high priority surveillance systems. In this paper, a novel framework based on Symbolic Pattern Recognition (SPR) has been developed. This has two main components which are learning and detection which works together as a joint unit to perform situation assessment. The detection component act as a watchdog, monitoring current activities and feeding the learning system

to learn new objects and patterns. Learning component uses the information from the detection component to learn the activities and classifying it as a threat or non-threat behaviour using symbols and grammar based rules. Qualitative and quantitative comparisons are made to evaluate the performance of this algorithm using standard CAVIAR dataset and real-time experiment in indoor domestic environment.

9647-5, Session 2

The use of composite fence with integrated sensors in security systems

Mieczyslaw Szustakowski, Piotr Markowski, Wieslaw Ciurapinski, Marek Zyczkowski, Mateusz Karol, Military Univ. of Technology (Poland)

This paper presents possibilities of using the composite fence in the security systems. The fence made entirely of dielectric materials is neutral for electromagnetic waves. Thus, the fence does not introduce disturbances in propagation of electromagnetic waves. The use of composite fences reduces reflections of electromagnetic waves which cause negative effects on fence sensors, microwave barriers and radars. Additionally, the sensing part of the fence sensors can be integrated in the composite fence structure. Thus, the detecting elements mounted on the fence are invisible for potential intruder. This paper presents the composite fence with integrated fiber for fiber optic sensors. By arranging the fiber into fence grid it is possible not only discreet installation of the sensors, but also better transfer movements of the fence to sensitive optical fiber. By using the fiber as a sensing element the whole fence remain dielectric. Thereby obtaining a fence entirely transparent to electromagnetic waves which is also monitored for forcing attempts. Another way to use the dielectric properties of the composite fence is possibility of use electromagnetic sensors. Installation of the electromagnetic sensor directly on the fence allows to create a monitored zone in the close surroundings on both sides of the fence. The use of two types of sensors based on different physical phenomena provides an improvement in the detection properties of the entire security system by reducing the number of false alarms and increasing level of safety by increasing the probability of detection an attempt to force the fence.

9647-6, Session 2

Doppler micro sense and avoid radar

Ashok Gorwara, Planar Monolithic Industries, Inc. (United States); Pavlo A. Molchanov, Planar Monolithic Industries (United States); Olha V. Asmolova, U.S. Air Force Academy (United States)

No Abstract Available

9647-7, Session 2

Small arms corrosion protection comparison study

Slobodan Rajic, William R. Lawrence, Panos G. Datskos, Oak Ridge National Lab. (United States)

No Abstract Available

9647-8, Session 2

Unattended and remote inertial sensors on surface acoustic waves

Dmitry Lukyanov, Sergey Y. Shevchenko, Alexander S. Kukaev, Maria Khivrich, Roman Telichkin, Saint Petersburg Electrotechnical Univ. “LETI” (Russian Federation)

Modern defense industry is interested in highly robust sensors of movement parameters. Traditional MEMS accelerometers and gyros cannot satisfy requirements of several applications due to their low shock and vibration resistance. This problem is rising because traditional vibration-type sensors have elastic suspensions and moving parts in their construction. That is why solid-state sensors are of a great interest. A possible way to construct such a sensor is to use surface acoustic waves (SAW). Excellent effectiveness of this sensors production and a high level of structural integration provides basis for increased accuracy, size reduction and significant drop in total production costs. SAW-based sensors are intended to work in the conditions of shocks larger than 25 000 g and rotation velocities of 10 000 deg/s. Existing principles of SAW-based sensors (accelerometers and gyroscopes) are based on the theory of SAW propagation in stressed and rotating wafers. The effect comes from the change in wave propagation properties induced by a stressed state of a sound conductor or the Coriolis effect. A short introduction to the basics of observed effects is provided in the report.

New opportunities are opening if the sensors do not require any power sources and provide an opportunity of a remote sensing. Surface acoustic waves is, probably, the only way to construct a gyro or an accelerometer with such features. The main idea is to use an RF signal for a SAW excitation as it is done in radio frequency identification (RFID) systems. In this case the sensor works as a reflector that reconfigures the coming signal according to an applied loading and sends it back to a measurement station. Several design concepts incorporating reflective delay lines were proposed in recent years, but faced some criticism. Still, the concept is promising and is being of interest in St. Petersburg Electrotechnical University. Several experimental models were developed and tested to find the minimal configuration of a passive and wireless SAW-based gyro. Structural schemes, potential characteristics and known limitations are stated in the report. Special attention is dedicated to a novel method of a FEM modeling with piezoelectric and gyroscopic effects simultaneously taken into account. Such a method is unique and might be used for any type of a SAW-based devices.

9647-10, Session 3

Robotics and robot-assisted search and rescue *(Keynote Presentation)*

John G. Blitch, Colorado State Univ. (United States)

No Abstract Available

9647-11, Session 3

Cost efficient unmanned aircraft systems in crisis management and modern hybrid warfare: Ukrainian case study *(Keynote Presentation)*

Andre Samberg, EU IMG-S TA7 (Finland)

No Abstract Available

9647-12, Session 4

Developing command and control for cross-domain unmanned vehicle operations

Lynn Ewart, Naval Undersea Warfare Ctr. (United States)

No Abstract Available

9647-15, Session 4

A system concept for persistent, unmanned, local-area Arctic surveillance

Bruce McArthur, Defence Research and Development Canada, Atlantic (Canada)

This paper describes a system concept for persistent (up to 365 days, 24/7), unmanned, local-area surveillance of air and maritime surface and sub-surface objects in the Canadian Arctic. The system concept is based on unmanned, remotely controlled and monitored Arctic Surveillance Systems that could be deployed at one or more maritime chokepoints, at locations in the Canadian Arctic Archipelago. The Artic Surveillance Systems would be operated over a satellite communication channel from a Southern Control Centre located in the south of Canada. Surveillance information for each detected platform and environmental reports for the local operating area would be compiled semi-automatically, from the integration of data transmitted from multiple above-water and underwater sensors and self-reporting systems, and be disseminated, in near real-time, to defence, security, and public safety clients. Potential sensors and self-reporting systems include radar, radar intercept receiver, underwater acoustic arrays, electro-optical/infrared camera system, Automatic Identification System (AIS), Automatic Dependent Surveillance - Broadcast (ADS-B), and a meteorological sensor system. The Arctic Surveillance System includes a Habitat System, to provide power, safety, security and physical structures to house the Arctic-deployed surveillance system components. The system concept is being used in support of the specification of functional requirements for a concept demonstration system for Arctic surveillance, currently under development by Defence R&D Canada.

The system concept is comprised of a surveillance concept, which considers the high-level surveillance requirements for persistent, unmanned, local-area Arctic surveillance, and a system operating concept, which considers the system capabilities and operating modes required to achieve the surveillance concept. Significant aspects of the surveillance concept include: geographic and environmental factors; platform types under potential surveillance; supported surveillance functions; end-user information requirements, in terms of both the type and quality of surveillance information products; information integration and the contribution of individual sensors to surveillance; and, the role of local-area surveillance within the broader context of Arctic Domain Awareness.

The system operating concept takes into consideration the sensor and Habitat capabilities required to support unmanned operation, the sensor and telemetry data types to be transmitted between the Artic Surveillance System and Southern Control Centre; and, options for the management of that data in a bandwidth-constrained communications environment. A data model is presented for an integrated surveillance information product, as well as options for dissemination of information products using formatted messages or web services. As a baseline, the operating concept for the production of surveillance information products and for remote monitoring and control of the Arctic Surveillance System assumes a semi-automated process, with manning of the Southern Control Centre occurring on a periodic basis or on-demand, in response to system alarms or the detection of events of interest. Specific consideration is given to the interplay between the automation level, the quality and timeliness of the resulting information productions, the allocation of processing functions between the Control Centre and the Arctic Surveillance System, and transmitted data volumes.

9647-16, Session 4

Detection and tracking of drones using advanced acoustic cameras

Joel Busset, Florian Perrodin, Distran GmbH (Switzerland); Peter Wellig, Beat Ott, Armasuisse (Switzerland); Kurt Heutschi, EMPA (Switzerland); Torben Rühl, Thomas Nussbaumer, RUAG Defence (Switzerland)

Recent events of drones flying over city centers, official building and nuclear installations in the USA, France, Belgium and the UK stressed the growing threat of uncontrolled drone proliferation and the lack of real countermeasure. Indeed, even detecting and tracking them can be difficult with traditional techniques. A system to acoustically detect and track small moving objects such as drones or ground robots using acoustic cameras is presented. The described sensor, completely passive, is composed of a 120 element microphone array and a video camera. The acoustic imaging algorithm determines in real-time the sound power level coming from all directions using the phase of the signals acquired by the microphones. A tracking algorithm is then able to follow the sound sources. Additionally, a beamforming algorithm can selectively extract the sound coming from each tracked sound source canceling the others and the background noise. This extracted mono-channel sound signal can be used to identify sound signatures and determine the type of object. The acoustic system is integrated in a multi-sensor system comprising a pan-tilt camera, an omni-directional infra-red camera and a omni-directional visible light camera.

The described techniques can be used to detect and track any object that produces noise (engines, propellers, tires, etc). It is a good complementary approach to more traditional techniques such as (i) optical and infrared cameras for which the small size of the object may only be equivalent to few pixels and be hidden by the blooming effect of a bright background, and (ii) radar or other echo-localization techniques suffering from the fact that the echo signal coming back to the sensor is very weak.

The distance of detection depends on the type (frequency range) and volume of the noise emitted by the object, and on the environment background noise. Detection range and resilience to background noise were tested both in laboratory environments and in outdoor conditions. It was determined that drones can be tracked up to 160 to 250 meters depending on the type of drone. Extraction of speech was also experimentally investigated: for a typical noise scenario, the speech signal of a person being 80 to 100 meters away can be captured by the system with sufficient quality and acceptable speech intelligibility.

9647-17, Session 4

UAS network testbed in national civil protection in Ukraine

Andre Samberg, EU IMG-S TA7 (Finland); Sergey G. Chumachenko, Ukrainian Research Institute of Civil Protection (Ukraine); Stanislav Valuiskyi, Nokia Networks (Ukraine); Sergiy Kashuba, Bogdan Trach, Technische Univ. Dresden (Germany)

No Abstract Available

Conference 9647B: Advanced Free-Space Optical Communication Techniques and Applications

Thursday 24 September 2015

Part of Proceedings of SPIE Vol. 9647 Unmanned/Unattended Sensors and Sensor Networks XI; and Advanced Free-Space Optical Communication Techniques and Applications

9647-31, Session PS

Study on rejection characteristic of current loop to the base disturbance of optical communication system

Yao Mao, Institute of Optics and Electronics (China) and Chinese Academy of Sciences (China); Yun-Xia Xia, Qi-liang Bao, Yong-mei Huang, Institute of Optics and Electronics (China)

As laser is narrow in transmitting beam and small in divergence angle, the LOS(Line of Sight) stabilization of optical communication system is a primary precondition of laser communication links. Compound axis control is usually adopted in LOS stabilization of optical communication system, in which coarse tracking and fine tracking are included. Rejection against high frequency disturbance mainly depends on fine tracking LOS stabilization platform.

Limited by different factors such as mechanical characteristic of the stabilization platform and bandwidth/noise of the sensor, the control bandwidth of LOS stabilization platform is limited, effective rejection of high frequency disturbance can not be achieved, so it mainly depends on the isolation characteristic of the platform itself.

It is proposed by the paper that current loop may reject the affect of back-EMF, through adopting the method of electric control, high frequency isolation characteristic of the platform can be improved, the improvement effect is similar to increasing passive vibration reduction devices. Adopting the double closed loop control structure of velocity and current, combining with the rejection effect of back-EMF caused by current loop, it is equivalent to reducing back-EMF coefficient, which can enhance the isolation ability of the LOS stabilization platform to high frequency disturbance.

Although closing of the current loop can enhance the isolation ability of the LOS stabilization platform to high frequency disturbance, the LOS stabilization platform can produce a resonant peak in middle-frequency of disturbance transfer characteristics, which can amplify the disturbance of this frequency. As local great-gain of the object characteristics of the system near resonant peak can overcome local disturbance amplifying of angular disturbance transfer characteristics automatically, it can compensate the resonant peak of disturbance transfer characteristic produced by LOS stabilization platform, which can get a better disturbance stabilization performance than single speed loop.

9647-32, Session PS

Multiloop control method for large aperture fast steering mirror

Yong-mei Huang, Tao Yang, Xiang Liu, Qiang Wang, Bo Liu, Institute of Optics and Electronics (China)

High precision fast steering mirror (FSM) is a key component for beacon alignment accuracy between laser communication terminal in free space laser communication system. Due to the weak power and narrow beam divergence angle of the beacon laser in satellite communication terminal, it is necessary that the high accuracy FSM controlling while the fine sensor is working in a low frame rate. This paper proposed a multiloop control method of the FSM, which is combined with high frame frequency FSM location signal feedback loop, velocity signal feedback loop and axis deviation signal feedback loop of the fine sensor. This method overcomes the limitations by low frame rate of the fine sensor and large aperture reflecting mirror structure. It effectively improves the errors inhibiting bandwidth of the FSM, and can obtain sub-micro-radian precision of ground telescope tracking and aiming the beacon in a satellite-ground laser communication system.

9647-21, Session 6

Preliminary results of Terabit-per-second long-range free-space optical transmission experiment THRUST *(Invited Paper)*

Dirk Giggenbach, Juraj Poliak, Ramon Mata-Calvo, Christian Fuchs, Deutsches Zentrum für Luft- und Raumfahrt e.V. (Germany); Nicolas Perlot, Ronald Freund, Fraunhofer-Institut für Nachrichtentechnik Heinrich-Hertz-Institut (Germany); Thomas Richter, Fraunhofer - Heinrich Hertz Institute (Germany)

Future Very High Throughput Satellite Systems (VHTS) will perform at several Tbps throughput and thus face the challenge of limited feeder-link spectrum. While with conventional RF feeder links several tens of ground gateway stations would be required, the total capacity can alternatively be linked through a single optical ground station using Dense Wavelength Division Multiplexing (DWDM) techniques as known from terrestrial fiber communications. While intermittent link blockage by clouds can be compensated by ground station diversity, the optical uplink signal is directly affected by scintillation and beam wander induced by the atmospheric index-of-refraction turbulence. The transmission system must be capable to mitigate these distortions by according high-speed tracking and fading compensation techniques. We report on a near-ground long-range (25km) atmospheric transmission test-bed which is, with its relatively low elevation of approx. 2 degrees, exemplary for a worst case GEO uplink scenario. The transmitting side of the test-bed consists of a single telescope with a coarse- and a fine pointing assembly in order to track the atmospheric angle-of-arrival and precisely aim towards the beacon of the receiver. On the other side of the test-bed, the receiver telescope is also capable of fine pointing by tracking the transmitted signal. The GEO uplink scenario is modelled by a precise scaling of the beam divergence and the receiver's field-of-view (FoV) as well as by the beacon offset to model the point-ahead-angle (PAA). In order to make the experimental test-bed correspond to an actual feeder link scenario, the link budget as well as the turbulence profile of the experimental scenario are modelled and compared to the GEO uplink. Several DWDM channels are multiplexed to reach the total link capacity of above one Tbps.

We report on the lab preparations, the free-space test-bed design, and preliminary results, of the Terabit Throughput Satellite Technology Project THRUST carried out at the German Aerospace Center.

9647-22, Session 6

Ground stations for aeronautical and space laser communications at German Aerospace Center

Florian Moll, Christian Fuchs, Amita Shrestha, Deutsches Zentrum für Luft- und Raumfahrt e.V. (Germany)

Free-space laser communications are subject of current research and development in many research and industrial bodies because of its high potential for application in long distance air-ground and space-grounds links. These can be implemented in future communication networks as feeder, backbone and backhaul links for various air- and space-based

scenarios. Experimental investigation of system performance and channel characteristics is important to support, evaluate and improve common analytical treatments. For that purpose, the Institute of Communications and Navigation of the German Aerospace Center (DLR) operates two optical ground stations – the Optical Ground Station Oberpfaffenhofen and the Transportable Optical Ground Station – which serve as measurement and technology demonstration receiver stations. The first one is a fixed installation and is operated as experimental station with focus on channel measurements and tests of new developments. Various measurement devices, communication receivers and optical setups can easily be installed for different objectives. The facility includes an astronomical clamshell dome for housing, an azimuth-elevation mounted 40 cm telescope setup and infrastructure for its operation. Past and current deployments in several research projects are described and selected measurement achievements are presented. The former installations comprise different scintillometers, pupil and focal plane imagers, a wave-front sensor, a differential image motion monitor and receiver front-ends. Obtained results are measurements of intensity and power scintillation (scintillation index, correlation time, covariance function) and wave-front distortion (Fried parameters, phase field). The second ground station is developed for semi-operational use and demonstration purposes. Based on experience with the experimental ground station, this one is developed with higher integration level and system robustness. The focus application is the space-ground and air-ground downlink of payload data from Earth observation missions. Therefore, it is also designed to be easily transportable for worldwide deployment. The concept of system integration is explained and main components are discussed. These are the mount construction and actuators, the telescope system, the communication transceiver and the concept of transportation. The deployment in demonstration campaigns for satellite- and aircraft-ground communication is outlined and the performance discussed.

The design and characteristics of both ground stations are presented and discussed. Further advancements in the equipment and their capabilities are also presented. A concept for extension of the fixed ground station with a Coudé focus is discussed as well as and equipment of the transportable ground station with laser systems for bi-directional communication are outlined.

9647-23, Session 6

LCT for EDRS: LEO to GEO optical communications at 1,8 Gbps between Alphasat and Sentinel 1a

Herwig Zech, Frank Heine, Daniel Tröndle, Stefan Seel, Matthias Motzigemba, Tesat-Spacecom GmbH & Co. KG (Germany); Rolf Meyer, Sabine Philipp-May, Deutsches Zentrum für Luft- und Raumfahrt e.V. (Germany)

The European Data Relay System (EDRS) relies on optical communication links between Low Earth Orbit (LEO) and geostationary (GEO) spacecrafts. Data transmission at 1,8 Gbps between the S/Cs will be applied for link distances up to 45000 km. EDRS is foreseen to go into operation in 2015. As a precursor to the EDRS GEO Laser Communication Terminals (LCT), a LCT is embarked on the Alphasat GEO S/C, which was launched in July 2013. Sentinel 1A is a LEO earth observation satellite as part of ESAs Copernicus program. Sentinel 1A also has a LCT on board. In November 2014, the first optical communication link between a LEO and a GEO Laser Communication Terminal at gigabit data rates has been performed successfully [1]. Data generated by the Sentinel 1A instrument were optically transferred to Alphasat. From Alphasat, the data were transmitted via Ka-band to a ground station. In the ground station, the original data were recovered successfully. So the whole chain from LEO to ground was verified. Since then, many optical communication links between the Alphasat LCT and the Sentinel 1A LCT were performed. During these tests, the acquisition and tracking performance was investigated. The first communication links showed a very robust link acquisition capability and tracking errors in the sub-µrad range. The communication link budget was verified and compared to the predictions, showing excellent overall system behavior with sufficient margin to support future GEO GEO link applications.

In this presentation, the architecture of the European Data Relay System and the design principle of the LCT applied for EDRS will be outlined. The test results of the LEO to GEO optical communication link campaign will be presented. The behavior of the optical communication system for various parameters in terms of acquisition, tracking and communication system will be shown. Statistics of the performed links will be presented. Measuring the far-field pattern of a LCT is possible for the first time in orbit at 40000 km distance. Measurement results and a comparison to the predictions will be shown.

[1] http://www.esa.int/Our_Activities/Observing_the_Earth/Copernicus/Sentinel-1/Laser_link_offers_high-speed_delivery

9647-24, Session 7

Evaluation of Error Correcting Code performances of a free space optical communication system between LEO satellite and Ground Station

Marcin Chochol, Angelique Rissons, Jerome Lacan, Institut Supérieur de l'Aéronautique et de l'Espace (France); Nicolas Vedrenne, ONERA (France); Geraldine Artaud, Ctr. National d'Études Spatiales (France)

Nowadays, the computation of mutual information (MI) is known to provide an excellent approximation of the error correcting code (ECC) performances. An accounted length of the free space optical link easily accomplishes a transmission between LEO satellite and optical ground station (OGS). Therefore, an original communication system based on optical transmission of 10 Gb/s between LEO satellite and OGS has been proposed and modelled by means of simulations.

This system exhibited an overall functionality of the transmission based on physical layer. Every part of the system interacting with each other accounted for the special property since the moment of data generation until detection and data recovery. Intermediate steps were including digital signal processing, electro-optical conversion and transmission finally terminated with proper data collection. The transmission of following OOK and 2-DPSK signals was manifested. Various detections methods, mainly single photo-detector, delay-interferometer balanced-detection and coherent homodyne detection have been applied. The transmission using single carrier system was exploited based on electro-optical field analysis. As a consequence, an optical signal was properly combined with time series emulating time samples distribution of attenuation spread in time over the LEO-ground link. Various time series have been investigated depending on the propagation conditions. Among several time series discussed, the most crucial were those based on no-correction, tip-tilt and adaptive-optics (AO) approach. The non-correction approach accounted for the incoming flux coupled into the fiber before Rx with no correction of the wave front. In case of tip-tilt, a partial correction with a tip tilt mirror was employed, depending on the correction frequency. Meanwhile, a full AO (tip-tilt mirror and deformable mirror) featured a full correction of the wave after coupling that let to limit dynamical injection losses. After detection based on various configurations of photodetector, data was carefully managed to compute MI.

Actually various methods to compute MI are given. In this paper, the original way to calculate MI was proposed. In short, the method drove to estimate the probability density function of any variable by simulating the transmission of a large set of symbols unlike other theoretical methods which are extremely difficult to apply due to the large number of processing steps at the physical layer of the decoder. In our method, MI is retrieved first by composing the matrix linking the transmitted data bits and the received data symbols. Both data were the two chosen variables. Then, 2-D histogram allows the estimation of the probability density functions leading to

the computation of joint and marginal entropies of individual variables.

As follows, the collected MI values were crucial for calculating several packet error rates (PERs) of a given ECC. Those outcomes simplified the final ECC estimation on proposed space optical link. Additionally, two cases of physical layer and higher layer interleaving have been implemented providing an excellent diversity to the propagation channel seen by the codeword of ECC. The convolutional interleaving was proposed and data memory sufficiently extended for both the transmitter and the receiver.

9647-25, Session 7

Code design for laser ethernet transceiver for free space optical communications

Amita Shrestha, Julio Cesar Ramirez Molina, Dirk Giggenbach, Jorge Pacheco-Labrador, Christopher Schmidt, Deutsches Zentrum für Luft- und Raumfahrt e.V. (Germany)

The Laser Ethernet Transceiver (LET) being developed by the Institute of Communications and Navigation of the German Aerospace Center (DLR) is a networking device that is able to provide a free-space optical bi-directional, transparent (on Ethernet-level) communication link between different types of networks. For this purpose, it implements Forward Error Correction (FEC) and protects the Ethernet packets (EP) and successfully decodes them even after being affected by the atmospheric Free-Space Optical (FSO) fading channel. The current LET is in full compliance with 802.3 IEEE Gigabit standards, providing an effective 1 Gigabit Ethernet connection to the user. It receives Ethernet packets from the partner, does the flow control and creates proprietary LET frames which are then sent through the FSO channel. At the receiver side, it receives the LET frames which are affected by the atmospheric disturbances and regenerates the transmitted Ethernet packets. LET is implemented in high-end Arria V Altera FPGAs.

The free space optical channel has various atmospheric effects that cause outages. Implementation of various coding schemes can help to mitigate these effects. In order to design a suitable coding scheme, it is crucial to understand the channel model. The objective of this paper is to adequately model the FSO channel based on measured received power vectors and design suitable coding scheme for this channel. As a starting point, we used the measured data from several ground-to-ground horizontal links of 4.3 km and 12 km and the receiver apertures of size 5cm and 127mm. These data are then used to evaluate the atmospheric parameters and fading statistics like, power distribution function (pdf) and cumulative distribution function (cdf) of the fades, fraction of fade, and fade duration for the scenario. Based upon these statistics, we designed and implemented a suitable bit-level forward error correction (BL-FEC) scheme in LET and tested it for various FSO scenarios using an optical fading test bed. The fading test bed is a laboratory device that emulates the FSO channel based on the measured data. For the BL-FEC code, we selected Reed-Solomon (RS) codes because of its low-complexity and availability as “off-the-shelf” IP cores.

Our results showed that the Reed-Solomon BL-FEC provides required link budget gain. However, slow fading FSO scenarios cause outages which go beyond the capability of simple BL-FECs. Therefore, we designed a packet level coding scheme which is able to cope with signal outages of different lengths. This paper discusses a suitable packet level code design and discusses the tradeoff between its complexity and ability to mitigate different qualities of outages, i.e. longer and more frequent fades require more complex coding schemes. The packet level codes designed are based on product codes. This solution presents the advantage that the already implemented RS BL-FEC can be simply used as the outer code of the product code data matrix. The main idea of the product code is such that the first layer RS code (inner code) encodes the incoming data bytes serially and creates a matrix such that each row contains a code word. Additional RS code (outer code) encodes the data column wise. Under this scheme and considering a typical maximum fade length of 10ms the implementation of such a product code would not require more than 100 Megabyte of the memory for guaranteeing an effective Gigabit Ethernet link to the user.

9647-27, Session 7

HgCdTe APDs for free-space optical communications

Johan Rothman, Julie Baergel, CEA-LETI (France)

HgCdTe avalanche photodiodes are capable of detecting and amplifying a photon flux with a close to negligible loss of the spatial or temporal information contained in the flux. This makes them suitable for most applications that require the detection of a few photons, both in imaging and time resolved single element detection, and they have been used to increase the sensitivity in applications ranging from astrophysical observations to free space optical telecommunication (FSO). The latter was demonstrated during NASAs and ESAs joint Lunar Laser Communication Demonstration (LLCD) which illustrated that HgCdTe APDs are the most sensitive solid state photodetector that exists up to date for FSO, if cooling power and/or cost is limited. In the communications we will present our most recent advances in the development of high operating temperature HgCdTe APDs with potential use for FSO. In particular, we will present the performance of large area HgCdTe APDs with a cut-off wavelength 2.5 μm and 3.7 μm. The performance of the detectors and their use for FSO will be discussed in terms of sensitivity bandwidth as a function of operating temperature.

9647-28, Session 8

Al0.52In0.48P as a detector for wireless underwater communication

Jeng Shiuh Cheong, Liang Qiao, The Univ. of Sheffield (United Kingdom); Jennifer S. L. Ong, The Univ. of Sheffield (United Kingdom) and The Univ. of Malaya (Malaysia); Jo Shien Ng, Andrey B. Krysa, John P. R. David, The Univ. of Sheffield (United Kingdom)

Free-space optical (FSO) light communication may be an alternative to the acoustic techniques for underwater communication systems due to its higher data transmission rate. However, light suffers from severe attenuation and scattering in water, even at the best transmission wavelength of ~480 nm. Therefore, a large photosensitive area is desired for maximum collection efficiency of photons, but this then comes at the expense of response speed. To improve the signal to noise (SNR) ratio while utilising smaller area detectors, we can utilise impact ionisation to provide amplification via avalanche gain. The stochastic nature of the ionization process means that this gain is accompanied by an “excess” noise, limiting the maximum useful gain that is available.

Short wavelength silicon photodiodes are relatively cheap and have good responsivity of ~ 0.27 A/W around 480 nm. These can provide high avalanche gain with low multiplication excess noise. However, a band-pass filter is required to reject the ambient light due to its broad spectral response. Recently, we showed that a homo-junction Al0.52In0.48P SAM-APD has a spectral response peak at 482 nm with an inherently narrow full-width-half-maximum (FWHM) of 21 nm. This device can operate at a gain of 167 giving high responsivity of 18 A/W at 480 nm and has a dark current performance similar to that of commercial silicon APDs, with a dark current density of 5 nA cm-2. It was also found that AlInP has a very low breakdown voltage temperature coefficient of -12 mV/K, which is typically half that of silicon. This reduces the requirement for stringent temperature control.

To optimise the APDs SNR, knowledge of the maximum useful avalanche gain is necessary, which means determining the

excess noise performance of AlInP. Excess noise measurements as a function of avalanche gain were performed on a series of homo-junction AlInP PINs and NIPs with nominal i-region thicknesses from 1.0 μm down to 40 nm. The dark current densities in these devices were also determined as a function of reverse bias voltage. An effective ionisation coefficient ratio, k of 0.15 and 0.30 was found in the thinnest PIN and SAM-APD respectively. In this paper, we will discuss the material properties of AlInP with a view of using it as an underwater communication optical detector with avalanche gain.?

9647-29, Session 8

LiFi developments within the UPVLC project

M. Dawson, Univ. of Strathclyde (United Kingdom); Harald Haas, Dominic C. O'Brien, The Univ. of Edinburgh (United Kingdom)

No Abstract Available

9647-30, Session 8

A responsive space: multimission satellites, a look to 2030

Laura Samso Pericon, Centurion Technologies Consulting LLC (Spain)

"A responsive space is the capability of space systems to respond rapidly to uncertainty" this is how O. Brown and P. Eremenko describe this concept.

Apart from responsiveness needs, complexity in missions is increasing: high data volume demand, better resolution, near-real time data availability between others ... thus the large and monolithic spacecraft could not cover all these requirements using the classical paradigm. In order to solve these needs, a shift is taking place from large and costly spacecraft carrying multiple payload capabilities to distributed low-cost small satellite systems working together and generating multi-mission opportunities.

Some common architectures are constellations, formations, clusters and trains; but satellite mission concepts are becoming convoluted and require outstanding capabilities such responsiveness as commented above, flexibility, scalability, real time fault-tolerant resource sharing and maintainability to name a few.

Think about different concepts, the concepts of fractionated and federated systems. Fractionated systems were formulated by the Defense Advanced Research Projects Agency (DARPA) and defined as systems composed by clusters of different on-orbit wirelessly interconnected spacecraft that work cooperatively exchanging resources to obtain the same overall mission capability of a large space system. These new concepts implies a cost reduction in the overall mission but other advantages are multi-point imaging capability reducing time of data gathering (advanced ISR), low-light imaging, system reliability using redundancy, for example.

Not only architecture concepts are changing the game but also new manufacturing processes, materials, communication links, efficient control algorithms, distributed Artificial Intelligence (AI) and decision making processes, power transfer techniques and standardization, to name a few. At the same time one of the challenges is to obtain regular, affordable and reliable access to space but one of the main problems is space debris management.

The world-first optical intersatellite communication link was stablished in 2001 between the SPOT-4 and the Advanced Relay and TEchnology MIssion Satellite (ARTEMIS) satellites.

Different types of communication links could be space-space such Low Earth Orbit (LEO)-LEO, Geostationary Orbit (GEO)—LEO and Intersatellite Links (ISL) LEO-LEO or GEO-GEO; and space-ground links.

Changing environments and conditions are spurring a complete new set of frameworks in the definition of business models.

NASA has a small spacecraft technology program focused in developing and demonstrating new capabilities. The European Space Agency (ESA) is also working and developing small satellite concepts. In another order of magnitude we can find for example the United Nations Programme on Space Applications Activities and their activities.

On the other hand, the industry is moving fast and different companies are already implementing some disruptive business models such Planet Labs, Satellogic, Skybox , not only offering imaging but video in near-real time.

Conference 9648A: Electro-Optical and Infrared Systems: Technology and Applications

SPIE. SECURITY+ DEFENCE

Tuesday - Wednesday 22–23 September 2015

Part of Proceedings of SPIE Vol. 9648 Electro-Optical and Infrared Systems: Technology and Applications XII; and Quantum Information Science and Technology

9648-1, Session 1

Simulation of a multispectral, multicamera, off-road autonomous vehicle perception system with Virtual Autonomous Navigation Environment (VANE) *(Invited Paper)*

David R. Chambers, Jason Gassaway, Southwest Research Institute (United States); Christopher T. Goodin, Phillip J. Durst, U.S. Army Engineer Research and Development Ctr. (United States)

We present a case-study in using specialized, physics-based software for high-fidelity environment and electro-optical sensor modeling in order to produce simulated sensor data that can be used to train a multi-spectral perception system for unmanned ground vehicle navigation. This case-study used the Virtual Autonomous Navigation Environment (VANE) to simulate filtered, multi-spectral imaging sensors. The VANE utilizes ray-tracing and hyperspectral material properties to capture the sensor-environment interaction. In this study, we focus on a digital scene of the U.S. Army Engineer Research and Development Center (ERDC) test track in Vicksburg, MS that has extremely detailed representations of the vegetation and ground texture. The scene model is used to generate imagery that simulates the output of specialized terrain perception hardware developed by Southwest Research Institute (SwRI), which consists of a stereo pair of 3-channel cameras. Rather than providing typical RGB outputs, the two cameras utilize special filters that allow one camera to have a half-blue channel (cutting off the shorter wavelengths) and the other to have a half-red channel (cutting off the longer wavelengths). The green channel in each camera is left as a common channel to enable more reliable stereo-matching. The perception system utilizes stereo processing for ground plane segmentation and object height estimation, the multi-spectral responses, and a large array of image texture features in order to create a 3-dimensional world model suitable for off-road vehicle navigation, providing depth information and an estimated terrain class label for every pixel by utilizing machine learning. The high performance material classification function serves as an enabling technology for off-road scenarios in which certain materials represent only minor obstacles (e.g. tall grass, sparse foliage). While the process of training the perception system generally involves hand-labeling data collected through manned missions, the ability to automatically generate labeled data for certain environments and lighting conditions represents an enabling technology for deployment in new theaters. We demonstrate an initial capability to simulate data and train the perception system and present the results compared to the system trained with real-world data from the same location, providing results of common off-road classes (e.g. grass, dirt, wood, foliage, sky, asphalt) in confusion matrix form. We also present discussion of the system's current limitations as well as plans for future experimentation and development.

9648-2, Session 1

Time-resolved multispectral imaging of combustion reactions

Alexandrine Huot, Marc-André Gagnon, Karl-Alexandre Jahjah, Pierre Tremblay, Simon Savary, Vincent Farley, Philippe Lagueux, Telops (Canada); Éric Guyot, Telops (France); Martin Chamberland, Frédérick Marcotte, Telops (Canada)

Thermal infrared imaging is a field of science that evolves rapidly. Scientists have used for years the simplest tool: thermal broadband cameras. This allows to perform target characterization in both the longwave (LWIR) and midwave (MWIR) infrared spectral range. Infrared thermal imaging is used for a wide range of applications, especially in the combustion domain. For example, it can be used to follow combustion reactions, in order to characterize the injection and the ignition in a combustion chamber or even to observe gases produced by a flare or smokestack. Most combustion gases such as carbon dioxide (CO2) selectively absorb/emit infrared radiation at discrete energies, i.e. over a very narrow spectral range. Therefore, temperatures derived from broadband imaging are not reliable without prior knowledge about spectral emissivity. This information is not directly available from broadband images. However, spectral information is available using spectral filters. In this work, combustion analysis was carried out using Telops MS-IR MW camera which allows multispectral imaging at a high frame rate. A motorized filter wheel allowing synchronized acquisitions on eight (8) different channels was used to provide time-resolved multispectral imaging of combustion products of a candle in which black powder has been burnt to create an explosion. It was then possible to estimate the temperature profile by modeling spectral profile derived from information obtained with the different spectral filters. Comparison with temperatures obtained using conventional broadband imaging illustrates the benefits of time-resolved multispectral imaging for the characterization of combustion processes.

9648-3, Session 1

Stand-off detection of liquid thin films using active mid-infrared hyperspectral imaging

Luke Maidment, Heriot-Watt University (United Kingdom) and Defence Science and Technology Laboratory (United Kingdom); Zhaowei Zhang, Heriot-Watt University (United Kingdom); Christopher R Howle, Defence Science and Technology Laboratory (United Kingdom); Stephen T Lee, Alan Christie, Thales Optronics (United Kingdom); Derryck T Reid, Heriot-Watt University (United Kingdom)

Stand-off chemical detection is desirable in situations where the chemical being analyzed could be dangerous, for example in the identification of chemical warfare agents from a safe distance. One possible embodiment of stand-off detection is active hyperspectral imaging, in which a tunable laser source illuminates a scene and images are recorded at different wavelengths, allowing chemicals to be identified by examining the relative brightness of each pixel and comparing this to the infrared absorption spectra for different chemicals. To our knowledge, no active hyperspectral imaging using flood illumination and staring-mode detection has been reported for the 3–4 μm wavelength band, and here we present a study based on a Catherine MP MW thermal imager from Thales UK, using an ultrafast periodically-poled lithium niobate optical parametric oscillator (OPO) as the illumination source.

The broadband OPO idler output was focused into a monochromator reducing its bandwidth to approximately 15 nm (11 cm-1). The OPO beam illuminated the target surface, which was laid flat on the optical bench and was situated 7.5 m away from the camera. The camera was not optimized for the detection of characteristic C-H absorption features which occur in the 3.0 – 3.6 μm range. As a result, we examined two chemicals with absorption in the 3.7 – 4.0 μm band, deuterium oxide (D2O) and deuterated methanol (methanol-4d). Thin films of liquid were prepared by placing small drops (40 - 45

μL) on a painted chemical agent resistant coating (CARC) surface and placing microscope cover slips over the drops. As the illumination is tuned from 3.75 – 4.1 μm, methanol-4d becomes darker compared to methanol in a series of recorded images. The average pixel value for both liquids was plotted at each illumination wavelength along with reference spectra, recorded using Fourier transform IR spectroscopy. The pixel brightness correlates well with the reference data in each case. We could also distinguish between water and D2O, which appear identical without active illumination, for a range of incident angles and with an illumination area up to 80 cm^2.

We have demonstrated the ability to distinguish liquids based on their mid-IR absorption properties at a stand-off range of 7.5 m. While the wavelength range of the specific camera used was not optimized for hydrocarbon sensing, our results show the potential of femtosecond-OPO illumination for active imaging in the mid-IR for standoff identification of liquids. By using a camera with a wider sensitivity range, our system has the potential to detect absorption features with sufficient resolution to distinguish between many different liquid chemicals. The sensitivity and field-of-view available using this approach should allow stand-off chemical sensing of liquid drops and films over many tens of meters.

9648-4, Session 1

Performance assessment of simulated 3D laser images using Geiger-mode avalanche photodiode: tests on simple synthetic scenarios

Antoine Coyac, Laurent Hespel, Nicolas Rivière, Xavier Briottet, ONERA (France)

In the past few decades, laser imaging has demonstrated its potential in delivering accurate range images of objects or scenes, even for long range ones and under bad weather conditions (due to rain, fog or simply during the night). As a matter of fact, the number of applications based on such a technology is rapidly growing due to a huge improvement of performance (acquisition time, range, spatial resolution and compacity). Several experimental systems have since been developed, with single or multiple detectors, covering many different applications.

Among a large variety of technologies in laser imaging, it is often difficult to compare their performance for a given application. The most popular way is based on experiments. But the main drawnback of experimentation is due to the difficulty of disposing of all the instruments to be compared. An alternative way is based on the simulation, offering a higher flexibility to perform this comparison, plus being time and cost efficient.

None such simulation tool being available outside the USA, we chose to build up our own end-to-end simulator generating high accurate 3D laser images, to evaluate the capabilities of numerous sensors (3D scanning laser, 3D focal plane arrays) depending on applications (enhanced vision, DSM generation, long distance target detection and reconnaissance). 3D arrays based on Geiger-mode Avalanche PhotoDiodes (GmAPD) have already demonstrated their high potential, especially with extremely low signal strength (i.e. in long range target detection (> 3 km) and bad weather conditions cases).

This paper presents our end-to-end simulator, named LANGDOC*, using such detection technology. LANGDOC is constructed according to photon's journey following each step between laser transmission and 3D image generation. It reproduces in particular (i) the whole Poisson's statistics process of photon absorption on the array, after transmission and backscattering on a target, and (ii) photoelectron detection, occurring independently on each pixel of the matrix. This allows the use of probabilistic methods to reach back to the object distance, if a detection occurs. According to acquisition conditions, no detection or noise detection can indeed occur on a pixel, randomly distributed within the gate width, even in the presence of a target. The high frame rate of the pulsed laser is then fully exploited to discriminate laser signal over noise, GmAPD being very sensitive to noise contributions (dark counts, solar background and crosstalk effects). The program runs until the 3D point cloud reconstruction after filtering of false alarms. This detector model will also communicate with an existing program in our lab, and adapted for our case, MATLIS, to deal with laser beam propagation including illumination variations on the target (speckle) and real atmospheric perturbations (turbulence), spatial and temporal signal-target interactions (full-waveform signal generation).

Results of 3D laser images simulated with the end-to-end simulator will be presented in this paper, for static scenarios first employing simple objects such as patterns, vehicles, etc. The entire physical process being managed, the simulator will be used to highlight the scientific interest of this new kind of sensor, mainly for the reconstruction of accurate DSMs, at high frame rate, from terrestrial or aerial mobile platforms.

*Laser imAge simulatioN with Geiger Detection for tOpography and surveillanCe

9648-5, Session 1

Long-range concealed object detection through active covert illumination

Ian J. Hales, Univ. of the West of England (United Kingdom); David R Williamson, University of the West of England (United Kingdom); Mark F. Hansen, Univ. of the West of England (United Kingdom); Laurence Broadbent, Aralia Systems Ltd. (United Kingdom); Melvyn Smith, Univ. of the West of England (United Kingdom)

A common surveillance problem is the automatic detection of objects concealed under clothing and the identification of those carrying them. As many 2D methods rely on texture information, the application of patterned clothing can be used to camouflage features that may provide a clue as to the shape of the object hidden beneath.

By examining 3D features, one may gather better insight as to hidden shapes, but the level of detail required is beyond traditional stereo imaging or structured light techniques. Photometric stereo (PS) is a method for dense surface reconstruction utilising several images of an object, lit from multiple directions. A particular advantage of this technique that it reliably separates textural elements, such as printed patterns, from physical shape, which in combination with the extremely detailed surface information it provides, offers many possibilities for concealed object detection.

As one may imagine, the success of such a technique is primarily dependent on the ability to artificially illuminate the subject considerably more brightly than the ambient lighting. Clearly at night, such a situation is entirely plausible, and longer wavelength, near-infrared (nIR) lighting allows us to capture the images covertly. However under daylight conditions, ambient lighting from the sun, even within the nIR spectrum, can far outweigh our ability to sufficiently illuminate the subject to calculate the surface image, especially at long range.

Not all wavelengths of light are attenuated equally within the atmosphere. Prior research suggests that certain wavelengths are attenuated by airborne moisture considerably more than others. By choosing the wavelength of light we use to illuminate the scene to one with high attenuation, in combination with a narrow bandpass filter, we show that it is possible to provide sufficient lighting contrast to perform PS over much longer distances than in previous work.

In this paper, we examine the 940nm wavelength, which falls within one of these high attenuation regions of the spectrum. This has a particular advantage that, not only do many off-the-shelf security cameras still have some degree of sensitivity at this wavelength, new sensor technology using a "black silicon" CMOS has recently become available with much higher sensitivity at visible and nIR wavelengths. We examine the response of this new technology against cameras using traditional silicon sensors, with application to surface

reconstruction using PS over long distances (up to 100m).

Having shown that the reconstructions we can produce are of considerably better quality than those possible using traditional cameras, we present several methods for the reliable detection of concealed objects and recognition of faces, using the high level of surface detail that PS can provide.

9648-6, Session 2

Use of algorithmic behavioral transfer functions in parametric EO system performance models *(Invited Paper)*

Duncan L. Hickman, Moira I. Smith, Tektonex Ltd. (United Kingdom)

The use of mathematical models to predict the overall performance of an electro-optic (EO) System is well-established as a methodology and is used widely to support requirements definition, system design, and produce performance predictions. Traditionally these models have been based upon cascades of transfer functions based on established physical theory, such as the calculation of signal levels from radiometry equations, as well as the use of statistical models. However, the performance of an EO System is increasing being dominated by the on-board processing of the image data and this automated interpretation of image content is complex in nature and presents significant modelling challenges.

Models and simulations of EO systems tend to either involve processing of image data as part of a performance simulation (image-flow) or else a series of mathematical functions that attempt to define the overall system characteristics (parametric). The former approach is generally more accurate but statistically and theoretically weak in terms of specific operational scenarios, and is also time consuming. The latter approach is generally faster but is unable to provide accurate predictions of a system's performance under operational conditions. An alternative and novel architecture is presented in this paper which combines the processing speed attributes of parametric models with the accuracy of image-flow representations in a statistically valid framework. The approach uses a Monte-Carlo simulation framework whose input is a mission file that comprises time-varying and statistically varying mission parameters. The EO system is represented as a combination of transfer functions and radiometric-based calculations together with a look-up table (LUT) which represent the performance of the algorithmic processing design. The LUT metrics are determined from pre-calculated image sequences and accessed using mission-specific pointers.

An additional dimension needed to create an effective simulation is a robust software design whose architecture reflects the structure of the EO System and its interfaces. As such, the design of the simulator can be viewed as a software prototype of a new EO System or an abstraction of an existing design. This new approach has been used successfully to model a number of complex military systems and has been shown to combine improved performance estimation with speed of computation. In all cases, an object-orientation design approach was adopted.

Within the paper details of the approach, which can be rapidly adapted to other scenarios, and the architecture are described in detail. Example results based on practical applications are then given which illustrate the performance benefits. Finally, potential improvements are discussed which would further widen the use of the modelling and simulation approach.

9648-8, Session 2

Compressive sensing applications for single detector rosette scanning infrared seekers

Hande Uzeler, Serdar Cakir, Tayfun Aytaç, TÜBITAK BILGEM ILTAREN (Turkey)

Compressive sensing is a novel signal processing technique which enables a signal that has a sparse representation in a known basis to be reconstructed using fewer measurements obtained in a specific way below the Nyquist rate. Single detector image reconstruction applications using compressive sensing have been shown to be successful. In this paper, we investigate the application of compressive sensing theory to single detector rosette scanning infrared seekers. Single detector infrared seekers suffer from low performance compared to costly focal plane array detectors. The single detector, pseudo-imaging rosette scanning seekers scan the scene with a specific pattern and process the resultant signal with signal processing methods to estimate the target location without forming an image. In this context, this type of old generation seekers can be converted to imaging systems by utilizing the samples obtained by the scanning pattern in conjunction with the compressive sensing theory framework. This paper is an extension of the work presented in [1]. In this paper, we focus on ground-to-air missile seekers hence the targets are airborne. We also include test images containing flares and investigate the reconstruction results. Furthermore, the sampling model of the rosette scanning seeker is modified from a point based model to a circular model to provide more realistic results. Similar to our previous work, in this study infrared images have been reconstructed from samples obtained by the rosette scanning pattern for different sample numbers and it has been shown that the results obtained are comparable to the results obtained by other sampling methods proposed in the literature.

[1] Hande Uzeler; Serdar Cakir and Tayfun Aytaç, "Image generation for single detector infrared seekers via compressive sensing", Proc. SPIE 8896, Electro-Optical and Infrared Systems: Technology and Applications X, 88960T (October 25, 2013)

9648-9, Session 2

A probabilistic blur detection approach for the autofocus of infrared images

Serdar Cakir, TUBITAK BILGEM ILTAREN (Turkey); A. Enis Cetin, Bilkent University (Turkey)

Infrared (IR) cameras play an important role in the measurement and analysis of object signatures in the latest surveillance systems. However, most of the scientific IR cameras used in military applications have manual focusing systems which reduce the level-of-detail and reliability of the measurements. To overcome this problem, many autofocus algorithms have been proposed that extract various features from the images in order to define a measure for determining the most focused camera image instance. In this work, a no-reference image quality measure is modified and this measure is proposed for the autofocus of infrared cameras. Experimental results show that the proposed measure can be used successfully and reliably in the problem of autofocus of infrared cameras.

9648-25, Session PS

Test and analysis of spectral response for UV image intensifier

Yunsheng Qian, Jian Liu, Cheng Feng, Nanjing Univ. of Science and Technology (China); Yang Lv, Nanjing University of Science and Technology (China); Yijun Zhang, Nanjing Univ. of Science and Technology (China)

The UV (Ultra Violet) radiation of spectrum range at 200 nm to 280 nm is nearly zero on the earth surface, because UV radiation is greatly absorbed by ozone in atmosphere. The optical power density of solar radiation in the spectrum range of 200 nm to 280 nm is less than 10-13W/m2. It is several orders of magnitude smaller than the solar radiation in visible

light and near-UV wave band, so as to provides good detection conditions for UV detectors whose spectral response is around 200~280 nm. The 200~280 nm spectrum range is usually called "Solar Blind Range". As is often true that the UV signal is in the presence of a large solar radiation background, and the solar blind UV wave band can't be influenced by atmosphere, it is easy to detect them as soon as solar blind UV radiation objects appear in the earth surface. The UV image intensifier, consisting of UV photocathode, MCP (Micro-channel plate), fluorescent screen and other components, is one kind of electric vacuum imaging device based on principle of photoelectronic imaging. It can achieve imaging detection of weak UV signals, and has widespread application in UV guiding, UV warning, and corona detection. Currently, the photocathode material in the practical UV image intensifier is Te-Cs. As for Te-Cs photocathode, a UV filter is necessary when utilizing this UV image intensifier for solar-blind detection as a result of weak response in 400nm.To achieve solar-blind detection, the spectral response characteristic is extremely desirable. Accordingly, a broad spectrum response measuring instrument is developed. This measuring instrument uses EQ-99 laser-driven light source in light system so as to get broad spectrum in the range of 200 nm to 1700 nm. The system of two grating monochromators is utilized to reduce the influence of stray light. Because of the weak response for Te-Cs photocathode when reaching 320nm wavelength, coherent detection technology is applied. This measuring system also contains a SR540 modulator, a SR830 lock-in amplifier, and a special preamplifier as well as a test software is work out. The spectral response of the UV image intensifier can be tested in the range of 200~1700 nm, and the test accuracy can reach up to 10-6 mA/W. Using this broad spectrum response measuring instrument, a UV image intensifier made by North Night Vision Technology Co. Ltd (NVT) is tested. This image intensifier containing Te-Cs photocathode uses a dual micro channel plate structure. The radiation gain at 254 nm wavelength and the spectral response at the spectral range of 200 nm to 600 nm are tested. By solving the quantum efficiency formula, the quantum efficiency values of the UV image intensifier at the wavelength of 254 nm, 280 nm, 320 nm, 400 nm, 500 nm and 600 nm are given respectively. It is found that the quantum efficiency above 280nm wavelength still exists, especially at 280 nm to 320nm. Therefore, high-performance UV filter system is required for solar blind UV detection. In this paper, we analyze solar spectral characteristics, calculate and talk about the filter system for solar blind UV detection in UV warning and corona detection.

9648-26, Session PS

High precision of LOS stabilization of shipboard ATP system using a novel second stabilization method

Yun-Xia Xia, Qi-liang Bao, Yao Mao, Yong-mei Huang, Institute of Optics and Electronics (China); Hai-feng Yang, Southwest China Research Institute of Electronic Technology (China)

Compared to ground based Electro-optical acquisition, tracking, pointing system (ATP), the line-of-sight (LOS) of ATP which mounted on a moving platform will be affected by platform vibration, and this greatly reduces precision of tracking. So, high stabilization precision of LOS is the key of the ATP system on moving base. As the most important application field, the LOS of shipboard ATP system is mainly subjected to two parts vibration, one is low frequency (usually 0.1~0.3Hz) and large amplitude disturbance which is caused by wave, the other is high frequency jitter (several tens Hz or more than one hundred Hz) caused by propeller, engine and so on. Conventional LOS stabilization method is inertial stabling the gimbal. Two single axis gyros mounted on gimbal and measures the velocity of its elevation axis and azimuth axis respectively and these signal feedback to control loop to suppress the vibration of the moving base, it is called velocity loop or stabilization loop. However, it is difficult or even impossible to obtain a high control bandwidth (usually no more than 10Hz) of the gimbal velocity loop because it is limited to low resonant frequency, large inertia of gimbal and so on. Thus the gimbal stabilization loop mainly useful for low frequency, large amplitude disturbance but performs inability in the rejection of high frequency vibration.

This paper proposed a novel control strategy which is called second stabilization to compensate high frequency vibration of moving base and improve the LOS stabilization precision of the ATP system. The main idea of the method is to make full use of the high frequency signal of gyro, feedforward the residual vibration of gimbal stabilization to Fast Steering Mirror (FSM, it is the executive mechanism of compound axis ATP system) and make the FSM action reverse to compensate these vibration. Because the gimbal rejects most large amplitude vibration and FSM compensates the residual jitter, so we called its second stabilization. First, we must obtain the high frequency jitter from gyro, this is the most important part of second stabilization. The signal from gyro includes two parts, the target velocity and the residual vibration. Because the target motion frequency is rather low and the residual vibration is rather high, so a very useful method is adopted high bandwidth filter to separate target velocity and vibration. Second, feedforward these vibration to the input of the FSM fast position loop. The FSM control includes two closed loops: the outer loop, which is tracking loop, and the inner loop, which is position loop. The position loop for the FSM is produced by using eddy current sensor and can achieve a wide bandwidth. In this way, the characteristic of controlled object is rebuilt into a relatively simple system and has fast transient response.

Based on this novel method, simulation and experiment were both carried out by a shipboard ATP system. The experiments include a shaking platform which can generate vibration as ship sailing and a compound axis ATP system which is mounted on the shaking platform. Both the simulated and experimental result indicated that the second stabilization control strategy is accurate and effective. Precision of stabilization is greatly improved by adding second stabilization loop, and it mainly improves the ability of vibration rejection between 1Hz to 100Hz. In addition, the second stabilization control strategy doesn't need any extra sensors or extra mechanism so it's easy to realizeIt can be concluded that the second stabilization control strategy is a new and extremely effective approach for high stabilization precision of LOS and have broad application prospect.

9648-27, Session PS

Adaptive iverse control for gyro stabilized platform of electro-optical tracking system

Yun-Xia Xia, Qi-liang Bao, Institute of Optics and Electronics (China); Hai-feng Yang, Southwest China Research Institute of Electronic Technology (China); Yao Mao, Yong-mei Huang, Institute of Optics and Electronics (China)

Electro-optical acquisition, tracking, pointing system (ATP) is widely used in public security, fire protection, surveillance, laser communications and so on. The design of ATP based on moving platform is more and more difficult due to platform moving and vibration as well as atmospheric turbulence will result in jitter of Line-of-Sight (LOS). So a gyro stabilized platform subsystem must be designed to insulate the effect of platform vibration. There are two problems, one is the control system should have good performance in disturbance rejection and in target tracking at the same time. The other is because the disturbance and the gyro stabilized platform characteristics often change with time or with the changes of attitude, optimal performance of gyro stabilized platform system requires an adaptive control system.

In this paper, a novel control approach so called Adaptive Inverse Control (AIC) for line-of-sight stabilized system is proposed. The most important parts in the control strategy are three adaptive filters, including plant model, tracking controller and disturbance controller. All the adaptive control loops are based on recursive least squares lattice filter and are

identified online. This paper adopts Adaptive Inverse Control, the inverse of the plant model is used as the tracking controller and the plant model together with the plant inverse model are used to cancel disturbance. So it processes target tracking and disturbance rejecting separately. At the same time, LTI feedback control is used as the inner loop of AIC. The LTI feedback control adopts cascade control strategy, including current loop rate gyro stabilization loop. The current loop is used to improve the linearity of motor and make sure the motor as an ideal motor. LTI feedback control has two functions, one is making the characteristic of the AIC control object rebuilt into a relatively simple object and nearly unchanged, the other is the rate gyro stabilization loop of LTI feedback also rejects disturbance and the AIC rejects the residual disturbance of inner loop. In this way, it greatly improve the ability of disturbance rejection.

Based on this novel method, Simulations and experiments were carried out for a gyro stabilized platform of electro-optical tracking system. The system includes a shaking platform which can generate vibration as the moving platform and a gyro stabilized platform which is mounted on the shaking platform. Simulation and experiment results indicate that the gyro stabilized platform using AIC method is accurate and effective. Comparing with PID control, the disturbance rejecting error is greatly improved at low-frequency and mid-frequency by adopting AIC method. The improvement of precision is more than 20dB nearly over the control bandwidth . It can be concluded that the AIC method is a new approach for the high-performance gyro stabilized platform and might have broad application prospect.

9648-29, Session PS

Some design considerations for high-performance infrared imaging seeker

Jinxiang Fan, Jianxiong Huang, Shanghai Mechanical-Electronic Engineering Institute (China)

In recent years , precision guided weapons play more and more important roles in modern warfare. The development and applications of infrared imaging seekers have been paid more and more attention. With the increasing of complexity of mission and environment , precision guided weapons make more and more strict demands for infrared imaging seekers. The requirements for infrared imaging seekers included: high detection sensitivity, large dynamic range, having better target recognition capability, having better anti-jamming capability, and better environment adaptability. To meet the strict requirements of weapon system, several important issues should be considered in the design of high-performance infrared imaging seeker. The mission, targets, environment of infrared imaging guided missile must be regarded. The tradeoff among performance goal, design parameters, infrared technology constraints and missile constraints should be considered. The optimized application of IRFPA and the implement of ATR in complicated environment should be concerned. In this paper, some design considerations for high-performance infrared imaging seeker were discussed.

9648-30, Session PS

An kind of the long service life integration CES

Zhijun Tu, Loulou Deng, Zhiwu Mei, Xinchao Hu, Beijing Institute of Control Engineering (China)

The design life of the conical scanning infrared earth sensor device (CES) is two years, and the traditional CES is applicable to the low and middle orbit satellites. The traditional CES adopts the split structure; the optical head and the circuit box are connected through a long cable, and the attitude and orbit control system provides the secondary power supply. The traditional CES has the following drawbacks: susceptible to the electromagnetic interference due to transmit the analog signal through a long line; the traditional CES shares the secondary power supply with the other equipment leading to the poorer power quality; larger weight; higher power dissipation; and the traditional CES has more constraints in the layout of satellite. In order to satisfy the reliability demand of the 1ong-1ife satellite, and solve the weak links, we design an kind of the long service life integration CES (LFICES).

In order to solve the problem from the resistance increased in the later life of the LFICES, we have researched the high torque motor, and we improved the stall torque from 550g.cm to 1100g.cm, then we performed the accelerated life test of the slewing gear. In the accelerated life test, we imitated operation of eight years, and the test results showed that the slew-ing gear meet the design life of eight years.

By using the low-noise power supply to the LFICES, we improved the LFICES's noise ratio of the weak signal processing system. The secondary power supply is arranged in the independent cavity body.

In this paper, we gives the design scheme of the LFICES. The telemetering data of the 26th remote sensing satellite in-orbit flight shows that the LFICES stable work, proving the LFICES can realize the function of eliminating the electromagnetic interference.

9648-31, Session PS

Fast measurement of temporal noise of digital camera's photosensors

Pavel A. Cheremkhin, Nikolay N. Evtikhiev, Vitaly V. Krasnov, Vladislav G. Rodin, Rostislav S. Starikov, Sergey N. Starikov, National Research Nuclear Univ. MEPhI (Russian Federation)

Currently photo- and videocameras are widespread parts of both scientific experimental setups and consumer applications. They are used in optics, radiophysics, astrophotography, chemistry, and other various fields of science and technology such as control systems and video-surveillance monitoring. One of the main information limitations of photo- and videocameras are noises of photosensor pixels. Camera's photosensor noise can be divided into random and pattern components. Temporal noise includes random noise component while spatial noise includes pattern noise component. Spatial part usually several times lower in magnitude than temporal. At first approximation spatial noises might be neglected. For measurement of camera noise characteristics, the most widely used method is EMVA Standard 1288. It allows accurate dark and light temporal noise measurement but difficult in implementation and time-consuming. Earlier we proposed modification of the automatic segmentation of non-uniform targets (ASNT) method for measurement of temporal noise of photo- and videocameras. Only two frames are sufficient for noise measurement with the modified method. In result, proposed ASNT modification should allow fast and accurate measurement of temporal noise. In this paper, we estimated light and dark temporal noises of four cameras of different types using the modified ASNT method with only several frames. These cameras are: consumer photocamera Canon EOS 400D (CMOS, 10.1 MP, 12 bit ADC), scientific camera MegaPlus II ES11000 (CCD, 10.7 MP, 12 bit ADC), industrial camera PixeLink PL-B781F (CMOS, 6.6 MP, 10 bit ADC) and video-surveillance camera Watec LCL-902C (CCD, 0.47 MP, external 8 bit ADC). Experimental dependencies of temporal noise on signal value are in good agreement with fitted curves based on a Poisson distribution excluding areas near saturation. Compared to the EMVA Standard 1288 we can obtain temporal noise characteristics significantly faster. We measured elapsed time for processing of shots used for temporal noise estimation. The results demonstrate the possibility of fast obtaining of dependency of camera full temporal noise on signal value with the proposed ASNT modification.

9648-32, Session PS

Modeling of digital information optical encryption system with spatially incoherent illumination

Alyona P. Bondareva, Pavel A. Cheremkhin, Vitaly V. Krasnov, Vladislav G. Rodin, Rostislav S. Starikov, Sergey N. Starikov, National Research Nuclear Univ. MEPhI (Russian Federation)

At present time methods of optical encryption are actively developed. The majority of existing methods of optical encryption use not only light intensity distribution, easily registered with photosensors, but also its phase distribution which require application of complex holographic schemes in conjunction with spatially coherent monochromatic illumination. This leads to complex optical schemes and low decryption quality. To eliminate these disadvantages it is possible to implement optical encryption using spatially incoherent monochromatic illumination which requires registration of light intensity distribution only.

Encryption is accomplished by means of optical convolution of image of scene, displayed with first spatial light modulator (SLM), and point spread function (PSF) of encryption diffractive optical element (DOE), displayed with second SLM. DOE'S PSF serves as encryption key. Encryption process described as follows. First SLM is illuminated with spatially-incoherent monochromatic light. In the absence of encryption DOE, lens forms scene image in photosensor plane. DOE serves as encryption element, while its PSF serves as encryption key. Light passing through DOE forms convolution of first SLM image and DOE'S PSF. Convolution registered by photosensor is encrypted image.

State of the art micromirror DMD SLMs offer unprecedented framerate up to 30000 frames per second. This, in conjunction with high speed digital camera, should allow to build high speed optical encryption system. Results of modeling of digital information optical encryption system with spatially incoherent illumination are presented. Factors taken into account are: resolution of SLMs and camera, holograms reconstruction noise, camera noise and signal sampling. Input information in binary code is presented as binary data pages consisting of black and white pixels and then displayed on first SLM. Encryption DOE displayed on second SLM might be changed every time data page changes, or once for several data pages to decrease computing power requirements. Encrypted image is registered with camera and stored on a hard drive or sent over network. Numerical decryption of a single data page requires computing of inverse filter with regularization based on a key corresponding to this page. Every change of encryption key requires new decryption filter to be computed, thus, making cracking attempts extremely time-consuming. Results of numerical simulation demonstrate high speed (several gigabytes per second), low bit error rate and high crypto-strength.

9648-10, Session 3

Areal density and systems implications of primary mirror material choices *(Invited Paper)*

Tony B. Hull, The Univ. of New Mexico (United States)

One of the key early decisions in architecture of spaceborne payloads is the selection of the optical material for the Optical Telescope Assembly (OTA). If this choice is made on the basis of assuming steady state thermal conditions, or fails to recognize the important second order effects of material used, there are strong implications on the mass or thermal efficiency of the overall OTA architecture. This in turn has a large effect on system mass, complexity, ancillary assemblies, testing error budget and even operational duty cycle. These drive the observational efficiency of the mission, and its risks, schedules and costs. The ideal choice for certain thermal environments may not be materials that have the lowest E/rho or the lowest areal density. Several thermal scenarios are considered.

9648-11, Session 3

ZERODUR®: an ideal optical material for future spaceborne missions

Thomas Westerhoff, SCHOTT AG (Germany); Tony B. Hull, The Univ. of New Mexico (United States)

SCHOTT has made ZERODUR® for over 35 years, and in this time it has been flown on over 30 missions, including NASA flagships Chandra and the secondary mirror of HST. ZERODUR® is produced in large quantities for a variety of ultra-stable applications, and will be produced by SCHOTT well into the future. Presently Schott offers ZERODUR® blanks with isogrid lightweighting. A 1.2m flight-like mirror has been produced demonstrating lightweighting to 40 kg/m2, or 88% lightweighted. The process used on this mirror is discussed, and how this process can be scaled to mirror requirements less than 0.25m diameter to greater than 4m diameter. While lower areal densities can be achieved, this process is optimized for maximum cost-efficiency and minimum production lapse time. The process is also suitable for making hex and other shape segments for future very large deployable telescope mirrors.

9648-12, Session 3

Thickness and air gap measurement of assembled IR objectives

Bernd Lueerss, Patrik Langehanenberg, TRIOPTICS GmbH (Germany)

The imaging quality of an optical assembly depends on several aspects. Besides the material and manufacturing quality of the individual components the alignment of the optical elements represents a critical factor is. In the assembly process mechanical positioning errors can occur resulting either in centration errors (e.g. shift or tilt) relative to a reference axis or in deviations of the surface positions along the reference axis. With increasing sensor resolutions and a need for cost-efficiency, opti cal metrology tools become an important factor for research and production. In this context the determination of air spacings and center thicknesses within complete assemblies is of special interest not only to improve image quality but also to reduce alignment and fabrication costs.

So far, only systems optimized for measurements of VIS samples with a working wavelength in the near infrared for were available on the market. Nowadays a growing number of applications use IR optics for thermography, surveillance or automotive. As these systems often use materials that are only transparent beyond a wavelength of 2 µm, the transfer of an existing technique to longer wavelength regions opens up new technical opportunities.

In this contribution we present the determination of lens center thicknesses and air gaps of optical assemblies in a non-contact manner. The measurement technique is based on time-domain low coherent interferometry. Here, a low coherent interferometer signal is recorded in a Michelson-type setup as a function of a variable optical delay in the reference arm. Whenever the path length in the reference arm matches the path length to a lens surface, interference fringes occur. After determining the positions with maximum modulation in the interference signal, the relative surface distances can be derived from the optical delay between two peaks. For a highly-accurate measurement a precise determination of the optical delay length with minimized Abbe-errors is required.

However, simulations have shown that the high chromatic dispersion of IR materials leads to a broadening of the interference envelope. This effect scales with the lens thickness and directly reduces the axial resolution. In addition, it might deteriorate the overall accuracy. While larger lenses were unavailable at the time of test we demonstrate the performance on a 2-element IR objective lens. The dispersive

effect could not yet be observed here.

We present a new instrument consisting of a time-domain low coherence interferometer that is especially designed for all kinds of IR materials. This setup allows the measurement of air spacing, as well as center thicknesses of IR lenses and uses a fast data acquisition to reduce sampling time even for larger assemblies. First measurements have shown that accuracy in the range of few micrometers can be achieved. The obtained data can then be used for quality control of high-precision IR objectives or the compensation of air spacing errors during the assembly process.

9648-13, Session 3

Digital holographic interferometer with correction of distortions

Alexander A. Sevryugin, Saint Petersburg Electrotechnical Univ. "LETI" (Russian Federation); Sergey A Pulkin, St.-Petersburg State University (Russian Federation); Ibrohim M Tursunov, St Petersburg State Electrotechnical Univ (Russian Federation); Dmitriy V Venediktov, St.-Petersburg State University (Russian Federation); Vladimir Y. Venediktov, Saint Petersburg Electrotechnical Univ. "LETI" (Russian Federation)

In many measuring interferometers the elements of the interferometer itself induce residual distortions of the wavefront and thus lead to systematic measurement errors. In 70-80-es there were developed and investigated the holographic approaches to correction of these distortions. The reported experiment revisits these ideas and describes some novel opportunities of these techniques, resulting from the use of modern matrix photosensors, matrix light modulators and from the possibility to combine in one system analogous and digital techniques.

9648-14, Session 4

Light harvesting structures for sensing infrared radiation

Fernando de León-Pérez, Centro Univ. de la Defensa Zaragoza (Spain)

One-dimensional light harvesting structures (LHS) can be integrated into a standard photodetector, increasing both the operational speed and the sensitivity of the detector [1]. Potential applications of LHS as chemical sensors at the infrared are discussed.

LHS with a realistic geometry nano-patterned on an opaque metallic film are theoretically optimized to render high transmission efficiencies at infrared frequencies. Simple design rules are developed for the particular case of a slit-groove array with a given number of grooves that are symmetrically distributed with respect to a central slit [2]. These rules take advantage of the hybridization of Fabry-Perot modes in the slit and surface modes of the corrugated metal surface. Same design rules apply for optical and infrared frequencies. The parameter space of the groove array is also examined with a conjugate gradient optimization algorithm that used as a seed the geometries optimized following physical intuition. Both uniform and nonuniform groove arrays are considered. The largest transmission enhancement, with respect to a uniform array, is obtained for a chirped groove profile. Such relative enhancement is a function of the wavelength.

Mechanisms for one-dimensional photon sorting are also theoretically studied. A double-Pixel structure is optimized to resolve two different frequencies in the near infrared [3]. Finally, we show how the transmission efficient of SLH can be improved by focusing the light on the aperture [4].

References

[1] T. Ishi et al., Jap. J. Appl. Phys. 44, L 364 (2005). L. A. Dunbar et al., Appl. Phys. Lett. 95, 011113 (2009)

[2] F. Villate-Guío et al., Opt. Express 20, (2012) 25441-25453

[3] F. Villate-Guío et al., Photon Nanostruct: Fundam Appl. 13, 58-65 (2015)

[4] F. Villate-Guío et al., J. Opt. Soc. Am. B 31, 1653-1659 (2014)

9648-15, Session 4

A true differential pyroelectric IR detector with improved D*

Alan P. Doctor, Laser Components Pyro Group, Inc. (United States)

Pyroelectric infrared detectors are used in many commercial and industrial applications. These devices are physically capacitors and are modeled with a current source in parallel. By nature these devices present a high impedance to any measuring circuit. Thus they require an impedance converting amplifier to measure the current produced by the detector. These by nature are "single ended" and thus any electronic perturbation from an external or internal source such as line frequency interference or from a nearby oscillator or other sources of electronic noise can be coupled onto the detector's output signal. This is in contrast to many other types of IR detectors such as thermopiles, thermistor bolometers and others which are characteristically much lower in impedance and don't require these impedance converters and thus are often used in the differential mode.

In practice each "side" or electrode forming the capacitor is directly connected to an impedance converting amplifier. While being exposed to a changing IR signal the capacitor produces charge and over time a current which flows out of the positive electrode and must be balanced by an equal but opposite charge/current from the negative electrode. When these are two signals are connected to separate impedance conversion circuits the outputs are the same but of opposite sense. When these two outputs are connected to a differential amplifier the output is doubled while all the common mode artifact is canceled out.

The electrical noise in this configuration is basically the noise in the input circuitry of the impedance converters. However as this noise is random in nature it only adds vectorally as the square root of the sum of the squares of the noise in each output thus the total noise is only increased by a factor of 1.41. Thus the D* of a detector connected as described will be increased by this factor

This connection will work with any pyroelectric material (LTO, DLATGS, PLZT, PVDF etc.) with current or voltage mode impedance conversion and configurations such as parallel or series with and without temperature fluctuation compensation and of course with standard single elements. We present this connection scheme and test data proving its efficacy.

9648-16, Session 4

A new generation of small pixel pitch SWaP cooled infrared detectors

Laurent Espuno, Yann Reibel, Laurent Rubaldo, Alexandre Kerlain, Nicolas Péré-Laperne, SOFRADIR (France); Aurelien Petit dit Dariel, CEA-LETI (France); Gilbert Decaens, Vincent Badet, Laurent Baud, Regis Cotte, Julien Roumegoux, Antoine Kessler, Patrick Maillart, Nicolas Ricard, Olivier Pacaud, SOFRADIR (France); Olivier Gravrand, Pierre Castelein, CEA-LETI (France)

Following clear technological trends, the cooled IR detectors market is now in demand for smaller, more efficient and higher performance products. This demand pushes products developments towards constant innovations on detectors,

read-out circuits, proximity electronics boards, and coolers.

Sofradir was first to show a 10µm focal plane array (FPA) at DSS 2012, and announced the DAPHNIS 10µm product line back in 2014. This pixel pitch is a key enabler for infrared detectors with increased resolution at a controlled cost. Sofradir recently achieved outstanding products demonstrations at this pixel pitch, which clearly demonstrate the benefits of adopting 10µm pixel pitch focal plane array-based detectors.

Daphnis products also benefit from a global video datapath efficiency improvement by transitioning to digital video interfaces. Moreover, innovative smart pixels functionalities drastically increase product versatility.

The latest results and their associated gain in detection performance are discussed in this paper.

In addition to this strong push towards a higher pixels density, Sofradir acknowledges the need for smaller and lower power cooled infrared detector. Together with straightforward system interfaces and better overall performances, latest technological advances on SWAP-C (Size, Weight, Power and Cost) Sofradir products enable the advent of a new generation of high performance portable and agile systems (handheld thermal imagers, unmanned aerial vehicles, light gimbals etc...)

This paper focuses on those features and performances that can make an actual difference in the field.

9648-17, Session 5

Vehicle tracking in wide area motion imagery from an airborne platform *(Invited Paper)*

Adam van Eekeren, Jan Baan, Pieter T. Eendebak, Jasper van Huis, TNO (Netherlands)

Airborne platforms with Wide Area Motion Imagery (WAMI) sensors can cover multiple square kilometers and produce large amounts of video data. Analyzing all data for information need purposes becomes increasingly labor-intensive for an image analyst. Furthermore the capacity of the data connection in operational areas may be inadequate to transfer all data to the ground station. Automatic detection and tracking of people, vehicles and buildings is useful to send the most relevant footage to the ground station and assists the image analysts for effective data searches.

In this paper, we propose a method for detecting and tracking vehicles in high-resolution WAMI images from a moving airborne platform. For the vehicle detection we use a cascaded set of classifiers, using an Adaboost training algorithm on Haar features. This detector works on individual images and therefore does not depend on image motion stabilization. For the vehicle tracking we use a local template matching algorithm. This approach has two advantages. In the first place it does not depend on the quality of the image motion stabilization and it counters the inaccuracy of the GPS data that is embedded in the video data. In the second place it can find matches when the vehicle detector would miss a certain detection. This results in long tracks even when the imagery is of low frame-rate. In order to minimize false detection, we also integrate height information from a 3D reconstruction that is created from the same images. By using the locations of buildings and roads, we are able to filter out false detections and increase the performance of the tracker.

In this paper we show that the vehicle tracks can also be used to detect more complex events, such as traffic jams and fast moving vehicles. This enables the image analyst a faster and more effective search of the data.

9648-18, Session 5

Information hiding techniques for Infrared Images: exploring the state-of-the art and challenges

Victor V. Pomponiu, Singapore Univ. of Technology & Design (Singapore); Davide Cavagnino, Marco Botta, Univ. degli Studi di Torino (Italy); Hossein Nejati, Singapore Univ. of Technology & Design (Singapore)

The proliferation of Infrared technology and imaging systems enables a different perspective to tackle many computer vision problems in defense and security applications. Infrared images are widely used by the law enforcement, Homeland Security and military organizations to achieve a significant advantage or situational awareness, and thus is vital to protect these data against malicious attacks. Concurrently, sophisticated malware are developed which are able to disrupt the security and integrity of these digital media. For instance, illegal distribution and manipulation are possible malicious attacks to the digital objects. In this paper we explore the use of a new layer of defense for the integrity of the infrared images through the aid of information hiding techniques such as watermarking. In this context, we analyze the efficiency of several optimal decoding schemes for the watermark inserted into the Singular Value Decomposition (SVD) domain of the IR images using an additive spread spectrum (SS) embedding framework. In order to use the singular values (SVs) of the IR images with the SS embedding we adopt several restrictions that ensure that the values of the SVs will maintain their statistics. For both the optimal maximum likelihood decoder and sub-optimal decoders we assume that the PDF of SVs can be modeled by the Weibull distribution. Furthermore, we investigate the challenges involved in protecting and assuring the integrity of IR images such as data complexity and the error probability behavior, i.e., the probability of detection and the probability of false detection, for the applied optimal decoders. By taking into account the efficiency and the necessary auxiliary information for decoding the watermark, we discuss the suitable decoder for various operating situations. Experimental results are carried out on a large dataset of IR images to show the imperceptibility and efficiency of the proposed scheme against various attack scenarios.

9648-19, Session 5

A multiscale contrast direction adaptation approach for the fusion of multispectral and multifocus infrared images

Onur A. Karali, Serdar Cakir, Tayfun Aytaç, TÜBITAK BILGEM ILTAREN (Turkey)

Infrared (IR) imaging devices are commonly used in the most recent surveillance systems since spectral characteristics of objects provide valuable information for object/background separation. Fusing images in IR band is proposed in order to assist the surveillance system operator and automatic image processing tasks that increases the level of situational awareness. Since image content may vary dramatically depending on the spectral range, the optical properties of the cameras, the spectral characteristics of the scene, and the spatial resolution of the interested targets in the scene proposed techniques are generally developed for specific scenarios. In this work, a general purpose IR image fusion technique that can support different scenarios by applying multi-scale detail detection and can be applied to images captured from different spectral regions of the spectrum by adaptively adjusting the contrast direction through cross checking between the source images is proposed. The proposed technique can is suitable for real-time implementations. The proposed algorithm is tested on several sets of registered multi-spectral and multi-focus IR images. The performance of the proposed technique is compared with the other well-known fusion techniques through objective and subjective tests. The test results show that the proposed method outperforms baseline techniques in the subjective tests and provides promising results in objective quality metrics with an acceptable computational load. In addition, the proposed technique preserves object details and prevents undesired artificial effects better than the baseline methods on the fusion scheme that contains four source images.

9648-21, Session 5

Graph Laplacian regularization based edge-preserving background estimation for single frame small target detection

Kun Bai, Yuehuan Wang, Qiong Song, Huazhong Univ. of Science and Technology (China); Mingna Liu, Jiandong Wu, Institute of Shanghai Aerospace Control Technology (China)

Lots of background estimation methods are proposed to segregate background and foreground for small target detection in last decade. In these background estimation methods, local gray level distribution are used to predict background. The background gray value of a pixel in image is predicted by its neighborhood gray value distribution, and it can get good prediction results in flat background region. However, edges in background usually are smoothed using this model. Addressing this problem, various edge-preserving background estimation methods are proposed. The edge direction is detected by analyzing the surrounding blocks around current background estimation window. But if edges with various direction exist in the estimation window, such as at corner, they will get bad edge-preserving results. And some algorithms such as modified mean filter are only proposed to preserve the horizontal edge, this method preserves edges along preferred directions. Unfortunately, the infrared images with complicated background generally contain the junction of edges. What's more, the TDLMS filter is usually used in these background estimation method, and the TDLMS filter is L2-norm which is well known to be sensitive to outliers. This sensitivity causes these background estimation methods to produce visually unsatisfying results. If the small target exists in one patch, the estimated background will bias and affect the SCR. So the effective and robust edge-preserving background estimation method for single frame small target detection is still needed.

In order to deal with problems, we propose a novel semi-supervised learning based edge-preserving background estimation model for small target detection. First, the accurate edge estimation ability will be specially taken into account when we design clutter background estimation method. And we both know that pixels on the same graph structure have more probability to share similar gray value in infrared image. So this feature of infrared image can be used in background estimation to preserve accurate edges. And this similarity feature of graph structure is independent on directions of graph structure, so it is capable of preserving edges with different directions in background estimation window. This similarity feature of graph structure in image data domain will be formulated using Graph Laplacian regularization model to preserve edges in infrared image. Then, in order to avoid the drawback of L2-norm in background estimation model, only part of pixels in patch image are selected as labeled samples in semi-supervised learning model to predict the background in our method. So our proposed background estimation based on Graph Laplacian regularized and semi-supervised learning is capable of getting a precise edge estimation and precluding the effect of small target on background estimation.

The experiment results demonstrate that our proposed method can achieve edge-preserving background estimation significantly and efficiently, and get better small target detection results.

Conference 9648B: Quantum Information Science and Technology

Tuesday 22 September 2015

Part of Proceedings of SPIE Vol. 9648 Electro-Optical and Infrared Systems: Technology and Applications XII; and Quantum Information Science and Technology

9648-41, Session 10

Practical security of a quantum key distribution transmitter *(Invited Paper)*

Marco Lucamarini, James F. Dynes, Toshiba Research Europe Ltd. (United Kingdom) and Toshiba Corp. (Japan); Iris Choi, Toshiba Research Europe Ltd. (United Kingdom) and Univ. of Oxford (United Kingdom); Martin B. Ward, Toshiba Research Europe Ltd. (United Kingdom); Bernd Fröhlich, Toshiba Research Europe Ltd (United Kingdom); Zhiliang Yuan, Andrew J. Shields, Toshiba Research Europe Ltd. (United Kingdom) and Toshiba Corp. (Japan)

Any cryptographic system whose security is based on Quantum Key Distribution (QKD) has to take reality into account. QKD's security stems from the laws of quantum physics, which are enforced in the implementation by using real, necessarily imperfect, physical systems and devices. If such devices are modeled as ideal, a security breach opens up and the inherent security of QKD can be circumvented by exploiting the gap between the ideal description and the real performance.

A well-known example is the "Trojan-horse attack" (THA) [1,2], where photons are injected by the attacker (Eve) into the transmitting unit (Alice) in an attempt to read the information direct from the encoding devices. Because the reflectivity of the optical components in Alice's module is not exactly zero, a fraction of the injected photons is reflected back to Eve and conveys useful information to her about the supposedly secure key.

Here we discuss a novel, quantitative, countermeasure to the THA in QKD. We interpret the THA as an information leakage problem [3]. This lets us quantify the security of a QKD system running the decoy-state BB84 protocol [4,5] and connect it to parameters that are directly measurable or controllable by the legitimate users. Our results are loss-tolerant [6] and allow to guarantee the security of most of the existing QKD setups using only additional passive, cost-effective, components such as optical isolators, filters and fibre loops. The upper bound to the Trojan photons injected by Eve is provided by the ISO-defined Laser Induced Damage Threshold (LIDT), which will be briefly presented.

As an additional example of a QKD transmitter's implementation imperfection, we consider the photon statistics of the light source. This is assumed to be Poissonian when attenuated lasers emitting well above threshold are used as light source. We test this assumption by measuring the correlation functions up to the fourth order of the light emitted by a 1GHz-clocked gain-switched laser diode. We find that the assumption about the Poissonian photon statistics is almost perfectly met in the practice. Nevertheless, the key rate is decreased by a non-negligible amount, in the order of 5%, when a rigorous treatment of the worst-case scenario is carried out.

Other potential flaws in the transmitting unit are related to the imperfect modulation of the phase and the intensity of the emitted light. We discuss a unified treatment to encompass all the mentioned imperfections in the finite-size regime. The result constitutes the backbone of the security-hardened QKD system installed between Otemachi and Koganei in the Tokyo QKD network [7].

[1] A. Vakhitov, V. Makarov, and D. R. Hjelme, J. Mod. Opt. 48, 2023 (2001).

[2] N. Gisin, S. Fasel, B. Kraus, H. Zbinden, and G. Ribordy, Phys. Rev. A 73, 022320 (2006).

[3] D. Gottesman, H.-K. Lo, N. Lütkenhaus, J. Preskill, Quant. Inf. Comput. 5, 325 (2004).

[4] X.-B. Wang, Phys. Rev. Lett. 94, 230503 (2005).

[5] H.-K. Lo, X. Ma, and K. Chen, Phys. Rev. Lett. 94, 230504 (2005).

[6] K. Tamaki, M. Curty, G. Kato, H.-K. Lo, and K. Azuma, Phys. Rev. A 90, 052314 (2014).

[7] A. Dixon et al., Opt. Express 23, 7583 (2015).

9648-42, Session 10

Practical aspects of security certification for commercial quantum technologies

Nino Walenta, Battelle Memorial Institute (United States); Mathilde Soucarros, Damien Stucki, Dario Caselunghe, Mathias Domergue, id Quantique SA (Switzerland); Michael A. Hagerman, Randall E. Hart, Don T. Hayford, Battelle Memorial Institute (United States); Raphael Houlmann, Matthieu Legré, id Quantique SA (Switzerland); Todd A. McCandlish, Battelle Memorial Institute (United States); Jean-Benoît Page, id Quantique SA (Switzerland); Maurice A. Tourville, Richard L. Wolterman, Battelle Memorial Institute (United States)

Quantum random number generation (QRNG) and quantum key distribution (QKD) are the first applications of quantum physics at the level of individual quanta which have matured into commercial products. Both have been commercially available for over 10 years, and increasingly adopted in information security systems. Current efforts focus on standardization and certification of QRNG and QKD devices and their components in order to validate the technology and enable more widespread adoption. Since no official certification scheme specific to quantum devices has been devised so far, alternative options must be investigated. This paper describes our approaches and efforts to enable compliance of commercial QRNG and QKD network devices with security standards such as AIS 20/31, FIPS140-2 or Common Criteria.

Firstly, we present the approach taken for a standalone commercial quantum random number generator (IDQ Quantis AIS31) so that it complies with the BSI AIS 20/31 standard. This standard describes a methodology for the evaluation of random number generators (RNGs), where RNGs are grouped under different categories. Under this classification, a QRNG falls under the category of physical true generators (PTG) that possesses a physical source of entropy without restriction on the physical processes involved. For the purpose of our product evaluation, we chose the class that guarantees the highest degree of security (PTG.3) of the generator's output. In practice, a cryptographic post-processing procedure, as well as health tests were therefore added to the random number generation process, and a rigorous mathematical model of the entropy source based on quantum phenomena derived in order to explain the amount of produced entropy. By describing and documenting the entire generation process, we were able to justify the correct generation of random numbers. The QRNG's conformity assessment to the AIS 20/31 standard was performed by an independent evaluation laboratory and confirmed the compliance of our QRNG product with the security standard.

Secondly, we present our approach for developing and certifying QKD-Trusted Node (QKD-TN) network architecture and hardware, which enables QKD-based key distribution amongst multiple users over arbitrarily long distances. Importantly, this approach strives, for the first time, for compliance of QKD with security standards for information systems, including FIPS 140-2 Level 3, ISO/IEC 19790 and Common Criteria EAL 4, in order to allow its use in e.g.

governmental networks and agencies. In the QKD-TN network, user keys are distributed between any two users by hopping over intermediate nodes, while being two-fold encrypted with QKD keys as well as conventional keys. The QKD keys are generated by the Coherent One-Way QKD protocol, with the entropy of all keys derived from the certified QRNG described above. Our approach presented here appends approved cryptographic functions to QKD to achieve compliance of QKD with FIPS 140-2 while maintaining the information-theoretical security of the QKD keys. The hardware is compactly integrated in ATCA-compatible blades, and all cryptographic security functionalities, including the QKD hardware, are protected by a tamper-proof enclosure with active zeroization response. The QKD-TN architecture can realize any network topology, with adjacent nodes separated by up to 100 km.

9648-43, Session 10

Quantum hacking on a practical continuous-variable quantum cryptosystem by inserting an external light

Hao Qin, Rupesh Kumar, Romain Alléaume, Télécom ParisTech (France)

We report here a new side channel attack on practical continuous-variable (CV) quantum key distribution (QKD). Inspired by blinding attack in discrete-variable QKD, we formalize an attack strategy by inserting an external light into a CV QKD system implemented Gaussian-modulated coherent state protocol and show that our attack can compromise its practical security. In this attack, we concern imperfections of a balance homodyne detector used in CV QKD. According to our analysis, if one inserts an external light (pulse or continuous wave) into Bob's signal port, due to the imperfect subtraction from the homodyne detector, the leakage of the external light contributes a displacement on the homodyne signal which causes detector electronics saturation. In consequence, Bob's quadrature measurement is not linear with the quadrature sent by Alice. By considering such vulnerability, a potential Eve can launch a full intercept-resend attack meanwhile she inserts an external light into Bob's signal port. By selecting proper properties of the external light, Eve actively controls the induced displacement value from the inserted light which results saturation of homodyne detection. In consequence, Eve can bias the excess noise due to the intercept-resend attack and the external light, such that Alice and Bob believe their excess noise estimation is below the null key threshold and they can still share a secret key. Our attack shows that the detector loopholes also exist in CV QKD, and it seems influence all the CV QKD systems using homodyne detection, since all the practical detectors have finite detection range.

9648-44, Session 10

Preventing side-channel effects in continuous-variable quantum key distribution

Ivan D. Derkach, Vladyslav C. Usenko, Radim Filip, Palacky Univ. Olomouc (Czech Republic)

Continuous-variable Quantum Key Distribution (CV QKD) is the new approach in establishing secure communication based on fundamental properties of multiphoton quantum states of light. Security of CV QKD protocols suffers from losses and noise that can be present in communication link as well as at trusted sides. It was shown that preparation noise can already break the security and detection noise confines the key rate, but can help to make protocol more robust against noise in quantum channel. Since equipment used by the trusted parties cannot be perfectly shielded, the possibility for external noise infusion will unavoidably be present and can be advantageously used by an eavesdropper to control measurements carried out at the receiver station in order to improve the knowledge about the generated key. Side channel considered in this research is an auxiliary channel, which is coupled to the signal prior to detection, input of such channel is under control of an eavesdropper, while the output cannot be blocked but can be measured by trusted receiver. Moreover, control of side-channel coupling strength is inaccessible to an eavesdropper.

We estimate security of the protocol by analyzing security against individual and collective attacks of QKD protocols based on coherent and squeezed states of light. In case of individual attacks in purely attenuating channel, an eavesdropper is measuring the output mode of the main communication channel and concurrently controls the input of the side channel conducting noise infusion using an entangling cloner attack. In this scenario even for purely attenuating untrusted channel, presence of additional noise in side channel can compromise the security of the protocol. In case of collective attacks, we consider purification scheme based on entangling source that is used for generation of the states and information encoding by homodyne or heterodyne measurements by one of the trusted parties. For collective attacks case the side-channel noise decreases the tolerance of the protocol to noise in the untrusted channel and can as well lead to security break of the protocol.

We suggest a method of reducing the negative impact of side channel presence for coherent and squeezed states protocols. In order to compensate the negative influence of side-channel noise infusion the monitoring of the output of the side channel should be conducted. Applying the proper manipulation on the data from the main detector as well as from the monitoring detector allows to recover the performance of the protocol. By weighed subtraction of the data from the main detector and the monitoring detector, we show that resulting measurement is free from the influence of the side channel. The method also allows to fully restore Gaussian entanglement even if it was broken by the presence of noise in the side channel. Optimal settings of the suggested method do not require channel estimation, entanglement or non-Gaussian operations, but depend only on parameters of local trusted operating station. Our result describes the promising method of shielding the quantum side channels in continuous-variable quantum key distribution.

9648-45, Session 11

Bridging the gap between theory and practice in quantum cryptography *(Invited Paper)*

Marcos Curty, University of Vigo (Spain); Kiyoshi Tamaki, NTT Basic Research Laboratories, NTT corporation (Japan); Feihu Xu, Research Laboratory of Electronics, Massachusetts Institute of Technology (United States); Akihiro Mizutani, Osaka Univ. (Japan); Charles Ci Wen Lim, Bing Qi, Oak Ridge National Laboratory (United States); Hoi-Kwong Lo, University of Toronto (Canada)

In theory, quantum key distribution (QKD) offers information-theoretic security based on the laws of physics. In practice, however, it does not, because the device models used in security proofs do not match the actual devices employed in real systems. As a result, we face implementation loopholes, or so-called side channels, which may be employed by adversaries to hack QKD without being detected. This raises the importance of developing security proof techniques that can tackle modelling discrepancies.

The most well-known example of such security proof technique is (full) device independent QKD (diQKD), which does not require a description of how QKD apparatuses operate. Given that certain assumptions are satisfied, its security can be proven based solely on the violation of a Bell inequality. Its main drawback, however, is that it requires a loophole-free Bell test which at the moment is still unavailable. Also, its secret key rate at practical distances is very limited with current technology.

The diQKD approach might be, however, over-pessimistic.

This is so because it assumes that the legitimate users of the system (called Alice and Bob) cannot trust their sources. In principle, however, the state preparation process could be monitored in a protected environment outside the influence of the adversary. This is one key idea of a novel solution known as measurement-device-independent QKD (mdiQKD), which can provide a secret key rate that is many orders of magnitude higher than that of diQKD. Also, this solution removes all side-channels from the measurement unit, arguably the most vulnerable part in QKD systems. Moreover, mdiQKD can be implemented with standard optical components, including low detection-efficiency detectors and highly lossy channels, and its feasibility has been promptly demonstrated both in laboratories and via field-tests. Its security is based on the idea of time reversal. Alice and Bob send quantum states to an untrusted relay (Charles/Eve) who is supposed to implement a Bell state measurement that projects the incoming signals into a Bell state. Importantly, Alice and Bob can verify whether or not Charles/Eve is honest by comparing a randomly chosen portion of their data.

The mdiQKD approach offers a practical and feasible avenue towards secure QKD realisations with flawed optical receivers. To take care of source flaws, one may use a novel protocol based on the so-called "rejected data analysis". Importantly, the security of this scheme is almost independent of any encoding flaw (even in the presence of high quantum channel loss) and it is compatible with both the decoy state method and mdiQKD. This means, in particular, that the usual stringent demand on precise state preparation can be considerably relaxed without affecting the performance of the system. Most importantly, when they are combined with mdiQKD, these results suggest the feasibility of long distance provably-secure communication with arbitrarily flaw devices. Here, we review the latest developments in this framework together with its assumptions, strengths and weaknesses.

9648-46, Session 11

Establishing security of quantum key distribution without monitoring disturbance *(Invited Paper)*

Masato Koashi, Univ of Tokyo (Japan)

In conventional quantum key distribution (QKD) protocols, the information leak to an eavesdropper is estimated through the basic principle of quantum mechanics dictated in the original version of Heisenberg's uncertainty principle. The amount of leaked information on a shared sifted key is bounded from above essentially by using information-disturbance trade-off relations, based on the amount of signal disturbance measured via randomly sampled or inserted probe signals. Here we discuss an entirely different avenue toward the private communication, which does not rely on the information-disturbance trade-off relations and hence does not require a monitoring of signal disturbance. The independence of the amount of privacy amplification from that of disturbance tends to give it a high tolerance on the channel noises. The lifting of the burden of precise statistical estimation of disturbance leads to a favorable finite-key-size effect.

Rather unexpectedly, a protocol based on the novel principle can be implemented by only using photon detectors and classical optics tools: a laser, a phase modulator, and an interferometer. The protocol resembles the differential-phase-shift QKD protocol in that both share a simple binary phase-coding on a coherent train of weak pulses from a laser. The difference lies in the use of a variable-delay interferometer in the new protocol, which randomly changes the combination of pulse pairs to be superposed. This extra randomness has turned out to be enough to upper-bound the information extracted by the eavesdropper, regardless of how she has disturbed the quantum signal. The complementarity in quantum mechanics plays an important role in the proof of security. The receiver has an alternative choice of measuring photon numbers instead of the phase, which could make it difficult for every party, including the eavesdropper and the receiver himself, to guess the value of the sender's sifted key bit.

9648-47, Session 11

Quantum cryptography with an ideal local relay *(Invited Paper)*

Gaetana Spedalieri, Carlo Ottaviani, Samuel L. Braunstein, The Univ. of York (United Kingdom); Tobias Gehring, Christian S. Jacobsen, Ulrik L. Andersen, Technical Univ. of Denmark (Denmark); Stefano Pirandola, The Univ. of York (United Kingdom)

No Abstract Available

9648-48, Session 11

Continuous-variable quantum key distribution with a single quadrature modulation

Vladyslav C Usenko, Palacky Univ Olomouc (Czech Republic); Frederic Grosshans, Laboratoire Aimé Cotton, UPR CNRS (France)

Quantum Key Distribution (QKD) is the method of sharing a cryptographic key between two trusted parties so that its security is provided by the very laws of quantum physics. The key can then be used in the one-time cipher therefore providing the cryprographic solution with information-theoretically provable security. While the first theoretical ideas and practical realizations were based on the use of the discrete-variable encoding of key bits into the parameters of the quantum systems with finite-dimensional energy spectrum (such as single photons, typically emulated by weak coherent pulses, or entangled photon pairs), the recent developments in the field are concerned with the use of the continuous-variable (CV) encoding of key bits in the continuous observables of the modes of electromagnetic radiation such as amplitude or phase quadratures of the field, subsequently measured by the homodyne detector with the shared phase reference (local oscillator) or by double homodyne (heterodyne) detection. It was in particular shown, that using continuous Gaussian encoding and one-way reverse reconciliation of the classical information shared between the trusted parties, the security of the key can be provided against collective and subsequently the most general attacks in the asymptotic limit using just semi-classical coherent states of light. The practical realization of the protocol is limited by the imperfections of the quantum communication channel and the devices used for the state preparation and detection. It is typically assumed that both of the complementary quadratures need to be modulated and measured (either subsequently or simultaneously). However, the Gaussian security proofs based on the purification of the state shared between the trusted parties in principle allow asymmetrical modulation if the channel properties are properly estimated or the pessimistic assumptions about the abilities of a potential eavesdropper are done. Therefore we suggest a CV QKD protocol based on the modulation of a single quadrature of coherent states which is aimed at simplifying the practical realization of CV QKD. The measurement of the complementary quadrature is still required for monitoring the channel noise. We derive the pessimistic security bounds in terms of the correlation elements of the covariance matrices based on the verification of physicality of the state shared between the trusted parties. We then consider the typical case of the Guasssian phase-insensitive channels and compare our protocol with the conventional coherent-state one where both of the quadratures are modulated. We show that suggested single-quadrature protocol is feasible at the distances and levels of noise limited but comparable to these of the standard protocol. We also consider the case when the key is not encoded, but the channel loss is estimated in a complementary quadrature. Such intermediate case provides better performance than the protocol which does not rely on the full estimation of channel transmittance. We therefore suggest the feasible and simplified coherent-state CV QKD protocol, which can be particularly useful when the local oscillator is

reconstructed locally (e.g. due to strong attenuation in a very long-distance link) and does not provide the phase reference for measuring correlations between both the quadratures.

9648-49, Session 12

Deploying quantum light sources on nanosatellites II: lessons and perspectives on CubeSat spacecraft *(Invited Paper)*

Alexander Ling, Robert Bedington, Edward Truong-Cao, Yue Chuan Tan, Cliff Cheng, Kadir Durak, James Grieve, National Univ of Singapore (Singapore); Jesper Larsen, Aalborg University (Denmark); Daniel Oi, University of Strathclyde (United Kingdom)

Due to fundamental challenges in establishing a global QKD network using optical fibres, several communication protocols using satellites have been proposed. To enable these space-based proposals, the Centre for Quantum Technologies (CQT) is developing SPEQS (Small Photon Entangling Quantum System), a source of entangled photons ruggedized to survive deployment in space and greatly miniaturised so that it conforms to the strict form factor and power requirements of a 1U cubesat.

Entangled photon pairs are generated through spontaneous parametric down conversion in BBO crystals, the optical pump being provided by a wavelength-stabilised laser-diode. A photo-diode based feedback system is implemented to maintain constant pump power, which is a function of the laser-diode junction temperature. The photon pairs generated are detected on board using single-photon Avalanche Photo Diodes (APDs) operating in Geiger mode.

Since APD operation is affected by temperature fluctuations along the orbit, thermo electric coolers would be desirable, except that they exceed the typical power budget allowed for scientific payloads on a cubesat. Consequently an alternative, more power efficient temperature compensation mechanism has been designed for APD operation.

Our system is also capable of monitoring the quality of the entangled photons produced in orbit. This is achieved through an opto-electronic design which changes the polarisation states of the photon pairs without using motor based polarisers. In addition to being power efficient, this does not interfere with the attitude control mechanisms of the satellite.

The fully autonomous system has undergone thermal, vacuum and vibration qualification tests and has been tested in a weather balloon in near space conditions, confirming the robustness of the system ahead of upcoming in-space demonstrations.

The successor to SPEQS, SPEQS2 is now also under development. This will be a bigger and brighter entangled photon source than SPEQS1, yet maintain CubeSat-compatibility and will be demonstrated on the CQT-led SpooQySat programme.

9648-50, Session 12

On-chip self-referenced continuous variable QKD *(Invited Paper)*

Ryan Camacho, Sandia National Labs. (United States)

No Abstract Available

9648-51, Session 12

A low bias variation SPAD-based pixel for a quantum random generator

Nicola Massari, Leonardo Gasparini, Alessandro Tomasi, Fondazione Bruno Kessler (Italy); Alessio Meneghetti, Univ. degli Studi di Trento (Italy); Daniele Perenzoni, David Stoppa, Fondazione Bruno Kessler (Italy)

Quantum random number generators (QRNG) based on photonics have been shown to be a promising technique because of their compactness, low cost and performance. While many works in the literature have limited output bit rate due to the use of a single detector [1-4], recent papers proposed to exploit the parallelism of an array of SPADs to implement high speed QRNG [5-6]. The work proposed by Burri et al. [5] declared to operate up to 500Mbs of random bits. Nevertheless, main drawback of this solution is the dependency of the bias on light variation, compelling the use of algorithms for data “whitening” [6].

The dependency of the bias on the photon flux variation have three main effects on the array of SPADs: 1. the need of a strong feedback in order to maintain the flux of photons constant; 2. the impracticality to implement the algorithm to all pixels of the array because of mismatches among pixels; 3. the need of a uniform distribution of light over the entire sensor. The goal of the present solution is to reduce at minimum the impact of the photon flux variation on the bias.

The basic idea is to extract random bits from a couple of SPADs. The pixel consists of two independent SPADs with related quenching circuits, connected together to an arbiter circuit. The pixel works in three different phases: the two SPADs are switched off during the reset phase and simultaneously enabled in the evaluation phase. Each detected photons is sent to the arbiter, which has to discriminate the winning SPAD and extract the bit ‘1’ or ‘0’ depending on the winner (if SPADA or SPADB) during the extraction phase. Supposing a uniform photon flux on both SPADs, the output sequence of bits can be considered ideally random. Main source of bias can be due to possible mismatches between the two SPADs and the arbiter offset. Simulation shows that the impact of the SPAD efficiency mismatch on the final bias is estimated lower than 0,05%. The DCR contribution, instead, can be considered negligible due to the good SNR and short evaluation phase. The proposed solution allows to extend the pixel functionality for higher values of photon flux maintaining the peak of rate constant until of the arbiter offset becomes predominant.

A test chip was fabricated and experimental results will be available at the time of the conference.

[1] M. Ren, E. Wu, Y. Liang, G. Wu, H. Zeng, “ Quantum random-number generator based on a photon-number-resolving detector”, Phys. Rev. A, 83, 023820 (2011).

[2] M. Furst et al, “High speed optical quantum random number generator”, Optics Express, 18(12), 13029 (2010).

[3] M.Wayne et al., “Low-bias high-speed quantum random number generator via shaped optical pulses”, Optic Express, 18 (9), 9351-9357 (2010).

[4] M.Wahl et al., “An ultra-fast quantum random number generator with provably bounded output bias based on photon arrival time measurements”, Appl. Phys. Lett., 98, 171105 (2011)

[5] S. Burri, et al. “Jailbreak Imagers: Transforming a Single-Photon Image Sensor into a True Random Number Generator”, in proceedings of 2013 International Image Sensor Workshop, Snowbird Resort, Utah, USA June 12-16, 2013.

[6] Stucki D. et al., “Towards a high-speed quantum random number generator”,Proc. SPIE 8899, Emerging Technologies in Security and Defence and Quantum Security II and Unmanned Sensor Systems X, October 29, 2013;

9648-52, Session 12

Heralded single-photon source from spontaneous four-wave mixing process in lossy waveguides

Nuno A. Silva, Instituto de Telecomunicações (Portugal) and Univ. de Aveiro (Portugal); Armando N. Pinto, Instituto de Telecomunicações (Portugal) and Unvi. de Aveiro (Portugal)

Single photon sources are important resources in many quantum communication technologies, such as quantum key distribution. Nevertheless, truly single photon sources are typically difficult to implement since they usually demand cryogenic temperatures or must be operated in vacuum. A different approach to perfect single photon sources is based on the generation of quantum-correlated photon pairs inside of nonlinear materials. In that scenario, the detection of one photon of the pair heralds the presence of the other photon. This kind of sources are known as heralded single photon sources, and uses a laser and a second-or third-order material to obtain the photon pairs. In third-order materials such as the chalcogenide glass, those quantum-correlated photon pairs can be obtained through the spontaneous four-wave mixing (FWM) process. Due to the strong spatial-temporal confinement of the light in those waveguides and the presence of an almost zero-dispersion frequency, it is possible to generate efficiently photon pairs through spontaneous FWM process over very short distances, and at telecom wavelengths. This is essential to implement on-chip single photon sources for integration with other components of the communication system. Nevertheless, waveguides with high values of nonlinear parameter (such as the chalcogenide glass) also tends to present a non-negligible loss coefficient.

In this work we investigate the generation of time-correlated photon pairs through the spontaneous FWM process inside a chalcogenide based optical waveguide in a non-negligible loss regime. Moreover, the theoretical model also accounts with the Raman scattering that inevitably accompanies the FWM process, and create time-uncorrelated photon pairs. After, we investigate the spontaneous FWM process as a heralded single photon source in a chalcogenide glass waveguide in both regimes lossless and high loss. We evaluate the quality of the heralded single photon source from its statistical characterization. That statistical characterization was obtained through the evaluation of the conditional second order coherence function at chalcogenide waveguide output. For a perfect heralded single photon source we will observe a conditional second order coherence function with null value, and values less than one means the nonclassical nature of the source. Our goal is to evaluate the impact of the waveguide loss on the statistics of the heralded single photon source.

The results obtained indicate that the presence of a non-negligible loss coefficient tends to improve the quality of the heralded single photon source, even considering the presence of uncorrelated photons from the Raman scattering process. From our findings we observe a decrease on the value of the conditional second order coherence function for high values of loss coefficient, when compared with lossless regime. In a non-negligible loss regime, the conditional second order coherence function is almost null over a high wavelength bandwidth. In that sense, the obtained results can help to guide the implementation of on-chip heralded single photon sources for quantum communication technologies applications.

9648-53, Session 13

Benchmarking D-Wave quantum annealing systems: some challenges *(Invited Paper)*

Catherine McGeoch, D-Wave Systems Inc. (Canada) and Amherst College (United States)

No Abstract Available

9648-54, Session 13

Quantum annealing on Ising spin glasses *(Invited Paper)*

Troels Rønnow, Nokia Research Ctr. UK (United Kingdom)

No Abstract Available

9648-55, Session 13

Locking capacity vs private capacity of quantum channels *(Invited Paper)*

Andreas Winter, Universitat Autonoma de Barcelona (Spain)

Guha et al. [arXiv:1307.5368] have recently defined the locking capacity of a quantum channel as the largest rate of a uniformly distributed bit string, which Alice can share with Bob over the channel while an eavesdropper, Eve, who has access to the channel environment, can only gain negligible accessible information about the string. We show that this relaxation of the private capacity of a channel, can be much larger than the latter; in fact, if a sub-linear size key is shared between Alice and Bob, there are channels with zero private capacity but positive locking capacity.

This gives a quantitative meaning to the information locking effect [DiVincenzo et al., PRL 92:067902, 2004], and answers an open question of Guha et al. The difference between private and locking capacity can also be related to non-zero discord, at least in some cases.

9648-57, Session 13

A complete classification of quantum public-key encryption protocols

Chenmiao Wu, Li Yang, Institute of Information Engineering (China)

A complete classification of quantum public-key encryption (QPKE) protocols is presented. A QPKE contains six elements: plaintext, ciphertext, public-key, private-key, encryption algorithm and decryption algorithm. According to the property of each element which either belongs to quantum space or classical space, there are 64 kinds of QPKE. 8 kinds are constructed, 52 kinds can be proved to be impossible to construct and the remaining 4 kinds have not been presented effectively yet. Thus, we classify these protocols into three types: type E, type N and type O.

Type E refers to the existed QPKE protocols. In our paper, we give examples of these 8 feasible protocols: 1. All the six elements belong to classical space. This presents the classical public-key encryption protocol; 2. Only decryption algorithm belongs to quantum space and others are classical. Quantum attack to the classical public-key encryption protocol is this kind; 3. Only plaintext is classical and other elements are belong to quantum space. This kind uses entangled state as public-key and private-key[1]; 4. Private-key and public-key are classical and the remaining elements are quantum. Fujita's McEliece cryptosystem[2] represents this kind; 5. Plaintext, public-key and private-key are classical and others are quantum. This kind of QPKE protocol can be realized by using Fujita's QPKE[2] to transmit classical plaintext ; 6. Only private-key is classical and other elements are quantum. Gotteseman's protocol[3] based on telepotation is one representative; 7. Plaintext and private-key are classical and others belong to quantum space. The protocol proposed by Liang[4] is one representative; 8. All the six elements are quantum. Such protocol also uses entangled pair as public-key and private-key.

The protocols which are unable to construct are classified into type N. We analyze the reasons for type N as follows: 1. If one of the two inputs, plaintext and public-key, is belong to quantum space, encryption algorithm must have the ability to process quantum information. If encryption algorithm is classical, such protocol is not existed; 2. The decryption algorithm also includes two inputs: ciphertext and private-key. If one input is quantum, the decryption should be quantum. If not, it's non-existed. 3. If one of inputs of encryption algorithm is quantum, the ciphertext should be quantum. If not, it means most of quantum components are missing during the processing. Such protocol is inefficient in transmitting message; 4. Similar to point 3, if the inputs for decryption algorithm have any quantum element, the plaintext should be quantum.

Type O includes protocols with uncertain existence. This indicates that the research on QPKE protocol should be focus on the existed kinds and the unproposed kinds.

[1] X. Li and D. Zhang, Quantum Public-key Cryptosystem Based on Super Dense Coding Technology, Journal of Computers, 8(12): 3168-3175, 2013.

[2] H. Fujita, Quantum McEliece Public-key Cryptosystem, Quantum Information & Computation 12(3-4): 181-202, 2012.

[3] D. Gottesman, Quantum public key cryptography with information-theoretic security, unpublished, 2005.

[4] M. Liang and L. Yang, Public-key encryption and authentication of quantum information, Science China Physics Mechanics and Astronomy, 55(9): 1618-1629, 2012.

Conference 9649: Electro-Optical Remote Sensing, Photonic Technologies, and Applications IX

SPIE. SECURITY+ DEFENCE

Monday - Tuesday 21–22 September 2015

Part of Proceedings of SPIE Vol. 9649 Electro-Optical Remote Sensing, Photonic Technologies, and Applications IX

9649-1, Session 1

SWIR laser gated-viewing at Fraunhofer IOSB *(Invited Paper)*

Benjamin Göhler, Peter Lutzmann, Fraunhofer-Institut für Optronik, Systemtechnik und Bildauswertung (Germany)

In this paper, we give a review of the work that has been done in the past ten years at Fraunhofer IOSB in the area of laser gated-viewing in the short-wavelength infrared (SWIR) band. Experimental system demonstrators in various configurations have been built up in order to show the feasibility for different applications and to investigate specific topics. The wavelength of the pulsed illumination laser is around 1.57 μm and lies in the invisible, retina-safe region allowing much higher pulse energy values than for wavelengths in the visible or near-infrared band concerning eye safety. All systems built up, consist of gated Intevac LIVAR(R) cameras based on EBCCD/EBCMOS detectors sensitive in the SWIR band. This review comprises military and civilian applications in maritime and land domain like long-range target identification, improvement of vision during bad visibility, 3-D imaging, speckle reduction and support in search and rescue missions. In addition, theoretical studies that were conducted – for example for estimating 3-D accuracy or for modelling range performance – are presented. Finally, an outlook for future work in the area of SWIR laser gated-viewing at Fraunhofer IOSB is given.

9649-2, Session 1

Accuracy evaluation of 3D lidar data from small UAV

H. M. Tulldahl, Fredrik Bissmarck, Håkan Larsson, Christina Grönwall, Gustav Tolt, FOI-Swedish Defence Research Agency (Sweden)

An UAV (Unmanned Aerial Vehicle) with an integrated lidar can be an efficient system for collection of high-resolution and accurate three-dimensional (3D) data. In this paper we evaluate the accuracy of a system consisting of a lidar sensor on a small UAV. High geometric accuracy in the produced point cloud is a fundamental qualification for detection and recognition of objects in a single-flight dataset as well as for change detection using two or several data collections over the same scene. Our work presented here has two purposes; the first is to relate the point cloud accuracy to data processing parameters and the second purpose is to examine the influence on accuracy from the UAV platform parameters. The UAV platform parameters studied are the platform speed and its orientation movements (roll-, pitch-, yaw-rates). The results are important as indicators of conditions where a certain accuracy limit is not achieved. These conditions can indicate the need for recollecting data, reprocessing data, or further developing of the processing algorithms. In our work, the accuracy is numerically quantified as local surface smoothness on planar surfaces, and as distance and relative height accuracy using lidar data from a terrestrial laser scanner as reference data. The UAV lidar system used in our work is the Velodyne HDL-32E lidar on a multirotor UAV with a total weight of 7 kg. For processing of data into a geographically referenced point cloud, positioning and orientation of the lidar sensor is based on inertial navigation system (INS) data, and on INS data combined with lidar data. The INS sensors consist of accelerometers, gyroscopes, GPS, magnetometers, and a pressure sensor for altimetry. The combination of INS and lidar data is achieved in a dynamic calibration process that minimizes the navigation errors in six degrees of freedom, namely the errors of the absolute positioning (x, y, z) and the orientation (roll-, pitch-, yaw) measured by GPS/INS. Our results show that low-cost and light-weight MEMS based (microelectromechanical systems) INS equipment with a dynamic calibration process can obtain significantly improved accuracy compared to processing based solely on INS-data. The system is rapid to deploy and the cost is relatively low compared to manned airborne sensor systems. The system has advantages over ground based laser scanning. It collects data much faster than scanning from movable tripod mounted systems. It reaches a larger survey area and also detects other objects or regions of interest (e.g. obscured by high vegetation) than systems based on ground vehicles.

9649-3, Session 1

Pulsed, tunable, single-frequency OP-GaAs OPO for the standoff detection of hazardous chemicals in the longwave infrared

Quentin Clément, Jean-Michel Melkonian, Jean-Baptiste Dherbecourt, Myriam Raybaut, ONERA (France); Arnaud Grisard, Eric Lallier, Thales Research & Technology (France); B. Gérard, III-V Lab. (France); Basile Faure, Grégoire Souhaité, Teem Photonics S.A. (France); Antoine Godard, ONERA (France)

Optical coherent sources with a narrow spectral linewidth and a broad tunability are of primary interest for chemical detection by optical spectrometry, especially in the longwave infrared (LWIR) range between 7 and 14 ?m. Optical parametric oscillators (OPOs) can fulfil these requirements, especially when a tunable high-peak-power emission is required to carry out standoff detection at an extended range.

Orientation-Patterned GaAs (OP-GaAs) is a nonlinear crystal that offers unique advantages to generate such a tunable radiation in the infrared with an optical parametric oscillator (OPO). We report here on LWIR single-frequency emission in OP-GaAs using a nested cavity OPO (NesCOPO) configuration and its use in a preliminary short-range integrated-path Lidar experiment to detect ammonia vapour at 10.4 μm.

The OP-GaAs crystal is 10 mm-long, 0.5 mm-thick, has a quasi-phase matching period ? = 72.6 μm, and is set in an oven to enable temperature tuning of the emitted wavelengths. The NesCOPO is pumped by a compact single-frequency Tm:YAP microlaser, also specially designed and manufactured for that purpose. This laser emits 36 ns pulses with a repetition rate of 100 Hz at 1938.5 nm and delivers a maximum output energy of 170 μJ.

We measure an oscillation threshold of 10 μJ at 10.3 μm. The maximum extracted idler energy is 2 μJ, with a typical pump depletion of 28%, and the idler wavelength can be tuned in the 10.3–10.9 μm range by changing the crystal temperature in the 25–75°C range. Single-frequency operation is obtained by a careful design of the NesCOPO signal-idler cavity length difference.

In order to demonstrate its potential for standoff chemical detection, the OP-GaAs NesCOPO is then implemented in an ammonia gas detection experiment. We target a cluster of absorption lines of ammonia, spreading from 10.32 μm to 10.45 μm. The output idler beam is split in three parts. The analysis beam passes through a cell with polyethylene windows containing ammonia gas, obtained by evaporation of an ammonium hydroxide solution. The beam then hits a diffusive non-collaborative target and the off-axis scattered light is collected by a 40 mm diameter germanium lens onto a nitrogen-cooled HgCdTe (MCT) detector. The reference beam directly hits a diffusive surface and scattered light is detected by another MCT detector to get a reference signal. The absorption measurement can thus be corrected from the idler

energy variation during wavelength scanning. The third beam part is sent to the monochromator with a third MCT detector that measures the wavelength with a ± 1 nm resolution, i.e., less than ± 0.1 cm-1. Successful detection of ammonia at a stand-off distance of 2 meters is demonstrated. Moreover, we are able to discriminate absorption from interfering atmospheric species such as atmospheric water vapor. Considering an equivalent optical depth of ammonia vapor over a 1-m distance and the absorption measurement relative uncertainty of ± 5 %, the typical sensitivity is 50 ppm with our current setup. Longer-range detection at the ppm level would be achievable with an improved setup (higher energy and larger receiver aperture).

9649-4, Session 1

Reconstruction of time-correlated single-photon counting range profiles of moving objects

Per M. Jonsson, Julia Hedborg, Markus Henriksson, Lars J. Sjöqvist, FOI-Swedish Defence Research Agency (Sweden)

Time-correlated single-photon counting (TCSPC) is a laser radar technique that can provide range profiling with subcentimetre range resolution. The method relies on accurate time measurements between a laser pulse sync signal and the registration of a single-photon detection of photons reflected from an object. The measurement is performed multiple times and a histogram of photon arrival times is computed to gain information about surfaces at different distances within the field of view of the laser radar. TCSPC is a statistic method that requires an integration time and therefore the range profile of a non-stationary object (target) may be corrupted. Here, we present results showing that it is possible to reconstruct the corrupted range profile of a moving target and receive range profiles close to that of a stationary object. The technique also gives the velocity of the target during a measurement.

A TCSPC range profiling system with subcentimetre range resolution was used for the experiments. The system consists of a picosecond pulsed laser, a monostatic transceiver unit for emittance of laser pulses and collection of reflected photons, a single-photon silicon detector and the timing acquisition hardware. The resolution of system is approximately 50 ps which corresponds to a range resolution of 7.5 mm. Corner cube retro reflectors with strong reflections, optical assemblies, e.g. rifle scopes, with a mixture of strong and weak reflections and geometrical forms with weak reflections were mounted on rails. Series of measurements on the objects with constant or non-linear velocities up to 0.5 m/s were done and compared with stationary measurements.

The timing acquisition hardware is recording both the photon detection time relative to the latest sync pulse and the number of sync pulses from the start of the measurement. By dividing the series into time intervals much shorter than the total acquisition time and cross-correlating the histogram from each time interval with the first one, it was possible calculate how long the target has moved relative to the first time interval. This distance as a function of time was fitted to a polynomic function. The result was used to calculate a distance correction of every single detection event and the equivalent stationary histogram could be reconstructed.

The results show that it is possible to reconstruct range profiles of moving object with this technique. Reconstruction of the signal requires no prior information of the original range profile and the instantaneous and average velocity of the object can be calculated. The technique works even when the necessary integration time is longer than the period where the movement is negligible, i.e. for objects with low signal strength compared to the velocity.

9649-5, Session 1

Lidar measurement as support to the ocular hazard distance calculation using atmospheric attenuation

Ove K. S. Gustafsson, Rolf Persson, Frank Gustafsson, Folke Berglund, FOI-Swedish Defence Research Agency (Sweden); Jonas Malmquist, Försvarets Materielverk (Sweden)

The reduction of the laser hazard distance range including atmospheric attenuation within the calculations of nominal ocular hazard distance (NOHD) have been tested with series of lidar measurements accomplished at the Vidsel Test Range, Vidsel, Sweden. The question addressed was “How low is the atmospheric attenuation as function of height in this area, using the wavelength of 1064 nm?” The objective was to find a lowest level of aerosol backscatter during this campaign, with the implications of low extinction coefficient for this particular wavelength, since the lowest atmospheric attenuation gives the highest ocular hazards. Assuming as an example: A designator laser of the type Nd:YAG, with wavelength 1064 nm, power 0.180 W, pulse length 15 ns, PRF 11.5 Hz and beam divergence of 0.08 mrad. This laser will have a NOHD of 48 km using multi-pulse situation with an exposure time of 10 sec.

The work included building a ground based backscatter lidar, performing a series of measurements and analyzing the results. During the time June to November, 2014, sixteen lidar measurements were performed and analyzed. Since the objective was to find atmospheric condition with low attenuation, only situations with clear air and good weather were chosen. The new lidar instrument was compared with an old aerosol UV-lidar system, using the third harmonic of Nd:YAG laser, at a test running both system at the same time at the same location (3m apart). The UV-lidar system has been compared to the MPI aerosol lidar in Hamburg within the former EARLINET-program. The differences in the results from the IR and UV lidar systems could be explained by the difference in wavelength and noise level.

The results of lidar measurements showed at several occasions very low atmospheric attenuation as a function of height to an altitude of at least 10 km. The lowest limit of aerosol backscatter coefficient possible to measure with this instrument is less than 0.3·10-7 m-1 sr-1. Assuming an aerosol lidar ratio between 30 – 100 sr leads to an aerosol extinction coefficient of around 0.9 - 3·10-6 m-1. The measured aerosol extinction coefficient and the assumed molecule extinction coefficient of 5·10-6 m-1, calculated using MODTRAN (Ontar Corp.) assuming an atmosphere without any aerosol, have the consequence of reducing the laser hazard distance with 51 – 58 %, depending on the lidar ratio assumption.

The conclusion from the work is that reducing the laser hazard distance using atmospheric attenuation within the NOHD calculations is possible but preferably with measurements of the atmospheric attenuation as function of altitude if possible. The extreme clear air condition in this area, especially during situation with polar air moving in to the area in combination with high pressure weather, happened occasional. Since the clear air and good weather situation is often demanded during training and test situation this can diminish the effect of reducing the atmospheric attenuation calculated NOHD values.

9649-6, Session 2

Evaluating uniformity of IR reference sources

Catherine Barrat, Sébastien Violleau, HGH Systèmes Infrarouges (France)

Infrared reference sources such as blackbodies are used to calibrate IR sensors and cameras. Applications requiring a high thermal uniformity over the emissive surface become more and more frequent. This is particularly required for two major applications:

• Non uniformity correction of infrared cameras: a camera is facing an extended area blackbody, the aperture and the field of view being entirely covered by the radiation of the blackbody. The non uniformity coefficients are calculated for each pixel of the IR camera detector. This procedure may be carried out at several temperatures of the source. Vacuum dedicated blackbodies are for example usually required to have an extremely high uniformity of radiation.

• Uniform calibration of a set of IR sensors facing a single large area blackbody: massive use of uncooled detectors for thermographic applications on a large scale of production requires procedures of calibration and test of several sensors in parallel. Lining up a set of IR sensors in front of a large emissive area blackbody is a solution frequently used by camera manufacturers. This solution of course requires that all the sensors receive the same level of radiation from the blackbody and consequently, a high level of uniformity.

The evaluation of the uniformity of a blackbody consists in measuring the thermal radiation of each point of the emissive surface. The use of an infrared camera for this purpose turns out to be absolutely inefficient since the uniformity of response of this camera has been itself corrected through the use of a blackbody which uniformity is usually unknown. Moreover, most of the time, the uniformity of response of this camera reveals to be worse than the uniformity of the measured blackbody.

Facing this demanding challenge and to match the high uniformity specification on extended area blackbodies, HGH has developed a testing bench based on a single element IR detector radiometer mounted on translating stages. Thanks to this low noise sensor and to an exclusive measurement drift correction method, we are able to draw an accurate thermal map of any kind of blackbodies: from low temperature extended area blackbodies up to high temperature cavity blackbodies with an accuracy of 30 mK at 50°C.

9649-7, Session 2

An approach to select the appropriate image fusion algorithm for night vision systems

Gabriele Schwan, Norbert Scherer-Negenborn, Fraunhofer-Institut für Optronik, Systemtechnik und Bildauswertung (Germany)

Usually night vision systems utilize short-wave infrared (SWIR) imagery from detectors based on InGaAs technology. Complementing this imagery with further imagery from the mid-wave infrared (MWIR) or the long-wave infrared (LWIR) frequency band respectively is advantageous. The combination of two bands should benefit from the specific properties of each band. Thus the importance of image fusion has increased. In the past many fusion algorithms were developed and published. Some attempts were made to assess the results from several fusion algorithms automatically with the objective of gaining the best suited output for human observers. But it was shown, that such objective machine-assessment does not always correlate with the observer's subjective perception.

In this paper a novel approach is presented, which selects the appropriate fusion algorithm to receive the best image enhancement results for human observers. As a starting point some characteristic fusion algorithms were selected for implementation. Among these are complex algorithms such as pyramidal algorithms (Laplace, wavelet, gradient, etc.), Computationally Efficient Pixel-level Image Fusion (CEMIF), Principal Component Algorithm (PCA), and Spatial Frequency algorithm (SF), as well as simple methods, such as pixel-wise Minimum, Maximum, Average, Summation, and Difference. For the evaluation of these algorithms a relevant data set of registered images from both the visual and the thermal spectrum showing human beings was set up. The ability to detect human beings was taken as the key topic to prove the advantage of image fusion.

Assessment of the fusion algorithms' results was done based on the local contrasts. The outcome of a fusion algorithm is expected to retain at any image-location always the image content from the input channel with higher local contrast respectively. To what extent a specific fusion algorithm is able to achieve this is evaluated by comparison of the local contrasts in the fusion results and the corresponding local contrasts in the input images. To avoid imbalance between the input contrasts and the fusion contrasts in case of equal contrasts in both input images weighting factors were introduced. The used assessment criterion is defined as the averaged sum of all differences in the local contrasts of the fusion image and the input images. All implemented fusion algorithms were subject to this assessment. By means of observer trials the matching of this objective assessment and the perception of human observers was compared. The result is that positive evaluation of fusion algorithms was confirmed by the observers.

In the proposed system setup the selection of the appropriate fusion algorithm can be carried out as follows. Prerequisite is 1) a representative data set covering different use cases and image contents, 2) the human observers' assessments of selected fusion algorithms used on this data, 3) a set of adapted assessment criterion for the fusion results, and 4) the implemented algorithms. First the input data has to be registered. Then a similar scenario is searched in the image data base. With the found reference image the stored assessment values of the algorithms are retrieved. The assessment algorithm with the best fit to the visual perception is used to select the best fusion algorithm for comparable scenarios. If the image contents changes, a new request can be sent to the image data base.

9649-8, Session 2

Field trials for development of multiband signal processing solutions to detect disturbed soil

Henrik Petersson, David K. J. Gustafsson, FOI-Swedish Defence Research Agency (Sweden); Julia Hedborg, Dietmar Letalick, Swedish Defence Research Agency (Sweden)

This paper describes a pair of field trials aiming to support the development of multi-band signal processing methods for detecting disturbed soil; an indirect indicator of the potential presence of buried landmines or IED's.

At first, a controlled environment was setup in which a sandbox containing homogenous sand was prepared and where the top layer of the soil was disturbed in different ways; e.g. by brushing, digging and walking. In this setup, measurements were made with a single band long wave infrared imager (LWIR) (7.5?m-13?m), a dual band medium wave infrared imager (MWIR) (3.5?m-4.25?m and 4.5?m-5.5?m), a single band short wave infrared imager (SWIR) (0.9?m-1.7?m) and single band polarized MWIR (3.7?m-4.9?m). All measurements were made in a short time-span and no temporal effects were hence included.

Analysing data from the above mentioned setup, different statistical properties were indicated when comparing pixels sampled from areas of undisturbed versus disturbed soil. Statistical hypothesis tests were also made on data. By such tests, it was possible to automatically detect areas with different statistical properties compared to a pre-defined reference patch of undisturbed soil.

Given the positive results above, a second phase of measurements was then made. In this phase, more attention was given to reflect a more realistic scenario in terms of temporal aspects, natural variations in soil properties, concept of operation etc. The sensor set-up was this time composed of a visual camera, a single band SWIR (1.5?m-2.8?m), a single band MWIR (3?m-5?m) and a single band LWIR (7.5-13?m). All sensors where co-mounted on the roof of a vehicle in a forward looking orientation and imaging the roadway from approximately 10 to 25 meters ahead of the vehicle. With this sensor platform, measurements where performed along a short section of a gravel road. The road section was divided in two sub-sections: the first 50 meters was used as an unaltered

reference road and the last 65 meters were prepared by placing pressure plates, batteries and diesel cans underneath its surface. Measurements were made at two meters intervals while the vehicle was standing still. To organize and enable image registration of all data, reference markers where placed along both sides of the road at 2 meter intervals. To enable studies in how the signature of disturbed soil change with time, measurements were made directly after the road was prepared with hidden objects, and then 1, 3, 14 and 16 days afterwards. During the complete measurement campaign, weather data was collected for reference.

Based on the trials described above, first visual inspections of sensor imagery has been made with the purpose of exploring how signatures of disturbed soil show-up in various wavelength bands and how these signatures change with time. The extent to which the studied different wavelength bands visually complement each other was also studied. An initial analysis on uni- and multivariate statistical properties of pixel-values sampled from disturbed vs undisturbed soil have also been made.

9649-9, Session 2

Classification of vegetation types in military region

Miguel Gonçalves, Jose Silvestre Silva, Academia Militar (Portugal); José M. Bioucas-Dias, Instituto Superior Técnico (Portugal)

In decision-making process regarding planning and execution of military operations, the terrain is a determining factor. The knowledge of the situation on the ground can be decisive for the success of a mission by gaining terrain's knowledge advantage over the enemy. In this context, aerial photographs may play a relevant role, namely when the cartographic information behind enemy lines is scarce or non-existent, constituting itself a source of vital information for the success of an operation in hostile region.

The objective of present work is the development of a tool capable of processing aerial photos containing information on the visible light band, detailing the various densities in vegetation and its elements.

The methodology implemented in this work starts with feature extraction, which is followed by the application of an automatic selector of features. The next step, using the k-fold cross validation technique, is an estimate of the input parameters for the following classifiers: Sparse Multinomial Logist Regression (SMLR), KNearest Neighbor (KNN), Linear Classifier using Principal Component Expansion on the Joint Data (PCLDC), and Multi-Class Support Vector Machine (MSVM).These classifiers are used in two different studies with distinct objectives. The first objective is to perform the vegetation's density discrimination, and the second objective is the identification of vegetation's main components.

It was found that the best classifier on the first approach is the Sparse Logistic Multinomial Regression (SMLR). On the second approach, the implemented methodology applied to high resolution images showed that the better performance was achieved by KNN classifier and PCLDC. It was concluded the use of automatic feature selection leads to an improvement in classifiers performance of more than 10 % of correct classifications, reaching to an increase of 25.7% for SMLR classifier. The achieved results show that the best performance occurs using between the 15 and 25 features for all classifiers with the exception of PCLDC.

We concluded that, to a good approximation, the used features are linearly separable, and the better performance was achieved by KNN classifier and PCLDC. Comparing the two approaches there is a multiscale issue, in which for different resolutions, the best solution to the problem requires different classifiers and the extraction of different features.

9649-10, Session 2

Hue-preserving local contrast enhancement and illumination compensation for outdoor color images

Marco Tektonidis, David Monnin, Frank Christnacher, Institut Franco-Allemand de Recherches de Saint-Louis (France)

Computer vision applications which are used to increase the situational awareness (e.g., object recognition, change detection, tracking, video surveillance) are based on the automatic or supervised analysis of color images of outdoor scenes. Illumination effects (e.g., shadows) affect the image quality and illumination variations introduce color and lightness differences between the different images. It is essential to perform image enhancement to improve the quality of single images (e.g., enhance details within shadows), and illumination normalization for compensating color and lightness differences between images.

In this work, we propose a new approach for simultaneous image enhancement and illumination normalization of color images of outdoor scenes. Our approach is based on the processing of the intensity and the saturation components of the images and exploits information from a proposed shadow detection method. We employ a hue preserving retinex-based approach which processes the intensity channel in the HSI (Hue-Saturation-Intensity) color space of an image to preserve the original color appearance and to avoid color distortions. The local surround function used for the retinex computation enhances details and improves the lightness consistency between corresponding regions of different images. The retinex for each pixel is computed based on a weighted average of a shadow retinex and a non-shadow retinex. These retinex values, as well as the corresponding weights, are obtained based on information determined by a shadow detection approach. The shadow-detection-based weighted retinex processing scheme significantly reduces the halo effect on shadow boundaries and suppresses smaller shadows, compared to the classic retinex processing scheme. For shadow detection we propose an efficient approach which is based on the RGB image normalization and on automatic histogram segmentation. The color information of the original image is assigned to the target intensity image employing a transformation method which avoids the gamut problem. To improve the color consistency we reduce the color differences between the different images using a hue and intensity preserving saturation processing method. The saturation level of the result can be adjusted based on the amount of color which is required by the application. The use of summed area tables (SAT) for the local surround function of the retinex processing scheme results to low computation times which allow the use of the approach for real time applications. Moreover, our approach is fully automatic since it does not require manual adjustments as, e.g., manual calibration.

We have quantitatively evaluated the approach based on image sequences acquired by a stationary camera as well as image pairs depicting the same scene from image sequences acquired with a non-stationary camera. Additionally, we have performed an experimental comparison with previous retinex-based approaches which have been used for image enhancement and illumination normalization.

9649-11, Session 3

3D sensing and imaging for UAVs *(Invited Paper)*

Christina Grönwall, FOI-Swedish Defence Research Agency (Sweden) and Linköping Univ. (Sweden); Gustav Tolt, Håkan Larsson, Patrik Lif, Fredrik Bissmarck, H. M. Tulldahl, FOI-Swedish Defence Research Agency (Sweden); Markus Henriksson, Per Wikberg, Mirko Thorstensson, Swedish Defence Research Agency (Sweden)

This paper summarizes on-going work on 3D sensing and imaging for unmanned aerial vehicles UAV carried laser sensors. We study sensor concepts, UAVs suitable for carrying the sensors, and signal processing for mapping and target detection applications. We also perform user studies together with the Swedish armed forces, to evaluate usage in their mission cycle and interviews to clarify how to present data.

Two ladar sensor concepts for mounting in UAV are studied. The discussion is based on known performance in commercial ladar systems today and predicted performance in future UAV applications. The small UAV is equipped with a short-range scanning ladar. The system is aimed for quick situational analysis of small areas and for documentation of a situation. The large UAV is equipped with a high-performing photon counting ladar with matrix detector. Its purpose is to support large-area surveillance, intelligence and mapping operations. Based on these sensors and their performance, signal and image processing support for data analysis is analyzed. Generated data amounts are estimated and demands on data storage capacity and data transfer is analyzed.

We have tested the usage of 3D mapping together with military rangers. We tested to use 3D mapping in the planning phase and as last-minute intelligence update of the target. Feedback from these tests will be presented. We are performing interviews with various military professions, to get better understanding of how 3D data are used and interpreted. We discuss approaches of how to present data from 3D imaging sensor for a user.

9649-12, Session 3

Comparison of high-speed imaging technique to laser vibrometry for detection of vibration information from objects

Gabriela Paunescu, Peter Lutzmann, Benjamin Göhler, Daniel Wegner, Fraunhofer-Institut für Optronik, Systemtechnik und Bildauswertung (Germany)

The development of camera technology in the recent years made high speed imaging a reliable method in vibration and dynamic measurements. The passive recovery of vibration information from high speed video recordings was reported in several recent papers. A highly developed technique, involving decomposition of the input video into spatial subframes to compute local motion signals, allowed an accurate sound reconstruction. A simpler technique based on image matching approach for vibration measurement was also reported as efficient in extracting audio information from a silent high speed video.

In this paper we investigate and discuss the sensitivity but also the limitations of high speed imaging technique for vibration detection in comparison to the well-established Doppler vibrometry technique.

9649-15, Session 3

A proposal for combining mapping, localization and target recognition

Christina Grönwall, FOI-Swedish Defence Research Agency (Sweden) and Linköping Univ. (Sweden); Gustaf Hendeby, Linköping Univ. (Sweden); Kristian Sinivaara, Cybercom Sweden (Sweden)

Simultaneous localization and mapping (SLAM) is a well-known positioning approach in GPS denied environments such as urban canyons and inside buildings. Autonomous/aided target detection and recognition (ATR) is commonly used in military applications to detect treats and targets in outdoor environments. This papers present approaches to combine SLAM with ATR in ways that compensate drawbacks in the respective methods. The methods use physical objects that are recognizable by ATR as unambiguous features in the SLAM map, while SLAM provides the ATR with better position estimates. Landmarks in the form of 3D point features based on normal aligned radial features (NARF) are used in conjunction with identified objects and 3D object models that replace landmarks when possible. This leads to a more compact map representation with fewer landmarks, which partly compensates for the introduced cost of the ATR.

We analyze three approaches to combine SLAM and 3D-data; point-point matching ignoring NARF features, point-point matching using the set of points that are selected by NARF feature analysis, and matching of NARF features using nearest neighbor analysis. The first two approaches are is similar to the common iterative closest point (ICP). We propose an algorithm that combines EKF-SLAM and ATR based on rectangle estimation.

We propose an algorithm that combines EKF-SLAM and ATR based on rectangle estimation, ATR-SLAM. We perform a comparison of an ATR-SLAM algorithm with ATR and an EKF-SLAM algorithm. NARF was used for landmark detection in both algorithms. Results show that ATR-SLAM outperforms SLAM when there are objects/targets that can be recognized in the scene, as ATR-SLAM delivers a more consistent map with smaller uncertainties in the sensor position estimates. The introduction of ATR into the SLAM algorithm helps to suppress incorrect association of features, which otherwise tend to degrade SLAM performance. The ATR-SLAM approach allows for fewer landmarks in the map, as a highly informative ATR objects efficiently substitute all regular landmarks associated with the object. The tests indicated that in a scene with many targets, typical for residential buildings and office premises, the memory footprint of the SLAM algorithm is substantially decreased by the introduction ATR. A drawback associated with the ATR function is the computation complexity.

Experiments performed using point clouds generated from a time-of-flight laser scanner show that a combination of ATR and SLAM produces more consistent maps and more robust loop closures than EKF-SLAM using only NARF landmarks. The intended application is to improve the positioning of a first responder moving through an indoor environment, where the map offers localization and simultaneously helps locate people, furniture and potentially dangerous objects like gas canisters.

9649-16, Session 4

Active-imaging-based underwater navigation *(Invited Paper)*

David Monnin, Gwenaël Schmitt, Colin Fischer, Martin Laurenzis, Frank Christnacher, Institut Franco-Allemand de Recherches de Saint-Louis (France)

Global navigation satellite systems (GNSS) are widely used for the localization and the navigation of unmanned and remotely operated vehicles (ROV). In contrast to ground or aerial vehicles, GNSS cannot be employed for autonomous underwater vehicles (AUV) without the use of a communication link to the water surface, since satellite signals cannot be

received underwater. However, underwater autonomous navigation is still possible using self-localization methods which determines the relative location of an AUV with respect to a reference location using inertial measurement units (IMU), depth sensors and even sometimes radar or sonar imaging. As an alternative or a complementary solution to common underwater reckoning techniques, we present the first results of a feasibility study of an active-imaging-based localization method which uses a range-gated active-imaging system and can yield radiometric and odometric information even in turbid water.

9649-17, Session 4

Passive and active EO sensing of small surface vessels

Ove Steinvall, Folke Berglund, Lars Allard, Johan Öhgren, Håkan Larsson, FOI-Swedish Defence Research Agency (Sweden); Elias Amselem, Uppsala Univ. (Sweden); Frank Gustafsson, FOI-Swedish Defence Research Agency (Sweden); Endre Repasi, Peter Lutzmann, Benjamin Göhler, Marcus Hammer, Fraunhofer-Institut für Optronik, Systemtechnik und Bildauswertung (Germany); Kennedy McEwen, SELEX Galileo Infrared Ltd. (United Kingdom); Kenneth J. McEwan, Defence Science and Technology Lab. (United Kingdom)

The detection and classification of small surface targets at long ranges is a growing need for naval security. This paper will present an overview of a measurement campaign which took place in the Baltic Sea in November 2014. The purpose was to test active and passive EO sensors (10 different types) for the detection, tracking and identification of small sea targets. The passive sensors were covering the visual, SWIR, MWIR and LWIR regions. Active sensors operating at 1.5 µm collected data in 1D, 2D and 3D modes. Supplementary sensors included a weather station, a scintillometer, as well as sensors for positioning and attitude determination of the boats.

Three boats in the class 4-9 meters were used as targets. After registration of the boats at close range they were sent out to 5-7 km distance from the sensor site. At the different ranges the target boats were directed to have different speed and aspect angles relative to the direction of observation.

Staff from IOSB Fraunhofer in Germany and from Selex (through DTSTL) in UK took part in the tests beside FOI who was arranging the trials.

A summary of the trial and examples of data and imagery will be presented.

9649-18, Session 4

Experiences from long range passive and active imaging

Christina Grönwall, David K. J. Gustafsson, Ove Steinvall, Gustav Tolt, FOI-Swedish Defence Research Agency (Sweden)

We present evaluations on algorithms for ATR of small sea vessels. The targets are on km distance from the sensors, which means that the algorithms have to deal with images affected by turbulence and mirages.

We evaluate earlier developed algorithms for registration of 3D-generating laser radar. The evaluations indicate that some robustness to turbulence and mirage induced uncertainties can be handled by our probabilistic registration method. We also assess methods for target classification and target recognition on these new 3Ddata.

An algorithm for detecting moving vessels in infrared image sequences is presented; it is based on optical flow estimation. Detection of moving target with an unknown spectral signature in a maritime environment is a challenging problem due to: camera motion, background clutter, turbulence and the presence of mirages. First, the optical flow caused by the camera motion is eliminated by estimating the global flow in the image. Second, connected regions containing significant motions that differ from camera motion is extracted. It is assumed that motion caused by a moving vessel is more temporally stable than motion caused by mirages or turbulence. Furthermore, it is assumed that the motion caused by the vessel is more homogenous with respect both magnitude and orientation, than motion caused by mirages and turbulence. Sufficient large connected regions with sufficient large flow magnitude with sufficient homogenous flow orientation are considered as a target region. The method is evaluated on newly collected sequences containing SWIR and MWIR, with varying targets, target ranges and background clutter.

Finally we discuss a concept for combining passive and active imaging in an ATR process. The main steps are that passive imaging is used for target detection, active imaging is used for target/background segmentation and a fusion of passive and active imaging is used for target recognition.

9649-19, Session 4

Maritime target identification in gated viewing imagery

Marcus Hammer, Marcus Hebel, Michael Arens, Fraunhofer-Institut für Optronik, Systemtechnik und Bildauswertung (Germany)

The growing interest in unmanned surface vehicles, accident avoidance for naval vessels and automated maritime surveillance leads to a growing need for automatic detection, classification and pose estimation of maritime objects in medium and long ranges. Laser radar imagery is a well proven tool for near to medium range, but up to now for higher range neither the detection range nor the sensor resolution was satisfying. As a result of the mentioned limitations of laser radar imagery the potential of laser illuminated gated viewing for automated classification and pose estimation was investigated. Laser illuminated gated viewing has a higher operating distance and in addition the resolution on the object is much higher than in current focal plane array laser radar systems. Due to the adjustable range gate the problem of object separation from the background, which is extremely difficult for passive imagery, can readily be resolved.

The paper presents new techniques for segmentation, pose estimation and model-based identification in gated viewing imagery of naval vessels in comparison with the corresponding results of long range data acquired with a focal plane array laser radar system.

The pose estimation in the gated viewing data is directly connected with the model-based identification which makes use of the outline of the object. By setting a sufficient narrow gate the distance gap between the upper part of the ship and the background leads to an automatic segmentation. By setting the gate the distance to the object is roughly known. With this distance and the imaging properties of the camera, the width of the object perpendicular to the line of sight can be calculated. For each ship in the model library a set of possible 2D - appearances in the known distance is calculated and the resulting contours are compared with the measured 2D - outline. The result is a match error for each reasonable orientation of each model of the library. The model with the least match error is therefore assigned to the measured object. However there are always two orientations of the ship with a similar match error, because the contour is similar for positive and negative orientation angles relative to the axis perpendicular to the line of sight.

The model library consists of the models of the observed ships based on CAD-models and additional 46 vessels as disrupters, generated out of laser radar imagery data from another field trial.

The result gained from the gated viewing data is compared

with the results of target identification by laser radar imagery of the same maritime objects. The data was taken on a field trial in Sweden were it was possible to get comparable data of both sensors in a range between 2000 m to 4000 m. Due to poor weather conditions during the field trial the quality of the sensor data is suboptimal; therefore the obtained classification results do not represent the ideal case, but they give a good impression of the achievable accuracy.

9649-20, Session 5

Methodology for the conception of speckle reduction elements in the case of short pulse illumination *(Invited Paper)*

Yves Lutz, Jean-Michel Poyet, Institut Franco-Allemand de Recherches de Saint-Louis (France)

One of the most efficient ways to decrease the speckle contrast in the field of laser illumination is to increase the spatial diversity of coherent laser sources. For very short laser pulses such as those required for flash laser imaging where the recording time corresponds to the illumination pulse length, the spatial diversity should take place instantaneously and no time averaging effect can be used. The spatial diversity is realized by sampling the laser beam into m sub-beams or beamlets with increased optical path length. This path length has to be greater than or equal to the coherence length of the laser beam. In this case, the beamlets are no longer able to create interferences which each other. According to the Goodman's theory of speckle reduction, the speckle contrast is then reduced by a factor of 1/√m. Unfortunately, in the case of multimode lasers, the number of uncorrelated beamlets is not infinite but is limited by a periodicity function resulting from the laser resonator length itself. The speckle reduction possibility is therefore limited and is directly linked to each laser source where the coherence length and cavity length are defined.

In this work, we present a methodology to determine experimentally the optical path length difference as well as the number of beamlets for despeckling a laser source. An experimental realization is presented where both coherence length and periodicity function are measured with a Michelson interferometer where only the speckle contrast of the two beamlets from each arm is analyzed. For the validation of the method, the chosen laser source is a single emitter 640nm laser diode with a coherence length close to 2 mm and a cavity length of 6.25mm. Two cylindrical steppers made with diamond turned PMMA have been realized and adapted for the speckle reduction of this laser. Cylindrical steppers are very interesting speckle reducing elements since they are easy to use, nearly insensitive to alignment and able to conserve the brightness of the input beam. A first stepper of 6 steps with path differences of 2 mm between each step and a second one with 12 steps and path differences of 1mm were tested experimentally. After expanding and homogenizing process, the laser beam is lunched through the stepper which results in rings of equal intensities but with different path lengths. The beamlets are then overlapped on a target with a focusing lens and the speckle contrast is recorded with a high resolution camera. The camera is devoid of its optic in order to record only the objective speckle produced by the interferences of the reflected wavelets. Both elements yield interesting results with close values and in accordance with the theory of spatial diversity. The speckle contrast could be reduced from an initial value of about 10% to a value close to 4%. These values confirm and validate the methodology presented in this work.

9649-21, Session 5

Automatic structural matching of 3D image data

Svjatoslav Ponomarev, S.I. Vavilov State Optical Institute (Russian Federation) and National Research Univ. of Information Technologies, Mechanics and Optics (Russian Federation); Vadim R. Lutsiv, S.I. Vavilov State Optical Institute (Russian Federation) and Saint-Petersburg State Univ. of Aerospace Instrumentation (Russian Federation) and National Research Univ. of Information Technologies, Mechanics and Optics (Russian Federation); Igor A. Malyshev, S.I. Vavilov State Optical Institute (Russian Federation)

A new image matching technique is described. It is implemented as an object-independent hierarchical structural juxtaposition algorithm based on an alphabet of simple object-independent contour structural elements. The structural matching applied implements an optimized method of walking through a truncated tree of all possible juxtapositions of two sets of structural elements. The algorithm was initially developed for dealing with 2D images such as the aerospace photographs, and it turned out to be sufficiently robust and reliable for matching successfully the pictures of natural landscapes taken in differing seasons from differing aspect angles by differing sensors (the visible optical, IR, and SAR pictures, as well as the depth maps and geographical vector-type maps). At present (in the reported version), the algorithm is enhanced based on additional use of information on third spatial coordinates of observed points of object surfaces. Thus, it is now capable of matching the images of 3D scenes in the tasks of automatic navigation of extremely low flying unmanned vehicles or autonomous terrestrial robots. The basic principles of 3D structural description and matching of images are described, and the examples of image matching are presented.

9649-22, Session 5

Results of implementation of the dynamic laser goniometer for non-contact measurement of angular movement

Eugeni D. Bokhman, Mikhail N. Burnashev, Yuri V. Filatov, Petr A. Pavlov, Saint Petersburg Electrotechnical Univ. "LETI" (Russian Federation)

The dynamic laser goniometer is well known instrument for precision calibration of optical polygons and optical encoders. Another mode of operation of the laser goniometer is the non-contact measurements of an object's angular position. An important feature of this mode is an extremely large range of measurement with high accuracy. With the usual resolution of about 0,1 arcs the laser goniometer has in this mode of operation an essential advantage against photo-electric autocollimators with their rather small measuring range.

The report presents the results of implementation of the dynamic laser goniometer in the measurements of the different kinds of angular movement. One of them is determination of the time dependence of the scanning mirror angular position using in some kinds of photography, for example, satellite imagery. The measurements made it possible to determine the instant angular position of scanning mirror with the accuracy of 0,2 arcs and the angular speed of scanning mirror with the accuracy of 0.001 arcs/s.

Another kind of implementation is connected with determination of parameters of a test table oscillatory movement. One of such tables was the standard setup providing the reproduction of vibration and angular accelerations in the frequency range 0.02 – 0.1 Hz and the amplitude range 20 – 200 arcs. Results of measurements obtained by the laser goniometer was compared with the data provided by laser interferometer included in the standard setup. The error of evaluation of angular oscillation amplitude obtained with the laser goniometer was beyond 0.1 arcs.

The measurements of another test table oscillatory movement with the frequency range up to 4.0 Hz and the amplitude up to 1,5 deg have shown that discrepancy from nominal values can reach several arc seconds. The report contains the analysis of possible sources of dynamic errors.

9649-23, Session 6

Modern fibre-optic lidars for remote sensing *(Keynote Presentation)*

Chris Hill, Malvern Lidar Consultants (United Kingdom)

This talk surveys some growth areas in optical sensing that exploit near-IR coherent laser sources and fibre-optic hardware from the telecoms industry. Advances in component availability and performance are promising benefits in several military and commercial applications. Previous work has emphasised Doppler wind speed measurements and wind / turbulence profiling for air safety, with recent sharp increases in numbers of lidar units sold and installed, and with wider recognition that different lidar / radar wavebands can and should complement each other. These advances are also enabling fields such as micro-Doppler measurement of sub-wavelength vibrations and acoustic waves, including non-line-of-sight acoustic sensing in challenging environments.

To shed light on these different applications we review some fundamentals of coherent detection, measurement probe volume, and parameter estimation – starting with familiar similarities and differences between “radar” and “laser radar”. The consequences of changing the operating wavelength by three or four orders of magnitude – from millimetric or centimetric radar to a typical fibre-optic lidar working near 1.5 ?m – need regular review, partly because of continuing advances in telecoms technology and computing.

Modern fibre-optic lidars tend to be less complicated, more reliable, and cheaper than their predecessors; and they more closely obey the textbook principles of easily adjusted and aligned Gaussian beams. The behaviours of noises and signals, and the appropriate processing strategies, are as expected different for the different wavelengths and applications. For example, the effective probe volumes are easily varied (e.g. by translating a fibre facet) through six or eight orders of magnitude; as the average number of contributing scatterers varies, from <<1 through ~1 to >>1, we should review any assumptions about “many” scatterers and Gaussian statistics.

Finally, some much older but still relevant scientific work (by A G Bell, E H Armstrong and their colleagues) is recalled, in the context of remote sensing of acoustic vibrations.

9649-24, Session 6

AlGaInN laser diode technology and systems for defence and security applications

Stephen P. Najda, Piotr Perlin, Tadek Suski, Lucja Marona, Michal Bockowski, Mike Leszczynski, Przemek Wisniewski, Robert Czernecki, George Targowski, TopGaN Ltd. (Poland); Scott Watson, T. Kelly, Univ. of Glasgow (United Kingdom)

The latest developments in AlGaInN laser diode technology are reviewed for defence and security applications. The AlGaInN material system allows for laser diodes to be fabricated over a very wide range of wavelengths from u.v., ~380nm, to the visible ~530nm, by tuning the indium content of the laser GaInN quantum well. Ridge waveguide laser diode structures are fabricated to achieve single mode operation with optical powers of >100mW. Visible light communications at high frequency (up to 2.5 Gbit/s) using a directly modulated 422nm Gallium-nitride (GaN) blue laser diode is reported in free-space and underwater.

High power operation of AlGaInN laser diodes is also reviewed. Low defectivity and highly uniform GaN substrates allow arrays and bars of nitride lasers to be fabricated. Laser bars of up to 5mm with 20 emitters have shown optical powers up to 4W cw at ~395nm with a common contact configuration. An alternative package configuration for AlGaInN laser arrays allows for each individual laser to be individually addressable allowing complex free-space and/or fibre optic system integration within a very small form-factor.

9649-25, Session 6

Microoptical gyros on the base of passive ring cavities

Yuri V. Filatov, Egor V. Shalymov, Vladimir Y. Venediktov, Saint Petersburg Electrotechnical Univ. “LETI” (Russian Federation)

The review paper is devoted to properties and performance of prospective microoptical gyros, based on multi-beam interference in ring cavities (resonators). We consider various integral and 3D optical technologies and various schemes of data collection from such gyros, including 1- and 2-channel connections, amplitude, phase and hybrid data analysis, quantum noise sensitivity limits of such devices, other possible source of errors etc.

9649-27, Session 7

Compact full-motion video hyperspectral cameras: development, image processing, and applications *(Invited Paper)*

Andrey V. Kanaev, U.S. Naval Research Lab. (United States)

Emergence of spectral pixel-level color filters has enabled development of hyper-spectral Full Motion Video (FMV) sensors operating in visible (EO) and infrared (IR) wavelengths. The new class of hyper-spectral cameras opens broad possibilities of its utilization for military and industry purposes. Indeed, such cameras are able to classify materials as well as detect and track spectral signatures continuously in real time while simultaneously providing an operator the benefit of enhanced-discrimination-color video. Supporting these extensive capabilities requires significant computational processing of the collected spectral data. In general, two processing streams are envisioned for mosaic array cameras. The first is spectral computation that provides essential spectral content analysis e.g. detection or classification. The second is presentation of the video to an operator that can offer the best display of the content depending on the performed task e.g. providing spatial resolution enhancement or color coding of the spectral analysis. These processing streams can be executed in parallel or they can utilize each other’s results. The spectral analysis algorithms have been developed extensively, however demosaicking of more than three equally-sampled spectral bands has been explored scarcely. We present unique approach to demosaicking based on multi-band super-resolution and show the trade-off between spatial resolution and spectral content. Using imagery collected with developed 9-band SWIR camera we demonstrate several of its concepts of operation including detection and tracking. We also compare the demosaicking results to the results of multi-frame super-resolution as well as to the combined multi-frame and multi-band processing.

9649-28, Session 7

Inter-instrument registration for the airborne hyperspectral system, Sysiphe

Sophie Fabre, Laurent Rousset-Rouviere, ONERA (France)

Sysiphe is an airborne hyperspectral imaging system with a spectral range from 0.4µm to 11.5µm and a spatial resolution of 0.5m at a ground height of 2000m. Sysiphe includes two components : the infrared hyperspectral instrument Sieleters covers the spectral range [3-11.5µm] and the visible and shortwave infrared reflective hyperspectral instrument Hyspex ODIN-1024 is related to the [0.4-2.5µm] spectra domain. The STAD, the post processing and archiving system, is developed

to provide spectral reflectance and temperature products from calibrated georeferenced and inter-band registered spectral radiance products provided by each instrument. The STAD is decomposed in many processing modules including the inter-instrument registration module. This one allows to generate a georeferenced radiance product covering the whole spectral domain with the georeferenced radiance products related to each hyperspectral instrument used as input.

Image registration is the process of transforming an image into the frame of the other image. In this case, the reference image is Hyspex ODIN-1024 radiance image and the Sieleters radiance image is the target image projected in the reference space. The problematic of registration is then related to the very high spatial resolution (0.5m) and the distinct spectral range covered by each instrument.

The proposed method operates in the image domain and is an intensity and feature-based method. It finds correspondence between image features such as points, lines, and contours and compares intensity patterns in images via correlation metric. The transformation model used to relate the target image space to the reference image space includes linear transformations (translation, rotation, scaling) used to model local geometric differences between images. The defined transformation model is applied on the target image by using a robust and reliable resampling tool that involves the extraction and interpolation of gray levels from pixel locations in the target image and their relocation to the approximate matrix coordinate location in the rectified image corresponding to the reference space. The registration method is automatic and can be used to register spectral radiance images or spectral reflectance and emissivity images (before or after the atmospheric compensation).

In this paper, the registration method and the associated resampling tool are described. The performance is analyzed by using simulated data set provided by real data acquired by an airborne hyperspectral instrument different from the Sysiphe system. Finally, preliminary registration results obtained with real data set acquired by the Sysiphe system are presented.

9649-29, Session 7

Airborne thermal infrared hyperspectral imaging of buried objects

Marc-André Gagnon, Philippe Lagueux, Jean-Philippe Gagnon, Simon Savary, Pierre Tremblay, Vincent Farley, Telops (Canada); Éric Guyot, Telops France (France); Martin Chamberland, Telops (Canada)

Characterization of hazardous lands using ground-based techniques can be very challenging. For this reason, airborne surveys are often preferred. The use of thermal infrared imaging represents an interesting approach as surveys can be carried out under various illumination conditions and that the presence of buried objects typically modifies the thermal inertia of their surroundings. In addition, the burial or presence of a buried object will modify the particle size, texture, moisture and mineral content of a small region around it. All these parameters may lead to emissivity contrasts which will make thermal contrast interpretation very challenging. In order to illustrate the potential of airborne thermal infrared hyperspectral imaging for buried object characterization, various metallic objects were buried in a test site prior to an airborne survey. Airborne hyperspectral images were recorded using the targeting acquisition mode, a unique feature of the Telops Hyper-Cam Airborne system which allows recording of successive maps of the same ground area. Temperature-emissivity separation (TES) was carried out on the hyperspectral map obtained upon scene averaging. The thermodynamic temperature map estimated after TES highlights the presence of hot spots within the investigated area. Mineral mapping was carried out upon linear unmixing of the spectral emissivity datacube obtained after TES. The results show how the combination of thermal information and mineral distribution leads to a better characterization of test sites containing buried objects.

9649-30, Session 7

Design of a compact hyperspectral imaging spectrometer for mid-infrared applications

Armande Pola Fossi, Nicolas Guérineau, ONERA (France); Hervé Sauer, Lab. Charles Fabry (France); Yann Ferrec, ONERA (France); Nicolas Roux, Marc Bousquet, Emmanuel Kling, Sagem (France)

Hyperspectral imaging consists in the acquisition of a scene at many wavelengths. Thanks to the capability to associate each point of the scene to its spectrum, hyperspectral imaging offers the possibility to identify interesting objects in the observed scene. Among the concepts generating the “hypercube”, we are developing at ONERA static Fourier Transform imaging spectrometers using lateral shearing interferometers. These interferometers duplicate the incident wavefront, displace it laterally by a small amount and obtain interference pattern localized at infinity between the original and the displaced wavefronts.

Among this family of interferometers, we chose the birefringent lateral shearing interferometer (BLSI) because it is a one way interferometer and can be therefore miniaturized. Common BLSI are the Savart plates made of two uniaxial plates with optical axis oriented at 45° in orthogonal principal sections (plane containing the optical axis and the normal the diopter) and the double-Wollaston made of two bounded Wollaston prisms. Our work consists in designing a static Fourier transform compact hyperspectral imaging spectrometer using one of the above mentioned BLSI.

The first part of this work was to validate the concept in the visible by using a Double-Wollaston made of Calcite. More precisely, the purposes here were to understand how BLSI works and to anticipate the difficulties in the conception of an infrared instrument. Among the difficulties we wanted to anticipate, there was the quality of the interferogram (contrast, fringe spacing, linearity of the fringes and so on) when manufacturing defects appear. This study also allowed to experimentally validate an algorithm which predicts the optical path differences and the intensity of interference created by a stack of anisotropic media. This algorithm is based on a matrix formulation of Maxwell equations and continuity of electric and magnetic fields at an interface. Thanks to this study, we have validated the Matlab code in particular by observing and characterizing stray rays created at anisotropic-anisotropic interface. They have been characterized as stray interference and stray light which intensity is a thousand smaller than the intensity of nominal light. The study also pointed out the importance of rigorous tolerancing of the future prototypes.

The second part of the work consists in developing the MWIR prototype. For this prototype the BLSI which is used is the Savart plates for two reasons. First, the Matlab code predicts that the stray rays intensity is a million smaller than the nominal ray intensity and second, the number of manufacturing parameters is smaller compare to the double-Wollaston which reduces the risk of degrading the interferences patterns. We are currently manufacturing a prototype using TeO2 uniaxial crystal. The expected resolution of the imaging spectrometer is 10 cm-1. The Savart plate will be mounted in front of a miniaturized MCT camera with a field of view of 60°x48°. Outdoor measurements are planned for June 2015.

9649-31, Session PS

Range-intensity coding under triangular and trapezoidal correlation algorithms for 3D super-resolution range-gated imaging

Xinwei Wang, Yan Zhou, Institute of Semiconductors (China); Youfu Li, City Univ. of Hong Kong (Hong Kong, China)

Three-dimensional super-resolution range-gated imaging (3D SRGI) is a new technique for high-resolution 3D sensing. It has good real-time performance and range super-resolution far beyond the classical 3D range-gated imaging based on time slicing, and has great potential in intelligent surveillance, automatic navigation and 3D underwater imaging. Up to now, 3D SRGI has been developed with two range-intensity correlation algorithms, including trapezoidal algorithm and triangular algorithm. To obtain high depth-to-resolution ratio of 3D imaging, coding method was developed for 3D SRGI based on the trapezoidal algorithm by the French-German Research Institute of Saint-Louis (ISL) in 2011. Here the depth-to-resolution ratio is defined as the ratio between the depth of 3D imaging and the product of the depth resolution and raw gate image number. Higher depth-to-resolution ratio means better capability of 3D imaging. In the ISL's coding method, the sensor gate time and the time delay between laser pulses and gate pulses were coded according to the trapezoidal algorithm, and then multiple coded range-gates sampled a targeted 3D scene and yielded coding gate images. Finally 3D images were decoded from coding gate images under the trapezoidal algorithm. In this paper, we investigate range-intensity coding based on triangular and trapezoidal correlation algorithms, and propose range-intensity coding based on the triangular correlation algorithm and hybrid range-intensity coding based on the two algorithms. The coding rules under the triangular algorithm and the hybrid algorithm are respectively established, and their theoretical models to predict the coding bin number are also developed. In fact, the triangular and trapezoidal algorithms both utilize the specific shapes of range-intensity profiles (RIP) to reconstruct depth information collapsed in gate images. From the coding perspective, one coding bin based on two gate images with triangular RIPs is the simplest case of the triangular algorithm, and two coding bins based on two gate images with trapezoidal RIPs is the simplest case of the trapezoidal algorithm. The depth of a coding bin is determined by the laser pulse width. For the case of three coding gate images, the typical coding bin number was proved to be 12 under the trapezoidal algorithm by ISL. Our research demonstrates that the maximum coding bin number is 7 for three coding gate images under the triangular algorithm, and the maximum number reaches 16 for three gate images under the hybrid algorithm. The coding examples of 7 bins and 16 bins mentioned above are given in this paper, and 3D images are successfully decoded. Large coding bin number for given gate images results in high depth-to-resolution ratio. The research of this paper is beneficial to enlarge depth-to-resolution ratio for the coding method of 3D SRGI.

9649-32, Session PS

A space debris removal system with solar pumped laser

Pingping Luo, Chen Li, Yuzhao Wang, Beijing Institute of Space Mechanics and Electricity (China)

One result of nearly 60 years human space activity is that about 15000 trackable pieces of space debris in the earth orbits, accounting for approximately 5800 tons of on-orbit mass, the total population is exceed 20000 objects larger than 10cm, and there are also countless small debris(<10cm) distribution in the space. The debris in near earth orbits poses significant danger to spacecraft, satellites, human flights and future space exploration activities. Long term forecasting predicts about 20 catastrophic collision during the next 200 years, and shows that if immediately stop all launch activity from now on, the debris population would continue to grow, leading to the result of the space environment would essentially unusable by 2100.

Nowadays, maneuvering of spacecraft in orbit to avoid collision with debris is the main adoption methods, which requires accurate position and path information of the object to be avoided. Consider with the prediction mentioned above, it is necessary to adopt the active debris removal technology to mitigate the growth of the debris population.

Various approaches to remove debris from space have been proposed, e.g. electro-dynamic tether, capture and removal, laser and so on. Among these methods, we choose laser technology to remove debris smaller than 10cm. For the small size debris, current radar and space telescopes cannot track and identify, preventing steer avoidance for lager debris pieces, meanwhile, additional layer of metal foil on the outside of the spacecraft is not work. Our approach is use powerful laser pulses to create a series of plasma plumes from the targeted surface of debris. The incident pulse laser beam generates a sequence of detonation plumes opposite the direction of the debris, the evaporated plasma eject with a velocity of roughly 105m/s in vacuum, this opposite velocity will reduce the debris' orbital velocity and cause it to re-enter the atmosphere and disintegrate.

In this paper, the integrated space based debris removal system is analyzed. The system is composed of ATP system, high power laser system and beam control system. The ATP is used to capture and lock the target all along, once the object is judged to be debris, and in the work distance of laser system, the high power laser system will turn on, and emit the laser pulses to the debris.

The laser parameters for space debris removal are analyzed in detail. According to the analysis of relationship between velocity increment and deorbit, and the relationship among single pulse energy, pulse frequency, pulse width, laser aperture, the parameters of the laser system are determined. With regard to space debris with approximately diameter of 10cm and distance of 50km, using high power laser with repetition frequency of 10Hz, pulse width of 5ns, the laser pulse energy of 50J, the space debris can be deorbited in the action time of about 420s. In this paper, a foldable space-based solar pumped laser system is proposed. The solar focus system is composed by the Fresnel lenses, which are with the most important advantages in space application: light weight. In order to reduce the volume of the system, the large size of the Fresnel lens is designed to be foldable. Compared with space-based traditional laser which completely relies on the electricity generated from solar cells, space-based solar pumped laser directly utilize solar energy and therefore reduce energy consumption significantly.

9649-33, Session PS

Structural and optical properties of TiO2–Al2O3 nanolaminates produced by atomic layer deposition

Viktoriia Fedorenko, Department of Experimental Physics, Odessa National I.I. Mechnikov University (Ukraine); Igor Iatsunskyi, Adam Mickiewicz Univ. (Poland) and Odessa I.I. Mechnikov National Univ. (Ukraine); Nikolay Pavlenko, Odessa I.I. Mechnikov National Univ. (Ukraine); Mariusz Jancelewicz, Adam Mickiewicz Univ. (Poland); Emerson Coy, NanoBioMedical Centre, Adam Mickiewicz University (Poland); Roman Viter, Institute of Atomic Physics and Spectroscopy, University of Latvia (Latvia)

In this work, optical and structural properties of Al2O3/TiO2 nanolaminates prepared by atomic layer deposition (ALD) were investigated. Al2O3/TiO2 nanolaminates were grown on Si (100) and glass substrates by ALD at 200°C using trimethylaluminum, titanium(IV) chloride, and deionized water as precursors. All prepared multilayers are nominally 100 nm thick with a varying number of alternating TiO2 and Al2O3 layers. Sample thickness and ellipsometric spectra were measured using a spectroscopic ellipsometer, X-Ray reflectivity, and the parameters determined by computer simulation matched with the experimental results well. The effect of nanolaminate structure on the optical transmittance is investigated using an ultraviolet–visible-near-infrared spectrometer. Band gap energy of TiO2 with different layer thickness in nanolaminates was estimated. Spectroscopic ellipsometry showed that the refractive index could be tuned between the two extremes of the individual constituents. X-ray reflectivity studies showed the Kiessig fringes and Bragg peaks, indicating the well defined formation of individual layers and bilayer periodicity in the multilayer films. The experimental results on the optical properties of Al2O3/TiO2 nanolaminates obtained in the present investigation have technical importance in UV optical coatings, and multilayer optical coatings as antireflective coatings.

Conference 9650A: High-Power Lasers 2015: Technology and Systems

SPIE. SECURITY+ DEFENCE

Monday 21 September 2015

Part of Proceedings of SPIE Vol. 9650 Technologies for Optical Countermeasures XII; and High-Power Lasers 2015: Technology and Systems

9650-1, Session 1

Recent Advances in Er3+:YAG solid-state heat-capacity technology *(Invited Paper)*

Stefano Bigotta, Karsten Diener, Thierry Ibach, Lothar Geiss, Georg Stoeppler, Joerg Schoener, Michael von Salisch, Marc Eichhorn, ISL (France)

The concept of a Solid State Heat-Capacity Laser (SSHCL) as a source for medium and high energy laser systems operating in the “eye-safe” range is currently under investigation at ISL. The aim is to obtain a robust laser source with low complexity, scalable to 100 kW and beyond and at the same time high beam quality (M?<3).

The main characteristic of the SSHCL is its operation scheme: the laser medium is cooled only after the laser action has ended, resulting in low temperature gradients in the laser medium itself during the laser operation. Previous investigations demonstrated the scalability of the heat-capacity laser principle and up to 4.65 kW and 440 J in less than 800 ms have been achieved using optimized doping levels for up-conversion reduction in this resonantly-diode-pumped Er3+:YAG SSHCL. Optical-to-optical efficiencies of over 41% and slope efficiencies of over 51% are obtained with respect to the incident pump power.

The presence of residual thermal gradients, due to non perfect pumping homogeneity of the crystal, negatively affect the laser performance in terms of laser pulse energy, duration and beam quality. The ideal resonator configurations are those which allow an extraction of the laser energy as homogeneous as possible. Using an intra-cavity adaptive optics system beams with phase wavefronts as flat as possible, on the order of less than 1/10 of the wavelength for each of the considered Zernike polynomials have been generated, and the shot duration has been lengthened by ~50%.

In this paper we investigate how to further increase the pulse duration of the SSHCL. The influence of the crystal geometry on the pump distribution homogeneity, the extraction efficiency and the pulse duration are analysed. Then we consider the use of a mechanical crystal changer for extending the laser pulse duration. By using a revolver with several crystals, we were able to correctly position the crystal inside the cavity and we demonstrated that crystals can be changed in less than 100 ms allowing a quasi-cw operation that can large exceed the time constraints imposed by the heating of the crystal.

Finally, we address the problem of measuring the laser beam quality, the standard way being to estimate the M? parameter of the laser. However the standard techniques currently used are suitable only for stable cw laser, and cannot be used for the SSHCL, where the crystal temperature is constantly increasing during the laser shot. A new kind of device, capable of measuring the M? at intervals of less than 100 ms, is presented in this report.

9650-2, Session 1

Considerations of a ship defense with a pulsed COIL

Kiwamu Takehisa, O2 Laser Laboratory (Japan)

Ship defense system with a pulsed COIL (Chemical Oxygen-Iodine Laser) is considered. One of the greatest threats for a battle ship and a carrier in warfare is a supersonic sea-skimming anti-ship missile. The counter measure is considered to be a supersonic RAM (Rolling Airframe Missile) at first. And a CIWS (Close-In Weapon System) is used as the last defense. However since a sea-skimming missile can be detected only at a 30-50km away due to the radar horizon, using a speed-of-light weapon is desirable as the first defense, especially when a sea-skimming missile with Mach >10 is realized.

Previous report explained the advantages of a giant pulse from a chemical oxygen laser (COL) to shoot down a supersonic aircraft.1) But the first defense requires the beam propagation length of ~30km, using a pulsed COIL is better considering its good air transmissivity. Therefore efficient operation for a giant-pulsed COIL is investigated with a simulation.

Ref.1) K. Takehisa, “Proposal of a defense application for a chemical oxygen laser,” SPIE Defense + Security 2015, Baltimore, to be published.

9650-3, Session 1

High-power sequence beam combining of pulsed lasers based on electro-optic deflection

Yongliang Zhang, Ying Deng, Shaoqi Wang, Minqiang Kang, China Academy of Engineering Physics (China)

When high energy pulsed lasers are applied in security and defense field, high pulse energy and repetition work is required simultaneously. But directly improving the repetition rate of a high energy laser will regularly result in a decline in the energy of a single pulse. When high average power lasers are applied in security and defense field, a power of above 100 kW class is required. Beam combining is necessary to achieve such a power class. A sequence beam combining technology based on electro-optic deflection is brought out in this paper. First the pulse sequences of the pulsed lasers are staggered by synchronizator and delay device, and then deflected differently by an electro-optic deflector. By adjusting the deflection paths and the incidence paths, the pulsed lasers can be deflected to a same path and consequently combined as one laser beam. The repetition and average power of the combined laser is the sum of that of the pulsed lasers, while the energy of a single pulse and the beam quality does almost not decline. The sequence beam combining technology will excel in preventing beam quality decline and reducing the demands for the lasers to be combined. In this paper the key issues have been studied, which include the beam quality of the combined laser, the power scaling ability, the demands for the lasers and the key related technologies. It is indicated that the sequence beam combining technology is a new high efficiency and high quality combining technology both for high energy lasers and high average power lasers.

9650-5, Session 2

Power scaling and beam combination of fiber lasers *(Invited Paper)*

Till Walbaum, Thomas Schreiber, Jens Limpert, Ramona Eberhardt, Andreas Tünnermann, Fraunhofer IOF (Germany)

Fiber lasers are known for their highly efficient generation of diffraction limited light with high average power levels. In order to reach such power levels, the complete process of fabrication of the rare-earth doped preform, the fiber drawing, implementation in a laser setup as well as the characterization requires a detailed understanding.

Firstly, we review this process chain and highlight several aspects in order to scale the power in these systems. This includes the preform preparation by modified chemical vapor deposition (MCVD). Its refractive index control is varied by different aspects during the process and it is shown, how these

influence the transverse profile and longitudinal homogeneity. After measuring the 3D profile and evaluating it by numerical means, the preform and boundary conditions are selected for fiber drawing.

Measurement methods for the final fiber characterization include absorption and laser efficiency measurements, but also novel devices for mode content measurements (S?-method) and photodarkening characterization. This allows verifying the conditions of the laser tests.

With this knowledge it is possible to draw a connection to the limitation of modal instability and recent experimental results to overcome it. Modal instabilities occur in high power fiber lasers at a power level of several 100 W or above depending on the system architecture. It is understood that they are a result of a thermally induced index grating generated by lower order mode interference that enables highly dynamic energy exchange between transverse modes. We will motivate recent explanation of this effect and show how passive mitigation strategies can help to increase the MI threshold.

Another method to scale the power of laser systems is beam combination, if single emitting systems are limited. Examples will be shown for continuous-wave as well as short-pulse fiber lasers based on coherent and incoherent combination.

While fiber laser are a very good approach for avoiding thermo-optical issues, the question arises, how to transfer this power to novel spectral regions. After the discussion of coherent combining, the approach of harmonic generation is explained to show how to reach higher photon energies.

On the other hand, by combining fiber lasers with another power scalable approach, we will show, how longer wavelength than generated by the laser can be efficiently created. This approach is based on Raman-conversion in diamond. Unlike other nonlinear crystals, diamond has a huge transparency region up to 4.5 μm as well as thermo-optical parameters that dramatically reduce thermal-lensing, which typically limits the performance of nonlinear crystals at high average powers. We will indeed show that a high power cw-fiber laser can be converted with up to 60% of efficiency from 1.06 μm to 1.24 μm in diamond, at an output power level of 360 W at the Stokes wavelength. As an outlook, spectral coverage is indicated at wavelength of 2.4-3.1 μm with average power levels well above 10 W.

9650-6, Session 2

High-power optical phased arrays for space debris tracking and manoeuvring

Lyle E. Roberts, Robert L. Ward, The Australian National Univ. (Australia); Andrew J. Sutton, Jet Propulsion Lab. (United States); Roland Fleddermann, Shasidran Raj, The Australian National Univ. (Australia); Craig Smith, EOS Space Systems Pty. Ltd. (Australia); David E. McClelland, Daniel A. Shaddock, The Australian National Univ. (Australia)

The performance of existing ground based space debris laser ranging systems can be improved by directing more light onto space debris targets using a high-power optical phased array (OPA). If the power delivered to target is sufficiently high then these systems may also permit remote manoeuvring of space debris via photon radiation pressure and/or ablation. In contrast to incoherent laser combination, an OPA actively controls the relative phase of multiple lasers, forming a contiguous and coherent optical wave front in the far field. Optical phased arrays are therefore able to support higher total delivery of power to a point in the far field beyond the limits of conventional lasers, without significant penalty on beam quality and cost. We present a scalable OPA architecture that can potentially support the total deliver of over 1 kW continuous wave (CW) optical power, which has been designed to improve the sensitivity of an existing ground-based space debris tracking system operating in Australia. It may also eventually provide the capability to remotely manoeuvre space debris in low-earth orbit.

The technique for coherent beam combination presented here scales power by co-phasing the outputs of multiple phase-locked lasers or fiber amplifiers. This technique does not require externally sampling the outgoing beam using free-space optics, and instead infers the relative phase of each emitter by measuring the light that is reflected back into the fibre at the OPA's glass-air interface. This internally sensed OPA can be implemented entirely in fiber, eliminating any need to use free-space sampling optics, and offering potential robustness in the presence of shock and vibration. The ability to independently control the phase of each emitter is enabled using digitally enhanced heterodyne interferometry, which simultaneously isolates the phase information from each emitter using spread-spectrum modulation techniques similar to those used in the global positioning system. Digitally enhanced heterodyne interferometry's inherent multiplexing capability reduces the complexity of the optical system, and instead relies on the efficient utilisation of digital signal processing resources. Digitally enhanced interferometry is resilient to noise and interference caused by spurious reflections in fiber, is readily scalable, and well suited to the computational power of field-programmable gate-arrays. Asymmetric power splitters are used to protect sensitive optical elements (e.g., electro-optic modulators and waveguide components) from sufficiently high optical powers (>100 mW) that would destroy them, whilst also allowing a small fraction of the back reflected light to return through the system for detection and measurement. This internally sensed optical phased array has been experimentally demonstrated at 500 mW with over 99.9% combination efficiency and kHz bandwidth beam steering. A 45 W OPA using three 15 W fiber amplifiers is currently being tested, which will provide the technology platform from which to scale to kW level CW optical powers.

9650-7, Session 2

High-power near-infrared supercontinuum source generated in an ytterbium-doped fiber amplifier

Aijun Jin, Sheng-Ping Chen, Lei Si, National Univ. of Defense Technology (China); Bin Zhang, National Univ. of Defense Technology (China) and College of Optoelectronic Science and Engineering, National University of Defense Technology (China); Jing Hou, Zong-Fu Jiang, National Univ. of Defense Technology (China)

In this report, we build a high power supercontinuum (SC) source system based on a four-stage master-oscillator power-amplifier (MOPA) configuration and obtain a higher than 200 W near infrared SC source, which is to our knowledge the highest SC output power. A passively mode-locked nanosecond pulsed seed laser at 1064 nm is amplified by two fiber amplifiers as the signal light of a master power amplifier. Then the signal light is augmented to higher than 200 W with 440 W pump power and broadened to be an SC source with the final spectrum covers a wavelength range from 1 ?m to beyond 1.7 ?m. The pulse duration of the seed laser can be changed through adjusting the pump power. Thus the process of power amplification and spectral evolution during SC generation and the influence of pulse duration on this process can be investigated in detail.

Because the signal light is at 1064 nm which is in the normal dispersion region of the gain fiber, in the first phase of power amplification and spectral broadening, Raman effect plays a dominant role. When the laser power is higher than the Raman threshold, the first Raman peak appears around 1120 nm. With the increase of pump power, more orders of Raman peaks are stimulated. Owing to the wide signal spectrum and Raman gain spectrum, the generated Raman-continuum is flat and no discrete Stokes peaks can be observed in the spectrum. Because of the high efficiency of stimulated Raman scattering (SRS) effect, most of the pump power is transferred to long wavelength spectral components and the power of signal light

at 1064 nm is not high significantly.

When the spectrum is extended across the zero-dispersion wavelength into anomalous dispersion region, modulation instability and soliton effect become the main effect for spectral broadening. With the increase of pump power and the output power, the power of signal light at 1064 nm is amplified dramatically and in the final output spectrum with pump power 440 W it becomes a prominent peak. This indicates that nonlinear effects in the anomalous dispersion region cannot drag the power of signal light obtained from the pump power to long wavelength spectral region adequately.

With similar average output power, narrower seed pulse leads to higher peak power and can induce Stokes waves earlier. Thus longer fiber left for soliton propagating. Due to the relationship of soliton self-frequency shift effect and fiber length, the spectrum can be shifted to longer wavelength. However, the signal light becomes a higher spike. In a word, narrower seed pulse leads to higher signal peak and wider SC source.

9650-8, Session 3

High-average-power narrow-line-width sum frequency generation 589 nm laser

Yanhua Lu, Huaijin Ren, Institute of Applied Electronics (China); Lei Zhang, Institute of Applied Electronics, China Academy of Engineering Physics (China); Gang Xie, Institute of Applied Electronics (China); Xiafei Xu, Institute of Applied Electronics, China Academy of Engineering Physics (China)

Sodium beacon lasers, which work at the wavelength exactly matched to the D2a line (589.159 nm) of the sodium atoms, have far-reaching applications both in Astronomy adaptive optics system and the transmission of high-energy lasers. To avoid temporal overlap with Rayleigh scattering backwards light in the lower atmosphere, high-repetition-rate 589 nm pulsed sodium beacon lasers will be of greater significance than CW lasers. In the paper we describe an 81 W, near diffraction-limit beam quality all-solid-state quasi-continuous-wave sodium beacon laser with a novel sum frequency generation (SFG) idea, based on a 1064 nm single frequency, good beam quality (M2 ≈1.8)laser and a 1319 nm multi-longitudinal-modes (MLM), bad beam quality (M2 ≈3.0) laser.

Both of two fundamental lasers of 1064 nm and 1319 nm are in the structure of master oscillator and power amplifiers (MOPA). To get super stable central wavelength, narrow line width and good beam quality, the seed lasers are both well controlled in longitudinal and transversal mode. The average-power of 1064 nm seed laser is 150 mW with the repetition rate of 250 Hz and the ultra-narrow line width (< 100 kHz). It is amplified to 150 W by two stages of Nd:YAG rods amplifiers. The beam quality M2 is about 1.8 while the beam quality M2 of the seed laser is 1.1. The average-power of 1319nm seed laser is 5.0 W with the line width of ~0.3 GHz. A LBO second harmonic generation crystal is inserted into the 1319 nm oscillator to suppress the spikes of the 1319 nm time waveform. It is amplified to 100 W with the beam quality M2 of about 3.0 also by two stages of Nd:YAG rods amplifiers. The whole pulse widths of the 1064 nm and 1319 nm lasers are 150 ?s and 155 ?s, respectively.

The 1064 nm and 1319 nm lasers which are re-shaped and beams-combined, then focused on a LBO slab crystal with the size of 3 mm?12 mm?50 mm. The 589 nm sodium beacon laser is caused by nonlinear SFG in the crystal. The pulse energy is 325 mJ with M2 < 1.3, 150?s pulse width and repetition rate of 250 Hz. The SFG efficiency is about 32.5 %.

The central wavelength of the 589 nm is locked to 589.159 nm in closed loop, which is well matched to D2a line of sodium atoms. The experimental measured result of 589 nm line width is ~0.3 GHz and just equivalent to the sum of the two infrared lasers' line widths.

9650-9, Session 3

High-energy 1064 nm single frequency long-pulse laser

Huaijin Ren, China Academy of Engineering Physics (China)

Single frequency lasers have many applications in gravitational-wave detecting, atom trapping, laser cooling, coherent lidar, and so on. Researchers have developed very high power single frequency lasers working in continuous format and Q-switched format. However, because of relaxation oscillation, the single frequency long-pulse laser at the level of hundreds of microseconds generated directly by oscillator is usually unstable in both time domain and frequency domain.

We report on a new method to get the single frequency long-pulse laser. The whole experimental system is a master oscillator power-amplifier (MOPA) structure composed of a 1064 nm seed laser, a pre-amplifier and a main amplifier. Different from the traditional pulse laser technologies, the 1064 nm pulse seed laser is generated by external modulating of a continuous-wave (CW) single frequency fiber laser through an electro-optic modulator (EOM). The modulated laser has a rectangle pulse shape with 250 Hz repetition rate, 200 ?s pulse width, 0.8 mJ pulse energy and excellent beam quality, M2 < 1.1.

The pulse seed laser is then amplified by two stages of Nd:YAG rods amplifiers. The first stage amplifier consists of two 25 Bar (5 sides by 5 circles) diodes pumped modules with a double-pass configuration. The peak pump power of each module is 3.8 kW with a pump width of 250 ?s. The diameter of the Nd:YAG rod is 4 mm and the length is 96 mm. A quartz rotator (QR) and a negative lens (NL, f= -400 mm) are inserted between the modules to compensate for the depolarization and the thermal lens effect. After the first stage amplifier, the pulse energy of 1064 nm laser becomes 21 mJ, and the beam quality M2 is about 1.3. The second stage amplifier is a single-pass configuration, and the gain modules are two 108 Bar (9 sides by 12 circles) diodes pumping modules with the peak pump power of 13 kW. In this module, the Nd:YAG rod has a diameter of 10 mm and a length of 190 mm. The final amplified energy is 2040 mJ with the beam quality M2 = 1.8. The total optical-to-optical efficiency is about 19 %. The pulse shape is modified to be trapezium with a pulse width of 150 ?s in FWHM.

Remarkably, there is no obvious line width broadening in the MOPA system. The line width of the 1064 nm is measured by the delayed self-heterodyne interferometer (DSHI) method. The bandwidth of the beat spectrum at -3 dB is 71.42 kHz, which means that the actual line width of 1064nm laser is less than 35 kHz, limited by the precision of our measuring system.

9650-10, Session 4

Supersonic diode pumped alkali lasers: Computational fluid dynamics modeling *(Invited Paper)*

Salman Rosenwaks, Eyal Yacoby, Karol Waichman, Oren Sadot, Boris D. Barmashenko, Ben-Gurion Univ. of the Negev (Israel)

Three-dimensional computational fluid dynamics (3D CFD) modeling of supersonic diode pumped alkali lasers (DPALs), taking into account fluid dynamics and kinetic processes in the lasing medium, is reported. For a supersonic Cs DPAL with parameters similar to those of the 1-kW flowing-gas subsonic Cs DPAL [A.V. Bogachev et al., Quantum Electron. 42, 95 (2012)] the maximum value of lasing power, ~ 7 kW, for the former is 25% higher than for the latter. Comparison between semi-analytical and 3D CFD models for Cs shows that just as in the subsonic laser [K. Waichman et al. J. Opt. Soc. Am. B 31, 2628 (2014)] the latter predicts much higher maximum achievable laser power than the former. Optimization of the He/CH4 buffer gas composition, flow parameters and the output mirror reflection using 3D CFD modeling shows that

for the resonator geometry of Bogachev et al., extremely high power and optical-to-optical efficiency, 35 kW and 82%, respectively, can be achieved in the Cs supersonic device. The main processes limiting the power of Cs supersonic DPAL pumped by a collimated (~5 mm diameter) beam are saturation of the D2 transition and large ~ 40% losses of alkali atoms due to ionization, whereas the influence of the gas heating is negligibly small. Application of end- or transverse-pumping by broad beam makes it possible to obtain much higher output power, > 250 kW, for ~ 350 kW pumping power for both the end- and transverse-pumping. These values of the power are by more than 40% higher than those predicted for the subsonic DPAL. For supersonic K DPAL both the gas heating and ionization effects are shown to be unimportant. Therefore the power calculated by the 3D CFD and semi-analytical models are very close to each other. Maximum values of the power ~40 kW and 350 kW for pumping by collimated and broad beam, respectively, are higher than those achievable in Cs supersonic laser. The power achieved in the supersonic K DPAL is two times higher than for the subsonic version with the same resonator and K density at the inlet, the maximum optical-to-optical efficiency being 82%. Estimates of the gas dynamics of a closed cycle supersonic DPALs are reported. They show that in K DPAL a closed cycle operation mode is feasible if a variable-geometry diffuser is employed and the mechanical pump power, required for maintaining the circulation is ~ 50-70 kW for flow conditions corresponding to 2-3 atm static pressure in the resonator, where lasing power of 25-30 kW can be achieved. At the same time for Cs and Rb high pressure devices, closed cycle supersonic operation mode requires unrealistically large values of mechanical pump power, > 100 kW, which means that only quasi CW operation mode, where the high pressure gas is expanded in the supersonic nozzle and collected in a storage tank, is possible for these atoms.

9650-11, Session 4

Modeling of pulsed K DPAL taking into account the spatial variation of the pump and laser intensities in the transverse direction

Boris D. Barmashenko, Ilya Auslender, Salman Rosenwaks, Ben-Gurion Univ. of the Negev (Israel); Boris Zhdanov, Matthew Rotondaro, Randall J Knize, US Air Force Academy, Laser and Optics Research Center (United States)

Diode pumped alkali lasers (DPALs) have recently been extensively studied [1]. Of special interest is the K DPAL which has very high quantum efficiency (99.6%). It can operate with low pressure He buffer gas [1], whereas Cs and Rb DPALs can operate with hydrocarbon buffer only or, the latter, also with high pressure (several atmospheres) He. Recently a highly efficient static, pulsed K DPAL with slope efficiency of 52% was demonstrated in USAFA [2]. In spite of the high efficiency, its threshold power was rather high, 22 W. This value could not be fitted by simple standard models [3,4] assuming uniform intensities of the pump and laser beams in the transverse direction. Here we report on a model of K DPAL where Gaussian spatial shape of the pump and laser intensities in any cross section of the beams are assumed. The full widths at half maximum (FWHM) of the pump beam in the two orthogonal directions in the beam cross section and its spectrum are taken from the experimental data [5]. The FWHM of the laser beam fundamental transverse mode (which is axially symmetrical) is calculated using the resonator parameters. Mirror reflections of 100% and 60% and window transmissions of 98.5% were used in the experiments and the computations. The assumed spectrum of the pumping laser was bimodal with two maxima; the distance between the maxima being 10.5 GHz [5]. The He pressure at the room temperature was assumed to be equal to the measured value of 600 Torr [2]. Good agreement between the measured and calculated dependence of the lasing power on the pump power is obtained under assumption that the liquid K temperature is 193 C, i.e., 8 C higher than the initial cell temperature before the pulse onset measured in [2]. The calculated temperature dependence of the small signal transmission through the alkali cell is also in good agreement with the measured data. First, a monochromatic approximation, assuming that the effective absorption cross section is calculated by the convolution of the pumping laser and absorption spectrum, was applied. Then the model was modified to take into account the spectral distribution of the pump intensity in different locations in the laser cell. In the modified model, propagation of each spectral component of the broadband pumping beam in the gain medium is calculated. The calculated results are obtained for different assumed temperatures and pressures. It was found that increasing the pressure results in decrease of both the laser threshold power and slope efficiency.

1. B.V. Zhdanov and R.J. Knize, Optical Engineering 52, 0210101-10 (2013).

2. B.V. Zhdanov, M.D. Rotondaro, M. K. Shaffer and R. J. Knize, Optics Express 22(14), 17266 (2014).

3. G.D. Hager and G.P. Perram, Applied Phys. B 112, 507 (2013).

4. B. D. Barmashenko and S. Rosenwaks, J. Opt. Soc. Am. B 30, 1118 (2013).

5. B.V. Zhdanov, private communication.

9650-12, Session 4

CFD assisted simulation of temperature distribution and laser power in pulsed and CW pumped static gas DPALs

Karol Waichman, Boris D. Barmashenko, Salman Rosenwaks, Ben-Gurion Univ. of the Negev (Israel)

An analysis of radiation, kinetic and fluid dynamic processes in diode pumped alkali lasers (DPALs) is reported. The analysis is based on a three-dimensional, time-dependent computational fluid dynamics (3D CFD) model. The Navier-Stokes equations for momentum, heat and mass transfer are solved by a commercial ANSYS FLUENT solver based on the finite volume discretization technique. The CFD code which solves the gas conservation equations includes effects of natural convection and temperature diffusion of the species in the DPAL mixture. The gas flow conservation equations are coupled to the equations for DPAL kinetics and to the Beer-Lambert equations for pump and laser beams propagation. The DPAL kinetic processes in the Cs/He/C2H6 (K/He) gas mixtures considered involve the three low energy levels, (1) n2S1/2, (2) n2P3/2 and (3) n2P1/2 (where n=4,6 for K and Cs, respectively), three excited alkali states and two ionic states. The kinetic processes include absorption due to the D2 transition followed by relaxation 3 to 2 fine structure levels and stimulated emission due to the D1 transition 2?1. Levels 2 and 3 are excited to the higher electronic states n2D3/2,5/2 and (n+2)2S1/2 by pump and laser photons and by energy pooling collisions followed by spontaneous emission, photoionization and Penning ionization of these levels and ion-electron recombination. The recombination proceeds via the sequence including fast conversion of Cs+ (K+) to Cs2+ (K2+) and dissociative recombination of Cs2+ (K2+). Using the CFD model, the gas flow pattern and spatial distributions of the pump and laser intensities in the resonator were calculated for end-pumped CW and pulsed Cs and K DPALs. The laser power and DPAL medium temperature were calculated as a function of pump power and pump pulse duration. The CFD model results for laser power were compared to experimental results of Cs and K DPALs. The model results for the gas temperature were compared to experimentally measured radial distribution of Cs DPAL temperature.

9650-13, Session 4

Low pressure Cesium and Potassium Diode Pumped Alkali Lasers: pros and cons *(Invited Paper)*

Boris V. Zhdanov, Matthew Rotondaro, Michael Shaffer, Randall Knize, U.S. Air Force Academy (United States)

This talk presents the results of our experiments on a comparative study of Cesium and Potassium based DPALs aimed to determine which of these two lasers has better potential for scaling to high powers. For both lasers we have chosen a so called "low pressure DPAL approach", which uses buffer gas pressure of about 1 atm for spin-orbit mixing of the exited states of alkali atoms to provide population inversion in the gain medium. This approach has several advantages compared to "high pressure (more than 10 atm) DPAL approach", but requires significant narrowbanding of the emission line of the pumping laser diodes (to the value less than 20 GHz), which was done using a technique developed in our lab. The goal of this study was to determine power limiting effects, which affect performance of these DPALs, and find out how these limiting effects can be mitigated. We paid special attention to possible thermal effects in gain medium and laser cell windows, ionization in gain medium, energy pooling and cell window damage. The experiments were performed using both static and flowing gain medium. For the second case we designed and built a closed cycle flowing system to circulate the gain medium through the laser cell. Also, we used a variety of buffer gases (hydrocarbons and noble gases) and varied buffer gas pressure, gain medium temperature and flow rate. In our experiments, we studied the performance of both lasers in CW and pulsed modes with different pulse duration and observed output power degradation in time from the initial value to the level corresponding to the CW mode of operation. To study possible contribution of thermal effects we used low power probe beam from HeNe laser propagating through the lasing gain medium. Also we recorded a fluorescence spectrum from the lasing gain medium which allowed us to analyze contribution of such effects as energy pooling collisions and ionization + recombination. As a result of this study, we revealed some essential positive and negative features of both DPALs, which can be taken into account for power scaling experiments.

9650-14, Session 4

3D CFD modeling of subsonic and transonic flowing-gas DPALs with different pumping geometries

Eyal Yacoby, Oren Sadot, Boris D. Barmashenko, Salman Rosenwaks, Ben-Gurion Univ. of the Negev (Israel)

No Abstract Available

Conference 9650B: Technologies for Optical Countermeasures

SPIE. SECURITY+ DEFENCE

Wednesday - Thursday 23–24 September 2015

Part of Proceedings of SPIE Vol. 9650 Technologies for Optical Countermeasures XII; and High-Power Lasers 2015: Technology and Systems

9650-21, Session 5

Technical advancement of high-power in 2-5m sources *(Invited Paper)*

Eric D. Park, Q-Peak, Inc. (United States)

No Abstract Available

9650-22, Session 5

Semiconductor lasers for DIRCM *(Invited Paper)*

Hans-Dieter Tholl, Diehl BGT Defence GmbH & Co. KG (Germany)

No Abstract Available

9650-23, Session 6

Potential of preemptive DIRCM systems *(Invited Paper)*

Ove Steinvall, FOI-Swedish Defence Research Agency (Sweden)

Manpads offer a severe threat to both civilian and military airborne platforms. The present countermeasure systems include platform maneuver, flares and DIRCM systems. Recently an increasing interest is aimed at preemptive measures e.g. to detect, identify and counter the threat before any missile has been launched. This will emphasize the importance of detecting and analyzing other signatures than this treated in conventional DIRCM systems. These may include laser emission from the target, detection of retro-reflections from optical sights and seekers as well as the optical signatures of the weapon and operator including the aiming and tracking activity.

We will exemplify some of the concepts by experimental results and discuss some of the system and technology challenges.

9650-24, Session 6

Quantification of helicopter rotor downwash effects on electro-optical defensive aids suites

Dirk P. Seiffer, Christian Eisele, Fraunhofer-Institut für Optronik, Systemtechnik und Bildauswertung (Germany); Markus Henriksson, Lars J. Sjöqvist, Sebastian Möller, FOI-Swedish Defence Research Agency (Sweden); Fabio Togna, Aeronautica Militare Italiana (Italy); Marie-Thérèse Velluet, ONERA (France)

The performance of electro-optical platform protection systems can be degraded significantly by the propagation environment around the platform. This includes aero-optical effects and zones of severe turbulence generated by engine exhausts. For helicopters rotor tip vortices and engine exhaust gases that are pressed down by the rotor airflow form the so called downwash phenomena. The downwash is a source for perturbations. A wide range of spatial and temporal fluctuations in the refractive index of air can occur. The perturbations from the turbulent flow cause detrimental effects on energy delivery, angle of arrival fluctuations, jam-code transmission, tracking accuracy and imaging performance in general. Therefore the effects may especially have a severe impact on the performance of laser-based protection systems (DIRCM). The chain from passive missile detection and warning to obtaining an optical break-lock by the use of an active laser system will be influenced.

To anticipate the installed performance of an electro-optical defensive aids suite (DAS) for helicopter platforms it is necessary to develop models for the prediction of the perturbations. Modelled results have to be validated against experimental findings. However, the data available in open literature on the effects of rotor downwash from helicopters on optical propagation is very limited. To collect necessary data and to obtain a first impression about the magnitude of occurring effects the European defence agency group (EDA) on “airborne platform effects on lasers and warning sensors (ALWS)” decided to design and perform a field trial on the premises of the Italian Air Force Flight Test Center in Pratica di Mare, Italy. ALWS is a technical arrangement under the Europa MoU among France, Germany, Italy, Sweden and the United Kingdom.

The objective of the trial was to investigate the impact of the downwash on both passive missile warning and active laser jamming, respectively. Several laser sources and imaging systems were used to characterize the effects under relatively controlled conditions. Motivation, trial limitations, trial setup and first impressions from the experimental analysis will be shown.

9650-25, Session 7

Tm, Ho, Op:GaAs, for high-power CW and high-pulse energy mid-IR *(Invited Paper)*

Eric D. Park, Q-Peak, Inc. (United States)

No Abstract Available

9650-26, Session 7

High-power low divergence semiconductor laser with circular beam

Cunzhu Tong, Lijie Wang, Lijun Wang, Changchun Institute of Optics, Fine Mechanics and Physics (China)

The Diode lasers show many advantages including the high electro-optical efficiency, small volume, low weight, long lifetime and low cost etc. It has been widely used for pumping of solid state lasers and fiber lasers, material processing, security, optical countermeasures and laser weapon, typically coupled into a fiber for easy use by beam shaping and combining techniques. Currently, the direct diode laser source with emission power of 8kW coupled into a 100micron fiber had been demonstrated. However, if continue to improve the performance, it seems have to start from the point-view of device structure to solve the issue of large divergence and elliptical beam, which are recognized as the main drawbacks since the first edge-emitting diode laser was demonstrated in 1962. It requires the use of expensive optical elements with high numerical aperture (NA) for focusing and coupling of diode lasers due to these drawbacks. Furthermore, the serious asymmetry of the vertical (~40°) and lateral (~10°) far-field (FF) angle also needs sophisticated circularly re-shaped optics for efficient coupling. Therefore, diode lasers with low divergence and circular beam emission would be valuable for the direct applications.

Many approaches have been proposed to improve the vertical beam divergence of edge-emitting diode laser, including the super large optical cavity (SLOC), asymmetric waveguide,

double barrier separate confinement heterostructures, inserting anti-guiding layers and longitudinal photonic bandgap crystal (LPBC) structure. These methods have reduced the vertical beam divergence with the definition of full-width at half-maximum (FWHM), down to below 5°, however, the FF angle with 95% power content is still high (>15°), which is more meaningful for the description of FF angle in the realistic applications and must be minimized to eliminate unwanted stray light effects in the application such as pumping of the fiber cladding.

Recently, we demonstrated the high power circular beam emission from the diode lasers with low divergence based on a modified Bragg reflection waveguide, which consists of a mode-localized optical defect layer, sandwiched between the top and bottom distributed Bragg reflector (DBR). When the guided mode with the effective index localized between the high index and low index of DBR, the corresponding FF pattern will be single-lobed. Through controlling the thickness of core layer, the light can propagates in the layers with high index but is evanescent in the layers with low index. This method could achieve large optical mode expansion in the waveguide and thus narrow beam divergence. We had demonstrated the low vertical divergence of 9.8° with 95% power content and 4.91° with the full-width at half-maximum was realized in the devices with 150 ?m stripe width. The packaged devices demonstrated a maximum continuous wave (CW) power of 4.6 W at 10oC. A direct fiber coupling efficiency of 90.6% had been achieved with a common fiber of 105 ?m core diameter. We believe that our work will contribute to the development of low divergence diode lasers.

9650-27, Session 8

Experimental and numerical analysis of atmospheric propagation of high energy laser

Carsten Pargmann, Thomas Hall, Frank Duschek, Thomas Fischbach, Karin M. Grünewald, Kirsten Klaffki, Jim Thieser, Jürgen Handke, Deutsches Zentrum für Luft- und Raumfahrt e.V. (Germany)

Powered by industrial demands solid-state high power lasers are getting more and more sophisticated. Hence, nowadays commercially available laser systems reach power levels of 10kW and above with noteworthy beam qualities. These systems deliver high power stability and availability and operate in the 1 μm wavelength region, yielding a high transmission through the atmosphere. Due to these specifications solid-state high power laser systems are interesting for applications outside of industrial use, too. Power beaming through air over large distances can be taken as an example. Security relevant applications of power beaming include the powering of aircrafts and satellites as well as selective counter measures against hostile projectiles.

The advent of high energy laser systems with emission wavelengths in the near infrared range reduced the effect of atmospheric absorption. Nevertheless, the laser beam is still exposed to beam wandering, beam deterioration and scattering processes. In order to analyze the atmospheric influence on the laser beam propagation the DLR operates at Lampoldshausen a free transmission laser test range. The beam propagates in a height of 1 m above asphalt ground along a path of 135 m between transmitting and receiving station. A variety of sensors continuously monitor temperature, pressure, relative humidity, wind, visibility, ozone content, uv-radiation, turbulence strength and aerosol particle distribution of the atmosphere in order to get a detailed picture of the current status of the weather conditions.

The laser source is a TruDisk 6001 (4C) disk laser fabricated by the company Trumpf. The emitted wavelength is 1.03 μm, the maximum power is 6 kW and the beam quality is about 4 mm?mrad. The laser radiation is coupled to a 40 m long optical fiber with a core diameter of 100 μm and transferred to the transmitting station. A telescope consisting of two off-axis parabolic mirrors enlarges the beam width to about 200 mm and focusses the radiation to the receiving station. Both stations contain sensors to measure the transmitted power and cameras to measure beam wandering, power-in-the-bucket and beam distortion values.

The turbulent motion of the air caused by convection and wind speed induces random fluctuations in the refractive index of the atmosphere. Although these variations are very small, a large propagation distance generates a considerable effect to the optical quality of the laser beam. The Kolmogorov turbulence model states that atmospheric temperature variations and wind-speed fluctuations create local unstable air masses. These consist of turbulent cells of different scale sizes. The energy determining the turbulence is fed into the large scale cell and then cascades down to small scales where it is dissipated by molecular viscosity. A numerical analysis of laser beam propagation is performed by the software TALAP (Turbulent Atmosphere and Laser Beam Propagation), developed at TP/DLR.

The test facility is operational at all weather conditions. First measurement results are obtained and compared to simulation results. Future measurements will be performed at different weather conditions and seasons. Experimental results will be used to modify the simulation software, if necessary.

9650-28, Session 8

Helicopter engine exhaust rotor downwash effects on laser beams

Markus Henriksson, Lars J. Sjöqvist, FOI-Swedish Defence Research Agency (Sweden); Dirk P. Seiffer, Fraunhofer-Institut für Optronik, Systemtechnik und Bildauswertung (Germany)

The hot exhaust gases from engines on helicopters are pushed down by the rotor in a turbulent flow. When the optical path of a laser beam or optical sensor passes through this region severe aberrations of the optical field may result. These perturbations will lead to beam wander and beam distortions that can possibly limit the performance of optical countermeasure systems.

To quantify these effects the Italian Air Force Flight Test Centre hosted a trial for the “Airborne platform effects on lasers and warning sensors” (ALWS) EDA-project, comprising ONERA (France), Fraunhofer IOSB (Germany), ITAF CSV (Italy) and FOI (Sweden). Lasers were placed on a balcony of the airport control tower and the laser beams propagated to a target screen in a 286 m long slant path with the helicopter hovering over this path. Collimated laser beams at 1.55, 2 and 4.6 μm wavelength were imaged with high speed cameras. Large increases in beam wander and beam divergence were found, with beam wander up to 200 μrad root-mean-square and increases in beam divergence up to 1 mrad. The temporal scale of the beam wander was 1-2 ms.

To allow scaling to other laser beam parameters and geometries formulas for propagation in atmospheric turbulence were used even though the turbulence may not follow Kolmogorov statistics. By assuming that the plume is short compared to the total propagation distance the integrated structure parameter through the plume could be calculated. Values in the range 10-10 to 10-8 m1/3 were found when the laser beams passed through the exhaust gases below the helicopter tail boom. Values calculated from beam wander were consistently lower than those calculated from long term spot size, indicating that the method is not perfect but provides information about order of magnitudes.

The measured results show that the engine exhaust will dominate over atmospheric turbulence even for kilometer path lengths from a helicopter at low altitude. How severe the effect is on system performance will depend on beam and target parameters.

9650-29, Session 9

Different pulse pattern generation by frequency detuning in pulse modulated actively mode-locked ytterbium doped fiber laser

He Chen, Sheng-Ping Chen, Lei Si, National Univ. of Defense Technology (China); Bin Zhang, National Univ. of Defense Technology (China) and College of Optoelectronic Science and Engineering, National University of Defense Technology (China); Zong-Fu Jiang, National Univ. of Defense Technology (China)

Actively/passively mode-locked fiber lasers generating short optical pulses have attracted considerable attention because of their distinct advantages such as cost effectiveness, alignment-free structure and compact design over their bulk counterparts. Applications in diverse fields including precise optical measurement, bio-medical study, and optical communications have been found with the employment of mode locking fiber laser. In the investigations of the mechanism of mode-locked fiber lasers, the diverse output pulse dynamics have been found to meet the requirements of different kinds of applications, such as soliton mode locking, dissipative soliton mode locking, and noise like mode locking. However, most of the investigations were conducted in passively mode locked fiber lasers. In our recent experimental investigation, we found different optical pulse pattern generation in pulse modulated actively mode-locked ytterbium doped fiber laser by modulation frequency detuning

Here, we report the results of our recent experimental investigation of the modulation frequency detuning effect on the output pulse dynamics in a pulse modulated active mode-locked ytterbium doped fiber laser. Our experimental study, which was carried out over a wide frequency detuning range under different modulation pulse width and fundamental/harmonic frequency modulation, shows the existence of five different mode-locking states that mainly depend on the modulation frequency detuning, which are: (a) amplitude-even harmonic/fundamental mode-locking, (b) Q-switched harmonic/fundamental mode-locking, (c) a sinusoidal wave modulation mode, (d) pulses bundle state, and (e) noise-like state.

For one particular experimental laser configuration, the amplitude-even mode-locking mode is maintained over the frequency detuning range within 10 kHz, and then the Q-switched harmonic/fundamental mode-locking mode appears over the frequency detuning range from 11 to 20 kHz. The Q-switched harmonic/fundamental mode-locking mode always produces both harmonic and fundamental repetition rate mode-locked pulses within a Q-switching envelope. When the frequency detuning increases beyond 20 kHz, more pulse patterns can be achieved. Afterwards, sinusoidal envelope harmonic/fundamental mode-locking mode can be observed. Then several pulses form a pulse bundle, which presents in a periodic order. When the frequency detuning approaches the limit, the pulse becomes unstable and behaves like noise, which is called noise-like pulse. A detailed experimental characterization of the output pulses in each operating mode is performed in terms of average power, pulse peak power, pulse width, and temporal width and repetition rate of the Q-switching envelope/the pulse bundle.

The simple and convenient method of generating diverse pulse patterns from a single mode-locked fiber laser might find plenty of applications in many fields of interests, such as material machining, optical signal processing and nonlinear optics research.

9650-30, Session 9

IRCM spectral signature measurements instrumentation featuring enhanced radiometric accuracy

Florent M. Prel, ABB Analytical Measurement (Canada); Cornelius J. Willers, Airbus Defence and Space (South Africa); Stéphane M. Lantagne, Louis M. Moreau, Claude B. Roy, ABB Analytical Measurement (Canada)

Hyperspectral Infrared signature measurements are performed in military applications including aircrafts and ships stealth characterization, detection/lock-on ranges, and flares efficiency characterization. Numerous military applications require high precision measurement of infrared signature characterization. For instance, Infrared Countermeasure (IRCM) systems and Infrared Counter-Countermeasure (IRCCM) system are continuously evolving; Infrared flares defeated IR guided seekers, IR flares became defeated by intelligent IR guided seekers and Jammers defeated the intelligent IR guided seekers.

A precise knowledge of the target infrared signature phenomenology is crucial for the development and improvement of countermeasure and counter-countermeasure systems and so precise quantification of the infrared energy being emitted from the targets requires accurate spectral signature measurements. Errors in the Infrared characterization measurements can lead to weakness in the safety of the countermeasure system and errors in the determination of detection/lock-on range of an aircraft from IR sensor. The infrared signatures are analyzed, modeled and simulated to provide a good understanding of the signature phenomenology in order to improve the IRCM and IRCCM technologies efficiency. The need of infrared spectral signature measurement technology is also raising in order to further improve and validate the models and simulations.

The addition of imagery to the Spectroradiometers is improving the measurement capability of complex targets because each element of the scene can now be measured simultaneously. However, the limited dynamic range of the CCD sensors used in these instruments confines the ranges of measurable radiance intensities. This ultimately affects the radiometric accuracy of these complex signatures. We will describe and demonstrate how the ABB hyperspectral imaging spectroradiometer features enhanced radiometric accuracy of military targets infrared spectral signature measurements.

Conference 9651: Millimetre Wave and Terahertz Sensors and Technology

SPIE. SECURITY+ DEFENCE

Tuesday 22 September 2015

Part of Proceedings of SPIE Vol. 9651 Millimetre Wave and Terahertz Sensors and Technology VIII

9651-2, Session 1

Terahertz time-domain spectroscopy for studying the kinetics of tissue adhesives

Marie Tobolova, Tomas Bata Univ. of Zlin (Czech Republic) and Brno Univ. of Technology (Czech Republic); Vojtech Kresalek, Tomas Bata Univ. of Zlin (Czech Republic); Zdenek Adamik M.D., Tomas Bata Regional Hospital (Czech Republic); Ivo Provaznik, Brno Univ. of Technology (Czech Republic)

Terahertz time-domain spectroscopy is a modern method suitable for studying variety of materials. Therefore, it finds useful applications in many technical areas. The techniques using terahertz radiation are non-invasive, non-destructive, and usually contact-free. The measurement is quite fast and no special procedure of sample preparation is needed. The mentioned advantages make this approach appropriate especially for biological and medical sciences. This study is focused on the kinetics of tissue adhesives.

Tissue adhesives are used in surgery for supporting the hemostasis and for wound closure. They can be sorted into three groups according to the main compound they include – cyanoacrylate glue, fibrin and thrombin glue. Effect of each type of glue is based on different mechanism. Fibrin and thrombin glues are usually derived both from human or bovine plasma. Their effect is based on their participation in the physiologic clotting cascade but there are some potential risks of transmitting viral infections. Cyanoacrylates are of synthetic origin and are known as superglues used for fast bonding of variety of materials. Because of toxicity of the cyanoacrylates themselves, there are used their derivatives. The mechanism of action is based on rapid solidification when in contact with weak bases, such as water or in this case - blood. To monitor the polymerization kinetics of cyanoacrylate glues, we have used the terahertz time-domain spectroscopy system TPS Spectra 3000 by TeraView Ltd.

Samples of chosen cyanoacrylate glue were prepared for preliminary transmission measurement. The parameters of the spectrometer must be set up for fast measurement because of the curing reaction rate. Some special substances can be added to the samples to slow the reaction and to allow better characterization of the whole process. The defined amount of cyanoacrylate sample or its mixture is applied on the appropriate underlayer and the optical parameters are measured in time. The parameters are evaluated at defined frequencies and their time dependences are analyzed to find time constants for mathematical description of the glue kinetics.

The other research of the tissue adhesives is needed for better insight of their mechanism of action. The kinetics of each type of glue can be different and the time of curing can be also influenced artificially when needed. The time of curing is very important because some applications require the fast wound closure but some of them need slower solidification because of longer manipulation with the glue during surgery or possible damage of the surgical instrument during injection of the glue (adherence to catheters and endoscopes).

9651-3, Session 1

Examining pharmaceuticals using terahertz spectroscopy

Katerina Sulovska, Vojtech Kresalek, Tomas Bata Univ. of Zlin (Czech Republic)

Pharmaceuticals trafficking is common issue in countries where they are under stricter dispensing regime with monitoring of users. Such pharmaceuticals contain precursors of drugs or addictive substances which are usually misused by drug addicts or producers. Most commonly smuggled pharmaceuticals include trade names Paralen Plus, Modafen, Clarinase repetabs, Aspirin complex, etc.; and are transported from eastern Europe (e.g. Slovakia, Ukraine, Russia, etc.) to countries like the Czech Republic, which is said to have one the highest number of methamphetamine producers, which can be made from above mentioned pharmaceuticals. The aim of this paper is to describe the possibility of terahertz spectroscopy utilization as an examining tool to distinguish between pharmaceuticals containing pseudoephedrine compounds and those without it. Materials: Six samples of commercially available pharmaceuticals with pseudoephedrine compound were used for the initial study – Paralen Plus, Modafen, Clarinase repetabs (three samples differing by expiration date) and Aspirin complex. Pills were ground to powder to be easily measured as a thin uniform layer glued on office paper. Selected medicaments contain as an active ingredient pseudoephedrini hydrochloridum or pseudoephedrini sulfas (Clarinase repetabs). Another sample was made from pharmaceutical with similar content (Recoxa tabs.) but with no pseudoephedrine. These samples were prepared via similar procedure. Methods: All of the measurements were done by the TPS Spectra 3000 instrument. The instrument was set to resolution 1.2 cm-1 with scanning frequency 30 and 1800 scans. Terahertz region was set to 0.2 – 2.5 THz. Prepared samples were measured on transmission module in ambient conditions and in the vacuum. As the reference, the paper with glue was chosen in both scanning conditions. Results: Results obtained from transmission module (absorbance, refractive index) show possibility of distinguishing between each sample, moreover, the spectra also differs in case of pills with various expiration date, where the signal is attenuated in contrast to the non-expired sample. During the initial study, the possibility of recognizing unknown sample was also studied. As the instrument is sensitive to the thickness of the sample, it is necessary to abide the same amount of sample to get proper spectra. This possibility was also studied with interesting results. Conclusion: Terahertz spectroscopy can be used in many application beginning from remote sensing of terrestrial phenomena, biomedical imaging, airport security checks, intermolecular forces study and many other applications. Using terahertz spectroscopy for distinguishing between different pharmaceuticals may be a promising technique considering further study of spectra by chemometric techniques as was shown by our results.

9651-24, Session 1

An enhanced MMW and SMMW / THz imaging system performance prediction and analysis tool for concealed weapon detection and pilotage obstacle avoidance

Steven R Murrill, U.S. Army Research Lab. (United States); Eddie L Jacobs, University of Memphis (United States); Charmaine C Franck, NASA - Langley (United States); Douglas T Petkie, Wright State University (United States); Frank C De Lucia, Ohio State University (United States)

The U.S. Army Research Laboratory (ARL) has continued to develop and enhance a millimeter-wave (MMW) and terahertz (THz)-band imaging system performance prediction and analysis tool for both the detection and identification of concealed weaponry, and for pilotage obstacle avoidance. The details of the MATLAB-based model which accounts for the effects of all critical sensor and display components, for the effects of atmospheric attenuation, concealment material attenuation, and active illumination, were reported on at the

2005 SPIE Europe Security & Defence Symposium (Brugge). An advanced version of the base model that accounts for both the dramatic impact that target and background orientation can have on target observability as related to specular and Lambertian reflections captured by an active-illumination-based imaging system, and for the impact of target and background thermal emission, was reported on at the 2007 SPIE Defense and Security Symposium (Orlando). Further development of this tool that includes a MODTRAN-based atmospheric attenuation calculator and advanced system architecture configuration inputs that allow for straightforward performance analysis of active or passive systems based on scanning (single- or line-array detector element(s)) or staring (focal-plane-array detector elements) imaging architectures was reported on at the 2011 SPIE Europe Security & Defence Symposium (Prague). This paper will provide a comprehensive review of a newly enhanced MMW and THz imaging system analysis and design tool that now includes an improved noise sub-model for more accurate and reliable performance predictions, the capability to account for post-capture image contrast enhancement, and the capability to account for concealment material backscatter with active-illumination-based systems. The reengineered noise sub-model now has a reformulated noise power spectral density (PSD) calculation to properly utilize the U.S. Army Night Vision and Electronic Sensors Directorate (NVESD) model's Noise Factor calibration constant (?). Additionally, a Noise Factor temporal scaling element has been devised to accurately account for increased detector integration time in the regime where the system frame time is greater than the human eye integration time. A new capability to account for scenarios where the application of post-capture, image contrast enhancement through contrast stretching (normalization) could positively impact probability-of-detection/identification range performance has been added and allows the user to select a contrast stretching gain factor between 1 and 10. This new feature allows the user to essentially trade-off (reduce) displayed image signal-to-noise ratio(s) (SNR) with (increased) target-to-background contrast ratio(s) for better overall target visibility. The radiometric sub-model has also been enhanced and now accounts for a user-definable level of Lambertian reflection (backscatter) from intervening target/weapon concealment materials that occurs in active illumination systems/scenarios. The final version of this paper will also provide example system component (active-illumination source and detector) trade-study analyses using the new features of this user-friendly THz imaging system performance analysis and design tool. Present plans for additional expansion of the model's predictive capabilities to include a more accurate and sophisticated Bidirectional Reflectance Distribution Function (BRDF)-based radiometric approach will also be outlined.

9651-4, Session 2

Improved design of a passive millimeter-wave synthetic aperture interferometric imager for indoor applications *(Invited Paper)*

Xianxun Yao, Kai Liu, Jungang Miao, BeiHang Univ. (China); Anyong Hu, School of Electronic and Information Engineering, Beihang University (China)

Passive millimeter-wave imaging technique is potentially the most effective and safe approach in concealed contraband detection for human bodies, because it has the ability to detect objects under clothes and only makes use of spontaneous radiations from objects and human bodies. Beihang University has involved in this technique for many years and already developed a series of prototype imagers based on synthetic aperture interferometric radiometer (SAIR) technique. The most recent SAIR prototype, developed by the Beihang University, operates at 8mm-band, with 22°? 40° field of view (FOV), 5 cm spatial resolution for 3 m imaging distance, 25 frame/second imaging rate and about 1 K radiometric sensitivity for 1 second integration time. For outdoor situations, this prototype provides satisfactory imaging performance, due to the high contrast between the background radiation and the human body radiation. However, in order to get a satisfactory inspection result for indoor situations, the prototype needs to improve its sensitivity when other specifications remain the same.

To do this, Beihang University is now devoted to the developing next-generation SAIR imager prototype. By improving the number of receiving channels and system bandwidth, this imager will be capable of achieving sufficient radiometric sensitivity for indoor human body inspection (about 1 K) at video rate imaging. Primarily, in order to obtain about 1 K radiometric temperature sensitivity with video rate imaging, 256 receiving channels with 1 GHz bandwidth operating at 34 GHz followed by a high performance digital signal processing subsystem is required. Secondly, the antenna array design is optimized for redundant visibility samples while including all necessary sample points for the image reconstruction operation. By averaging the redundant visibility samples, the signal to noise ratio (SNR) of measured visibility samples can be greatly enhanced, that in turn improve the radiometric temperature sensitivity. Moreover, the data signal processing subsystem of this prototype requires an analogue-to-digital unit to sample the 256 received channel synchronously with 1 GHz sampling rate, and an ultra large scale digital correlator array to compute 32640 (256?255/2) complex cross-correlations simultaneously with 1 GHz working frequency. For the purpose of reducing the complexity and cost of the analogue-to-digital unit, a specialized chip is designed for 1-bit quantization with 1 GHz sampling rate and power measurement. To realize the digital correlator array, a distributed correlation calculation architecture by using a group of FPGA chips is presented. In this architecture, about 2000 complex cross-correlations with 1 GHz working frequency and 128 Gbps transmission rate are required for each FPGA chip, which is feasible for existing FPGA chips.

9651-5, Session 2

The three-dimensional near-field aperture synthesis imaging algorithms applied to extended targets in a millimetre wave security screening portal

Neil A Salmon, MMW Sensors Ltd (United Kingdom) and Manchester Metropolitan University (United Kingdom)

The aperture synthesis technique offers a route to passive millimetre wave imaging that enables a conformally deployable sensor technology that can be integrated into surfaces of opportunity. This offers a very flexible deployment capability, as the imager thickness need only be a centimetre, comprising printed circuit antennas, receivers and a cross-correlator. Radiometric electric fields at arbitrary surfaces are sampled, cross-correlated and processed into an image using aperture synthesis algorithms. The system requires no moving parts and can take snap-shot time frames on a millisecond timescale. Integrating the sensor into surfaces at the deployment site means the aperture size can be as large as the available infrastructure, providing the highest possible image resolution.

For the security screening application, the radio astronomy aperture synthesis imaging algorithms are modified for the near-field, thereby providing a three-dimensional (3D) imaging capability. In a portal screening scenario (for entry to transport networks/public buildings), where antennas are deployed around the subject, these algorithms deliver the half-wavelength Abbe microscope resolution in three-dimensions. This means that by operating at the low frequency of just 20 GHz (to minimise costs) the commensurate spatial resolution of ~8 mm is suitable for the recognition of most threats. This architecture of imager has an attractive simplicity, as it requires only single bit digitisation of radiometric fields and requires no artificial radiation sources to illuminate subjects. This bypasses health-and-safety issues associated with irradiating subjects and offers a potentially low cost solution. With a suitable number of receivers the system will have sufficient sensitivity to generate a 3D video image of a walking subject, making threat concealment more difficult for subjects.

This paper presents details of the 3D imaging algorithm. It investigates how well forward simulation (creating synthetic cross-correlations) and the (near-field aperture synthesis) inversion algorithms work to create 3D images. The spatial resolution limits in and around an envisaged security screening portal are examined by simulating point sources of radiation. The effect of the size on an extended target in the portal on the resulting image quality is investigated. It does this by combining the techniques of computer graphics hidden facet removal with the coherence properties of passive thermal radiators. To understand capabilities of this technique, simple 3D geometrical shapes are simulated, having sizes and physical properties characteristic of human subjects. As a means to improving image quality, a technique is investigated which mosaics separate image volumes together, each generated with a difference aperture synthesis phase reference.

9651-6, Session 2

Vehicle screening in three dimensions using aperture synthesis passive millimetre wave imaging

Neil A Salmon, MMW Sensors Ltd (United Kingdom)

No Abstract Available

9651-7, Session 2

Ultrawide band 3D microwave imaging scanner for the detection of concealed weapons

Nacer Ddine Rezgui, David A Andrews, Nicholas J Bowring, Manchester Metropolitan Univ (United Kingdom)

The threat of concealed weapons, explosives and contraband in footwear, bags and suitcases has led to the development of new devices that can be deployed for security screening and to facilitate the baggage checking process at airports, train stations and other venues. Metal detectors are regularly employed to detect metallic objects, but cannot detect or locate non-metallic objects, such as ceramic guns or knives and explosives. Passenger luggage is x-rayed to reveal any concealed weapons or illicit contraband such as drugs and skilled operators look for any anomalies in the images. Both metal detectors and x-rays are not able to detect targets at standoff distances. To address these deficiencies, an UWB 3D microwave imaging scanning apparatus using FMCW stepped frequency working in the K and Q bands and with a planar scanning geometry based on an x y stage, has been developed to screen suspicious luggage and footwear. To obtain the 2D cross section or 3D microwave images of the concealed weapons, the targets are placed above the platform and the single transceiver horn antenna attached to the x y stage is moved mechanically to perform a raster scan along and across the target to create a 2D synthetic aperture array. The S11 reflection signal of the transmitted sweep frequency from the target is acquired by a VNA in synchronism with each position step. The scans are combined to form a three-dimensional data array. To enhance and filter the raw data from clutter and noise and to obtain 2D and 3D microwave images of the concealed weapons or explosives, data processing techniques are applied to the acquired signals. These techniques include background subtraction, Inverse Fast Fourier Transform (IFFT), thresholding, filtering by gating and windowing and deconvolving with the transfer function of the system using a reference target. The deconvolution algorithm is used to remove the effects of the transceiver horn antenna, VNA and cables out of the raw data reflected from the target. The 3D microwave image quality depends on the bandwidth, sampling resolution and the aperture of the system. A sharp image of the target requires the use of a focusing transceiver horn antenna and lens combination with a large aperture and a high frequency. To focus the 3D reconstructed microwave image of the target in range and across the x y aperture without using focusing elements, 3D Synthetic Aperture Radar (SAR) techniques are applied to the post-processed data. The K and Q bands, between 15 to 40 GHz, show good transmission through clothing and dielectric materials found in luggage and footwear. The UWB 3D microwave image scanner has a 25 GHz frequency bandwidth giving a depth resolution of 6 mm and good lateral resolution and can detect and locate a hidden weapon within the luggage and footwear. A description of the system, algorithms and some results with replica weapons, knives and simulant explosives and a comparison of microwave images obtained by IFFT, 2D and 3D SAR techniques are presented.

9651-9, Session 3

Discrimination and identification of RDX/PETN explosives by chemometrics applied on terahertz time-domain spectral imaging *(Invited Paper)*

joyce bou sleiman, Jean-baptiste Perraud, Bruno Bousquet, Jean-paul Guillet, University of Bordeaux (France); Norbert Palka, Military University of Technology (Poland); Patrick Mounaix, University of Bordeaux (France)

Recently, terahertz spectroscopy and imaging have been extensively investigated regarding their potential advantages for military and homeland security applications. Till now, different techniques have been used to detect explosives such as laser-induced breakdown spectroscopy, ion mobility spectrometry, gas chromatography, etc. Terahertz Chemical imaging has been used for discrimination and identification of chemical substances including explosives. In order to automate the procedure of reconnaissance, chemometrics applied on terahertz can be an important and promising tool. Different chemometric technics can be investigated for different needs. Principal Component Analysis (PCA) is one of the basic unsupervised chemometric methods used to describe the data, to observe whether the samples are similar or not. Partial Least Squares-Discriminant Analysis (PLS-DA) is a supervised method used for classification of different substances. In order to identify and classify RDX and PETN explosives, we applied these two techniques on terahertz absorbance images.

MATERIALS AND METHOD

Three samples were prepared as pressed pellets of 400 mg. Two of them contained 80 mg of hexogen (RDX) and 80 mg of penthrite (PETN) respectively, and 320 mg of polyethylene (PE) selected as binder for its low absorption in the THz range. The third sample was made of a RDX/PETN mixture containing 40 mg RDX + 40 mg PETN and 320 mg of polyethylene (PE) as binder. 2D THz spectral images were recorded for each sample, meaning that a spectrum ranging from 0.2 to 3 THz was recorded for each pixel. For that, terahertz time-domain spectroscopy measurements were realized in transmission mode via TDS-THz spectrometer from Teraview (TPS 3000) combined with imaging tools. Then absorption spectra were extracted from measurements and classed in matrix that was used in chemometric analysis.

DISCRIMINATION BY PCA

Instead of sweeping all the spectrum of all the substances and searching for fingerprints to extract images that reveals the presence of one of the substances among others, PCA allows automatically evaluation of all the frequencies and then the possibility to automatically distinguish all the substance in the image. These results are achieved by using the first scores of the PCA analysis. The obtained images show good contrast between the three pellets of RDX, PETN and their mixture. In addition, the study allows the identification of the frequency that reveals this contrast.

IDENTIFICATION BY PLS-DA

On the other hand, for identification of these explosives, each pixel in the image is predicted using PLS-DA. In this order, the PLS-DA model is created and calibrated with three classes,

where each of them consists on limited number of pixels for each sample. Then all the pixels on the entire image, which are unknown to the model, was predicted and classed in one of these three classes. Good classification of all the pixels enables the identification of the RDX, PETN and their mixture.

CONCLUSION

PCA and PLS-DA was successfully applied on THz absorbance images. Thus chemometrics is an important automatic tool for discrimination and classification, and is very promising in detection illicit and dangerous substances for homeland security.

9651-10, Session 3

New way for concealed object detection using passive THz images without their viewing

Vyacheslav A. Trofimov, Vladislav V. Trofimov, Lomonosov Moscow State Univ. (Russian Federation)

We developed new real-time algorithm, based on the correlation function, for concealed object detection by using computer processing of the passive THz images without their viewing. This algorithm allows us to make a conclusion about presence of forbidden objects on the human body. To increase the quality of THz images we proposed one more algorithm in comparison with new algorithms which have developed by us early.

We apply new algorithms with success to the images captured by passive THz camera TS4 manufactured by ThruVision Inc. Microsemi Corp. and other. The distance between the camera and person is changed from 4 to 10 metres.

9651-12, Session 3

Millimetre waves sensor modeling and simulation

Jean Latger, Thierry Cathala, Nicolas Douchin, OKTAL Synthetic Environment (France)

Guidance of weapon systems relies on sensors to analyse targets signature. Defence weapon systems also need to detect then identify threats also using sensors. One important class of sensors are millimetre waves radar systems that are very efficient for seeing through atmosphere and/or foliage for example. This type of high frequency radar can produce high quality images with very tricky features such as dihedral & trihedral bright points, shadows and lay over effect. Besides, image quality is very dependent on the carrier velocity and trajectory. Such sensors systems are so complex that they need simulation to be tested.

This paper presents a state of the Art of millimetre waves sensor models. A short presentation of asymptotic methods shows that physical optics support is mandatory to reach realistic results.

SE-Workbench-RF tool is presented and typical examples of results are shown both in the frame of Synthetic Aperture Radar sensors and Real Beam Ground Mapping radars.

SE-RAY-EM software is based on a combination of Shooting and Bouncing Rays (SBR) technique, that has been optimized to calculate efficiently the intersections between rays from a transmitter towards a 3D database and back to a receiving point, and EM models for computing propagation, reflection and diffraction. These models are the formulations of Geometrical Optics (GO), Physical Optics (PO) and Equivalent Current Method (ECM). An operating strategy enables unified calculation for the near or far EM scattered fields from the scenes. The “forward scattering” approach based on the equivalence principle is also used to compute EM fields in the shadow region. Since it relies on asymptotic methods SE RAY-EM is well suited for computing the EM interactions of an incident wave with complex 3D models of large scale environments and objects at high frequencies typically in the 1 – 100 GHz range.

Several technical topics are then discussed, such as the rendering technique (ray tracing vs. rasterisation), the implementation (CPU vs. GP GPU) and the trade off between physical accuracy and performance of computation.

Examples of results using SE-Workbench-RF are showed and commented.

9651-13, Session 4

Modulation and frequency response of GDDs in the millimeter wave/THz region

Namig Alasgarzade, Taylan Takan, Ilker U. Uzun-Kaymak, Middle East Technical Univ. (Turkey); Asaf B. Sahin, Yildirim Beyazit Univ. (Turkey); Hakan Altan, Middle East Technical Univ. (Turkey)

Recent studies suggest that commercially available Glow Discharge Detectors (GDD) can be used in detecting millimeter waves for imaging applications [1]. For the study described here, various types of GDDs otherwise known as Neon indicator lamps were commercially obtained (International Light Technologies, Peabody, MA, USA). To understand the interaction mechanism between plasma created inside a GDD and the millimeter wave, two different millimeter wave/THz measurement systems are employed. In one set-up, a Schottky diode multiplied (Virginia Diodes Incorporated-VDI, Charlottesville, VA, USA) source with an output at a frequency of 113GHz was reconfigured such that the Dielectric Resonator Oscillator (DRO) could be modulated up to tens of MHz frequencies. The response of GDDs at modulation frequencies up to 100 kHz is analyzed by utilizing a lock-in amplifier while a pre-amplifier electronic circuit was used for higher frequencies. In addition, using the same transmitter, the response of a GDD is tested for two different scenarios by rotating the GDD, i.e. making its structure parallel and perpendicular to the optical axis. Results show that data obtained in the perpendicular orientation agrees well with the Malus’ Law.

In another configuration a VDI multiplied source (WR2.8AMC) which was driven by a frequency tunable Yttrium Iron Garnett (YIG) oscillator was used to analyze frequency dependent GDD-THz interactions in the 240-380 GHz frequency range. These measurements were compared to our previous studies where when the GDD was turned on and placed at the focus of a broadband THz beam, the THz transmission was attenuated for certain frequencies. These frequencies are thought to be resonant with the dimensions of the structure of the device [2].

Both systems allow us to understand the response of GDDs with respect to modulation frequency, RF frequency and polarization orientation with respect to the native electric field inside the plasma. Resonance effects, frequency sensitivity and geometrical structures of GDDs are studied for the purpose of obtaining better performance in THz-GDD interaction for applications including general THz wave detection and imaging. In the latter, these measurements can aid the development of a new imaging system by employing an array of GDDs, each accompanied with a preamplifier circuit. These circuits will replace the lock-in amplifier and provide a cheaper solution with a wider frequency performance.

References

[1] A. Abramovich, N. S. Kopeika, D. Rozban, and E. Farber, “Inexpensive detector for terahertz imaging,” Applied Optics, vol. 46, no. 29, pp. 7207–7211, (2007).

[2] K. Çınar, H. M. Bozacı, and H. Altan, “Characterization of a Glow Discharge Detector with Terahertz Time Domain Spectroscopy,” IEEE Sensors J., 13, 2643-2647 (2013).

Acknowledgements

This work is supported under The Scientific and Technical Research Council of Turkey (TUBITAK) grant # 113F321

9651-14, Session 4

Millimeter-wave signal detection technique using a vector network analyser (VNA) for solid state sources

Ata Khalid, Jue Wang, Khalid Alhar Alharbi, Afesomeh Ofiare, Edward Wasige, David R S Cumming, University of Glasgow (United Kingdom)

Our experimental results show that a Vector Network Analyser (VNA) can be used to identify oscillation frequency of a signal source with moderate or low RF power if certain care is taken. We have used this technique for the first time to test Resonant Tunnelling Diodes (RTD) based oscillators. At frequencies above 100 GHz it is challenging to accurately identify and measure RF signal from these embryonic devices because the power generated from these devices is often in nW. The VNA is a powerful and widely used tool available to most microwave and mmwave laboratories and a simple scan to observe the s11 would reveal the existence of an oscillatory behaviour in device under test. We have used this for the first time to measure D-band RTD oscillators. We report that by observing the magnitude change of one-port reflection coefficient across the entire swept frequency range, a sudden peak or a dip corresponds to an oscillation frequency. In addition, using modern VNA as a signal detection method can significantly reduce measurement time and increase measurement accuracy to VNA capability for developing emerging signal generating devices at early stage, especially for planar, large quantity and operating in a wide frequency range.

In conclusion, VNA application has been investigated to experimentally prove this instrument as an effective and efficient tool to accurately identify the oscillation frequency of one-port RF signal from RTD oscillators up to 190GHz. This technique will benefit modern signal source development, which has many new features such as miniaturized planar structure, large quantity, moderate or low RF power and operating in a wide frequency range etc.

9651-15, Session 4

High frequency resonant tunnelling diode oscillator with high output power

Jue Wang, Khalid Alharbi, Afesomeh Ofiare, Ata Khalid, David Cumming, Edward Wasige, University of Glasgow (United Kingdom)

Terahertz (THz) technology has wide applications in such as imaging systems, wireless communication systems and spectroscopy systems, etc. Due to the absence of reliable and compact coherent-wave sources, there is a terahertz gap defined by frequencies between 100GHz to 3 THz. Resonant tunneling diode (RTD) is considered to be one of the promising solid-state THz sources which can operate at room temperature. The published highest frequency of RTD oscillator is 1.55 THz with 0.4 ?W output power. The main factor that prohibits RTD oscillator applications is its low output power.In this paper, a prototype monolithic microwave integrated circuit (MMIC) resonant tunneling diode (RTD) oscillator operated at 166 GHz G-band (140 GHz-220 GHz) with 0.34 mW (-4.7 dBm) output power is reported. The results indicate the potential of applying the same design approach to further increase RTD oscillator output power for THz applications.

9651-16, Session 4

Electrically tunable graphene-enabled THz metadevices

Taylan Takan, Mehmet A. Nebioglu, Middle East Technical Univ. (Turkey); Nurbek Kakenov, Osman Balci, Coskun Kocabas, Bilkent Univ. (Turkey); Hakan Altan, Middle East Technical Univ. (Turkey)

Through the use of metamaterials, control and manipulation of electromagnetic waves and their interaction with matter has been possible beyond what can be done with conventional matter [1]. Active metadevices, which incorporate passive metamaterials with various tuning mechanisms provide unique functionalities [2]. Electrical tunability with large dynamic range is a challenging requirement for practical applications of metadevices. In this study electrically tunable metadevices working at THz region which use large area graphene capacitors incorporated with resonant metal-mesh array of cross-shaped apertures is demonstrated.

Recently, Bilkent Group discovered a simple device structure consisting of an electrolyte medium sandwiched between two large area graphene electrodes, permitting an efficient mutual gating between two graphene electrodes that yield charge densities on the order of 1014 cm-2 [3]. Using this supercapacitor structure various optoelectronic devices including optical modulators [4], electrochromic devices and switchable radar absorbing surfaces [4] were fabricated. In this work we demonstrate a new type of electrically controllable metadevices, using graphene supercapacitors incorporated with metal-mesh array of cross-shaped apertures. Electrical tunability is achieved via tuning high mobility free carries on graphene, which in turn controls the magnitude of dissipation in the resonator coupled to graphene electrodes.

The device consists of an ionic liquid electrolyte sandwiched between two large area graphene electrodes which is coupled to the metal-mesh array with PVC substrate in between.

Using chemical vapor deposition technique graphene electrodes were synthesized on copper foils and then transferred onto flexible PVC substrates using hot lamination technique. The metal-mesh array was fabricated on the other side of the graphene-coated PVC by printing the cross aperture shapes on 10 μm thick copper foil followed by chemical etching of copper. Gating between graphene electrodes is achieved by electrolyte without any metallic gate electrodes. The electrolyte gets polarized and dopes the graphene electrodes under external bias voltage which in turn allows the resonance of the metamaterials to be tuned.

The whole device is modeled and simulated using commercially available EM simulation software and the spacing between metal mesh and graphene is optimized.

A VDI Schottky diode based, multiplied mm-wave/THz emitter is used as a tunable frequency signal source. Driven by a voltage-controlled frequency-tunable YIG oscillator, the system can provide a minimum average output power of about 1 mW, in the frequency region of 240-380GHz. The output of the source is amplitude modulated and measured via a Golay Cell. The output beam was collimated and focused onto the device with spot diameter about 3 mm at the device position. The radiation was then collected and focused onto the receiver with identical set of optical elements.

References:

1. Tao, H., Padilla, W. J., Zhang, X. & Averitt, R. D. Recent Progress in Electromagnetic Metamaterial Devices for Terahertz Applications. Ieee J Sel Top Quant 17, 92-101 (2011).

2. Shin, D. et al. Broadband electromagnetic cloaking with smart metamaterials. Nature communications 3, 1213 (2012).

3. Polat, E. O. & Kocabas, C. Broadband Optical Modulators Based on Graphene Supercapacitors. Nano Letters 13, 5851-5857 (2013).

4. Osman Balci, E. E. P., Nurbek Kakenov, Coskun Kocabas. Graphene-enabled electrically switchable radar absorbing surfaces. Nature communications 6, 6628 (2015).

9651-17, Session 4

Bolometric kinetic inductance detector technology for sub-millimeter radiometric imaging

Juha Hassel, Andrey V. Timofeev, Visa Vesterinen,

Hannu Sipola, Panu Helistö, Mika Aikio, Aki Mäyrä, VTT Technical Research Ctr of Finland Ltd (Finland); Arttu R Luukanen, Asqella Oy (Finland); Leif Grönberg, VTT Technical Research Ctr of Finland Ltd (Finland)

Kinetic inductance detectors (KIDs) have established their position as candidate technology in astronomical imaging missions. The most extensively developed line of KID technology is relying on superconducting materials properties in milli-Kelvin temperatures, which limits the operational temperature of the technology while ensuring the extreme radiometric sensitivity. The KID technology is naturally suitable for operation of large arrays thanks to its compatibility with RF or microwave multiplexing techniques. While milli-Kelvin KIDs reach the ultimate sensitivity levels needed in the imaging of cold astronomical objects, in terrestrial applications with radiometric temperature around 300 K the sensitivity requirement is not quite as limiting. The terrestrial applications include in particular the civil security applications such as concealed objects detection. For these ends we have recently demonstrated detectors based on KIDs operated at elevated cryogenic temperatures (~10 K) to address the need of large-scale detector array technology with compact cryogenics. The aim is to enable large 'staring' arrays to avoid optomechanical scanning in imaging as it introduces complexity in system level and degrades the sensitivity through reduced integration time per image pixel. The detectors are operated in thermal mode requiring the detectors to be integrated on sub-micron thick membranes. We will introduce the basic concepts of our technology, and provide characterization results yielding basic figures of merit such as noise equivalent power, noise equivalent temperature difference, detection band and response time. We also discuss the scaling issues related to the technology with respect to imaging area and spatial resolution. The status of our prototype imager development with about 2500 detectors is provided by introducing results on readout-band RF properties, optics and system integration aspects.

9651-18,

Comparison of objects detection capabilities in LWIR and THz ranges

Marcin Kowalski, Mariusz Kastek, Mieczyslaw Szustakowski, Military Univ. of Technology (Poland)

Multispectral systems for detection of concealed dangerous objects are becoming more popular because of their higher effectiveness compared to mono-spectral systems. So far, the problem of detecting objects hidden under clothing was considered only in the case of airports but it is becoming more and more important for public places like metro stations, and government buildings.

Exploration of new spectral bands and technology development result in introduction of new solutions – both mono and multispectral. It has been proved that objects hidden under clothing can be detected and visualized using terahertz (THz) cameras. However, passive THz cameras still offer too low image resolution for objects recognition. Limited range is another urgent challenge. On the other hand new infrared cameras offer sufficient parameters to detect objects covered with fabrics in some conditions, as well as high image quality and big pixel resolutions.

The purpose of the studies is to investigate and compare the possibilities of using passive cameras operating in long wavelength infrared (LWIR) and THz spectral ranges for detection of concealed objects. For the purpose of investigations, commercial imagers operating in 6.5-11.7 ?m and 250GHz (1.25mm) were used. In the article, we present the measurement setup and the results of measurements in various operating conditions. Theoretical studies of both spectral bands focused on detection of objects with passive imagers are also presented.

9651-19,

Textile influence on remote identification of explosives in the THz range

Michal J. Walczakowski, Norbert Palka, Mieczyslaw Szustakowski, Military Univ. of Technology (Poland)

Remote identification of explosives in the terahertz range has been studied in recent years. However, law requirements for tighter public safety puts pressure on improved solutions and progress in the detection of explosives and hazardous materials. To prevent threats security services must find substances of its interest which most of the time are concealed. This increase importance of textile influence on the process of spectral detection and identification. In this study common clothing and variety of textile materials were used in research on its influence on remote materials identification. Experimental setup was designed for the terahertz reflection spectroscopy of different materials located at a distance up to 5 m. The source of the radiation is a tunable solid-state optical parametric oscillator (OPO), which generates a narrow-band nanosecond pulses in the range of 0.7-2.7 THz. The signal is detected with hot electron bolometer (HEB). Investigations were carried out for three series – for 1 m, 3 m and 5 m distance between the examined sample and the system. Experiment was conducted in the 0.7 – 2.5 THz range for 1 m and 3 m distance. For 5 m distance lower power of the source above 2.1 THz limited examined spectral range to this value. Fabrics subjected to testing were varied in terms of the fibers kind which they were made from and weights of test materials ranged from 53 g/m2 up to 420 g/m2. Also textiles with a composition consisting of several fibers with differing percentage of the fibers composition of each sample were measured. Information about textiles reflectance was obtained in separate set of experiments. The main studies were performed in the THz range and supplemented research was conducted in the mid infrared region (MIR). In the terahertz range FTIR and TDS spectroscopy were used and in the MIR range textiles were characterized using FTIR spectroscopy. Optical microscope was used for the investigations of the visual features of tested fabric. The study fabrics were made of viscose, polyester, cotton, spandex, wool, nylon, leather, flax. Obtained spectra of selected materials, including explosives, were compared to the results received from a purged time domain spectroscopy system. To add more realism experiment was conducted in free space with relative humidity of about 30 - 40% depending on the weather conditions of the day.

9651-20,

Channel calibration for digital array radar in the presence of amplitude-phase and mutual coupling errors

Weixing Li, National Univ. of Defense Technology (China); Jianzhi Lin, Yue Zhang, Zengping Chen, National University of Defense Technology (China)

1. PURPOSE

Digital array radar (DAR) is remarkable for the characteristics of large instantaneous dynamic range, flexible control, multi-beams simultaneously and superior ability of anti-interference. Most array processing algorithms are based on ideal assumption of both the signals and channels. For actual systems, amplitude-phase errors as well as mutual coupling will lead to substantial performance degradation of digital processing such as digital beam-forming (DBF) and direction of arrival (DOA). This paper demonstrates a practical calibration algorithm that calibrates the amplitude-phase errors using interior calibration network and then realizes mutual coupling calibration by eigen-decomposition approach. Based on an 8-elements X-band DAR test-bed, experiments are carried out in the anechoic chamber and outdoors. The expected results of radiation pattern and DOA estimation of measured data illustrate that the algorithm is fairly effective and feasible in actual systems.

2. METHODS

The main contents in the paper can be summarized as follows:

Description of the 8-elements DAR test-bed.

The theories and realization of the proposed algorithm that combines amplitude-phase calibration and mutual coupling together.

Experiments setup in anechoic chamber and outdoors and the processing results of measured data.

In the first section, a flexible DAR test-bed with interior calibration network is demonstrated. The system contains 8 antenna elements which receive echoes with carrier frequency of 10GHz. After down-convert, the operation frequency is from 0.6GHz to 3.0GHz. The front-end is composed of a two-stage low noise amplifier (LNA) and an adjustable attenuator followed by four band-pass filters of 500MHz bandwidth. The digital receives integrate a four-channel ADC with the sampling rate of 1.2Gsps. The DBF processors and DSP processors are based on VPX standard which are powerful to carry out DBF, DOA and so on. A calibration network is installed on the back of antenna array panel for interior calibration. The calibration network is composed of a power divider and a coupler. Feed the calibration signal into the receive channels through the coupler, and the characteristics of the whole interior calibration path is obtained.

In the second section, the array signal model is studied, taking into consideration of the amplitude-phase errors and mutual coupling. The calibration is carried out by three steps. Step1, with the pre-knowledge of the characteristic of calibration network, interior calibration method can be used to eliminate the amplitude-phase errors caused by front-ends and ADC. Step2, emit calibration source from several positions. Then decompose the covariance matrix of received data, and find eigenvector corresponding to the maximum eigenvalue. Step3, according to subspace theories, there is a relationship between the eigenvector and distorted steering vector. As a result, the closed-form solution of mutual matrix is obtained.

In the third section, experiments are carried out in the anechoic chamber and outdoors based on the 8-elements DAR test-bed. In the anechoic chamber, interior calibration source is feed into the calibration network, and then signals are emitted from different directions and received by the DAR test-bed. The receive data are processed by the proposed algorithm. The radiation patterns are improved greatly after calibration. In the outdoor experiments, the measured data of ADS-B signals is captured. MUSIC algorithm is used to find the direction of the aviation. The results indicate that the proposed algorithm achieves good performance and is feasible to realize.

3. RESULTS &CONCLUSIONS

In this paper, a practical calibration algorithm that calibrates the amplitude-phase errors as well as mutual coupling calibration is demonstrated. Experiments are carried out in the anechoic chamber and outdoors. The radiation pattern of the array is similar to the ideal one, and the DOA resolution of measured data is improved greatly. The results indicate that the proposed algorithm achieves good performance and is feasible to realize.

9651-21,

Spatio-spectral characteristics and polarization of THz radiation from two-color femtosecond filament

Vera Andreeva, Lomonosov Moscow State Univ. (Russian Federation); Mikhail Esaulkov, Institute on Laser and Information Technologies (Russian Federation); Nikolay Panov, Petr Solyankin, Vladimir Makarov, Daniil Shipilo, Alexander Shkurinov, Olga Kosareva, Lomonosov Moscow State Univ. (Russian Federation)

One of the most promising and convenient sources of THz radiation is the plasma channel of femtosecond filament. THz radiation generated during filamentation has high field amplitude and broad spectrum ranged from 0.1 to 30 THz.

There are two physical mechanisms responsible for THz radiation generation during filamentation: nonlinear response of neutral gas and transient photocurrent due to tunnel ionization of gas atoms and molecules. These two mechanisms can be spectrally separated [1], but we were not able to prove the existence of the high-frequency THz radiation band because the spectral sensitivity of ABCD detection decreases at high frequencies as well as to describe propagation of THz radiation in our numerical model.

In this work, we use UPPE [2] for numerical investigation of THz pulse generation, which is based on the field approach and takes into account the components oscillating at optical and THz frequencies and derived without assumption of paraxial approximation.

For experimental investigation we use Michelson interferometer with a helium-cooled bolometer to study both the high- and low-frequency parts of the THz spectrum. For the polarization studies, we built a setup with separated beams for first and second harmonics so that we could control them independently.

According to our numerical modelling, first the high-frequency components with maximum spectral density appear in THz radiation spectrum due to nonlinear response of the bound electrons. Then, the lower-frequency part of the spectrum is formed due to the free electron density increase, which leads to shift of the maximum spectral intensity to lower frequencies.

Our experiments show increase in the detected bandwidth in comparison with ABCD detection method and observe the THz signal in spectral region governed by the nonlinear response of bound electrons. We study the spatial profile of the emitted radiation and reveal its broadband cone-like shape with maximum spectral intensity and bandwidth propagating at approximately 5° from the beam axis. Moreover, we observe substantial dependence of the emitted spectral bandwidth on the pulse duration and the sign of its chirp. The experimentally and numerically obtained angular-frequency spectra of THz radiation are in good agreement.

THz polarization measured for the case of both linear polarizations of ? and 2? beams was directed along ? beam polarization. This result cannot be explained using neither simple photocurrent nor bound electrons nonlinearity models separately. Our simulations also show how the pulse shape and polarization of both fundamental and second harmonic radiation is distorted during the propagation inside the filament region. Evolution of the 2? polarization results in generation of THz pulse polarized closer to ? than simplified theoretical models, which do not include the propagation effects, predict it. This is in perfect agreement with our experimental results.

[1] ?.V. Borodin, N.A. Panov, O.G. Kosareva, V.A. Andreeva, M.N. Esaulkov, V.A. Makarov, A.P. Shkurinov, S.-L. Chin, X.-C. Zhang. "Transformation of terahertz spectra emitted from dual-frequency femtosecond pulse interaction in gases" Optics letters 38, 1906-08 (2013)

[2] M. Kolesik, J.V. Moloney "Nonlinear optical pulse propagation simulation: From Maxwell's to unidirectional equations" Physical Review E 70, 036604 (2004)

9651-23,

Detection of the mm-wave radiation using a low-cost LWIR microbolometer camera from a multiplied Schottky diode based source

Basak Kebapci, METU-MEMS Research and Application Center (Turkey); Firat Tankut, MikroSens Elektronik San ve Tic A S (Turkey); Hakan Altan, Middle East Technical University (Turkey); Tayfun Akin, MikroSens Elektronik San ve Tic A S (Turkey) and Middle East Technical University (Turkey) and MikroSens (Turkey)

This paper presents the measurement and analysis method for detection of the mm wave signal at 96 GHz by using a low-cost microbolometer infrared (IR) camera with 70 μm pixel pitch optimized for detection in the 8 12 μm (LWIR) range. The mm wave beam derived from a multiplied Schottky diode based source is detected within ~65% of the whole area of a 160?120 pixel focal plane array microbolometer sensor. Under ~73 mW incident power, responsivity is measured as 7.3 V/W, and the average noise for the measurement is determined as 12 μV, which includes both detector and readout electronics contribution. From the measured parameters, the integrated Noise Equivalent Power (NEP) is calculated as 1.63 μW within the 7.8 kHz readout bandwidth. By using a simple setup, it is shown that a low cost microbolometer camera which is designed for LWIR range can detect a distinct mm wave beam at 96 GHz.

Conference 9652A: Optics and Photonics for Counterterrorism, Crime Fighting, and Defence

Monday - Tuesday 21–22 September 2015

Part of Proceedings of SPIE Vol. 9652 Optics and Photonics for Counterterrorism, Crime Fighting, and Defence XI; and Optical Materials and Biomaterials in Security and Defence Systems Technology XII

9652-1, Session 1

Detection of munitions grade G-series nerve agents using Raman excitation at 1064 nm

Eric G. Roy, Rigaku Raman Technologies, Inc. (United States); Phillip G. Wilcox, Soren Hoffland, U.S. Army Edgewood Chemical Biological Ctr. (United States); Ian Pardoe, EXCET, Inc. (United States)

Raman spectroscopy is a powerful tool for obtaining molecular structure information of a sample. While Raman spectroscopy is a common laboratory based analytical tool, miniaturization of opto-electronic components has allowed handheld Raman analyzers to become commercially available. These handheld systems are utilized by Military and First Responder operators tasked with rapidly identifying potentially hazardous chemicals in the field. However, one limitation of many handheld Raman detection systems is strong interference caused by fluorescence of the sample or underlying surface which obscures the characteristic Raman signature of the target analyte. Munitions grade chemical warfare agents (CWAs) are produced and stored in large batches and typically have more impurities from the storage container, degradation, or unreacted precursors. In this work, Raman spectra of munitions grade CWAs were collected using a handheld Raman spectrometer with a 1064 nm excitation laser. While Raman scattering generated by a 1064 nm laser is inherently less efficient than excitation at shorter wavelengths, high quality spectra were easily obtained due to significantly reduced fluorescence of the munitions grade CWAs. The spectra of these less pure, but more operationally relevant, munitions grade CWAs were then compared to spectra of CASARM grade CWAs, as well as Raman spectra collected using the more common 785 nm excitation laser.

9652-2, Session 1

Hyperspectral detection and scalable LTE technology-based alerting for CBRNE threats

Jaana R. Kuula, Univ. of Jyväskylä (Finland)

Hyperspectral technology can be used for automated and operated detection of CBRNE threats both in long distance and short range measurements. The quality and accuracy of the information received from hyperspectral sensors, however, varies depending on the distance of the target, environmental conditions, type of sensors, detected substances and on the surface or substrate on which they are found. The information received from sensors defines what kind of alerts can be given and to whom. For example, weak and unconfirmed signals need to be delivered immediately to the authorities, whereas civilians should be alerted only for confirmed threats and at that extent what the actual nature, size and area of the hazard in that particular case is. Most sensors cannot individually and reliably detect and identify CBRNE threats, define the hazard zone and give tailored alerts to the selected audiences. For that reason sensor based alerts to the civilians are not preferred, and authorized human decision making is required instead. This article proposes a detection and alerting system for CBRNE threats where illicit substances are detected with hyperspectral technology and alerts are given to the authorities and civilians at a needed range with a scalable LTE technology. The alerting system also creates an instant situational awareness map of the incident. Depending on the priorities, the location and status of various entities can be included on the map. For example, if an alert has been given to the civilians in a selected emergency area, their location, condition and need for help is shown on the map. The map will show the situation before the actualization of the threat and the location and status of casualties after the blast, depending on the point of time when the alert is given. The article demonstrates the proposed hyperspectral system by presenting the test results of detecting live CWA agents and their precursors and degradation products with three hyperspectral cameras in SWIR, MWIR and LWIR wavelength areas. The operation of the LTE technology based alerting and situational awareness system is demonstrated with simulated sensor based alerts in a school violence and chemical release incident, and with police experiments of alerting authorities and civilians for simulated threats. The two systems can be used together as a technically integrated detection and alerting system or separately with human decision making in between. Both systems are developed at the Department of Mathematical Information Technology of the University of Jyväskylä and they have been tested in several experimentations with the fire and rescue service, police and defence forces in Finland. All experiments have been made with commercially available technologies and university based software, and they have focused on crisis management, forensic investigation, counter terrorism and CBRNE. In alerting capabilities, accessibility and affordability LTE technology has exceeded all other technologies on the market.

9652-3, Session 1

Multispectral analysis of biological agents to implement a quick tool for stand-off biological detection

Mariachiara Carestia, Roberto Pizzoferrato, Jessica Gabriele, Gian Marco Ludovici, Michela Gelfusa, Andrea Malizia, Orlando Cenciarelli, Pasquale Gaudio, Univ. degli Studi di Roma “Tor Vergata” (Italy)

The deliberate use or the accidental dispersion of pathogenic biological agents (BAs) like bacteria, toxins, viruses and fungi, is a threat from a military and civilian point of view [1]. To maximize the effect of the proper countermeasures, a quick and effective detection of the presence of BAs is paramount.

Identification of BAs requires sampling and analysis using molecular biology techniques, among which, Real Time PCR and genomics remain the gold standard. Instead, optical techniques can be applied to achieve a fast detection of the presence of BAs in the form of aerosols, the most effective way of exposing a large number of people to this threat [2]. Furthermore, optical techniques can achieve stand-off distance detection, or be implemented on mobile platforms, without requiring sampling procedures.

To this extent, several features of biological aerosols can be exploited, ranging from particle size distribution to intrinsic fluorescence measurements [3]. The latter technique is one of the most promising route concerning BAs optical detection[4]. The ubiquity of biological endogenous fluorophores limits the definition of the specific optical features that can be used to distinguish between the different BAs, and between BAs and other organisms and molecules.

With the aim of identifying an approach to exploit differences of the fluorescence signatures of biological agents, this work investigated the response of some BAs simulants, to a set of different excitation wavelengths in the UV spectral range (i.e. 266, 273, 280, 300, 340, 355 nm).

Our preliminary results on bacterial spores and vegetative forms, dispersed in water, showed that appreciable differences occur in the fluorescence spectra under excitation with different wavelengths.

More in detail, the photo luminescence (PL) spectra coming from different species of Bacillus, in the form of spores (used

as simulants of Bacillus anthracis), show significant differences between the two species by excitation at all the wavelengths, with slightly larger differences at 300, 340, 355 nm.

On the other hand, the vegetative forms of two Bacillus species, did not show any appreciable difference, i.e. the PL spectra are virtually identical, for excitation wavelengths of 266, 273, 280 nm. Conversely, small yet appreciable difference appear at 300, 340, 355 nm.

Finally, large difference appear between the spore and the vegetative form of each species at all the wavelengths, with slightly larger variations at 300, 340, 355 nm.

Together, these preliminary results support the hypothesis that a multi-wavelength approach could be used to improve the sensitivity and specificity of UV-LIF based BAs detection systems.

The next step of this work will concern the application of a support vector regression method, as evaluated in our previous work [5], to define a methodology for the setup of a multispectral database for the stand-off detection of BAs.

[1] Cenciarelli, O., Rea, S., Carestia, M., D'Amico, F., Malizia, A., et al., "Bioweapons and Bioterrorism: A Review of History and Biological Agents," Defence S&T Tech. Bull., 2013, vol. 6, pp. 111-129.

[2] ?vábenská, E. . "Systems for detection and identification of biological aerosols," Defence Science Journal 62(6), 404-411 (2012).

[3] Greenwood, D.P., Jeys, T.H., Johnson, B., Richardson, J.M., and Shatz, M.P., "Optical techniques for detecting and identifying biological-warfare agents," Proceedings of the IEEE, 2009, vol. 97, pp. 971-989.

[3] Walt, D. R., & Franz, D. R. (2000). Peer Reviewed: Biological Warfare Detection. Analytical chemistry, 72(23), 738-A.

[4] NATO RTO Technical Report, [Laser Based Stand-off detection of biological agents], RTO-TR-SET-09S.

[5] Carestia, M., Pizzoferrato, R., Gelfusa, M., Cenciarelli, O., D'Amico F., et. al., "Towards the implementation of a spectral data base dot the detection of biological warfare agents," Proc. SPIE 9251, Technologies for Optical Countermeasures XI; and High-Power Lasers 2014: Technology and Systems, 92510I (October 7, 2014); doi:10.1117/12.2067227;

9652-4, Session 1

Tests of various colorants for application of a Fourier-transform infrared imaging system to deciphering obliterated writings

Shigeru Sugawara, National Research Institute of Police Science (Japan)

Obliterated writing is writing that has been obscured by differently colored materials. The decipherment of obliterated writing is an important field in forensic science. In general, obliterated writing is deciphered using the spectroscopic and fluorescent photographs of visible and near-infrared light in the wavelength range of 0.4–1 ?m. However, there are obliterated writings that cannot be deciphered using the conventional methods. The decipherment possibility depends on the optical characteristics of the colorants used to write the characters and those of the colorants used to obliterate the writing. A decipherment method for obliterated writings was developed in the present study. Mid-infrared spectroscopic imaging in the wavelength range of 2.5–14 ?m was considered for decipherment because, in forensic science, infrared spectroscopy is commonly used to identify ink, as the infrared spectrum differs among different brands. Subsequently, a Fourier-transform infrared imaging system (Spectrum Spotlight 300, Perkin Elmer Co.) was used for deciphering the obliterated writings. A sample obliterated writing that was made by pressing information-protection stamps on characters written by black water-dye ballpoint pens could be deciphered by drawing images using an absorption peak intensity of 1594 cm-1, and the result was presented at the previous SPIE DSS meeting [1]. After the meeting, various other colorants were tested for their ability to make obliterated writings, which we attempted to decipher using the Fourier-transform infrared imaging system. As a result, it was revealed that the absorption peak at different wavelengths and reflectance increase at a specific wavelength can also be used for deciphering obliterated writings that cannot be detected using the conventional methods.

[1] Sugawara S. Application of a Fourier-transform infrared imaging system to deciphering obliterated writings for forensic purposes. SPIE Defense+ Security. Baltimore: International Society for Optics and Photonics; 2014. p. D.

9652-5, Session 2

Laser desorption of explosives as a way to create an effective non-contact sampling device

Artem E. Akmalov, Alexander A. Chistyakov, Gennadii Kotkovskii, National Research Nuclear Univ. MEPhI (Russian Federation)

The problem of the detection of explosives in air, in view of their extremely low vapor pressure and influence of environment is still relevant. Required analytical detection thresholds belong to sub-ppt (particle per trillion) range. In some cases, one can detect traces of explosives by wiping a surface of an object with a napkin, followed by heating of the napkin and vaporization of a sample. Herewith it's necessary to provide both maximum effectiveness of the explosives transfer from an object to the napkin and quick heating. This is not always achievable. Also, a touch of a suspicious object can be dangerous. In this connection, the approach of using a laser pulse for contactless explosives desorption from a suspicious surface seems attractive.

In this paper the quantitative investigation of effectiveness of different laser sources during desorption of trace amounts of trinitrotoluene (TNT), cyclotrimethylenetrinitramine (RDX), pentaerythritoltetranitrate (PETN), cyclotetramethylenetetranitramine (HMX) from common surfaces has been performed. The YAG:Nd3+ nanosecond (?pulse=6 ns, ?=266,532,1064 nm), and picosecond (?pulse=300ps, ? = 266,532 nm) lasers, the continuous wave laser (? = 440nm) were used. The samples - substrates of quartz, paper, aluminum or polyethylene with traces of explosives (10-4 gr per 0.15 cm2 area) - were located in a specially designed vacuum-impenetrable laser rod. The rod through the direct sample injection module was introduced to the mass spectrometer ion source, followed by desorption of explosives under laser action. The dependencies of mass desorbed on the intensity 106-109 W/cm2 were investigated.

It was shown the most effective laser source is a nanosecond laser (? =266 nm). The desorbed quantities at the optimum intensity 6.108W/cm2 were 5-20 ng for TNT, 1-4 ng for RDX, 20-50 ng for PETN. Surprisingly, the action of a single laser pulse on HMX resulted in the NO2-output only. The HMX desorption was stimulated only by a series of 50 or more pulses as a result of substrate heating, and continued after the end of laser exposure.

It was also shown the desorption efficiency under nanosecond (?=532nm) radiation with intensity 4.108W/cm2 was comparable to that of ultraviolet radiation for TNT, RDX, PETN, even in the case of optically thin samples. Probably the absorption by impurities plays an important role in this case. Desorption of HMX also needed a series of pulses.

The nanosecond (? =1064nm) and picosecond radiation were entirely not effective.

The continuous wave radiation at the intensity 10W/cm2 produced desorption 50-1000 ng for all studied explosives under exposure of the same place of a sample for 90 seconds or more. The nanosecond (?=266nm) radiation at a comparable time of exposure was more effective.

The minimum mass of desorbed explosives was implemented on paper, the maximum mass - on polyethylene.

The NO-byproduct was observed for all used wavelengths. The NO-mass fraction in the desorption products was not more than 10%. The mechanism of NO appearance is thermal.

We discuss the possible changes in desorbed amounts under atmospheric conditions.

The perspectives to make the effective non-contact sampling device based on the chip nanosecond ultraviolet YAG:Nd3+ diode-pumped laser with mass ~2 kg are discussed.

9652-6, Session 2

Liquid explosive detection using near infrared LED

Hideo Itozaki, Shiori Ito, Hideo Sato-Akaba, Yuji Miyato, Osaka Univ. (Japan)

A bottle scanner to detect liquid explosive has been developed using technologies of near infrared. Its detection rate of liquid explosive is quite high and its failure rate of safety liquids quite low. It uses a light source with wide spectrum such as a halogen lump. Recently a variety of LED has been developed and some of them have near infrared spectrum. Here near infrared LED is tried to be used as a light source of liquid explosive detector.

An infrared LED that has a main peak of spectrum at 1028 nm has been used as a light source to scan liquids. Spectrum width of this LED is quite narrow such as less than 100 nm. Several liquid is evaluated by this LED and it can identify liquids very well. This experiment shows that the infrared LED can be used as a light source for a liquid scanner.

An LED has some merits, such as long life of more than some ten thousand hours and small consumption electric power of less than 0.2 W. When the LED is used as a light source for the liquid scanner, it comes more compact and handy.

9652-7, Session 2

CRIM-TRACK: sensor system for detection of criminal chemical substances

Jens K. Munk, Ole T. Buus, Jan Larsen, Technical Univ. of Denmark (Denmark); Eleftheria Dossi, Cranfield Univ. (United Kingdom); Sol Tatlow, Pro Design Electronic GmbH (Germany); Lina Lässig, Securetec Detektions-Systeme AG (Germany); Lars Sandström, Gammadata Holding AB (Sweden); Mogens H. Jakobsen, Technical Univ. of Denmark (Denmark)

The detection of illegal compounds is an important analytical problem. A high confidence-level sensing device requires a reliable, selective and sensitive detection method. The successful sensing device also features automated target acquisition, identification and signal processing of data. Furthermore, the sensing device is preferably portable, fast, user friendly, highly sensitive, specific, and cost efficient. At current, law enforcement agencies are left in need of such technology. This market gap is a security risk.

CRIM-TRACK is developing a working sensing device based on these requirements. This EU FP7 project has succeeded in engaging highly skilled specialists in all areas required for successful technological development and implementation thereof. We rely on our demanding, internal team of law enforcement end users to benefit maximally from our prototypes. At current we are 21 months into development and have successfully detected all compounds required from us by these end users. We can now detect minute quantities of drugs and explosives as well as precursors thereof in laboratory settings.

Using colorimetric technology we have developed prototypes that employ disposable sensing chips. The prototype series converge toward a miniaturized, automated, fast, cost efficient, highly sensitive, and simple “sniffer” and detection unit. Ease of operation and intuitive sensor response are highly prioritized features that we implement as we gather data to feed into our machine learning system, which itself develops with time. With machine learning our ability to detect threat compounds amidst harmless substances improves.

Different end users typically prefer their equipment optimized for their specific field. In some situations, such as an explosives-detecting scenario, the end user may prefer false positives over false negatives, while the opposite may be true in other situations such as a drug-detecting scenario. Because the signal processing in done in silico, such decisions will be programmed to match user preference. Likewise, sensor output can be as detailed as the sensor allows. Thus, the user can be informed of the statistics behind the detection, identities of any threat substances, identities of co-detected harmless substances, and possibly quantities of both. On the other hand, the response can also be simplified down to “yes” vs. “no”.

A marketable product suitable for the field requires further work and is beyond the project’s scope. However, the technology under development in CRIM-TRACK will provide custom officers, police and other authorities with an effective tool to control trafficking of illegal drugs and drug precursors.

9652-8, Session 2

Magnetic induction imaging with optical atomic magnetometers: towards applications to screening and surveillance

Luca Marmugi, Sarah Hussain, Univ. College London (United Kingdom); Cameron Deans, University College London (United Kingdom); Ferruccio Renzoni, Univ. College London (United Kingdom)

The evolving conflict against smuggling, trafficking and terrorism constantly demands new detection capabilities. Indeed, conventional techniques for cargo screening and earlier vessel or vehicle detection are often challenged, or of limited effectiveness with unpredicted targets and enclosures. We present here a proof-of-principle demonstration of a novel remote, non-invasive detector for conductive objects, based on Magnetic Induction Tomography (MIT) with Optical Atomic Magnetometers (OAMs).

The active nature of the technique and its scalability provide new practical solutions for fast underground and underwater mapping and surveillance, as well as for real-time cargo screening and non-destructive imaging.

MIT relies on the excitation of eddy currents in the object of interest and on the detection of the magnetic fields produced by them. Conductivity maps of conductive targets can be thus obtained. However, standard MIT systems are limited by the poor sensitivity of pick-up coils at low frequencies, which also limits the maximum range to a few tens of meters.

OAMs overcome these limitations: their sensitivity below 50 MHz is up to 10^(7) times higher than that of a coil of the same size, and their bandwidth is not limited by intrinsic factors. In addition, OAMs have an enormous potential for miniaturisation, and they do not require calibration, because their output is proportional to the magnetic field through fundamental physical constants only.

In order to demonstrate the detection capabilities of an OAM-based MIT detector for security and defence, in our setup, a small magnetic field (primary field), oscillating at a frequency down to the Hz band, propagates (in air, ground or water) and induces eddy currents in conductive objects. These currents generate a local oscillating magnetic field (secondary field) opposing to the driving one, whose properties depend on conductivity ?, permittivity ?_r and permeability ?_r of the target. A laser-driven 87Rb vapour OAM detects the secondary field, thus providing a position-resolved mapping of the region of interest. In detail, a pump laser creates long-living atomic orientation of the ground state of 87Rb atoms. Under the influence of the total magnetic field, atomic spins’ precession

in the external magnetic field modifies the optical properties of the atomic sample, as detected by a laser probe. By using a phase-sensitive detection scheme, both phase and amplitude of the secondary fields are measured, and the background is rejected without any shielding. The device does not require any physical contact between sensor, driving source, target and read-out electronics. The system can be operated either in single-sensor scheme, where a single sensing head is scanned through the sample, or in a steady array configuration, by exploiting inverse problem algorithms for image reconstruction.

The potential of OAMs for extreme sensitivity, miniaturisation, dynamic range and array operation, paves the path to a new generation of non-invasive, remote, active detectors, with "field-ready" capabilities for the detection of illegal, dangerous or unknown materials and their cases, and for ground- and water-penetrating monitoring and early detection.

9652-9, Session 3

An engineering approach towards creating ubiquitous THz applications *(Invited Paper)*

Stepan Lucyszyn, Imperial College London (United Kingdom)

No Abstract Available

9652-10, Session 3

Principal limitation of standard THz time-domain spectroscopy method of the detection and identification of substance and way of its overcoming

Vyacheslav A. Trofimov, Svetlana A. Varentsova, Lomonosov Moscow State Univ. (Russian Federation)

We demonstrate principal limitations of standard Time Domain Spectroscopy (TDS) based on a broadband THz pulse for the detection and identification of substance. To avoid these limitations we propose highly effective new algorithm for this purpose. We demonstrate its applicability in realistic situations for various substances under consideration.

9652-11, Session 4

Embedded security system for multi-modal surveillance in a railway carriage

Rhalem Zouaoui, Thales Research & Technology (France); Romaric Audigier, CEA LIST (France); Sébastien Ambellouis, Institut Francais des Sciences et Technologies des Transports de l'amenagement et des Reseaux (France); François Capman, Thales Communications S.A. (France); Hamid Benhadda, THALES, Advanced Studies Department, THALES-CEA VisionLab (France); Stéphanie Joudrier, Thales Research & Technology (France); David Sodoyer, IFSTTAR (France); Thierry Lamarque, Thales Research & Technology (France)

Public transport security is one of the main priorities of the public authorities when fighting against crime and terrorism. In this context, there is a great demand for autonomous systems able to detect abnormal events such as violent acts and vandalisms aboard coaches as well as intrusions when the train is stationed at the depot. To this end, we present an innovative approach which aims at providing efficient automatic detection of abnormal events in the public transport by fusing video and audio analytics and sending real time alerts to the security operators.

The objective of this work is to demonstrate that the fusion of video and audio detections can reduce the false alarm rate compared to classical detection systems based on video analytics only. A preindustrial prototype relying on a low power computing platform has been developed. This multi-modal detection system is composed of two omnidirectional microphones and of one camera and integrates onboard video and audio analytics as well as fusion capabilities. The algorithms are embedded on a dedicated platform based on an original combination of ARM and FPGA processors.

On the one hand, for detecting intrusion when the coach is at the depot, the system relies on the fusion of "abnormal audio events" detection by using an unsupervised approach with the detection of intrusion from video processing. It consists in modeling the normal ambience, and detects deviation from the trained models during testing. The implemented solution is based on clustering of automatically extracted segments of acoustic features and statistical GMM modeling of each cluster. During testing, abnormal events are detected when none of the GMM likelihoods is above a predetermined threshold. This audio detection is fused with an intrusion detector based on the 3D detection and tracking of individuals in the videos.

On the other hand, for violent events detection, the system fuses unsupervised and supervised audio algorithms with video detection of violent events. The supervised audio technique detects specific events. In this work, we focus on shout detection. We use a Gaussian Mixture Model to catch the formantic structure of a shout signal. Video analytics use an original approach for detecting aggressive motion by focusing on erratic motion patterns specific to violent events. As data with violent events is not easily available, a normality model with structured motions from non-violent videos is learned for one-class classification. A probabilistic inference framework is used to detect configurations of unstructured motion patterns and, consequently, violent events. The method is real-time and quite robust to the context in use. Indeed, it is independent of the learning scenes.

To provide one common alert based on multimodal detections, an innovative fusion algorithm is embedded on the dedicated platform. The algorithm is based on the theory of Dempster-Shafer and computes the degree of belief of each probable incident It handles combination of alerts and manages asynchronous detectors outputs.

In order to test and then improve the algorithms, a mix of real, laboratory and synthetic video scenes were recorded. Indeed, original synthetic scenes have been specifically produced to simulate violent events and test the approach before deploying the system in real life. Results from real environment testing will be provided to prove the approach efficiency.

9652-12, Session 4

Automatic inference of geometric camera parameters and intercamera topology in uncalibrated disjoint surveillance cameras

Richard J. M. den Hollander, Henri Bouma, Jan Baan, Pieter T. Eendebak, Jeroen H. C. van Rest, TNO (Netherlands)

Person tracking across non-overlapping cameras and other types of analytics benefit from spatial calibration information that allows an estimation of the distance between cameras and a relation between pixel coordinates and world coordinates within a camera. In a large environment with many cameras, or for mobile camera deployments, it is efficient to perform this calibration automatically. This increased efficiency allows for a short configuration time, and the improvement of person tracking in ad-hoc crisis situations or in a changed camera-setup due to maintenance. We show an autocalibration method entirely based on automatic pedestrian detections in surveillance video in multiple non-overlapping cameras. In this paper, we show the two main components of automatic calibration. The first shows the intra-camera geometry estimation that leads to an estimate of the pitch angle,

focal length and camera height, which is important for the conversion from pixels to meters and vice versa. The second aspect shows the inter-camera topology inference that leads to an estimate of the distance between cameras, which is important for spatio-temporal analysis of multi-camera tracking. This paper describes each of these methods and provides results on realistic video data.

9652-13, Session 4

Incremental concept learning with few training examples and hierarchical classification

Henri Bouma, Pieter T. Eendebak, Klamer Schutte, George Azzopardi, Gertjan J. Burghouts, TNO (Netherlands)

The number of networked sensors (e.g., CCTV and smartphones) is growing exponentially and the amount of surveillance video increases daily. Concept detection and localization is important to understand the content of video and allow flexible querying in a large number of cameras.

Typically, the concept detectors that perform well on public benchmarks are trained on large collections (e.g., Pascal VOC and ILSVRC which are both based on ImageNet). The deep convolutional neural network (CNN) has been demonstrated to be an effective approach of which several implementations have been proposed, such as Decaf/Caffe, Overfeat and R-CNN.

The following problems, which are relevant for incremental concept learning and localization, have not yet been addressed. While CNNs have proven to be highly effective in challenges that contain huge training collections, it is not yet clear how they perform on practical applications with only a few training samples. Furthermore, new classes may (initially) consist of a low number of positive examples, resulting in an unbalanced number of samples in each class. Finally, the user may start adding new classes that are very similar or closely related to existing classes. For example, in the case when 'barbie' and 'dress' are two concepts and the barbie is wearing a dress.

Our novel contribution is that we propose a concept-detection method with incremental learning that addresses these problems. Firstly, we show that for a focused application in a single domain, it is possible to reduce the number of training samples to a low number and that the performance benefits from a training set that is as specific as possible for the purpose. Secondly, we show that the addition of novel concepts is often possible without retraining existing concepts, which is important to minimize computational cost and to allow fast interaction. Thirdly, we show that an unbalanced number of positive training samples leads to biases in classifier scores that can be corrected by giving higher weight to the classes that occur less frequent. Fourthly, we observed the deterioration of the detector performance due to hard-negative mining for similar or closely related classes and investigated hierarchical classification as a solution.

9652-14, Session 4

Posture estimation for improved photogrammetric localization of pedestrians in monocular infrared imagery

Mikolaj E. Kundegorski, Toby P. Breckon, Durham Univ. (United Kingdom)

Target tracking within conventional video imagery poses a significant challenge that is increasingly being addressed via complex algorithmic solutions. The complexity of this problem can be fundamentally attributed to the ambiguity associated with actual 3D scene position of a given tracked object in relation to its observed position in 2D image space. Recent work has tackled this challenge head on by returning to classical photogrammetry, within the context of current target detection and classification techniques, as a means of recovering the true 3D position of pedestrian targets within the bounds of current accuracy norms (Kundegorski & Breckon 2014)?.

A key limitation in such approaches is the assumption of posture – that the observed pedestrian is at full height stance within the scene. Whilst prior work (Kundegorski & Breckon 2014)? has shown the effects of statistical height variation to be negligible, variations in the posture of the target may still pose a significant source of potential error. A non-cooperate pedestrian target may use variations within their posture to subvert accurate localization of their position within the scene (e.g. e.g. crawling or crouching). Despite this issue, in many applications the upright stance of a pedestrian target is indeed assumed (Peng et al. 2015; Besbes et al. 2010; Dalal & Triggs 2005)?.

Here we present a method that addresses this issue via the use of regression based pedestrian posture estimation. The current posture of a pedestrian detected within the scene is estimated as a percentage of full height (maximal posture) based on the use of a Histogram of Orientated Gradient (HOG) feature extracted from each detected scene target. Performance is compared against the use of varying feature inputs including direct methods (pixel values), Sobel gradient response and contour derived Hu shape moments with the use of Support Vector Machine (SVM) and Random Forest based machine learning regression.

In contrast to prior work in the field, we leverage the key advantages of thermal-band infra-red (IR) imagery for pedestrian localization with a tracking framework (Han et al. 2013)? and demonstrate robust target localization, independent of variations in target posture (i.e. behaviour), within the statistical error bounds outlined in (Kundegorski & Breckon 2014)?. This is demonstrated for variations in pedestrian target height ranging from 0.4-2m over a distance to target range of 7-30m.

We show that the robust localization and foreground target separation, afforded via infrared imagery, that facilities accurate 3D position estimation of targets to within the error bounds of conventional Global Position System (GPS) positioning (Kundegorski & Breckon 2014)? can be extended to maintain such accuracy bounds despite variations in target posture. Based on our improved photogrammetric estimation of target position, we then illustrate the efficiency of regular Kalman filter based tracking operating on actual 3D pedestrian scene trajectories.

9652-15, Session 4

Detecting Abandoned Objects using Interacting Multiple Models

Stefan Becker, David Münch, Hilke Kieritz, Wolfgang Hübner, Michael Arens, Fraunhofer-Institut für Optronik, Systemtechnik und Bildauswertung (Germany)

In recent years, the wide use of video surveillance systems has caused an enormous increase in the amount of data that has to be stored, monitored, and processed. As a consequence, the awareness of observing all relevant events is very hard for solely human operators. Hence, it is becoming crucial to support human operators with automatic surveillance applications for notifying potentially relevant events. In order to assist human operators, this paper presents an intelligent video analysis module for real-time alerting in case of abandoned object in public spaces. The overall processing pipeline consists of two major parts. The first processing stage is the detection and tracking of person in the scene. It is reasonable to assume that the motion model of a person can change over time. For example, a person can stand still, walk, or run. Such varying characteristics are hard to describe with one model. In order to better capture the complex dynamics of a person, an Interacting Multiple Model (IMM) filter is used. The estimated states of the IMM filter serves as input for the next processing stage. In the second processing stage, the states of IMM filter,

which change according to finite-state, discrete Markow chain, are used to recognize loitering persons. Their observed positions define a region of interest and conduce as context information for a background model. The context information is used for controlling the pixel-wise update probabilities of the background model with a dynamic parameter. Thereby a too fast integration of pixels corresponding to static persons inside the background model is avoided. Detected foreground regions from the proposed context aware background model are utilized to detect abandoned object.

In case of a detected abandoned object, an alarm event is triggered. The effectiveness of the proposed system is evaluated on the PETS 2006 dataset and an own dataset, both reflecting a prototypical surveillance scenario.

9652-16, Session 5

Video content analysis on body-worn cameras for retrospective investigation

Henri Bouma, Jan Baan, Frank B. ter Haar, Pieter T. Eendebak, Richard J. M. den Hollander, Gertjan J. Burghouts, Remco Wijn, Jeroen H. C. van Rest, TNO (Netherlands)

In the security domain, cameras are important to assess the situation. Besides fixed surveillance cameras we see an increasing number of sensors on mobile platforms, such as UAV's, vehicles and persons. Mobile cameras allow rapid and local deployment, enabling many novel applications and effects. For example, recent studies showed that bodycams at the police lead to a reduction of violence and complaints by civilians.

The increased use of bodycams creates several challenges and opportunities. The growing amount of video is challenging. How can we extract information from such video, how can we perform queries, when is it advantageous to extract the information, how can an officer retrieve information efficiently? Nevertheless, such video gives the opportunity to stimulate the professionals memory and support complete and accurate reporting.

In this paper, we show how video content analysis (VCA) can address these challenges and seize these opportunities. This is done by creating a complete summary of the video which allows quick retrieval of relevant fragments. The content analysis for summarization consists of several components, such as stabilization, scene selection, motion estimation, localization, pedestrian tracking and action recognition in the video from a bodycam. The different components and visual representations of summaries are compared to assess the added value for retrospective investigation.

9652-17, Session 5

Knowledge-based video surveillance for detection of infrastructure manipulation

David Münch, Barbara Hilsenbeck, Hilke Kieritz, Stefan Becker, Ann-Kristin Grosselfinger, Wolfgang Hübner, Michael Arens, Fraunhofer-Institut für Optronik, Systemtechnik und Bildauswertung (Germany)

We are living in a world dependent on sophisticated technical infrastructure. Malicious manipulation of such critical infrastructure poses an enormous threat for all its users. Thus, running a critical infrastructure needs special attention to log the planned maintenance or to detect suspicious manipulation. In the contribution at hand, we present a knowledge-based surveillance approach to log visual observable occurrences in such an environment.

Our approach is built on several generic computer vision modules and time-space data fusion using scene dependent knowledge.

As physical manipulation of infrastructure is assumed to be done by people, the core component is a person detector and tracker. This component is based on offline learning of a general person model and online learning of the individual person's model. A second component is a modified version of an abandoned object detection method to detect physical changes in the environment caused by a present person. Finally, simple skin detection or door-status detection methods support the visual observable events. Each component of its own does not allow to make any statements about the current situation in the observed area. Instead, the sum of all components and scene knowledge has to be considered together to infer manipulation behavior.

In order to do so, we bear a relation between the expected scene behavior and the underlying basic computer vision modules.

The whole approach is qualitatively evaluated on a prototypical scenario in a server room.

9652-18, Session 5

Versatile illumination platform and fast optical switch to give standard observation camera gated active imaging capacity

Regis Grasser, Benjamin Peyronneaud, Kevin YON, Marie AUBRY, CILAS (France)

Gated active imaging associates pulse laser illumination with fast integration sensor for imaging in extremes conditions. This topic has been explored since more than a decade. Several systems have been developed and technology is today mature. Among others, gated active imaging can bring significant improvement in long range identification, image quality enhancement for bad weather conditions, observation through obscurant such as fog or smoke and 3D reconstruction. Systems in the NIR region using reliable laser sources and multi-pulse exposure already demonstrate these advantages on the field. The spread of this valuable technology to demanding applications, such as homeland security, remains limited because of the complexity and cost of current technical solutions, on the illumination side as well as on the sensor side.

Cilas, subsidiary of Airbus Defense and Space, has been working in the field of active systems for threat detection and identification for the past 15 years. Many systems have been deployed in the field and are in operation today. In order to ease the access to this technology, Cilas is working on several fronts. On the illumination side, Cilas releases a new versatile illumination platform dedicated to active imaging. Based on a highly modular patented design, high peak power laser illumination suitable for gated active imaging is possible in the NIR and/or SWIR region through a single cost effective and small footprint solution.

On the sensor side, several suitable solutions are today available in the NIR region. On the SWIR spectral band, attractive for its eye-safe properties and good atmospheric transmission, solutions remains sparse. In fact, multi-pulses exposure isn't available today and SWIR gated active imaging requires complex and expensive high energy laser sources. In synergy with its versatile illumination platform, Cilas is developing a new patented detection concept to promote gated active imaging in applications that require eye-safe SWIR operation. In order to ease the constraint and cost burden of very specific sensors, we suggest moving the critical fast optical switch function required for the gated active imaging onto a simple independent apparatus included in the reception optical train. This approach allows gated active imaging capacity on virtually any camera in NIR and SWIR regions. Based on a proprietary design inspired from cost effective adaptive optics, the fast optical shutter presents itself as a slick window capable of quickly switching from a fully reflective to a fully transparent state. Aperture time under 1µs has been obtained in NIR or SWIR region with a repetition rate above 10kHz. Because of its small form factor, this new optical shutter can be placed at the entrance pupil of a standard objective. Once synchronized with a compact illumination platform, gated

active imaging through multi pulses exposure is enabled no matter the actual camera sensor that keeps grabbing images as usual.

The association of the versatile illumination platform and the fast optical switch presents itself as an independent body, so called the "flash module", giving to classic imaging system the gated active imaging capacity in NIR and SWIR.

9652-19, Session 5

Towards a real-time wide area motion imagery system

Rob Young, Stephen B. Foulkes, QinetiQ Ltd. (United Kingdom)

It is becoming increasingly important in both the defence and security domains to conduct persistent wide area surveillance (PWAS) of large populations of targets. Wide Area Motion Imagery (WAMI) is a key technique for achieving this wide area surveillance. The recent development of multi-million pixel sensors has provided sensors with wide field of view replete with sufficient resolution for detection and tracking of objects of interest to be achieved across these extended areas of interest. WAMI sensors simultaneously provide high spatial and temporal resolutions, giving extreme pixel counts over large geographical areas. The high temporal resolution is required to enable effective tracking of targets. The provision of wide area coverage with high frame rates generates data deluge issues; these are especially profound if the sensor is mounted on an airborne platform, with finite data-link bandwidth and processing power that is constrained by size, weight and power (SWAP) limitations. These issues manifest themselves either as bottlenecks in the transmission of the imagery off-board or as latency in the time taken to analyse the data due to limited computational processing power.

This paper describes recent research to address these limitations and realise for the UK a WAMI system capable of providing real time situational awareness. The WAMI Project developed a processing architecture for applying the automatic Video Moving Target Indicator (VMTI) processing developed for ground-based applications to airborne video imagery. The aim was to achieve situational awareness over a wider area than visible from ground-based assets and to automate the analysis of airborne imagery that would be slow to analyse by human viewers.

The processing architecture was developed around a Dell Precision M6800 laptop that was used to run the QinetiQ WAMI algorithms. These algorithms were designed to track in real time moving objects observed by the Selex VigilX sensor system. The activity culminated in a trial in which the WAMI tracker was integrated into the VigilX sensor system and then deployed on board a Piper Navajo aircraft and flown in the UK during March 2014. The air trial included a data collect in short wavelength infra-red (SWIR) and long wavelength infra-red (LWIR) modalities. The laptop was used with both an on-board composite image for real time processing during collect and on the ground by the parallel processing of individual camera feeds. This demonstration proved that the Dell was capable of providing tracks at a speed commensurate with the VigilX update rate. The processing architecture is such that it can scale linearly with increasing pixel count.

In the WAMI air trial, the modified video tracking algorithms were successfully demonstrated in an airborne collect and shown to be capable of extracting salient track information, in real time, from a composite live streaming video source. This result has de-risked a key technical component on the route to realising a WAMI system that can exploit all its gathered information in real time.

9652-20, Session 5

Sensor for real-time determining the polarization state distribution in the object images

Barbara Kilosanidze, George Kakauridze, Institute of Cybernetics (Georgia); Teimuraz Kvernadze, Georgi Kurkhuli, Abastumani Astrophysical Observatory of the Ilia State University (Georgia)

An innovative real-time polarimetric method is presented based on the integral polarization-holographic diffraction element developed by us. This element is suggested to be used for real time analysis of the polarization state of light, to help highlight military equipment in a scene. In the process of diffraction, the element decomposes light incoming on them onto orthogonal circular and linear basis. The simultaneous measurement of the intensities of four diffracted beams by means of photodetectors and the appropriate software enable the polarization state of an analyzable light (all the four Stokes parameters) and its change to be obtained in real time. The element with photodetectors and software is a sensor of the polarization state. Such a sensor allows the point-by-point distribution of the polarization state in the images of objects to be determined. The spectral working range of such an element is 530 – 1600 nm. This sensor is compact, light-weight and relatively cheap, and it can be easily installed on any space and airborne platforms. It has no mechanically moving or electronically controlled elements. The speed of its operation is limited only by computer processing. This sensor is proposed to be use for the determination of the characteristics of the surface of objects at optical remote sensing by means of the determination of the distribution of the polarization state of light in the image of recognizable object and the dispersion of this distribution, which provides additional information while identifying an object. A theoretical model showing the connection of the Stokes parameters of light reflected from a recognizable object with the characteristics of the material of the reflecting surface of the object has been developed that allows the appropriate correlation connections to be set. Experimentally the possibility of obtaining the distribution of the values of the Stokes parameters is shown for the samples from different materials and of a different geometric form. The possibility of detection of a useful signal of the predetermined polarization on a background of statistically random noise of an underlying surface is also possible with presence of appropriate database. The application of such a sensor is also considered for the determination of the distribution of stressed state in different constructions based on the determination of the distribution of the polarization state of light reflected from the object under investigation. A compact laboratory model was developed for the realization of this method. The correlation relations between the change in the polarization state of light reflected from the sample with the distribution of the dosated mechanical stresses is considered. The theoretical model is developed. The experimental results are shown for different samples with stress distribution from different materials both transparent and opaque, metals and dielectrics. The method is nondestructive and will enable the distance monitoring and diagnosis of already existing constructions and objects to be carried out that is important for the prevention of natural disasters. In comparison with existing methods of nondestructive stress analysis the proposed method will differ by universality, simplicity, technological effectiveness, high speed and comparative cheapness, which conditions its competitiveness.

9652-24, Session 5

Multi-feature based robust face detection and coarse alignment method via Multiple Kernel Learning

Bo Sun, Di Zhang, Jun He, Lejun Yu, Xuewen Wu, Beijing Normal Univ. (China)

Abstract- Face detection and alignment are two crucial tasks to face recognition which is a hot topic in the field of defense and security, whatever for the safety of social public, personal property as well as information and communication security. Common approaches toward the treatment of these tasks in recent years are often of three types: template matching-based, knowledge-based and machine learning-based, which are always separate-step, high computation cost or fragile robust. For deep study, we first collected about 5000 face images without hats of 150 Chinese via webcams or cameras in wild, whose sample figures are given in the paper. After analyzing, we propose a novel face detection and coarsely alignment method, which is inspired by those three types of methods. Firstly, different features of shape, color and texture are extracted from forehead sample images, based on which more discriminative ones are selected and combined by the Multiple Kernel Learning (MKL) algorithm. Thus, a model for effectively detecting a forehead is trained, with which a head can be roughly located. Then with skin detection and ellipse fitting methods, we can obtain a face and its offset parameters, hence coarsely align. For testing, we train our model with 1000 images (half positive, half negative samples). Finally, we take 500 face images as test samples, and compare the result of the proposed method along with some related methods (Viola and Jones, 2004; Felzenszwalb et al,. 2010; Xiangxin Zhu et al,. 2012). This demonstrates that the proposed method to outweigh the state-of-art methods for its highly-effective detection rate as well as the simultaneously aligning face function. Except for the method, experimental scheme and result, the application conditions and further research of the proposed method are also given in the paper.

This work is supported by the Fundamental Research Funds for the Central Universities of China (2014KJJCA15, 2012YBXS10).

9652-21, Session 6

Robust heuristic features for face recognition

Dakshina Ranjan R. Kisku, National Institute of Technology, Durgapur (India); Phalguni Gupta, Indian Institute of Technology Kanpur (India); Jamuna K. Sing, Jadavpur Univ. (India)

Face recognition is considered as one of the most dynamic and complex research areas in machine vision and pattern recognition due to the variable appearance of face images. Changes in appearance may occur due to many factors, such as facial attributes compatibility complexity, the motion of face parts, facial expression, pose, illumination and partly occlusion. As a result face recognition problem become ill-posed. SURF (Speeded up robust features) descriptor is a robust image descriptor. It can be used in computer vision tasks like object recognition or 3D reconstruction. It is known as the improved version of the SIFT (Scale Invariant Feature Transform) descriptor. The standard version of SURF is several times faster than SIFT and more robust against different image transformations than SIFT. SURF is based on sums of 2D Haar wavelet responses and makes an efficient use of integral images. As basic image features it uses a Haar wavelet approximation of the determinant of Hessian blob detector. Differences in facial expression, head pose, illumination, and partly occlusion may result to variations of facial characteristics and attributes. To capture the face variations, face characteristics of dynamic and static parts are further fused by concatenation with the detected SURF interest points extracted from localized mouth, eyes and nose facial parts. The proposed technique has made an attempt to handle this problem. It has been determined that when the face matching accomplishes with the whole face region, the global features (whole face) are easy to capture and they are generally less discriminative than localized features. In the proposed face recognition method, local facial landmarks are considered for further processing. The optimal face representation using SURF descriptor on local landmarks then allows matching the localized facial features efficiently.

This paper proposes a local feature based face recognition technique which makes use of dynamic (mouth) and static (eyes, nose) salient features as limited physiological information of face obtained through SURF descriptor. It makes use of standard facial component detection algorithm to extract salient facial parts such as eyes, mouth and nose from face image. Scale and rotation Invariant SURF feature descriptor is then used on each of these facial parts to detect invariant points and further a heuristic algorithm is applied to invariant features set to select best features from each salient area. Finally, algorithm fuses best heuristic features determined from all salient parts. Matching of two faces is accomplished by using distance metrics with a pair of corresponding fused feature vectors. Matching scores obtained from verification module are then characterized by Doddington's user-dependent matcher reliability method and the relevance of individual matchers towards more efficient and robust performance is determined by wolf and lamb factors. It has been estimated that, both these factors can decrease the performance of any biometric system by accepting more and more imposters as false accept. In Doddington's concept, for user weighting, the users who can imitated labeled as lambs, i.e., imposters can provide biometric cues that are similar to that of lambs. Wolves on the other hand can successfully imitate some other users. The proposed techniques are evaluated with three face databases, namely, FERET, ORL, BANCA and IITK face databases.

9652-22, Session 6

SIFT fusion of kernel eigenfaces for face recognition

Dakshina Ranjan R. Kisku, National Institute of Technology, Durgapur (India); Massimo Tistarelli, Univ. degli Studi di Sassari (Italy); Phalguni Gupta, Indian Institute of Technology Kanpur (India); Jamuna K. Sing, Jadavpur Univ. (India)

Faces are highly challenging and dynamic objects used as biometric evidences which have been successfully used in various application areas such as identity verification of human beings, face matching, face detection in gatherings, face image retrieval, etc. There are various ways to represent face characteristics which have sufficient information to distinguish two faces. Amongst the most popular techniques of face descriptions for face recognition, feature based techniques are found to be quite impressive.

In this paper, we investigate an application that integrates holistic appearance based method and feature based method for face recognition. The automatic face recognition process which makes use of multiscale Kernel PCA characterized approximated face image and reduced number invariant SIFT keypoints extracted from face projected feature space. To achieve higher variance in the inter-class face images, we compute equidistant principal components to project a face image onto some approximated kernel eigenfaces and reduced feature spaces. As long as feature spaces retain their distinctive characteristics, reduced number of SIFT points are detected for a number of principal components and keypoints are fused in terms of matching scores determined from face matching processes on a set of feature vectors. The proposed method is tested on UMIST and ORL face databases, and the efficacy of the system is proved by the test results computed in cloud computing environment.

9652-23, Session 6

FRIT characterized hierarchical kernel memory arrangement for multiband palmprint recognition

Dakshina Ranjan R. Kisku, National Institute of Technology, Durgapur (India); Phalguni Gupta, Indian Institute of Technology Kanpur (India); Jamuna K. Sing, Jadavpur Univ. (India)

Due to low-cost, user-friendly and reliable one, palmprint recognition has been established itself a very accurate solution for a range of access control applications and identity verifications. Several studies on palmprint recognition have been made for improving performance of the system by palmprint images taken under visible light. However, in the last few years, thrust for robust palmprint system has begun with multispectral palm images. These multispectral palm images which are captured under visible and infrared light with different wavelengths show best substitution of visible ones by improving system performance further with very little error rates.

In this paper, we advocate a hierarchical kernel associative memory (KAM) based computational model for robust multispectral palmprint recognition with finite Ridgelet transform representation. To characterize multispectral palmprint image, Finite Ridgelet Transform is used to achieve a very compact representation of linear singularities and the FRIT captures the singularities along lines and edges. Finite Ridgelet Transform is used to represent the multispectral palmprint image and it is then modeled by Kernel Associative Memories. Finally recognition scheme is thoroughly tested with a benchmarking multispectral palmprint database CASIA. For recognition purpose Bayesian classifier is used. The experimental results exhibit robustness of the proposed system under different wavelengths.

Conference 9652B: Optical Materials and Biomaterials in Security and Defence Systems Technology

Wednesday 23 September 2015

Part of Proceedings of SPIE Vol. 9652 Optics and Photonics for Counterterrorism, Crime Fighting, and Defence XI; and Optical Materials and Biomaterials in Security and Defence Systems Technology XII

9652-48, Session PS

Luminescence properties of new heavy metals complexes *(Invited Paper)*

Gabriela Wiosna-Salyga, Ewelina Witkowska, Beata Łuszczynska, Ireneusz Glowacki, Ireneusz Kownacki, Bogdan Marciniec, Jacek Ulanski, Lodz Technical Univ. (Poland)]

No Abstract Available

9652-45, Session PS

Optical properties of polymethacrylate with styrylquinoline side chains

Beata J. Derkowska-Zielinska, Nicolaus Copernicus Univ. (Poland); Viviana Figà, University of Palermo (Italy); Oksana Krupka, Vitaliy Smokal, National Taras Shevchenko Univ. of Kyiv (Ukraine)

Photochromic materials have potential applications for information storage, the controlled on/off digital switching of synthesized molecules by photo-irradiation. Styrylquinolines and their analogues are well-known for their photochemical and photophysical properties. The interesting aspect concerning styrylquinoline and polymers based on them due to their possibility to transform between the generally stable trans form and the metastable cis form upon exposure of the light or thermal stimulation. The isomerization process of styrylquinoline containing compounds plays significant role in the unique optical properties of materials. Therefore, styrylquinoline containing compounds can be used in advanced micro- and nanotechnologies.

The styrylquinaline containing derivatives were synthesized and their structures determined by UV- and HNMR- spectroscopies. The polymerization was carried out in DMF with AIBN as initiator. The products of polymerization were characterized by HNMR, GPC, DSC. The trans – cis isomerisation for styrylquinaline containing polymers have been investigated in solutions and solid state at 365 nm wavelength

9652-46, Session PS

Proposal of all-optical sensor based on nonlinear MMI coupler for multi purpose usage

Mehdi Tajaldini, Mohamad Zubir Mat Jafri, Univ. Sains Malaysia (Malaysia)

In this study, we propose an all-optical sensor based on consideration the nonlinear effects on modal propagation and output intensity based on ultra-compact nonlinear multimode interference (NLMMI) coupler. The sensor can be tuned to highest sensitivity in the wavelength and refractive index ranges sufficient to detect water- soluble chemical, air-pollutions, and heart operation. The results indicate high output sensitivity to input wavelength. This sensitivity guides us to propose a wave sensor both transverse and longitudinal waves such as acoustic and light wave, when an external wave interacts with input waveguide. For instance, this sensor can be implemented by long input that inserted in the land, then any wave could detected from earth. The visible changes of intensity at output facet in various surrounding layer refractive index show the high sensitivity to the refractive index of surrounding layer that is foundation of introducing a sensor. Also, the results show the high distinguished changes on modal expansion and output throat distribution in various refractive indices of surrounding layer.

9652-47, Session PS

Controlled release of anti-cancer agents from nanoparticle surface by optimizing the prodrug designs

Yoshikazu Ikuta, Yoshitaka Koseki, Tsunenobu Onodera, Hidetoshi Oikawa, Hitoshi Kasai, Tohoku Univ. (Japan)

Controlled release of anti-cancer agent from nano-sized drug have very important role for cancer treatment by drug delivery systems (DDS) so as to decrease the drug dose and side effects. One of the possible strategy for controlled release of active agent is optimization of prodrugs designs composed of nanoparticles. In this article, we prepared four kinds of podophyllotoxin (PPT) dimer (C4, C10, C18 and SS) having different carbon chain length or bonding mode in linker and fabricated the nanoparticles consisting of only resulting PPT dimers by the reprecipitation method, which is a fabrication technique of organic nanocrystals. As a result, the cytotoxicities of PPT dimer nanoparticles became increasing as the linker length of PPT dimer became shorter, and PPT dimer SS nanoparticles showed the effective anti-cancer activity, compared with that of PPT dimer C10 in spite of having same linker length. And then, it was found that the release rate of PPT from PPT dimer nanoparticles was increased when the length of linker was decreased and the disulfide bond was incorporated into linker by evaluation of degradation rate using esterase and reductant agent. Those results indicated that cytotoxicity of PPT dimer nanoparticles well agreed with release rate of PPT. In other words, control of anti-cancer activity and degradation rate of PPT dimer nanoparticles could be easily achieved by changing the linker types of dimer compounds. In the future, this strategy can be potent tool for cancer treatment as DDS.

9652-30, Session 5

DNA as a novel material toward electronics and photonics *(Keynote Presentation)*

Norihisa Kobayashi, Chiba Univ. (Japan)

DNA, a unique one-dimensional biopolymer with the sequence of four bases, plays an important role for all livings, and is well known to have information in itself with an address of 0.34 nm base-pair pitch. DNA has been collecting a lot of interest as a functional material since DNA forms complex with functional molecules such as organic dyes, metal complexes and conductive polymers through electrostatic binding, intercalating and groove binding. These interaction modes in DNA with highly ordered structure give unique complex structure, resulting in the attractive electronic and photonic functions. In this paper, we would like to introduce our recent results on the application of DNA to several aspects of electronics and photonics such as light emitting materials and device, memory devise and so on. These devices have demonstrated attractive performance which exceeds that of common devices made with currently available organic based materials.

9652-31, Session 5

Bio-mediated synthesis and spectroscopic studies of gold nanoparticles *(Invited Paper)*

Katarzyna Matczyszyn, Magdalena Klekotko, Irena Maliszewska, Joanna Olesiak-Banska, Wroclaw Univ. of Technology (Poland); Jakub Siednienko, Krzysztof Pawlik, Institute of Immunology and Experimental Therapy (Poland); Marek Samoc, Wroclaw Univ. of Technology (Poland)

This work presents the bio-mediated synthesis of gold nanoparticles (GNPs) using plant (Mentha piperita) extract or fungi cell-free filtrate (Trichoderma koningii) [1]. The synthesis was monitored by UV–Vis absorption spectroscopy and transmission electron microscopy (TEM) and the best conditions of forming various shapes were found. Reduction of gold ions with the plant extract results in the production of nanoparticles with spherical, triangular and hexagonal shapes and sizes ranging from 10 to 200 nm. The kinetics of the reaction was studied in various conditions of the synthesis. We have separated different sizes and shapes of gold nanoparticles from the obtained mixture using centrifugation in sucrose density gradient. The cytotoxicity of the obtained GNPs was studied by performing MTT assay. The results revealed that the biologically synthesized nanoparticles are less toxic than those synthesized using the chemical methods. Moreover the nanoparticles made with the use of the cell-free filtrate of Trichoderma koningii were applied, in combination with methylene blue, for an effective phototherapy of Staphylococcus epidermidis. We compared the results of the phototoxicity of the chemically synthetized gold nanoparticles and those made with the use of Trichoderma koningii, with the addition of methylene blue molecules, upon irradiation with a Xe lamp and He-Ne laser light. The effective kill of bacteria was achieved after illumination of the system containing bacteria, biogenic gold nanoparticles and methylene blue, this being the best result obtained for this kind of therapies. We observed also the luminescence of the biosynthesized nanoparticles, not seen in the chemically made nanostructures. Our results constitute important information about the behavior of biosynthesised colloidal gold nanoparticles under Xe lamp and laser illumination.

Acknowledgements

The authors acknowledge financial support from the National Science Centre Opus grant no. DEC-2013/09/B/ST5/03417. The work was financed by a statutory activity subsidy from the Polish Ministry of Science and Higher Education for the Faculty of Chemistry of Wroc?aw University of Technology.

References

[1] I. Maliszewska, A. Le?niewska, J. Olesiak-Ba?ska, K. Matczyszyn, M. Samo?, Biogenic gold nanoparticles enhance methylene blue-induced phototoxic effect on Staphylococcus epidermidis, Journal of Nanoparticle Research 16 2457 (2014)

9652-32, Session 5

Image processing by protein-based visual receptive fields *(Invited Paper)*

Yoshiko Okada-Shudo, Univ of Electro-Communications (Japan)

The potential ability of photo-sensitive protein bacteriorhodopsin (bR) to exhibit both excitation and inhibition has been applied to construct bR receptive field. We have exploited bR characteristics to fabricate artificial ganglion and simple receptive fields consisting of two oppositely coated bR films. We have demonstrated that such receptive fields, DOG and Gabor filter, are capable of analog image processing. Such bR receptive fields can subtract and differentiate operations without an additional external connection. In the computational approach, it was shown that it can mimic some functions that is used in the brain.

9652-33, Session 5

Different strategies for the detection of bioagents using electrochemical and photoelectrochemical genosensors

Ilaria Palchetti, Diego Voccia, Francesca Bettazi, Univ. degli Studi di Firenze (Italy)

The need for rapid, reliable, specific, and sensitive methods of detecting pathogens, at low cost, is the focus of a great deal of research [1]. To meet expectations of users, analytical methods for pathogen detection must have the specificity to distinguish between different bacteria, the adaptability to detect different analytes, and the sensitivity to detect bacteria on-line and directly in real samples without preenrichment [1]. The device must also be simple and inexpensive to design and manufacture. (Bio)sensor technology is claimed to satisfy these requirements [1].

In recent years various kinds of electrochemical biosensors based on identification of the bacterial nucleic acid have been developed [2]. The development of DNA-based biosensors for the detection of specific nucleic acid sequences consists in the immobilization, onto the surface of a chosen transducer, of an oligonucleotide with a specific base sequence called the probe. The complementary sequence (target) present in the sample solution is recognized and captured by the probe through the hybridization reaction. The evaluation of the extent of the hybridization allows one to confirm whether the sample solution contains the complementary sequence of the probe or not. Electrochemical transducers have received considerable attention in connection with the detection of DNA hybridization. Moreover, recently, with the emergence of novel photo- electrochemically active species and new detection schemes, photoelectrochemistry has resulted in substantial progress in its analytical performance for biosensing applications.

Different electrochemical approaches of pathogen and toxin detection using nucleic acid based electrochemical biosensors have been proposed by our group, recently [3]. In this work, we propose a photoelectrochemical method for DNA/RNA detection based on a semiconductor electrode and an elaborate in situ production of ascorbic acid (AA) as electron donor under alkaline phosphatase (ALP) catalytic activity. Increased DNA/RNA concentration leads to the enhanced ALP loading and thus boosts the AA generation from phosphorylated ascorbic acid. In presence of AA, the enhanced anodic photocurrents can be monitored upon visible-light irradiation at 450 nm. Different DNA/RNA targets have been investigated. The main part of the work has been devoted to the characterization of the proposed method in terms of reproducibility and sensitivity.

[1] I. Palchetti, M. Mascini, Anal Bioanal Chem, 2008, 391, 455–471

[2] I. Palchetti, M. Mascini, Nucleic Acid Biosensors for Environmental Pollution Monitoring, 2011, Palchetti & Mascini eds., RSC, London DOI 10.1039/9781847559524

[3] S. Laschi, R. Miranda-Castro, E. González-Fernández, I. Palchetti, F. Reymond, J. S. Rossier, G. Marrazza, Electrophoresis, 2010, 31, 3727-3736

9652-34, Session 6

Bio-inspired materials for electrochemical devices *(Keynote Presentation)*

Agnieszka Pawlicka, Univ. de São Paulo (Brazil); Alessandra Firmino, Franciani C Sentanin, Rodrigo C Sabadini, David Q Jimenez, Cristiano C Jayme,

Universidade de Sao Paulo (Brazil); Mihaela Mindroiu, Roxana G Zgarian, Gratiela Tihan, Ileana Rau, University Politehnika of Bucharest (Romania); Maria M. Silva, Univ. do Minho (Portugal); Anna Flavia Nogueira, UNICAMP (Brazil); Jerzy Kanicki, Univ. of Michigan (United States); François Kajzar, Ecole Normale Supérieure de Lyon (France)

Natural macromolecules are very promising row materials to be used in modern technology including security and defense. There are abundant in nature, easy extracted and possess biocompatibility and biodegradability properties. Besides medical applications, they started to be tested in electrochemical devices, mainly as ionically conducting membranes. These membranes can be obtained using polysaccharides, proteins and DNA throughout chemical or physical modifications, such as crosslinking or plasticization processes. The membranes can be doped with different inorganic salts, including lithium and rare earth ones, ionic liquids, organic and inorganic acids or other macromolecules. As an example, the gelatin-, polysaccharides- and DNA-based membranes show very good ionic conductivity values of about 10-3-10-5 S/cm, have predominantly amorphous structure, high transparency in the visible range of 80-90% and 3 to 5 V electrochemical window. Blends of gelatin, polysaccharides and DNA with other macromolecules such as poly(ethylene dioxythiophene) (PEDOT), poly(ortho etoxy aniline) (POEA) and gelatin, among others were also obtained and characterized by electrochemical measurements, thermal analysis and microscopy. The membranes can be colored or colorless and can be applied in electrochemical devices, such as electrochromic (ECDs) or dye sensitized solar cells (DSSC). ECDs change the color under applied potential, so they can modulate the intensity of transmitted light of 15 to 35%. As the electrochromic materials are usually blue colored, such as WO3 or Prussian blue (PB), the color change is from transparent to blue. However, new researches show that it is possible to combine colors and obtain green-yellow reflective ECDs, which can be applied in active camouflage. DNA, DNA-CTMA, DNA-DODA and DNA-PEDOT:PSS were also investigated as either hole carrier material (HTM) or polymer electrolytes in dye-sensitized solar cells (DSSC). The DNA-based samples as HTM in small DSSCs revealed a solar efficiency of 1.49%. Polymer electrolytes of DNA-CTMA and DNA-DODA, both with 9 and 10 wt% of LiI/I2 applied in small DSSC exhibited the efficiency of 0.14, 0.31, 0.18 and 0.66%, respectively. The obtained results show that natural macromolecules-based membranes are not only environmentally friendly but also promising materials to be investigated for several electrochemical devices; however, to obtain better results still more research should be performed.

9652-35, Session 6

Absorption spectrum analysis based on singular value decomposition for photoisomerization and photodegradation in organic dyes *(Keynote Presentation)*

Yutaka Kawabe, Toshio Yoshikawa, Toshifumi Chida, Kazuhiro Tada, Chitose Institute of Science and Technology (Japan); Masuki Kawamoto, Takashi Fujihara, Takafumi Sassa, RIKEN (Japan); Naoto Tsutsumi, Kyoto Institute of Technology (Japan)

In order to analyze the spectra of inseparable chemical mixtures, many mathematical methods have been developed to decompose them into their components from series of spectral data obtained under different conditions. We formulated a method based on singular value decomposition (SVD) in linear algebra, and applied it to two example systems of organic dyes, being successful in reproducing absorption spectral components assignable to cis/trans azocarbazole dyes after photoisomerization and to monomer/dimer of cyanine dyes in photodegaradation process. From the temporal evolution of each component, we discussed the mechanism of holographic characteristics of azocarbazoe derivatives, and the origin of superior durability of fluorescent dyes in DNA-complexes.

For the example of photoisomerization, polymer films containing azocarbazole dyes, namely 3-[(4-nitrophenyl)azo]-9H- carbazole-9-ethanol (NACzEtOH) and 3-[(4-cyanophenyl) azo]-9H- carbazole-9-ethanol (CACzEtOH) were prepared, since these materials have showed updatable holographic stereogram for real images with high performance. Origin of their mechanism had been mainly attributed to the photoorientation processes triggered by photoisomerization from the holographic characteristics like optical diffraction and photoinduced birefringence. Recently, we made continuous monitoring of absorption spectrum after optical excitation and found that their spectral shapes varied slightly during recovery process, of which fact suggested the contribution from a generated photoisomer. Application of the method was successful to identify two spectral components due to trans and cis forms of azocarbazoles which were coincident with the theoretical results obtained by a molecular orbital calculation. Temporal evolution of their component weight factors suggested important roles of long lifetimed cis states in both azocarbazole derivatives instead of photoorientation effects as having been believed.

We also applied the method to the photodegradation of cyanine DiQC2(1) and carbocyanine DiQC2(3) doped in DNA-lipid complexes which have shown more efficient and durable optical amplification and/or lasing under optical pumping than the same molecules embedded in a conventional PMMA matrix. When concentration of the dyes was high, their absorption spectra were composed of spectra due to monomer and H-type aggregation which might be dimer. Although their initial spectral shapes and their temporal evolution strongly depended on the type of matrix, the same SVD method was successful in extraction of two spectral components originating in monomer and dimer, showing that monomer population was initially greater in DNA-complex but the dimer occupied larger part in PMMA. During the photodegradation process, absorption magnitude gradually decreased due to decomposition of molecules and their decaying rates strongly depended on the spectral components, that is, dimer band in PMMA diminished much faster than monomer, suggesting that the long persistency of the dyes in DNA-complex related to weak tendency of aggregate formation.

9652-36, Session 6

Hybrid, organic-inorganic composites for applications in Vis-NIR photodiodes *(Invited Paper)*

Beata Luszczynska, Jacek Ulanski, Lodz University of Technology (Poland); Piotr Bujak, Adam Pron, Warsaw Univ. of Technology (Poland)

Near-infrared (NIR) and short-wave infrared (SWIR) photodiodes are the main constructive element of the light sensing devices for multiple applications such as telecommunications, short-wave infrared imaging, and night vision. The use of the inorganic nanocrystals for the construction of photodiodes offer the extending of the sensitivities to the longer wavelengths up to 3000 nm. The nanocrystals may act as the sensitizers in the photosensing system, not taking part in the charge transport. Nevertheless the use of nanocrystalline photosensitizer require appropriately designed polymeric compounds, acting as the matrix for nanocrystals. Such matrix provide functional interface extracting charge carriers and effectively transporting them to the proper electrodes. The majority of QDs reported in literature contain chemical elements such as Cd, Pb or Hg that are hazardous for human health and the environment, what constitute an important problem to dissolve. The main aim of this project is to obtain solution-processable active materials for Visible and NIR-sensitive photodiodes based on greener NPs compositions (Cd- and Pb- free) combined with conjugated polymers whose chemical structure allows efficient photodiode operation and long-term stability of the

devices in air-working conditions. We will present of novel synthetic strategies of: Cd- and Pb-free semiconducting colloidal nanoparticles with controlled size and morphology for the application in photodiodes. We will also present the work parameters of the selected type of photodiodes containing Cd- and Pb-free nanoparticles.

9652-37, Session 6

Fabrication and characterization of an inkjet-printed DNA biopolymer-based UV photodetector *(Invited Paper)*

Jack P. Lombardi III, Air Force Institute of Technology (United States); Roberto S. Aga Jr., Emily M. Heckman, Carrie M. Bartsch, Air Force Research Lab. (United States)

The performance of a printable, ultraviolet (UV) photoconducting biopolymer is investigated for UV photodetectors of varying layer thicknesses. The biopolymer is formed from deoxyribonucleic acid (DNA) with the addition of the Clevios P formulation of poly(3,4-ethylenedioxythiophene)-poly(styrenesulphonate) (PEDOT:PSS) and hexadecyltrimethyl-ammonium chloride (CTMA); it is then combined with phenyl-C61-butyric acid methyl (PCBM) to make a printable, UV photoconducting material. The highest measured responsivity of the photodetectors is 1.2 mA/W at 20 V bias using a 260 nm source.

9652-38, Session 7

High sensitive magnetic sensors from organic nonlinear magneto-optic materials *(Keynote Presentation)*

André P. Persoons, KU Leuven (Belgium) and Univ. of Arizona (United States)

The extremely large Faraday rotation, even a ferromagnetic transition at cryogenic temperatures, as observed in regioregular poly(3-alkyl)thiophenes has resulted in the development of extremely sensitive magnetic sensors even if the mechanism of these magnetic effects remain still largely unexplained. These remarkable results, and the quality of the sensors already realized, spurred intense research for new materials with still higher magnetic sensitivities for Faraday rotation.

New and recently developed materials based upon macrocycles of thiophenes in solution will be discussed. As guidance for their synthesis we used an extremely simple model to explain the magnetic effects. This model, an electron-on-a-conducting ring, stresses the importance of persistent currents in nano- or mesoscopic rings which can be realized as macrocycles from (semi)conducting thiophenes by chemical synthesis. Synthesis and properties of such rings will be discussed. The expected magnetic properties of organic macrocycles and cyclic structures are potentially related to the strong Faraday rotation effects observed in these polymers.

Detailed calculation on the ϖ-electron distribution in macrocycles of regioregular and regiodefect 10-ring thiophenes will be presented and related to persistent currents as previously shown to be present in mesoscopic rings of (not superconducting) metals. The use of SQUID measurements on these macrocycles to investigate the possibility of fluctuating magnetic moments in these new molecular structures will be presented. These magnetic moments, fluctuating or even persistent, could be the cause of the giant Faraday rotation effects observed, as well as the ferromagnetism observed in regioregular poly(3-alkyl)thiophenes.

The potential of the ultrasensitive magnetic sensors already developed will be highlighted by examples in the biomedical field. An example of the use of these sensors for adult and fetal Magnetic Cardio Graphy (MCG) will be presented, as well as the important applications for Magneto Encephalo Graphy (MEG). The extreme sensitivity of these new sensors, allowing measuring to 100 femtoTesla, may supersede SQUID techniques for MEG, with the important bonus of ease of applicability and low cost.

9652-40, Session 7

Influence of various solvents on the nonlinear optical properties of metallophthalocyanines (MPcs) *(Invited Paper)*

Beata J. Derkowska-Zielinska, Nicolaus Copernicus Univ. (Poland)

The aim of this work was to learn how the influence of various solvents correlates with nonlinear optical properties of metallophthalocyanines (MPcs). The methods, which were used to measure nonlinear optical properties, were degenerate four wave mixing (DFWM) and nonlinear transmission (TNL) [1-2]. We used ethanol, chloroform, DMSO and THF as solvent of metallophthalocyanines.

The absorption spectra of MPcs solutions present a narrow Q-band in the visible region and a relatively wide B-band in the near ultraviolet. Nonlinear optical properties of MPcs solutions change with using different solvent. In all cases we observed the solvatochromism effect.

9652-49, Session 7

Ultrafast conformational changes in biomolecules studied by time-resolved circular dichroism *(Invited Paper)*

Pascale Changenent-Barret, Francois Hache, Lab. d'Optique et Biosciences (France)

Circular dichroism (CD), the difference in absorption for a left or a right circularly polarized light, is with optical rotation a unique optical characteristics of chiral molecules. Because chirality is primarily a geometrical property, CD is in turn very sensitive to the conformation of molecules. This feature makes CD an attractive probe for stereochemistry and especially for the study of biomolecules. Taking advantage of our knowledge in ultrafast optics and nonlinear optical properties of chiral molecules, we have developed new experimental schemes allowing such time-resolved CD measurements in order to investigate the dynamics of the conformational changes in molecules or biomolecules. In particular, we have extended the wavelength range to the far-UV where much information about the secondary structure of proteins is available.

For very short time resolution, we have developed a classical pump-probe set-up with a sub-picosecond laser source tunable in the far ultraviolet. The laser source is based on several stages of optical parametric amplification and sum-frequency generation and yields pulses tunable between 220 and 350 nm. The originality of the set-up is that it is CD and not merely absorption which is measured as a function of the pump-probe delay. Two techniques were implemented, either by directly modulating the probe polarization from right to left circular with a longitudinal Pockels cell, or by measuring the probe beam ellipticity with a Babinet-Soleil compensator. The first technique is more direct but it suffers from many artifacts whereas the second one which requires more acquisitions, is much more robust. Comparison of the two techniques will be addressed. The time resolution of the set-up is about 2 ps. Application to the very first step of photoinduced conformational changes in Photoactive Yellow Protein will be presented.

We have also developed a T-jump experiment allowing the study of protein denaturation. T-jump consists in heating up the water with a nanosecond pulse. Monitoring the CD as a function of time (> 10 ns) allows us to follow quantitatively

the helicity of the samples and to observe the very first steps of protein folding. In this experiment, UV probe is obtained by frequency-quadrupling the output of an 82 MHz Titanium-Sapphire laser. This set-up is used to investigate the thermodynamic and kinetic parameters of thermal denaturation of model polypeptides.

F. Hache, "Invited featured article : Application of time-resolved circular dichroism to the study of conformational changes in photochemical and photobiological processes" J. Photochem. Photobiol. A 204, 137-143 (2009).

L. Mendonça, F. Hache, P. Changenet-Barret, P. Plaza, H. Chosrowjan, S. Taniguchi, and Y. Imamoto, Ultrafast carbonyl motion of the Photoactive Yellow Protein chromophore probed by femtosecond circular dichroism, J. Am. Chem. Soc. 135, 14637 (2013).

J. Duboisset, A. Deniset-Besseau, E. Benichou, I. Russier-Antoine, N. Lascoux, C. Jonin, F. Hache, M. C. Schanne-Klein, and P. F. Brevet, A bottom-up approach to build the hyperpolarizability of peptides and proteins from their amino acids, J. Phys. Chem. B 117, 9877-9881 (2013).

L. Mendonça, A. Steinbacher, R. Bouganne, and F. Hache, Comparative study of the folding/unfolding dynamics of poly(glutamic acid) in light and heavy water, J. Phys. Chem. B 118, 5350-5356 (2014).

9652-41, Session 8

Photoisomerisation, luminescent and nonlinear optical properties of selected derivatives of pyrazoline *(Keynote Presentation)*

Jaroslaw Mysliwiec, Adam Szukalski, Andrzej Miniewicz, Wroclaw Univ. of Technology (Poland)

Currently, main topic of the research is related to the useful and multifunctional materials for photonic applications. Materials which have interesting optical and nonlinear optical (NLO) properties can be used in many kinds of applications, e.g., all optical switches and memories or in laser technology. Moreover, mainly the organic compounds are the most desirable type of photonic materials because of their features (easy manufacturing, low costs of fabrication and biodegradability).

Inspiration of studies in this specific group of materials was (1,1-dicyanoethenyl)-1-phenyl - 4,5 -dihydro-1H-pyrazole (DCNP) compound, which characterized by interesting and useful optical properties described in literature. New synthesized group of pyrazoline derivatives (PRDs) were investigated. They have different kind of additional electron acceptor groups (nitrile or nitro). PRDs were suspended in poly(methyl methacrylate), which serves as a matrix.

Here we report on experimental results of dynamic photoinduced changes of birefringence done in Optical Kerr Effect experimental set-up and light amplification such a stimulated emission and random lasing. Results obtained from the conducting third order nonlinear process and light amplification indicate broad field of possibly applications.

9652-42, Session 8

Plasmonic fluorophores: influence of the nanoantenna shape and cristallinity *(Invited Paper)*

Céline Fiorini-Debuisschert, Commissariat à l'Énergie Atomique (France)

No Abstract Available

9652-43, Session 8

Pharmacological activities of pure nanodrugs created by the reprecipitation method

Hitoshi Kasai, Tohoku Univ. (Japan)

Generally, chemical compounds that are synthesized for use as drugs are modified by introducing hydrophilic substituents to the compounds to increase their water solubility. On the contrary, we have worked up our plan that the compounds whose solubility to water becomes as low as possible can be useful for making drug nanoparticles. This novel idea goes in the contrary of the conventional approach undertaken in the synthetic chemistry of medicine: nevertheless will get to the core point of the size control in organics.

Based on the completely opposite idea to the conventional one, in this presentation, we propose a new concept, termed "pure nano-drugs" (PNDs), which are comprised of drug ingredient and are delivered into cells in a carrier-free state without using polymer. As the first model of PNDs, the nanoparticles of dimer compounds of SN-38 having the high anticancer activity were fabricated with approximately 50 nm in size by chemical nanotechnology, which was combined with (a reprecipitation method developed at our laboratory) and chemical modification of the dimerization in order to decrease the solubility to water. This aqueous dispersion of SN-38 dimer nanoparticles has been shown to exhibit an extremely effective anti-cancer activity, when compared to irinotecan, a prodrug of SN-38 and a widely used water-soluble anticancer monomer. And then the PNDs composed of the drug compounds with hydrophobic substituents also were fabricated and their pharmacological activities were clarified. The use of the PNDs with lower concentration is expected to reduce the harmful side effects commonly associated with conventional anticancer agents. In the future, the concept and technology of PNDs would be applicable to various other types of compounds in addition to drugs.

9652-44, Session 8

Enhanced nonlinearity of nonlinear optic polymers using nucleobases as charge blocking layers *(Invited Paper)*

François Kajzar, Univ. Politehnica of Bucharest (Romania); Fahima Ouchen, Emily M. Heckman, Air Force Research Lab. (United States); Larry R. Dalton, Univ. of Washington (United States); James G. Grote, Air Force Research Lab. (United States)

No Abstract Available

Conference 9653: Target and Background Signatures

Wednesday - Thursday 23–24 September 2015

Part of Proceedings of SPIE Vol. 9653 Target and Background Signatures

9653-32, Session PS

A road extraction algorithm with saliency analysis in high-resolution remote sensing images

Libao Zhang, Shuang Wang, Shiyi Wang, Beijing Normal Univ. (China)

There is plenty of complex ground information in high-resolution remote sensing images. The direct segmentation-based extraction of roads in that kind of images will cause low accuracy and cannot rule out inferences such as residential areas. In this paper, we propose a road extraction method based on saliency analysis for high-resolution remote sensing images, which can remove the interference of residential areas effectively and acquire roads accurately. Firstly, the Otsu segmentation is employed to remove the background information so that we can acquire a feature map of residential areas and roads. Then, we use the human visual system to obtain a saliency map of residential areas. The feature map of residential areas is generated by segmenting the saliency map. Finally, the roads are extracted by the logical XOR operation of the two feature maps. Experimental results show that our proposed method can remove the residential areas effectively and extract roads perfectly and will have both theoretical and practical significance for road extraction in remote sensing images in the future.

9653-1, Session 1

A systems approach to stealth on the ground revisited *(Invited Paper)*

Kent E. Andersson, The Swedish National Defence College (Sweden); Hans Kariis, FOI-Swedish Defence Research Agency (Sweden); Gunnar Hult, The Swedish National Defence College (Sweden)

The worsening security environment in Northern and Eastern Europe increases the need to give priority to national defence tasks. This in turn increases the interest for high-end technology. The procurement of new army materiel during the first decade of this century has been characterized by states purchasing off -the shelf products, and thereby sponsoring only incremental development. The armed forces focus has been on force protection in asymmetric warfare. Hence, though there has been great development in sensor technology, thereby increasing the potential threat, and in materials science, thereby increasing the possibilities to reduce signatures, the interest in signature management and camouflage for combat vehicles has been modest. The new security development, however, is expected to increase interest from North European states in supporting development of conceptually new stealthy ground platforms, incorporating a decade of advances in technology and experiences from stealth platforms at sea and in the air. The scope of this case-study is to draw experience from where we left off. At the end of the nineties there was a growing interest in stealth for combat vehicles in Sweden. An ambitious technology demonstrator project was launched. One of the outcomes was a proposed Systems Engineering process tailored for signature management presented to SPIE in 2002. (Olsson et.al, A systems approach..., Proc. SPIE 4718) The process was used for the Swedish/BAE Systems Hägglunds AB development of a multirole armored platform (The Swedish acronym is SEP). Before development was completed there was a change of procurement policy in Sweden from domestic development towards Governmental Off-The Shelf, preceded by a Swedish Armed Forces change of focus from national defense only towards expeditionary missions. Lessons learned, of value for future development, are presented. They are deduced from interviews of key-personnel, at the procurer and the industry side respectively, and from document reviews.

9653-2, Session 1

Evaluation criteria for spectral design of camouflage

Christina Åkerlind, FOI-Swedish Defence Research Agency (Sweden) and Linköping Univ. (Sweden); Jan Fagerström, FOI (Sweden); Tomas Hallberg, Hans Kariis, FOI-Swedish Defence Research Agency (Sweden)

In development of VIS-IR camouflage for signature management, the aim is the design of surface properties of an object to spectrally match or adapt to a background and thereby minimizing the contrast. For this purpose, six criteria to put requirements on and to evaluate a good camouflage standard have previously been suggested [1]. The criteria correspond to properties of low reflectance, low gloss, emissivity, dynamic properties, degree of polarization and broadband or multi spectral properties. Diffuse reflectance and low gloss are related and can be achieved through surface roughness. However, these properties are wavelength dependent, and must be viewed in a broad band perspective. Both reflected and emitted radiation has polarization properties, which can be affected by the surface properties.

The six criteria have previously been investigated individually and exemplified on different types of materials. In this work we describe them in relation to one another, and discuss in terms of spectral design, choices of materials and characterization methods for future work, where prioritization between different properties could be necessary. The criteria and their interconnection are compared using sensitivity analysis in evaluation software. Examples are given on effects of parameters on materials and structures for tactically relevant targets.

[1] Kent Andersson, and Christina Åkerlind, "A review of materials for spectral design coatings in signature management applications", Proc. of SPIE Vol. 9253 92530Y-19, 2014, doi: 10.1117/12.2067167.

9653-3, Session 1

Camouflage effectiveness of static nets in SAR images

Johan Jersblad, Saab Barracuda (Sweden); Christer Larsson, Saab Bofors Dynamics AB (Sweden) and Lund Univ. (Sweden)

We present a methodology to determine the camouflage effectiveness of static nets in a SAR image. There is currently no common international recognized methodology within the signature management community in this research topic. One step towards establishing a common methodology is to use a standardized target to be camouflaged. We use the STANdard Decoy for CAmouflage Materials (STANDCAM) target developed by the German Army, WTD 52, Oberjettenberg. STANDCAM is constructed from metal laminated glass fiber and resembles a typical modern vehicle. One side of the target is tracked and the other is wheeled. The signature is non-classified.

An ISAR measurement of the STANDCAM with a camouflage configuration is acquired as the first step of the method. The ISAR data is then blended with SAR data acquired in field trials. The blended data is transformed to match the performance of a typical threat SAR sensor in terms of resolution and noise. In the final SAR image a contrast metric between the target and background is extracted. The contrast measure is then the

measure of the camouflage effectiveness.

The ISAR and SAR measurements should be performed with overlapping frequencies, polarizations and elevation angles for a realistic SAR blending. The ISAR images of the target with or without camouflage are decomposed into scatterers using ideas from compressed sensing. The same procedure is used to decompose measured backgrounds into scatterers. Collections of scatterers are then used to create the blending of the target (with or without camouflage), background and shadow.

As an example of result we present ISAR measurements and determine the camouflage effectiveness in a SAR image using SAR blending for static nets with different electrical conductivity and design.

This methodology presents a qualitative measure to determine the effectiveness of a static net on the STANDCAM target. However, it does not take into account the full performance of ATR algorithms used in SAR radar. A good model for ATR performance is of course also important in order to determine camouflage effectiveness.

The ISAR measurements were performed by the Swedish Defense Research Agency (FOI) at their radar facility Lilla Gåra. The STANDCAM target was positioned on a turntable where a wooden support structure created fixing points outside the turntable for the static nets. The net was erected using standard support poles. The SAR measurements were performed by Saab Dynamics. The SAR data was acquired using a ground-based rail system for the antennas. Data was collected in the X-band at zero degrees elevation in both trials. Both measurement campaigns were funded by the Swedish Defense Material Administrations (FMV) Research and Technology Program.

9653-4, Session 1

Discriminating between camouflaged targets by their time of detection by a human-based observer assessment method

Gorm K. Selj, Morten Søderblom, Norwegian Defence Research Establishment (Norway)

Detection of a camouflaged object in natural sceneries requires the target to be distinguishable from its local background. The development of any new camouflage pattern therefore has to rely on a well-founded test methodology – which has to be correlated with the final purpose of the pattern – as well as an evaluation procedure, containing the optimal criteria for i) discriminating between the targets and then eventually ii) for a final rank of the targets.

In this study we present results from a recent camouflage assessment trial where human observers were used in a search by photo methodology to assess generic test camouflage patterns. We conducted a study to investigate possible improvements in camouflage patterns for battle dress uniforms. The aim was to do a comparative study of potential, and generic patterns intended for use in arid areas (sparsely vegetated, semi desert).

We developed a test methodology that was intended to be simple, reliable and realistic with respect to the operational benefit of camouflage. Therefore we chose to conduct a human based observer trial founded on imagery of realistic targets in natural backgrounds. Inspired by a recent and similar trial in the UK, we developed new and purpose-based software to be able to conduct the observer trial. Our preferred assessment methodology – the observer trial – was based on target recordings in 12 different, but operational relevant scenes, collected in a dry and sparsely vegetated area (Rhodes). The scenes were chosen with the intention to span as broadly as possible. The targets were human-shaped mannequins and were situated identically in each of the scenes to allow for a relative comparison of camouflage effectiveness in each scene. Test of significance, among the targets' performance, was carried out by non-parametric tests as the corresponding time of detection distributions in overall were found to be difficult to parameterize.

From the trial, containing 12 different scenes from sparsely vegetated areas we collected detection time's distributions for 6 generic targets through visual search by 148 observers. We found that the different targets performed differently, given by their corresponding time of detection distributions, within a single scene. Furthermore, we gained an overall ranking over all the 12 scenes by performing a weighted sum over all scenes, intended to keep as much of the vital information on the targets' signature effectiveness as possible. Our results show that it was possible to measure the targets performance relatively to another also when summing over all scenes.

We also compared our ranking based on our preferred criterion (detection time) with a secondary (probability of detection) to assess the sensitivity of a final ranking based upon the test set-up and evaluation criterion. We found our observer-based approach to be well suited regarding its ability to discriminate between similar targets and to assign numeric values to the observed differences in performance. We believe our approach will be well suited as a tool whenever different aspects of camouflage are to be evaluated and understood further.

9653-5, Session 1

Adaptive camouflage in the VIS and IR spectral range: Main principles and mechanisms *(Invited Paper)*

Alexander Schwarz, Fraunhofer-Institut für Optronik, Systemtechnik und Bildauswertung (Germany)

Conventional camouflage materials, devices or systems like covers, nets, suits, colors, coatings, patterns etc. are used usually if the signature of the uncamouflaged object is conspicuous and has to be adjusted to the actual background.

These solutions are passive, i.e. camouflage properties cannot be changed or adapted if necessary.

But better technologies in combination with smart materials make adaptive camouflage more and more applicable in future conflicts.

In this paper several possible principles, mechanisms and materials for rapid configuration of signatures in the VIS and IR spectral range will be presented.

Not all existing principles and mechanisms are described in this paper, because some of them are non-relevant or have small physical adaptive effects proven in a lab under special conditions and are very far from any realistic integration into military systems.

In this paper the most promising principles and mechanisms are described, that have a realistic chance (even though a small chance in some cases) and the potential in not to far future to be realized in adaptive camouflage devices for military application.

These basic adaptive principles are based on the fact that a relevant camouflage property can be influenced or changed by varying another physical or technical parameter.

Beside the working principle and a basic description additional qualities are given such as the operative spectral range, the degree and speed of adaptation, versatility, weight, size, power consumption, robustness, usability and lifetime.

As far as available suppliers, expected costs and the technology readiness level (TRL) are given.

Examples and an overall assessment of each principle complete the paper.

If no clear or detailed information is available or published explicitly a reasonable estimate is given.

9653-6, Session 2

New impressive capabilities of SE-workbench for EO/IR real-time rendering of animated scenarios including flares

Alain Y. Le Goff, DGA Maitrise de L'Information (France); Thierry Cathala, Jean Latger, OKTAL Synthetic Environment (France)

In the field of optronics warfare, DGA Information superiority provides DGA program managers with technical assessments of risk management for various topics including IR flares and self-protection systems for aircraft. It resorts to synthetic image generation to model the operational battlefield of an aircraft, as viewed by IR threats, in order to search for efficient IR flare deployment, specify a self-protection system and then evaluate its capabilities in numerous scenarios. For this purpose, DGA Information superiority completed the SE-Workbench suite from OKTAL-SE with functionalities to predict a realistic aircraft IR signature using highly trustable COTS like Gasturb for gas-turbine modeling or Fluent for CFD. The next step is the physical modeling of flare IR signature by Lacroix Defense using OKTAL-SE technology and the integration of the real-time IR rendering engine of SE-Workbench called SE-FAST-IR

SE-FAST-IR is a set of physics-based software and libraries that allows preparing and visualizing a 3D scene for the EO/IR domain. It takes advantage of recent advances in GPU computing techniques that have significantly increased the capabilities of real-time image simulation and that enable to include complex physical phenomena in a 3D animated scenario, ensuring a high realism in the rendered sequences. It makes intensive use of OpenGL Shader state-of-the-art technology. Some physics computations are processed on the graphics board, resulting in a minimal CPU load that thus remains available for other simulation tasks. The recent past evolutions that have been performed concern the realistic and physical rendering of reflections on both smooth and rough surfaces (e.g. canopy and paint), the rendering of both radiative and thermal shadows, the use of procedural techniques for the managing and the rendering of very large terrains (especially for helicopter applications), the implementation of Image-Based Rendering for plumes with preparation of static signatures and their interpolation for dynamic exploitation, and lastly for objects (aircraft targets and flares) the preparation of several thermal states and their interpolation for dynamic exploitation.

The on-going software development is yet the representation of the spectral, directional, spatial and temporal signature of flares, for both realistic and real time rendering, in the IR spectrum but also near IR and extended visible. This representation is prepared from experimental data that are acquired during windblast tests and high speed track tests. It is based on particle system mechanisms in order to model the different components of a flare (burning core, hot plume, "cold" smoke and scories). The validation of a flare model will comprise a simulation of real trials and a comparison of simulation outputs to experimental results concerning the flare signature and above all the behavior of the stimulated threat.

9653-7, Session 2

Multisensors signature prediction workbench

Jean Latger, Thierry Cathala, OKTAL Synthetic Environment (France)

Guidance of weapon systems relies on sensors to analyse targets signature. Defence weapon systems also need to detect then identify threats also using sensors. The sensors performance is very dependent on conditions e.g. time of day, atmospheric propagation, background ... Visible camera are very efficient for diurnal fine weather conditions, long wave infrared sensors for night vision, radar systems very efficient for seeing through atmosphere and/or foliage ... Besides, multi sensors systems, combining several collocated sensors with associated algorithms of fusion, provide better efficiency (typically for Enhanced Vision Systems). But this sophisticated systems are all the more difficult to conceive, assess and qualify. In that frame, multi sensors simulation is highly required.

This paper focuses on multi sensors simulation tools.

A first part makes a state of the Art of such simulation workbenches with a special focus on SE-Workbench. SE-Workbench is described with regards to infrared/EO sensors, millimetre waves sensors, active EO sensors and GNSS sensors.

SE-WORKBENCH achieves the synthesis of 3D scene observed by a sensor, in four steps:

- first, the physical characterization of the 3D scene behaviour,

- then, the scenario edition (definition of the objects of the scenario, the 3D scene and objects, assignment of trajectories to moving objects, definition of atmospheric and thermal conditions, parameterization of the sensors),

- then, the computation of the physical radiance signal received by the sensor

- at last, the sensor effects modelling.

The SE-WORKBENCH realizes the multi-spectral unification of optronics, electromagnetism and GNSS (Global Navigation Satellite System), using a common kernel and physical extensions assignment both aimed at a unique 3D scene and a common technology.

The first development was in 1994 and has been strongly boosted by the French SCALP missile program and the qualification of the IR tracking system. At the beginning, the SE-WORKBENCH was focused on the IR domain. In 2001, an electromagnetic version of the workshop was initiated, with the help of ONERA French research centre, mainly focused on millimetre waves and wide scenes, typically for SAR applications. A new GNSS version for satellite application has started in 2009. The control of the SE-WORBENCH-EO validity domain is based on both a theoretical validation approach (development of physical models, general modelling and simulation knowledge, elementary tests and validity assessment) and a validation process based on comparisons with experiments (SCALP/EG missile [FR], AASM missile [FR])

Then a general overview of simulation of targets and backgrounds signature objectives is presented, depending on the type of simulation required (parametric studies, open loop simulation, closed loop simulation, hybridisation of software simulation and hardware ...). After the objective review, the paper presents some basic requirements for simulation implementation such as the deterministic behaviour of simulation, mandatory to repeat it many times for parametric studies ...

Several technical topics are then discussed, such as the rendering technique (ray tracing vs. rasterisation), the implementation (CPU vs. GP GPU) and the trade off between physical accuracy and performance of computation.

Examples of results using SE-Workbench are showed and commented.

9653-8, Session 2

Image simulation for hardware In the loop simulation in EO domain

Thierry Cathala, Jean Latger, OKTAL Synthetic Environment (France)

Infrared camera as a weapon sub system for automatic guidance is a key component for military carrier such as missile for example. The associated Image Processing, that controls the navigation, needs to be intensively assessed. Experimentation in the real world is very expensive. This is the main reason why hydride simulation also called HardWare In the Loop (HWIL) is more and more required nowadays.

In that field, IR projectors are able to cast IR fluxes of photons directly onto the IR camera of a given weapon system, typically a missile seeker head.

Though in laboratory, the missile is so stimulated exactly like in the real world, provided a realistic simulation tool enables to perform synthetic images to be displayed by the IR projectors. The key technical challenge is to render the synthetic images at the required frequency.

This paper focuses on OKTAL-SE experience in this domain through its product SE-FAST-HWIL.

The technique associated to SE-FAST-HWIL is called "rasterization". It runs on the GPU using pixel "shaders". A shader is a piece of code that enables to control the way of drawing pixels. Rasterization consists in projecting triangles of the 3D scene onto the 2D screen and then to draw pixels to fill the triangles. It has no correlation at all with any physical process.

The advantage is the performance. For simple images, frequency of some hundreds Hz can be reached.

HWIL is a very tricky activity because it is very hardware dependent. In that frame, Image Generation is the bottleneck because every customer wants to simulate more and more complex 3D scenes, with more and more special effects, for more and more high frequency and accurate sensors. Actually, it is very difficult to assess the trade-off that is necessarily made between the PC hardware performance, and the DataBase complexity.

In order to help the Client to assess this complexity, OKTAL-SE provides within the SE-FAST-HWIL package a set of tools that enables one to prototype the expected performance for a given hardware and a given 3D DataBase complexity.

With SE-FAST-HWIL package, the customer can play on several parameters:

- The type of PC and especially of 3D graphic board
- The type of OS (Windows versus Linux)
- The type of antialiasing and 3D graphic board configuration
- The amount of polygon
- The size of polygons
- The amount of texture

Examples are given, in the frame of the SE-Workbench. The presentation focuses on trials on real operational complex 3D cases. In particular, two important topics, that are very sensitive with regards to IG performance, are detailed: first the 3D sea surface representation and then particle systems rendering especially to simulate flares. Beyond "projection mode", some information will be given on the SE-FAST-HWIL new capabilities dedicated to "injection mode".

9653-9, Session 2

Simulation of atmospheric and terrestrial background signatures for detection and tracking scenarios

Caroline Schweitzer, Karin Stein, Fraunhofer-Institut für Optronik, Systemtechnik und Bildauswertung (Germany)

In the fields of early warning, one is depending on reliable image exploitation: Only if the applied detection and tracking algorithms work efficiently, the threat approach alert can be given fast enough to ensure a timely evacuation and an automatic initiation of the countermeasure. In order to evaluate the performance of those algorithms for a certain electro-optical (EO) sensor system, test sequences need to be modelled as realistic and detailed as possible. Since the signature of background and target are both influenced by the atmospheric conditions that the future system will be exposed to, the application of comprehensive atmospheric modelling tools is essential.

This paper gives an introduction of the atmospheric modelling tools that are currently used at Fraunhofer IOSB to simulate spectral background signatures in the infrared (IR) range. It is also demonstrated, how those signatures are affected by changing atmospheric and climatic conditions. In conclusion – and with a special focus on the modelling of different clouds types - sources of error and limits are discussed.

9653-11, Session 2

Modelling the combined infrared and radar signature of the wake of a vessel

Miranda van Iersel, Bernadetta Devecchi, TNO Defence, Security and Safety (Netherlands)

Each vessel moving in the sea, imprints a perturbation on the wave structure of the sea and forms a so-called wake. These wakes can be used in the detection of a target, but can also help in identifying its characteristics. Several studies concentrated on detection of a target wake by making use of either radar or infrared sensors. We model the infrared and radar signature of the wake and sea surface background and investigate the synergy between the two bands. The primary goal of this work is to make a comparative study between the two bands in order to be able to discriminate which sensor gives a more reliable detection in which scenario.

9653-12, Session 3

Spectral analysis of the vegetative background in the NIR and SWIR spectral range

Max E. Winkelmann, Fraunhofer-Institut für Optronik, Systemtechnik und Bildauswertung (Germany)

The conspicuity of a target is always regarded in relation to a background. Therefore it is necessary to define and analyse the background. In moderate climate the natural background consists heavily of vegetation. In the Near Infrared (NIR) spectral range (from 750 nm to 1200 nm) the red edge (chlorophyll becoming transparent) is known to dominate the spectra increasing reflection significantly. The spectra in the Short Wave Infrared (SWIR) spectral range (from 1200 nm to 2500 nm) is dominated by the decrease of the reflectivity to values less than 0.1 and water absorption (at 1490 nm and 1950 nm). This absorption features can be exploited with imagery as the atmospheric water absorption is smaller than the absorption in a liquid with several other ingredients as plants show it. Furthermore the maximum of the absorption is shifted due to the liquid effects on the water molecules.

The data from the ASTER library can be used to qualify the spectral behaviour of vegetative background. This data is measured for a direct reflection for several undefined leaves with canopy and a grass sod. To assess the conspicuity, the variation of the background has also to be taken into account. There are several publications (for example from Sims et.al. and Danson et.al.) to address the dependency of the reflectance of vegetation on the internal leave structure. To get an idea of this variation of the reflectance in vegetative backgrounds, we have measured the spectral characteristics in the lab and field with various devices. Aerial imagery suffers from the influence of soil effects (see Huete et.al.) and should not be taken into account for such a survey.

The effect of varying water content will be described and an estimation of the variation of vegetative backgrounds will be given. Furthermore there will be a comparison to other background materials with and without water content.

The difference between measurements of directional reflectance measured in field measurements and the integrated hemispherical reflectance is discussed together with the angular dependence of reflection of a structured surface.

Literature:

F. M. DANSON, M. D. STEVEN, T. J. MALTHUS & J. A. CLARK (1992): High-spectral resolution data for determining leaf water content, International Journal of Remote Sensing, 13:3, 461-470

Daniel A.Sims, John A. Gamon (2003): Estimation of vegetation water content and photosynthetic tissue area from spectral reflectance: a comparison of indices based on liquid water and chlorophyll absorption features, Remote Sensing of Environment 84 (2003) 526–537

A.R. HUETE, R.D. JACKSON, D.F. POST (1985): Spectral

response of a Plant Canopy with Different Soil Background, Remote Sensing of Environment 17:37-53 (1985)

9653-13, Session 3

Iranian Seijil III: extraction of gradient intensities of asymmetric exhaust plumes in boost phase

Clifford A. Paiva, BSM Research Associates (United States)

Research addresses asymmetric missile exhaust plume, ionization/plasma effects, in ascent (boost-phase). Functions of hard-body ascent, divert attitude control systems, plume expansions, and Prandtl-Meyer reverse exhaust plume flows, confirm detection algorithms' potential difficulties. Specifically it is demonstrated that these algorithms adversely affect multi-wavelength (SWIR-MWIR-LWIR) discrimination interception methodologies, since these are based exclusively upon symmetric gradient edge intensities. Selected target case study is the Iranian Seijil-3, two stage solid propellant (HTPB/aluminum/NH4-CLO4) missile system with post-boost vehicle (PBV) hydrazine/N2O4, liquid propellant, attitude control systems. Boost-phase and early mid-course (late ascent) missile exhaust plumes have been shown to generate a variety of very challenging ionization and plasma spectral effects, and these tend to degrade automatic target detection, acquisition, classification and identification (ATDCI) algorithms. Missile plume intrinsic core detection and acquisition in SWIR prior to MWIR-LWIR transfer to classification and identification, remain the primary challenge.

9653-15, Session 3

The Havemann-Taylor Fast Radiative Transfer Code (HT-FRTC) and its application within Tactical Decision Aids (TDAs)

Jean-Claude Thelen, Stephan Havemann, Gerald J Wong, Met Office (United Kingdom)

The HT-FRTC is a component of the Met Office Neon Tactical Decision Aid (TDA). Within Neon the HT-FRTC has for a number of years been used to predict the IR apparent thermal contrasts between different surface types as observed by an airborne sensor. To do this, the FRTC is supplied with the inherent temperatures and spectral properties of these surfaces (i.e. ground target(s) and surrounding background).

A strength of the HT-FRTC is its ability to take into account the detailed properties of the atmosphere, which in the context of Neon tends to be provided by a Numerical Weather Prediction (NWP) forecast model. Incorporated into the HT-FRTC is an exact treatment of atmospheric scattering based on spherical harmonics. This allows the treatment of different aerosol and cloud types. Recent developments even account for rain and falling snow.

The HT-FRTC has been extended to cover the spectral range of the Photopic and NVG sensors. One aim here is to give the user guidance on the expected light levels, especially at night, again taking the atmospheric conditions into account. A recent development allows such predictions during twilight.

The user of the code can add new sensors by simply supplying files that contain their sensor's spectral properties.

The HT-FRTC works in Principal Component space which significantly reduces the computational requirements regarding memory and time.

Other applications of the HT-FRTC include simulations of satellite and airborne hyperspectral sounders. The HT-FRTC is also used as the forward model in variational retrieval schemes of atmosphere and surface parameters.

9653-16, Session 3

FTOM-2D: a two-dimensional approach to model the detailed thermal behavior of nonplanar surfaces

Berndt Bartos, Karin Stein, Fraunhofer-IOSB (Germany)

The Fraunhofer thermal object model (FTOM) predicts the temperature of an object as a function of the environmental conditions. The model has an outer layer exchanging radiation and heat with the environment and a stack of layers beyond modifying the thermal behavior. The orientation of the layer is defined by the normal vector of the surface. The innermost layer is at a constant or variable temperature called core temperature. All the layers have a heat capacity and a thermal conductivity. The outer layers properties are color (visible), emissivity (IR), coefficients for free and forced convection, and a factor for latent heat. The environmental parameters are air temperature, wind speed, relative humidity, irradiation of the sun, and thermal radiation of the sky and ground. The properties of the model (7 parameters) are fitted to minimize the difference between the prediction and a time series of measured temperatures. The size of the time series is one or more days with 288 values per day (5 minute resolution). The model can be used for very different objects like backgrounds (meadow, forest, stone, sand) or objects like vehicles.

The two dimensional enhancement was developed two model more complex objects with non-planar surfaces and heat conduction between adjacent regions. In this model we call the small thermal homogenous interacting regions thermal pixels. A simple array is used to define the geometry, which can be edited by hand and does not need a difficult geometry editor. For each thermal pixel the orientation and the identities of the adjacent pixels are stored in the array. In this version the heat conductivity between adjacent thermal pixels is the same for all pairs of pixels and the properties of all outer layers are the same summing up to 8 parameters to fit. The model is limited to a convex geometry to reduce the complexity of the heat exchange and allow for a higher number of thermal pixels.

For the test of the model time series of thermal images of a test object (Cubi) were analyzed. The test object is made of steel plates forming an L-shaped arrangement of three cubes with length of the edges of 50 cm. The square sides of the cubes were modeled as 25 thermal pixels (5 x 5). In the time series of thermal images small areas (10 cm x 10 cm) were analyzed to generate data files that can easily be read by the model. For the fit only a selected number of thermal pixels were compared to the thermal time series.

The program was developed with Matlab. The differential equation for the heat transfer is the time consuming part in the computation and was programmed in C. The fit used the Nelder-Mead simplex method available in Matlab. The algorithm needed typically 500 cycles and about 20 minutes of time for a single run. The core temperature in the Cubi was not constant but varies with the temperature of the outer plates and had to be estimated. The comparison showed a good agreement of the fitted and not fitted thermal pixels with the measured temperatures. This indicates the ability of the model to predict the temperatures of the whole object.

In the future the model will be enhanced to model thermal regions of different sizes. The speed will be optimized using C++ and using parallel processing (OpenMP) on multi-processor server systems.

9653-17, Session 3

Comparison of the relative merits of the midwave and longwave infrared bands for various target types using detected thermal contrast

Seán M. Stewart, Nazarbayev Univ. (Kazakhstan)

The two most important atmospheric transmission bands in the infrared occur at the midwave band of 3–5 ?m and the

longwave band of 8–12 ?m respectively. For a given infrared detector, which of the two spectral bands, if any, gives the better performance is often asked but is a question steeped in controversy. Despite a number of different approaches having been attempted in the past, no definitive answer to this question has been reached. In the literature one continues to find conflicting and often contradictory results even in cases where similar formulations using the simplest of models have been used. In this study an analysis designed to assess the relative merits of detectors operating in the midwave and longwave infrared bands based on the recently defined thermal figure of merit known as the detected thermal contrast for a range of different target types is undertaken. As a concept, thermal contrast provides an important measure of performance as it allows a target to be distinguished from its background on the basis of temperature alone. Under ideal limiting conditions typical of those found for many industrial and scientific applications, by considering a range of targets whose spectral emissivities vary linearly as a function of both wavelength and temperature, closed-form expressions for the detected thermal contrast for both thermal and quantum based detectors are calculated in terms of polylogarithm functions. When used as a measure of performance the detected thermal contrast is found to be very robust as it is more heavily influenced by changes in temperature occurring over the surface of the target rather than from small changes in the spectral content of the emitted radiation. The detected thermal contrast is therefore less affected by ill-defined spectral target emissivities, one of the greatest sources of uncertainty in any thermal-imaging system. In agreement with our earlier work, where spectral target emissivities linearly dependent on temperature for tungsten targets were considered, the midwave band for either detector type is found to give the better performance for a range of different target types while differences between the two types of detectors is not as significant as others have previously claimed. The work not only confirms earlier work performed using simpler models for the spectral target emissivity, it also impugns several results previously reported in the literature relating to the behaviour of the detected thermal contrast within a given spectral interval and for the type of detector used.

9653-18, Session 4

An approach to optimal hyperspectral and multispectral signature and image data fusion for detecting hidden targets on shorelines *(Invited Paper)*

Charles R. Bostater Jr., Florida Institute of Technology (United States)

Hyperspectral and multispectral imagery of shorelines collected from airborne and shipborne platforms are used to correct pushbroom imagery using inertial motion motions units and augmented global positioning data. Corrected reflectance image types are then used to optimize the new high spatial resolution spectral signatures. The process demonstrated utilizes littoral zone features from imagery acquired in the Gulf of Mexico and shoreline imagery using a newly developed technique that makes use of numerically embedded targets in the higher spatial resolution multispectral images. The fusion process utilizes a optimization procedure to obtain the new higher spatial resolution spectral resolution signatures of obscured embedded targets within shoreline vegetation. Results presented and demonstrated suggest the ability to refine difficult targets within vegetation, shoreline vegetation and in submerged littoral zone airborne imagery using a combination of sensor data types, image fusion, and simulation techniques. The techniques hold promise for enhancing situational awareness during environmental surveillance and monitoring activities.

9653-19, Session 4

Assessment of target detection limits in hyperspectral data

Wolfgang Gross, Fraunhofer-Institut für Optronik, Systemtechnik und Bildauswertung (Germany); Jonas Böhler, Univ. Zürich (Switzerland); Hendrik Schilling, Wolfgang Middelmann, Fraunhofer-Institut für Optronik, Systemtechnik und Bildauswertung (Germany); Jörg Weyermann, Univ. Zürich (Switzerland); Peter Wellig, Roland Oechslin, Armasuisse (Switzerland); Mathias Kneubühler, Univ. Zürich (Switzerland)

Hyperspectral remote sensing data can be used for civil and military applications to detect and classify target objects that cannot be reliably separated using broadband sensors. The comparably low spatial resolution is compensated by the fact that small targets, even below image resolution, can still be classified.

The goal of this paper is to determine the target size to spatial resolution ratio for successful classification of different target and background materials. Airborne hyperspectral data is used to simulate data with known mixture ratios and to estimate the detection threshold for given false alarm rates.

The data was collected in July 2014 over Greding, Germany, using airborne aisaEAGLE and aisaHAWK hyperspectral sensors. On the ground, various target materials were placed on natural background. The targets were four quadratic molton patches with an edge length of 7m in the colors black, white, grey and green. Also, two different types of polyethylene with an edge length of approximately 5.5m were deployed.

Synthetic data is generated from the original data using spectral mixtures. Target signatures are linearly combined with different background materials in specific ratios. The simulated mixtures are appended to the original data and the target areas are removed for evaluation. Commonly used classification algorithms, e.g. Matched Filtering, Adaptive Cosine Estimator etc. are used to determine the detection limit. Fixed false alarm rates are employed to find and analyze certain regions where false alarms usually occur first. A combination of 18 targets and 12 backgrounds is analyzed for three VNIR and two SWIR data sets of the same area.

9653-20, Session 4

Utilization of hyperspectral camera for determination of camouflage surfaces spectral characteristics homogeneity

František Racek, Univ. of Defence (Czech Republic); Adam Jobánek, Military Research Institute (Czech Republic); Teodor Baláž, Univ. of Defence (Czech Republic)

The paper deals with description of newly developing method of Hyperspectral camera utilization for determination of camouflage surfaces spectral characteristics homogeneity. The color patterns of camouflage surfaces are usually checked pointwise. It is assumed subsequently that the spectral characteristics of the pattern are the same for whole area of camouflage surface. The essential properties of hyperspectral camera allow to determine the level of spectral qualities homogeneity of the surface. Although the respective snapping of hyperspectral image is fairly easy, the evaluation of HS datacube features specific problems connected with homogeneity of illumination, optical system aberrations, transformation to reflectance and spectral unmixing. All the measurement aspects have to be taken into account to correctly determine the homogeneity of camouflage surfaces spectral characteristics.

1. INTRODUCTION

Camouflage could be, among others, understood as an effort to provide subject with the spectral signatures similar to

its background. Spectral-wise this process exceeded visual band long ago mainly towards the IR area. Validation of the camouflage materials (e.g. prints) spectral requirements fulfilment in lab conditions plays crucial role on the way to better camouflage. Hyperspectral techniques described in this paper could improve the quality control by changing the concept of spectral defects identification on the camouflage prints and thereby increase the effectiveness of camouflage.

2. HYPERSPECTRAL IMAGING AND DATA PROCESSING

The principal of hyperspectral (HS) imaging is established on exploitation of a portion of the electromagnetic spectrum segmented into narrow bands for the purpose of additional analysis. Image created this way is called hyperspectral datacube. Possible interpretation of the datacube is a set of image vectors, where any image vector is recognized as a spectrum pertains to pixel spatial element. Simply expressed, the overall spectral reflectance of the object in the pixel spatial element is known in the case of HS imaging contrary to the color or intensity only in the case of traditional imaging.

The measurement chain has to be properly prepared to reach the goal of the task, to judge the aerial spectral qualities of camouflage surfaces correctly. The main attention is focused on both spatial and spectral resolution of eventual HS datacube. In the ideal case of snapping the HS image we assume the uniformly widespread illumination and aberrationless optical imaging system of HS camera. The HS datacube processing than consists of the suitable HS datacube conversion to reflectance and spectral unmixing for the color spot edges. Since the ideal conditions cannot be fulfilled the additional effects like non-uniform illumination, chromatic aberration of imaging system has to be taken into account.

3. RESULT

The HS imaging is proper way of the camouflage surfaces spectral qualities validation. It allows the sufficiently accurate, quick and cheap measurement. Nonetheless the HS datacube processing has to be made properly, under assumption of all possible effects, to judge the aerial spectral qualities of camouflage surfaces correctly.

9653-21, Session 4

Analysis of exploitable spectral features of target and background materials

Max E. Winkelmann, Fraunhofer-Institut für Optronik, Systemtechnik und Bildauswertung (Germany)

The development of hyperspectral cameras and the increasing sensitivity of detectors are enabling the exploitation of spectral features. As object detection is done by comparing the radiation originating from an object and its background the task of camouflage is not only to analyse the spectral features of the objects but also the features of the background. In the reflection dominated electro-optical spectral range (from 0.4 μm to 2.5 μm) the spectral reflectivity is usually used to describe the signature. In the emission dominated electro-optical spectral range (from 3 μm to 12 μm) not only reflectivity/emissivity are relevant but also the temperature of the objects resulting from environmental influence and thermal properties of the material incorporating surface structures. Nonetheless, some features of spectral reflectivity will influence the detectability of an object in relation to certain backgrounds.

The visual (VIS) spectral range can usually be neglected in this analysis according to the colour impression in this spectral range. In the visual spectral range there are already multispectral sensors in use (both the human eye and cameras) and therefore patterns including different spectrally reflecting materials (colours) are used for camouflage issues. The use of camouflage patterns might also be an opportunity to camouflage objects in other spectral ranges if the spectral background characteristics can not be reproduced by a single camouflage material.

Results from several spectral measurements will be presented. Some results are:

Adjustment of the reflectance of camouflage textiles to both the Near Infrared (NIR) spectral range (from 750 nm to 1200 nm) and Short Wave Infrared (SWIR) spectral range (from 1200 nm to 2500 nm) to match a vegetative background is difficult.

The reflectance of a textile is influenced by its colours for the VIS, NIR and SWIR spectral range; contrary to the thermal spectral range where the reflectance is dominated by the fibres it consists of.

The reflectivity of sand in the thermal longwave (LW) and the thermal midwave (MW) spectral range depends on the grain size which makes it difficult to predict the spectral appearance of sand in a realistic environment. The effect can be seen in both quartzite samples and collected samples from operational areas.

Water absorption features in the SWIR spectral range will be difficult to be reproduced by camouflage materials.

As a consequence of these results, methods will be discussed how these spectral differences between camouflage materials and the background can be exploited and how camouflage materials can be improved to avoid these exploitations.

9653-22, Session 5

Precision targeting in guided munition using IR sensor and MmW radar

Sreeja S., Indian Institute of Technology Bombay (India); Hari B. Hablani, Indian Institute of Technology Gandhinagar (India); Hemendra Arya, Indian Institute of Technology Bombay (India)

The miss distance in conventional munitions can be improved by incorporating sensors for target detection and guidance during the flight. Then a guided munition will have a higher probability of disabling target. The advantage of a PGM compared with other types of munition is that it provides a very low collateral damage and a high probability of hitting the target.

This paper is concerned with a Precision Guided Munition equipped with an Infrared sensor and Millimeter Wave radar [IR and MmW, for short]. The IR sensor is passive and it responds to the temperature difference between target and background. The IR sensor is a part of the infrared search and track (IRST) system of the munition guidance system. The IRST delineates the hot region of the target and tracks it. The two-dimensional imagery of the target is obtained through a two-dimensional scanning of the target area by linear detector array. The infrared sensor and the millimeter wave radar sensor suite lends robustness to the guidance system of the munition. In an inclement weather, the impaired operation of the IR sensor will be compensated for by the MmW radar, which operates in all weathers. Conversely, a degraded operation of the MmW radar in jamming environment will be compensated for by the passive IR sensor measurement. An IR sensor measures angular co-ordinates (azimuth and elevation) of a target and MmW radar measures the range.

The target under consideration is a low maneuvering tank. For the present study, the tank motion is modeled as a second-order Gauss-Markov Process. The IRST system collects temperature distribution of the target and background area as pixel intensity in focal plane image. The existence of the target is detected from the measurements extracted from the focal plane image of the IR sensor. Segmentation is used to separate background from the target image using pixel intensity variation. A tracking window is generated in the image, in pixel units, after segmentation process. The precise detection of the target is by the detection of the centroid of a hot spot target. The centroid is estimated by calculating the centre of mass of high pixel intensity area, i.e., pixels inside the tracking window. The integration of guidance, control, and target sensing is achieved by combining the state space model of vehicle dynamics and engagement kinematics. To filter the target sensing noise and to estimate the target line-of-sight rate, an integrated state space model is considered along with an extended Kalman Filter for estimation. The miss distance achieved by including by image processing delays

is 1.65 m, which is greater than miss distance by without considering image processing i.e.,1.20 m. The IR sensor senses the target image every 25 msec but the centroid estimation is at a frequency of 10 Hz. Every 100 msec, centroids of four consecutive images are averaged, yielding a time-averaged centroid, implying some measurement delay. The centroid measurement is used to estimate the line-of-sight rate required for the guidance law to precisely guide the munition to the target.

9653-23, Session 5

Real-time object detection and tracking in omni-directional surveillance using GPU

Florian Depraz, Vladan Popovic, Ecole Polytechnique Fédérale de Lausanne (Switzerland); Beat Ott, Peter Wellig, Armasuisse (Switzerland); Yusuf Leblebici, Ecole Polytechnique Fédérale de Lausanne (Switzerland)

Recent technological advancements in hardware systems have made better quality and more powerful cameras with higher resolutions available. Modern panoramic systems use multiple cameras to produce videos with a resolution of 9000 x 2400 pixels at a rate of 30 frames per second (fps) [1]. Isolating and detecting movements of all objects present in a scene require analysis of all the information contained in the pixels within the frames. Many modern applications use object tracking to determine the speed and the path taken by each object moving through a scene. This is done by analyzing the difference between two or more consecutive frames. In fields like surveillance systems, crowd analysis or traffic control, processing lots of individual pixels must be done in real time. All items in the scene should be detected with the least amount of false recognitions. False recognitions can

be due to tree movements, clouds, or waves which are part of the background and should be discarded.

Several state-of-the-art algorithms are used to extract the pixels composing the objects from the background ones [2]. This paper only concentrates on Background Subtraction Techniques [3], from the basic implementation with a learning rate to the One-Gaussian and Gaussian Mixture Model (GMM) implementations [3]. Using this approach we generate a model of the background scene containing all the pixels considered as background. This step is known as background modeling. The foreground pixels are extracted from the processed frame and compared to the corresponding ones of the model. Using a connected-component detector, neighboring pixels are gathered in order to form blobs which correspond to the detected foreground objects. The new blobs are compared to the ones formed in the previous frame to see if the corresponding object has moved.

Graphics Processing Units (GPUs) are powerful devices with lots of processing capabilities for parallel jobs and oating points operations. The detection of objects requires a large amount of pixel operations on the video frames that can be done in parallel, making GPU a good choice for the processing platform. The connected-component detector is also suitable for a parallel implementation using the GPU's shared memory to merge the temporary results. During the detection, some foreground pixels may not be properly detected. To resolve this issue, morphological operations, such as erosion and dilation, are used. Similarly, these algorithms are implemented in parallel manner to decrease processing time and increase the quality of the results.

In this paper, we present real-time implementations of Background Subtraction Techniques and a connected component detector using a GPU, by parallelizing the processing pipeline. Furthermore, we talk about real-time processing techniques to cope with environment changes, image noise, camouflage/obfuscation and detection of false positives. We present the results of our object detection implementation on omni-directional videos acquired by the system presented in [1]. Finally, we compare the detectability of the objects in the scene depending on their shape, size and speed, using various methods chosen to detect the foreground pixels, and the processing speed for each of the selected methods.

[1] Omer Cogal, Abdulkadir Akin, Kerem Seyid, Vladan Popovic, Alexandre Schmid, Beat Ott, Peter Wellig, and Yusuf Leblebici. A new omni-directional multi-camera system for high resolution surveillance. Proc. SPIE 9120, Mobile Multimedia/Image Processing, Security, and Applications 2014, 91200N, 9120, May 2014.

[2] Alper Yilmaz, Omar Javed, and Mubarak Shah. Object tracking: A survey. ACM Comput. Surv., 38(4), Dec 2006.

[3] M. Piccardi. Background subtraction techniques: a review. In Systems, Man and Cybernetics, 2004 IEEE International Conference on, volume 4, pages 3099{3104 vol.4, Oct 2004.

9653-24, Session 5

RecceMan®: an interactive recognition assistance for imaging reconnaissance: synergistic effects of human perception and computational methods for object recognition, identification and infrastructure analysis

Nadia El Bekri, Susanne Angele, Elisabeth Peinsipp-Byma, Fraunhofer-Institut für Optronik, Systemtechnik und Bildauswertung (Germany); Martin Rückhäberle, Fraunhofer IOSB (Germany); Bruno Haelke, Ausbildungszentrum für Abbildende Aufklärung der Luftwaffe (Germany)

In this paper, we introduce an interactive recognition assistance system for imaging reconnaissance. This system supports aerial image analysts on missions during three main tasks: Object recognition, object identification and infrastructure analysis. Based on satellite or aerial images, aerial image analysts are able to extract single object features and thereby recognize different object types. It is one of the most challenging tasks in the imaging reconnaissance. Currently there are no high potential ATR (automatic target recognition) applications available, as consequence the human observer cannot be replaced entirely. State of the art ATR applications cannot assume in equal measure the human perception and the ability of his interpretation. Why is this still such a critical issue? First, cluttered and noisy images make it difficult to automatically extract, classify and identify object types. Second, due to the changed warfare and the rise of asymmetric threats it is nearly impossible to create an underlying data set containing all features, object or infrastructure types. Many other reasons like environmental parameters or aspect angles compound the application of ATR supplementary. Due to the lack of suitable ATR procedures, the human factor is still important and so far irreplaceable. In order to use the potential benefits of the human perception and computational methods in a synergistic way, both are unified in an interactive assistance system. RecceMan® offers two different modes for aerial image analysts on missions: the object recognition mode and the infrastructure analysis mode. The aim of the object recognition mode is to recognize a certain object type based on the object features that originated from the image signatures. The infrastructure analysis mode pursue the goal to analyze the function of the infrastructure. The image analyst extracts visually certain target object signatures, assigns them to corresponding object features and is finally able to recognize the object type. The system offers him the possibility to assign the image signatures to features given by sample images. In order to distinguish the weak signal of a target object sample images are offered for different sensor types (e.g. visible, infrared) in order to compare the signatures. The underlying data set contains a wide range of objects features and object types for different domains like ships, land vehicles. Each domain has its own feature tree developed by aerial image analyst experts. By selecting the corresponding features, the possible solution set of objects is automatically reduced and matches only the objects that contain the selected features. Moreover we give

an outlook of current research in the field of ground target analysis in which we deal with partly automated methods to extract image signatures and assign them to the corresponding features. This research includes methods for automatically determining the orientation of an object and geometric features like width and length of the object. This step enables to reduce automatically the possible object types offered to the image analyst by the interactive recognition assistance system.

9653-25, Session 5

Evaluation of UAV video change detection using simulation tools

Günter Saur, Jan Bartelsen, Fraunhofer IOSB (Germany)

Change detection is one of the most important tasks when applying unmanned aerial vehicles (UAV) for video reconnaissance and surveillance. Here we address changes of short time scale, i. e. the observations are taken in time distances from several minutes up to few hours. Each observation is a short video sequence corresponding to the near-nadir overflight of the UAV over the interesting area and the relevant changes are e.g. recently parked or moved vehicles/objects. The change detection algorithm has to distinguish between relevant and non-relevant changes. Examples for non-relevant changes are 3D structures of the scene and compression or transmission artifacts.

Before an automatic change detection component can be operationally used as part of an UAV video exploitation system, an evaluation and assessment process has to be accomplished. Basis for the evaluation is a large video data set containing many relevant objects with varying scene background and altering influence parameters. Results of the evaluation are performance characteristics of the change detection components when applied to data satisfying certain specifications, e.g. minimum object size, minimum ground sampling distance and minimum image quality. An important influence parameter is the relation of the relevant objects to their scene background, e.g. if they are salient or (partially) occluded or camouflaged or simply not obvious since many other irrelevant changes (e.g. 3D effects) are present. The generation of real test data for performing an overall evaluation is limited for practical reasons of expense and by the fact that many influence parameters in practice cannot be varied independently from each other.

Simulation tools such as VBS3 offer a convenient means to create systematically a large amount of video data including ground truth. In this paper we develop some conceptual aspects of how to use simulation tools to evaluate a change detection processing chain. we use a change detection component of the video exploitation system ABUL of Fraunhofer IOSB, Saur & Krüger [1]. The processing chain consists of 3 steps applied to the input consisting of 2 selected video clips each containing an overflight over the scene: (1) Video mosaicking for each video clip. (2) Image referencing and geometric and radiometric adaption. (3) Change detection between the video mosaics.

As initial scene model a road segment was selected which passes through an urban and rural landscape with vegetation such as trees, bushes and meadows. To a second instance of this scene various objects (small to large) at different locations (on, near, off the road) are added. By selecting flightpaths with suitable sensor orientation, video clips are created in which the sensor footprint follows the road. Many instances of video clip are generated by varying the flightpath, sensor parameters, and the objects. For evaluation, a pair of video clips is selected, the video change detection is applied and the result was compared to the ground truth.

Starting by using two identical flight paths we analyze the influence of object appearance in different scene background. In a further step, varying flightpaths leading to 3D parallax will be investigated.

9653-26, Session 5

Spectral anomaly detection in radiological search

Thomas L. McCullough, John Hague, National Security Technologies, LLC (United States)

Radiological search and mapping depends on the successful recognition of anomalies in large data sets which contain varied and dynamic backgrounds.

We present a new algorithmic approach for real-time anomaly detection which is resistant to common detector imperfections, avoids the limitations of a source template library and provides immediate -- and easily interpretable -- user feedback.

This algorithm is based on a continuous wavelet transform for variance reduction and evaluates the deviation between a foreground measurement and a local background expectation using methods from linear algebra.

We also present a technique for recognizing and visualizing spectrally similar clusters of data.

This technique uses Laplacian Eigenmap Manifold Learning to perform dimensional reduction which preserves the geometric “closeness” of the data while maintaining sensitivity to outlying data.

We illustrate the utility of both techniques on real-world data sets.

9653-27, Session 6

Human factors of target detection tasks within heavily cluttered video scenes

Samuel W. Huber, Forventis-GmbH (Switzerland); Peter Wellig, Armasuisse (Switzerland)

Background: Algorithms show difficulties in distinguishing weak signals of a target from a cluttered background, a task that humans tend to master relatively easily. But still, human performance has its limitations. We conducted two studies to identify how various degrees of clutter influence operator performance and search patterns in a visual target detection task. We believe that the results may help to optimize the design and functionality of support algorithms intended to help human operators to better perform surveillance tasks.

Methods: In the first (explorative) study 8 male subjects had to look for specific female targets within a heavily cluttered public area. The area was crowded with averagely 140 persons. Subjects were supported by differing amounts of markings that helped them to identify females in general. We presented short video clips together with still images and analyzed the search patterns in relation to the number of markings presented using eyetracking technology (SMI REDm, Sensomotoric instruments) and a tachistoscopic procedure (VisalyserTM). For the second (quantitative) study, 18 male UAV pilots, payload operators and FLIR operators were tasked to identify 22 specific trucks on a heavily frequented motorway intersection. We presented them with video material from a UAV surveillance mission. The video image was subdivided in three zones: The central zone (CZ), a circle area of 10°, representing the parafoveal region. The peripheral zone (PZ) corresponded to a 4:3 format while the hyper peripheral zone (HPZ) represented the region left and right to the 4:3 area specific to the 16:9 format. We analyzed fixation densities and task performance using eyetracking technology (Eyetracker SMI REDm, Sensomotoric Instruments) and task protocols.

Results: In the first study, we found an approximately U-shaped correlation between the number of markings in a video and the degree of structure in search patterns as well as performance. The subjects showed a rather erratic scan pattern for the video material containing 0 and 40 markings while they developed a more structured approach when presented with material containing 5, 10 or 20 markings. Also mean detection times (MDT) were best for the 5, 10 and 20 markings conditions (MDT0=24.2s, MDT5=1.8s, MDT10=4.9s,

MDT20=3.6s, MDT40=14.9s). For the motorway surveillance task we found a difference in MDT for CZ vs. HPZ (p=0.01) and PZ vs. HPZ (p=0.003) but no difference for CZ vs. PZ (p=0.491) (MDTCZ=2.72s; MDTPZ=2.4s; MDTHPZ=4.73s). There were no differences in detection rate for the respective zones. We found the highest fixation density CZ decreasing towards the HPZ.

Conclusion: We were able to demonstrate that markings could increase surveillance operator performance in a cluttered environment as long as their number is kept in an optimal range. When performing a search task within a heavily cluttered environment, humans tend to show rather erratic search patterns and spend more time watching central picture areas.

9653-28, Session 6

Evaluation of statistical methods for the evaluation of observer trials for the assessment of the effectiveness of signature measures

Patrick Dunau, Daniel Fitz, Karin Stein, Fraunhofer-Institut für Optronik, Systemtechnik und Bildauswertung (Germany)

An observer trial represents a sophisticated method for the assessment of the effectiveness of camouflage measures. When analyzing the effectiveness or quality of signature measures, the quantity sought for, is subject to the purpose, the signature measure was developed for. Depending on the intention the signature measure was generated for, e.g. camouflage in different spectra or deception, the effectiveness considers different characteristics. Inferring from that, evaluating the potential of a signature measure by observer trials is subject to individual planning. In order to extract the quantities of interest, statistical evaluations have to be performed on the results of the observer trials. If observer trials are used for the analysis of the effectiveness of signature measures, the yield of statistical evaluations is subject to limits. Different statistical methods are analyzed in order to identify these limits.

In order to achieve statistical relevance, at least 40 observers are required for carrying out statistical analyses on observer trials. The individual observer's results can be interpreted as a sample of all possible trial results. Using methods of the descriptive statistics, the statistical parameters variance, median and range can be calculated from the sample. If multiple samples exist, e.g. for different object or different observer classes, further analysis can be performed. In order to evaluate the differences between two samples, a statistical hypothesis test can be applied. The test analyzes if the differences between the samples are statistically significant or insignificant. Statistical parameters of the samples and the information about the statistical significance of the difference of two or more samples do not directly contribute to the evaluation of effectiveness.

Another possibility for the evaluation of observer's results is offered by the "receiver operating characteristic" (ROC). The ROC curve plots the true positive rate against the false positive rate by altering the discrimination threshold of the classifier, deciding whether some result data point is called a true or false positive. Each point on the ROC curve belongs to a certain discrimination threshold. This threshold yields specific values for specificity, i.e. the portion of wrong decisions for the true data points, and for the sensitivity, i.e. the portion of correct decisions for the true data points. On the basis of these values the false alarm rate and the true positive rate are computed. The point on the ROC curve is given by the ratio of sensitivity and specificity, where the x value denotes the false alarm rate and the y value gives the sensitivity, i.e. true positive rate. The curve can be interpreted using the area under curve (AUC) value, which can be recognized as the probability of detecting an object. In signal detection theory the AUC value is called "detectability". The ROC curve and the AUC value yield a representation for the effectiveness of a certain signature measure.

Consequently methods mentioned above, will be evaluated by considering their capabilities for the use in signature evaluation.

In this paper two different observer trial situations will be depicted and the methods will be used in order to evaluate the trial results. The methods will be analyzed to show their applicability for the evaluation of the effectiveness of signatures.

9653-29, Session 6

Performance of target distinctness metrics evaluated against colour and monochromatic photosimulation results

Vivienne C. Wheaton, Joanne B. Culpepper, Defence Science and Technology Organisation (Australia)

The TNO Human Factors Search_2 dataset (Toet et al., 1998) is a valuable resource for studies in target detection, providing researchers with observational data against which image-based target distinctness metrics and detection models can be tested. The observational data provided with the Search_2 dataset was created by human observers searching colour images projected from a slide projector to an effective 10-times magnification. Often, target distinctness metrics studies (Nyberg and Bohman, 2001, Chang and Zhang, 2006) are however carried out not on colour images but on images that are processed into greyscale by various means. This is usually done for ease of analysis and meaningful interpretation. Utility of a metric for modelling target detection performance is usually assessed by analysing the correlation between metric results and observational results recorded from the Search_2 observer experiment. However, the question remains of how well the results from the target distinctness metrics analysed from monochromatic images could be expected to compare to the observational results from colour images.

We present results of a photosimulation experiment conducted using a monochromatic representation of the Search_2 dataset and an analysis of several target distinctness metrics. The greyscale images presented to observers were created by processing the Search_2 images into L*, a* and b* colour space representations, and presenting the L* (lightness) image. The results of this experiment are compared with the original Search_2 results, comparing the effect of viewing monochromatic and colour images. Good correlation is obtained between the monochrome photosimulation and the original data in terms of the probability of correct detection (correlation of 0.83)and the mean search time (correlation of 0.83). Two common target distinctness metrics, Root Sum of Squares (RSS) and the standard Doyle metric (Copeland et al., 1996), and two newer metrics, Pixel Contrast (Culpepper and Wheaton, 2014) and target variance, are applied to these monochrome images. The target distinctness metrics results are compared to the results of the monochrome photosimulation experiment, and the original Search_2 results, examining which contrast metrics perform differently when evaluated against colour or monochrome observational results.

References:

CHANG, H. & ZHANG, J. 2006. New metrics for clutter affecting human target acquisition. IEEE Transactions on Aerospace and Electronic Systems, 42, 361-368.

COPELAND, A. C., TRIVEDI, M. M. & MCMANAMEY, J. R. 1996. Evaluation of image metrics for target discrimination using psychophysical experiments. SPIE Opt. Eng., 35, 1714-1722.

CULPEPPER, J. B. & WHEATON, V. C. A target detection model predicting field observer performance in maritime scenes. Proc. SPIE 9249, Electro-Optic and Infrared Systems: Technology and Applications XI, 7 October 2014 2014. 92490C.

NYBERG, S. & BOHMAN, L. 2001. Assessing camouflage methods using textural features. SPIE Opt. Eng., 40, 1859-1876.

TOET, A., BIJL, P., KOOI, F. L. & VALETON, J. M. 1998. A high-resolution image data set for testing search and detection models, Soesterberg, The Netherlands, TNO Human Factors Research Institute.

9653-30, Session 6

Disruptive camouflage tricks the human eye: a study of detection times of two near-similar targets in natural backgrounds

Gorm K. Selj, Norwegian Defence Research Establishment (Norway)

Our current understanding of camouflage, in military as well as in evolutionary perspectives, has evolved during the last 100 years. In that period of time several underlying principles have emerged. It has turned out in the recent decade that background pattern matching alone may not be sufficient to conceal targets because of the ubiquitous and revealing information contained by the edges of a target. In this paper we have studied one concealment strategy, the so-called disruptive coloration, further as it predicts that high contrast patches placed at the target's outline will impede detection, by creating false target edges when exposed to the observer. This is thought to be due to the patches' abilities to distract the observer's attention, hindering detection. Such disruptive coloration is contra-intuitive as it may impede detection in spite of the fact that the patches themselves may be poorly concealed.

In military environments the "disruptive approach" within camouflage has been textbook material for decades. Still, little has been reported, supporting this idea, especially when it comes to the concealment of human targets in natural sceneries. We report here experimental evidence from a field study, containing detection data from 12 unique natural scenes (5 testing the disruptive effect, 7 as reference tests), with both human targets and human observers, showing that disruptively colored camouflage patches along a human's outline (its head) may increase detection time significantly as when compared to a similar (human) target concealed only with background matching.

An inspection of the detection times distributions for the two (near identical) targets in 5 different natural scenes, show that the target (T1) with the disruptive patch at the head periphery had significantly longer detection times (p never exceeding 0.064) in 3 of the scenes as when compared to the other target (T2) with no such patch. In the two remaining scenes, we found no significant difference between the two target's performances. However, in these two scenes, the targets were in overall poorly adapted to the background and likely to be revealed so quickly that any disruptive effect was difficult to assess. In 7 of 7 reference scenes, with no disruptive patch in either of the two targets, we found no significant performance in any of the 7 scenes, indicating that the two near identical targets were similar in performance whenever the disruptive patch was not present in any of the targets.

Hence, our results support the idea that disruptive coloration may impede detection and similarly that the best concealment is achieved when disruptive coloration is added to a target that matches the background (reasonably) well.

This study raises important question to the current understanding of human vision and concealment in natural backgrounds as well as to any approach to describe the human visual system mathematically.

9653-31, Session 6

A comparison between maritime field observations and photosimulation for developing and validating visible signature evaluation tools

Joanne B. Culpepper, Vivienne C. Wheaton, Defence Science and Technology Organisation (Australia); Qi T. Shao, Defence Science and Technology Organisation (Australia) and YTEK Pty Ltd. (Australia); Alistair Furnell, Defence Science and Technology Organisation (Australia)

Over the past 50 years, the majority of detection models used to assess visible signatures have been developed and validated using static imagery. Some of these models are the German developed CAMAELEON (CAMouflage Assessment by Evaluation of Local Energy Spatial Frequency and OrieNtation) model and the U.S. Army's Night Vision and Electronic Sensors Directorate (NVESD) ACQUIRE and TTP (Targeting Task Performance) models. All these models gathered the necessary human observer data for development and validation from static images in photosimulation experiments. In this paper, we compare the results of a field observation trial to a static photosimulation experiment.

A field observation trial was conducted in 2013 using eleven Royal Australian Navy observers. The observers were tasked to search for a small maritime target in an entirely open ocean scene from an elevation of approximately 33 m. After viewing the scene for 60 s, observers rated confidence in detection on a four point scale and recorded bearing to the target using a compass. Simultaneously, imagery of the small maritime target was taken. This imagery was used in a static image photosimulation trial conducted in 2014. Eight Royal Australian Navy observers participated in the static photosimulation trial, three of which also participated in the original field observation trial. In the photosimulation trial, the observers were tasked to search each scene and to identify the target location. A time limit of 50 s was placed on the visual search task, after which the next image was presented.

The probability of detection obtained from the field observation trial was compared to the detection probability obtained from the static photosimulation trial. The comparison showed no correlation between the field trial and the static image photosimulation detection probabilities, where a Spearman correlation coefficient of -0.3 was calculated. These results question the validity of using static photosimulation to develop and validate maritime visible signature evaluation tools. Instead, a more valid approach may be to source the necessary perception data from field observations.

SPIE. REMOTE SENSING

SPIE. SECURITY+ DEFENCE

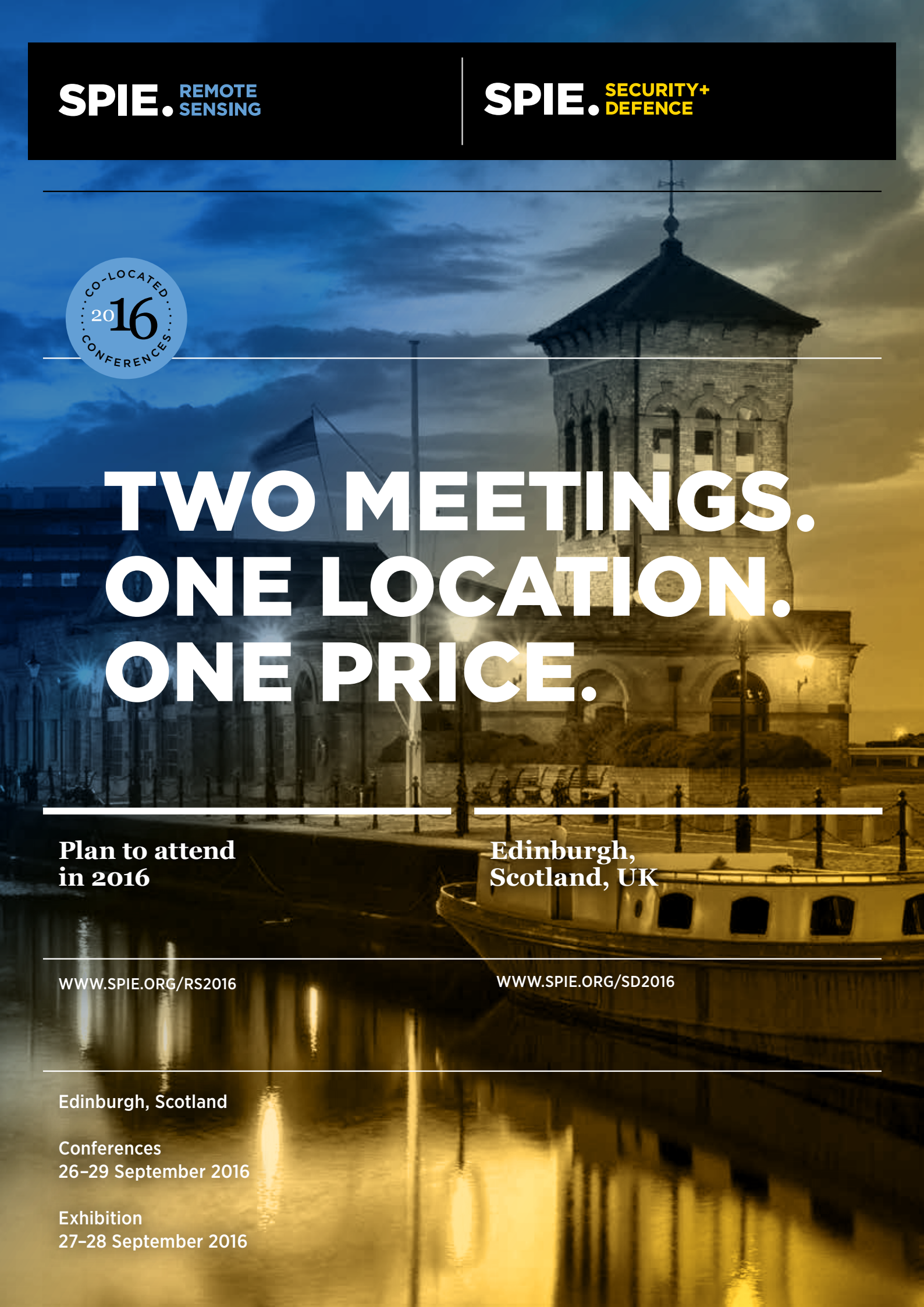

TWO MEETINGS. ONE LOCATION. ONE PRICE.

Plan to attend in 2016

Edinburgh, Scotland, UK

WWW.SPIE.ORG/RS2016

WWW.SPIE.ORG/SD2016

Edinburgh, Scotland

Conferences
26–29 September 2016

Exhibition
27–28 September 2016